Fossil Fuels Utilization

Environmental Concerns

ACS SYMPOSIUM SERIES **319**

Fossil Fuels Utilization

Environmental Concerns

Richard Markuszewski, EDITOR
Ames Laboratory
Iowa State University

Bernard D. Blaustein, EDITOR
U.S. Department of Energy
Pittsburgh Energy Technology Center

TD 196 .F67A44 1985 copy 1

American Chemical Society.
 Meeting 1985 :
 Fossil fuels utilization

ACS Symposium Series

M. Joan Comstock, *Series Editor*

FOREWORD

The ACS SYMPOSIUM SERIES was founded in 1974 to provide a medium for publishing symposia quickly in book form. The format of the Series parallels that of the continuing ADVANCES IN CHEMISTRY SERIES except that, in order to save time, the papers are not typeset but are reproduced as they are submitted by the authors in camera-ready form. Papers are reviewed under the supervision of the Editors with the assistance of the Series Advisory Board and are selected to maintain the integrity of the symposia; however, verbatim reproductions of previously published papers are not accepted. Both reviews and reports of research are acceptable, because symposia may embrace both types of presentation.

PREFACE

CONCERNS ABOUT THE ENVIRONMENTAL EFFECTS of emissions resulting from the combustion of fossil fuels, particularly coal, continue to increase as the utilization of these fuels grows. The large amounts of sulfur dioxide and nitrogen oxides emitted into the atmosphere and the attempts to tie these fossil-fuel-derived pollutants directly to the undeniably difficult problem of acid rain have caused heated debates, numerous research studies, government actions, and serious efforts to reduce pollution. The issues are extremely complex, and our understanding of the origin, properties, behavior, and effects of these pollutants is incomplete. Often, theories are contradictory.

Yet it seems that emissions of all pollutants, including acid rain precursors, particulates, trace elements, and organics, should be limited as much as possible, even if the interrelationships of cause and effect are not yet clearly defined. The question is, however, how to limit emissions in a timely, economical, and technically effective manner without disrupting the industrial or social fabric of our nation.

The efforts at mitigating pollution caused by fossil fuel utilization encompass a broad spectrum of environmentalists, legislators, and concerned citizens, as well as a multidisciplinary array of scientists, engineers, and health officials. The diversity of approaches to solve this serious problem is reflected in the wide range of topics covered by the contributions to this volume.

In the first three sections, 19 chapters relate different methods that address the main options for reducing pollutants: (1) removal of sulfur, ash, and trace elements prior to combustion; (2) control of emissions by various techniques or adjustment of conditions during combustion; and (3) cleanup of combustion effluents in various gas streams. In the last section, 10 chapters describe the characterization, reactions, transport, and effects of pollutants emitted during the combustion of fossil fuels.

Most chapters are reports of original research, and as such provide insight into possible solutions or problems in a narrow field. However, several chapters review the current state of technology and point to future directions for necessary research. No one chapter provides a complete answer to the elusive and controversial question of how to limit emissions, yet each chapter contributes to our understanding of the science and technology involved in achieving this goal. As a group, the chapters in this

ix

volume represent the complex nature of the problem and the necessity for interdisciplinary approaches to addressing environmental concerns in fossil fuel utilization.

RICHARD MARKUSZEWSKI
Fossil Energy Program
Ames Laboratory
Iowa State University
Ames, IA 50011

BERNARD D. BLAUSTEIN
Pittsburgh Energy Technology Center
U.S. Department of Energy
P.O. Box 10940
Pittsburgh, PA 15236

July 23, 1986

1

Advanced Physical Coal Cleaning
A Strategy for Controlling Acid Rain Precursor Emissions

Thomas J. Feeley, III, and Bernard D. Blaustein

Pittsburgh Energy Technology Center, U.S. Department of Energy, Pittsburgh, PA 15236

The United States has made impressive strides in reducing atmospheric emissions of sulfur dioxide since passage of the Clean Air Act Amendments of 1970. However, significant amounts of SO_2 continue to be emitted and these emissions may increase. A large percentage of these emissions are produced by coal-fired electric utilities, and these sources have been targeted for further SO_2 reductions in numerous acid rain control proposals. Advanced physical fine-coal cleaning to remove pyrite may provide a viable strategy for reducing future SO_2 emissions. There is a large research effort to develop advanced coal-cleaning technologies as a cost-effective means to control acid rain precursor emissions from coal-fired power plants and large industrial sources.

In recent years there has been increased concern about emissions of sulfur dioxide (SO_2) and nitrogen oxides (NO_x) from fossil fuel combustion and about the role that SO_2 and NO_x play in the formation of acid precipitation. With the passage of the Clean Air Act Amendments in 1970 and 1977, regulations were enacted to control the major emitters of SO_2 and NO_x ([1,2]). New Source Performance Standards (NSPS) were established in 1971 to limit SO_2 emissions from coal-fired power plants. The NSPS were later revised in 1979 to include a percentage reduction requirement. These regulations proved to be an effective tool in protecting air quality. After reaching a peak in 1973, national annual emissions of SO_2 declined by 28 percent between 1973 and 1983. This decline is all the more impressive because electric utility coal consumption increased by about 60 percent during the same period. Relatively large amounts of pollutants continue to be emitted, however, and emissions are projected to increase. Table I gives the National Acid Precipitation Assessment Program's 1980 emissions estimates for SO_2 and NO_x by source category ([3]). As shown, sources in the United States emitted 24.6 teragrams of SO_2 and 21.5 teragrams of NO_x in 1980. Table II presents projected U.S. emissions estimates ([4]). The data

Table I.   Pollutant Emissions in 1980 by Source Category

	Pollutant (Tg/Yr)	
Source Category	SO_2	NO_x
Electric Utilities	15.7	7.3
Industrial Combustion	3.4	4.1
Residential/Commercial Combustion	0.8	0.6
Non-ferrous Smelters	1.1	Neg.
Other Industrial Processes	2.7	0.9
Transportation	0.8	8.3
Miscellaneous	0.1	0.3
Total	24.6	21.5

Data taken from reference 3, page 34.   Note change in units.

Table II.   U.S. Current and Projected SO_2 and NO_x Emissions

Source Category	Current 1980 (Tg/Yr)		Projected 1990 (Tg/Yr)		Projected 2000 (Tg/Yr)	
	SO_2	NO_x	SO_2	NO_x	SO_2	NO_x
Electric Utilities	15.0	5.6	15.9	7.2	16.2	8.7
Industrial Boilers and Process Heaters	2.4	3.5	3.4	3.0	6.5	4.0
Nonferrous Smelters	1.4		0.5		0.5	
Residential/Commercial	0.8	0.7	1.0	0.7	0.9	0.6
Other Industrial Processes	2.9	0.7	1.2	0.8	1.5	1.1
Transportation	0.8	8.5	0.8	7.8	1.0	9.7
TOTALS	24.1	19.0	22.8	19.5	26.6	24.1

Source: Reference 4, page 2-94.

cited by Homolya and Robinson (page 2-94 in reference 4) show an increase in both SO_2 and NO_x for the year 2000 as compared to 1980.

Acid Deposition

The level of emissions of SO_2 and NO_x, and their effects in the United States and in other industrialized countries have been the target of considerable debate.   When SO_2 and NO_x are emitted into the atmosphere, a large fraction of these pollutants can be oxidized to sulfate and nitrate during atmospheric transport, and then deposited as acidic compounds (4-8).   Acid rain is the popular term to describe this complex phenomenon.   Acidic compounds can be deposited in both wet and dry forms, and this process is more properly referred to as acid deposition or acid precipitation.   The wet forms of acid deposition include rain, snow, fog, and dew.   Dry deposition occurs via absorption of SO_2 and NO_x on surfaces and via

the gravitational settling (deposition) of fine particulate aerosols, some of which are acidic. For a discussion of dry deposition, see the chapter by Hicks in reference 4.

The question of what to do about acid deposition is a very complex and controversial one. The controversy surrounding acid deposition is fueled by a less-than-perfect understanding of its sources, chemistry, transport, effects, and mitigation. Numerous overviews on acid deposition have been published (3-13) and much research is currently being carried out (14,15). Field studies have indicated that large portions of the eastern United States and southeastern Canada are subject to deposition of environmentally significant amounts of sulfate and nitrate, as shown in Figures 1 and 2. In some locations, these acidic compounds have contributed to an average annual precipitation pH as low as 4.2 (see Figure 3). (Figures 1 to 3 are adapted from Figures 8-14, 8-15, and 8-17 in reference 4.) In the eastern United States, sulfur compounds are responsible for about two-thirds of the acidity of precipitation, with nitrogen compounds accounting for the remaining one-third. This relative contribution to acid precipitation is essentially reversed in the western United States.

Many of the areas currently receiving high levels of acid deposition contain aquatic and terrestrial ecosystems susceptible to acidification (16-21). The adverse effect of acid deposition has been most clearly documented in the acidification of lakes and streams located in these sensitive areas. Acidification can alter biological populations and communities, as well as reduce the number of species within them. Often, acidified waters are found in regions that have little or no natural capacity to neutralize acidity. The insufficient buffering capacity of these lakes, streams, and surrounding soils serves to exacerbate the problem. There is further concern about impacts on forests, although the extent to which acid deposition contributes to forest damage and decline is not at all clear. Our incomplete understanding of acid deposition is underscored by our lack of knowledge of the sequence of events involved in its formation. It is generally agreed that SO_2 and NO_x emitted from human activities are the primary precursors of acid deposition in the United States. Once in the atmosphere, these pollutants undergo a complex series of chemical reactions as they are converted to their acidic forms. During this conversion, SO_2 and NO_x can be transported long distances, so that for a given receptor site, remote sources can add significantly to the contribution of local sources (22). Therefore, emissions from one region of the United States can contribute to deposition of acidic materials in another region hundreds of kilometers downwind. However, because of the complex chemical transformation and atmospheric transport processes involved, there is as yet no accepted method to establish with certainty the specific sources that give rise to acid deposition in a given receptor area.

Only a few papers in this symposium directly address the issue of acid deposition. Almost all, however, are related to some aspect of the problem. The chemistry and effects of combustion-derived air pollutants, as well as methods for characterizing these emissions, are reported. In addition, a number of papers focus on the three categories of control options available for reducing SO_2 and NO_x: precombustion, during combustion, and postcombustion.
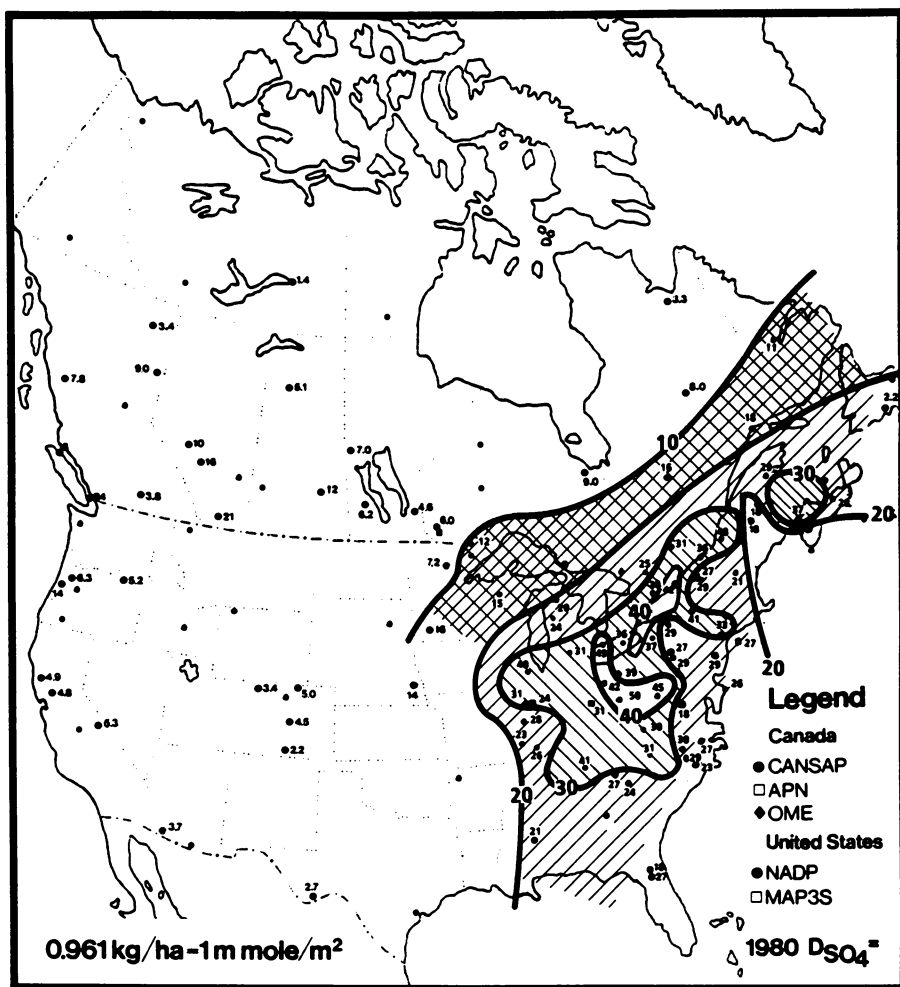
Figure 1. Precipitation amount - weighted mean sulphate ion deposition for 1980 (m moles per square metre).
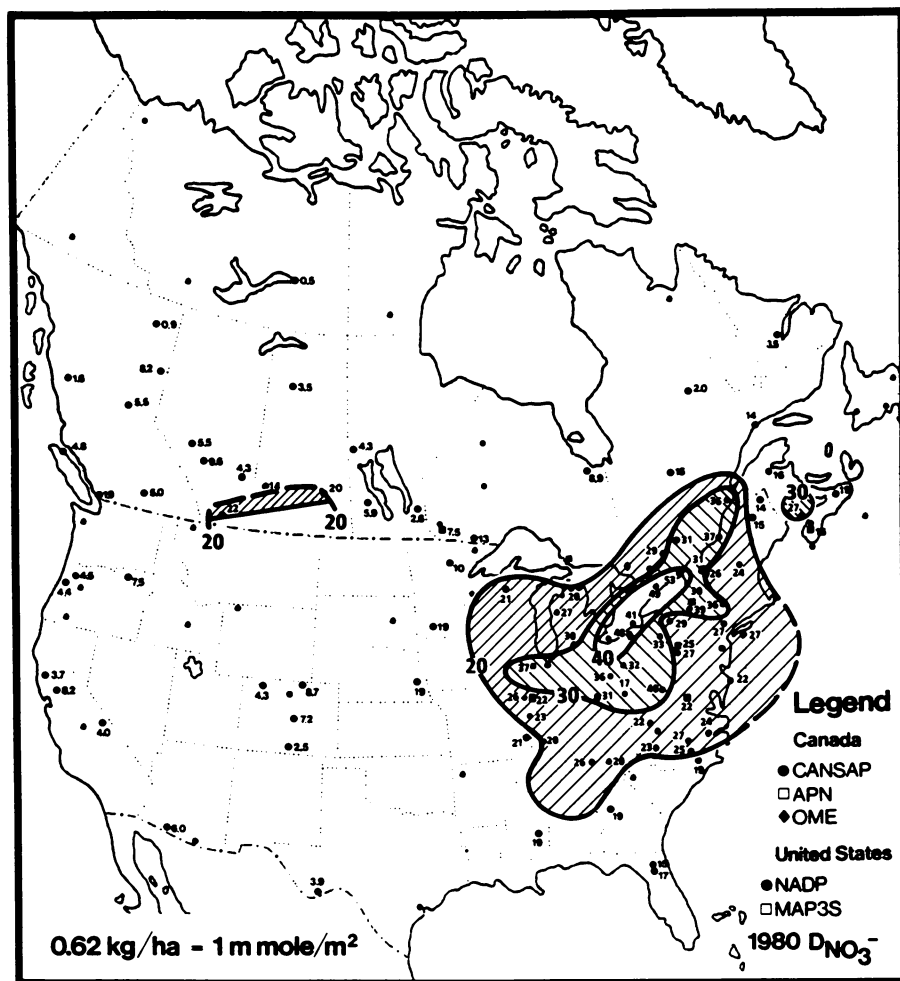
Figure 2.   Precipitation amount - weighted mean nitrate ion
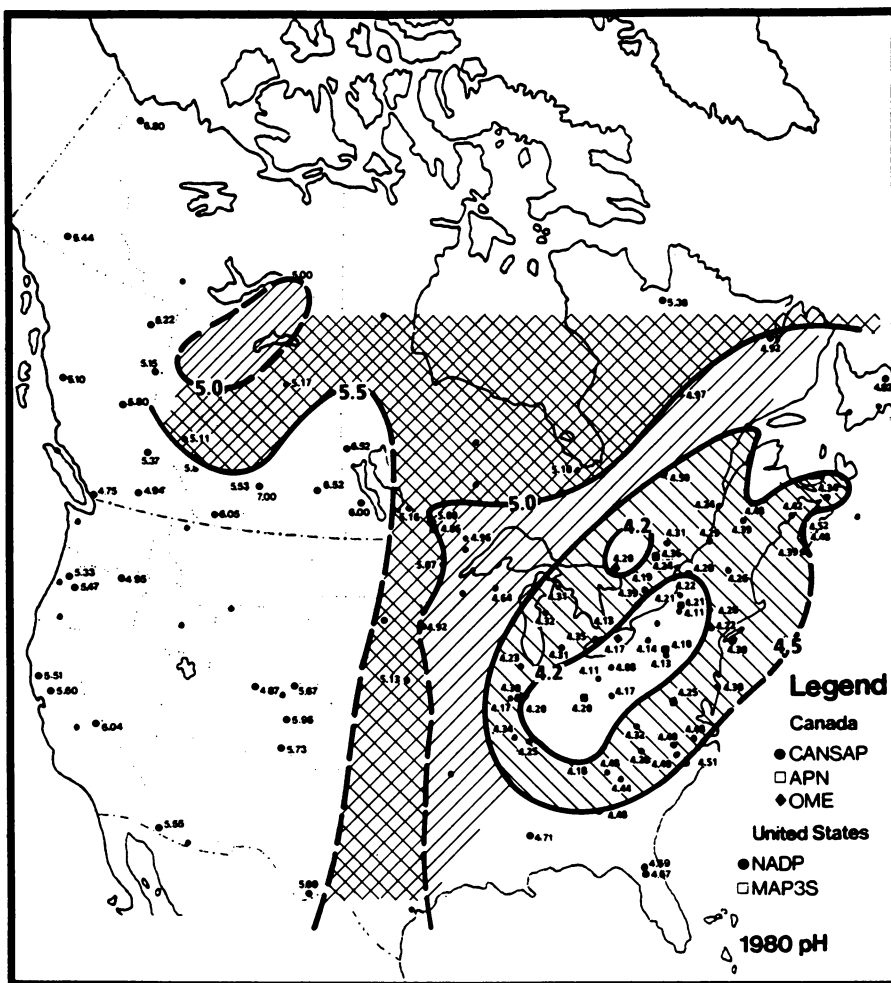deposition for 1980 (m moles per square metre).

Figure 3.   Precipitation amount - weighted mean annual pH in North America for the calendar year 1980.

Precombustion control involves removal of sulfur compounds from fuel prior to combustion. Control during combustion employs techniques to minimize the formation and/or release of SO_2 and NO_x during the combustion process. Finally, SO_2 and NO_x can be removed from the combustion flue gas using various postcombustion control methods. This chapter discusses the potential of mitigating acid deposition through precombustion cleaning of coal to remove sulfur compounds.

Sulfur Dioxide Emissions

Although both SO_2 and NO_x are precursors to acid deposition, SO_2 has been targeted most often for reduction. Of the approximately 25 teragrams (27 million tons) of SO_2 emitted in 1980, coal-burning electric utilities were responsible for nearly two-thirds. As mentioned, the 1971 and revised-1979 NSPS are designed to curb emissions of SO_2 from coal-fired utilities. These performance requirements have been quite successful in controlling SO_2 emissions from new coal-burning units brought on line since 1971. However, it is the relatively uncontrolled emissions from older coal-fired power plants that have called attention to these boilers for further control measures. Numerous legislation has been offered at both the state and federal level to achieve a reduction in SO_2, much of which will come from further restrictions on coal-fired utility emissions. Some bills call for as much as an 8-12 million ton reduction in annual SO_2 emissions from 1980 levels.

There are a number of options available for controlling SO_2 from coal-fired power plants. Selection of a control strategy should further reductions in SO_2 be required will be contingent on a number of factors specific to each utility. Not the least important are the cost and reduction efficiencies of the available options. Table III presents cost and performance estimates for various SO_2 control technologies from a recent Office of Technology Assessment (OTA) report ([8]). As shown, with the possible exception of switching to a lower sulfur coal, there is a general increase in cost (mills per kilowatt hour) as reduction efficiencies increase. The relationship between SO_2 reduction and cost is also illustrated in Figure 4 from the OTA report, which shows utility SO_2 control costs for various reduction scenarios. There is considerable scatter in the estimates, but the eight studies cited agree sufficiently to show that for SO_2 reductions of several million tons per year, total annualized costs will be in the billions of dollars.

The potentially high cost of reducing current SO_2 emissions has prompted continued development of pollution control technologies. One practical method for controlling SO_2 emissions from coal-fired power plants is physical coal cleaning ([23-26]). Although greatly coal-specific, coal cleaning can in some cases produce coal that is in compliance with the 1971 NSPS of 1.2 pounds of SO_2 emitted per million Btu heat input ([24]). The 1971 and 1979 NSPS for SO_2 for coal-burning electric utilities, and the percentage reduction requirements used to classify coals into four categories, each subject to a different level of SO_2 reduction, are shown in Table IV. Allowable sulfur dioxide emissions to the atmosphere range from a high of 1.2 lb/10^6Btu heat input to a low of 0.6 lb/10^6Btu heat input or less, depending on the amount of

Table III. Overview of Control Technologies for Sulfur Dioxide

Control Technology	Reduction Efficiencies (percent)	Revenue Requirements (mills/kWh)	Stage of Development
Fuel switching	30-90	0-7	In use
Physical coal cleaning	5-40	1-5	In use
Chemical coal cleaning	60-85	NA	Emerging
Wet flue gas desulfurization	70-95	10-17	In use
Dry flue gas desulfurization	40-90	9-15	In use
Regenerable flue gas desulfurization	70-90	12-25	Available

Source: Reference 8, page 157.

Table IV. New Source Performance Standards for SO_2, 1971 and 1979

Source	Potential SO_2 in Raw Coal, lb/SO_2/10^6 Btu	SO_2 Reduction Required, %	Sulfur Dioxide Emission Limits lb SO_2/10^6 Btu
Coal-Fired Boilers, >250 million Btu/hr, for which construction commenced after 08/17/71	---	---	1.2
Coal-Fired Utility Boilers, >250 million Btu/hr, for which construction commenced after 09/19/78	<2	70	0.6
	2 to 6	70 to 90	0.6
	6 to 12	90	1.2
	>12	>90	1.2

sulfur in the raw coal. For low-sulfur coals, only a 70 percent reduction in potential SO_2 emissions is required when actual emissions are less than 0.6 lb/10^6Btu heat input. The 1979 NSPS permit a sliding scale of 70 percent to 90 percent SO_2 reduction for intermediate-sulfur coals (see Table IV). At present, as shown in Table III, flue gas desulfurization is the only technology available for achieving 70 to 90 percent SO_2 reductions. Coal cleaning followed by flue gas desulfurization is one possible strategy for meeting the 1979 NSPS's more stringent percentage reduction requirements (25).

Figure 4. Comparisons of utility SO_2 control costs -- estimates of 31-State aggregate control costs made by OTA and other groups.

Coal Cleaning

Coal cleaning, or coal preparation, involves the removal of sulfur compounds prior to combustion. The primary forms of sulfur in coal are inorganic (mostly pyrite) and organic. Organic sulfur, which can constitute as much as one-half or more of the total sulfur in some U.S. coals, is chemically bound in the coal structure and cannot be removed by physical cleaning processes. Consequently, physical coal cleaning alone is unable to meet the 1979 NSPS and would have to be used in combination with flue gas scrubbing to meet these standards. Research is currently under way also on chemical cleaning methods that remove essentially all the organic sulfur in coal and thus produce a clean coal that can meet the new NSPS without need for flue gas cleanup.

Present day coal cleaning physically removes the inorganic (pyritic) sulfur in coal. Commercial coal-cleaning plants typically employ several physical cleaning techniques, depending on the size and type of coal to be cleaned and on the desired end use for the product. The plants are most commonly equipped with jigs, dense-medium vessels, dense-medium cyclones, concentrating tables, and flotation cells (26). All except the latter rely on the difference between the density of coal and its mineral impurities. Coal has a lower specific gravity (approximately 1.3-1.5) than the mineral matter associated with it (specific gravity in the range of 2.0-5.0), including pyrite. By placing coal in a liquid of intermediate specific gravity, it can be separated from its mineral matter. For instance, dense-medium vessels use a suspension of magnetite in water to separate, or "float", the lighter coal particles from the heavier mineral matter, which sinks to the bottom as refuse (see Figure 5).

Currently, about 70 percent of the coal mined east of the Mississippi River is cleaned in commercial preparation plants (27). This includes both metallurgical and steam coal. Although coal cleaning has not traditionally been a means to control SO_2 emissions but rather has been a way to control coal quality, it can remove up to 40 percent of the pyritic sulfur in coal. Hence, for utilities using "washed" coal, SO_2 discharged to the atmosphere is less than would be the case if as-mined coal was burned. Other benefits from burning a cleaned coal include reduced transportation cost per Btu of material shipped, reduced coal-pulverizing and boiler-maintenance costs, increased boiler reliability and availability, and reduced waste disposal requirements (23,28).

Physical Coal Cleaning

There have been several assessments of the potential of physical coal cleaning for reducing SO_2 emissions (29-31). Maronde and Deurbrouck (31) estimated the maximum potential sulfur reduction that could be achieved through extensive cleaning of coals from the Northern Appalachian Region: Maryland, Ohio, Pennsylvania, and northern West Virginia. The study focused on the 11 highest producing coal seams, which accounted for approximately 94 percent of the 168.4 million tons of coal mined in the region in 1982. (The United States produced about 833 million tons of coal in 1982 (32).) The Northern Appalachian Region has a reserve base
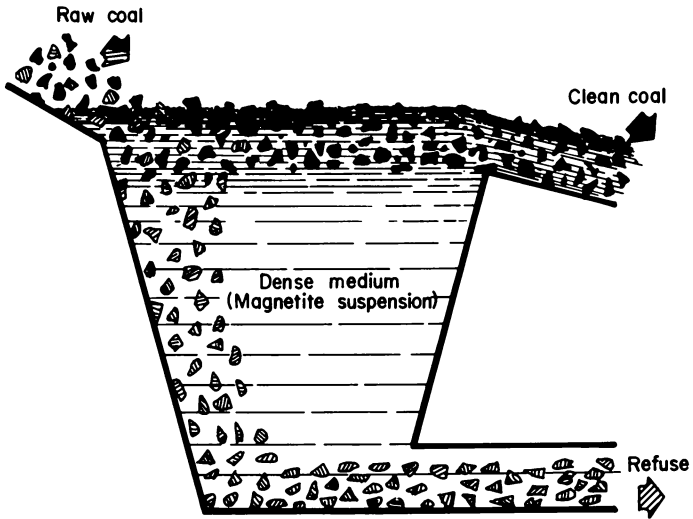
Figure 5.   Schematic diagram of a dense-medium coal-cleaning
vessel.

in excess of 64 billion tons of high-quality medium- to high-sulfur coal. This compares to a total U.S. reserve base of more than 488 billion tons (32). On the average, two-thirds of the sulfur in the coal from this region is pyritic, making these coals excellent candidates for physical coal cleaning.

Table V presents sulfur reduction data for two of the major coal seams in the region: the Pittsburgh Seam and the Lower Kittanning Seam. Laboratory washability (float-and-sink) analyses of representative samples of these coals were used to determine potential sulfur reductions at various levels of cleaning. To assess the impact on regional SO_2 emissions, sulfur reduction potentials were estimated for only those coals both produced and utilized in the Northern Appalachian Region. The "Present Level" of cleaning shown in the table represents estimated base-line values for the amount of sulfur in the coal product. These values take into consideration any coal cleaning that occurred, and are compared to coal sulfur contents that would result from more intense levels of cleaning. Each of the 11 major coal-producing seams in the region were evaluated in this manner.

Table V. Theoretical Effects of Coal Cleaning on Sulfur Reduction for Two Northern Appalachian Coals Mined in 1982

Level of Cleaning	Clean Coal Product - Thousands of Tons -	Sulfur	Sulfur Reduction (Percent)	Mining Requirement, Thousands of Tons
Pittsburgh Seam				
Present Level	33,769	987	--	43,429
1 1/2" x 0 at 1.40 sp. gr.	32,238	743	24.7	47,381
3/8" x 0 at 1.40 sp. gr.	32,061	672	31.9	48,495
14 mesh x 0 at 1.30 sp. gr.	31,088	514	47.8	68,862
Lower Kittanning Seam				
Present Level	13,391	368	--	15,864
1 1/2" x 0 at 1.40 sp. gr.	12,408	197	46.5	18,240
3/8" x 0 at 1.40 sp. gr.	12,290	169	54.1	18,597
14 mesh x 0 at 1.30 sp. gr.	11,930	136	63.0	30,116

Source: Reference 31.

As shown in Table V, the sulfur reduction potential for these two coals is significant. At 1982 production levels, the sulfur content of Pittsburgh Seam coal would be reduced by almost 48 percent, from 987,000 tons to 514,000 tons, through intensive cleaning. This level of cleaning was simulated in the laboratory by crushing coal to 14 mesh x 0 (the largest particle would pass through a screen opening of 1.40 mm). The crushed coal was then placed in a liquid medium of 1.30 specific gravity to separate the clean coal from the pyrite. Cleaning Lower Kittanning Seam coal in the same manner would potentially result in even greater sulfur reduction. Again using 1982 production figures, the sulfur content of this coal would be reduced by 63 percent from estimated 1982 levels, from 368,000 tons to 136,000 tons. A summary analysis of the 11 highest producing seams in the region indicated that the sulfur content of the coal could be reduced by more than one-half through extensive physical coal cleaning. If cleaned at 14 mesh x 0 size and at 1.30 specific gravity, total theoretical sulfur reduction would be approximately 1.7 million tons from 1982 levels, from 2.9 million tons down to 1.2 million tons. Assuming that all of the sulfur is converted to SO_2, this would be equivalent to a decrease in SO_2 emissions of 3.4 million tons.

This potential for increased SO_2 reduction through extensive physical coal cleaning is impressive but would be difficult and too costly to accomplish given the present state of development of commercial coal-cleaning equipment. Present day coal-cleaning plants are not designed or equipped to clean coal to the levels achieved in washability tests, which are carried out in the laboratory so as to maximize the separation of coal and pyrite for a given size consist and specific gravity. Conventional cleaning processes cannot duplicate the laboratory conditions used to demonstrate this level of sulfur reduction. As previously mentioned, the primary objective of most coal cleaning practiced in the United States is to improve overall quality of the fuel (i.e., remove mineral matter) rather than reduce SO_2 emissions. As such, commercial coal preparation performs a more or less "rough" cleaning of the coal in terms of sulfur removal.

Another necessary consideration in coal preparation is the trade-off between improved coal quality and the total heating value recovered in the cleaned product. Examination of Table V shows that for Pittsburgh Seam coal, cleaning at 1.30 specific gravity and 14 mesh x 0 particle size (so called "deep" cleaning) would result in a 47.8 percent reduction in sulfur. However, to achieve a total Btu content in the clean product equivalent to that in the original coal, the mining requirement would have had to be increased from about 43 million tons to almost 69 million tons. For the Northern Appalachian Region as a whole, the total mining requirement would increase from 125 million tons to more than 249 million tons, or by 100 percent, to achieve the maximum sulfur reduction of 1.7 million tons at the same total Btu recovery in the clean coal product.

The increased mining requirement is due to a decrease in clean coal recovery at lower specific gravities of separation. Although the specific gravity of coal is less than its mineral impurities, some coal is lost with the refuse material (mineral matter) as the specific gravity at which the coal is cleaned decreases. The rela-

tionship between specific gravity of separation, Btu recovery, and sulfur reduction in a cleaning plant is shown in Table VI for four coals (23). As the specific gravity of separation is lowered, the sulfur content of the cleaned coal decreases, as expected. However, improved coal quality is achieved at the expense of a reduction in Btu recovery. This "non-recovered" coal has a significant impact on the cost of coal cleaning. Thus, commercial coal preparation plants are not only technology-limited but also constrained by a decrease in total Btu recovery in the clean coal product that is associated with an increase in sulfur removal.

Table VI. Sulfur Reduction and Btu Recovery by Coal Cleaning

	Raw Coal	Coal-Cleaning Operating, Specific Gravity			
		1.4	1.5	1.6	1.8
Illinois No. 6 Coal					
lb SO_2/MBtu[1]	8.97	3.86	4.18	4.38	5.08
Sulfur reduction, %	--	57	53	51	43
Btu recovery, %	--	78	88	92	96
Pittsburgh Coal					
lb SO_2/MBtu[1]	6.05	3.79	4.18	4.37	4.68
Sulfur reduction, %	--	37	31	28	23
Btu recovery, %	--	82	92	95	97
Upper Freeport Coal					
lb SO_2/MBtu[1]	3.97	1.76	1.93	2.03	2.35
Sulfur reduction, %	--	56	51	49	41
Btu recovery, %	--	78	89	93	97
Cedar Grove Coal					
lb SO_2/MBtu[1]	1.45	1.17	1.20	1.23	1.25
Sulfur reduction, %	--	19	17	15	14
Btu recovery, %	--	91	93	95	96

[1] Assuming 100% conversion of sulfur to SO_2.

Source: Reference 23.

In any development of advanced physical coal-cleaning (PCC) techniques, an important consideration is the heterogeneous nature of coal and, in particular, the variable manner in which pyrite occurs in coal. This variability influences the behavior of coal with regard to cleaning (26). In some coals, pyrite is distributed throughout the coal matrix as particles only microns in size. Thus, to separate pyrite from these coals, the coal must be crushed to very fine size in order to "liberate" the pyrite from the coal particles. However, conventional commercial PCC techniques cannot

efficiently (nor economically) separate coal from mineral matter at
these fine sizes. Thus, there is a need to develop advanced
physical fine-coal-cleaning processes, which might use techniques
such as froth flotation, selective agglomeration, true-heavy-liquid
cycloning, electrostatic separation, or high-gradient magnetic
separation (33,34).

     Development and application of these advanced PCC processes
could play a significant role in reducing sulfur dioxide emissions,
particularly from older, uncontrolled coal-fired power plants. The
U.S. Department of Energy has initiated additional research to
complement the ongoing programs directed toward control of acid
rain precursor emissions from newer coal-burning facilities built
in compliance with current NSPS. One important part of this new
acid rain initiative involves a cooperative effort with the
Electric Power Research Institute (EPRI) to evaluate advanced
physical fine-coal-cleaning technologies. The performance of
advanced cleaning processes at a scale of one ton per hour will be
tested at EPRI's Coal Cleaning Test Facility (CCTF) located at
Homer City, Pennsylvania (35).

     Selection will be based on a number of criteria, including
technical performance, process economics, and commercialization
potential. Specifically, DOE and EPRI are interested in processes
capable of (1) producing a clean coal with pyritic sulfur content
significantly lower than that achievable with conventional cleaning
equipment; (2) operating at Btu recoveries of 80 percent or
greater; (3) producing a clean coal with 2 percent or less ash; and
(4) producing a final product with less than 30 percent moisture.

Microbubble Flotation

One technology to be tested at the CCTF will be a microbubble
flotation process developed by Bechtel National, Inc., of San
Francisco. Microbubble flotation is a further development of con-
ventional froth flotation of coal. Froth flotation is a physico-
chemical process that uses the difference in the surface properties
of coal and its associated mineral impurities to effect a
separation. An aqueous coal slurry is fed into an aerated tank,
where the hydrophobic coal particles become attached to, and are
buoyed to the surface by, finely dispersed air bubbles and are
collected as a clean-coal-froth product. The mineral matter, being
hydrophilic, is wetted by water and remains in suspension to be
carried off as refuse.

     For flotation to be most effective, reagents such as oil
(collector) and surfactant (frother) must be added to the aqueous
coal slurry. The collector adsorbs on the coal surface and makes
it more hydrophobic, while the surfactant facilitates production of
a stable froth. According to Leonard (26), the optimum coal sizes
for froth flotation are between 50 and 140 mesh (0.3 and 0.106 mm).
While conventional froth flotation will successfully remove
minerals from coal, it has limited effect on the pyrite content, as
pyrite tends to float almost as well as coal. Because of this,
researchers have been looking for better ways to remove pyrite from
coal. In addition, as previously mentioned, it is necessary to
grind coal to very fine sizes in order to sufficiently liberate the
mineral matter and pyritic sulfur. But, at these very fine sizes,

conventional froth flotation exhibits poor separation of coal and
mineral matter.

In froth flotation, in addition to coal mineral character-
istics and the chemical reagents used, air bubble size plays a
critical role. Flotation of ultrafine coal requires extremely
small bubbles and the means to impart adequate forces at the
bubble-solid interface to effect attachment of the coal particles
to the bubble. The Bechtel process to be tested uses a unique
flotation cell developed by Bergbau Forschung in Germany in which
micron-sized bubbles are generated, along with proprietary addi-
tives developed by Energy International that make pyrite more
hydrophilic and also improve coal product recovery. The flotation
cell consists of a conical vessel into which pre-aerated slurry is
introduced through several inlets. The aerator placed outside the
separation vessel generates microbubbles and provides the solid-
bubble contact. The bubble loading takes place with adequate force
to ensure maximum bubble loading of the fine coal particles. With
the introduction of the aerated slurry into the separator, the
bubbles rise to the surface without being disturbed by turbulence
within the vessel. The froth level is adjusted to permit effective
settling of the mineral refuse. As part of the development, it was
shown that very fine mineral particles adhere to the surfaces of
larger coal particles, thus contributing to the ash content of the
coal. However, by selecting the proper dispersant and introducing
it into the process where fresh surfaces are generated in the
grinding step, separation of pyrite and other mineral matter from
the coal can be maximized.

Depending on the characteristics of the coal to be processed,
Bechtel's unit has the flexibility to be operated in a number of
modes. One such mode of operation involves a 3-stage, "reverse"
flotation process. In this case, clean coal will be floated in the
first two stages. In the final, or reverse-flotation, stage the
clean coal product will be conditioned with reagents so that pyrite
particles will float to the surface, and the clean coal will sink
to the bottom of the cell, where it is collected as the final
product.

Conclusion

The full potential for removing pyritic sulfur from various coals
by physical coal cleaning is significant but difficult to achieve.
However, SO_2 control by precombustion removal of pyrite could be an
important SO_2-emissions reduction strategy. The cleaned coal pro-
duced could be used in coal-fired utilities, constructed both pre-
and post-NSPS, as well as in industrial boilers. To realize the
potential for coal cleaning in actual practice, however, new tech-
niques must be demonstrated in the laboratory and then at the
"proof-of-concept" scale (approximately one ton of coal per hour).
These new coal beneficiation techniques could be advanced physical-
coal-cleaning (PCC) processes, or they could employ microbial
desulfurization or chemical desulfurization to remove organic
sulfur. These latter processes could be used by themselves or in
concert with PCC processes.

Disclaimer

Reference in this report to any specific commercial product, process, or service is to facilitate understanding and does not necessarily imply its endorsement or favoring by the United States Department of Energy.

Literature Cited

1. "Standards of Performance for New Stationary Sources," Environmental Protection Agency. Federal Register, Vol. 36, No. 247, December 23, 1971.
2. "New Stationary Sources Performance Standards: Electric Utility Steam Generating Units," Environmental Protection Agency. Federal Register, Vol. 44, No. 113, June 11, 1979.
3. "National Acid Precipitation Assessment Program," Annual Report 1984 to the President and Congress, EOP Publications, 726 Jackson Place, N.W., Washington, DC 20503.
4. "The Acidic Deposition Phenomenon and Its Effects, Critical Assessment Review Papers," Volume 1: Atmospheric Sciences. EPA - 600/8-83-016AF, Washington, DC, July 1984.
5. "Acid Deposition: Atmospheric Processes in Eastern North America," National Research Council, National Academy Press, Washington, DC, 1983.
6. "The Acidic Deposition Phenomenon and Its Effects, Critical Assessment Review Papers," Volume 2: Effects Sciences. EPA-600/8-83-016BF, Washington, DC, July, 1984.
7. "Atmosphere-Biosphere Interactions: Toward a Better Understanding of the Ecological Consequences of Fossil Fuel Combustion." National Research Council, National Academy Press, Washington, DC, 1981.
8. "Acid Rain and Transported Air Pollutants: Implications for Public Policy," OTA-O-204, U.S. Congress, Office of Technology Assessment, Washington, DC, June 1984.
9. "An Analysis of Issues Concerning 'Acid Rain,' Report to the Congress," GAO/RCED-85-13, U.S. General Accounting Office, Washington, DC, December 11, 1984.
10. "Acid Rain: A Review of the Phenomenon in the EEC and Europe," Environmental Resources Limited, UNIPUB, 1983, New York, NY 10157.
11. "Acid Precipitation: An Annotated Bibliography," D.A. Wiltshire and M.L. Evans, U.S. Geological Survey Circular 923, 1984.
12. Acid Rain: Sharing the Cost, J.H. Sununu, Issues in Science and Technology, 1985, 1 (2), 47-59.
13. European Concern About Acid Rain Is Growing, D.A. O'Sullivan, Chem. Eng. News, Jan. 28, 1985, 12-18.
14. "National Acid Precipitation Assessment Program Operating Research Plan 1984." Vol. I, Research Framework; Vol. II, Inventory of Research. EOP Publications, 726 Jackson Place, N.W., Washington, DC 20503.
15. "Acidic Deposition Research." EA-4027-SR-LD, R.M. Perhac, Special Report, April 1985, Electric Power Research Institute, Palo Alto, CA.

16. "Acid Deposition: Processes of Lake Acidification," National Research Council, National Academy Press, Washington, DC, 1984.

17. "The Integrated Lake-Watershed Acidification Study," EA-3221, Electric Power Research Institute, Palo Alto, CA, 1984.

18. Report on Effects of Acidifying and Other Air Pollutants on Forests (English edition). F. Scholz, UN Economic Commission for Europe reprint from Mitteilungen der Bundesforschungsanstalt für Forst- und Holzwirtschaft, Hamburg, April 1984.

19. "Effects of Acidic Deposition on Forest Ecosystems in the Northeastern United States: An Evaluation of Current Evidence," R.L. Burgess, ed. ESF-84-016, State University of New York, College of Environmental Science and Forestry, Syracuse, NY, January 1984.

20. Effects of Air Pollution on Forests: Critical Review, S.B. McLaughlin, J. Air Pollution Control Assoc., 1985, 35 (5), 512.

21. Effects of Air Pollution on Forests: Critical Review Discussion Papers, B. Prinz, W.H. Smith, E.B. Cowling, P.D. Manion, and S.B. McLaughlin, J. Air Pollution Control Assoc., 1985, 35 (9), 913.

22. Pollution Aerosol in the Northeast: Northeastern-Midwestern Contributions, K.A. Rahn and D.H. Lowenthal, Science, 1985, 228, 275-284.

23. Computer Economics of Physical Coal Cleaning and Flue Gas Desulfurization, C.R. Wright, T.W. Tarkington, and J.D. Kilgroe, Presented at EPA/EPRI Symp. on Flue Gas Desulfurization, New Orleans, LA, November 1-4, 1983.

24. "Use of Coal Cleaning for Compliance with SO_2 Emission Regulations," Battelle Columbus Labs, OH, PB81-247520, September 1981.

25. "Physical Coal Cleaning for Utility Boiler SO_2 Emission Control," EPA- 600/7-78-034, February 1978.

26. "Coal Preparation," 4th edition, J.W. Leonard, ed. Am. Inst. Mining, Metall. Petrol. Engrs., Inc., New York, NY, 1979.

27. "Annual Energy Outlook 1984, with Projections to 1995." Energy Information Admin., U.S. Dept. of Energy, Washington, DC, January 1985.

28. "Impact of Coal Cleaning on the Cost of New Coal-Fired Power Generation," EPRI CS-1622, Electric Power Research Institute, March 1981.

29. "Sulfur Reduction Potential of the Coals of the United States," J.A. Cavallaro, M.T. Johnston, and A.W. Deurbrouck. Report of Investigations 8118, U.S. Bureau of Mines, Washington, DC, 1976.

30. "Sulfur Reduction Potential of the Coals of Ohio," J.T. Wizzard, J.A. Cavallaro, and A.W. Deurbrouck, DOE/PETC/TR-83/7, U.S. Department of Energy, Pittsburgh, PA, 1983.

31. Sulfur Reduction Potential of the Coals of the Northern Appalachian Region, C.P. Maronde, and A.W. Deurbrouck, <u>Proc. 2nd Annual Coal Preparation Exhibition and Conference</u>, Lexington, KY, April 1985.

32. "Coal Production 1984," DOE/EIA-0118(84), U.S. Department of Energy, November 1985.

33. "Physical Cleaning of Coal: Present and Developing Methods," Y.A. Liu, ed., M. Dekker, Inc., New York, NY, 1982.
34. "Processing and Utilization of High Sulfur Coals," Y.A. Attia, ed., Proc. 1st Int'l. Conf. on Proc. Util. High Sulfur Coals, Columbus, OH, October 1985, Coal Science and Technology, Vol. 9, Elsevier Science Publ., New York, NY, 1985.
35. "Coal Cleaning Test Facility: 1985 Plan." CS-4071, Interim Report, July 1985, Electric Power Research Institute, Palo Alto, CA.

Separation of Ultrafine Pyrite from High Sulfur Coals by Selective Dispersion and Flocculation

Yosry A. Attia

148 Fontana Laboratory, Metallurgical Engineering Department and Mining Engineering Division, The Ohio State University, Columbus, OH 43210

A novel technique for separating ultrafine pyrite par-
ticles (minus 40 micrometers) from coal fines has been
conceptually developed and tested. The technique invol-
ves the use of a selective polymeric dispersant for
pyrite, while flocculating coal particles with a poly-
meric flocculant. The suspended pyrite can then be
removed from the flocculated coal fines which settle
preferentially by gravity.

The key to this separation was the design and prepara-
tion of the selective dispersant for pyrite (PAAX).
This was achieved by incorporating xanthate groups into
the structure of a low molecular weight acrylic acid
polymer (PAA). Testing this reagent on individual sus-
pensions of coal and pyrite confirmed its selective
dispersion action towards pyrite, while it had no dis-
persion action on coal suspension when using Purifloc-
A22 flocculant. Preliminary tests on high sulfur coals
from Kentucky No. 9 seam, Meigs Creek, and Ohio No. 6
also confirmed this selectivity. Further process de-
velopment is needed, however, before this promising
technique can become commercially feasible.

Most of the Eastern U.S. coals suffer from high sulfur content, which
on burning emit sulfur dioxide in excess of the EPA limit of 1.2 lb
SO_2/million Btu. Specifically, there are three broad regions that
suffer from severe sulfur problems. These are: Northern Appalachia
(Pennsylvania, Ohio, West Virginia) with average sulfur content of
about 3%; the Midwest region (Indiana, Illinois, Kentucky) with
average sulfur of 3.9%; and Central Midwest (Iowa, Missouri, Kansas,
Oklahoma) with average sulfur of 5.25%.
    The presence of sulfur in coal is generally attributed to two
forms, organic sulfur and pyritic sulfur. The proportion of pyritic
sulfur to organic sulfur varies significantly from one coal seam to
another, but it appears that pyritic sulfur generally represents
about 70 percent or more of the total sulfur ($\underline{1}$). The pyrite is

found in coal in a wide size distribution, with a significant pro-
portion in the very fine size fraction (less than 25 micrometers).
For example, the mean particle size of pyrite in the Midwest region
is about 37μm (400 mesh), for the Central to Western Midwest region
is about 107μm (150 mesh), and in the Appalachian regions is about
68-100μm. This can only mean that a significant amount of the pyrite
is in the very fine to colloidal fractions. In fact, there are coal
seams, such as Kentucky No. 9, where almost all of the pyrite par-
ticles are often smaller than about ten micrometers (2).

It is believed, therefore, that the separation-removal of pyrite
from coal prior to its combustion would greatly reduce the sulfur
dioxide emission and render many coal deposits within the new
source performance standards.

For separation of coal from relatively coarse shale and pyrite,
gravity-based techniques have been effectively utilized. For sizes
below 300 micrometers to about 100 micrometers, froth flotation has
been used satisfactorily for separating coal from shales (3). Even
separation of pyrite from coal has been achieved by flotation (4).
However, most of these processes become less effective when the
particle size of the coal suspension is significantly below 100
micrometers.

One of the promising new technologies for separation of very
fine particles is selective flocculation. The selective floccula-
tion process has been used effectively to separate very finely dis-
seminated minerals from mixed ore suspensions (5). The process is
based on the preferential adsorption of an organic flocculant on
the wanted minerals, thereby flocculating them, while leaving the
remainder of the suspension particles dispersed. The dispersion
of certain components in the suspension such as pyrite can be en-
hanced by using more selective or powerful dispersants. Methods for
achieving selective flocculation and dispersion have been recently
described by Attia (6).

The objective of this research was to investigate the feasi-
bility of separating coal fines from mixed suspensions with pyrite
by selective flocculation. In this work, the separation of pyrite
from coal was based on the distinct differences in their surface
chemical properties. Pyrite being a sulfide mineral has an affinity
for xanthate-containing reagents, while coal does not have such an
affinity towards xanthates. Therefore, if xanthate groups could be
incorporated into the structure of long-chain polymers, selective
polyxanthate flocculants or dispersants for pyrite might thus be
achieved. The use of polyxanthates for selective flocculation of
sulfide minerals, particularly for copper, was first reported by
Attia and Kitchener (7). The separation of pyrite from coal using
polyxanthate dispersants was initially reported by Attia and
Fuerstenau (8) and more recently described by Attia (9).

Preparation and Characterization of Polyxanthate Dispersants

As reported earlier (8), polyxanthate dispersants can be prepared by
reacting low molecular weight polyacrylic acid solutions with
sodium hydroxide and carbon disulfide. Thus, to a 50-ml 1 percent
solution of PAA supplied by Scientific Polymer Products, Inc. (mol.
wt. = 2000), 5.4g NaOH pellets were added and dissolved. Then 15 ml

CS_2 was added, and the solution was shaken in a water bath at 55°C for 2.5 hours. The crude reaction product was carrot-red in color and was referred to as PAAX.

Purification of the reaction products of PAAX was made by mixing 50 ml of the carrot-red solution with excess amounts of methanol (up to 300 ml) to produce a pale yellow precipitate. After standing for a period of time, the suspension was filtered off to recover this precipitate. The purified PAAX precipitate was readily soluble in distilled water. Great care was exercised to minimize decomposition of the polyxanthate during the purification process. This was partly achieved by maintaining the solution pH highly alkaline.

Characterization of purified PAAX solutions was made by uv visible spectroscopy technique using a Model Carey-17 Spectrometer (Varian). The uv spectra of the purified and unpurified reaction products of the xanthated polyacrylic acid are shown in Figure 1. Table 1 shows the molar extinction coefficients for the reaction products of the xanthated cellulose (viscose) for comparision (<u>10</u>). From the uv spectra and Table 1, it was concluded that the xanthate groups were present in both the purified and the crude PAAX products. It was also clear that the purification method used rejected most of the secondary reaction products (the polysulfides) from the xan-thated product. Most of the secondary reaction products mentioned in Table 1 are present in the uv spectrum of the crude product of PAAX in Figure 1, but not in the purified product. However, it seemed that the xanthate absorption peaks were slightly shifted to the higher wavelengths of 305 to 308µm, as compared with 303µm for most lower molecular weight xanthates. It is important to note that the unmodified polyacrylic acid solution, although not shown here, did not exhibit absorption peaks in this region of wavelength (i.e., 300 to 308µm).

Table 1. Molar Extinction Coefficients of Viscose Compounds (<u>10</u>)

Compounds	Wavelength					
	336µm	303µm	272µm	250µm	226µm	206µm
Sodium cellulose xanthate		17508			10928	
Sodium cellulose dixanthogen		6862			12396	
Sodium dithio-carbonate		600	10500	3250		
Sodium trithio-carbonate	18200	3440			12230	
Sodium sulfide				1690	7730	
Carbon disulfide						60,000–70,000

Xanthates are usually formed by reacting an alcohol or a raw material containing alcoholic hydroxyl groups with an alkali and carbon disulfide (<u>10</u>). However, in the case of the acrylic acid polymer used here, it is not clear how this reaction would proceed. But whatever the mechanism, it appears from the uv spectra and from

the flocculation tests that the polyacrylic acid was modified to
contain xanthate groups in its structure. Attia (9) has recently
proposed the possible structure of this polyacrylic acid/xanthate
(PAAX) dispersant as sodium polyacrylate-acrylodithiocarbonate.
He also pointed out that the ratio of acrylate to xanthate groups
in the polymeric structure depends primarily on the degree of xan-
thation.

Testing of PAAX on Individual Coal and Pyrite Suspensions

Selective flocculation of coal from pyrite was investigated using
the newly developed polyxanthate dispersant in conjunction with
Purifloc-A22 flocculant (a polystyrene sulfonate). Thus, 50 ml
mineral suspensions of each of the coal and pyrite containing 2
percent solids of less than 37μm (400 mesh) particle size were
treated with certain amounts of the PAAX dispersant (50 to 400 mg/l),
while stirring continued for 5 minutes at high shear rate. The
initial suspension pH before the addition of dispersant was about
10. The final suspension pH after the addition of the crude solu-
tion of PAAX was sometimes higher due to its high sodium hydroxide
content and ranged between pH 10.7 and 11.5. At the end of disper-
sant conditioning time (5 minutes), 4 mg/l Purifloc-A22 was admini-
stered into the suspension, and stirring was continued for 10
seconds at high shear, then lowered to a gentle agitation for an
additional 10 seconds. The suspension was transferred into a 100-ml
graduated cylinder and was allowed to stand still for 5 minutes.
At the end of the settling period, the suspended solids were de-
canted, and the settled solids were recovered. Each fraction was
placed in an evaporating dish, oven dried and weighed. Selective
flocculation of coal mixtures with pyrite was made on suspensions
containing equal proportions of coal and pyrite, using 200 mg/l
PAAX dispersant at pH 10. The flocculation procedure was the same
as described above, except that the products were qualitatively
analyzed by visual inspection of both fractions. The coal samples
used in these experiments were anthracite coal, supplied by Wilkes-
Barre, Pennsylvania, and the pyrite used was pure crystals from
Wards Natural Sciences, Inc., Rochester, N.Y.
    The flocculation results on the individual mineral suspensions
are shown in Figure 2 (A & B). These graphs show the effect of
polyacrylic acid dispersant before (PAA) Figure 2A, and after
xanthation (PAAX) Figure 2B, on the flocculation-dispersion behavior
of individual suspensions of coal and pyrite with Purifloc-A22
flocculant.
    From Figure 2(A), it appeared that PAA inhibited or restrained
the flocculation action of Purifloc-A22 on both coal and pyrite
suspensions at PAA concentrations of 100 mg/l and above. The dis-
persive action of PAA in this case was therefore unselective. How-
ever, the PAAX crude reaction product in Figure 2(B) only dispersed
the pyrite suspension to the same level as PAA, while the coal sus-
pension was totally flocculated even at high PAAX concentrations.
The polyxanthate dispersant, rather than improving the dispersion
of pyrite, simply did not adsorb on the coal particles, thereby
creating a selective dispersion action for the pyrite. These obser-
vations in Figure 2(B) were repeated and noted several times, even
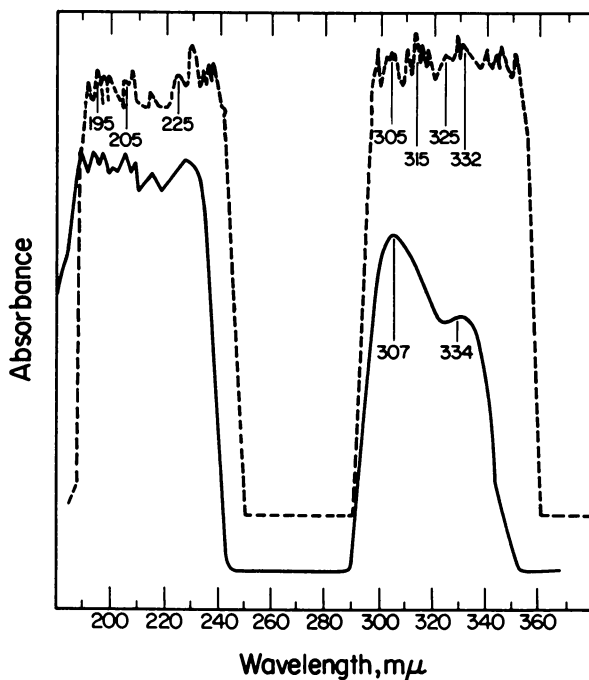with purified PAAX solutions. Selective dispersion of pyrite or

Figure 1. UV Spectrum for Purified and Unpurified Polyxanthate PAAX Dilute Solution.
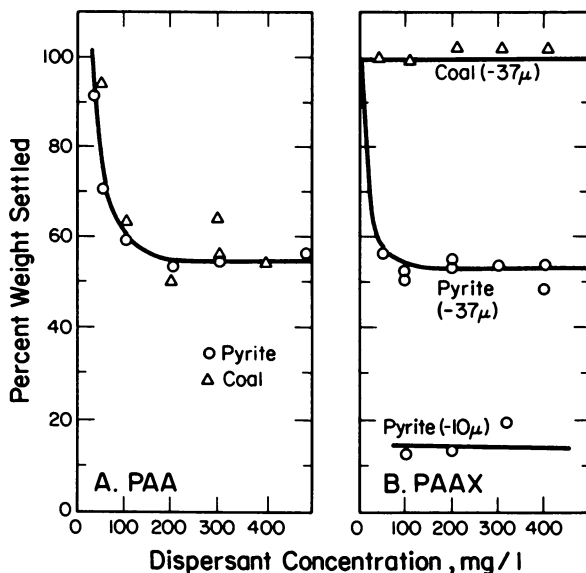
Figure 2. Effect of (A) Polyacrylic Acid (PAA) and (B) Xanthated Polyacrylic Acid (PAAX) Dispersants on the Flocculation of Anthracite Coal and Pyrite Suspensions with Purifloc-A22 (2 mg/l) at pH 10. Reproduced with permission from Ref. 9, Copyright 1985, Elsevier.

selective flocculation of coal from pyrite using PAAX reagents
appeared, therefore, possible.

   In order to ascertain that the selective dispersion effect of
PAAX was truly due to the modified polymer itself and not to the
associated poly-sulfides in the crude reaction, the flocculation
testing was repeated with the purified PAAX solution. By using 300
mg/l of the purified PAAX solution, about 96 percent of the coal
suspension flocculated in 5 minutes, while the pyrite suspension
remained stable. These tests confirmed that the selective dis-
persion action was due to the PAAX (polyxanthate polymer) itself.

Effect of Pyrite Particle Size on Dispersion. It was suspected that
a lot of the apparently non-dispersed pyrite particles shown in
Figure 2 was due to the settling of "coarse" particles between 10
and 37 micrometers. Pyrite has a specific gravity of about 5.0,
while that of coal is around 1.2-1.3. Therefore, a pyrite suspen-
sion having only particle size below 10 micrometers was prepared
and tested. The results, which are also shown in Figure 2(B), showed
that the minus 10 micrometer pyrite suspension remained very stable,
with only 10 - 20% weight of the particles settled or flocculated.
From these observations, it is believed that the selective disper-
sion of pyrite will be more effective for the smaller particle sizes.

Selective Flocculation of High Sulfur Coals

Preliminary testing of the unpurified polyxanthate dispersant men-
tioned earlier, during the selective flocculation of three high
sulfur coals, is described here. The coal samples used for the
study were Kentucky No. 9, Meigs Creek, and Ohio No. 6. The coal
samples were wet ground in a steel ball mill and screened to obtain
the minus 400 mesh (-37μm) fraction for testing in the case of
Kentucky No. 9 coal tests, and to minus 500 mesh (-25μm) fraction
in the case of Meigs Creek and Ohio No. 6 coals.

   Single-step selective flocculation tests were conducted on
dilute coal suspensions (about 3% wt), using F1029-D flocculant
(a partially hydrophobic polymer prepared by Dai-Ichi Kogyo Sieyaku,
Japan) at pH 10 to 10.5. The test procedure was as follows: The
coal suspension was dispersed at a moderate shear for 5-10 minutes,
during which the required amounts of PAAX solution were added and
the pH was adjusted to 10 or 10.5. The flocculant was then admini-
stered while the suspension was stirred at high shear for 10
seconds. The suspension was thereafter stirred at a low shear for
one minute, followed by gentle rotation in an inclined cylinder for
5 minutes. At the end of this step, the suspension was decanted,
and the flocculated fraction was recovered. Both fractions were
dried, weighed and analyzed for total sulfur. The results of these
preliminary studies are shown in Tables 2, 3 and 4 for Kentucky
No. 9, Meigs Creek, and Ohio No. 6 coals, respectively.

Table 2. Material Balance for One-Step Selective
Flocculation of Kentucky No. 9 Coal Using PAAX Dispersant
and Fl029-D Flocculant at pH 10 (9)

Product	Weight%	Total Sulfur%	Total Sulfur Distribution%	Remarks
Dispersed	3.7	13.74	20.3	500 mg/l PAAX
Flocculated	96.3	2.08	79.7	2 mg/l F1029-
Feed	100.0	2.52	100.0	D
Dispersed	2.7	9.96	9.7	300 mg/l PAAX
Flocculated	97.3	2.56	90.3	2 mg/l F1029-
Feed	100.0	2.76	100.0	D

Table 3. Material Balance for One-Step Selective
Flocculation of Meigs Creek Coal Using PAAX Dispersant
and Fl029-D Flocculant at pH 10.5*

Product	Weight%	Total Sulfur%	Total Sulfur Distribution%	Remarks
Dispersed	22.7	7.00	26.0	2 mg/l F1029-
Flocculated	77.3	5.86	74.0	D
Feed	100.0	6.12	100.0	500 mg/l PAAX
Dispersed	16.5	11.53	27.7	5 mg/l F1029-
Flocculated	83.5	5.94	72.3	D
Feed	100.0	6.86	100.0	500 mg/l PAAX
Dispersed	12.4	12.97	24.4	10 mg/l F1029-
Flocculated	87.6	5.69	75.6	D
Feed	100.0	6.59	100.0	500 mg PAAX

*Sodium hexametaphosphate was also added (500 mg/l) to disperse
the ash minerals

These results show that the sulfur content of the dispersed
(reject) product was significantly higher than the feed or the floc-
culated fractions. For example, with Kentucky No. 9 coal, at the
higher PAAX dispersant concentration (500 mg/l), the sulfur content
in the dispersed fraction was 13.74% compared with 2.08% in the
flocculated fraction. Similarly, with Meigs Creek coal, the dis-
persed fractions contained about twice as much sulfur as the floc-
culated fractions, except at the lower (2 mg/l) flocculated dosage.
The total sulfur rejection (24-28%) was somewhat higher than that
achieved with Kentucky No. 9 coal (10-20%). With Ohio No. 6 coal,
similar results were again observed. The sulfur content in the
dispersed fractions was at least twice as much as in the flocculated

Table 4. Material Balance for One-Step Selective
Flocculation of Ohio No. 6 Coal Using PAAX Dispersant and
F1029-D Flocculant

Product	Weight%	Total Sulfur%	Total Sulfur Distribution%	Remarks
Dispersed	6.9	11.6	16.0	200 mg/l PAAX
Flocculated	93.1	4.8	84.0	10 mg/l
Feed	100.0	5.3	100.0	F1029-D
Dispersed	14.3	10.0	28.0	300 mg/l PAAX
Flocculated	85.7	4.3	72.0	2 mg/l
Feed	100.0	5.1	100.0	F1029-D
Dispersed	23.0	8.9	39.3	500 mg/l PAAX
Flocculated	77.0	4.1	60.7	2 mg/l
Feed	100.0	5.2	100.0	F1029-D

fractions. The total sulfur rejection ranged between 16 and 39%.
The lower rejection ratio of 16% was accompanied by high selectivity
in pyritic sulfur dispersion. This was due to the higher (10 mg/l)
flocculant concentration which resulted in higher coal yield (93.1%
wt) in the flocculated fraction. On the other extreme, when higher
dispersant concentration (500 mg/l) was used with lower flocculant
concentration (2 mg/l), much less coal was flocculated (77% wt) and
more sulfur was apparently rejected (39%). The intermediate con-
ditions of 300 mg/l PAAX dispersant and 2 mg/l flocculant produced
correspondingly intermediate results.
     While these results present a definite evidence for the
selectivity of flocculating coal and dispersing pyrite with the
reagents mentioned above, the total sulfur removal was rather low.
The low sulfur removal could be due to the fact that a significant
portion of the pyrite is known to be very finely disseminated, for
example minus 10 micrometers in Kentucky No. 9 coal seams (2). In
the brief tests mentioned here, no attention was paid to the liber-
ation characteristics of pyrite from coal. It was hoped that
grinding to minus 400 mesh (37 micrometers) or to minus 500 mesh
(25 micrometers) would liberate a significant amount of pyrite.
Another possible reason for the low sulfur removal was the presence
of "coarse" pyrite or pyrite-containing coal particles which would
settle at a similar rate as the pure coal flocs, thus interfering
in their separation. As mentioned earlier in this article, the
process is expected to be more effective for the 10 micrometer
size pyrite than for the 37 micrometer size pyrite particles, if
gravitational settling was used for separation of flocs from suspen-
sion. Other floc separation methods such as flotation might extend
the effectiveness of this selection flocculation method to coarser

sizes. Alternatively, the coarser pyrite particles (greater than
25 micrometers, for example) could be separated by other techniques
prior to applying selective flocculation.

Conclusions

From the preceeding discussion, it can be concluded that the addition
of the polyxanthate dispersant (PAAX) during the selective floccu-
lation of coal with F1029-D or Purifloc-A22 presents a promising
approach for the removal of ultrafine pyrite particles from coal
suspensions. This would be especially true, however, if future
investigations could improve the overall pyrite removal, while still
obtaining high coal (Btu) recovery. It is anticipated that by
applying multi-stage selective flocculation (i.e., the flocs from
the first separation step are re-dispersed and re-flocculated several
times), most of the liberated ultrafine pyrite particles would be
removed.

Literature Cited

1. "Analysis of Ohio Coal", Information Circular No. 47, State of
    Ohio Department of Natural Sciences, Division of Geological
    Survey, 1978.
2. Albaugh, E., Gulf Research and Development, Pittsburgh,
    Pennsylvania, private communications with Y. Attia, 1982.
3. Aplan, F. F., in "Beneficiation of Mineral Fines";
    Somasundaran, P., and Arbiter, N., Eds., NSF workshop,
    New York, 1978.
4. Miller, K. J., "Flotation of Pyrite from Coal", U.S.
    Patent 3,807,557, April 30, 1974.
5. Attia, Y. A., "Selective Flocculation Technology, State
    of the Art Review", 111th AIME Annual Meeting, Dallas, 1982.
6. Attia, Y. A., "Fine Particle Separation By Selective
    Flocculation", Separation Science and Technology, 17 (3),
    1982, 75-83.
7. Attia, Y. A., and Kitchener, D. A., "Development of Complexing
    Polymers for the Selective Flocculation of Copper Minerals",
    Eleventh Inter. Miner. Process. Cong., Cagliari, Italy, 1974.
8. Attia, Y. A., and Fuerstenau, D. W., "Feasibility of Cleaning
    High Sulfur Coal Fines by Selective Flocculation", Fourteenth
    Intern. Miner. Process Congr., Toronto, Canada, 1982.
9. Attia, Y. A., in "Processing and Utilization of High Sulfur
    Coals"; Attia, Y. A., Ed., Elsevier, Amsterdam, 1985, pp. 267.
10. Rao, S. R., "Xanthates and Related Compounds", Marcel Dekker,
    New York, 1971.

3

Chemical Cleaning of Coal with Hot Alkaline Solutions

C.-Y. Chi, C.-W. Fan, Richard Markuszewski, and T. D. Wheelock

Ames Laboratory, Iowa State University, Ames, IA 50011

Various bituminous coals were demineralized by an ex-
perimental two-step leaching process in which the ball-
milled coals were first treated with a hot alkaline
solution and then with a dilute mineral acid. Differ-
ent alkalis and acids were studied to determine their
relative effectiveness. In addition, the effects of
alkali concentration, treatment temperature, and treat-
ment time were evaluated. Under the best conditions,
the process reduced the ash content of the coals by
85-90% and the total sulfur content by 70-90%. As the
temperature of the alkaline treatment was raised from
150 to 345°C, the removal of sulfur increased greatly
whereas the recovery of organic matter declined. When
a 1 $\underline{M}$ sodium carbonate solution was employed for the
treatment, the recovery of organic matter was 91-97%
for various coals treated at 250°C and 79-89% for the
same coals treated at 300°C.

The use of hot aqueous caustic solutions for the demineralization of
coal dates back to German research during World War II, in which the
objective was to produce a low-ash product suitable for conversion to
electrode carbon ($\underline{1}$). Subsequent work at the U. S. Bureau of Mines
demonstrated that treatment of coal with 10% NaOH solutions at 225°C,
followed by washing with dilute HCl, could decrease the ash content
to 0.7% from an original level of 9.8% ($\underline{2}$). Since that time, several
workers have addressed the chemical cleaning of coal using aqueous
caustic under various conditions. Some treated the coal with caustic
at 300°C, followed by washing with hot H_2SO_4 and then HNO_3 ($\underline{3}$).
Others used a mixture containing 10% NaOH and 2-3% $Ca(OH)_2$ at
250-300°C and high pressure for their treatment ($\underline{4}$). Recent work in
Australia ($\underline{5}$) and in India ($\underline{6}$) also employed leaching with aqueous
NaOH and washing with acid to achieve low levels of ash in the final
product.

Our own work started with the use of dissolved oxygen in hot aqueous solutions of sodium carbonate to desulfurize coal (7). Since then, our efforts were redirected towards cleaning of coal by using aqueous alkaline solutions, under non-oxidizing conditions, with subsequent acid treatment to remove the ash-forming mineral matter from coal. The extraction of most of the mineral matter from coal was accomplished recently by treating fine-size coal with a hot alkaline solution to dissolve quartz and to convert clay minerals and iron pyrite into acid-soluble compounds which were extracted with dilute acid in a second step (8). Although various alkalis and acids may be utilized, Na_2CO_3 and H_2SO_4 are advantageous because of low cost and ready availability. Preliminary work has shown that hot Na_2CO_3 solutions readily convert kaolinite into sodium hydroaluminosilicates which are acid-soluble (9). That work has also shown that hot sodium carbonate solutions will dissolve quartz and convert iron pyrite into hematite, but not as readily as sodium hydroxide solutions.

In this work, the characteristics of the two-step process were studied in greater detail using three different bituminous coals under a variety of conditions, with particular attention being given to the first step. The relative effectiveness of various alkalis was studied as well as the effects of alkali concentration, alkaline treatment time, and temperature. The alkali-treated coals were subsequently leached with hot HNO_3 to remove mineral matter. Nitric acid was employed because it dissolves iron pyrite and is used for that purpose in ASTM Method D2492 (10) for determining various forms of sulfur in coal. Since only organically bound sulfur should remain in coal which has been leached with HNO_3, it was possible to obtain an indication of how much organic sulfur was removed by the two-step treatment.

Experimental Methods

The bituminous coals used in this study were obtained from several sources (Table I). Much of the work was done with high volatile C bituminous coal from the Cherokee seam at the Lovilia No. 4 underground mine in Iowa. The other two coals were somewhat higher in rank. The different coals were ground to -200 mesh (U.S. Standard); a portion of each product was ball-milled further to approximately 90% -400 mesh. A sample of each prepared coal was leached with boiling dilute HNO_3 to remove inorganic sulfur so that the sulfur content of the residue would reflect the organic sulfur content of the raw coal. The leaching procedure with HNO_3 was similar to that of ASTM Method D2492 (10) and was described in more detail elsewhere (11).

For the first step, 12 g. of ground coal and 120 ml. of alkaline solution were mixed and placed in a 300-ml. stainless steel autoclave equipped with a turbine agitator. The system was flushed with nitrogen and then heated to the desired temperature while the mixture was stirred continuously. After a period of treatment at constant temperature and pressure, the autoclave was cooled quickly, and the contents were filtered to recover the coal. The filter cake was washed with 400 ml. of distilled water, dried at 90°C for 4 hr., weighed, and analyzed for total sulfur and ash. A portion of the alkali-treated coal (usually 2.5-3.0 g) was leached for an additional

Table I. Bituminous coals used in leaching experiments

Coal Seam	Location	Size mesh	Ash, %	Tot. S %	HNO$_3$ leached Ash, %	HNO$_3$ leached Tot. S %
Cherokee group	Monroe County, Iowa	-400	8.24	2.65	3.05	1.13
Illinois No. 6	Trivoli County, Illinois	-200	12.75	3.71	5.55	1.66
		-400	8.90	3.14	4.99	1.66
Lower Kittanning	Armstrong County, Pennsylvania	-200	18.07	10.44	7.94	1.88
		-400	18.44	10.24	8.29	1.69

30 min. with boiling 2.1 M HNO$_3$ in a stirred, three-neck Pyrex flask
fitted with a reflux condenser. In most cases, 250-300 ml. of acid
was employed. After the acid treatment, the flask was cooled quickly
to room temperature, and the contents were filtered. The filter cake
was washed, dried, weighed, and analyzed as above. The ash content
of the raw and treated coals was determined by ASTM Method D3174
(10), while the sulfur content was determined with a Fisher model 475
total sulfur analyzer.

Reporting Basis

The ash content of raw and treated coals is reported on a moisture-
free basis and the sulfur content on both a moisture- and ash-free
basis. The ash reduction achieved corresponds to the overall change
in moisture-free ash content divided by the moisture-free ash content
of the raw coal. The reduction in total sulfur content corresponds
to the change in total sulfur content divided by the total sulfur
content of the raw coal, all on a moisture- and ash-free basis. The
apparent reduction in organic sulfur content corresponds to the dif-
ference between the sulfur content of the acid-leached raw coal and
the final sulfur content of the acid-leached, alkali-treated coal
divided by the sulfur content of the acid-leached raw coal, all on a
moisture- and ash-free basis. Coal recovery corresponds to the mass
ratio of coal recovered during the alkaline treatment step to coal
charged, all on a moisture- and ash-free basis.

Experimental Results

The results of leaching ground raw coals with HNO$_3$ alone are indi-
cated in Table I. The sulfur content of the acid-leached coal is
indicative of the organically bound sulfur, while the ash content
reflects the removal of iron pyrite and other minerals such as car-
bonates which are soluble in nitric acid. It can be seen that acid
leaching alone reduced the sulfur content of Cherokee coal by 57%,

Illinois No. 6 coal by 44-55%, and Lower Kittanning coal by 84-87%; also for these coals the ash content was reduced by 63%, 44-56%, and 55-57%, respectively.

For the alkaline treatment experiments, a relatively long time was needed to heat the reactor and its contents to the required temperature. Typically, it took 20 min. to reach 150°C, 25 min. to reach 200°C, and 45 min. to reach 300°C. While the temperature was being raised, the alkaline attack on the coal and its mineral matter got underway. This attack can be seen from the changes which took place when ball-milled Cherokee coal was heated in 1.0 M Na_2CO_3 from room temperature to 300°C (Figure 1). Subsequent changes which occurred as the treatment was continued at 300°C are also reflected in Figure 1. The data in this diagram represent the results of nine different runs conducted for various time intervals. The results show that by the time the reaction mixture had reached 300°C the sulfur content of the coal had been reduced by 56% which was equivalent to removing all of the inorganic sulfur. As the treatment was continued at 300°C, the sulfur content of the coal was further reduced until a reduction of 69% was achieved. Further treatment was counterproductive as the sulfur content of the product actually increased slightly. Thus, for maximizing sulfur removal, the optimum treatment time was 85 min. total or 40 min. beyond the initial heat up period. For the optimum treatment time, the total sulfur content of the alkali-treated coal was 27% below the apparent organic sulfur content of 1.13% indicated in Table I for the raw coal. Hence, it appeared that some of the organic sulfur had been removed.

The ash content of the alkali-treated coal was slightly higher than that of the raw coal which was probably due to the formation of sodium hydroaluminosilicates. Coal recovery on a moisture- and ash-free basis declined gradually as the treatment time was extended (Figure 1). Moreover, the rate of decline increased beyond a total treatment time of 70 min.

When the alkali-treated coal which had provided the data for Figure 1 was subsequently leached for 30 min. with boiling HNO_3, the overall results shown in Figure 2 were obtained for the two-step process. The time and temperature of the alkaline treatment step are indicated. Since the HNO_3 leaching step by itself was capable of removing the inorganic sulfur and reducing the total sulfur content of the coal by 57%, treating the coal with alkali first had a relatively small effect on the total sulfur content of the coal after the combined treatment. For the optimum alkaline treatment time, the total sulfur content was reduced by 77.5% for the combined treatment, as compared to 69% for the alkaline leaching step alone. On the other hand, the combined treatment seemed to account for a significant reduction in the apparent organic sulfur content. For an extended treatment time, the reduction in organic sulfur content exceeded 45% for the combined treatment which seemed significantly greater than the 27% reduction noted for the alkaline leaching step alone.

The alkaline treatment step had a pronounced effect on what happened to the ash content of Cherokee coal when it was subsequently leached with acid. As Figure 2 indicates, HNO_3 leaching of the raw coal reduced the ash content by 63%. Pretreating the coal with alkali for short intervals at temperatures up to 200°C had little
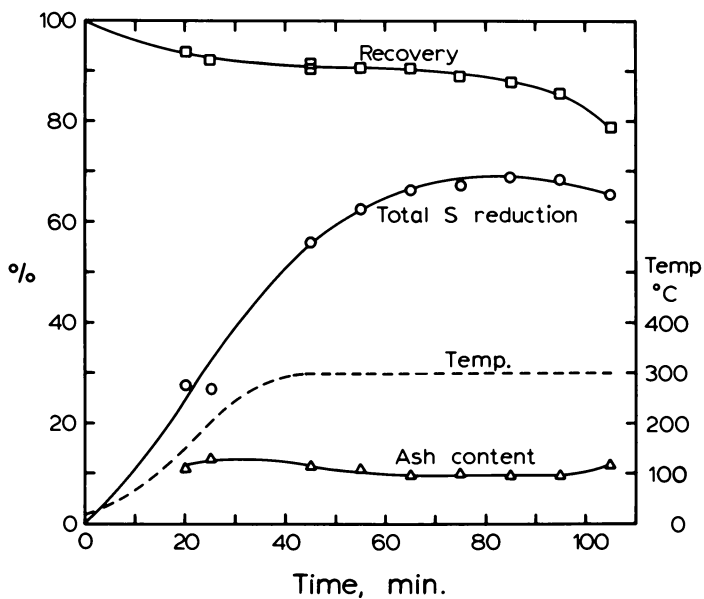
Figure 1. Results of treating -400 mesh Cherokee coal with 1 $\underline{M}$ Na_2CO_3.
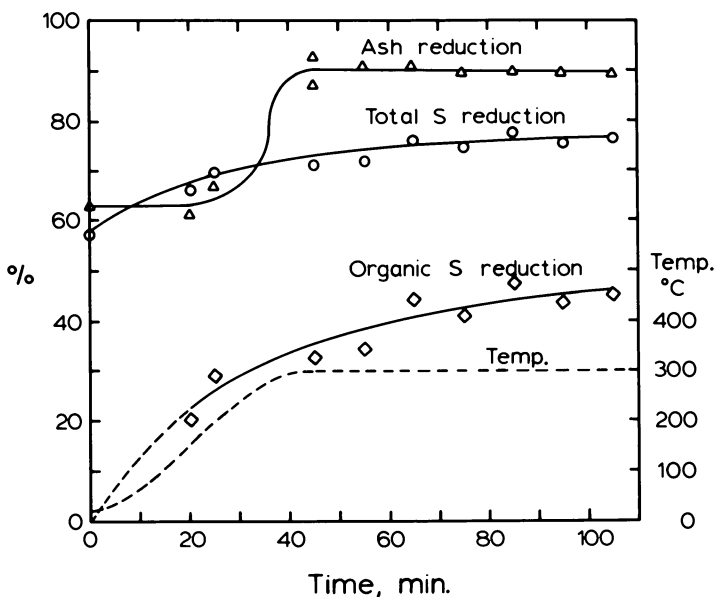

Figure 2. Overall results of applying the two-step process to Cherokee coal. Time and temperature are for the alkaline treatment step.

effect on the results of subsequent acid leaching. But pretreating the coal at 300°C for even a short time resulted in lowering the ash content 90% when the coal was leached with acid.

To determine the effect of the final temperature during the alkaline leaching of Cherokee coal, several runs were carried out in which different portions of the coal were treated with 1.0 $\underline{M}$ Na_2CO_3 for 1.0 hr. at various final temperatures. The alkali-treated coal was then leached with HNO_3. The results of the alkaline leaching step are indicated in Figure 3 and the overall results in Figure 4. As the treatment temperature was raised, the quantity of sulfur removed by the first step increased greatly while coal recovery declined. The decline in recovery was gradual up to 250°C and then more precipitous beyond. The overall reduction in total sulfur content for both steps increased slightly and the reduction in apparent organic sulfur content somewhat more as the temperature of the first step was raised. The overall reduction in ash content for both steps also rose but then reached a plateau at 250°C.

The effects of alkali type and concentration were studied by treating different portions of Cherokee coal with various alkaline solutions for 1 hr. at 300°C (Table II) and then by leaching with HNO_3. The sulfur reduction achieved in the first step was nearly the same for a majority of the alkalis; however, it was slightly lower for coal treated with either $NaHCO_3$ or $KHCO_3$. Coal recovery in the first step was similar with most alkalis except that it was slightly higher for coal treated with $NaHCO_3$ and greatly lower for coal treated with NaOH. Because of the low recovery, the caustic-treated coal was not subjected to the second step. When the second step was applied to the other alkali-treated portions, the lowest sulfur and ash contents were obtained with coal treated with 1.0 $\underline{M}$ Na_2CO_3. Lower concentrations of Na_2CO_3 achieved similar overall reductions in sulfur and ash contents and provided a higher recovery.

Other coals were also subjected to the two-step treatment (see Table III). The results obtained with ball-milled Illinois No. 6 coal were similar, in general, to those achieved with Cherokee coal. When the alkaline treatment step was applied to either coal, sulfur reduction increased and coal recovery declined as the temperature was raised. However, for any given temperature the recovery and sulfur content of the alkali-treated product were higher for Illinois coal than for Cherokee coal. The high sulfur content of the treated Illinois coal appeared to be largely due to the higher organic sulfur content of the raw coal, while the higher recovery of this material seemed to be related to a difference in coal rank. When the alkali-treated Illinois coal was treated with HNO_3, most of the ash-forming minerals were removed to give a low ash content. Also, the total sulfur content of the final product was lower than the apparent organic sulfur content of the raw coal, indicating removal of some organic sulfur. As with Cherokee coal, the results with Illinois coal were not affected greatly by alkali concentration, but in both cases the final ash content achieved with the two-step process declined slightly as the alkali concentration increased. The results with Illinois coal were also not affected greatly by particle size. The first-step recovery was slightly lower and the ash-content of the final product was slightly higher for -200 mesh coal than for -400 mesh coal. The sulfur content of the final product was nearly the same in both cases.
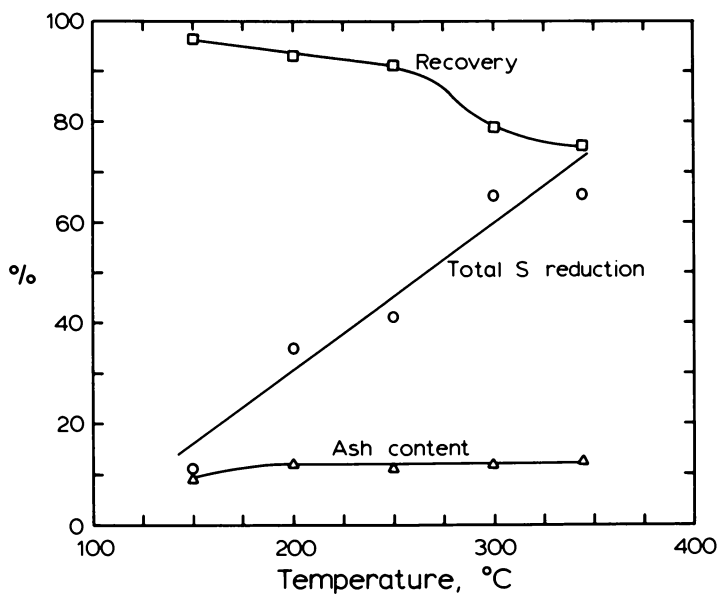
Figure 3. Results of treating -400 mesh Cherokee coal with 1 $\underline{M}$ Na_2CO_3 for 1 hr. at indicated temperature.
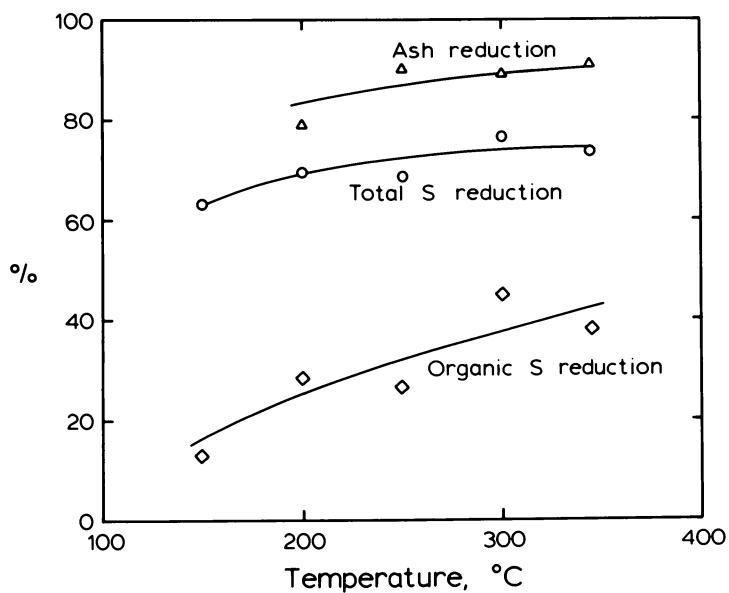

Figure 4. Overall results of applying the two-step process to Cherokee coal which was treated with Na_2CO_3 at the indicated temperature.

Table II. Results of treating Cherokee coal with different alkali at 300°C for 1 hr. followed by leaching with HNO_3

	Alkaline treatment step				Product[a]		Overall reduction		
Alkali	Recov., %	Ash, %	Tot.S %	S redn., %	Ash, %	Tot.S, %	Ash, %	Tot.S, %	Org.S, %
0.2 M Na_2CO_3	85.8	10.04	0.94	64.5	1.21	0.62	85.3	76.6	45.1
0.6 M Na_2CO_3	85.4	10.32	0.84	68.3	0.95	0.62	88.5	76.6	45.1
1.0 M Na_2CO_3	78.7	11.90	0.92	65.3	0.88	0.62	89.3	76.6	45.1
1.0 M $NaHCO_3$	84.0	10.42	1.35	49.1	1.10	0.84	86.7	68.3	25.7
1.0 M K_2CO_3	79.4	11.84	1.02	61.5	1.63	0.83	80.2	68.7	26.5
1.0 M $KHCO_3$	75.4	13.13	1.27	52.1	2.15	0.80	73.9	69.8	29.2
2.8 M NaOH	35.6	13.42	1.02	61.5	--	--	--	--	--

[a] Ash and total sulfur contents of final acid-treated product.

Compared to the other coals, Lower Kittanning coal responded similarly in some ways to the two-step treatment but differently in other ways (Table III). The differences seemed related to the high ash and sulfur contents of the coal and possibly to a difference in mineral species. Sulfur removal was affected by the alkaline treatment time and temperature much as for the other coals. However, because of the very high iron pyrite content, the alkaline leaching step never succeeded in reducing the total sulfur content to the level of the apparent organic sulfur content. On the other hand, after applying both steps, the final sulfur content was always below the apparent organic sulfur content of the raw coal, again indicating organic sulfur removal. Sulfur removal in the first step was affected somewhat by alkali concentration and a 1.0 M concentration appeared optimum. Coal recovery was affected by changes in various parameters as for the other coals, but it was slightly higher for any given set of conditions in the case of Lower Kittanning coal. The greatest difference in results with this coal occurred with the removal of ash-forming minerals, because the two-step treatment appeared ineffective except under relatively mild alkaline leaching conditions. Only by carrying out the first step at a relatively moderate temperature (i.e., 250°C) or with the smallest alkali concentration or for the shortest time did the alkaline leaching step appear to have a beneficial effect on the overall results. Consequently, it seemed as though the Lower Kittanning coal was unique in containing some component which reacted with alkali under more rigorous conditions to form a nitric acid-insoluble material.

Table 3. Results of applying different alkaline treatment conditions to coal followed by leaching with HNO_3.

Coal	Na_2CO_3 M	Temp., °C	Alkaline treatment step[a]					Acid trtd. prod.		Overall reduction		
			Time, min.	Recovery, %	Ash, %	Tot. S, %	S red., %	Ash, %	Tot. S, %	Ash, %	Tot. S, %	Org. S, %
Ill. No. 6	0.2	300	60	89.8	11.73	2.03	35.4	1.44	1.43	83.8	54.5	13.9
Ill. No. 6	0.6	300	60	89.5	11.66	1.68	46.5	1.04	1.43	88.3	54.5	13.9
Ill. No. 6	1.0	250	60	96.8	11.34	1.91	39.2	1.03	1.30	88.4	58.6	21.7
Ill. No. 6	1.0	300	60	86.8	12.09	1.78	43.3	0.77	1.44	91.3	54.1	13.3
Ill. No. 6	1.0	344	60	80.8	11.36	1.36	56.7	0.71	1.02	92.0	67.5	38.6
Ill. No. 6[b]	1.0	300	60	81.2	19.42	1.95	47.4	1.43	1.39	88.8	62.5	16.3
Low. Kit.	0.2	300	60	91.5	20.67	5.74	43.9	4.02	1.52	78.2	85.2	10.1
Low. Kit.	0.6	300	60	90.0	21.80	3.16	69.1	8.92	1.26	51.6	87.7	25.4
Low. Kit.	1.0	300	60	88.8	23.40	3.03	70.4	8.98	1.31	51.3	87.2	22.5
Low. Kit.	2.0	300	60	89.8	22.94	3.30	67.8	8.62	1.27	53.3	87.6	24.9
Low. Kit.	3.0	300	60	87.2	24.57	3.96	61.3	8.15	1.44	55.8	85.9	14.8
Low. Kit.	1.0	200	60	97.0	18.99	9.23	9.9	3.29	1.62	82.2	84.2	4.1
Low. Kit.	1.0	250	60	96.5	20.78	7.88	23.0	2.88	1.45	84.4	85.8	14.2
Low. Kit.	1.0	344	60	85.2	22.58	1.87	81.7	10.14	1.20	45.0	88.3	29.0
Low. Kit.	1.0	300	0	92.0	22.36	5.61	45.2	6.29	1.43	65.9	86.0	15.4
Low. Kit.	1.0	300	30	88.9	23.66	3.42	66.6	8.70	1.25	52.8	87.8	26.0
Low. Kit.	1.0	300	90	81.7	30.00	3.83	62.6	8.24	1.32	55.3	87.1	21.9
Low. Kit.[b]	1.0	300	60	87.8	23.85	4.21	59.7	7.96	1.36	56.8	87.0	27.7

[a] Net treatment time at constant temperature is indicated. [b] -200 mesh.

In order to explain the unusual results of leaching Lower Kittanning coal, the nature of the ash-forming minerals in coal after the alkaline leaching step and after the acid/water washing step was characterized by x-ray diffraction (XRD) with a Siemens D500 diffractometer using copper $K\alpha$ radiation. Examination by XRD showed that the principal mineral impurities in raw Lower Kittanning coal were iron pyrite, kaolinite, and quartz. Leaching this coal with $1\underline{M}$ sodium carbonate at 300°C for 1 hr. appeared to convert essentially all of the kaolinite to sodium hydroaluminosilicate and a large portion of the pyrite to hematite; also, most of the quartz was extracted or converted. After washing the alkali-treated coal with nitric acid, hematite appeared to constitute most of the remaining mineral matter. This is probably due to the low solubility of hematite in dilute nitric acid. However, since hematite is dissolved rapidly by hot hydrochloric acid, the removal of ash-forming minerals from Lower Kittanning coal could be improved by adding a hydrochloric acid washing step after the two-step treatment. The results of additional leaching experiments, in which the coal was subjected to hot alkaline treatment followed by both nitric and hydrochloric acid leaching, showed that the final ash content of the Lower Kittanning coal was reduced to about 1% in most cases. XRD analysis showed that only traces of the original mineral impurities remained in the final product. Comparable results were achieved also with the Cherokee and Illinois No. 6 coals.

Discussion and Conclusions

A two-step process for extracting mineral matter and sulfur from coal was demonstrated with three different coals under a variety of treatment conditions. The first step involves treatment with a hot alkaline solution which extracts part of the sulfur and generally converts much of the mineral matter to an acid-soluble form. The second step involves leaching with an acid to extract the converted mineral matter. Although H_2SO_4 would likely be used in the second step of a commercial process, HNO_3 was chosen for the present study in order to shed some light on the disposition of organic sulfur.

Under our experimental conditions, nitric acid dissolved iron pyrite but not the hematite which was formed during the alkaline treatment step. More rigorous alkaline treatment conditions were more effective than less rigorous conditions for converting the iron pyrite into hematite which could not be easily removed by the nitric acid. Consequently, when rigorous alkaline treatment conditions were applied to Lower Kittanning coal, the residual hematite more than made up for the other minerals which were extracted so that the overall reduction in ash content for the two-step process was no better than for HNO_3 leaching alone.

A major concern of the present study was the effect of various parameters involved in the alkaline treatment step. Early in the investigation it was observed that Na_2CO_3, K_2CO_3, and NaOH were equally effective for removing sulfur in the first step while $NaHCO_3$ and $KHCO_3$ were less effective. On the other hand, coal recovery suffered greatly when NaOH was used. For the combined two-step treatment, the lowest sulfur and ash contents were achieved with Na_2CO_3. In view of this result and various economic advantages,

Na_2CO_3 was selected for studying the effects of other parameters. The effects of alkali concentration appeared relatively minor in most instances. However, for Lower Kittanning coal an alkali concentration of 1.0 M appeared optimum for removing sulfur in the first step whereas a smaller concentration (0.2 M) resulted in a lower ash content overall for the two-step process.

Alkali-treatment time and temperature affected the results greatly. Sulfur removal increased and coal recovery decreased in the first step with rising temperature, and above 250°C coal recovery decreased disproportionately. Removal of mineral matter in the second step was affected by the temperature of the first step. With both the Iowa and Illinois coals, the overall reduction in ash content for both steps increased with temperature up to 300°C and then leveled off. But with Lower Kittanning coal, 250°C seemed to be the optimum temperature for reducing the ash content. Increasing the alkaline treatment time up to a point resulted in increasing sulfur removal in the first step, but beyond this point less sulfur was removed. Coal recovery declined as the alkaline treatment time was extended, and the rate of decline accelerated after prolonged treatment.

The apparent removal of organic sulfur by the two-step treatment observed with all three coals was of considerable interest. Since the total sulfur content of the treated coal was below that which could be achieved by leaching with HNO_3 alone, it appeared that the alkaline leaching step either removed a significant quantity of organic sulfur or converted some of the organic sulfur into a form which was extractable with HNO_3. In several instances, the total sulfur content of Iowa or Illinois coal treated by the alkaline leaching step alone was below the apparent organic sulfur content of the raw coal, indicating organic sulfur removal as well as inorganic sulfur removal, but usually the apparent reduction in organic sulfur content was slight and may not have been significant.

Acknowledgments

Literature Cited

1. Crawford, A., "The preparation of ultra-clean coal in Germany," Trans. Inst. Min. Eng., 111, 204 (1951).
2. Reggel, L.; Raymond, R.; Wender, I.; Blaustein, B. D. "Preparation of ash-free, pyrite-free coal by mild chemical treatment," Am. Chem. Soc. Div. Fuel Chem. Preprints 17(1), 44-48 (1972).
3 Yang, R. T.; Das, S. K.; Tsai, B. M. C. "Coal demineralization using sodium hydroxide and acid solutions," Fuel 64(6), 735-742 (1985).

4. Stambaugh, E. P. "Hydrothermal coal process," in Coal Desulfur-
    ization: Chemical and Physical Methods (ACS Symp. Series 64),
    T. D. Wheelock, ed., Am. Chem. Soc., Washington, D. C. 1977, pp.
    198-205.
5. Waugh, A. B.; Bowling, K. McG. "Removal of mineral matter from
    bituminous coals by aqueous chemical leaching," Fuel Processing
    Technol. 9, 217-233 (1984).
6. Venkataswamy, Y.; Chandra, D.; Chakrabarty, J. N. "Removal of
    sulphur from Indian coals by sodium hydroxide leaching," J.
    Inst. Energy, Dec. 1984, pp. 438-443.
7. Wheelock, T. D. "Oxydesulfurization of coal in alkaline solu-
    tions," Chem. Eng. Commun. 12(1-3), 137-160 (1981).
8. Fan, C.-W.; Markuszewski, R.; Wheelock, T. D. Process for
    producing low-ash, low-sulfur coal, Am. Chem. Soc. Div. Fuel
    Chem. Preprints, 29(1), 114-119 (1984).
9. Fan, C.-W.; Markuszewski, R.; Wheelock, T. D. Behavior of
    mineral matter during alkaline leaching of coal, Am. Chem. Soc.
    Div. Fuel Chem. Preprints, 29(4), 319-325 (1984).
10. American Society for Testing and Materials, Annual Book of ASTM
    Standards, Part 26, Philadelphia, PA, 1975.
11. Markuszewski, R.; Miller, L. J.; Straszheim, W. E.; Fan, C.-W.;
    Wheelock, T. D.; Greer, R. T. Evaluation of the removal of
    organic sulfur from coal, in New Approaches in Coal Chemistry
    (ACS Symp. Series 169), B. D. Blaustein, B. C. Bockrath, and
    S. Friedman, eds., Am. Chem. Soc., Washington, D.C., 1981, pp.
    401-414.

4

Coal Desulfurization and Demineralization by Molten Caustic Mixtures

Richard Markuszewski, D. R. Mroch, G. A. Norton, and W. E. Straszheim

Ames Laboratory, Iowa State University, Ames, IA 50011

Several bituminous coals have been treated with molten
mixtures of NaOH plus KOH at 350-370°C in a 1:10 coal-
to-caustic ratio for 1 hour and then washed with water,
dilute acid, and finally with water again. By this
procedure, which is similar to that of the TRW Gravi-
melt Process, 80-90% of the ash and 70-80% of the total
sulfur have been removed with a recovery of 80-90% of
the coal on a moisture- and ash-free basis. The desul-
furization could be improved by using a finer grind of
coal, better washing procedures, or a recleaning step.
Samples of raw and cleaned coals produced at the Ames
Laboratory and obtained from TRW have been character-
ized for the mineral matter content and distribution
among various particle sizes. The sulfur forms before
and after treatment have been determined by convention-
al ASTM techniques and a direct SEM method.

The use of molten caustic to remove pyrite and other mineral matter
from coal was first reported by Masciantonio who discovered that
treating 1 part of coal with 4 parts of 1:1 NaOH/KOH mixture at 250°C
or higher removed all of the pyrite within 5 minutes (1). At temper-
atures above 250°C, organic sulfur was also removed. In recent
years, the technique was refined by TRW and became known as the Grav-
imelt Process (2-4). By using 10 parts of molten caustic to treat 1
part of coal at 370°C, followed by washing with dilute H_2SO_4, almost
all of the pyritic sulfur and about 80% of the organic sulfur could
be removed. In addition, the final ash contents were generally less
than 1%. Further studies on the effects of retention time, tempera-
ture, coal-to-caustic and NaOH/KOH ratios, particle size, and rank of
coal resulted in sulfur and ash reductions which met the New Source
Performance Standards (5,6). Some fundamental aspects of cleaning
coal with molten caustic were also studied by Maijgren et al. (7,8),
who investigated the behavior of some organosulfur model compounds

in addition to the effect of caustic composition, reaction time, temperature, and particle size.

The overall objectives of our own DOE-sponsored work at the Ames Laboratory are to propose, test, and develop methods for regenerating the spent caustic and other reagents used in the TRW Gravimelt Process in order to make this chemical cleaning method economical. As a preliminary step to our investigations, the thermodynamics, phase equilibria, and other properties of proposed reaction schemes were tested in order to develop flow diagrams incorporating the desulfurization and regeneration schemes (9,10). Furthermore, in order to ensure that our samples of cleaned coal and spent caustic are comparable to those produced by the Gravimelt Process, similar procedures were used in the cleaning steps. In the course of our work, the effect of various washing procedures as well as of particle size and recleaning was investigated. In addition, some fundamental chemistry and behavior of the mineral matter during cleaning were studied on our own samples and on samples provided by TRW.

Experimental

For our own work, channel samples of Pittsburgh No. 8 coal from the Grafton Mine, Churchville, WV, and Illinois No. 6 coal from the Captain Mine, Percy, IL, were used. Two separate batches, IL6 and IL6A, of the Illinois coal were used. The characteristics of the 2 bituminous coals are listed in Table I.

Table I. Analyses for Pittsburgh No. 8 (PT8) and Illinois No. 6 (IL6 and IL6A) Coals (on a dry basis, except for moisture)

	% H_2O	% Ash	% S	Sulfur Forms			Volatile Matter, %	Heating Value, Btu/lb
				(Pyr.	Sulf.	Org.)		
PT8	2.18	7.02	3.12	(1.48	0.26	1.38)	39.27	13,482
IL6	8.25	13.26	4.10	(1.82	0.29	1.99)	36.55	11,833
IL6A	8.70	14.17	4.52	(2.21	0.23	2.08)	38.50	12,245

The desulfurization experiments were run in a batch reactor designed and constructed at the Ames Laboratory. The reaction crucible (8 in. x 3.5 in. o.d.) was constructed from Inconel tubing. A basket to hold the coal was fashioned from -20 mesh stainless steel screen. The chromel-alumel thermocouple was sheathed in stainless steel.

For the experiments, 50g of coal (usually 12 mesh x 0) were placed in the basket and covered with 400g NaOH and 100g KOH. The basket, thermocouple, and stirring rod were placed in the crucible, and the crucible was lowered into the preheated furnace. The coal-caustic mixture was stirred and kept at 370°C for 1 hour while a continuous flow of nitrogen above the crucible provided an inert atmosphere. After the reaction, the basket containing the coal cake was removed from the reactor. The cake contained about 2 parts of

caustic adhering to 1 part of coal by weight. The cake was first washed with 2L of water, followed by 1L of 10% H_2SO_4 or HCl, and then a final wash with 2 or 4L water.

The cleaned coal was dried at 110°C overnight and then sampled for analysis. Moisture, ash, and pyritic and sulfate sulfur were determined by ASTM procedures (11). Total sulfur was determined by high-temperature combustion using a Fisher Total Sulfur Analyzer. Organic sulfur was determined by difference.

For comparison, samples of another Pittsburgh No. 8 coal were obtained in March, 1983, from the TRW Gravimelt Benchscale Run #2 performed in California. The samples included raw coal, water-washed caustic-treated coal (intermediate product), and the final clean product (after additional acid and water wash) from the Gravimelt Process. In addition to the standard analyses described above, the samples were also analyzed directly for organic sulfur by a technique utilizing scanning electron microscopy (SEM) and energy-dispersive x-ray spectrometry as described by Straszheim et al. (12). Furthermore, they were characterized for various mineral phases and their distribution among different particle sizes by SEM and automated image analysis (SEM-AIA), a technique described previously by Straszheim and Markuszewski (13).

Results and Discussion

Standard Conditions. The results for several cleaning experiments on the Pittsburgh No. 8 (PT8) and Illinois No. 6 (IL6 or IL6A) coals are presented in Table II. For the Pittsburgh coal cleaned under standard conditions (runs #3 and #16), 77-82% ash removal and 65-72% sulfur removal were achieved with recoveries around 85-90%. For the Illinois coal, (IL6 #6, IL6A #1, and IL6A #2), the ash and sulfur removal was better at 87-89% and 72-78%, respectively, while recovery was lower at 75-79% on a moisture- and ash-free (MAF) basis.

Improved Conditions. When more water was used for the washing step (PT8 #10) or when the wash water was heated to 100°C (PT8 #12), both ash and sulfur removals were improved for each step without appreciable decrease in recovery. When 10% HCl was substituted for 10% H_2SO_4 (PT8 #9), the sulfur removal was improved, but the ash removal was worse than for run PT8 #3 in which 10% H_2SO_4 was used.

Best results were obtained when cleaned coal from run PT8 #10 was cleaned again under the same conditions. The final ash content of 0.30% and final sulfur content of 0.38% represent removals of 96 and 88%, respectively. The overall recovery, however, decreased to 73%. The lower recovery may be partially due to increased coal handling and the associated mechanical losses.

The 12 mesh x 0 IL6 coal, sized as 80% plus 60 mesh, was used in run #6. When the sample was ground to 85% minus 70 mesh and used in run #10, the final ash content of 0.56% and final sulfur content of 0.57% achieved represent significant improvements in removal, to 96% and 86%, respectively. The lower recovery of 65% can again be attributed in part to mechanical losses of the finer coal through the mesh of the basket.

Table II. Removal of Sulfur and Ash from Pittsburgh (PT8) and Illinois (IL6 or IL6A) Coals Under Standard[1] or Modified Conditions

Sample Run #	Conditions[1]	% Ash[2]	% Removal	% S[2]	% S Removed	% Recov.[3]	H.V., Btu/lb
PT8	Untreated	7.02	----	3.12	----	----	13,482
PT8 #3		1.27	82.4	1.09	65.1	89.7	13,699
PT9 #9	Same as #3, but 10% HCl wash	2.27	67.6	0.91	70.8	87.9	13,581
PT8 #10	4L Wash	1.50	78.6	0.87	72.1	89.6	13,581
PT8 #12	4L Hot Wash	1.07	84.8	0.68	78.5	91.0	13,176
PT8 #16		1.61	77.0	0.89	71.5	84.6	13,510
PT8 #13	#10 recleaned	0.30	95.8	0.38	87.8	72.8 (overall) 81.1 (2nd step only)	13,962
IL 6	Untreated	13.26	----	4.10	----	----	12,825
IL 6 #6	+60 mesh (80%)	1.79	86.5	1.16	71.7	74.5	12,450
IL6 #10	-60 mesh (85%)	0.56	95.8	0.57	86.1	64.7	12,489
IL6A	Untreated	14.17	----	4.52	----	----	12,245
IL6A #1		1.85	86.9	1.01	77.7	79.1	12,312
IL6A #2		1.53	89.2	1.12	75.2	79.1	13,004

[1] Standard conditions are: 10:1 caustic/coal ratio, 4:1 NaOH/KOH ratio, 370°C for 1 hour, 2L hot water (100°C) wash, 1L 10% H_2SO_4 wash (60°C), 4L hot H_2O wash (100°C). Only nonstandard conditions are listed.

[2] % Sulfur and % ash are reported on a dry basis.

[3] % Recovered = % $\frac{\text{grams MAF coal out x 100}}{\text{grams MAF coal in}}$

Effect of Various Washings on Sulfur Forms. The total sulfur content of cleaned PT8 coal was analyzed by observing the various sulfur forms after different washing procedures. Results of these analyses are presented in Table III. Use of a 2L wash under standard conditions (run #3) showed an appreciable residue of sulfate in the cleaned coal, greater than the amount of sulfate present in the original, untreated coal. Such incorporation of sulfate after treatment with H_2SO_4 of chemically cleaned coals has been observed before in our laboratories (14). It may be due to the formation of organic sulfate esters, formation of inorganic sulfates, or some other mechanism for adding sulfate. When more thorough washing was used in run #10, the sulfate content was decreased significantly. When 10% HCl was used for the acid wash in run #9, there was no chance of sulfate incorporation, and thus the final sulfate content was almost zero.

Table III. Effect of Washing Improvements on Sulfur Forms

Sample Run #	Conditions	% Pyritic Sulfur	Sulfatic Sulfur	Organic Sulfur	Total Sulfur
PT8	Untreated	1.48	0.26	1.38	3.12
PT8 #3	Standard 2L wash	0.02	0.47	0.60	1.09
PT8 #9	10% HCl wash	0.06	0.02	0.83	0.91
PT8 #10	4L wash	0.01	0.13	0.73	0.87

Effect of Molten Caustic on Particle Size. The Pittsburgh No. 8 coal used in run #3 was sized, using U. S. standard sieves and a portable sieve shaker, before and after the molten caustic treatment. The results of the sieve analyses are presented in Table IV. For the untreated coal, 20.1% of the particles were -60 mesh. After the treatment, 38.6% of the coal particles were -60 mesh, indicating comminution of the sample by action of the molten caustic. When the same cleaned and sieved sample was sieved again, the -60 mesh fraction increased to 44.4%, indicating that the treated coal particles were friable and continued to break down further by even simple sieving. When the raw coal was sieved for a second time, results showed that the particle size distribution was unaffected. The degradation of coal matter by molten caustic can occur by pitting due to removal of mineral grains as well as by direct attack on the coal macerals. Observations of such attacks have been made previously by Oder et al. (15) on samples prepared by TRW. In addition, sudden release of moisture and volatile matter during contact with molten caustic can also contribute to the comminution process.

Table IV. Sieve Analysis for Pittsburgh No. 8 Coal Before and After Cleaning With Molten Caustic at Ames Laboratory

| Mesh Size | RAW COAL | | CLEAN COAL | |
	PASS #1 Wt. %	PASS #2 Wt. %	PASS #1 Wt. %	PASS #2 Wt. %
>12	15.0	14.6	4.5	3.3
12-60	65.0	65.6	56.9	52.2
60-120	9.8	9.8	20.6	24.9
120-170	3.2	3.1	5.0	5.9
170-200	1.2	1.2	1.9	2.2
200-325	2.7	2.7	4.7	5.2
<325	3.2	3.0	6.4	6.2

Effect of Gravimelt Process on Mineral Matter in Coal. The samples of Pittsburgh No. 8 coal obtained from TRW, representing raw coal, the intermediate product and the final cleaned coal, were analyzed by ASTM and other procedures. The results are presented in Table V. In the final product, the total and organic sulfur were reduced by 70-80% from the levels observed in the raw coal, and the pyritic sulfur was reduced by about 99%, while levels of sulfate sulfur were not significantly affected. The organic sulfur concentrations

Table V. Analysis of Raw and Gravimelt Treated Pittsburgh No. 8 Coal. Values are in % unless otherwise noted and, except for moisture, are corrected to a dry basis).

	RAW			INTERMEDIATE PRODUCT			FINAL PRODUCT		
	TRW Data[a]	Ames Data	Org. S. by SEM[b]	TRW Data	Ames Data	Org. S. by SEM[b]	TRW Data	Ames Data	Org. S. by SEM[b]
H_2O	6.46	0.89	----	3.27	2.98	----	2.55	1.25	----
Ash	10.15	9.88	----	30.46	29.22	----	1.26	1.00	----
Tot S	4.28	4.22	----	0.43	0.32	----	0.75	0.86	----
Pyr S	2.20	1.78	----	----	0.02	----	----	0.01	----
Sulf S	0.02	0.20	----	----	0.06	----	----	0.26	----
Org S	2.06	2.24	1.99	----	0.24	0.08	----	0.59	0.41
Elem S (ppm)	----	29	----	----	<1	----	----	4	----
H.V. BTU/lb	13,282	----	----	8,454	----	----	13,780	----	----
MM[c]	12.50	12.00	----	----	33.03	----	----	1.13	----

[a] Analysis of head sample.
[b] Procedure in Reference 11.
[c] Mineral matter = (1.13 x ash) + (0.47 x pyritic S), as defined in Reference 3.

determined directly by the SEM technique were consistently lower than the indirect ASTM values. The deviation was most pronounced for the treated coals, which may indicate the formation of unusual minerals such as sulfides or jarosites during the Gravimelt process. Possibly, incomplete dissolution of pyrite in the ASTM method may also have inflated the ASTM organic sulfur values. These apparent discrepancies are being studied further. The magnitude of the reductions in levels of the various sulfur forms was generally better than the reductions for the Pittsburgh No. 8 coals observed at the Ames Laboratory (see Tables II and III).

In addition, the TRW samples were analyzed by the SEM-AIA technique described previously (13). The SEM-AIA data on the mineral phase identification and distribution between the size fractions are presented in Table VI for all three samples of raw and treated coal. The SEM-AIA data show the nearly complete removal of many minerals and a reduction of more than 90% in the overall content of the coal as a result of treatment by the TRW Gravimelt Process. No major changes in particle size distribution were observed, although the pyrite distribution shifted somewhat towards the coarse fraction after processing.

A significant change in mineralogy can be observed for the cleaned coals. The processed coals showed a much greater percentage of material classified as "miscellaneous" than did the raw coal, indicating formation of unusual minerals. For the washed, Gravimelt-treated coal, this miscellaneous portion contained significant amounts of Ca, K, and/or Na. SEM-EDX examination showed also a

Table VI. SEM-AIA Classification of Mineral Matter in Pittsburgh
           No. 8 Coal Samples Obtained from TRW. The mineral
           phases are described by chemistry and area-equivalent
           diameter (in μm), expressed as weight percent of the
           total coal.

Raw Coal
Particle size, μm

Mineral Phase	< 6.3	6.3-20	20-63	63-200	Total
Pyrite	0.25	1.67	1.63	0.96	4.50
Kaolinite	0.15	0.75	0.62	0.50	2.02
Illite	0.29	0.92	0.71	0.51	2.43
Quartz	0.13	0.58	0.25	0.37	1.32
Iron-rich	0.01	0.04	0.22	0.71	0.98
Calcite	0.00	0.00	0.01	0.00	0.01
Silicates	0.08	0.13	0.03	0.14	0.39
Misc. & Unknown	0.10	0.21	0.02	0.00	0.34
Total	1.01	4.30	3.50	3.19	12.00

Water-Washed Gravimelt-Treated Coal (Intermediate Product)
Particle size, μm

Mineral Phase	< 6.3	6.3-20	20-63	63-200	Total
Pyrite	0.13	0.18	0.08	0.00	0.40
Kaolinite	0.01	0.02	0.00	0.00	0.03
Illite	0.19	0.59	0.42	0.12	1.32
Quartz	0.01	0.07	0.00	0.00	0.08
Iron-rich	0.33	1.05	1.15	1.14	3.67
Calcite	0.05	0.07	0.00	0.00	0.11
Silicates	0.12	0.18	0.20	0.46	0.95
Misc. & Unknown	4.33	9.31	5.67	3.35	22.66
Total	5.17	11.46	7.53	5.07	29.22

Final Gravimelt Product
Particle size, μm

Mineral Phase	< 6.3	6.3-20	20-63	63-200	Total
Pyrite	.006	.010	.074	.173	.262
Kaolinite	.019	.054	.025	.154	.252
Illite	.023	.030	.008	.000	.060
Quartz	.023	.037	.014	.017	.091
Iron-rich	.004	.004	.000	.000	.008
Calcite	.003	.005	.002	.000	.010
Silicates	.007	.007	.003	.000	.017
Misc. & Unknown	.093	.147	.060	.000	.300
Total	.176	.295	.185	.343	1.000

general enhancement of these cations in the coal rather than in a separate phase or in components enriched in these elements, indicating that they could be associated with the organic portion of coal (possibly with carboxylate or phenolate functions). Such enhancement in the level of cations associated with the organic portion of coal has been observed previously in coals after treatment by the Ames Oxydesulfurization Process (16) and in lower rank and severely weathered coals (17). In the final product from the Gravimelt treatment, the "miscellaneous" material contained appreciable amounts of Cr, Mn, and Ni or Fe (or both), suggesting contamination from nickel and stainless steel components. For several mineral categories, the relative weight percent decreased after the caustic treatment and then increased after the acid treatment. It appears that the caustic treatment altered much of the original mineral matter while forming unusual minerals. The iron-rich phase, for example, in the intermediate product could be $NaFeO_2$ which has been shown to be the principal product from the reaction of FeS_2 with fused NaOH (18). The subsequent acid treatment removed much of the unusual mineral matter in the "miscellaneous and unknown" category, thereby increasing the relative percentages in the other mineral categories. The final product in Table VI contained also 800 ppm Na, 500 ppm K, and 0.03% Ca, thus indicating that these troublesome elements are below levels of concern.

Conclusions

Coal treated at the Ames Laboratory with molten caustic by a procedure similar to that of the Gravimelt Process resulted generally in 80-90% reductions in ash and 70-80% reductions in total sulfur. The recoveries of coal on a moisture- and ash-free basis were 80-90%. The removal of sulfur and ash could be improved by better washing, finer grind, or additional cleaning. SEM-AIA data on samples treated by TRW showed the formation of unusual minerals in the treated samples, as well as enrichment of these minerals in certain elements. The decrease of 90% in the ash content could be explained by the removal of individual mineral phases in all particle sizes. Removal of organic sulfur was corroborated by a direct SEM-EDX technique.

Acknowledgments

Literature Cited

1. Masciantonio, P. X. Fuel 1965, 44, 269-275.
2. Meyers, R. A.; Hart, W. D. "Chemical Removal of Organic Sulfur from Coal;" Symp. on Removal of Heteroatoms from Fuel, ACS Meeting, Houston, TX, March 23-28, 1980.

3. TRW, "Laboratory Study for Removal of Organic Sulfur from Coal;"
    Final Report to U.S. DOE, DE-AC-80PC30141, July 1, 1981.
4. Hart, W. D. Proc. Resources from Coal, Coal Wastes, and Ash
    Workshop, 1982, pp. 66-75.
5. TRW Energy Development Group, "Gravimelt Process Development;"
    Final Report, DOE/PC/42295-T7 (DE84013743), Redondo Beach, CA,
    June 1983.
6. Meyers, R. A. Proc. First Annual Pittsburgh Coal Conference,
    1984, pp. 381-384.
7. Maijgren, B.; Hübner, W.; Norrgard, K.; Sundvall, S.-B. Fuel
    1983, 62, 1076-1078.
8. Maijgren, B.; Hübner W. Proc. International Conference on Coal
    Science, 1983, pp. 256-259.
9. Chiotti, P.; Markuszewski, R. "Regeneration of Alkali in the
    Fused Salt Desulfurization System;" Fossil Energy Annual Report
    (Oct. 1, 1981 - Sept. 30, 1982), IS-4816, Ames Laboratory, Iowa
    State University, Ames, IA, pp. 39-56.
10. Chiotti, P.; Markuszewski, R. J. Chem. Eng. Data 1985, 30,
    197-201.
11. Annual Book of ASTM Standards, Part 26, ASTM, Philadelphia, PA,
    1982.
12. Straszheim, W. E.; Greer, R. T.; Markuszewski, R. Fuel 1983,
    62, 1070-1075.
13. Straszheim, W. E.; Markuszewski, R. Am. Chem. Soc. Div. Fuel
    Chem. Preprints 1984, 29(4), pp. 310-318.
14. Fan, C. W.; Markuszewski, R.; Wheelock, T. D. Am. Chem. Soc.
    Div. Fuel Chem. Preprints 1984, (29)1, pp. 114-119.
15. Oder, R. R.; Murthy, B. N.; McGinnis, E. L. Separation Science
    and Technology 1983, 18, 1371-1393.
16. Markuszewski, R.; Miller, L. J.; Straszheim, W. E.; Fan, C. W.;
    Wheelock, T. D.; Greer, R. T. In "New Approaches in Coal
    Chemistry"; Blaustein, B. D., Bockrath, B. C., Friedman, S.,
    Eds., ACS SYMPOSIUM SERIES NO. 169, American Chemical Society:
    Washington, D.C., 1981; pp. 401-414.
17. Huggins, F. E.; Huffman, G. P. Proc. International Conference
    on Coal Science, 1983, 679-682.
18. Chiotti, P.; Markuszewski, R. Ind. Eng. Chem. Process Des. and
    Dev. 1985, 24, 1137-1140.

RECEIVED March 6, 1986

5

Molten Hydroxide Coal Desulfurization Using Model Systems

Bruce R. Utz, Sidney Friedman, and Steven K. Soboczenski[1]

Pittsburgh Energy Technology Center, U.S. Department of Energy, Pittsburgh, PA 15236

The chemistry for the removal of organosulfur from coal, using fused caustics (molten hydroxides), was examined. Benzothiophene and dibenzothiophene were chosen as model compounds that simulate organosulfur compounds in coal. Results indicate that the desulfurization of thiophene-ring systems involves initial ring opening to form an intermediate aromatic thiol, followed by a slower sulfur-elimination step that produces the desulfurized product. The reactivities of the two hydroxides (NaOH and KOH) used were also studied. The relative amount of each hydroxide in the mixture may be critical in removing organosulfur, and potassium hydroxide is the reactive species. This suggests that the rate of decomposition/desulfurization may be enhanced by hydroxides containing the larger alkali cation, potassium. The sulfur-elimination step was further examined by conducting decomposition experiments with thiophenol, sodium thiophenolate, or potassium thiophenolate. These compounds were chosen because they have the same functionality as the intermediate aromatic thiol formed from the decomposition of benzothiophene. Preliminary results show that potassium thiophenolate is more readily desulfurized than sodium thiophenolate and provides further evidence to support the important role of the potassium cation. Additional evidence for the role of the potassium cation was obtained by replacing KOH with other potassium salts. Similar rates of benzothiophene desulfurization were obtained with the K_2CO_3-NaOH fused salt mixture. The

---

[1]Current address: E.I. du Pont de Nemours & Co., Inc., LaPorte, TX 77571

possible role of water in molten hydroxide desul-
furization was examined by varying the amount of
water present in certain hydroxides. Results dem-
onstrate that water does not play an important role
in the removal of sulfur from organosulfur moieties.

The removal of mineral matter, including pyritic sulfur, and some
of the organic sulfur with molten hydroxides is a known tech-
nique (1).   The TRW "Gravimelt" Molten Hydroxide Desulfurization
Process is now being developed by the Department of Energy to
improve the removal of sulfur from coal (2,3). Other methods have
been used (4), but none have been as effective as the Gravimelt
Process. This particular process is attractive because it removes
much of the organic sulfur as well as pyritic sulfur. While the
chemistry of inorganic sulfur removal (primarily pyrite) by caustic
is being examined actively (5), little research has been done on
the corresponding removal of sulfur from organosulfur moieties in
coal. Two model compounds that are being used initially to examine
the chemistry of organosulfur removal are benzothiophene and
dibenzothiophene. Characterizations of organosulfur in coal (6-8)
suggest that thiophene-type ring structures are the prevalent
organosulfur forms in many coals. The objective of this study is
to determine how molten hydroxides remove organosulfur from these
model compounds and to relate these results to coal. Results of
studying the chemistry of molten-hydroxide desulfurization, using
thiophene-type ring systems, may lead to innovative approaches to
utilization of this hitherto unexplored area of organosulfur
chemistry, such as, the use of other fused salts to enhance
desulfurization.

Experimental

All molten hydroxide desulfurization reactions were performed using
1/2-inch Monel Swagelok unions as reactors. Similar 316-
stainless-steel reactors developed cracks and leaks, resulting in
loss of volatile components. In a typical reaction, 3.1 to 4.0 g
of powdered sodium hydroxide and/or potassium hydroxide, 0.3 to
0.6 g of an organosulfur compound, and a 1/4-inch-diameter Monel
ball (to ensure adequate mixing) were added to the reactor under a
nitrogen atmosphere in a glove box. In some cases, the hydroxide
mixture was added in two steps to reduce the free volume of the
reactor, which ensured that the reactant would be in the condensed
phase and in intimate contact with the molten hydroxide. This was
accomplished by melting most of the powdered base in the reactor at
$350^{o}C$, followed by cooling the reactor to ambient temperature and
subsequently adding the organosulfur compound and 0.3 to 0.5 g of
additional base. The end caps were tightened to 35 ft lb; and for
each additional experiment, the caps were tightened an additional 3
to 5 ft lb until 75-80 ft lb was reached.
    The reactor was bolted to a bracket assembly and immersed in a
Tescom SBL-2 fluidized sand bath that was preheated to reaction
temperatures. Reaction temperatures ranged from $350^{o}C$ to $400^{o}C$,
and reaction times varied from 10 minutes to 3 hours. Vigorous
mixing (≈ 240 shakes/min) was effected by using a Burrell mechanical

wrist-action shaker. The reactors were cooled rapidly by immersion in ambient-temperature water.

After reaction, the vessels were opened, placed in 50 mL of CH_2Cl_2, and shaken for 5 minutes. This partially removed neutral organics and minimized evaporative losses of volatile organics. The CH_2Cl_2 solution was decanted into a flask containing 0.1 g of an internal standard. The reactor was then shaken with 50 mL of deionized water until the base was dissolved (20-30 minutes). The strongly basic solution was decanted and the reactor was washed with an additional 10 mL of water to ensure complete removal of its contents. The aqueous solutions were combined and extracted with two 25-mL portions of CH_2Cl_2 to remove any of the remaining neutral and basic organics. Using litmus paper as the indicator, the water layer was acidified to a pH of 4-5 with 4 to 6 mL of concentrated HCl. The acidified solution contained acidic products that had previously remained in the aqueous phase as soluble salts. The neutralized water layer was then extracted with two 25-mL portions of CH_2Cl_2. Internal standards were added to each portion to determine quantitatively the individual components and permit calculation of the material balances. Material balances of approximately 85%-95% were achieved.

The three methylene chloride portions were individually analyzed using an HP 5740 gas chromatograph with a 50-meter SE-54 phenylmethylsilicone capillary column. In most cases, flame ionization was sufficient to detect the individual components of the extracts, although in certain instances a mass selective detector (MSD) was also used to assist in the identification of products. The CH_2Cl_2 was removed using a rotoevaporator, and the products were further characterized by proton NMR, FTIR, and low-voltage, high-resolution mass spectrometry. Some loss of the more volatile components was observed.

Thermal decomposition reactions were conducted using thiophenol and its salts. The aromatic thiol (0.2-0.6 g) and a stainless-steel ball were added to the reactor, and the reactor was heated to 375°C for 30 minutes. Sodium thiophenolate and potassium thiophenolate were prepared by mixing equivalent amounts of a 1 M NaOH or KOH solution and thiophenol in a round-bottomed flask sparged with nitrogen. The solution was stirred for approximately 1 minute and then rotoevaporated until the water had been removed. Residual water was removed by adding absolute ethanol and distilling the water-ethanol azeotrope. The solid product was dried in a vacuum oven for 1 hour at 100°C. Experiments designed to examine the decomposition characteristics of the thiophenolate salts were performed with the "neat" salts, as well as with the free acid (thiophenol). Experiments to examine decomposition characteristics of thiophenolate salts were also performed using 0.6 g of thiophenol and 3.0-3.5 g of the KOH:NaOH mixture (60:40).

Results and Discussion

Reaction of Benzothiophene. A weight ratio of 1:1 (KOH:NaOH) was chosen for the initial model-compound study, which was based on one of the ratios that the TRW process is using for bench-scale experiments with coal (2). Preliminary experiments with benzothiophene at 375°C and 30-minute reaction times indicated that benzothiophene

had reacted with the molten hydroxide to form two principal products. Capillary GC, high resolution mass spectrometry, FTIR, and NMR techniques identified the major product as o-thiocresol and the minor product as toluene.

Extending the reaction times to 3 hours gave a considerably different distribution of products. Not only was the benzothio-phene consumed, but the major product was toluene. These results indicate that the overall reaction of benzothiophene with molten hydroxide involves a ring opening and elimination of a one-carbon fragment to form o-thiocresol (Equation 1), followed by a slower sulfur elimination to form toluene (Equation 2).

$$\text{benzothiophene} \xrightarrow[\text{375°C/30 min}]{\substack{\text{KOH: NaOH} \\ (60:40)}} \text{o-thiocresol anion } (Na^+, K^+) + H_2 + \text{1 carbon fragment} \quad (1)$$

$$\text{o-thiocresol anion } (Na^+, K^+) \longrightarrow \text{toluene} + Na_2S, K_2S \, (?) \quad (2)$$
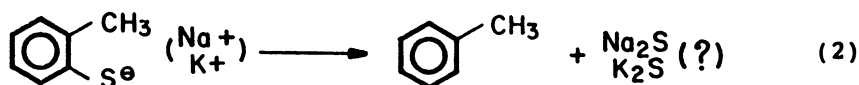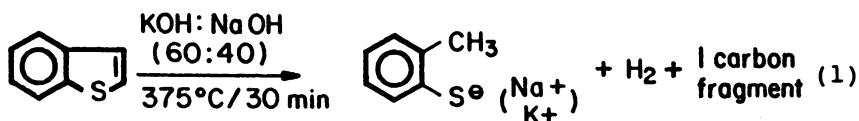
These results are supported by the observations of Weissgerber and Seidler (9), who identified small amounts of o-thiocresol and formic acid when reacting benzothiophene with KOH at 300°C-310°C. Preliminary results indicate that the one-carbon fragment may be carbon monoxide or formic acid. Apparently higher temperature, as well as extended reaction time, are effective in removing sulfur from the species completely.

Effect of KOH:NaOH Ratio. Because of inconsistencies in product yield, a series of experiments was conducted to determine the reactivity of each hydroxide. Mixtures having different ratios of KOH and NaOH were prepared, and their activities were compared by determining the extent of benzothiophene conversion to the initial product, o-thiocresol, or to the subsequent product, toluene. Weight percents of KOH:NaOH used for this study were as follows: 0:100, 40:60, 45:55, 48:52, 50:50, 52:48, 55:45, 60:40, 75:25, 90:10, and 100:0. Figure 1 shows the results of these experiments. Note that at approximately a 45:55 ratio of KOH:NaOH, the conver-sion of benzothiophene to o-thiocresol increases dramatically. The lack of any significant reaction at lower percentages of KOH was unexpected. Increasing the weight percent of KOH in the hydroxide mixture beyond approximately 50% resulted in a decrease in the con-centration of o-thiocresol and a corresponding increase in toluene formation, consistent with the proposed mechanism where toluene is a decomposition product of the intermediate (o-thiocresol). Maximum yields of desulfurized product (toluene) were obtained by using pure KOH. Conversions varied dramatically at approximately a 45:55 ratio; therefore all subsequent experiments were done with a 60:40 ratio of KOH:NaOH, since reactions were occurring at a sig-nificant rate in this mixture. The 60:40 ratio was used as the "standard" ratio for most of the study.

The lack of reactivity for hydroxide mixtures containing less than 40 wt% of KOH was believed to be caused by the existence of an

induction or inhibition period. Experiments were conducted using the standard KOH:NaOH mixture at reaction temperatures of 375°C and reaction times between 5 and 30 minutes in order to determine if an induction or inhibition period exists. The results (Figure 2) demonstrate that at shorter reaction times, no reaction occurs. The existence of an induction or inhibition period would explain why benzothiophene was unreactive when using hydroxide mixtures containing less than 40 wt% KOH. In the previous set of experiments (Figure 1), all experiments were conducted for 30 minutes. At lower KOH concentrations, 30-minute reaction times fell within the induction or inhibition period, and therefore no reaction occurred.

A hydroxide mixture containing less than 40 wt% of KOH was chosen arbitrarily (30 wt%) and allowed to react at 375°C for 1 hour to determine if benzothiophene would decompose at longer reaction times. After 1 hour, benzothiophene completely decomposed to o-thiocresol and toluene. These results demonstrate that hydroxide mixtures containing lesser amounts of KOH have an induction or inhibition period longer than 30 minutes. Additional evidence to support this hypothesis was obtained by conducting reactions with benzothiophene and pure KOH at different reaction times. These results (Figure 2) show that the induction or inhibition period decreases significantly when KOH alone is used and further suggests that the relative amount of KOH can influence the length of the induction or inhibition period.

Most important, the existence of an induction or inhibition period suggests a free-radical step in the decomposition of the thiophene ring. Further evidence for the free-radical nature of the reaction was obtained from experiments conducted under less severe conditions in order to isolate the initial ring-opened intermediate before subsequent loss of the one-carbon fragment. Efforts to isolate the initial decomposition product were unsuccessful. Apparently, the loss of the one-carbon fragment occurs rapidly, consistent with a free-radical chain reaction of some type.

While some specific role of the K^+ cation may account for the increased reactivity of benzothiophene with increasing amounts of KOH in the hydroxide mixture, the possible role of the total base, KOH, cannot be neglected. Potassium hydroxide is a stronger base and nucleophile in this system than NaOH is (10), and the increased basicity and nucleophilicity could account for increased reactivity toward benzothiophene decomposition. The chemical nature of ionic melts is not fully understood. While the hydroxide melts are believed to be fully dissociated (11), explanations have also been given for the formation of "quasicrystalline states" (12), where order within the melt exists and dissociation is not complete. It is difficult to deduce how much independent freedom K^+ and OH^- have and if either the K^+ cation or KOH or both are the important species.

To determine the potential role of the potassium cation, experiments were conducted in which different potassium salts were substituted for KOH. The two salts examined were KCl and K_2CO_3. The possible role of KOH cannot be eliminated because of the reactions shown in Equations 3 and 4.
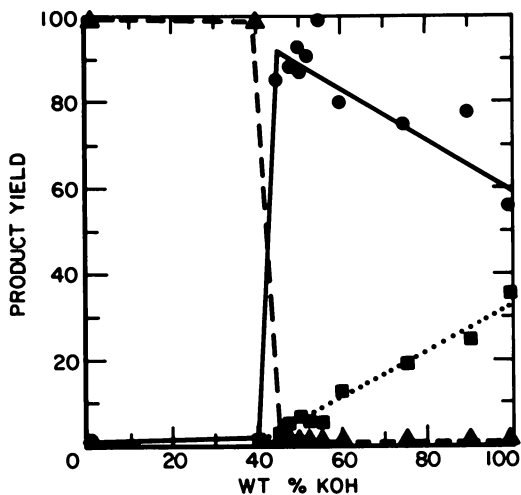
Figure 1. Reactions of benzothiophene with molten KOH/NaOH mixtures at 375°C for 30 minutes. benzothiophene, --- ▲ ----; o-thiocresol, —— ● ——; toluene, ····· ■ ·····.
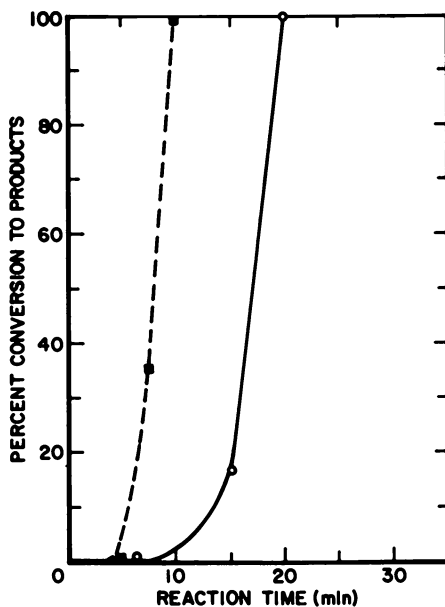
Figure 2. Induction Period - molten hydroxide treatment of benzothiophene (reaction temperature - 375°C).   KOH:NaOH (60:40), —— ○ ——; KOH, --- ■ ---.

$$NaOH + KCl \rightleftharpoons KOH + NaCl \qquad (3)$$

$$2NaOH + K_2CO_3 \rightleftharpoons 2KOH + Na_2CO_3 \qquad (4)$$
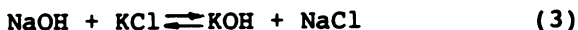
By calculating the enthalpy of the reaction and assuming no significant entropy change, the ΔH (based on heats of formation and heats of fusion) of Equation 3 is approximately +5.2 kcal/mole and of Equation 4 is approximately +10.5 kcal/mole. While both reactions are not favored thermodynamically, at high temperatures (i.e., 375°C), these reactions will establish an equilibrium where significant amounts of KOH and/or K^+ and OH^- may exist.

Benzothiophene experiments conducted at 375°C for 30 minutes with KCl-NaOH mixtures (70:30 by wt) resulted in no decomposition or desulfurization. Experiments conducted with K_2CO_3-NaOH mixtures (70:30 by wt) resulted in complete decomposition of benzothiophene, yielding o-thiocresol and toluene as products. Relative amounts of the two products were similar to those found in experiments that used the KOH-NaOH mixture. Experiments with the KCl-NaOH mixture were repeated at longer reaction times (1 and 3 hours). After 1 hour, very little decomposition of benzothiophene had occurred. After 3-hour reaction times, the majority of benzothiophene had decomposed to toluene (4%), o-thiocresol (26%), and tolyldisulfide (23%). While the yield of tolyldisulfide (an oxidation product of o-thiocresol) was somewhat unexpected, the longer reaction times demonstrate that KCl-NaOH mixtures can cause benzothiophene decomposition. Again, the induction or inhibition period may account for the lack of KCl-NaOH reactivity using 30-minute reaction times.

Results of experiments with benzothiophene and pure NaOH serve to emphasize the difference between NaOH and KOH. Even at reaction times of 6 hours, no benzothiophene decomposition was observed with NaOH. These results not only emphasize the role of K^+/KOH but suggest that K^+/KOH is a necessary part of the hydroxide mixture for decomposition and ultimate desulfurization of thiophene-ring systems.

From this, it can be seen that the amount of KOH within the hydroxide mixture would probably be critical in removing organo-sulfur from coal. While the particular role of KOH has not been determined, evidence from the literature has shown that the size of the cation may be important in stabilizing intermediate carbanions. Wallace et al. (13) conducted a series of base- catalyzed, beta-elimination reactions with isopropyl sulfide and measured the amount of olefin production. The proposed mechanism involved initial abstraction of a proton by the t-butoxide base, and formation of a carbanion, with subsequent elimination of the sulfur moiety (which can be considered a good leaving group) to form the olefin (Equation 5).

$$(5)$$
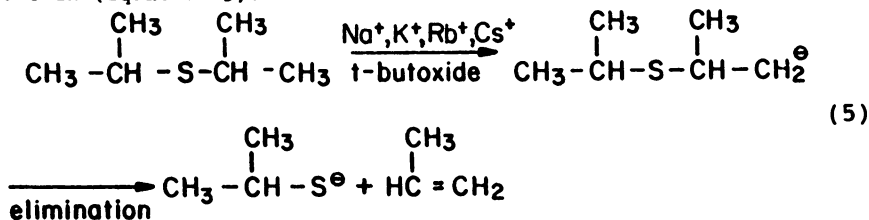
It was shown that the rate of olefin production was dependent on the size of the metal cation (Li$^+$, Na$^+$, K$^+$, Rb$^+$, and Cs$^+$) of the base. The increase in olefin production with an increase in cation size was explained as an increase in cation solvation by solvent with the larger cations, making t-butoxide a stronger base and thus increasing the rate of proton abstraction. Possibly these differences in cation solvation influence the reactivity of the carbanion intermediate for the conversion of benzothiophene and account for increased reactivity with the larger cation, potassium.

Thiol Decomposition. As explained previously, the elimination of sulfur from benzothiophene occurs stepwise after the aromatic thiol (o-thiocresol) has formed and not in a concerted fashion from the thiophenic ring system. Extrapolation of this implies that thiophenic sulfur in coal is eliminated by conversion to an aromatic thiol that subsequently undergoes desulfurization. Since the aromatic thiol is the apparent organosulfur species that undergoes desulfurization, it is of interest to understand the chemistry involving the elimination of sulfur from aromatic thiols. Thiophenol was used as a model compound to examine reactions, primarily the thermal decomposition reactions that might lead to sulfur elimination. In the experiments with caustic and benzothiophene, the intermediate (o-thiocresol) most likely exists in the salt form, since the aromatic thiol group is acidic. Because of this, the thermal chemistry of the sodium and potassium salts of thiophenol was also examined.

The bond dissociation energy (BDE) of the S-H bond of aryl thiols is approximately 75 kcal/mole (14), which would result in the formation of a resonance-stabilized phenylthio radical. The BDE of the aromatic C-S bond is approximately 85 kcal/mole (14), and cleavage of thiophenol at the C-S bond would result in the formation of an unstable and reactive phenyl radical. Very little decomposition of neat thiophenol occurred at a reaction temperature of 375°C for 30 minutes, confirming a report in the literature (14). The only two products observed (Equation 6) were diphenyl sulfide (3%-5%) and diphenyl disulfide (3%-5%).

Phenyl Sulfide (3-5 %)   Phenyl Disulfide (3-5 %)   (90-94 %)   (6)
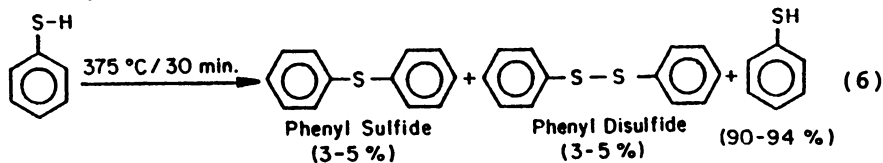
The products are believed to be formed by S-H bond cleavage resulting in phenylthio radicals that subsequently couple to form diphenyl disulfide. Ipso attack by a phenylthio radical on thiophenol (via a free-radical aromatic substitution) would produce diphenyl sulfide (Equation 7).

(7)
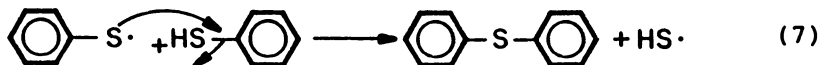
This proposed reaction would be facilitated because the leaving group would be the stable HS radical (15), and arylthio radicals

are known to attack substituted aromatics (16) via a free-radical aromatic substitution mechanism.

Thiophenol was allowed to react with the standard KOH-NaOH mixture under the same conditions used for most other experiments (375°C for 30 minutes), and the observed reaction products (Equation 8) were

$$\text{S-H} \xrightarrow[\text{(60:40)}]{\substack{375°C/30 \text{ min.} \\ \text{KOH: NaOH}}} \text{benzene} + \text{SH} + \text{OH} + CH_2Cl_2\text{-Insoluble Material} \quad (8)$$

(25-30%)   (≈8%)   (≈10%)   (≈6%)
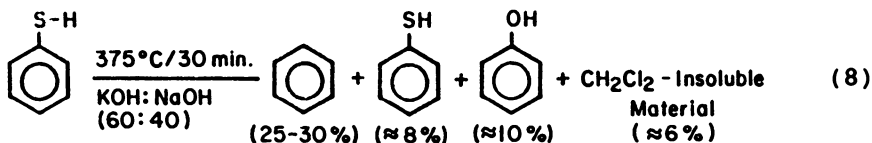
completely different than those that resulted from the simple thermal decomposition of thiophenol (Equation 6). The major products were benzene (25%-30%), thiophenol (8%), phenol (10%), and CH_2Cl_2-insoluble material (6%-10%). Even though the material balances were poor (50%-60%), the presence of the KOH and NaOH, probably as reactants, dramatically affected the reaction pathway. Since the major product observed was benzene, it is obvious that the C-S bond is more labile in the presence of the caustic than under simple thermal conditions.

Since thiophenol is a moderately strong acid, it was expected that potassium and sodium salts of thiophenol would be present in the molten KOH-NaOH mixture. Both the sodium and potassium thiophenolate salts were prepared in order to examine their thermal stability. Reaction products with the neat sodium salt were essentially the same as with thiophenol. Only diphenylsulfide (<1%) and diphenyldisulfide (1%-3.5%) were found, along with recovered starting material. Results using the neat potassium salt of thiophenol were completely different. The potassium salt underwent substantial decomposition (Equation 9), producing benzene (25%-30%) as the major identifiable product, 36%-38% CH_2Cl_2-insoluble material, and 11%-15% recovered thiophenol (as unreacted potassium salt).

$$\text{S}^{\ominus}\text{K}^{\bullet} \xrightarrow{375°C/30\text{ min.}} \text{benzene} + \text{SH} + \text{CH}_2\text{Cl}_2\text{-Insoluble Material} \quad (9)$$

(25-30%)   (11-15%)   (36-38%)
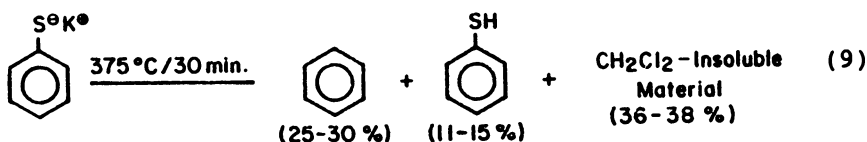
These results were similar to those of the reaction of thiophenol with the KOH-NaOH mixture, wherein benzene was also the major product. The similarity in the two sets of results suggest that the potassium salt of thiophenol is probably the active species in the desulfurization step of the reactions of benzothiophene and molten caustic.

The change in the lability of the C-S bond may be due to a change in BDE of the C-S bond with formation of the potassium salt. If homolytic cleavage of the C-S bond is occurring, then a free-radical polymerization or condensation reactions could explain the insoluble material that was recovered from the thermal decomposition reaction of the potassium salt. To examine this possibility,

thiophenol was reacted with the KOH and NaOH mixture, and sodium formate. Formate ion is known to react with hydroxide to generate hydrogen, carbon monoxide, and carbonate salts (17). This in situ generation of H_2 might then cap intermediate free radicals (phenyl radicals) and thus inhibit free-radical polymerization reactions. In most cases, the material balances varied between 60% and 70%, but most important, the benzene yields increased to 50%-63%, and little CH_2Cl_2-insoluble material was observed. These results are consistent with homolysis of the C-S bond and capping of the phenyl radical by hydrogen to form benzene before any free-radical polymerization reactions could occur. Experiments with the potassium salt of thiophenol, conducted in the presence of gaseous H_2, also gave benzene yields of 55%-65%.

These results support the hypothesis that the formation of specific salts of aromatic thiols completely changes the thermal decomposition desulfurization mechanism and that thermal elimination of sulfur may be best accomplished by forming specific salts of the aromatic thiols. A possible explanation for the increased rate of desulfurization with increasing amounts of KOH, for reactions involving benzothiophene and molten caustics, is that larger amounts of K^+ allow more of the intermediate aromatic thiol to be converted to its potassium salt rather than to the unreactive sodium salt. Based on these results, it is suggested that the conjugate base of the intermediate o-thiocresol, produced from benzothiophene, undergoes thermal decomposition to toluene.

Reaction of Dibenzothiophene. Dibenzothiophene was much less reactive than benzothiophene. Reactions in the standard KOH/NaOH mixture (60:40) at 375°C for 30 minutes in our laboratories demonstrated that dibenzothiophene was unreactive and quantitatively recovered. Using dibenzothiophene as a model, Maijgren and Hubner (18) observed that under similar reaction conditions (75%KOH and 25%NaOH, 370°C for 60 minutes), 81% of dibenzothiophene was recovered, but no reaction products were identified. Wallace et al. (19) found also that dibenzothiophene was unreactive when heated at 200°C for 20 hours in a mixture of KOH and white oil. The severity of the reaction conditions in our laboratory was increased by raising the temperature to 400°C and allowing the reaction to occur for 6 hours. Under these conditions, using the standard KOH/NaOH mixture, dibenzothiophene reacted completely, producing approximately 62% o-phenylphenol and 6% biphenyl (approximately 30% of the material was unaccounted for). Apparently even dibenzothiophene will react with molten hydroxide and desulfurize if the reaction conditions are sufficiently severe.

Role of Moisture. Previous results have shown that benzothiophene was not desulfurized in molten sodium hydroxide. Since A.C.S. reagent-grade KOH has a moisture content of 13%-15% and reagent-grade NaOH contains only 1-2 wt% moisture, experiments were completed to test whether water might be playing an important role in the desulfurization reaction. An equivalent amount of water (13 wt%) was added to experiments conducted in NaOH, and in each case, no conversion occurred. Based on these preliminary results, it appears that water does not have an advantageous effect on the removal of sulfur from organosulfur compounds using molten sodium

hydroxide.   More recent results have shown that the addition of
13 wt% moisture to the standard KOH/NaOH does have an effect on the
rate of desulfurization, and while the recycled caustic (in a
process) will not require complete drying, it will require some
drying.

Conclusions

Experiments carried out in microautoclaves have demonstrated that
sulfur can be removed from organosulfur model compounds using
molten hydroxides.   It has been shown that the ratio of KOH to NaOH
is critical in removing sulfur from organosulfur compounds and that
the reaction temperatures and times determine the rate of reaction
and final products.   Extrapolating these results to coal, a large
improvement in sulfur removal using the molten hydroxide desulfuri-
zation process might be possible by varying the amount of KOH and
NaOH.   Understanding the importance of the cation in the decomposi-
tion and ultimate desulfurization of thiophene-type ring systems
should allow us to enhance the elimination of sulfur from organo-
sulfur compounds and should extend to the removal of organosulfur
from coal.   While sulfur might be removed from benzothiophene
moieties in coal at $375^{o}C$, it appears that more severe conditions
may be necessary to remove sulfur from dibenzothiophene moieties.
Efficiency of organosulfur removal may be partially dependent on
the type of organosulfur species in coal, and therefore continued
efforts to characterize the types of organosulfur moieties in coal
are necessary.

Acknowledgments

Disclaimer

Reference in the report to any specific commercial product,
process, or service is to facilitate understanding and does not
necessarily imply its endorsement or favoring by the United States
Department of Energy.

Literature Cited

1.   Masciantonio, P.X., Fuel 1965, 44, 269.

2.   TRW Energy Development Group; "Gravimelt Process Development,"
     DOE Final Report, No. DOE/PC/42295-T7, June 1983.

3.   Meyers, R.A.; McClanathan, L.C.; Hart, W.D. Proceedings of the
     Pittsburgh Coal Conference, Pittsburgh, Pa., September 16-20,
     1985, 112.

4. Morrison, G.F., "Chemical Desulphurisation of Coal," IEA Coal
    Research, Report No. ICTIS/TRIS, June 1981, London SWIW OEX.

5. Chiotti, P.; Markuszewski, R. Ind. Eng. Chem. Proc. Des. Dev.
    1985, 24(4), 1137.

6. Attar, A. "An Analytical Method for the Evaluation of Sulfur
    Functionalities in American Coals," DOE Final Report #DOE/PC/
    30145-T1 (DE 84007770) 1984.

7. LaCount, R.B.; Anderson, R.R.; Friedman, S.; Blaustein, B.D.
    Am. Chem. Soc. Div. Fuel Chem. Preprint 1986, 31(1), 70.

8. Spiro, C.L.; Wong, J.; Lytle, F.W.; Greegor, R.B.;
    Maylotte, D.H.; Lamson, S.H. Science 1984, 226, 48.

9. Weissgerber, R.; Seidler, C. Ber. Dtsch. Chem. Ges. B. 1927,
    60, 2088.

10. Whaley, T.P. In "Comprehensive Inorganic Chemistry"
    Bailor, J.C., Jr.; Nyholm, Sir R.; Emeléus, H.J.; Trotman-
    Dickenson, A.F., Eds; Permagon Press:Oxford 1975, p. 423-427.

11. Copeland, J.L. "Transport Properties of Ionic Liquids,"
    Gordon and Breach Science Pub.: New York, 1974, Ch. 1.

12. Ubbelohde, A.R.   In "Ionic Liquids," Inman, D.;
    Lovering, D.G.; Eds.; Plenum Press: New York, 1981, Ch. 1.

13. Wallace, T.J.; Hofmann, J.F.; Schriesheim, A. J. Am. Chem.
    Soc. 1963, 85, 2739.

14. Shaw, R. In "The Chemistry of the Thiol Group," Patai, S.,
    Ed.; John Wiley and Sons: N.Y. 1974, Part 1, p. 151-161.

15. Thompson, C.J. J. Am. Chem. Soc. 1952, 74, 3284.

16. Benati, L. J. Chem. Soc. Perkin Trans. 1. 1972, 2817.

17. Boswell, M.C.; Dickson, J.V. J. Am. Chem. Soc. 1918, 40,
    1779.

18. Maijgren, B., and Hübner, W. Proceedings of the International
    Conference on Coal Science, International Energy Agency,
    Pittsburgh, Pa., April 15-19, 1983, 256.

19. Wallace, T. J.; Heimlich, B.N. Tetrahedron 1968, 24, 1311.

Chemical Cleaning of Coal
Effect on the Removal of Trace Elements

G. A. Norton, Richard Markuszewski, and H. G. Araghi

Ames Laboratory, Iowa State University, Ames, IA 50011

Levels of many trace elements in Illinois No. 6 and
Pittsburgh No. 8 coals were significantly reduced by
treatments with molten caustic mixtures or aqueous alkali
solutions, followed by washing with acid. Treating run-
of-mine Illinois No. 6 coal with aqueous Na_2CO_3 at ele-
vated temperatures and pressures and washing the product
coal subsequently with acid reduced Mn, Pb, and Zn con-
centrations by 75% or more, while levels of Cd and Ni
were reduced by lesser amounts. In one of these sam-
ples, substantial reductions in levels of Ba, Cr, Rb,
and Sr were also observed. Coals which were treated with
molten NaOH/KOH mixtures at atmospheric pressure showed
substantial reductions in concentrations of As, Cd, Hg,
Pb, Rb, Se, Sr, and Zn. The amounts of several elements,
such as Cr, Cu, and Ni, were elevated in some of the
treated coals, but this can be attributed to corrosion of
reactor components.

Coal contains most of the elements of the periodic table, the major-
ity of which are present in concentrations of 100 ppm or less. Many
of these trace elements are toxic to plant and animal life, even at
low levels. Because U.S. power plants consume on the order of 600
million tons of coal annually for the production of electricity ([1]),
coal combustion can mobilize thousands of tons of potentially haz-
ardous trace elements into the environment each year. Due to the
large quantities of coal combusted, even trace amounts of toxic ele-
ments present in the coals can accumulate to hazardous levels. Also,
potentially deleterious effects of particulate emissions from coal
combustion may be enhanced since many trace elements are surface-en-
riched ([2]) and concentrate preferentially in the smaller, more res-
pirable particle sizes ([3]). Substantial amounts of some elements,
such as As, Hg, and Se, are in the vapor phase in flue gases from
coal combustion and are essentially unaffected by most particle con-
trol devices. Aside from the potential detrimental environmental
aspects, trace elements in coal can pose adverse technological

problems, such as catalyst poisoning in catalytic hydrogenation and gasification reactions (4,5,6).

Physical methods can effectively remove some trace constituents from coal, especially if deep cleaning methods are employed (7). However, such methods do not adequately remove finely disseminated minerals or organically bound elements, thereby necessitating chemical treatments for removing such components.

Background

A literature survey was conducted to acquire information pertinent to the removal of trace elements from U.S. coals during physical and chemical cleaning. This survey included trace element associations with minerals and their affinities for organic or inorganic components in coal. Literature was also searched to ascertain the trace elements of concern with respect to coal utilization and for data reported previously on the removal of trace elements during physical and chemical coal cleaning. Results of these literature searches are discussed below.

Trace Elements of Environmental Concern. In a list prepared by a panel of scientists and engineers involved with environmental aspects of coal utilization, As, B, Cd, Hg, Mo, Pb, and Se were considered to be of primary environmental concern (8). The elements Cr, Cu, Ni, V, and Zn were of moderate concern, while Ba, Co, Ge, and Mn were believed to be of minor concern. Despite the toxicity of Ag, Be, Sn, and Tl, the panel believed concentrations of these elements in coal and coal residues are negligible and that the likelihood of health hazards associated with these constituents is remote. This list served as a guide in choosing the elements to be determined in raw and treated coals in this study. However, some of the elements, such as B, were not studied in this work due to the inherent difficulties with the analytical procedures and instrumental methods employed.

Occurrence of Trace Elements in Coal. Based on the reviewed literature, it is evident that modes of occurrence in U.S. coals vary considerably, although several generalizations can be made. Many elements of environmental concern, including As, Cd, Hg, Pb, and Zn, have an affinity for the mineral portion of the coal and tend to be associated with pyrite or accessory sulfide minerals (6,9-12). Other elements which have been reported as being at least partially associated with pyrite include Co, Mn, and Se. The element Zn appears to occur as sphalerite in most coals. Although Mo has a general inorganic association, its mode of occurrence is uncertain. The element As has been found to occur in solid solution in pyrite (13), while Cd has been found in solid solution in sphalerite (14,15). The predominant mineral species containing a particular element can vary. In one example, Pb seems to be present mostly as PbSe in Appalachian Basin coals, but it tends to exist in the form of PbS in coals from other regions (13,16).

Although most trace elements appear to be largely inorganically associated, several of them have a strong affinity for the organic portion of the coal and are believed to be present as metal chelates. Among the elements in this category are B, Be, and Ge (6,9-12).

Although the majority of B appears to be associated with the organic matrix in most coals, B has also been reported occurring in illite (13-17). Many elements, such as Cr, Cu, Ni, and Se, appear to have a mixed or highly variable organic/inorganic affinity in some coals. Again, these are only generalizations, since organic/inorganic associations of trace elements can vary widely from coal to coal and can show both extremes in their affinities.

Trace Element Removal During Physical Cleaning. Commercial coal cleaning processes employ physical means for beneficiation and are aimed at removing ash forming minerals and sulfur, although removal of the mineral matter also results in reduced levels of some trace elements. Trace element extraction efficiencies for various physical cleaning processes have been reported.

In one study, eight geographically diverse coals were ground and cleaned subsequently with a wet concentrating table (18). Cleaning efficiencies with respect to trace elements varied widely between coals. For the elements of environmental concern, average percent removals were less than 50%. In studies where coal was physically cleaned by float/sink separation in static baths of known specific gravity, reductions in trace element concentrations were also generally less than 50% (1,7,19).

Physical cleaning of various coals by oil agglomeration reduced levels of As, Cr, Pb, Mn, Mo, Ni, and V by 50-80%, while levels of some other trace elements were reduced by lesser amounts (20). Oil agglomeration appeared to be more effective at removing trace elements than the wet concentrating table or float/sink density separations. This may be related to an increase in the liberation of mineral matter associated with grinding to produce the relatively fine particle sizes required in the oil agglomeration technique.

Levels of various elements such as As, Cd, Cr, Cu, Pb, Mn, Se, and Zn were reduced by 50% or more in some coals cleaned by combinations of heavy media cyclones, froth flotation cells, and hydraulic classifiers (21-24). Cleaning was less effective for other coals. In general, average reductions in overall trace element content corresponded to reductions in ash levels.

Trace Element Removal During Chemical Cleaning. The literature on trace element removal from coal by chemical cleaning methods alone is sparse. There are some indications, however, that leaching physically cleaned coals with various acids can effectively remove many trace elements of interest. In one study, for example, various coals from eastern, central, and western coal regions were cleaned by a combination of physical and chemical means, and extraction efficiencies for numerous elements were ascertained by analyzing the raw and treated coals (25). Cleaning was performed by floating the coals at a specific gravity of 1.40, grinding the float fraction to -325 mesh, and then successively leaching with 10% HNO_3, 49% HF, and 25% HCl. Based on average concentrations in raw and treated coals from a given region, levels of Be were reduced by 90% or more, while levels of As, B, Cr, Cu, Mo, Ni, Se, and V were reduced by at least 70%. In that study, physical separation by flotation followed by acid leachings was found to be much more efficient at removing trace elements than flotation alone, although this may be partially attributed to the

liberation of mineral matter during grinding prior to the chemical leaching step.

Only a few of the chemical cleaning processes studied in the past or currently being developed present trace element data in addition to the conventional sulfur, ash, and heating values. One of the exceptions is the Jet Propulsion Laboratory Chlorinolysis Process, in which cleaning was generally accomplished by bubbling chlorine through a mixture containing 100 grams of finely ground coal, 200 grams of solvent (either methylchloroform, carbon tetrachloride, or tetrachloroethylene), and 20-70 grams of water (26). The chlorination step was conducted at 50-100°C at atmospheric pressure for 10-20 minutes. The coal was then hydrolyzed by washing with water for 60-120 minutes at 60-100°C and subsequently dechlorinated at 350-550°C in a steam atmosphere. For some coals treated under these conditions, levels of As, Be, Pb, and V were reduced by 50-90% (26,27). Analytical data on the raw and treated coals are shown in Table I. In another one, the Battelle Hydrothermal Process (28-30), an aqueous slurry of finely ground coal, NaOH, and Ca(OH)$_2$ was heated for 10-30 minutes at 250-350°C at pressures of 600-2500 psig. Trace element data for several Ohio coals are shown in Table II. Based on averages from these coals, this process reduced levels of all reported trace elements by 70-90%. In yet another chemical cleaning process, the Meyers Process, crushed coal was leached with an acidic solution of ferric sulfate at 100-130°C for several hours (31). If the leaching time was long enough, almost all of the pyritic sulfur was extracted. At the same time, levels of As, Cd, Cr, Mn, Ni, Pb, V, and Zn were significantly reduced (32). Still, the data discussed above represent only a small fraction of the chemical processes that have been studied.

Table I. Elemental Data for Coals Before and After Treatment by the Low-Temperature Chlorinolysis (26,27)[1]

	Kentucky #4 (26)			Upper Freeport (26)		Illinois #5 (27)	
	Raw	Treated[2]		Raw	Treated	Raw	Treated
As	73	25	49	85	9	2	1
Ba	5	5	--	<10	92	38	30
Be	8	4	13	5	4	3	1
Cd	1	<1	--	--	--	--	--
Hg	<1	<1	--	<0.5	<0.5	0.6	<0.5
Li	<10	5	--	20	21	9	3
P	131	68	68	1040	700	736	126
Pb	46	4	5	0.5	3	18	4
Se	<1	<1	--	<1	<1	<1	<1
Ti	1086	510	680	1400	700	476	460
V	46	12	48	<25	<25	15	<1

[1] Values are in ppm.
[2] Results from two separate runs are presented.

Table II.   Trace Element Levels In Coals Before and After Treatment
            by the Battelle Hydrothermal Process (29,30)[1]

	Raw (ppm)	Treated (ppm)
As	25	2
B	75	4
Ba	25	4
Be	10	3
Li	15	3
Mo	20	5
Pb	20	5
Th	3	0.5
V	40	2

[1]   Values are averages from three Ohio coals.

        In our own work, the effectiveness was examined of trace element removal by two chemical coal cleaning methods being studied for possible large-scale application. One method involved treatment with aqueous Na_2CO_3 solutions, and the other involved treatment with molten NaOH/KOH mixtures. In each case, acid washes were used as subsequent cleaning steps to decrease the ash content, followed by water washes in the final step. Although the primary objective of these treatments was to remove sulfur and ash-forming minerals, the extraction of trace elements from these coals was examined as an additional benefit of chemical coal cleaning.

Experimental

Aqueous Na_2CO_3 Treatments. Two samples of treated Illinois No. 6 run-of-mine coal were studied. One sample was treated in an autoclave under a pressure of 600 psi for one hour with 1.0 $\underline{M}$ Na_2CO_3 at 250°C in a nitrogen atmosphere and washed subsequently with hot 2.0 $\underline{M}$ HCl and then with water to obtain the final product (33). The other sample was first pretreated with 0.2 $\underline{M}$ Na_2CO_3 at 150°C for one hour under an oxygen partial pressure of 200 psi, then treated with 1.0 M Na_2CO_3 as in the above sample, and washed subsequently with hot 1.8 $\underline{M}$ H_2SO_4 and finally with water. The run-of-mine coal was ground to -200 mesh prior to the treatments.

Molten Caustic Treatments. Two additional samples were obtained from a different Illinois No. 6 coal used for molten caustic treatments at Ames Laboratory under conditions simulating the TRW Gravimelt Process (34). For these samples, 12 x 0 mesh coal was treated with a molten 4:1 NaOH/KOH blend using a 10:1 caustic-to-coal ratio for one hour at 370°C under a nitrogen atmosphere. After separating and washing the coal with water, the coal was treated with hot 10% H_2SO_4 and then with a final water wash. Two runs were made, one in the normal manner and the other with powdered reagent-grade iron included in the coal/caustic mixture. The iron was added in hopes that it would act as a sulfur scavenger and improve desulfurization.

In addition to these samples, several coal samples were provided by TRW Systems, Inc., from the San Juan Capistrano test plant in California. The samples included Illinois No. 6 and Pittsburgh No. 8 coals before and after treatment by the Gravimelt Process. The raw Illinois and Pittsburgh coals were -14 mesh and -6 mesh, respectively.

Analytical Methodology

All raw and treated coals were analyzed at Ames Laboratory for trace, major, and minor elements using energy-dispersive x-ray fluorescence (XRF), inductively coupled plasma-atomic emission spectroscopy (ICP-AES), and atomic absorption spectrophotometry (AA). General analytical procedures employed for each of these techniques are discussed separately below.

Atomic Absorption. For the determinations of Cd and Pb by AA, the coal samples were ashed at 500°C, and the ashes were subsequently dissolved in accordance with procedures described in ASTM Method D-3683 (35). Basically, the ash was dissolved in a mixture of HNO_3, HCl, and HF in a tightly capped plastic bottle in a steam bath. Saturated H_3BO_3 solution was then added to the mixture to complex the excess fluoride and to improve flame properties during AA measurements. For the AA determinations of As, Sb, and Se, sample solutions were prepared by treating the coal with hot HNO_3 and then with fuming H_2SO_4 in an Erlenmeyer flask-reflux cap apparatus (36). Conventional flame AA was used for the Cd and Pb determinations, while hydride generation AA was used for the As, Sb, and Se. For the Hg determination, a portion of the coal was placed in a Parr bomb containing 10% HNO_3. After ignition, the contents of the bomb were washed into an Erlenmeyer flask, and $SnCl_2$ solution was added to the mixture to reduce the Hg for conventional cold vapor AA measurements. Corrections were made for reagent blanks in all analyses by AA.

X-ray Fluorescence. For the coals analyzed by XRF, samples that were +60 mesh were first ground to -60 mesh with a boron carbide mortar and pestle. The samples were then prepared by mixing two grams of sample with 0.2 grams of Somar Mix, a granulated plastic binding agent. If less than two grams of sample were available, the amount of binding agent was scaled down proportionally. The powder was then pressed into disks at a pressure of about 5000 psi. The XRF analyses were performed using a Mo-target x-ray tube. An NBS coal, Standard Reference Material 1632(A), was used for instrument calibration.

For these samples, matrix corrections were not made. The matrix effects are most severe at the lower energy levels and are considered to be of almost negligible importance for elements having an atomic weight greater than that of iron. Thus, concentrations of Al, Si, S, and Cr may be in error by up to ±50% of the amount present because of matrix effects and relatively poor counting statistics. All other reported elements are estimated to be accurate to within ±10% of the correct values.

Inductively Coupled Plasma. Analyses by ICP were performed on the same dissolutions used for the AA analyses for Cd and Pb. The solutions were diluted as necessary and were then nebulized and introduced into the plasma. Line spectra were collected with a multichannel analyzer and corrections were made for reagent blanks and background shifts. For all analyses, NBS Standard Reference Material 1632 was used for instrument calibration.

Results and Discussion

Results of the analyses on coals before and after treatment with aqueous Na_2CO_3 solutions and molten NaOH/KOH mixtures at Ames Laboratory are shown in Table III. Levels of Cd, Pb and Zn were relatively high in the raw Illinois No. 6 run-of-mine coal used for the Na_2CO_3 treatments. The elevated Cd levels correlate well with the high Zn levels, since Cd in coal is commonly associated with sphalerite (ZnS). The Pb was probably present largely as galena (PbS). For the alkali-treated coal washed subsequently with HCl, levels of Mn, Pb, Rb, Sr, and Zn were reduced by 75% or more, while levels of Ba, Cd, Cr, Ni, and Se, were reduced by 30-60%. The coal that had been pretreated showed reductions of 75% or more for Mn, Pb, and Zn, while Cd and Ni were reduced by 60% or more. It is interesting to note that every alkali and alkaline earth metal determined was enriched in the pretreated coal relative to the coal that was leached with no pretreatment. Some of these, such as Ba and Ca, were more concentrated in the pretreated coal than in the raw coal. The high Cu concentration in the coal which was pretreated is a result of contamination from the stirrer used in the autoclave. The relatively high Cu levels in this sample caused an interference in the Zn determination. A different autoclave and stirrer was used for the non-oxidative treatments.

XRF data on coals treated with molten caustic at Ames Laboratory showed that levels of Fe, which is predominantly associated with pyrite in coal, were reduced by about 90% for each of the two runs. Reductions in concentrations of other elements which form abundant minerals in coal, including Al, K, and Si, were also substantial. Because roughly 90% of the ash was removed, substantial concentration reductions in the major mineral-forming elements are expected. Levels of Ba, Rb, Sr, and Zn were reduced by 70% or more, and Se was reduced by 30% or more in the coal treated in the normal fashion (Run 1). In the coal from the test containing the iron additive (Run 2), levels of Rb, Sr, and Zn were also reduced by 70% or more. Pb levels remained essentially constant for each of the treated coals. The elevated Cr and Ni levels are believed to be corrosion byproducts from the reactor.

In the coal treated by molten caustic in Run 2, the Cr and Ni levels are significantly higher than in Run 1, suggesting a more severe attack in the second test. If the attack were more severe, then levels of Fe, Al, Si, and ash would be anticipated to be somewhat lower than in Run 1. As can be seen from these data, this is indeed the case. However, because of the numerous variables involved, no definitive conclusions can be drawn. Overall trace element reductions did not seem to be significantly improved in Run 2.

Table III. XRF Data on Coals Before and After Treatment.[a]

	Molten NaOH/KOH Treatment			Aqueous Na$_2$CO$_3$ Treatment		
	Raw Ill. No. 6	Run 1	Run 2[b]	Raw Ill. No. 6	Run 1	Run 2[c]
Ash (%)	14.17	1.24	1.02	13.24	2.61	2.97
Al (%)	1.9	0.72	0.29	2.0	0.70	0.79
As	3.4	1.0	3.8	<5	2.1	<1.0
Ba	49	<10	36	27	17	59
Br	1.7	<1.0	<1	2.7	6.3	5.7
Ca	5650	<284	<247	4560	264	7180
Cd	<2	<20	<2	49	<20	20
Cr	27	58	144	26	18	98
Cu	12	<61	<113	38	53	2100
Fe (%)	1.19	0.189	0.142	1.50	0.87	0.12
Ga	2.9	5.4	1.4	<12	4.5	<4.5
Ge	<2	<1.0	<2	<17	5.1	5.3
K	1960	810	804	1775	65	1260
Mn	51	<18	22	62	14	9.5
Ni	20	241	344	24	14	<10
Pb	14	17	10	210	10	24
Rb	10	<1.0	<1	9.6	<1.0	7.5
S[d] (%)	4.52	0.96	0.84	3.71	2.40	1.8
Se	1.8	<1.0	<2	3.0	1.2	9.1
Si (%)	3.1	0.64	0.18	2.6	0.68	1.5
Sr	24	1.0	<2	11	<1.0	42
Ti	640	240	165	700	610	450
Zn	49	11	8.2	1100	36	<240

[a] Values are in ppm unless otherwise noted and are corrected to a dry basis.
[b] Powdered iron included in coal/caustic mixture.
[c] Pretreated with 0.2 M Na$_2$CO$_3$ and oxygen.
[d] Determined by a high-temperature combustion instrumental method.

    Results of chemical analyses on coals treated by the Gravimelt
Process at TRW are shown in Table IV. Ash contents were decreased to
1% or less, and levels of As, Be, Cd, Hg, Pb, Se, Sr, and Zn were
reduced by 75-95%. It is interesting to note that most of these
elements are commonly associated with pyrite. Thus, substantial
reductions in levels of these elements can be anticipated when most
of the pyrite is removed (as indicated for both coal samples). In
addition, the levels of Ba, Ge, Mn, and Rb were also reduced; how-
ever, the reduction levels for these elements are not as prominent
nor as clear-cut.

Table IV. XRF, AA, and ICP Data on Raw and Chemically Cleaned Coals Received from TRW Systems, Inc.[a]

	Illinois No. 6		Pittsburgh No. 8		
	Raw	Cleaned	Raw	Cleaned	
Ash (%)	9.23	0.53	9.88	1.00	
Pyr. S (%)	1.04	0.02	1.78	0.01	
Hg	0.28	0.04	0.15	0.10	A A
Pb	5.8	1.4	5.6	1.4	
Cd	0.70	0.16	0.44	0.024	
As	0.33	0.14	3.9	0.18	D A T A
Sb	0.09	0.08	0.06	0.06	
Se	1.5	0.6	1.6	0.19	
Al (%)	1.6	<0.7	1.2	<0.7	
As	<5	<10	<10	<5	
Ba	40	<40	~30	<40	
Ba*	<25	<0.4	13	<3.1	
Be*	0.77	<0.10	0.6	<0.06	
Br	9.9	16	7.9	3.4	
Ca (%)	0.16	0.015	0.18	0.027	
Ca*	978	63	545	72	
Cd	<20	<20	<20	<20	
Cr	23	62	23	152	
Cr*	10	54	<6	110	
Cu	16	I(Ni)	20	I(Ni)	
Cu*	16	28	12	16	I C P
Fe (%)	0.968	0.078	1.54	0.107	
Fe*(%)	1.1	0.051	~1.3	0.033	a n d
Ga	<1	<1	~2.3	<1	
Ge	5.0	3.6	4.5	3.1	X R F
K	1500	360	1100	620	
Mn	49	9.9	51	21	D A T A
Mn*	42	1.7	23	4.4	
Ni	17	100	15	132	
Ni*	4.8	47	4.3	58	
Pb	<10	<10	<10	<10	
Rb	10	<5	7.4	<5	
S (%)	2.6	0.47	2.4	0.78	
Se	<3	<3	<3	<3	
Si (%)	2.2	<0.2	2.0	0.23	
Sn	<20	<20	<20	<20	
Sr	17	<5	41	<5	
Ti	630	370	770	350	
Ti*	489	290	480	190	
V*	<2.5	<0.9	<14	1.5	
Zn	31	~3.9	23	~4	
Zn*	39	2.1	20	<0.6	

[a] Values are in ppm unless % is noted and are corrected to a dry basis. An "I" indicates an unsatisfactory determination due to an interference from another element (shown in parentheses).

* ICP data.

Conclusions

Based on the results of this study, the following conclusions can be drawn:

1) Trace element data on cleaned coals are sparse, particularly for chemically cleaned coals.
2) Based on literature data, physical cleaning methods generally seem to be less effective at trace element removal then chemical methods.
3) Trace element extraction efficiencies for a given cleaning process are highly variable between coals.
4) No data are available on reproducibility with respect to trace element removal during chemical cleaning.
5) Corrosion of reactor components during chemical coal cleaning can significantly elevate levels of various trace elements.
6) The aqueous Na_2CO_3 and molten NaOH/KOH treatments, followed by acid washes, effectively removed many trace elements from the coals studied.
7) Because of the large number of variables involved, results of this study should not be extrapolated to other coals.

Acknowledgments

Literature Cited

1. Harvey, R.D.; Cahill, R.A.; Chou, C.-L.; Steele, J.D. "Mineral Matter and Trace Elements in the Herrin and Springfield Coals, Illinois Basin Coal Field," Illinois State Geological Survey, April, 1983; pp. 3, 103.
2. Linton, R.W.; Loh, A.; Natusch, D.F.S.; Evans, C.A., Jr.; Williams, P. Science 1976, 191, 852.
3. Natusch, D.F.S.; Wallace, J.R.; Evans, C.A., Jr. Science 1973, 183, 202.
4. Ihnatowicz M.; Worsztynowicz, A. Proc. Intern. Conf. on Coal Science, 1983, pp. 790-793.
5. Valkovic, V. In "Trace Elements in Coal"; Vol. 1, CRC Press Inc., Boca Raton, Florida, 1983; p. 68.
6. Ruch, R.R.; Gluskoter, H.J.; N.F. Shimp "Occurrence and Distribution of Potentially Volatile Trace Elements in Coal," Illinois State Geological Survey, Environmental Geology Notes, Number 72, August 1974.
7. Cavallaro, J.A.; Deurbrouck, A.W.; Gibbon, G.A.; Hattman, E.A.; Schultz H. In "Analytical Methods for Coal and Coal Products";

Vol. I, Karr, C., Ed.; Academic Press, New York, 1978; pp. 435-464.

8. "Trace Element Geochemistry of Coal Resource Development Related to Environmental Quality and Health," U. S. National Committee for Geochemistry, National Academy Press, Washington, D. C., 1980.

9. Zubovic, P. In "Coal Science"; Gould, R. F., Ed.,; ADVANCES IN CHEMISTRY SERIES No. 55, American Chemical Society: Washington, D.C., 1966; pp. 221-231.

10. Zubovic, P.; Sheffey, N. B.; Stadnichenko, T. "Distribution of Minor Elements in Some Coals in the Western and Southwestern Regions of the Interior Coal Province," U.S.G.S. Bulletin 1117-D, 1967.

11. Zubovic, P.; Stadnichenko, T.; Sheffey, N. B. "The Association of Some Minor Elements with Organic and Inorganic Phases of Coal," U.S.G.S. Professional Paper 400-B, 1960.

12. Gluskoter, H.J.; Ruch, R.R.; Miller, W.G.; Cahill, R.A.; Dreher, G.B.; Kuhn, J.K. "Trace Elements in Coal: Occurrence and Distribution," Illinois State Geological Survey, EPA-600/7-77-064, June 1977.

13. Finkelman, R.B. Ph.D. Thesis, University of Maryland, Chemistry Dept., 1980.

14. Swaine, D.J. Trace Subst. Environ. Health 1977, 11, 107.

15. Gluskoter H.J.; Lindahl, P.C. Science, 1973, 181, 264.

16. Cecil, C.B.; Stanton, R.W.; Allshouse, S.D.; Finkelman, R.B. Proceedings: Symposium on Coal Cleaning to Achieve Energy and Environmental Goals, Vol. 1, 1979, pp. 110-125.

17. Bohor B.F.; Gluskoter, H.J. J. Sediment. Petrology 1973, 43, 945.

18. Ford, C.T.; Care, R.R.; Bosshart, R.E. "Preliminary Evaluation of the Effect of Coal Cleaning on Trace Element Removal"; Report 3, Trace Element Program, Bituminous Coal Research, Inc., 1976.

19. Schultz, H.E.; Hattman, E.A.; Booher, W.B. In "Trace Elements in Fuels"; Babu, S.P., Ed.; ADVANCES IN CHEMISTRY SERIES No. 141, American Chemical Society: Washington, D. C. 1975; pp. 139-153.

20. Capes, C.E.; McIlhinney, A.E.; Russell, D.S.; Sirianni, A.F. Environ. Sci. Technol. 1974, 8, 35-38.

21. Ford, C.T.; Moses, R.G. "Evaluation of the Effects of Coal Cleaning on Fugitive Elements, Phase I"; Bituminous Coal Research, BCR Report L-923, 1978.

22. Ford, C.T.; Price, A.A. "Evaluation of the Effect of Coal Cleaning on Fugitive Elements, Phase II, Part I"; Bituminous Coal Research, BCR Report L-1082, 1980.

23. Ford, C.T.; Price, A.A. "Evaluation of the Effect of Coal Cleaning on Fugitive Elements, Final Report, Phase III"; Bituminous Coal Research, BCR Report L-1304, 1982.

24. Ford, C.T.; Boyer, J.F. Proc. Symp. on Coal Cleaning to Achieve Energy and Environmental Goals, Vol I, 1979, pp. 59-90.

25. Kuhn, J.K.; Fiene, F.L.; Cahill, R.A.; Gluskoter, H.J.; Shimp, N.F. "Abundance of Trace and Minor Elements in Organic and Mineral Fractions of Coal," Illinois State Geological Survey, Environmental Geology Notes #88, August 1980.

26. Kalvinskas, J.J.; Hsu, G.C. Proceedings: Symposium on Coal Cleaning to Achieve Energy and Environmental Goals, Vol. 2, 1979, pp. 1096-1140.

27. Hsu, G.C.; Kalvinskas, J.J.; Ganguli, P.S.; Gavalas, G.R. In "Coal Desulfurization: Chemical and Physical Methods"; Wheelock, T. D., Ed.; ACS SYMPOSIUM SERIES No. 64, American Chemical Society: Washington, D. C., 1977; pp. 206-217.
28. Stambaugh, E.P.; Conkle, H.N.; Miller, J.F.; Mezey, E.J.; Kim, B.C. Proceedings: Symposium on Coal Cleaning to Achieve Energy and Environmental Goals, Vol. 2, 1979, pp. 991-1015.
29. Stambaugh, E.P. In "Coal Desulfurization: Chemical and Physical Methods"; Wheelock, T.D. Ed.; ACS SYMPOSIUM SERIES No. 64, American Chemical Society: Washington, D.C., 1977; pp. 198-205.
30. Stambaugh, E.P.; Miller, J.F.; Tam, S.S; Chauham, S.P.; Feldman, H.F.; Carlton, H.E.; Nack, H.; Oxley, J.H. Presented at the 12th Air Pollution and Industrial Hygiene Conference on Air Quality Management in Electric Power Industry, 1976.
31. Meyers, R.A "Coal Desulfurization"; Marcel Dekker, Inc. New York, 1977.
32. Hamersma, J.W.; Kraft, M.L.; Meyers, R.A. In "Coal Desulfuriza- tion: Chemical and Physical Methods"; Wheelock, T.D. Ed.; ACS Symposium Series No. 64, American Chemical Society: Washington, D.C., 1977, pp. 143-152.
33. Fan, C.-W. Ph.D. Thesis, Iowa State University, 1984.
34. "Gravimelt Process Development," Final Report, TRW Energy Devel- opment Group, DOE/PC/42295-T7, June, 1983.
35. "Annual Book of ASTM Standards, Part 26," American Society for Testing and Materials, 1982.
36. Slemer D.D.; Brinkley, H.G. Anal. Chem. 1981, 53, 750.

Removal of Organic Sulfur from Coal by Reaction with Supercritical Alcohols

C. B. Muchmore, J. W. Chen, A. C. Kent, and K. E. Tempelmeyer

Department of Mechanical Engineering and Energy Processes, Southern Illinois University at Carbondale, Carbondale, IL 62901

The processing of high organic sulfur content coals with methanol and ethanol as supercritical solvents has resulted in reduction in sulfur concentrations exceeding 50%. Since the total sulfur removed exceeds the mineral sulfur content of the coal processed, it is evident that organic sulfur is being removed during the reaction. The resulting solid product maintains over 50% of the concentration of volatile matter compared to that of the parent coal. A high BTU gas is also produced, and some conversion of coal to liquid products occurs. Pre-treatment of the coal with potassium hydroxide prior to the supercritical desulfurization reaction has resulted in improved sulfur removal. For some coals, the combination of a physical cleaning process for removal of pyritic sulfur, followed by supercritical desulfurization with an alcohol, can reduce sulfur emissions below 1.2 lb SO_2/ million BTU.

Growing concern over environmental effects of acid rain has resulted in increased interest in development of pre-combustion removal of sulfur from coal. Physical coal cleaning processes are effective for pyritic sulfur removal but do little to reduce the organic sulfur content of coal. This paper reports the removal of organic sulfur from coal, employing ethyl or methyl alcohols as the solvent/reactant. The process is based on the observation that, under supercritical conditions, reactions occur that selectively remove organic sulfur from the coal matrix.

Literature Review

The maximum conversion of coal to liquid products has been the primary objective of most work on supercritical extraction of coal reported in the literature. A 1975 article by Whitehead (1), one of the first references to supercritical coal extraction, presented data on supercritical extraction of coal by coal tar or petroleum

naphtha fractions. Tugrul and Olcay (2) reported in 1978 extraction
yields and analytical results obtained by supercritical-gas
extraction of 250 mesh lignite with toluene at 400 °C and 16 MPa.
They found extraction nearly complete after 30 minutes; extract
yields of about 24% were reported. Gas chromatography/mass
spectrometry analyses of several extract fractions indicated dozens
of paraffins, alkylated hydrocarbons, phenolic and oxygenated
compounds; however, no sulfur compounds were reported. A kinetic
study of a high-volatile bituminous coal utilizing supercritical
toluene was reported by Slomka and Rutkowski (3). A close fit of
their experimental data on time dependence of extraction yield was
found when a second order equation was used. The use of
supercritical toluene extraction of coal in pilot plant studies
supported by the British Coal Board was reported by Maddocks (4).
The major objective of that study was also maximum conversion of
coal to liquid products; reduction of sulfur in the unconverted
solid was not reported.
        Some work has been reported utilizing alcohols for
supercritical extraction of coal. Makabe et al.(5) reported
extraction of coal with ethanol-sodium hydroxide mixtures with the
objective of maximizing extraction yield; no sulfur data were
reported. Methyl alcohol reaction with a low volatile bituminous
West Virginia coal at higher temperatures (460-600 °C) was reported
by Garner et al.(6). Promotion of coal gasification was the
objective of that study; sulfur content of the resultant char was
not reported.
        An article by Amestica and Wolf (7) describes results of
experiments carried out in a batch reactor system similar to that
used in our investigations. These investigators utilized an Illinois
No. 6 coal, employing either toluene or ethanol as supercritical
extractants. A batch autoclave was utilized in their studies, and
temperature and pressure ranges (350-450 °C, 5.89-19 MPa) were
comparable to those we employ. As was the case with previous
investigations reported in the literature, the major objective of
their research was to study the dissolution of coal materials by the
supercritical phase. They studied the effects of temperature,
pressure, solvent/coal ratio, and reaction time. Similar to the
batch reactor system be employ, the fluid reaction products were
vented through a condenser for collection of liquid products, and
the non-condensable components were vented through a sulfur scrubber
system, employing zinc acetate solution. When ethanol was used as
the supercritical phase, sulfur rejection, expressed in terms of the
sulfur recovered in the gas scrubber system, was reported to vary
from 1.7% to 11.7% of the sulfur in the feed coal. However, no data
were presented on sulfur content of either the solid or liquid
products. They noted that at 400 °C their liquid yield was higher
than conversion, indicating incorporation of carbon from the
solvent. Incorporation in either the solid or liquid products could
account for this observation.
        In contrast to the previously reported work utilizing
supercritical solvent extraction of coal, the major objective of our
research effort is to develop a desulfurization process that will
result in a solid product suitable for combustion in existing coal
fired utility boilers.

Experimental

These experiments utilized a 300cc stirred autoclave reactor, with associated purging, venting and product collection equipment, Figure 1. The coal, previously dried and ground to the desired particle size (generally -40 mesh), is charged to the reactor and alcohol is added. Heating the stirred mixture to above the critical temperature and pressure of the solvent (for ethyl alcohol 243°C and 6.38 MPa) results in a sequence of extraction and reaction processes that remove organic sulfur from the coal. After the desired reaction time (generally one hour), the fluid phase is vented from the reactor through a condenser system and liquid and gaseous products are collected. After cooling, the solid product is collected from the reactor.

For some experiments, pre-treatment of the coal with potassium hydroxide was employed in amounts of 5% of the weight of the coal charged to the reactor. Other pre-treatment methods investigated include contact with 10% HCl under varying conditions and soaking in N,N – dimethylacetamide (DMA) to promote swelling of the coal prior to supercritical desulfurization in alcohol.

The total sulfur concentration of the coal charged to the reactor and that of the solid product were determined by use of a Fischer Total Sulfur Analyzer. Liquids were analyzed on a Perkin Elmer Sigma 3 gas chromatograph and gas analyses were performed on a Varian Model 3400 gas chromatograph.

Results and Discussion

Solvent effects. For one set of experiments, a comparison of ethyl and methyl alcohols as supercritical extractants was made over a temperature range of 275-450 °C, utilizing three different coals of varying ratio of organic to pyritic sulfur content. The coals were provided by the Illinois State Geological Survey (ISGS); they have been kept under a nitrogen atmosphere since the initial size reduction following mining of the coal. Analyses of these coals, provided by the ISGS, are given in Table I. Sulfur forms were determined by wet chemical analysis according to the ASTM D2492 standard method for organic sulfur. The organic sulfur/pyritic sulfur ratio varied from 0.72 to 2.82 for these coals. For all runs, the reaction time was 1 hr, and a solvent/coal ratio of 1/1 was used.

The results of these batch runs are summarized in Figure 2, where the sulfur reduction obtained (evaluated on a concentration basis, comparing the total sulfur in the product char to that of the original coal) is shown as a function of the organic sulfur/pyritic sulfur ratio of the original coal, with temperature as a parameter. Ethyl alcohol resulted in greater desulfurization (48%) than methyl alcohol at higher temperatures (400 °C) with the higher organic sulfur content coal, and methyl alcohol gave comparable desulfurization to ethyl alcohol at the lower temperature investigated (300 °C) with the lower organic sulfur content coal. The results with the high organic sulfur content coal confirm that organic sulfur is being removed by the supercritical
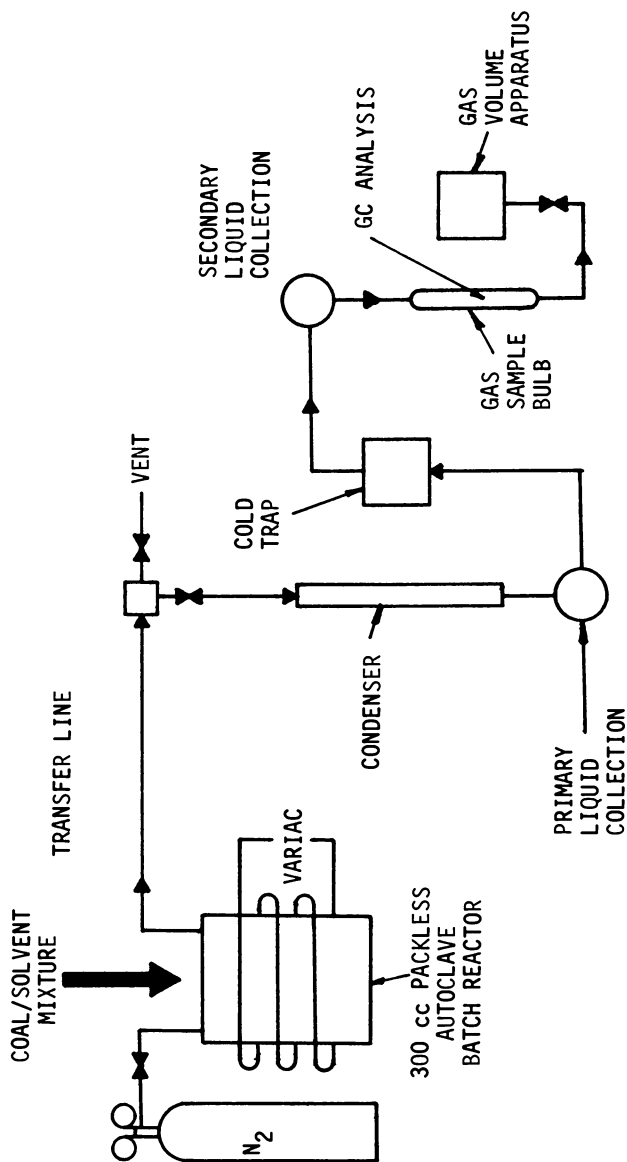
Figure 1. Flow diagram of batch reactor system.

extraction/reaction process, since the total sulfur removal was in excess of the pyritic and sulfate sulfur content of the coal.

Table I. Analyses of Coals (Mine Washed Coals Provided by the Illinois State Geological Survey)

ASTM ANALYSIS (as received basis)	Coal #1	Coal #2	Coal #3
MOISTURE	13.7	13.4	4.98
ASH	8.5	5.6	7.90
VOLATILE MATTER	37.7	37.0	37.18
FIXED CARBON	40.1	44.0	49.9
SULFATIC SULFUR	0.06	0.06	0.11
PYRITIC SULFUR	0.94	1.69	0.98
ORGANIC SULFUR	2.65	0.96	1.53
TOTAL SULFUR	3.65	2.71	2.62
FREE SWELLING INDEX	5.5	4.5	4.5
BTU(Parr Rapid Method)	10,903	11,562	12,630

[a]Herrin (No. 6) coal from a west central Illinois Underground mine, collected June 1, 1983
[b]Colchester (No. 2) coal from a north western Illinois strip mine, collected June 23, 1983
[c]Mixture of 80% Springfield (No. 5) coal with 20% Herrin (No. 6) coal from southern Illinois slope and strip mines, respectively, blended in the washing plant, collected July 15, 1983

Sulfur forms analyses on the product solids are not reported here, since results of the ASTM standard procedure can be misleading in terms of indicating which type of sulfur (pyritic, sulfate, organic) has been removed. Typically, both sulfate and pyritic sulfur are indicated to be present in low concentrations (generally less than 0.2%) when the ASTM procedure is applied to the solid product from supercritical desulfurization of coal with alcohols. The organic sulfur is defined as the difference between the total sulfur in the sample and the sum of the sulfur of the two mineral forms. It has been recognized that during pyrolysis of coal, pyrite decomposition can result in trapping of sulfur released from the pyrite within the coal matrix (8). Although the temperatures employed in this work are lower than those at which pyrite decomposition might be expected, microscopic examination of the solid product indicated conversion of pyrite to lower sulfur content mineral forms. Thus, it is likely that application of the ASTM procedure for determination of sulfur forms in the solid product measures this "new" organic sulfur, in addition to the remaining "original" organic sulfur.

Potassium hydroxide pre-treatment. Another series of four runs was performed to compare methyl and ethyl alcohols as supercritical fluid reactants, with and without KOH (5% of the coal charge). Previous studies had indicated enhanced desulfurization by pre-treatment of the coal with a potassium hydroxide-alcohol solution. Reaction time was 2 hours at a reaction temperature of 340 °C; maximum reaction pressures were 17.3 to 30.8 MPa. The high organic
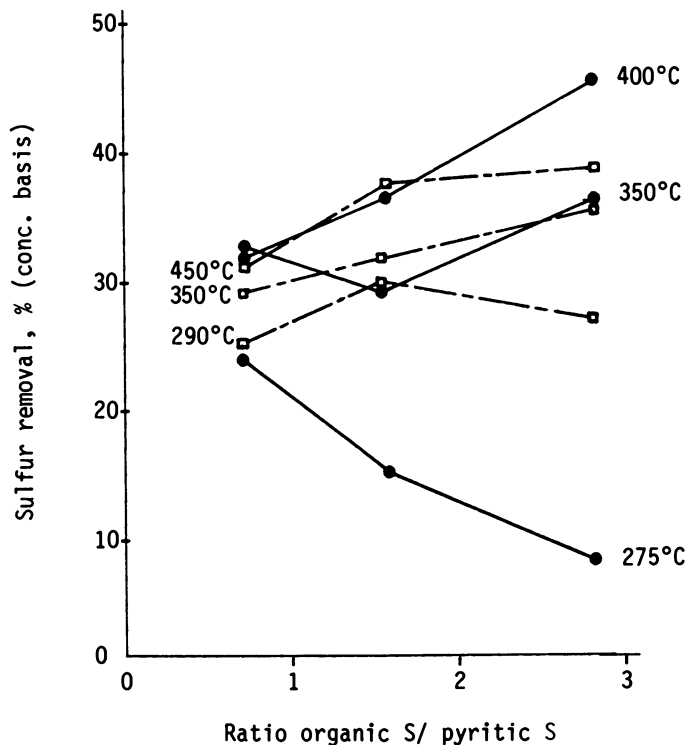
Figure 2. Comparison of ethyl and methyl alcohols as supercritical desulfurization fluids, for coals of varied organic sulfur/pyritic sulfur ratio. (ethanol ————, methanol —·—)

sulfur content coal (total sulfur content 4.23%, organic S/pyritic
S ratio = 2.82; i.e., 73 % of total sulfur being organic sulfur)
was used for these runs; results are summarized in Table II.
    Inspection of Table II indicates that total sulfur removals
exceed the amount of pyritic sulfur present in the coal processed,
indicating that organic sulfur is being removed under the reaction
conditions employed. Addition of potassium hydroxide decreased solid
product and liquid recoveries and increased gas production; this was
an anticipated result due to the reported influence of caustic on
decomposition rates of alcohol at the reaction temperatures
utilized. The greatest desulfurization (54.0% reduction in sulfur
concentration) resulted in the methanol-KOH system. It is of
interest to note that from 56 to 69% of the volatile matter is
retained in the solid product compared to that of the original coal,
on a concentration basis. Heating values of the solid products are
one to seven per cent greater than the original coal, in spite of a
slight increase in ash content. The higher ash resulting from the
KOH treatment reflects the greater conversion of coal, as well as
the KOH itself.

Gas and liquid product analyses. Analyses of the gas products
resulting from the batch experiments reported in Table II are also
given in that Table. The greater production of hydrogen when KOH
was used is evident for both ethanol and methanol. As anticipated,
no ethylene and much less ethane resulted from the methanol runs,
compared to the ethanol runs; methane concentration was higher in
the methanol runs.
    Gas chromatograms of the liquid products for two of the batch
experiments reported in Table II, were obtained where ethyl and
methyl alcohols were used without KOH addition. A capillary column
was used for the analyses, and the sample was split to two different
detectors after passing through the column, giving dual traces on
each chromatogram. A flame photometric detector (FPD), specific for
sulfur containing compounds, and a flame ionization detector (FID),
sensitive to essentially all organic compounds, were used. Of the
more than half dozen major sulfur-containing compounds observed on
the FPD chromatograms, several have been identified. Ethyl sulfide,
ethyl disulfide, thioacetal, and thiophene were indicated by GC/MS
analysis. The participation of the ethanol solvent (or a two
carbon degradation product) in the desulfurization reactions is
suggested by the structure of the sulfur-containing products thus
far identified. The gas chromatogram of the liquid product from the
methanol run indicates only two major sulfur compounds and lesser
amounts of coal-derived organic material, compared to the ethanol
run.

Effects of alternate pre-treatment procedures. A variety of pre-
treatment procedures, previously described, were performed to study
the effect on supercritical desulfurization. Table III presents the
elemental analyses of the solid products resulting from these runs.
All pre-treatment procedures resulted in greater desulfurization
than tests when no pre-treatment was used. In all cases the H/C
ratio was reduced compared to that of the coal processed, suggesting
that incorporation of the hydrogen-rich solvent in the coal

Table II. Comparison of Product Distributions for Methanol and
           Ethanol as Supercritical Extractants, and
           Effect of Potassium Hydroxide

	Solvent System[a]			
	Ethanol, No KOH	Ethanol, 5% KOH	Methanol, No KOH	Methanol, 5% KOH
Maximum Reaction pressure (KPa)	17.3	20.8	18.4	30.8
Solid yield (% of coal charged)	83.0	81.9	89.5	86.8
Liquid recovery (% of liquid charge)	83.5	74.8	90.3	59.8
Gas produced (liters at STP)	9.2	13.8	5.8	24.6
% desulfurization (conc. basis)	36.3	37.6	30.5	54.0
Overall material balance(%)	91.5	90.5	94.3	89.2

Solid analyses
  (Moisture free)
                   ISGS Std.
                   Coal #1
                   (moisture free)

	ISGS Std. Coal #1 (moisture free)	Ethanol, No KOH	Ethanol, 5% KOH	Methanol, No KOH	Methanol, 5% KOH
% Total Sulfur	4.23[b]	2.69	2.64	2.94	1.95
% Volatile matter	41.6	23.8	23.2	28.8	25.0
% Ash	10.4	12.2	17.4	11.3	17.9
Btu/lb	12,375	13,263	12,990	12,826	12,501

Gas Analyses
  (volume %)

	ISGS Std. Coal #1	Ethanol, No KOH	Ethanol, 5% KOH	Methanol, No KOH	Methanol, 5% KOH
H_2		9	17	4	38
CH_4		35	23	68	31
C_2H_4		1	1	0	0
C_2H_6		30	27	7	3
CO_2		20	22	17	25
Other		5	10	4	3

[a] Reaction Conditions: 60 g coal, 60 g ethanol, 2 hr. reaction at
    340°C.
[b] 3.07% organic sulfur

structure did not occur to a significant extent. Note that although
the total sulfur concentration was reduced in all cases, the
nitrogen content exhibits a very slight increase, due to conversion
of coal material to liquid and gaseous products less rich in
nitrogen than the parent coal. The greater increase in nitrogen
resulting from the DMA pre-treatment was likely the result of
contribution from the solvent. Oxygen content was reduced for all
the processing conditions employed.

Table III. Elemental Analyses of Solid Products from Supercritical
            Solvent Treatment of Coal under Various Reaction
                            Conditions

SOLVENT & CONDITION[a]	C	H	N	S	H/C RATIO
Coal Treated, ISGS std coal #1	66.05	4.85	1.17	4.23	0.881
EtOH	75.82	3.95	1.39	2.75	0.625
MeOH	72.63	4.04	1.31	2.99	0.667
EtOH + 5% KOH	73.90	3.32	1.24	2.60	0.539
MeOH + 5% KOH	70.37	3.72	1.25	1.96	0.634
DMA[b] soaked 24 hr; EtOH	70.97	4.42	2.56	2.41	0.747
Acid leached[c]; MeOH + 5% KOH	73.32	3.07	1.30	1.88	0.502
Acid leached[d]; MeOH + 5% KOH	71.91	3.96	1.23	1.53	0.661
HCl refluxed 1 hr; MeOH	77.17	3.05	1.32	2.16	0.474
MeOH + 5% KOH; Two stage	69.16	3.18	1.12	1.47	0.552

a All run at 350 C, 1 hr   b N,N-Dimethylacetamide
c Soaked for 4 hrs, in 10 % HCl   d Soaked for 48 hrs in 10 % HCl

Process potential. The potential for processing a typical high
sulfur coal to produce a solid product with less than 1% total
sulfur by a sequence of physical beneficiation for pyrite reduction,
followed by supercritical extraction for removal of organic sulfur,
is indicated by example in Table IV. A 3% total sulfur coal,
containing equal amounts of pyritic and organic sulfur, could be
processed by existing technologies for removal of pyritic sulfur to
give a total sulfur concentration of, say, 1.8%. An additional 50%
reduction of the remaining total sulfur would then give a final
total sulfur concentration of 0.9%.

     The technical feasibility of such an approach is demonstrated
in Table IV, where data obtained on a sample of Illinois No. 5 seam
cleaned coal from an Illinois Basin operating mine was processed by
supercritical extraction. The cleaned coal had a total sulfur
content of 1.5 %; processing this physically cleaned coal for 1 hour
at 350C in methanol with 5% KOH reduced the total sulfur
concentration to 0.75 %. The solid product, which retained 56 % of
the original volatile matter concentration, exhibited a value of 1.1
lb SO_2/ million BTU, thus meeting the existing new performance
standard of 1.2 lb SO_2/ million BTU.

Table IV. Example of Sequential Processing of Coal for Removal of
Pyritic and Organic Sulfur. (Current
experimental data are given in the lined
regions of the table.)

	PYRITIC S	ORGANIC S	SULFATE S	TOTAL S
COAL RUN OF MINE	1.5%	1.5%	---	3.0%
	---	--	---	>2.0%
PHYSICAL CLEANING	0.3%	1.5%	---	1.8%
	0.66%	0.76%	0.06%	1.48%
SUPERCRITICAL DESULFURIZATION	0.2%	0.7%	---	0.9%
	0.02%	0.61%	0.12%	0.75%

Conclusions

It is apparent from the data thus far obtained that both ethyl and
methyl alcohols are effective for desulfurization of high organic
sulfur content coals when used as extractants/reactants under
supercritical conditions. The data presented here does not indicate
if any significant amount of pyritic sulfur is being removed during
the supercritical desulfurization reactions; however this
possibility must be recognized in any proposed model of the system.
Although significant quantities of hydrogen sulfide have not been
detected in the gaseous products, the formation of hydrogen sulfide
as an intermediate compound when sulfur is released from organic
moities in the coal matrix, as well as from pyrite, is a likely
possibility. The detailed reaction pathways of the desulfurization
reactions occurring in the presence of supercritical alcohols has
yet to be determined.   The technical feasibility of producing a
compliance   solid fuel by   sequential processes of   physical
treatment for pyritic sulfur removal, followed by supercritical
desulfurization with an alcohol for removal of organic sulfur, has
been demonstrated.

Acknowledgments

Literature Cited

1. Whitehead, J.L.; Williams, D.F. Journal of the Institute of
    Fuel, December 1975.
2. Tugrul, T.; Olcay, A. Fuel, July 1978, 57.

3. Slomka, B.; Rutkowski, A. Fuel Processing Technology, 1982, 5.
4. Maddocks, R.R.; Gibson, J.; Williams,D.F. Chem. Engr. Progress, June 1979.
5. Makabe, M.; Hirano, Y.; Ouchi, K. Fuel, May 1978, 57.
6. Garner, D.N.; Huffman, W.J.; Parker, H.W., Coal Processing Using Methanol as a Reactant, 79th National Meeting, AIChE, 8th Petrochemical and Refining Exposition, 1975, Houston, TX.
7. Amestica, L. A; Wolf, E. E. Fuel, 1984, 63, 227.
8. Cleyle, P.J.; Caley, W.F.; Stewart, I.; Whiteway, S.G. Fuel, 1984, 63, 1579.

8

Microbial Desulfurization of Bituminous Coals

Charanjit Rai

Department of Chemical and Natural Gas Engineering, Texas A&I University, Kingsville, TX 78363

Microbial desulfurization of Illinois #6 and Indiana #
3 coal having a total sulfur content of 2 to 8% has
been investigated using acidophilic microogranisms,
T. ferrooxidans, in the laboratory shake-flask
experiments and in a two-inch pipeline loop. The results
indicate that about 80% pyritic sulfur removal was
achieved with 10 to 25% coal/water slurry recirculating
at 6 ft/sec. at room temperature in 7 to 12 days.
Results show that the rates of bacterial desulfurization
from coal samples are higher in the pipeline loop
under turbulent flow conditions as compared to the
shake-flask experiments for particle sizes 43 to 200µm.
It is visualized that the proposed coal slurry pipelines
could be used as biological plug flow reactors under
aerobic conditions. The laboratory corrosion studies
under dynamic test conditions show that use of a
corrosion inhibitor will limit the pipeline corrosion
rate to acceptable levels.

Our environment has constantly been polluted by the combustion of conventional fuels like petroleum, coal and natural gas. It is estimated that about 28 million tons of sulfur dioxide gas (SO_2) is discharged to the environment due to the combustion of fossil fuels. The Clean Air Act Amendment of 1977 set an emission limit of 1.2 lb SO_2 per million Btu of fuel combusted. Most bituminous coals contain 3 to 6 percent sulfur as inorganic or organic sulfur. The inorganic sulfur compounds are primarily metal sulfides, pyrite or marcasite, and sulfates formed by the air oxidation of metal sulfides ([1],[2]). The organic sulfur in coal is thought to be in the form of thiols, sulfides, disulfides, or condensed thiophenes, benzothiophenes, dibenzothiphenes and thioxanthenes having varying reactivities. Physical and chemical processes have been studied for coal desulfurization, some of them operate at high temperatures and are energy intensive. Removal of organic sulfur by these processes is difficult. Microbial desulfurization offers an effective means of precombustion sulfur removal ([3],[4],[5]).
    The scientific literature describes only a limited number of

studies dealing with microbial desulfurization of organic sulfur
compounds. Maliyantz (7) reported bacterial desulfurization of
Russian crude oil by a sulfate reducing bacteria, but similar
attempts by Davis and Updegraff (8) were not successful. Kirshebaum
(9) described aerobic microbial conversion of sulfur in petroleum
to water-soluble inorganic forms like sulfate or sulfuric acid.
Yamada (10) reported the isolation of a bacteria capable of utiliz-
ing petroleum sulfur compounds like dibenzothiophene. Sagadia (11)
isolated a bacteria on benzothiophenes, but due to the toxicity of
the compound and the oil components and metals the culture could not
reduce the sulfur content of the oil.

Microbial degradation of the aromatic nucleus of substituted
thiophenes has been demonstrated by Amphlett and Calley (12).
Dibenzothiophene is converted into a water-soluble form, 3-hydroxy-
2-formylbenzothiophene which imparts an orange-red color in the
culture broth. Finnerty (13) reported the use of microorganisms of
the genus <u>Acinetobacter</u> and <u>Micrococcus</u> to convert dibenzothiophenes
into water-soluble products that can be removed from high-sulfur
crude oil.

Colmer and Hinkle (14) identified <u>T. ferrooxidans</u> in acidic
mine waters. Subsequent studies by Silverman <u>et al</u>. (15,16) con-
firmed that <u>T. ferrooxidans</u> could be utilized to oxidize FeS_2 in coal
in 3 to 4 days, and the rate of oxidative dissolution was a function
of the particle size and rank of the coal. Dugan and Apel (4,5)
showed that a mixed culture of <u>T. ferrooxidans</u> and <u>T. thiooxidans</u>
was most effective at a pH of 2 to 2.5 when the nutrient was en-
riched with NH_4^+. They reported 97% removal of pyritic sulfur from
a coal sample with 3.1 weight percent sulfur. Norris and Kelly (17)
reported that other acidophilic bacteria, <u>Leptospirillum ferrooxidans</u>
in mixed cultures with <u>T. thiooxidans</u>, was effective for FeS_2 re-
moval.

Hoffman <u>et al</u>. (18) conducted a parametric study to determine
the effect of bacterial strain, N/P molar ratio, the partial pressure
of CO_2, the coal source and the total reactive surface area on the
rate and extent of oxidative dissolution of iron pyrite at a fixed
oxygen pressure. The bacterial desulfurization of high pyritic
sulfur coal could be achieved in 8 to 12 days for pulp densities upto
20% and particle size of less than 74μm. The most effective strains
of <u>T. ferrooxidans</u> were isolated from the natural systems, and the
most effective nutrient medium contained low phosphate levels, with
an optimal N/P molar ratio of 90:1.

Recent studies by Kargi (21) show that the thermophilic sulfur
oxidizing organism <u>Sulfolobus acidocaldarius</u> could remove pyritic
sulfur and could also oxidize dibenzothiophene (DBT) in a carbon-
free salt medium. Chandra <u>et al</u>. (22) have reported removal of
organic sulfur from dibenzothiophene (DBT) by using an organism iso-
lated from soil and grown in DBT-enriched culture. Isbister and
Koblinski (23) have mutagenically altered a naturally occuring micro-
organism that has exhibited capability for partially oxidizing organ-
ic sulfur in DBT.

<u>Mechanism of Microbial Desulfurization.</u> The microbial dissolution
of pyritic sulfur in coal by acidophilic bacteria has been
thoroughly investigated (17,18,29). The pyrite is readily oxidized
by oxygen or ferric ion, resulting in the ferrous state as follows:

$$FeS_2 + 3.5\ O_2 + H_2O \longrightarrow Fe^{++} + 2SO_4^{=} + 2H^{+} \qquad (1)$$

$$FeS_2 + 2\ Fe^{+++} \longrightarrow 3Fe^{++} + 2S \qquad (2)$$
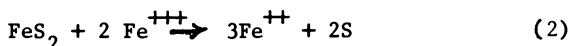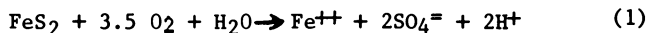
T. ferrooxidans derives energy by catalyzing the oxidation of the ferrous ions back to the ferric state (13):

$$Fe^{++} + 1/4\ O_2 + H^{+} \longrightarrow Fe^{+++} + 1/2\ H_2O \qquad (3)$$
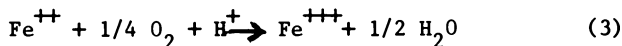
Ferric sulfate, a reaction product, reacts with FeS_2 to form more ferrous sulfate which is again catalyzed by _T. ferrooxidans_ to the ferric state.

$$FeS_2 + 14\ Fe^{+++} + 8H_2O \longrightarrow 15\ Fe^{++} + 2\ SO_4^{=} + 16H^{+} \qquad (4)$$
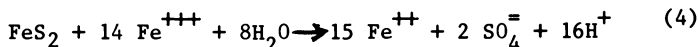
Elemental sulfur, likewise, is oxidized by _T. thiooxidans_ forming sulfuric acid.

$$2S + 2\ H_2O + 3O_2 \longrightarrow 4H^{+} + 2SO_4^{+} \qquad (5)$$
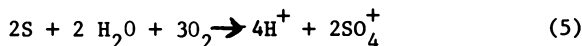
The oxidation reactions are dependent on the microbial reactions with the end result of accelerating the transformation of FeS_2 to ferrous sulfate, and thus equation (1) represents the overall reaction stoichiometry. Other reactions provide possible mechanistic pathways for the microbial pyritic dissolution.

   Most microbial desulfurization studies have been conducted in the laboratory shake-flask type experiments, and the major drawback cited against such a process has been that the rates of pyritic sulfur removal were not high enough to reduce the reactor size to a reasonable capacity (2,6). In this study an attempt has been made to determine the effectiveness of _T. ferrooxidans_ under simulated pipeline conditions for pyritic sulfur removal. Since the microbial desulfurization process is conducted under acidic environment, an attempt has been made to determine the corrosion rates under dynamic conditions using Illinois #6 and Indiana #3 bituminous coals and to investigate the effectiveness of a commercial corrosion inhibitor for controlling the corrosivity.

Experimental

Coal Samples. The samples of Illinois #6 and Indiana #3 were obtained from the Amax Coal Company's Delta and Midwest mines and Ziegler Coal Company's mine in the Randolph County of Illinois. Table I shows pyritic sulfur content data. The samples were ground in a ball mill and then sieved to obtain the desired particle size distribution.

   The shake-flask and two-inch pipeline experiments were initially conducted with various particle sizes, such as: As Received, 417 to 1651 μm, 208 to 417 μm, 147 to 208 μm, and 43 to 417 μm. However, for detailed study another sample size, 74 to 147 μm, was selected.

Microbial Procedures. A pure culture of _T. ferrooxidans_ obtained from the American Type Culture Collection (ATCC) was used in this study for the shake-flask experiments and the 2-inch slurry pipe-

Table I. Bituminous Coal Samples and Their Pyritic Sulfur Content

Coal Sample	FeS$_2$ (wt%)
Illinois #6, Delta Mine (CS-1280-004) Amax Coal Company	2.02
Illinois #6 (C22024) Herrin Coal, Northern Illinois Illinois State Geological Survey Champaign, Illinois	4.90
Illinois #6, Randolph County, Ziegler Coal Company	4.20
Indiana #3, Ayrshire Mine (CS-1180-007) Amax Coal Company	2.60

line experiments. A mineral salts medium having the following com-
position was used in these experiments: FeSO$_4$. 7 H$_2$O 20 g/l; (NH$_4$)$_2$
SO$_4$ 0.8 g/l; KH$_2$ PO$_4$ 0.4 g/l; Mg SO$_4$. 7 H$_2$O 0.16 g/l. The mineral
salts were dissolved in distilled water and the pH was adjusted to
2.8 by addition of 1N H$_2$SO$_4$. The medium was autoclaved at 20 psia
for one hour. The growth medium consisted of slurried coal samples
consisting of Illinois #6 or Indiana #3, as desired.

Analytical Procedures. The samples of bituminous coals were analyz-
ed for pyritic sulfur, sulfate sulfur and total sulfur using con-
ventional wet chemical procedures adapted from the American Society
of Testing Materials (23, 24). The ASTM D 3177-75, The Eschka
method was used for the total sulfur, and ASTM D-2492-79 was used for
sulfate and pyritic sulfur determinations. The treated samples were
filtered through a Whatman #2 filter paper to separate the coal
particles from the liquid medium. The filtered sample was washed
with 0.1 N HCl followed by distilled water to remove traces of ab-
sorbed sulfate and iron.
    The total sulfur content of the coal samples was determined by
the Eschka method. The sulfate sulfur content of the test samples
was determined by extraction of a one-gram sample with dilute
hydrochloric acid followed by turbidimetric determination of sulfate
(24). The pyritic sulfur content was determined by extraction of the
weighed coal samples with 2N nitric acid followed by titrimetric or
atomic absorption determination of iron in the extract. (25).

Laboratory Corrosion Test. The laboratory test procedure for the
determination of corrosion rates of coal slurry used in this study
was adapted from the method developed by Bomberger (26). The
corrosion rates were determined by using ASTM Standard Corrosion
Test, also known as the Total Immersion Method (27). The Bomberger
technique consists of keeping coal slurry in suspension in a two-
liter reaction vessel at a constant temperature. The corrosion
rates are determined either by actual weight loss of steel coupons

suspended in the reaction vessel or by the use of corrosometer
probe over a 24 to 72 hour period. The weight loss of steel coupons
is a measure of the corrosion rates expressed as Inch Per Year (IPY).
In the case of corrosometer probe, it is initially calibrated by
means of a weight loss measurement.

The ASTM Corrosion Test procedure by Total Immersion Method
requires that all specimens in a test series should have the same
dimensions when comparisons are to be made. In these experiments,
carbon steel was used representing the pipeline material. The coupons
were cleaned, polished and weighed. Coal-water slurry, 10 to 40
weight percent, was used in the corrosion tests. For the coal-water
slurry the intitial pH of the medium varied from 2.3 to 2.6 and the
test series containing the nutrient media, the microorganisms and the
inhibitors the pH varied from 2 to 2.5. Specimens were immersed in
the reaction vessel maintained at a constant temperature of 86°F for
72 hours or the specified time. The coupons were removed, washed
with deionized water, dried and weighed. The loss in weight of the
specimen, before and after the test was attributed to corrosion.
From the weight loss data, the corrosion rates were calculated as
Inch Per Year (IPY).

Results and Discussion

Shake-Flask Experiments with T. ferrooxidans. A limited number of
experiments were conducted using T.ferrooxidans to determine the
influence of process variables on the rate and extent of pyritic
sulfur release from the coal samples in shake-flask experiments
using a mechanical shaker. No attempt was made to optimize the
mineral salts medium composition since the influence of NH_4^+, N/P
molar ratio and the nitrogen requirements for the growth of T.
ferrooxidans have been thoroughly investigated by other workers
(4,7,8,10). A mineral salts medium with the composition described
earlier in the Microbial Procedures section was used in all the
experiments with T. ferrooxidans.

A number of samples of pulverized coals were used having the
following particle sizes: As received, 417 to 1651 μm, 147 to 208
μm, and less than 147 μm. Coal/water slurries (10 wt%) made from
the sterilized coal samples in mineral salts medium were inoculated
with a strain of T. ferrooxidans and were subjected to mechanical
shaking from three to twelve days. At the end of the desired test
period, (3, 6, 9 or 12 days), the coal samples were filtered,
thoroughly washed with deionized water and analyzed for pyritic
sulfur content. The data were plotted as mg/liter of pyritic sulfur
released as a function of time as shown in Figure 1 for a coal
sample of Illinois #6 from the Ziegler Coal mine. The data show
that a maximum reduction in pyritic sulfur content was achieved with
less than 147 μm particle size, the average rate being 377.4 mg/
liter x day during the nine-day oxidation period versus 199.0 mg/
liter x day for the 417 to 1651 μm particles. Indiana #3 coal from
the Ayrshire mine exhibited similar trends, the average pyritic
oxidation rate being 291.1 mg/liter x day for the 147 to 617 μm
particles over an eight-day period with T.ferroxidans.
Two-Inch Slurry Pipeline Experiments: (a) Slurry Pipeline System.
A two-inch PVC pipeline loop, 60 feet in length, was installed on a
laboratory wall and a 2-hoursepower positive displacement type Gould

pump, Model 3196, was incorporated in the flow system. The flow rate
through the pipeline could be varied from a low of 2 ft/sec to 15 ft
/sec. The system was designed to recirculate coal/water slurry
through an open drum where air was bubbled in the line. A copper
cooling coil was immersed below the slurry level in the drum for re-
circulating cold water through the medium in order to remove heat
from the system. The flow rate in the pipeline was monitored by the
use of a Polysonics flow meter, model UFM-P. The equipment was
capable of continuous operation. The critical velocity for flow of
slurries in the pipeline was calculated using a correlation develop-
ed by Oroskar and Turian (28). The critical velocity, defined as
the minimum velocity needed to keep the coal particles suspended in
the liquid medium, was calculated to be 5.5 ft/sec for a 50 wt%
coal/water slurry for the two-inch laboratory pipeline.
(b) Particle Size Distribution: A 6.6 wt% slurry, consisting of
Indiana #3 bituminous coal with 60.5% of 417 to 1651 μm and 39.5% of
147 to 417 μm particles, was recirculated through the pipeline loop
for 6 hours at 5.6 to 5.8 ft/sec at 85-95°F; deionized water was
used for preparation of the slurry. At the conclusion of the
experiment, the coal particles were filtered, dried and sieved to
determine the particle size distribution. The data for final size
distribution of the slurried coal are shown in Table II.

Table II. Slurry Recirculation in Laboratory Pipeline

Indiana #3 (Ayrshire)	417 to 1651 μm, 60.5%
(6.6% wt% slurry in	
deionized water)	147 to 417 μm, 39.%5
pH of slurry	2.5
Flow Rate:	5.6 to 5.8 ft/sec
Temperature:	85-95°F
Run, Hours:	6

Final Particle Size Distribution

Particle Size	Percent
+1651 μm	0.62
-1651 to +417 μm	4.69
-417 to +147 μm	40.45
-147 to +74 μm	39.40
-74 μm	14.79

(c) Microbial Desulfurization Experiments in the Two-Inch Pipeline.
Illinois #6 (Delta Mine) and Indiana #3 (Ayrshire Mine) bituminous
coals were used in the slurry pipeline desulfurization experiments
using T. ferrooxidans for inoculating the coal/water slurry used
in these experiments. A 10 wt% coal/water slurry was prepared
using deionized water and the mineral salts medium described earlier.
The coal particle size range was from 147 um to 1981 μm. The slurry
was controlled by recirculating cold water through the copper cool-
ing coils in the slurry drum. Duplicate samples of coal slurry were
taken once a day for the determination of pyritic sulfur content in
the slurry. The experiment was continued for seven days with recir-
culation of the slurry through the pipeline system continuously or

for 8 hours/day. The experimental data with Illionois #6 (Delta) are shown in Table 3, and the rate of pyrite desulfurization is shown in Figure 2. The desulfurization rates in the slurry pipeline experiments and the laboratory shake-flask experiments are in good agreement.

Another slurry pipeline desulfurization experiment was conducted using Indiana #3 (Ayrshire) coal as a 25 wt% slurry in deionized water. The other process variables were carefully controlled: flow rates 6-6.5 ft/sec, temperature 70-90°F, and pH 2.5-2.8. The experiment was continued for 14 days, and the slurry samples for pyritic sulfur determination were taken daily. The desulfurization rates with Indiana #3 coal in the pipeline experiment are shown in Table 4 and are in good agreement with the laboratory data and the results with Illinois #6 coal. As observed in the laboratory experiments, the rate of desulfurization of bituminous coals is directly proportional to the pyritic sulfur content and inversely to the particle size of the coal sample.

Corrosion Test Results: The corrosion rates were determined using a 10 wt% to 40 wt% coal water slurry with 147 to 417 μm coal particles. The corrosion rates ranged from 1.223 X 10^{-3} IPY for Illinois #6 to 1.272 X 10^{-2} IPY for Indiana #3 coal slurry consisting of 40 wt% each coal.

The addition of T. ferrooxidans in salt medium at the desired concentration to the coal/water slurry increased the corrosion rates for both the coals tested. The corrosion rates for the 72-hour and 500-hour experiments in the presence of T. ferrooxidans in salt medium with 10 wt% slurry of Illinois #6 ranged from 4.2 X 10^{-3} IPY to 1.41 X 10^{-2} IPY, respectively. However,the introduction of up to 10 ppm of a commercial corrosion inhibitor, Calgon T G-10, inhibited the corrosion rates with Illinois #6 and Indiana #3 coals to very low levels approaching those obtained with the deionized water. Balck Mesa pipeline has used this corrosion inhibitor on a regular basis with very satisfactory results.

Conclusions

About 80% pyritic sulfur removal has been achieved by microbial desulfurization of Illinois #6 and Indiana #3 coals using T. ferrooxidans in laboratory shake-flask experiments and in a two-inch pipeline loop. The 10 to 25 wt% coal/water slurry was recirculated at 6-7 ft/sec for 7 to 12 days at 70-90°F. Results also show that the rates of bacterial desulfurization are higher in the pipeline loop under turbulent flow conditions for particle sizes, 43 to 200 μm as compared to the shake-flask experiments. It is visualized that the proposed coal slurry pipelines could be used as biological plug flow reactors under aerobic conditions. The laboratory corrosion studies show that use of a corrosion inhibitor will limit the pipeline corrosion rates to acceptable levels.

Acknowledgments
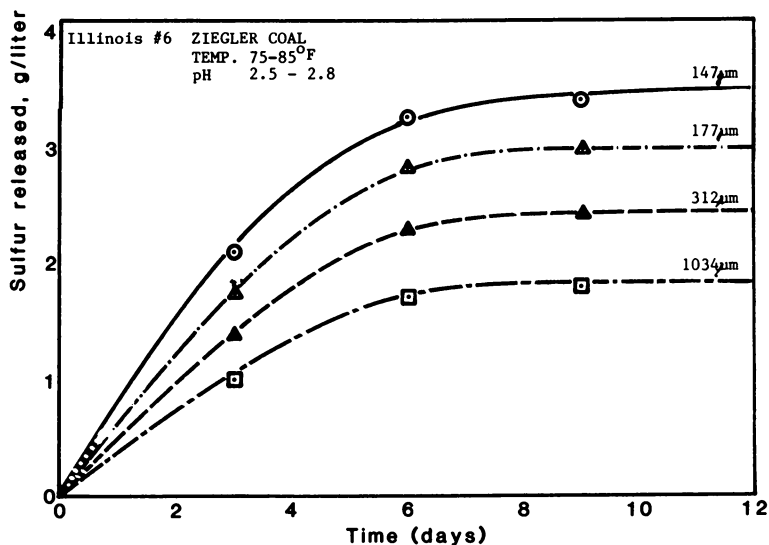
Figure 1. Effect of particle size on pyritic desulfurization. (Reproduced with permission from Ref. 30. Copyright 1985, American Institute of Chemical Engineers.)
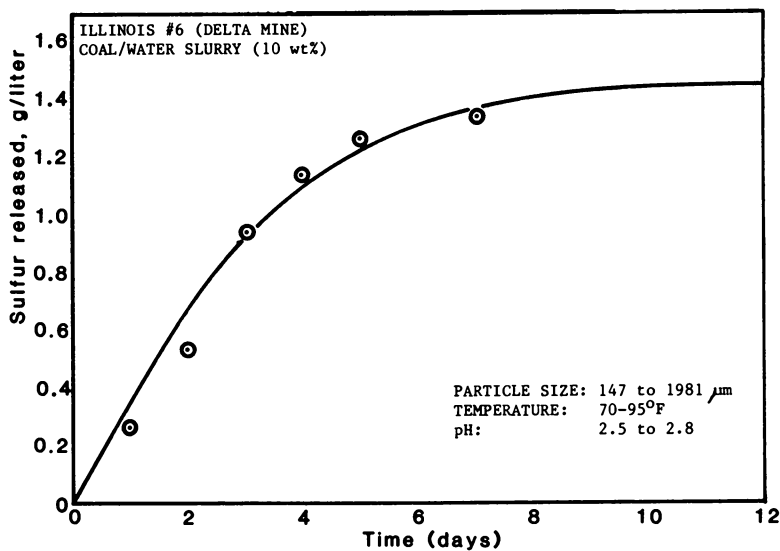
Figure 2. Slurry pipeline desulfurization. (Reproduced with permission from Ref. 30. Copyright 1985, American Institute of Chemical Engineers.)

Table III. Slurry Pipeline Desulfurization Coal/Water Slurry
(10 wt%) Illinois #6 Bituminous Coal (Delta Mine)
(Thiobacillus ferrooxidans)

Days	Pyritic Sulfur, wt%	Pyritic Sulfur Reduction, %	Rate of Desulfurization mg/Liter X Day
0	1.70	0.00	0.00
1	1.45	14.7	257.35
2	1.13	33.5	293.26
3	0.80	52.9	308.82
4	0.60	64.7	283.08
5	0.48	72.0	251.17
7	0.41	76.0	189.70

Slurry Flow Rate: 6 to 6.2 ft/sec
Slurry Temperature: 70-90°F
Coal Particle Size: 147 μm to 1981 μm
pH of Slurry: 2.5 to 2.8

Source: Reproduced with permission from Ref. 30. Copyright 1985
American Institute of Chemical Engineers.

Table IV. Slurry Pipeline Desulfurization Coal/Water Slurry
Indiana #3 Bituminous Coal (Ayrshire Mine)
(Thiobacillus ferrooxidans)

Days	Pyritic Sulfur, wt%	Pyritic Sulfur Reduction,%	Rate of Desulfurization mg/Liter X Day
0	2.58	0	0.00
4	1.75	32	558.57
5	1.55	40	554.53
7	1.82	30	292.26
9	1.03	60	463.60
11	0.645	75	473.53
12	0.516	80	463.01
13	0.52	80	426.56

Slurry Flow Rate: 6 ft/sec
Slurry Temperature: 70-90°F
Coal Particle Size: 147 μm to 1981 μm
pH of Slurry: 2.5 to 3.0

Literature Cited

1. Wheelock, T.D., Editor, 1977 "Coal Desulfurization Chemical and Physical Methods." American Chemical Society Symposium Series # 64, Washington, DC, pp. 101-102.
2. Rofmann, H.K. Proc. Inst. Environ.Sci. 1979, pp. 266-270.
3. Robert C. Eliot, "Coal Desulfurization Prior to Combustion," Noyes Data Corporation, New Jersey, 1978 pp.V-VI, 141-153.
4. Dugan, P.R.; and Apel, W.A. 1978. "Microbial Desulfurization of Coal." In Metallurgical Application of Bacterial Leaching and Related Microbial Phenomenon." Editors, L.E. Murr; Torma, A.E.; Brieley, J.A. Academic Press, N.Y.pp. 223-250.
5. Dugan, P.R.; Apel, W.A. U.S. Patent 4 456688, 1984.
6. Kargi, F. 1982. Microbial Coal Desulfurization. Microbial Enzyme Technol. 4(1): 13.20.
7. Maliyantz, A.A. Azerbaidzhanskoe Neftyanoe Khoz, 1935, 6, 89.
8. Davis, J.B., Updegraff, D.M., Bacteriol Rev. 1954, 18, 215.
9. Kirshenbaum, I. U.S. Patent 2,975,103 1961.
10. Yamada, K. Agr. Biol. Chem.,32, 840 1968.
11. Sagardia, F. Applied Microbiology 1975, 29,722.
12. Amphlett, M.J.; Calley, A.G. Biochem. J.1969, 112 12.
13. Finnerty, W.R., Symposium on Microbial Processes for Metals Accumulation and Sulfur/Nitrogen Removal from Fuels. American Chemical Society, Las Vegas, Nevada, August 1980.
14. Colmer, A.R., Hinkle, M.E., 1947. The Role of Microorganisms in Acid Mine Drainage, Science 106: 253-256.
15. Silverman, M.P.; Lundrgen, D.G.,1959, Studies on Chemosynthetic Iron Bacterium Ferrobacillus ferrooxidans. J.Bacteriol. 78: 326-331.
16. Silverman, M.P.; Faust, B.C.; Panda, F.A.;Koo, H.H.; Tsuchiya, H.M. 1981. Pyritic Sulfur from Coal by Bacterial Action. Fuel 42, 113-124.
17. Norris, P.R.; Kelly D.P. 1978. Toxic Metals in Leaching Systems. pp. 83-209. In L.E. Murr, Torma, A.E.; and Brierly J.A., Metallurgical Applications of Bacterial Leaching and Related Phenomena. Academic: New York, 1978.
18. Hoffman, M.R., Faust, B.C., Panda, F.A. and Koo H.H., Tsuchiya, H.M. 1981, Kinetics of the Removal of Iron Pyrite from Coal by Microbial Catalysis. Applied & Environ. Microbiology. 42: 259-271.
19. Andrews, G.F., Maczuga, J. 1984. Bacterial Removal of Pyrite From Coal, Fuel 63, 297-301.
20. Singer, P.C. and Stumm, W., 1970. Acidic Mine Drainage: The Rate Determining Step. Science 167: 1121-1123.
21. Kargi, F.; Robinson, J.M., Biotechnology and Bioengineering, XXIV, pp. 2115-2121, 1982.
22. Chandra, D., Roy, D., Mishra, A. K, Chakrabarti, J.N.; Sengupta, B., Fuel, 58, 549-550 1979.
23. Isbister, J.D.; Kobylinski, E.A., In,"Processing and Utilization of High Sulfur Coals." Attia,Y.A, Ed.; Elsevier, New York, 1985.
24. Karr, C. 1978. "Analytical Methods for Coal and Coal Products." Academic: New York Vo. I pp. 224, 280-321.
25. American Society of Testing Materials. Annual Book of ASTM Standards, Part 26, Methods D2492-79 and D3277-75, Philadelphia, PA, 1979.

26. Bomberger, D.R., "Hexavalent Chromium Reduces Corrosion in Coal-Water Slurry Pipeline." <u>Materials Protection</u>, Vol. 4, pp. 43-49, 1965.
27. American Society of Testing Materials. Annual Book of ASTM Standards, Part 10, pp. 913-943, 1979.
28. Oroskar, A.R., Turian, R.M., 1980. "The Critical Velocity in Pipeline Flow of Slurries", <u>AIChE J.</u> <u>26</u>, 550-558.
29. Rai, C., "Microbial Desulfurization of Coal and Texas Lignites." Presented at the AIChE Spring National Meeting, Houston, TX, March 1985.
30. Rai, C. "Microbial Desulfurization of Coals in a Slurry Pipeline Reactor Using Thiobacillus ferrooxidans." <u>Biotechnology</u> <u>Progress</u> <u>1</u>, pp. 200-204, 1985.

9

Pollution Control in Fluidized Bed Combustors

Robert C. Brown

Department of Mechanical Engineering, Iowa State University, Ames, IA 50011

Careful design of fluidized bed combustion systems can
reduce the deleterious emissions associated with coal
combustion. The expense of post-combustion removal of
SO_2 is eliminated by employing limestone sorbent for
bed material. SO_2 released from coal in the bed is
readily absorbed due to the high probability of gas-
solid contact. The low combustion temperatures em-
ployed in FBC for good sorbent utilization also sup-
press thermal NO_x emissions. Emissions associated
with fuel nitrogen can be controlled by changes in
operating conditions, staged combustion, or injection
of ammonia. Particles elutriuted from fluidized beds,
resulting in both poor combustion efficiency and emis-
sion of noxious pollutants if not controlled, are cap-
tured by cyclones, fabric filters, and electrostatic
precipitators. The low temperatures of FBC reduce
volatilization of alkaline compounds associated with
corrosion problems in fossil fuel boilers. Despite the
enormous advantages of FBC in emission control, several
problem areas remain to be solved.

Fluidized bed combustion (FBC) is rapidly becoming a commercially
attractive method for utilizing fossil fuel resources. Although FBC
has been under development for many years, only recently has its
ability to burn coal and low grade fuels in an environmentally ac-
ceptable manner given impetus to its application. In particular, the
prospect of FBC replacing expensive and complicated wet scrubber
desulfurization equipment with in-situ sulfur dioxide removal has
attracted widespread attention; however, careful design of FBC sys-
tems can also markedly reduce other deleterious emissions associated
with coal combustion. These include nitrogen oxides (NO_x), partic-
ulates, and alkalis.
   A fluidized bed is produced by passing a stream of gas vertical-
ly through a bed of solid particles at sufficient velocity to suspend
the particles. In this state, the bed takes on many of the proper-
ties of a fluid. Solid fuel injected into the bed will also be
fluidized until combustion is complete or until the solid fuel

particle is small enough to be elutriated from the bed by the gas
flow.

A number of variations on this basic scheme has been developed
to exploit or overcome particular features of FBC. The boiling bed
employs just sufficient air velocity to fluidize the bed material.
It has little lateral mixing in the bed and coal fines are too read-
ily elutriated from the bed, giving low combustion efficiency. In-
ternally circulating beds attempt to increase bed residence time by
increasing lateral circulation in the bed. Externally circulating or
entrained FBC employs large air flow velocities to intentionally
entrain bed material and coal particles with the air. Bed material
and coal are recovered by cyclones and reinjected into the bed.
Pressurized FBC (PFBC) has been developed to increase combustion
intensity and improve thermodynamic efficiency of power cycles. In
principle, PFBC can produce power both from steam raised by heat
extraction from the bed as well as from expanding the hot, pressur-
ized flue gas in the gas turbine. The gas turbine also provides
power to pressurize air entering the fluidized bed.

The potential for FBC to reduce sulfur dioxide (SO_2) emissions
has attracted considerable attention in the United States because of
the high sulfur content of many indigenous coal reserves and strict
environmental quality standards. Sulfur occurs in coal as both or-
ganically bound material and as iron pyrites. Most of the pyrites
can be removed by washing if the coal is ground fine enough to re-
lease the mineral crystals, but physical methods cannot remove organ-
ic sulfur. Although chemical methods have been proposed, they do not
appear economical at this time. Therefore, the only alternative is
to remove this sulfur after it has been oxidized to SO_2 in the com-
bustion process. Flue gas desulfurization by both wet and dry scrub-
bing processes is a well developed but expensive technology to build
and maintain. FBC eliminates post-combustion clean-up equipment by
employing an inexpensive SO_2 sorbent, limestone or dolomite, for bed
material. SO_2 released from coal in the bed is readily absorbed due
to the high probability of gas-solid contact. In order to achieve a
high degree of SO_2 removal, it is important that the sulfur be oxi-
dized in the bed rather than above the bed, in the freeboard, where
the probability of gas-solid contact is much smaller. Detailed un-
derstanding of FBC combustion and SO_2 sorption mechanisms is funda-
mental to achieving this condition.

The rapid heating of coal particles injected into a fluidized
bed will be accompanied by release of volatile gases from the parti-
cles. Combustion of these volatiles, which include sulfur-bearing
compounds such as hydrogen sulfide, occurs in the bed for well de-
signed systems. The char remaining after release of volatiles also
contains sulfur and will be oxidized in the fluidized bed until the
size of the char particles becomes small enough to be elutriated from
the bed. FBC systems designed to oxidize these small char particles
in the freeboard can also be expected to release SO_2 in the freeboard
where limited sorption may set the lower bound on sulfur emissions.
Sulfur in the volatiles and char will oxidize primarily to SO_2.
Although SO_3 will also be produced from SO_2, the maximum extent of
its conversion will be limited by equilibrium considerations to only
a few percent of SO_2 concentration (1), and the role of SO_3 in FBC is
usually considered to be unimportant. Limestone in the fluidized bed

must first be calcined to lime (CaO) before it can react as a sorbent:

$$CaCO_3 \longrightarrow CaO + CO_2 \qquad (1)$$

The decrease in molar volume during calcination of $CaCO_3$ to CaO has the effect of increasing the porosity of the sorbent which is important to the efficient utilization of limestone. The gas-solid reaction between SO_2 and limestone sorbent consists of a number of steps (2): diffusion of gaseous SO_2 through the pores of the calcined limestone, reaction of SO_2 with CaO to form calcium sulfate ($CaSO_4$), and diffusion of SO_2 through the calcium sulfate product layer to react with additional CaO in the particle. Unfortunately, the sulfation reaction:

$$CaO + SO_2 + 1/2O_2 \longrightarrow CaSO_4 \qquad (2)$$
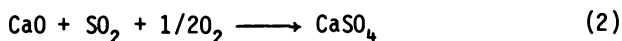
increases the molar volume of the sorbent with a corresponding decrease in the porosity of the sorbent to subsequent diffusion of gaseous SO_2 (3,4). This effect appears to limit limestone/sulfate conversion to about 50%. Absorption efficiency is a function of Ca/S mole ratio, with greater than stoichiometric ratios required for efficient sulfur dioxide reduction (5,6). The extent of sorbent utilization will depend on such factors as sorbent particle size, the size of diffusion pores, and the size of CaO crystallites where sulfation actually takes place. Attempts to correlate sorbent utilization with sorbent properties have not been successful (7,8), although the following general features can be noted. Fine limestone, with its large surface area, is well known to increase sorbent reactivity (6-9), but elutriation of sorbent also increases as particle size is made smaller. Bonn and Munzner (7,8) have shown that maximum absorption efficiency can be achieved with either fine limestone of 10-20 μm size, which reacts before it is elutriated from the bed, or coarse limestone of about 400 μm size, which is not elutriated from the bed. Generally, coarse limestone has been utilized commercially although FBC systems have been recently developed to exploit the advantages of fine sorbent particles. These include the internally circulating bed, designed by Westinghouse (10), which abrades limestone particles by high-velocity impact against an attrition device, and the Multi-Solids Fluidized Bed Combustion design of Battelle (11) which entrains fine limestone in an externally circulating bed. Limestones that easily abrade can substantially improve stone utilization, especially if coarse stone is employed (8). On the basis of Ca/S molar ratio, dolomite is usually more effective than limestone (7,8,12). Dolomite calcines to CaO·MgO, but for temperatures and pressures typical of atmospheric FBC, the MgO reacts only slowly with SO_2 to form $MgSO_4$ (12). Although this absence of reaction decreases the capacity of the stone on a mass basis, it improves the porosity of the partly spent stone and provides access to CaO located at the core of the stone. Several researchers (13-17) have observed that as pressure is increased in a fluidized bed, sulfur retention by limestone decreases. This effect is the result of a shift in the calcination reaction (Eq. 1) toward $CaCO_3$; hence, less calcined lime is available for sulfation. Although SO_2 can react directly with $CaCO_3$ (18):

$$CaCO_3 + SO_2 + 1/2\ O_2 \longrightarrow CaSO_4 + CO_2 \qquad (3)$$
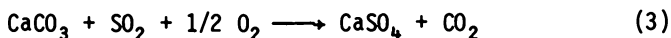
very little pore volume, hence surface area, exists in the uncalcined limestone. If dolomite is substituted for limestone, no loss in sulfur retention is observed. Dolomite undergoes "half-calcination" at temperatures considerably lower than for limestone:

$$CaCO_3 \cdot MgCO_3 \longrightarrow CaCO_3 \cdot MgO + CO_2 \qquad (4)$$

The decrease in molar volume associated with the conversion of $MgCO_3$ to MgO increases the porosity of the stone. Although the MgO is relatively inert toward reaction with SO_2, the increased porosity of the stone provides a greater surface area of $CaCO_3$ for the direct reaction with SO_2 described by Eq. (3). There is an optimum temperature for maximum sulfur retention in the range of 800-850°C which is more pronounced for limestone than it is for dolomite (15,19-21). This optimum temperature can be understood by noting that as temperature is increased, increased calcination improves sorbent porosity. As the optimum temperature is exceeded, SO_2 reacts with CaO before it can diffuse into the core of the sorbent particle and pores become blocked to further sorbent utilization. No such effect is observed at elevated pressures, where sulfur retention increases for temperatures at least to 900°C (15).

FBC has also been successful in reducing nitrogen oxide (NO_x) emissions produced during combustion. The term NO_x is intended to encompass all oxides of nitrogen formed during combustion, although at least 90% of NO_x represents nitric oxide (NO) with the balance consisting of nitrogen dioxide (NO_2). The NO emissions from coal combustion arise from both oxidation of atmospheric nitrogen (thermal NO) and oxidation of nitrogen-bearing compounds in the coal (fuel nitrogen). Thermal NO emissions increase with temperature (22); hence, low combustion temperatures characteristic of FBC (700-900°C) are expected to reduce thermal NO emissions compared to conventional combustion. In fact, the main source of NO emissions in FBC is fuel nitrogen (23-25), with the contribution from thermal NO being less than 5% of the total emission (26). In contrast to fuel sulfur, not all fuel nitrogen is converted to the oxide. Depending upon combustion conditions, the conversion is only 5-40% (24). Since no nitrogen is associated with ash, some fuel nitrogen must be converted directly or indirectly to molecular nitrogen. Significant reduction of NO_x emissions from FBC requires an understanding of the fate of fuel nitrogen during coal devolatilization and combustion.

Emissions of NO_x are significantly affected by FBC operating conditions. For bed temperatures less than 850°C, NO emissions increase with temperature (24,27-29). The rate of increase has been measured at between 1.5 ppm (29) and 2.6 ppm (27) per degree Celsius. Above 850°C, NO emissions appear to level off and even decrease. The concentration of NO in the flue gas decreases substantially as pressure is increased (13,15,16). Furusawa et al. (25) showed NO_x emissions to increase substantially as excess air increased from 0 to 50% with modest increases as excess air was further increased. Gibbs et al. (30,31) have found that lowest emissions are associated with shallow beds (depths less than 0.3 m) and surface-fed uncrushed fuels. The highest emissions occurred for deep beds and bottom-fed

crushed coals. Pereira et al. (24) and Gibbs et al. (27) found that
NO is formed preferentially near the fluidizing air distributor
plate. Fuel type is also important in determining the extent of fuel
nitrogen conversion to NO. Hampartsoumian and Gibbs (29) found that
emissions decreased as fuel volatile content of the coal increased.
     The mechanism of NO_x formation and reduction involves both
homogeneous and heterogeneous reactions between products of coal
devolatilization and combustion. Experiments have established that
NO is released from both volatiles and char during coal combustion
(22,24,27,32,33). For temperatures less than 750°C, char is primari-
ly responsible for NO, but as temperature is increased above 750°C
volatiles contain most of the fuel nitrogen. This result is to be
expected because the quantity of volatiles released increases with
temperature. Important to the understanding of NO emissions was the
discovery that char and volatiles can reduce NO released in the
fluidized bed. Measurements of NO concentration profiles in FBC have
shown that NO decreases 40-50% between the lower bed and freeboard
(24,27,34). The importance of NO-carbon reactions in producing this
effect has been well established (27,34,35). In addition, the re-
action between NO and char is significantly enhanced in the presence
of CO (36,37). Because CO and hydrocarbon concentrations can be high
immediately above the bed (38), their role in NO reduction may be
important. De Soete (39) proposed that fuel nitrogen released as
volatiles is converted into one of several intermediate nitrogen
compounds, including N, NH, NH_2, CN, and HCN, that are either oxi-
dized to NO or act to reduce NO to N_2. Hence, in a fluidized bed
reactor, both formation and reduction of NO take place simultaneous-
ly, with substoichiometric (low oxygen) conditions favoring low NO
emissions. The relative importance of NO-volatile and NO-char re-
actions has not been clearly established. A model of NO formation in
FBC by Beer et al. (40) predicts that 70% of NO is released from
volatiles whereas 65% of NO formed is reduced by NO-char reactions.
NO emission in FBC is further complicated by the apparent interaction
of NO with SO_2 and sulfated sorbents. Jarry et al. (23) observed NO
emissions to decrease by 40% when limestone was employed in FBC.
Hoke et al. (28) found NO and SO_2 reacted in contact with partially
sulfated limestone, and it was suggested that NO acted as an oxidant
for calcium sulfite ($CaSO_3$).
     Despite the intrinsically low thermal NO emissions of FBC, the
nitrogen content of coal results in total NO emissions that may
exceed air quality standards. A number of strategies can be adopted
to reduce NO emissions resulting from fuel nitrogen. Careful choice
of operating conditions can reduce NO emissions but there are limita-
tions to the effectiveness of this technique. For example, improve-
ments in NO emissions achieved by decreasing bed temperature are
attended by increased SO_2 emissions as the temperature drops below
the optimum 800-850°C range for limestone sorbent utilization. Com-
bustion efficiency will also decrease as the temperature drops be-
cause of reduced carbon burn-up. Use of a high volatility fossil
fuel can also reduce NO_x emissions, but this constraint would erode
the fuel flexibility characteristic of FBC. Experiments suggesting
that low emissions are favored in shallow beds with coal fed from
above the bed may have limited practical application if control of

coal elutriation and in-bed heat transfer area are more important economic considerations in bed design. NO_x reduction can also be achieved by controlling excess air. Because NO_x increases with excess air, limiting excess air to the minimum required for good combustion efficiency is important. If operating temperatures are high enough to assure calcination of limestone sorbent, this limitation on excess air should not effect SO_2 emissions.

Staged combustion has been suggested to exploit the advantages of substoichiometric operation in FBC. If the concentration of oxygen is intentionally limited, nitrogen intermediates released during coal devolatilization will preferentially reduce NO to N_2. Additional oxygen can be added in subsequent sections of the FBC unit to assure complete combustion of the fuel. Two designs for staged combustion in FBC have been proposed. The first consists of a single bed with primary and secondary air streams (41-43). The primary stream, supplied through the distributor plate at the bottom of the bed, is sufficient for fluidization. All fuel is injected into the bed which results in substoichiometric conditions favoring low NO_x emissions. The secondary air is typically injected in the freeboard just above the bed in quantities large enough to make overall combustion stoichiometric or excess air condition. Gibbs et al. (41) found that the extent of NO reduction increased as the proportion of primary air was reduced. Tatebayashi et al. (42) noted the importance of sufficient freeboard height for maximum NO reduction and attributed this to NO-char reactions. The major problem with this design is high elutriation rates for coal particles. An alternative design employs two fluidized beds in series (26,44,45). The lower bed operates substoichiometrically and serves to limit the conversion of fuel nitrogen to NO. The second receives the effluent of the first bed, including NO and elutriated char. Char in the second bed either reacts with NO, further reducing NO_x emissions, or is oxidized by air admitted to the second bed. Combustion efficiency is improved but at the cost of system complexity.

NO_x emissions have been reduced in pulverized coal combustors by injecting ammonia gas (NH_3) downstream of the flame zone (46,47). The process is controlled by complex free radical reaction chains (48), but the overall reaction is described by:

$$4NH_3 + 6NO \longrightarrow 5N_2 + 6H_2O \qquad (5)$$

$$4NH_3 + 4NO + O_2 \longrightarrow 4N_2 + 6H_2O \qquad (6)$$
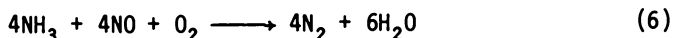
Unfortunately, the process is extremely temperature sensitive. If the temperature is too low, NH_3 passes through the boiler unreacted and is emitted as a noxious pollutant. If the temperature is too high, rather than reduce NO, the NH_3 is oxidized to NO. The optimum temperature range is 900-1000°C, although the presence of hydrogen or unburned hydrocarbons shifts this range to lower temperatures (49). The feasibility of using NH_3 injection in FBC has been investigated by Hampartsoumian (50). It was found that emissions were reduced 30-50% if NH_3 injection occurred in the freeboard immediately above the bed. Injection into the bed or higher in the freeboard was less effective. Injecting NH_3 into the air flow below the distributor plate increased NO_x emissions. Excess air was found to reduce the

effectiveness of NH_3 injection but varying the bed temperature be-
tween 770 and 900°C had little effect on NO reduction.

Emission of particulates is another area of concern in FBC. For
combustion of fine coal in FBC with fluidization velocities less than
0.5 m/s, concentration of coal in the bed is very low and combustion
inefficiency due to particle elutriation or incomplete combustion is
very low. Commercial FBC development emphasizes higher fluidization
velocities of around 4 m/s in an attempt to reduce boiler size. At
these high velocities, elutriation of coal fines becomes significant
(51). Even the use of large coal particles to feed the bed will not
eliminate coal fines arising from attrition and decrepitation, and it
is common practice to recover elutriated carbon with cyclones and
reinject it into the bed. Nevertheless, very fine particles, con-
sisting of unburned carbon, ash, and bed material must be captured
from the flue gas with additional stages of particle collection.
Fabric filters (bag houses) are most commonly employed, although hot
gas electrostatic precipitators can also be used. The electrical
resistivity of particles to be captured is an important consideration
in assessing the applicability of electrostatic precipitators to FBC.
Two factors appear to limit the resistivity of particulates in FBC
(52,53). Concentrations of SO_3, important in determining the resist-
ivity of particles in flue gas, are low in FBC. This may be the
result of highly reactive SO_3 being readily absorbed by elutriated
limestone or alkaline ash. The second factor is the high intrinsic
resistivity of sorbent materials. Offsetting these factors is the
strong influence of carbon content in lowering fly ash resistivity.

The release of alkaline compounds is also an important factor
in coal combustion. Most high-temperature corrosion problems in
fossil fuel boilers are the result of salt melts (54,55). Alkali
metal compounds volatilize from coal at the high temperatures of
conventional combustion and subsequently condense on heat transfer
surfaces. The lower temperatures of FBC are expected to reduce salt
volatility, a fact that has been confirmed by Vogel et al. (16).
This feature of FBC is very attractive for development of coal-fired
gas turbine power plants where the presence of alkaline material in
the turbine inlet gas produces unacceptable corrosion problems.

Despite enormous advances in pollution control through the rise
of fluidized beds, there remain several areas for improvement. The
power and steam requirements of utilities and large industries cul-
minated in atmospheric, externally circulating FBC which dominate the
market today. Research and development in emissions control have
recently concentrated on these designs; however, FBC is rapidly ex-
panding into new applications that require alternative design con-
cepts. Most prominent among these developments are pressurized FBC
and small-scale FBC boilers and furnaces. New or modified emission
control strategies may be required in these applications; several
areas for future research are discussed below.

Pressurized FBC may make possible the use of coal in turbo-
charged combustors and combined cycle power systems. Success is
dependent on reducing the erosive and corrosive character of hot,
pressurized flue gas generated from coal combustion before expanding
it through the system's gas turbine. The problems to be overcome are
manifold. The usual requirement for reducing particulate emissions
to environmentally acceptable levels is supplemented with stringent

in-plant limits. Particulate loading of flue gas must be substan-
tially reduced before entering the gas turbine. Clean-up operations
are complicated at these high temperatures; fabric filters cannot be
used and cyclones are inefficient at removing particles smaller than
10 μm. Research is needed to improve the design of hot gas clean-up
equipment such as high efficiency cyclones and electrostatic precipi-
tators. Gas turbines are also intolerant of alkali. Turbine manu-
facturers specify less than 0.024 ppm alkali in the entering gas
stream to prevent hot corrosion of turbine blades. Alkali emissions,
although low in FBC compared to pulverized coal combustion, are typi-
cally one to two orders of magnitude greater than gas turbines can
tolerate. Simple mechanical filtration preceding the turbine is not
adequate because much of the alkali exists as vapor. The mechanisms
of alkali vaporization and condensation must be better understood and
control strategies developed. Attempts to improve thermodynamic
cycle efficiency by raising turbine inlet temperature and lowering
turbine exit temperature must be accompanied by additional research
on emissions of SO_2 from fluidized beds and formation of SO_3 in free-
boards. Higher turbine inlet temperatures require correspondingly
higher bed temperatures which will move sulfation reactions beyond
the optimum range for good sorbent utilization. Lower turbine exit
temperatures demand lower acid dew point temperatures which are a
function of SO_3 levels in the flue gas. Pressurized FBC demands a
better understanding of sulfur kinetics both in the bed and free-
board.

Small-scale FBC units offer the prospect of coal regaining mar-
kets it once held in water and space heating for residential, com-
mercial, and light industry applications. However, such a revival
must be preceded by major rethinking of current FBC designs. Large-
scale FBC systems are driven by design criteria distinct from that
for small-scale boilers. It seems highly unlikely that lessons
learned in the evolution of externally circulating FBC can be direct-
ly applied to emissions control in units sized for a hospital or
shopping center. Simpler designs are required. A second look at
bubbling beds and their attendant problems may be in order. How can
carbon burn up and sorbent utilization be improved if external recir-
culation is not employed?

Several other topics deserve further investigation. The econom-
ic evaluation of FBC often hinges on the cost of limestone or dolo-
mite. Improvements in sorbent utilization would greatly improve the
commercial prospects for FBC. Another approach that has not received
a great deal of attention is the use of regenerable sorbents. This
neglect may reflect a widespread perception of such processes as
being uneconomical. Research on regeneration of sorbents might im-
prove this picture. A great virtue of FBC is its fuel flexibility;
emission characteristics of alternative fuels and coal-derived fuels
should be undertaken. For example, coal-water-mixtures (CWM), in
combination with additives, might be formulated to yield lower pollu-
tion emissions. There is already evidence that the agglomeration
behavior of CWM improves carbon burnout compared to dry coal. Final-
ly, the formation of toxic and mutagenic agents in FBC is a neglected
topic. When absorbed on fly-ash, these agents can pose a significant
inhalation hazard. Often it is assumed that low temperatures and
good carbon burn out in FBC reduce the formation of condensed

aromatics, but the small amount of available data is contradictory on this point.

Acknowledgment

Literature Cited

1. Burdett, N. A.; Gliddon, B. J.; Hottchkiss, R. C.; Squires, R. T. J. Inst. Energy 56, 119 (1983).
2. Kunii, D.; Levenspiel, O. Fluidization Engineering, John Wiley and Sons, 1969.
3. Hartmann, M.; Coughlin, R. W. A.I.Ch.E. J. 22, 490 (1976).
4. Hartmann, M.; Coughlin, R. W. Ind. Eng. Chem. Proc. Des. Dev. 13, 248 (1974).
5. Glenn, R. D.; Robison, E.B. Proceedings of the Second International Conference on Fluidized Bed Combustion, US EPA (1970).
6. Davidson, D. C.; Smale, A. W. Proceedings of the Second International Conference on Fluidized Bed Combustion, US EPA (1970).
7. Munzner, H.; Bonn, B. Proceedings of the Sixth International Conference on Fluidized Bed Combustion, US EPA (1980).
8. Bonn, B.; Munzner, H. Sulfur Capture with Limestones in Fluidized Bed Combustion, Inst. Energy Symp. Ser., No. 4 (1980).
9. Anastasia, E. L.; Carls, E. L.; Jarry, R. J.; Jonke, A. A.; Vogel, G. J. Proceedings of the Second International Conference on Fluidized Bed Combustion, US EPA (1970).
10. Newby, R. A.; Keairns, D. L.; Altine, H. K.; Hamm, J. R.; Ahmed, M. M.; Weeks, K. D.; Bachovchin, D. M.; Kececioglu, I.; Ulerich, N. H.; Yang, W. C. "Advanced Atmospheric Fluidized Bed Combustion Design: Internally Circulating AFBC," DOE Technical Report DOE/MC/19329-1405, January 1983.
11. Kim, B. C.; Litt, R. D.; Nack, H. Proceedings of the Seventh International Conference on Fluidized Bed Combustion, (1983).
12. Borgwardt, R. H.; Harvey, R. D. Environ. Sci. Tech. 6, 350 (1972).
13. Wright, S. J. Proceedings of the Third International Conference on Fluidized Bed Combustion, US EPA (1973).
14. O'Neill, E. P.; Keairns, D. C.; Kittle, W. F. Proceedings of the Third International Conference on Fluidized Combustion, US EPA (1973).
15. Roberts, A. G.; Stanton, J. E.; Wilkins, D. M.; Beacham, B.; Hoy, H. R. Inst. Fuel Symp. Ser. No. 1 (1975).
16. Vogel, G. J.; Swift, W. M.; Montagna, J. C.; Lenc, J. F.; Jonke, A. A. Inst. Fuel Symp. Series No. 1 (1975).
17. Hoke, R. C.; Bertrand, R. R. Institute Fuel Fluidized Combustion Conference, London (1975).
18. Jansson, S. A.; O'Connell, L. P.; Stanton, J. E. Proceedings of the Seventh International Conference on Fluidizied Bed Combustion (1982).
19. Ehrlich, S. Inst. Fuel Symp. Ser. No. 1 (1975).
20. Moss, G. Inst. Fuel Symp. Ser. No. 1 (1975).
21. Highley, J. Inst. Fuel Symp. Ser. No. 1 (1975).

22. Pershing, D. W.; Wendt, J. O. L. Sixteenth Symposium (International) on Combustion, The Combustion Institute (1977).
23. Jarry, R. J.; Anastasia, L. J.; Carls, E. L.; Jonke, A. A.; Vogel, G. J. Proceedings of the Second International Conference on Fluidized Bed Combustion, US EPA (1970).
24. Pereira, F. J.; Beer, J. M.; Gibbs, B. M.; Hedley, A. B. Fifteenth Symposium (International) on Combustion, The Combustion Institute (1975).
25. Furusawa, T.; Honda, T.; Takano, J.; Kunii, D. Proceedings of the Second Engineering Foundation Conference on Fluidization, Cambridge University Press (1978).
26. Horio, M.; Mori, S.; Furusawa, T.; Tamanuki, S. Proceedings of the Sixth International Conference on Fluidized Bed Combustion, US DOE (1977).
27. Gibbs, B. M.; Pereira, F. J.; Beer, J. M. Inst. Fuel Symp. Ser. No. 1 (1975).
28. Hoke, R. C.; Shaw, H.; Skopp, A. Proceedings of the Third International Conference on Fluidized Bed Combustion, US EPA (1973).
29. Hampartsoumian, E.; Gibbs, B. M. J. Inst. Energy (1984).
30. Gibbs, B. M.; Hedley, A. B. Seventeenth Symposium (International) on Combustion, The Combustion Institute (1978).
31. Gibbs, B. M.; Hampartsoumian, E. Inst. Energy Symp. No. 4 (1980).
32. Vogt, R. A; Laurendeau, N. M. "NO Formation from Coal Nitrogen: A Review and Model," Central States Section/The Combustion Institute, Ohio (1976).
33. Pohl, J. H.; Sarofim, A. F. Sixteenth Symposium (International) on Combustion, The Combustion Institute, (1976).
34. Pereira, F. J.; Beer, J. M. Deuxieme Symposium Européen sur la Combustion, Orleans, France (1975).
35. Furusawa, T.; Kunii, D.; Oguma, A.; Yamada, N. Proc. Soc. Chem. Eng. Japan 4, 562 (1978).
36. Chan, L. K. "Kinetics of the Nitric Oxide-Carbon Reaction Under Fluidized Bed Combustor Conditions," Dissertation, M. I. T., Cambridge, MA (1980).
37. De Soete, G. G. "Mechanisms of Nitric Oxide Reduction on Coal and Char Particles," Report on EERC Subcontract No. 8318-6, (Internal Report Institut Francais du Petrole, Ref. No. 28136), 1980.
38. Walsh, P. M.; Dutta, A.; Beer, J.M. "Freeboard Reactions in Fluidized Bed Combustion," US DOE Technical Report DOE/PC/30215-3, November 1981.
39. De Soete, G. G. European Combustion Symposium, The Combustion Institute, Sheffield (1973).
40. Beer, J. M.; Sarofim, A. F.; Lee, Y. Y. Proceedings of the Sixth International Conference on Fluidized Bed Combustion (1980).
41. Gibbs, B. M.; Pereira, F. J.; Beer, J. M. Sixteenth Symposium (International) on Combustion, The Combustion Institute (1977).
42. Tatebayashi, J.; Okada, Y.; Yano, K.; Ikeda, S. Proceedings of the Sixth International Conference on Fluidized Bed Combustion, US DOE (1980).

43. Taylor, T. E. Proceedings of the Sixth International Conference on Fluidized Bed Combustion, US DOE (1980).
44. Hirama, T.; Adachi, T.; Tomita, M.; Horio, S. Thirteenth Autumn Conference of the Chemical Engineering Assoc., Nagoya (1979).
45. Tomita, M.; Hirama, T.; Adachi, T.; Yamaguchi, H.; Horio, M. Proceedings of the Sixth International Conference on Fluidized Bed Combustion, US DOE (1980).
46. Lyon, R. K. U.S. Patent No. 3,900,554; 1975.
47. Muzio, L. J.; Arand, J. J.; Teixeira, D. P. Sixteenth Symposium (International) on Combustion, The Combustion Institute (1976).
48. Dean, A. M.; Hardy, J. E.; Lyon, R. K. Ninteenth Symposium (International) on Combustion, The Combustion Institute (1982).
49. Lyon, R. K. Hydrocarbon Proc. 58, 10 (1979).
50. Hampartsoumian, E. Ph.D. Thesis, The University of Leeds (1982).
51. Skinner, D. G. The Fluidized Combustion of Coal, National Coal Board, London (1970).
52. Bubenick, D.; Lee, D.; Hall, R.; Fenelly, P. The Proceedings of the Sixth International Conference on Fluidized Bed Combustion, US DOE (1980).
53. Shilling, N.; Morris, W. The Proceedings of the Sixth International Conference on Fluidized Bed Combustion, US DOE (1980).
54. Reid, W. T. External Corrosion and Deposits in Boilers and Gas Turbines, American Elsevier, N.Y. (1971).
55. Raask, E. Mineral Impurities in Coal Combustion, Hemisphere Publishing, N.Y. (1985).

Organic Compounds from Coal Combustion

G. A. Junk, J. J. Richard, M. J. Avery, R. D. Vick, and G. A. Norton

Ames Laboratory, Iowa State University, Ames, IA 50011

Organic compounds in the various effluents from the
efficient combustion of coal at power plants do not
appear to be an environmental problem. This conclu-
sion is based on interpretation of results obtained
during a four-year study of samples of stack gas and
fly, grate and stack ashes from the combustion of coal
alone and of mixtures of coal and refuse-derived fuel.
Dioxins and furans were not present in these samples
at the detection limit of 10 parts per trillion.
Alkanes, chlorinated benzenes, polychlorinated bi-
phenyls, polycyclic aromatic hydrocarbons, aliphatic
acids and other miscellaneous compounds were identi-
fied, but the amounts were below those reported for
ambient urban air. These low levels of organic com-
pounds are obtained only under steady state conditions
of high combustion temperature, excess oxygen, small
fuel particles and sufficient residence time. The
waters from the sluicing of the fly ash and grate
ashes to settling ponds were also analyzed. The re-
sults of these analyses and separate adsorption and
leaching experiments were used to conclude that fly
and grate ashes were not a probable source of organic
contamination of ground and surface waters.

The release of organic pollutants into the environment from the
burning of coal has been of periodic concern ever since the indus-
trial revolution in England. This concern has resurfaced recently
due to the shift to coal as the major fuel for generating electrici-
ty in the U.S.

Because of this environmental concern, an extended study of the
Ames power plant for generating electricity was begun in 1977. This
study included all types of pollutants such as NO_x, SO_x, total
suspended particles, fly ash, grate ash, and trace elements as well
as the organic compounds from the combustion of coal alone and mix-
tures of coal and refuse derived fuel (RDF). The results in this
report are confined to the organic compounds found in all of the

solid, liquid and gaseous effluents related to the combustion pro-
cesses.

At the start of this study in 1977, the analytical methodology
was inadequate for the characterization of organic compounds in the
various effluents. Thus, priority was given to: 1) identifying the
analytical difficulties; 2) devising methods to resolve the most
critical problems; and 3) using evolving methodologies to determine
those components judged to pose a threat to the environment.

As an aid in establishing the analytical problems, published
data were compiled and reviewed for coal combustion and waste incin-
eration (1). Important conclusions drawn from this review were: 1)
only a limited number of organic components had been identified in
the effluents; 2) the identified components reflected analytical
capabilities and interests rather than a true distribution; 3) reli-
able quantitative data were not available; and 4) the data base was
insufficient for predicting the probable environmental effects as-
sociated with the combustion of coal.

A critical examination of the analytical procedures used prior
to 1977 showed these to be inadequate for the determination of or-
ganic compounds in combustion effluents; of special concern were the
short-comings in sample collection methods. These short-comings are
delineated in a review published recently (2). Because of these
sampling uncertainties, the continuous development and validation of
new procedures and sampling systems was an essential element of this
study.

Coincident with the development of sampling procedures were the
constant iterative improvements in extraction, separation, identifi-
cation and quantitation of organic compounds. Special emphasis was
placed on selected compound classes such as the polycyclic aromatic
hydrocarbons (PAHs), polychlorinated biphenyls (PCBs), chlorinated
benzenes, and chlorinated dibenzo-p-dioxins (dioxins). The best
available procedures were used to determine these components because
they have known acute or chronic effects and previous studies sug-
gested that they might be present in effluents from the combustion
of coal alone and combination coal/RDF.

Sampling Procedures

Sampling points for all power plant influent and effluent streams
are shown in Figure 1. The procedures used to collect the stack
effluents, the fly and grate ash samples, and the waters are dis-
cussed separately below.

Stack Vapor. The major goal in sampling the stack effluent was to
obtain large samples representative of the components present in the
vapor phase and associated with suspended particles. Vapor phase
organic components present in the stack effluent were sampled by
three different procedures. An EPA Method 5 train was equipped with
an organic module and used during the early stages. This sampler
allowed the stack gas to pass over the accumulated particles during
the entire sampling period and thus gave rise to the possibilities
of adsorption, sublimation and chemical transformations of organic
components. When the equipment became available, the Method 5 train
was supplanted by a Source Assessment Sampling System (SASS). This
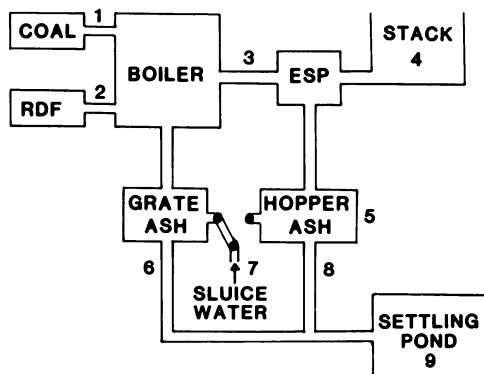
Figure 1. Sampling points for fuels (1 and 2), ESP fly ash (5), ash slurries (6 and 8), sluice water (7), sediment and water (9), organic vapors (3 and 4), and suspended particulate matter (4).

system allowed larger volumes of gas to be sampled and reduced the
contact between accumulated particles and the stack gas. The com-
plexity of the SASS made it undesirable for use when the only goal
was to obtain a sample of vapor phase components. A third sampling
system was the Ames Vapor Sampling System (AVSS) described by Junk
and Richard (3). This sampling system largely eliminated contact
between vapor phase components and particles. The AVSS provided a
simple and effective accumulation of organic components from very
mild atmospheres such as ambient air and very severe atmospheres
such as stack gas.

Stack Ash. Four procedures were used for obtaining samples of stack
ash. The EPA Method 5 train used initially did not protect ade-
quately the integrity of the samples because stack gas passed con-
tinuously over accumulated particles. The magnitude of this problem
could not be investigated because insufficient quantities of stack
particles were accumulated to allow for the accurate determination
of adsorbed organic components. The SASS provided adequate quan-
tities of particles and simultaneously lessened the contact between
accumulated particles and stack gas. However, even the SASS did not
collect enough of the small respirable particles to facilitate de-
terminations of many organic components that might pose a potential
health hazard. Two other procedures were used for obtaining large
quantities of stack ash for scouting analyses. In one procedure,
the particles that had accumulated in unused sampling ports were
simply retrieved, sized, and used as samples representative of stack
ash. Although these particles were obviously not truly representa-
tive of those emitted from the stack, they were available in larger
quantities for exploratory studies of analytical protocols and to
establish the types of compounds present in the particles. The
second procedure for obtaining larger amounts of stack ash consisted
of inserting a tray into the stack to collect the particles that
settled from the disturbed gas stream. As was the case with the
particles collected from sampling ports, the particles collected in
the tray were not truly representative of the stack effluent. How-
ever, these particles were useful for determining changes in the
organic emissions when firing conditions and fuels were varied.

Fly Ash. Fly ash samples were collected directly from the hoppers
of the cyclone and electrostatic precipitator used for particle
control.

Grate Ash. Grate ash samples from stoker-fired units were collected
from hoppers located below the grates. Grate ash from the tangen-
tially fired units was removed from the boilers by sluicing. Sam-
ples were obtained by filtering the sluice water collected at the
outlet of the pipe used to transport the sluiced ash to a settling
pond. Additional ash samples were collected from the settling pond
as sediment samples.

Waters. Sluice and settling pond waters were collected as four-
liter grab samples.

Extraction Procedures

The extractions of adsorbents, water condensates and ashes (particles) are described separately below.

Adsorbents. A macroreticular resin, XAD-2, was used as the adsorbent in the AVSS, the SASS and the EPA Method 5 sampling train. Organic compounds accumulated on the resin were recovered by elution with methylene chloride. Diethyl ether was used as an eluent, instead of methylene chloride, when subsequent determinations were performed by gas chromatography with electron capture detection. Other eluents and desorption techniques were tested and found to offer no significant advantages (3).

Water Condensates. When stack gas was cooled during sampling, water vapor condensed. The organic components in these condensates were extracted with methylene chloride. Diethyl ether, pentane and isooctane were used as alternative extraction solvents when subsequent gas chromatographic determinations required the use of electron capture detectors.

Ashes (Particles). Because there were no standard and accepted procedures among the many described in the literature for the extraction of organic components from particles, several techniques were critically evaluated. Soxhlet extraction with benzene, benzene-methanol, benzene saturated with hydrogen chloride, toluene, toluene-methanol, and methylene chloride were evaluated. Sonic extractions using a probe or a bath with a variety of solvents and pretreatment procedures using aqueous acids and water were also tested. No technique resulted in significant improvement in the extraction of the cross-section of different organic components associated with the various particle effluents. Consequently, the traditional Soxhlet extraction using benzene-methanol was used most frequently.

Class Separations

Chromatographic and solvent partitioning procedures were used to separate organic components recovered from particles into chemical classes to facilitate their ultimate determinations in less complex mixtures. The procedure included the separation of PAHs on Sephadex (4), the separation of components on the basis of polarity using alumina (5), silica gel (6), Florisil (7), the polystyrene-divinyl-benzene resin XAD-4 (8), and the traditional solvent partitioning into acid, base and neutral fractions. Preparatory scale, normal-phase, high-performance liquid chromatography with amine and cyano columns was also used to separate mixtures on the basis of polarity and to partially separate PAHs (9).

The Soxhlet extraction of particles with benzene-methanol yielded PAHs plus many polar and non-polar organic compounds which interfered with the gas chromatographic separations. The interfering compounds were removed using standard solvent partitioning with dimethylsulfoxide [DMSO] (10), dimethylformamide [DMF] (11), or nitromethane (12).

Compound Separations

Gas chromatography was used for the separation of individual organic
components. Columns packed with Dexsil 300 (Supelco Inc., Belle-
fonte, PA) provided the separation of the high boiling point PAHs
during the early stages of this study. Later, as the column tech-
nology advanced rapidly, capillary columns coated with SE-52 and
SE-54 (J&W Scientific, Rio Rancho, CA) were used almost exclusively.
These columns were found to be applicable to the efficient separa-
tion of a diverse assortment of organic components in complex mix-
tures.

Identification and Quantitation

Combination gas chromatography/mass spectrometry (GC/MS) was used
for the identification of the organic components extracted from the
various combustion effluents. Tentative identifications of the un-
known compounds were obtained by computer library searching or manu-
al interpretation of mass spectral data. Additional qualitative
information was obtained by gas chromatography on different polarity
columns using element-specific detectors. Quantitations were per-
formed by comparing the signal obtained for an identified peak with
the signal obtained for a known amount of the same compound chroma-
tographed under the same conditions in a similar matrix. In specif-
ic instances, internal standards and the method of standard addi-
tions were used for quantitation. The quantitation by gas chroma-
tography was periodically checked on randomly chosen samples using
appropriate techniques of combination GC/MS.

Confirmations and Validations

The presence of environmentally hazardous compounds, such as PCBs,
in samples was confirmed using as many independent pieces of infor-
mation as was possible. Ideally, each individual compound in a
sample would exhibit NMR, IR, UV and MS data identical to authentic
samples. In the real world of environmental samples, the compound
in question is usually present in a complex matrix consisting of
hundreds of other compounds in amounts far below those needed for
most of the above mentioned techniques. Thus, gas chromatography/
mass spectrometry (GC-MS) data are often all that are available.
       For positive identifications by GC/MS, the full mass spectrum
of a tentatively identified component was compared to the mass spec-
trum of an authentic sample. If the spectra were identical, within
experimental error, and if the gas chromatographic retention times
of standard and unknown components on a 30-meter SE-54 fused silica
capillary column agreed within two seconds, the identification was
considered positive. When the amount of material present was insuf-
ficient for detection using full scan GC/MS techniques, the more
sensitive single and multiple ion monitoring techniques were em-
ployed. Confirmation in these cases consisted of coincidences of
retention times of mass chromatograms of the unknown and of the
authentic sample. For chlorinated materials, the molecular ions
contained additional information about the chlorine isotope distri-
bution. Confirmation in those cases included the correct isotope

ratios for the number of chlorines in the molecule. An additional piece of information for chlorinated materials was the coincidence of retention times of standards and unknown components coupled with response towards the electron capture detector.

Validation of the methodology used for components that could not be detected in extracts of particle samples was obtained by extraction of surrogate samples. The surrogate sample for PAHs was soot generated from an air-starved methane flame. The positive results obtained from this soot sample have been reported elsewhere (13). The surrogate sample for dioxins was an incinerator ash obtained from Dow Chemical Company. Results obtained from analysis of extracts of this ash sample were ±50% of the published values for the tetra-, hexa-, hepta- and octachloro- isomers (14). This agreement substantiated the validity of the analytical protocol used to screen the effluent samples for dioxin compounds.

Results and Discussions

Results on the identification and quantitation of organic components in effluents from coal and coal/RDF combustion and on the analyses of sluice and settling pond water are presented and discussed below.

Identified Components

A combined listing of all the compounds identified in the vapor and on particles emitted during the combustion of coal at the Ames power plant are listed in Table I. Similar compounds have been identified in the emissions from a second coal-fired power plant located at Iowa State University. Therefore, this list may be partially representative of coal combustion in semi-modern boilers. Certainly, many more organic compounds than the listed 78 are present in these effluents, but so far these have not been positively identified. Indeed, a 1980 review of organic compounds from coal combustion (1) taken from all the literature reports had only 106 compounds identified.

Quantitation

It was not possible to obtain exact quantitative values for all the identified components associated with each of the effluents from coal combustion. The amounts varied because of the analytical problems mentioned in the experimental section and different firing conditions. Even when special efforts were made to achieve constant firing conditions, radically different amounts of gas chromatographable materials were obtained as shown by the two chromatograms in Figure 2. However, semi-quantitative values have been obtained for many of the components and these values are proposed to be reasonable estimates of the amounts of organic compounds expected from the efficient combustion of coal in a modern power plant. A discussion of some important compound classes and the amounts in the various effluents is given below. In general, the amounts are much lower than would be predicted from a review of the limited quantitative data available in the literature.

Table I. List of Organic Compounds Present in Effluents From
          Coal Combustion

ALKANES	AROMATICS	PAHs
Methane	Toluene	Benz(a)pyrene
Decane	Xylene	Anthracene
Undecane	Propylbenzene	Fluoranthene
Hexadecane	Butylbenzene	Fluorene
Heptadecane	Biphenyl	Pyrene
Octadecane	Terphenyl	Naphthalene
Nonadecane	Methylindene	1-Methylnaphthalene
Eicosane		2-Methylnaphthalene
Heneicosane		Acenaphthene
Docosane		Benz(a)anthracene
Tricosane		Benz(ghi)anthracene
Pentacosane		
Hexacosane		
Octacosane		
Triacontane		
Dotriacontane		
Trimethylcyclohexane		
Dimethylcyclohexane		

ACIDS	PHENOLS
2-Ethylbutanoic	Phenol
Nonanoic	o-Cresol
Decanoic	Ethylphenol
Dodecanoic	Butylphenol
Tridecanoic	2,4-Dichlorophenol
Tetradecanoic	2,4,6-Trichlorophenol
Pentadecanoic	
9-Hexadecenoic	
Hexadecanoic	
Heptadecanoic	
Octadecanoic	
Benzoic	

CL COMPOUNDS	O, N, P, S COMPOUNDS
Tetrachloroethylene	Acetophenone
Tetrachloroethane	Methylacetophenone
1,2-Dichlorobenzene	Phthalic Anhydride
1,3-Dichlorobenzene	Methylbenzoate
1,4-Dichlorobenzene	Indanone
1,2,4-Trichlorobenzene	Dibenzofuran
1,2,3-Trichlorobenzene	Diethylphthalate
1,2,3,4-Tetrachlorobenzene	Dibutylphthalate
1,2,3,5-Tetrachlorobenzene	Diisobutylphthalate
Pentachlorobenzene	Di(2-ethylhexyl)phthalate
Hexachlorobenzene	Diphenylamine
2,3,2',5'-Tetrachlorobiphenyl[a]	
2,5,3',4'-Tetrachlorobiphenyl	
2,4,5,2',5'-Pentachlorobiphenyl	
2,4,5,2',4',5'-Hexachlorobiphenyl	

[a] The characteristic Arochlor 1254 profile was observed but only
    four isomers were positively confirmed.

Polycyclic Aromatic Hydrocarbons (PAHs). The most highly studied
class of compounds in combustion effluents is the PAHs. However,
very little information about the amounts present in the vapor phase
and on particles in the effluents from the efficient combustion of
coal is available. The data in Table II partially fills this infor-
mational gap. The amounts in the vapor phase varied according to
the firing conditions and the stack temperature that was ~ 170°C.
Even if all these PAHs were to condense on the particles, the
amounts are well below the multiple µg/g quantities present on am-
bient air particles.

Table II. Summary of PAHs in Effluents From Coal-Fired Power
            Plants

| Compound | Concentration Range (ng/g)[a] | | Conc. Range Vapor Phase (ng/M³)[c] |
	Respirable Particles	Non-Respirable Particles	
Naphthalene	ND[b]-18	0.5-23	10-1800
Phenanthrene	NM	NM	26-640
Anthracene	NM	NM	0.4-100
Fluoranthene	0.2-0.3	0.05-1.5	0.5-240
Pyrene	0.2-7	0.08-1.1	0.2-2850
Chrysene	ND	ND-4	0.1-28
Benz(a)pyrene	ND	ND	0.1-120
Benz(a)anthracene	ND	ND-0.3	NM[d]
Benz(ghi)perylene	NM	NM	3-22

[a] Observed in 26 stack samples collected over a 4 year period.
[b] Not detected at the limit of 0.05 ng/g.
[c] Includes values reported by Midwest Research Institute (15,16).
[d] NM = Not measured.

Alkanes and Aromatics. The distinction between aromatic and poly-
cyclic was arbitrarily set at three conjugated six-member rings in
Table I. With this definition the alkanes and aromatic hydrocar-
bons, with 25 entries, dominate the list of identified components.
These compounds are also present in the highest concentration in the
different effluents. Ordinarily their concentrations were not
measured because of a low interest in these kinds of compounds but
in those instances where measurements were made, the amounts ranged
from 10-1500 ng/M³ in the vapor phase and from 10-90 ng/g on the
suspended particles in the stack effluents. These hydrocarbons were
not quantitated for any of the fly and grate ash samples.

Aliphatic Acids and Phenols. Eleven aliphatic acids and six phenols
were determined as constituents of the vapor phase and associated
with particle effluents. These acidic compounds and the amounts are
listed in Table III. A range of values from 20 different sampling
runs is shown for the C9, C12, C14, C16 and C18 acids and phenol to
illustrate the fluctuations that can occur in the amounts of organic
acids in the effluents. The extent of the variation attributed to
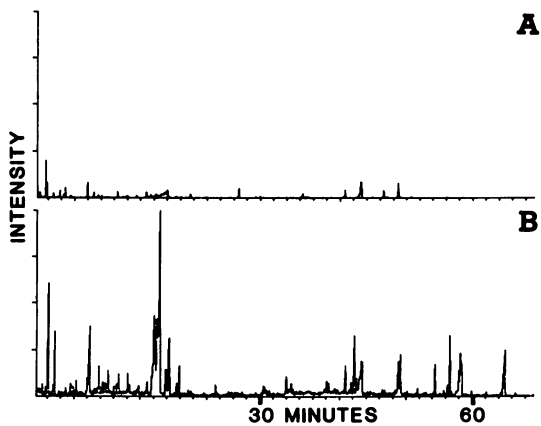
Figure 2. Gas chromatograms of organic material emitted during two different sampling days, A and B, when supposedly similar firing conditions were employed.

changes in firing conditions and analytical difficulties in the determinations is unknown and needs further study.

Polychlorinated Biphenyls (PCBs). The PCBs were observed in the stack effluents during the combustion of coal but these compounds were not produced in the combustion process by a de novo synthesis or from precursor compounds. The source of the PCBs was the indoor air used to support the combustion. This indoor air contained 0.11 $\mu g/M^3$ of PCBs; the concentration of PCBs in the stack gas was only 0.02 $\mu g/M^3$ when coal containing no detectable level of PCBs was burned. For perspective, this emission level should be compared to the average ambient outdoor air level of about 0.006 $\mu g/M^3$.

When the coal fuel was supplemented with RDF containing 8500 μg of PCBs/kg of RDF, the amount of PCBs in the stack remained at the low level of 0.02 $\mu g/M^3$.

Table III. Summary of Acidic Compounds in Effluents From Coal-Fired Power Plants

| | Concentration Range[a] | |
Acid	Vapor (ng/M^3)	Particles (ng/g)
2-Ethylbutanoic	200	NM[b]
Nonanoic	20-250	NM
Decanoic	10	20
Dodecanoic	80-800	90
Tridecanoic	NM	10
Tetradecanoic	100-300	8-600
Pentadecanoic	90	50
9-Hexadecenoic	50	NM
Hexadecanoic	40-300	40-270
Heptadecanoic	NM	20
Octadecanoic	80	40-150
Phenol	20-200	25-1000
o-Cresol	NM	NM
Butylphenol	NM	NM
2,4-Dichlorophenol	NM	0.1
2,4,6-Trichlorophenol	NM	0.05
Pentachlorophenol	NM	0.2

[a] Where a range is listed, these selected components were measured in 26 extracts.
[b] NM = Not measured.

Calculations based on fuel inputs, stack gas flow, support gas input and PCBs in all the inputs and effluents showed that >99% of the PCBs in the input RDF were destroyed in the combustion process. The details of this investigation of the co-combustion of coal and RDF containing PCBs have been published elsewhere (17).

The explanation of the high destruction efficiency for the PCBs in the RDF is efficient combustion based on a combination of high

temperature (~ 2000°F), excess oxygen at 22%, and adequate residence time and sufficient turbulence for the small coal and RDF particles in the combustion zone. This same combination of combustion conditions is the probable explanation for the undetectable levels of TCDD discussed below.

2,3,7,8-Tetrachlorodibenzo-p-dioxin (TCDD). At the detection limit of ten parts per trillion, no TCDD was found in the effluents from the combustion of coal in three different boilers at the Ames power plant (see summary table in reference 16 for description of boilers). This observation was confirmed at a second smaller coal-fired power plant located at Iowa State University. Even when the coal fuel was supplemented with RDF, which should contain the precursor compounds, no dioxins were observed in the vapor and particle samples taken from the effluents. Thus no de novo synthesis occurred during the combustion of coal alone and if dioxins were formed from precursor compounds in the co-combustion of coal and RDF, they were destroyed in the efficient combustion as explained above for the thermal destruction of the PCBs present in the RDF. The PCBs are reported to be completely destroyed at 1200°F (18) and a similar destruction temperature is expected for the dioxins. This is well below the 2000°F operation of the boilers used for this study (19).

Chlorinated Benzenes. Ten chlorinated benzenes were targeted for analysis in the stack effluents. The analytical results when coal alone was combusted are shown in Table IV. When the coal fuel was supplemented with RDF up to 20%, no consistent increase in the amounts of the chlorinated benzenes occurred although barely detectable amounts of the tetra-, penta- and hexa- isomers were observed during some of eleven different combustions of coal with 20% RDF. Based on these results it appears as if the dichlorobenzenes, reported to be present in the RDF at the 8000 μg/kg level (15,16), were thermally destroyed with high efficiency in much the same manner as that documented above for the PCBs present in the RDF. This suggestion has not been supported so far by experimental results. An additional speculation is that the origin of the chlorobenzenes observed in the effluents when coal alone was combusted was the indoor air used to support the combustion.
The environmental effects from the emission of these chlorinated benzenes are estimated to be insigificant because of the low levels and the further dilution by factors of 10^3 to 10^5 in the atmosphere before any human or plant exposure.

Summary of Identifications and Quantitations From Vapor and Particle Effluents. The identified compounds in each chemical class and the range in concentrations for different vapor and particle effluents from the combustion of coal and mixtures of coal and RDF are summarized in Table V. The range in concentrations is of the order of 10^3. This range occurs because of one or any combination of the following reasons: 1) individual compounds within a class are present at concentrations that vary by many orders of magnitude; 2) differences in firing conditions caused a real change in the emissions; 3) analytical and sampling methodologies changed over the

Table IV. Chlorinated Benzenes in Stack Effluent From Coal-Fired Power Plants

Chlorobenzene Isomer	Concentrations ng/M³
1,2-Dichloro-	0.5
1,3-Dichloro-	ND[a]
1,4-Dichloro-	80
1,2,3-Trichloro-	3.9
1,2,4-Trichloro-	1.2
1,2,3,4-Tetrachloro -	ND
1,2,3,5-Tetrachloro -	ND
1,2,4,5-Tetrachloro -	ND
Pentachloro-	ND
Hexachloro-	ND

[a] ND = Not detected at limit of 0.03 ng/M³; average of three runs.

Table V. Summary of Compounds in Vapor and Particle Effluents From the Combustion of Coal and Coal/RDF

Compound Class	Number Identified	Estimated Levels[a] Vapors (ng/M³)	Estimated Levels[a] Particles (ng/g)
Alkanes	18	10-1500	NM[b]
Aromatics	7	10-2000	10-90
PAHs	11	0.1-400	0.1-110
Acids	12	20-800	8-600
Phenols	6	5-7200	0.05-1100
CL Compounds	15	0.1-1000	1-16
O, N, P, S Compounds	11	70-2500	50-100

[a] From 26 combustion episodes over a four year period.
[b] NM = Not measured.

four-year duration of this project; and 4) the particle effluents include fly, grate and stack ash samples where the amounts vary considerably. Consequently, this summary table should be used only to get a very rough estimate of the kinds and amounts of compounds present in the vapor and particle effluents. Indeed, it was not possible to establish any differences in the kinds and amounts of organic emissions when the data from the 26 combustion episodes were separated into coal only and coal/RDF groups.

In addition to the rough estimate of emissions discussed above, the data in Table V can be used to show that the organic compounds in the stack effluents are emitted mostly in the vapor phase.

Sluice Water. There is a legitimate concern over the release of pollutants into the water environment following the utilization or

disposal of the huge amounts of fly and grate ash produced during the combustion of coal. Our studies were restricted to the investigation of the possible release of organic pollutants only when fly and grate ash are sluiced to settling ponds and retained there as a disposal site. The water in the settling pond was checked periodically for organic compounds known to be present at low concentrations on the ash.

None of these known components were detected in the water at the conservative limit of one ppB. Indeed, this pond water did not contain any gas chromatographable organic compounds at the detection limit of 0.1 ppB even though the well water used for sluicing contained multiple ppB levels of aromatic compounds indicative of the coal tar that had contaminated the aquifer (20). Thus, the ash effluents from coal combustion appear to adsorb rather than release organic compounds into the water.

This adsorption feature was examined in an experiment where water containing 20 to 50 ppB of five aromatic hydrocarbons was mixed with fly ash for ten minutes at a water to ash weight ratio of 10 to 1. In this short contact time, the fly ash completely removed the organic components; this is vividly illustrated by the two capillary column gas chromatograms shown in Figure 3. Going from left to right, the major peaks in the water sample prior to contacting the fly ash are indan, 3-methylindene, naphthalene, 1-methylnaphthalene and acenaphthylene. The effective adsorption is probably due to the active forms of carbon, aluminum and silicon expected to be present in fly ash. For organic compounds then, fly ash provided desirable clean-up rather than undesirable contamination of water.

Conclusions

Based on the results of this study, the following conclusions can be made:

1) Organic emissions quantified in this study are much lower in general than predicted from the literature.
2) Organic compounds in the various effluents from the efficient combustion of coal at power plants do not appear to be an environmental problem.
3) Under efficient combustion conditions, organic compounds in the fuel are destroyed.
4) No significant ground water contamination is expected to occur as a result of fly ash disposal and utilization.
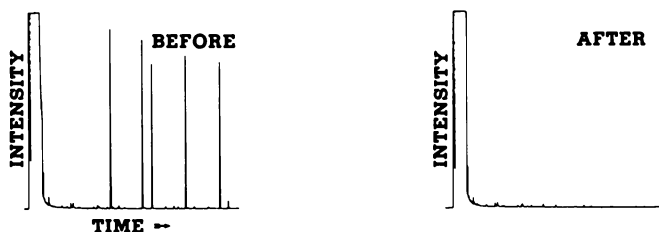
Figure 3. Gas chromatograms of water containing 20 to 50 ppB of five aromatic hydrocarbons before and after contact with coal combustion fly ash.

5) Additional work is needed on the identification and quanti-
   tation of organic emissions from coal combustion.
6) The low organic emissions from steady state combustion at
   power plants should not be extrapolated to small scale
   units such as woodstoves where the necessary conditions for
   efficient combustion are rarely achieved.

Literature Cited

1. Junk, G. A.; Ford, C. S. Chemosphere 1980, 9, 187.
2. Junk, G. A.; Jerome, B. A. Amer. Lab. 1983, 15, 16.
3. Junk, G. A.; Richard, J. J. In "Identification and Analysis of
    Organic Pollutants in Air"; Keith, L. H., Ed.; Butterworth Pub-
    lishers: Boston, MA, 1984, Chap. 5.
4. Klimisch, H. J. Z. Anal. Chem. 1973, 264, 275.
5. Klemm, L. H.; Reed, D.; Miller, L. A.; Ho, B. T. J. Org. Chem.
    1959, 24, 1468.
6. Cahnmann, H. J. Anal. Chem. 1957, 29, 1307.
7. Dinneen, G. U.; Smith, J. R.; VanMeter, R. A.; Albright, C. S.;
    Anthony, W. R. Anal. Chem. 1955, 27, 185.
8. Spitzer, T. J. J. Chromatogr. 1978, 150, 381.
9. Wise, S. A.; Bonnet, W. J.; May, W. E. In "Polynuclear Aromatic
    Hydrocarbons, Fourth International Symposium"; Bjorseth, A.;
    Dennis, A. J., Eds., Battelle Press: Columbus, OH, 1980, p.
    781.
10. Bjorseth, A. Anal. Chim. Acta. 1977, 94, 21.
11. Tomkins, B. A.; Kuboxa, H.; Griest, W. H.; Caton, J. E.; Clark,
    B.; Guerin, M. R. Anal. Chem. 1980, 52, 1331.
12. Hoffman, D.; Wynder, E. L. Anal. Chem. 1960, 32, 295.
13. Vick R. D.; Avery, M. J. "Extraction and Identification of Or-
    ganic Materials Present in Soot from a Natural Gas Flame"; Iowa
    State University Journal, IS-4329, 1978.
14. Lamparski, L. L.; Nestrick, T. J. Anal. Chem. 1980, 52, 2045.
15. Haile, C., Midwest Research Institute, personal communication.
16. Redford, D., US EPA, personal communication.
17. Richard, J. J.; Junk, G. A. Environ. Sci. Technol. 1981, 15,
    1095.
18. Sebastian, F. P.; Kronenberger, G. F.; Lombana, L. A.; Napoleon,
    J. M. Proc. Am. Ind. Chem. Eng. Workshop, 1974, 5, 67.
19. Joensen, A. L., Iowa State University, personal communication.
20. Burnham, A. K.; Calder, G. V.; Fritz, J. S.; Junk, G. A.; Svec,
    H. J.; Willis, R. Anal. Chem. 1972, 44, 139.

11

Emissions Sampling of Combustion Effluents from a Stationary Diesel Engine That Burns a Coal-Derived Liquid Fuel

W. Piispanen, P. Webb, and D. Trayser

Battelle Memorial Institute, Columbus Laboratories, Columbus, OH 43201

The emissions from a utility diesel engine burning a middle distillate Exxon Donor Solvent (EDS) coal liquid and diesel fuel (DF-2) were measured as part of a program designed to evaluate the feasibility of the use of coal derived fuels in utility diesels. The test program included various engine loads and EDS/DF-2 blend ratios. Also, higher and lower air manifold temperatures (AMT) were evaluated. The results indicated that an EDS/DF-2 blend of up to 66.7 percent EDS was usable in the engine. Full engine tests showed that the particulate emissions were increased with increasing amounts of the EDS fuel. The effect of EDS fuel on NO_x emissions was less clear. The SO_2 emissions were low and were unchanged by EDS/DF-2 blend ratios.

The purpose of this program was to define for utility diesel systems what engine and operating condition modifications might be necessary to accommodate the use of coal liquid fuels. Coal liquids (i.e., SRC II, EDS, etc.) have been shown to burn quite readily ([1,2]); however, certain of their known physical and chemical characteristics are likely to influence their suitability for engine use. Among these are:

o   Low cetane number
o   High flash and distillation points
o   High aromatic content
o   High nitrogen content
o   High sulfur content.

The low cetane number of coal liquid fuels could lead to poor starting and warm-up characteristics at low ambient temperatures and to engine roughness at part load operation.

In addition, low cetane fuels have been shown to result in increased combustion chamber deposits and higher smoke or particulate emissions.

A higher flash point might affect the safety of the fuel in storage but is not likely to influence engine operations. A higher distillation point, on the other hand, may lead to longer ignition delay, necessitating a change in injection timing, and poorer fuel vaporization and mixing of the injected fuel with the air charge in the combustion chamber.

The hydrogen content of coal is about 5 percent. In the conversion process (to liquid fuel) the partial hydrogenation increases the hydrogen content to about 10.6 percent for the EDS fuel. Petroleum-based distillate fuels have a hydrogen content in the range of 12 percent; however, the higher aromatic content in the raw coal generally results in an aromatic content in the coal liquid fuel, after hydrogenation, considerably higher than the petroleum fuel. This higher aromatic content could cause higher hydrocarbon and/or polycyclic aromatic (POM) emissions.

The emissions of NO_x from distillate oil fueled diesel generators represent a major air emission source. The use of synfuels presents an additional NO_x problem for diesel generators in that raw (unhydrotreated) liquids often contain significant levels of both sulfur and nitrogen with the heteroatom concentration increasing with boiling range. The fact that the EDS fuel has a low fuel nitrogen content (0.1 percent) could prove valuable in its use as a diesel fuel.

Manufacturers of diesel engines generally recommend that fuels which contain less than 0.5 percent sulfur be used in order to minimize corrosion problems. A typical diesel fuel has approximately 0.15 percent sulfur though there is a wide variation in different fuels. The use of EDS fuel with a sulfur content of 0.4 percent could present a possible problem with regard to both SO_2 and SO_3 emissions.

Technical Approach

For this program a Cooper LSV-16-GDT 16-cylinder, 4-stroke, turbocharged engine was used to evaluate various blends of EDS and a standard DF-2 fuel. The engine was owned and operated by a public utility company. Cooper Energy Services designed a test matrix for the evaluation of fuel blends at different engine operating conditions and supervised the actual engine test operations. Basically, three operating parameters were varied: the fuel blend ratio as EDS/DF-2, the air manifold temperature (AMT) and the engine/speed load conditions as kilowatts (kW) of electrical power at rated speed. In addition a specially designed sampling system was used to evaluate extreme blend ratios and test engine modifications applied to only one of the 16 cylinders. Baseline tests on the DF-2 fuel were made at the various test conditions for comparative purposes.

Sampling for gaseous emissions was conducted at two locations
of the engine exhaust. In one location a rake-type probe
with a heated sampling line was used to continuously withdraw
samples of the exhaust gas before it entered the silencer.
A special check-valve sampling probe was installed for alternative
single cylinder exhaust gas monitoring. Provision for SO_2/SO_3
sampling was included in both sample lines. The sampling for
SO_2/SO_3 was by a controlled condensation system based on an
original design by Goksoyr and Ross (3), followed by a hydrogen
peroxide impinger train. This system is now referred to as
the Goksoyr-Ross train and methods for operation are documented
by both the U.S. EPA and the APHA.
        Sampling for particulates was by a standard EPA Method
5 probe and impinger train. The method was modified by adding
NaOH to the second impinger to allow determination of chloride
emissions. The Method 5 sampling was conducted at the outlet
of the silencer using two perpendicular sampling ports and
multiple point traverses. For the program, replicate tests
were conducted when feasible. Duplicate measurements were
made of SO_2 (EPA Method 6 and an NDIR instrument) and of NO_x
(EPA Method 7 and chemiluminescence instrument). Analyses
of particulate, SO_2/SO_3 and Cl were made onsite. All gas mon-
itoring instruments were zeroed and spanned daily using certified
span gases.

Test Results

Fuel Analyses. Prior to actual sampling the fuel blends were
analyzed by Southwest Research Institute (SWRI) and reported
in their report to EPRI on this project (4). The cetane number
of the fuel blends ranged from 49.6 for 100% DF-2 to 21.0 for
100% EDS. The higher heating value (HHV) ranged from 19,500
Btu/lb (for 100% DF-2) to 18,569 Btu/lb (for 100% EDS). The
nitrogen and sulfur content were variable but reported by SWRI
as 0.09 percent sulfur and 0.12 percent nitrogen. This sulfur
content is lower and the nitrogen is higher than most conventional
diesel fuels. The DF-2 sulfur content was also low at 0.15
percent. The H/C ratio of the EDS was somewhat lower than
the DF-2 (approximately 0.11 compared to 0.16), indicating
a higher degree of aromatic constituents.

Baseline Tests. Baseline diesel tests were conducted at constant
speed (360 rpm) and four generating loads, No Load, 1800 kW,
2600 kW, and 3600 kW. All tests were conducted at 110° F AMT
except for the 3600 kW condition which also included 150° F
AMT and 95° F AMT tests. The results of particulate emissions
testing at four conditions of 0 Blend are listed in Table I.
The results include both the 95° F AMT and the 150° F AMT tests
which indicate the observed reduction in particulate emissions
with increased AMT.

Table I.   Baseline Test Particulate Emissions

Load (kW)	AMT (°F)	Fuel Rate (Btu/kWhr)	(lb/MM Btu)	(ng/J)
2,650	110	9,950	.018	7.7
3,570	110	9,910	.028	12.0
3,590	149	10,010	.016	6.9
3,590	95	9,900	.028	12.0

The gaseous emissions were comparable to those reported in other tests of diesel generators burning No. 2 diesel fuel (5). The O_2 ranged from 10.8 percent at 3600 kW to 18.2 percent at FSNL (Full Speed No Load). As expected, the CO_2 increased with load. The CO was slightly higher than expected, up to 195 ppm at 3600 kW, indicating less than optimum performance. The SO_2 concentrations were low, reflecting the low sulfur content of the fuel.

Gaseous Emissions from Blend Test.   Tests were conducted for the various blend ratios and load conditions. The results from the stack emissions measurements for the full engine tests are summarized in Table II. This table provides averages for each engine load condition as measured at the baseline fuel condition and for the three blend ratios. As was observed in the baseline tests, the CO_2 increased with engine load while O_2 decreased. There was no observed effect of blend ratio on SO_2 emissions, although SO_2 did increase slightly with increasing load as would be expected. The NO_x, when corrected to 15 percent O_2 (dry), showed a significant increase as load was increased to 1800 kW and then a more gradual increase up to the maximum load of 3600 kW. The results of gaseous monitoring for the baseline and maximum blend tests at AMT of 95°F and 150°F are included in Tables III and IV. The 3600 kW baseline emission tests for 95° F and 150° F AMT were comparable to the 110° F AMT tests. The gaseous emissions showed no significant changes between operating temperatures except that the corrected NO_x appeared to increase slightly at 110°F AMT compared to 95°F. The maximum blend tests were both slightly higher than the 110° F AMT 0 blend but an additional test at 2600 kW and 150° F AMT showed a corrected NO_x value of 946 ppm which was below the 110° F AMT value.

Particulate Emissions from Blend Tests.   The stack particulate emissions for the baseline and three blend ratios were measured. The effect of blend ratios on the particulate emission rate is shown graphically in Figure 1. In this representation the percent increase of the particulate emission rate over the baseline value for the various blend ratios is plotted for the two higher engine loads at 110° F AMT.

The effect of blend ratio on the particulate emissions is significant. The increase in the rate over baseline is

Table II. Average Stack Gaseous Emissions Data Summary For Full
Engine Tests (From Reference 6)

Load (kW)	CO$_2$ (percent)	CO (ppm)	O$_2$ (percent)	SO$_2$ (ppm)	NO (ppm)	NO$_x$ (ppm)	THC (ppm)
0 Percent Blend, AMT = 110°F							
FSNL	1.8	178	18.2	67	--*	453	206
1800	5.6	87	13.2	73	803	816	142
2600	6.2	93	12.0	72	833	983	153
3600	7.2	161	10.8	80	962	997	166
25 Percent Blend, AMT = 110°F							
FSNL	1.8	345	18.5	54	349	516	273
1800	7.8	105	13.3	60	766	835	155
2600	6.6	105	12.0	58	--	895	160
3600	7.2	175	11.1	55	--	1089	205
50 Percent Blend, AMT = 110°F							
FSNL	1.9	725	18.3	56	458	601	390
1800	6.0	110	13.0	56	--	907	117
2600	6.7	124	12.0	64	--	862	120
3600	7.4	162	11.0	62	--	1158	128
67 Percent Blend, AMT = 110°F							
FSNL	1.8	1200	18.5	50	388	540	750
1800	6.1	110	12.9	59	974	1007	108
2600	6.9	116	11.8	61	--	998	105
3600	7.3	170	11.2	62	--	1138	122

*Indicates data deleted due to malfunction of instrument.
Note: NO and NO$_x$ data are corrected to 15 percent O$_2$.

Source: Reproduced with permission from Ref. 6. Copyright 1983
Electric Power Research Institute.

Table III. Stack Emissions Data Summary For 3600 kW
at 95° F AMT

Blend (percent)	CO$_2$ (percent)	CO (ppm)	O$_2$ (percent)	SO$_2$ (ppm)	NO$_x$ (ppm)	THC (ppm)
0	7.0	145	11.0	82	894	140
67	7.0	115	11.5	70	1006	135

Table IV. Stack Emissions Data Summary For 3600 kW
At 150° F AMT

Blend (percent	CO$_2$ (percent	CO (ppm)	O$_2$ (percent)	SO$_2$ (ppm)	NO$_x$ (ppm)	THC (ppm)
0	7.4	170	10.5	71	858	185
75	7.2	130	11.3	67	1046	168
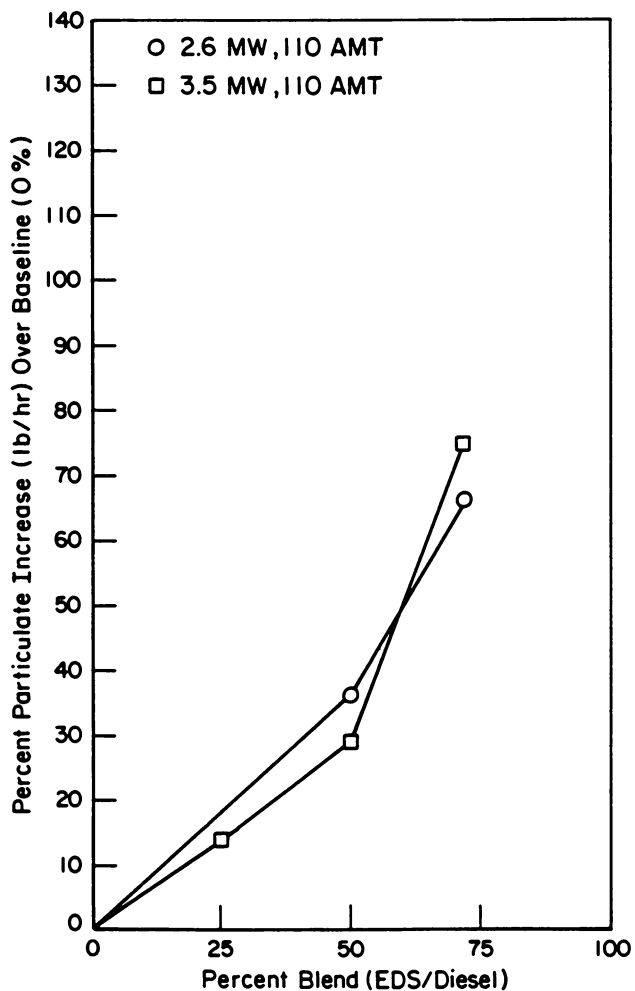
Figure 1.   Particulate mass rate increase as affected by blend
ratio, engine load, and AMT.

approximately the same for the two conditions load at 110°
F AMT. In terms of actual emissions rate based on mass of
particulate per heat input, the 50 percent blend at 2600 kW
and 110° F AMT was lowest (10.2 ng/J) while the 66.7 percent
at 3600 kW and 110° F AMT was the highest (20.9 ng/J). A test
of 75 percent blend at 3600 kW and 150° F AMT was observed
to have a lower particulate emission rate (16.1 ng/J) than
the reported highest value, and similarly a baseline test of
3600 kW and 150° F AMT showed a 42 percent lower particulate
emission rate than either the 95° F AMT or the 110° F AMT baseline
as shown in Table I. This suggests that increasing the AMT
may reduce the particulate emission rate.

Other Gaseous Emissions. Emissions samples for SO_3 and chlorides
measurements were also included in this program. In total,
12 samples for SO_2/SO_3 measurement were obtained; 6 were in
the stack location and 6 were in the single cylinder configura-
tion. No SO_3 was detected in any of the samples by the standard
titration with 0.02 N NaOH. In each of the tests for particulate
emissions conducted in this program, an impinger sample was
collected for Cl determination by AgCl gravimetric method.
In all cases there was no precipitate formation indicating
chlorides were less than the detectable limit.

Conclusions

The use of EDS/DF-2 fuel blends in utility diesels provides
an acceptable alternative of conventional petroleum-based fuel
operation. A blend ratio of approximately 66.7 percent EDS
and 33.3 percent DF-2 can be used without engine knocking at
an AMT of 110° F. At an AMT of 150° F this ratio can be extended
to 75 percent EDS. The major impact of the use of EDS blends
appears to be an increase in the particulate emissions rate.
The effect of EDS/DF-2 blends on particulate emissions was
significantly influenced by both blend ratio and engine load.
Increasing one or the other or both resulted in an increase
in the particulate emissions, though an increase in AMT may
reduce the particulate emission rates. No information on particle
size or morphology was obtained in this program.
      The results of the exhaust stack measurements of gaseous
emissions indicate that the use of EDS/DF-2 fuel blends under
engine load conditions resulted in a moderate increase in CO
emissions (25%) and a moderate decrease in THC emissions (26-31%)
when compared to baseline (0%) tests. The EDS/DF-2 fuel blends
all showed substantial increases in both CO and THC emissions
at the no-load condition.
      The emissions of NO_x from EDS blends are less than or
equal to the baseline over all engine loads except for the
maximum EDS/DF-2 blend where NO_x levels were slightly higher
at lower loads. A 150° F AMT slightly increased the NO_x for
baseline and the 66.7 percent blend at 3600 kW but lowered

the 2600 kW concentration. The overall average percent of
NO_2 in the NO_x at baseline conditions was approximately 9 percent.
Due to problems with the NO analyzer, the effect of AMT and
blend ratio on NO_2 could not be determined.

     There was little correlation between blend ratios and
SO_2 emissions, all of which were relatively low. Measurements
of SO_3 and Cl were below the expected lower limits and thus
the potential for corrosion should be minimal in the use of
EDS/DF-2 blends.

Acknowledgments

Literature Cited

1. Piper, B. F.; Hersch, S.; Nazimowitz, W. "Combustion
    Demonstration of SRC II Fuel Oil in a Tangentially
    Fired Boiler"; Report No. EPRI FP-1029, Electric
    Power Research Institute; Palo Alto, CA, 1979.
2. Downs, W.; Kubasco, A. J. "Characterization and
    Combustion of SRC II Fuel Oil", Report No. EPRI
    FP-1028, Electric Power Research Institute; Palo
    Alto, CA, 1979.
3. Goksoyr, H.; Ross, K. J. Inst. Fuel, 1962, 35, 177.
4. Ariga, S; Baker, Q. A. "Evaluation of Exxon Donor
    Solvent (EDS) Coal Liquid as a Utility Diesel Fuel";
    Report AP-3224, Electric Power Research Institute:
    Palo Alto, CA, 1983
5. Shih, C. C.; Hammersma, J. W.; Ackerman, D. G.;
    Beimer, R. G.; Kraft, M. L.; Yamada, M. M. "Emission
    Assessment of Conventional Stationary Combustion
    Systems: Volume II, Internal Combustion Sources,"
    U.S. EPA Report No. EPA-600/7-79-029C, 1979.
6. Piispanen, W.; Webb, P.; Trayser, D. "Emissions
    Sampling for Utility Diesel Synfuel Tests";
    Appendix B in Report AP-3224, Electric Power
    Research Institute: Palo Alto, CA, 1983.

RECEIVED March 31, 1986

12

Evaluation of Coal-Derived Liquids as Utility Boiler Fuels

David P. Burford and Steven M. Wilson

Research and Development Department, Southern Company Services, Inc., Birmingham, AL 35202

Over one million gallons of coal derived liquid fuel were tested at Mississippi Power Company's Plant Sweatt to determine their potential as viable replacements for liquid petroleum fuels. The six synthetic liquids [SRC-II (Middle Distillate), SRC-II (Full Range Distillate), H-Coal (Heavy), H-Coal (Light), H-Coal (Blend) and Exxon Donor Solvent] were combusted at various loads and burner configurations to determine optimum efficiencies, emission characteristics and supplementary operational requirements. A concerted effort to minimize NO_x emissions from the coal derived liquids by reducing combustion air and using burners out of service provided as much as 50% reduction in NO_x. Particulate emissions from the coal derived liquids were an order of magnitude less than those from No. 6 fuel oil. Overall, the synthetic fuels were more efficient, produced fewer emissions and were easier to handle than the No. 6 fuel oil normally used at the plant making them at least comparable as replacements for liquid petroleum fuels.

The synthetic fuels evaluation at Mississippi Power Company's Plant Sweatt is just one of a number of tests, sponsored by the Electric Power Research Institute (EPRI) under project RP 2112, to assess the potential of coal derived, liquid synthetic fuels as an alternative or substitute for liquid petroleum fuels. Specifically, the work done at Plant Sweatt examined the applicability of six liquid synthetic fuels to a full scale, wall fired utility boiler in terms of boiler efficiency and emission characteristics. EPRI sponsored testing with synthetic fuels at other sites included small scale combustors, a Combustion Engineering wall-fired utility boiler, a Combustion Engineering tangentially-fired utility boiler, a combustion turbine and diesel piston engines with generally favorable results.

    The testing at Plant Sweatt was sponsored by EPRI, Mississippi
Power Company (MPC) and Southern Company Services, Inc. (SCS).
EPRI also contributed 27,700 barrels of synthetic fuel to the test
effort. Due to funding constraints, the intensive testing of the
coal derived liquids could not be maintained for the entire
project. Therefore, the first phase of the testing on three of the
fuels was considered the "Intensive Test Matrix", while the last
three coal derived liquids were examined under normal plant
operation and are referred to as the "Longevity Tests".

Objectives

The objectives of the test were to:

- Demonstrate the use of coal derived liquids as potential
  substitutes for petroleum fuel oil in a full scale, wall
  fired utility boiler.
- Assess the potential for minimizing nitrogen oxide (NO_x)
  emissions from the six, high fuel-bound nitrogen liquids.
- Obtain data on the quantity and composition of other
  emissions from the combustion of the synthetic fuels such
  as particulate loading, particulate morphology,
  hydrocarbons, chlorides and flue gas acid dew point
  temperature.
- Assess the future utilization of coal derived liquids as a
  ossible re lacement fuel for other existing boilers or as
  a design basis for new boilers.
- Compare and contrast the combustion characteristics of the
  two baseline fuels and the six synthetic fuels in terms of
  combustion efficiency, regulated emissions and fuel
  handling.

Facilities

Mississippi Power Company's Plant Sweatt is located on Valley Road,
approximately five miles south of Meridian, Mississippi, in
Lauderdale County. This station has two identical steam units
labeled 1 and 2 which were placed in service in 1951 and 1953,
respectively. Although rated at 40 MW, each unit is capable of
generating 49 MW and with the onsite 39.4 MW combustion turbine,
represent 4.5% of Mississippi Power's generating capacity. The
boilers are Babcock & Wilcox (B&W), balanced draft, front wall
fired units (2 vertical x 3 horizontal burner matrix) with welded
cases. Each is designed to produce 425,000 pounds of steam per
hour at 850 psig and 900°F. Both are currently fired on either
natural gas or No. 6 oil and have no environmental controls of any
type. While this plant is normally restricted to providing peaking
capability during the summer, arrangements were made to isolate
Unit 1, the test unit, from economic dispatch and to set load based
on testing requirements from September 1983 through December 1983
to accommodate the project schedule.

Project Organization

The project at Plant Sweatt was organized with Southern Company
Services as EPRI's prime contractor responsible for project
management, project direction and subcontractor performance.
Subcontracted to Southern Company Services were Babcock & Wilcox
(B&W) and KVB. B&W provided technical consultation and boiler
performance evaluations, KVB provided combustion gas emission
characterizations and supplementary technical consultation.
Although not directly subcontracted to SCS, Radian, Inc. provided
fuel logistics support and Control Data Health Care Services (now
W. J. Keane and Associates) assisted with the industrial hygiene
program as part of the multi-site EPRI work with synthetic fuels
(RP 2112).

Plant Modifications

Before testing could begin in September of 1983, minor
modifications to Plant Sweatt were required to accommodate the
objectives of the work. Five areas were addressed:

   1)   Fuel forwarding system
   2)   Rail transloading site
   3)   Burner air registers
   4)   Exterior ductwork
   5)   Industrial hygiene program support

   The well documented aggressiveness of synthetic fuels toward
rubber-based gasketing material dictated the design of a redundant
fuel forwarding system of predominantly welded joints. The few
joints that were gasketed were done so with Flexitalic gaskets
(asbestos/metal) which are resistant to degradation from contact
with synthetic fuels. This redundant fuel system allowed Unit 1 to
operate concurrently on natural gas and a liquid fuel in any
configuration. It also provided the flexibility to transition
online from liquid synthetic fuel to either baseline fuel at the
burner front should Plant Sweatt have been needed for a production
type emergency. This redundant fuel system was designed to provide
the same liquid pressures and flow rates to the existing Racer
burner components at the boiler front as in normal No. 6 fuel oil
operation. Four, 7800 gallon commercial fuel hauling trailers
provided the onsite surge capacity for storing synthetic fuels and
were manifolded into the synthetic fuel forwarding system. When
emptied, each trailer was pulled out for refilling at the rail
transloading site.
   The six synthetic fuels were delivered to Plant Sweatt in
23,500 gallon "jumbo" railcars from their various origins. These
cars were temporarily sited on Illinois Central & Gulf Railways
Okatibbee siding approximately 1/4 mile from the plant. This
railsiding was the location for the second set of modifications.
An area approximately 200'x20' was graded and paved to support the
transloading operation from railcar to trailer. Curbing and a
drainage sump were included to contain any spillage. The trans-
loading was done with the fuel transporter's tractor power-take-off

pump, gravity fed from the railcar's bottom discharge. Fuel
transloading was a continuous process during testing over 25 MW due
to synthetic fuel consumption rates and the time constraint imposed
by incremental offloading at the remote railsiding.

The third area of modification was in the boiler windbox.
Although B&W had reworked the burners on Unit 1 in 1974, moderate
to severe warpage and misalignment were noted during the B&W Field
Service Engineer's inspection in November of 1982. Consequently,
the air register vanes in all six burners were replaced and
individually aligned for reliable air flow control. Partial
shrouds were also added around each burner to augment the control
of combustion air flow.

Corrosion penetrations in the flue gas ductwork downstream of
the air preheater necessitated the replacement of some ductwork as
the fourth modification. Although air inleakage on the suction
side of the ID fan was not operationally troublesome, any dilution
of the flue gas upstream of the proposed emission extraction grid
would bias the analytical results in measuring combustion
emissions. When this ductwork was replaced, an access platform for
the sampling crews was added around the flue gas extraction ports.

The last area of modification actually took place in several
locations around the plant to support the industrial hygiene
program. First, the plant employee locker room area was subdivided
into a clean side/dirty side concept similar to that found at
nuclear installations. All equipment or personnel involved in
synthetic fuel handling were segregated on the dirty side. In
order to pass to the clean side where street clothing was stored,
personnel were required to take a shower at the end of their
shift. A daily change of coveralls and laundry service were also
mandatory for synthetic fuel handlers. Personnel involved in the
testing were given baseline medical examinations and classes on
personal hygiene as a part of the project philosophy of "no
contact" with the synthetic fuels. Personnel not involved in
handling the synthetic fuels were denied access to those areas
where spills and contamination were most probable; the redundant
fuel system/trailer pad, the boiler front, the rail transloading
area and the dirty side locker room. Barricade tape and signs were
appropriately placed as a reminder. In order to contain any large
spillage, the stationary trailer pad and the rail transloading area
were paved and curbed. Fuel handling personnel were equipped with
hard hats, eye protection, face masks with organic vapor filters,
coveralls, a bib rainsuit, and elbow-length gloves. Individuals
were reimbursed at the end of the project if their work boots were
found to be contaminated. Fortunately, no major spills or gross
contamination occurred during the four months of testing.

Test Plan

Six synthetic fuels from three major research firms were provided
by EPRI for testing at Plant Sweatt:

- Gulf Research/Tacoma, Washington [DOE/OR/03055-72, Feb 82]
    Solvent Refined Coal-II (Full Range Mixture)
    Solvent Refined Coal-II (Middle Distillate Fraction)

- Ashland Oil/Catlettsburg, Kentucky [DOE/ET/10143-T37, Apr 84]
        H-Coal (Light Fraction)
        H-Coal (Heavy Fraction)
        H-Coal (Blended Mixture, 3:1 Light:Heavy)
- Exxon Research/Baytown, Texas [DOE/ET/2893-12, Nov 83]
        Exxon Donor Solvent

Mississippi Power Company provided both baseline fuels:
        Natural Gas
        No. 6 Fuel Oil

In satisfying the test objectives, it was necessary to "test" the single gaseous fuel and seven liquid fuels on as common a basis as possible for a meaningful comparison. Generally, the areas of investigation were:

    1) Limits of operability
    2) Operability at repeatable conditions
    3) Adaptability for combustion optimization.

The test points contemplated were based on each fuel's "smoke point" as the boundary between complete and incomplete combustion. Smoke point was operationally defined as the measured flue gas excess oxygen level at which drastic upswings in carbon monoxide (normally $\leq$ 30 ppm) and opacity (normally $\leq$ 15%) were noted on B&W and KVBs instantaneous monitors. This specific oxygen level is a function of each fuel's molecular composition and the boiler's particular combustion dynamics. It may also be influenced by burner type, tip placement, combustion air distribution, fuel viscosity/atomization and other adjustable factors. By operating just above the smoke point, the combustion losses associated with heating excess combustion air are minimized, thus raising boiler efficiencies. Three test points for each liquid fuel were originally established based on that fuel's smoke point:

    1) Smoke Point

    2) Low Excess Air - "LEA"
        Smoke point plus 0.5% excess oxygen in the flue gas

    3) Normal Excess Air - "NEA"
        Smoke point plus 1.0% excess oxygen in the flue gas

    4) High Excess Air - "HEA"
        Smoke point plus 2.0% excess oxygen in the flue gas

A fifth test point was also established later to give the test results commonality at one excess oxygen level. This last test point was set at the comparable excess oxygen level found for the baseline liquid fuel (No. 6 fuel oil) known as the Oil Comparable (OC) test point. These five points were established with normal burners in service at three loads; 40 megawatts, 25 megawatts and 15 megawatts and again with burners out of service. This satisfied the three areas of investigation outlined earlier. Testing was

limited on occasion by unstable combustion or fan capacity. These
occurrences caused the early termination or omission of some tests
in the interest of safety.

Coal liquefaction processes are designed to clean coal
chemically by removing ash, sulfur and to a lesser extent, nitrogen
from a feed coal. The principal differences between the fuels
tested at Plant Sweatt and their petroleum counterparts are that
synthetic fuels have a higher carbon/hydrogen molar ratio (C/H,
0.76 versus 0.66 typically) and a higher fuel-bound nitrogen
content (0.44% versus 0.29% by weight typically). A high C/H ratio
in liquid fuels is sometimes an indication of the undesirable
tendency to form soot during combustion. However, soot formation
during the Plant Sweatt testing was not significant and normally
tracable to a plugged atomizer sprayer plate. Increased fuel-bound
nitrogen in coal derived fuels can serve as the precursor for
another currently regulated emission, nitrogen oxides (NO and
NO_2 expressed as NO_x). One of the objectives of the Plant
Sweatt testing was to measure and reduce NO_x emissions through
combustion modifications. These modifications were limited to
operational changes to the combustion process within the boiler.
No additional low NO_x devices were installed or tested
(ie; selective catalytic reduction reactors). This was done to
examine the feasibility of "least cost" options for NO_x reduction
in existing liquid fueled boilers.

The combustion conversion of nitrogen to NO_x is dominated by
the oxidation of fuel nitrogen as opposed to the oxidation of the
elemental nitrogen from combustion air. Like any other chemical
reaction, this conversion can be stoichiometrically controlled by
limiting the availability of any of the reactants. To reduce NO_x
emissions at Plant Sweatt, the combustion was staged using the
technique of "burners out of service" (BOOS) which limits available
oxygen in the region of the burner flame where NO_x formation is
most likely. By optimizing each burner flame with air register
adjustments and then simply closing the fuel valve on selected
burners, the BOOS technique is accomplished. Burners remaining in
service (burners with fuel), are supporting combustion with minimal
amounts of oxygen since their relative fuel-to-air ratio increases
when fuel to other burners is shut off. This promotes the
conversion of fuel nitrogen compounds to N_2 rather than to
NO_x in the region of individual burner flames. Burners without
fuel (the BOOS) are contributing the balance of oxygen required for
efficient combustion by creating oxygen rich zones in the boiler
outside of the flame zone. The BOOS technique was complemented at
Plant Sweatt by operation at minimum excess air levels (LEA) as an
additional measure of NO_x reduction. The configuration of BOOS
that gave the least NO_x emission on each liquid fuel and each
load was determined by trial and error on the test unit. This
lowest NO_x BOOS configuration was then subjected to extensive
testing at the five excess air levels described earlier. It was
not desirable, however, to reduce NO_x emission rates at extreme
operating conditions if there were unacceptable consequences such
as increased particulate emissions or reduced combustion
efficiency. Although a primary objective of the project was to
maximize the reduction of NO_x, optimization of the combustion

conditions for efficient, environmentally acceptable operation was
a secondary goal in that it examined the potential for extended low
NO_x operation.

Data Acquisition

During the intensive test matrix, data acquisition at Plant Sweatt
was performed by Babcock & Wilcox and KVB. B&W used their
Computerized Boiler Diagnostic System (CBDS) programmed into a
Hewlett-Packard portable computer to gather and calculate boiler
operating data. This automated system was complemented by the
traditional checklist approach for non-automated control room
information. The CBDS recorded approximately 200 data points every
sixty seconds for refinement into single, ten-minute averages for
each test. Data measurement included extensive thermocouple grids,
differential pressure transmitters and extractive flue gas analysis
both before and after the air preheater. Instantaneous values
could be read on a CRT screen while scan values and averages were
permanently stored on magnetic disk. These averages were combined
later to provide a single, boiler efficiency value for each test.
B&W also calibrated the plant's combustion air flow orifice
readings with their Velocity/Pressure Averaging System (VPAS) prior
to testing.
     KVB acquired real time data on several emissions and gathered
many gaseous and particulate samples for later analysis. Included
in their matrix were the continuous monitoring of carbon monoxide,
carbon dioxide, excess oxygen, nitrogen oxides and sulfur dioxide.
Gas extraction sampling for sulfur trioxides and chlorides was done
intermittently as was measurement of acid dew point, particulate
loading, particulate morphology and particulate size
distributions. Testing for polycyclic hydrocarbons was not
successful due to errors in both sampling and analysis.
     During the longevity testing on the last three fuels, data
acquisition was done manually and with less frequency due to
constraints in funding and available manpower. Boiler efficiency
calculations for the longevity tests were done on the SCS Boiler
Performance Code (BPC) after BPC results were validated against the
B&W Computerized Boiler Diagnostic System. No data on particulates
were taken on these last three fuels for the reason stated above.

Results and Conclusions

Results on the first three synthetic fuels [SRC-II(Full range
mixture), H-Coal(Heavy fraction) and H-Coal(Blended mixture)]
indicate that all three have higher boiler efficiencies and
produced fewer emissions than the baseline No. 6 fuel oil and
required no preheating as does No. 6 fuel oil. Results of testing
on the last three synthetic fuels [SRC-II(Middle distillate
fraction), H-Coal(Light fraction) and Exxon Donor Solvent] indicate
comparable findings but lack the extensive investigation devoted to
the first three fuels. The burners out of service technique in
combination with reduced excess combustion air was very successful,
providing as much as a 50% reduction in NO_x levels. These coal
derived liquid fuels appear to be quite adequate as potential

replacements for petroleum liquids in existing units and should
certainly be considered in the design basis for utility boilers of
the future. These synthetic fuels offered definite advantages in
terms of emissions and handling properties. The only drawbacks to
the use of coal derived fuels are in their chemical aggressiveness
toward elastomeric materials and their uncertain potential for
human toxicity effects. Both problems should be surmountable
through simple design accommodations such as nonelastomer gaskets
and a 'closed' fuel forwarding system that limits personnel
exposure to the synthetic fuels.

Combustion efficiencies calculated for the test fuels ranged
from a low of 83.6% for natural gas at 15 MW to a high of 91.2% for
SRC-II at 25 MW (Figures 1 and 2). The efficiencies calculated for
all the coal derived liquids are on the order of one to two
percentage points higher than No. 6 fuel oil and five to seven
percentage points higher than natural gas. This is strongly
associated with the larger amount of excess combustion oxygen
required for natural gas and No. 6 fuel oil to operate above their
smoke points and the relatively higher hydrogen content of these
baseline fuels. Both conditions serve to reduce the heat available
for absorption on boiler surfaces and hence, reduce boiler
efficiency. Table I indicates the relative 'need' for additional
combustion oxygen for each fuel as determined by the fuel's
smokepoint:

<div align="center">

Table I
Experimentally Determined
Ranking of Low Excess Air (LEA) Limits
(at 40 MW, 6 burners in service)

</div>

1)	2.7%	H-Coal(Heavy)	3)	3.0%	H-Coal(Blend)
	2.7%	H-Coal(Light)	4)	3.5%	SRC-II(Middle Distillate)
	2.7%	Exxon Donor Solvent	5)	4.0%	Natural Gas
2)	2.9%	SRC-II(Full Range)	6)	5.8%	No. 6 Fuel Oil

Nitrogen oxide emissions (quantitatively expressed as nitrogen
oxide, NO) from unoptimized coal derived liquid combustion were
higher than that of No. 6 fuel oil or natural gas (Figure 3).
This was anticipated since the relative nitrogen content of the
coal derived liquids is higher than either baseline fuel (0.44%
versus 0.29% typically). However, the combination of burners out
of service and low excess air reduced NO_x emissions from the
coal derived liquid as much as 50% in some cases (Figures 4 and
5). Table II lists some typical NO_x reduction results for the
intensive test matrix.

It is interesting to note that NO_x emissions from the
synthetic fuels could be lowered to the same level as the NO_x
emissions from optimized No. 6 fuel oil combustion. From another
perspective, optimized synthetic fuel combustion (LEA, BOOS)
resulted in considerably <u>less NO_x</u> than unoptimized No. 6 fuel
oil operation (HEA, no BOOS). In terms of regulatory compliance,
the BOOS technique was successful in lowering NO_x emissions to
levels below the New Source Performance Standard (NSPS) for coal
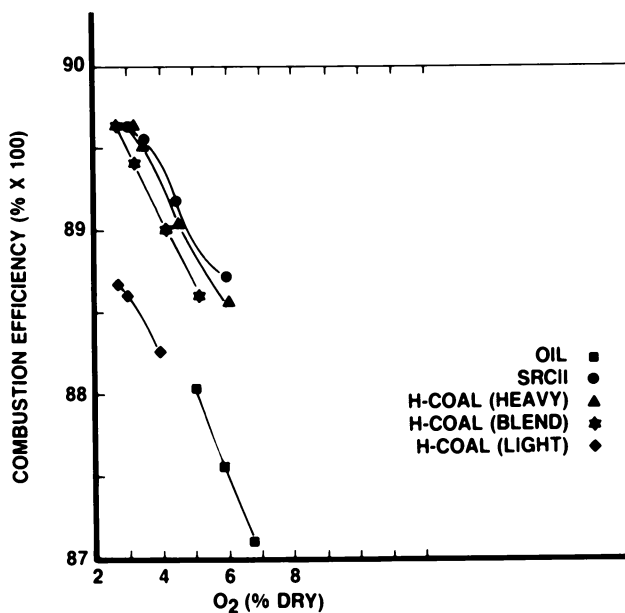
Figure 1. Liquid synthetic fuel combustion test; combustion efficiency vs. excess oxygen. 40 MW, 6 burners in service.
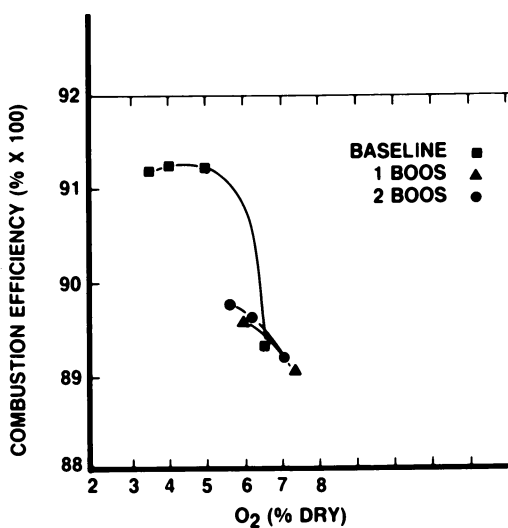
Figure 2. Liquid synthetic fuel combustion test; combustion efficiency vs. excess oxygen. SRC II Low NO_x at 25 MW.
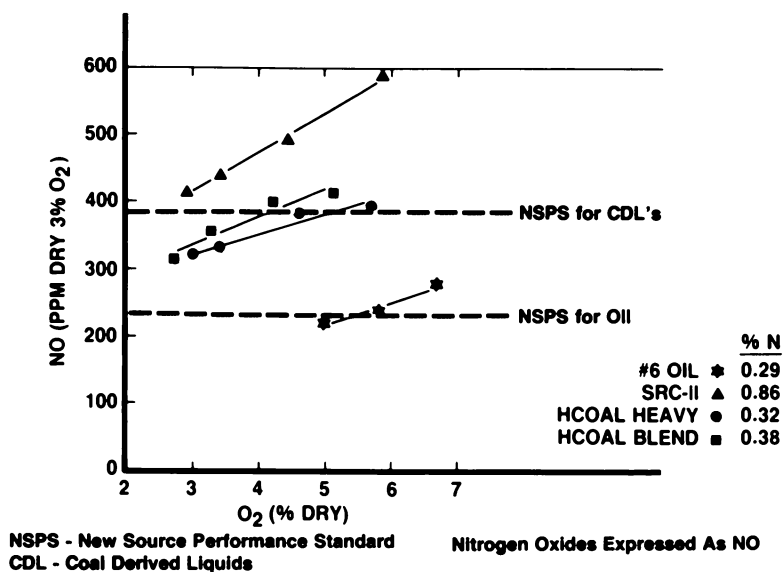
Figure 3. Liquid synthetic fuel combustion test; nitrogen oxides vs. excess oxygen. 40 MW baseline.
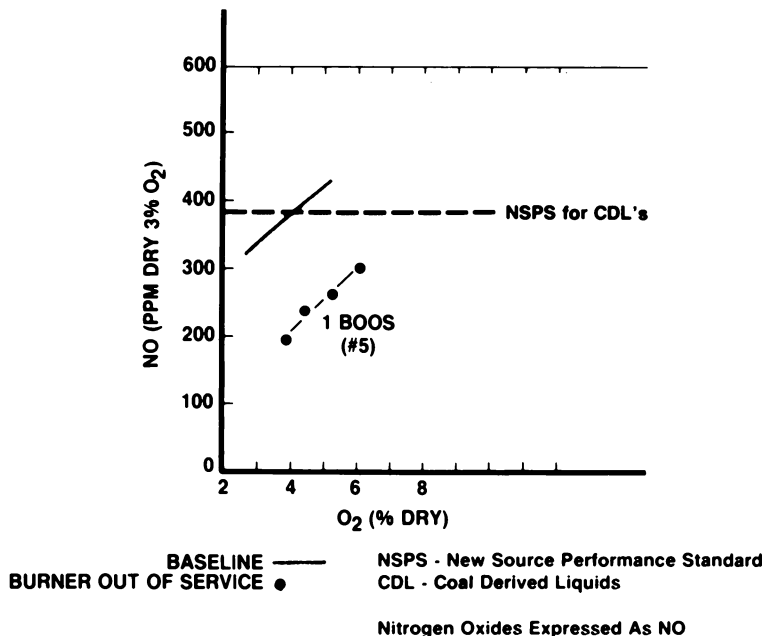
Figure 4. Liquid synthetic fuel combustion test; nitrogen oxides vs. excess oxygen. H-Coal (blend) low NO_x at 40 MW.

derived liquids (0.5 lb/10⁶ BTU, approximately 375 ppm) <u>and</u>
the NSPS for oil (0.3 lb/10⁶ BTU, approximately 225 ppm).

TABLE II
Selected NO_x Reduction Results

Fuel	Load	Burners	Excess O_2 Level	NO_x	% Reduction
SRC-II(Full Range)	25MW	no BOOS	HEA	403ppm.................	
					25%
		no BOOS	LEA	301ppm.....	53%
					37%
		2 BOOS	LEA	191ppm.................	
H-Coal(Blend)	40MW	no BOOS	HEA	398ppm.................	
					21%
		no BOOS	LEA	316ppm.....	51%
					30%
		1 BOOS	LEA	195ppm.................	
No. 6 Fuel Oil	40MW	no BOOS	HEA	275ppm.................	
					21%
		no BOOS	LEA	217ppm.....	33%
					15%
		1 BOOS	LEA	185ppm.................	

Particulate emissions from the synthetic fuels were very low,
on the order of 0.01 lb per million BTU, and approximately one
order of magnitude less than particulate emissions from No. 6 fuel
oil. Data on particulate morphology and submicron particle size
distributions indicate a unimodal size distribution for the No. 6
fuel oil and the SRC-II fuels while indicating a bimodal size
distribution for the H-Coals. Burners out of service and low
excess air (LEA) operation did not significantly contribute added
particulate emissions although it did tend to shift the unimodal
distributions toward a larger number of smaller particles.
Bimodal size distributions of the H-Coals showed little change at
reduce air conditions. Emissions of SO_2 from the coal derived
liquids were also quite low (with correspondingly low acid
dewpoints) as these chemically cleaned fuels contained only a
fraction of the sulfur normally found in petroleum liquids (0.15%
versus 2.29% typically).
One of the more interesting findings of the project was that
the coal derived liquids exhibited heat absorption profiles in the
Plant Sweatt boiler quite different from those associated with
conventional liquid fuels. With good repeatability, the coal
derived liquids gave furnace exit gas temperatures (FEGT)
approximately 250°F higher than those of comparable No. 6 fuel oil
tests (see Figure 6). These FEGT data were consistent between
coal derived fuels and were supported by calculated data showing a
simultaneous reduction in furnace heat absorption (see Figure 7).
This finding may be of some benefit to units that have difficulty
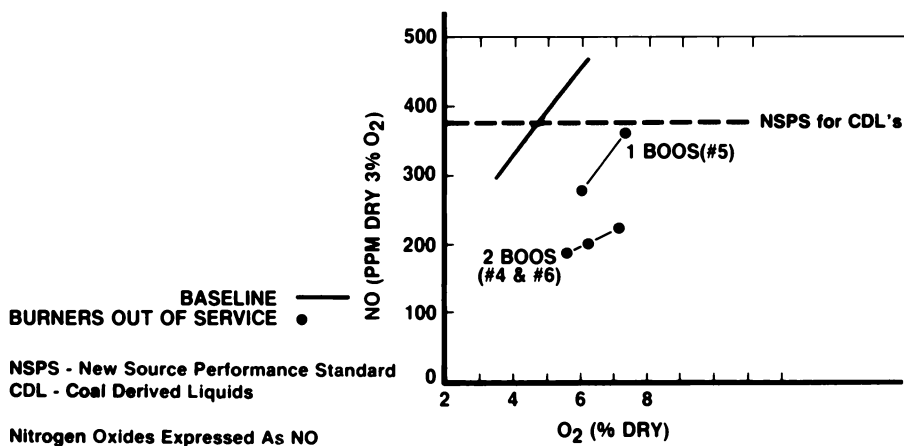
Figure 5. Liquid synthetic fuel combustion test; nitrogen oxides vs. excess oxygen. SRC-II low NO_x at 25 MW.
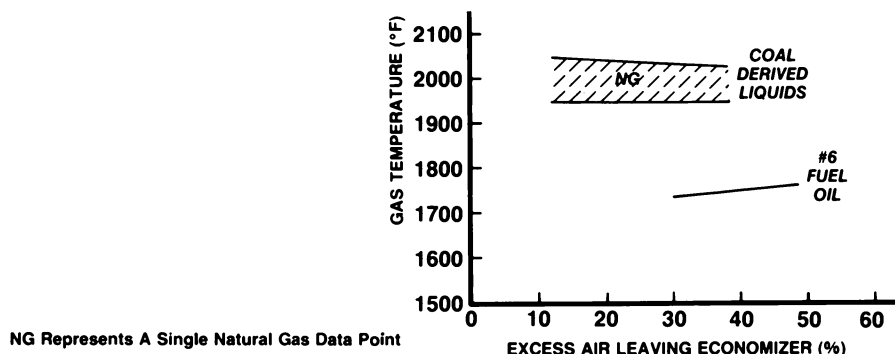
Figure 6. Liquid synthetic fuel combustion test; furnace exit gas temperature vs. excess air. At 40 MW.
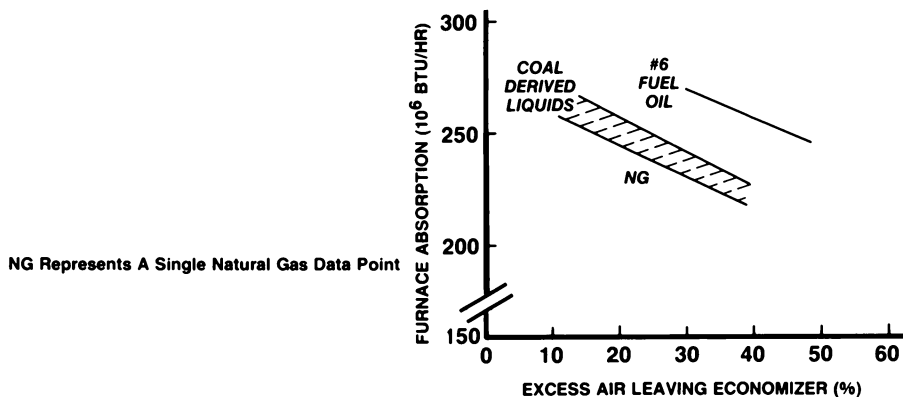
Figure 7. Liquid synthetic fuel combustion test; furnace absorption vs. excess air. At 40 MW.

reaching adequate superheater steam temperatures. The heat
absorption profiles at Plant Sweatt were also different from the
profiles recorded at other coal derived liquid test sites
indicating a strong dependency on individual boiler design and
combustion dynamics (see EPRI AP 3360 and AP 3986). The
difference, however, was not large enough to indicate a need for
changes in design or metallurgy in most existing boilers.

Although it would not be the method of choice at a unit
committed to synthetic fuel use, it was logistically necessary to
handle the coal derived liquid fuels in an incremental manner at
Plant Sweatt. Since there is still much to learn about the health
effects of these chemically altered, aromatic hydrocarbon liquids,
fuel handling was conducted in an extremely cautious manner and
followed the project guideline of "no human contact" with the
synthetic fuels. The project's personal hygiene requirements for
individual protection (clothing changes, restricted areas, and
mandatory raingear/facemask/gloves) proved to be a bit burdensome
but were not difficult to enforce. At a plant designed
specifically to use synthetic fuels, the potential for contact
with the fuel could be minimized through bulk liquid storage,
welded pipe joints, dry disconnect couplings and backflushing
filters. This would limit potential spillage (and human contact)
to normally infrequent fuel transfer operations and emergencies.

Overall, the consensus of the participants is that any of the
six coal derived liquids could be considered as an acceptable
replacement for liquid petroleum fuel in either Plant Sweatt
boiler with no equipment modifications, equipment additions or
environmental variances. The application or replacement usage of
these coal derived liquids in other utility boilers would not seem
to be any more difficult but should be prefaced by an extensive,
individual site assessment of candidate units. The few
modifications required at Plant Sweatt indicate that a limited
number of design criteria would be affected if these six synthetic
liquids were to be included in the fuel specifications of future
utility boilers. The handling and emission characteristics of coal
derived liquids may even be preferable to certain petroleum
liquids in some utility applications.

All the data reported here have been further reduced and
analyzed in EPRI report number AP 3985 (published in September,
1985). Copies of this five volume document are available to the
public through the EPRI Research Reports Center/Box 50490/Palo
Alto, California 94303, [(415) 956-4081]. Further specific
inquiries on the Plant Sweatt work can be made to the authors at
Southern Company Services, Inc. or to Mr. Henry Schreiber of the
the Advanced Power Systems Division of the Electric Power Research
Institute. No further work on coal derived liquids is currently
planned for Mississippi Power Company's Plant Sweatt at this time.

RECEIVED April 2, 1986

13

Research Strategy for the Development of Flue Gas Treatment Technology

Charles J. Drummond and Douglas F. Gyorke

Pittsburgh Energy Technology Center, U.S. Department of Energy, Pittsburgh, PA 15236

A discussion of the commercialization of advanced technology to control emissions from the combustion of coal for the production of electricity is presented. A historical summary of the development of flue gas treatment technology, some approaches to process development, the factors affecting the success of new flue gas treatment concepts, and a general strategy that may be applied to the development of these new concepts are provided. The scrubbing of utility flue gas is a relatively new practice. Even though the first application of flue gas scrubbing for sulfur dioxide control occurred in London, England, in 1933, the application of this technology to coal-fired utility boilers in the United States did not begin until the 1970's. The difficulty in controlling emissions from coal-fired utility boilers lies in the tremendous volume of flue gas to be treated. The scale is so large, and the capital and operating expenses are so great that utility companies enter into flue gas treatment with great caution. Most newly conceived flue gas treatment systems do not advance beyond laboratory or small-scale pilot testing. Factors affecting the success of these new concepts are capital equipment costs, operating costs, system reliability and performance, and waste disposal requirements. The acceptance of a novel flue gas treatment technology requires that confidence in system reliability be built through intense, large-scale testing.

Emissions from the combustion of fossil fuels have become an increasing concern to society over the past several decades. The amounts of sulfur dioxide, nitrogen oxides, and particulates placed

in the atmosphere by combustion processes have necessitated plans
and systems to alleviate the problems associated with these
pollutants. The billions of dollars spent over this time period on
legislation, research, development, and application have made an
impact on the problem. Yet the potential for pollution resulting
from the projected future use of fossil fuels, in particular coal,
provides the impetus for commercialization of advanced technology
to control these emissions. The search continues for low-cost
solutions to the problem.

   The path to commercialization for flue gas cleanup processes
is difficult; of 189 processes under development, only 10 processes
can claim 100 MW(e) or greater of total flue gas desulfurization
capacity (1). In light of the magnitude of the problem, and the
current costs of its solution, it is worthwhile to review the
reasons for these successes and failures. Examination of the
strengths and weaknesses of current process development practices
may suggest a more efficient research path for the future.

Background

Satriana (2) provides a summary of the development of flue gas
treatment technology. The first commercial application of flue gas
scrubbing for sulfur dioxide control was at the Battersea-A Power
Station [228 MW(e)] in London, England, in 1933. The process used
a packed spray tower with a tail-end alkaline wash to remove
90 percent of the sulfur dioxide and particulates. Alkaline water
from the Thames River provided most of the alkali for absorption.
The scrubber effluent was discharged back into the Thames River
after oxidation and settling. A similar process was also operated
at the Battersea-B Power Station [245 MW(e)] beginning in 1949.
The Battersea-B system operated successfully until 1969, when
desulfurization efforts were suspended due to adverse effects on
Thames River water quality. The Battersea-A system continued until
1975, when the station was closed.

   In an effort to avoid discharge of scrubber effluent into the
Thames River, Imperial Chemical Industries, Ltd., British Power
Authority consultants, and the Howden Construction Company together
developed the ICI Howden process, a closed-loop, lime-based system
for the removal of sulfur dioxide. This process was installed at
the Swansea Power Plant in 1935 and at the Fulham Power Plant in
1937. Both systems operated successfully until their shutdown
during World War II.

   A flue gas desulfurization (FGD) unit using tidal water to
absorb sulfur dioxide from zinc smelter tail gas was installed in
1949 in Tasmania. In 1952, the first unit of the Bankside Power
Station in London installed an improved version of the Battersea
system, again using water from the Thames River to provide alkali
for absorption. The first large-scale application of flue gas
scrubbing using lime or limestone was installed in 1964, scrubbing
1.8 million cfm (actual) of waste gas at an iron-sintering plant in

Russia. This facility was followed closely by an installation at a large sulfuric acid plant in Japan in 1966.

In the United States, FGD research began with small-scale pilot studies conducted by the Tennessee Valley Authority (TVA) in the 1950's. In 1966, Combustion Engineering, together with National Dust Collector, developed a process based on dry limestone injection in the boiler. By 1972, the Combustion Engineering process had been installed on five boilers, but these installations proved inadequate owing mainly to boiler plugging, low sulfur dioxide absorption, and reduced particulate collection efficiency in the electrostatic precipitator.

In 1970, the Clean Air Act Amendments were adopted. This legislation provided for enforcement, by the United States Environmental Protection Agency (EPA), of sulfur dioxide emissions limits for power plants constructed or modified after August 17, 1971. This Act, together with efforts already under way, spurred extensive FGD research that was sponsored by the Electric Power Research Institute (EPRI), EPA, and TVA. These research efforts, together with work conducted by private equipment vendors, have significantly improved the reliability and efficiency of flue gas desulfurization systems using lime or limestone. As of January 1984, calcium-based, wet, throwaway systems (including lime, limestone, and alkaline-ash systems) accounted for 84 percent of existing and planned FGD capacity (1). Lime and limestone flue gas desulfurization systems are clearly the most successful of any process developed for the control of sulfur dioxide emissions from coal-fired electric power generating facilities.

In 1977, the Clean Air Act was again amended to require even tighter control of sulfur dioxide emissions. The increasingly stringent federal regulations and the high cost to construct and operate existing wet FGD units, together with the unique requirements of the treatment of flue gases from electric power generating facilities, have encouraged continued research on new flue gas cleanup processes.

Perspective

While the scrubbing of industrial waste gas has been practiced for 150 years, the scrubbing of utility flue gas is a relatively new practice (3). Stack gas scrubbing in industry is required because of the presence of toxic gases or hazardous levels of pollutants. These extremely hazardous materials require stringent control at an expense per unit volume of gas that is much higher than required for utility operations. However, utility boilers produce a tremendous volume of flue gas to be treated. A 500-MW(e) power generating facility produces approximately 2-million cfm (actual volume at 300°F) of flue gas that must be treated to remove relatively low concentrations of specific pollutants. This utility flue gas would contain 2000-3000 ppm (0.2-0.3 percent) of sulfur dioxide, 300-500 ppm of nitrogen oxides, and 1.0-1.5 grains of fly ash per cubic foot (actual) when a high-sulfur coal with 10-15 percent ash is combusted. By comparison, the total exhaust volume treated by 50 to 60 waste gas scrubbers at the Ford Cleveland Foundry is equivalent to the flue gas volume that would be produced by a 300-MW(e) utility boiler (3).

A recent estimate of the potential reduction in sulfur dioxide emissions that could be achieved by applying current utility emissions restrictions to industrial boilers shows the great disparity in scale between these two applications. The emissions reductions achieved by applying these regulations to all industrial boilers with heat inputs greater than 100 million Btu/hr is equivalent to the total emissions of only five medium-sized utility boilers, each operating at the sulfur dioxide emissions limit of 1.2 pounds SO_2 per million Btu (4). This is less than 0.5 percent of current nationwide annual sulfur dioxide emissions. While certain economies of scale affect flue gas treatment for utility boilers, the scale is so large, and the capital and operating expenses so great that utility companies enter into flue gas treatment with great caution.

The federal clean air regulations for coal-fired electric power generating facilities provide for three levels of sulfur dioxide emissions control; the applicable regulation depends on when boiler construction was completed. For boilers completed before 1971, there are no federal regulations for sulfur dioxide or nitrogen oxides emissions. Coal-fired boilers constructed between 1971 and 1979 must reduce sulfur dioxide emissions to 1.2 pounds per million Btu or less, and nitrogen oxides emissions to 0.7 pounds per million Btu or less (5). Initially these regulations could be met solely by switching to coal with a sulfur level of 0.7 percent or less. The Clean Air Act Amendments of 1977 eliminated this solution by establishing New Source Performance Standards (NSPS) requiring coal-fired boilers that began construction after September 1979 to incorporate flue gas treatment to control sulfur dioxide emissions. If controlled emissions are between 1.2 and 0.6 pounds SO_2 per million Btu, these coal-fired utility boilers must achieve 90 percent or greater reduction of uncontrolled sulfur dioxide emissions. If controlled emissions are less than 0.6 pounds SO_2 per million Btu, these boilers require flue gas treatment to reduce uncontrolled emissions by 70 to 90 percent. The New Source Performance Standards of the Clean Air Act Amendments of 1977 also required more stringent control of nitrogen oxides to a level equivalent to 0.6 pounds per million Btu (5).

There are several approaches available to a utility to construct a boiler that will meet New Source Performance Standards. These approaches can be classified according to the position in the combustion system at which pollutant control technology is applied. Precombustion control involves removal of sulfur, nitrogen, and ash compounds from the fuel before it is burned. For coal combustion this approach involves the application of coal-cleaning technology. Combustion control relies on modifications to the combustion process itself or the addition of material to the combustion process to reduce pollutant formation or capture the pollutants formed in the combustion chamber. Examples of combustion control include staged combustion, boiler limestone injection, and fluidized-bed combustion with limestone addition. Post-combustion control involves removal of pollutants after they have been formed but before they are released into the atmosphere. Traditionally, flue gas desulfurization has meant the application of post-combustion control either alone or in conjunction with another

approach. Thus, emissions control may include any one or a combination of all of the above approaches depending on the specific requirements of the operating boiler or plant. From the perspective of the utility company, adherence to emissions regulations is a matter of minimizing costs and complexity to do the job.

Approaches to Process Development

There are many advantages and disadvantages to each newly conceived process that affect its commercial success. Most of these advantages and disadvantages are not unique to any one system but may be characteristic of a certain class of processes. In the development of new flue gas treatment processes, a design philosophy must be chosen that combines the most advantageous system elements in one process concept. Classification of common system elements, such as the reagent used, the eventual disposition of the pollutant, or the moisture content of the spent reagent, can aid in determining the most desirable attributes of a new design.

Flue gas treatment systems can be classified as either wet or dry based on the moisture content of the treated flue gas and the spent sorbent. Wet systems completely saturate the flue gas with water vapor. These systems contact the flue gas with a liquid or slurry stream. Dry systems contact the flue gas with a dry or wet sorbent but never include enough water for complete saturation of the flue gas. Dry systems result in a dry product or spent sorbent material, while wet systems result in either a slurry or a sludge containing appreciable amounts of water.

Another classification of flue gas treatment systems is based on the final disposition of the sulfur-containing product. Of all flue gas treatment systems in commercial use today, 95 percent result in a throwaway sulfur compound ($\underline{1}$). The remaining processes include regeneration of the sorbent and produce a by-product stream. The regeneration process yields a more concentrated sulfur stream that can be used to produce a salable by-product, such as elemental sulfur, sulfur dioxide, or sulfuric acid. Credit from the sale of these by-products can recover part of the cost of regeneration but currently cannot provide full compensation for the higher capital and operating costs of most regenerable systems because of the low value of recovered sulfur compounds.

Flue gas treatment systems can also be classified in terms of the reagent used in the process. Limestone and lime are the two most commonly used reagents for flue gas desulfurization. This is mainly because of the low cost of these reagents, especially limestone. Low reagent costs and simplicity of design make flue gas treatment systems using lime or limestone the most economical of the systems currently available.

The path to commercial success of flue gas treatment systems involves several steps, each increasing in complexity and requiring more stringent testing of system integration and reliability. The initial step in the development of any flue gas treatment concept is laboratory testing of the fundamental chemistry of the process to verify essential elements of the system. Typically, larger bench-scale tests follow that include as many parts of the system as possible. Pilot-scale tests are then performed with successively increasing size and system integration. Demonstration of

the flue gas treatment process consists of the sustained operation of a single full-sized process train at a utility site. For systems of this nature, the treatment of flue gas produced by 100 MW(e) of power generation would provide a basis for the design of replicate systems. Final acceptance of the system by the utility industry may require years of operation sufficient to assess factors relevant to determining expected plant life and operability, such as erosion, corrosion, component fatigue, and catalyst deactivation (if applicable). Initial application of new processes on non-utility boilers may be required to obtain the required operating experience. As utility confidence is paramount, testing must be rigorous. Most newly conceived flue gas treatment systems do not advance beyond laboratory or small-scale pilot testing; as of January 1984, there were only ten commercial flue gas treatment systems in use on utility boilers of 100 MW(e) or greater capacity in the United States (1).

Factors Affecting Success

The single overriding factor affecting the success of a flue gas treatment system is the total system cost. All elements of a flue gas treatment system either directly or indirectly affect the total cost to own and operate the system over its expected life. These systems are not installed by utility or industrial companies to produce a profit but instead are often viewed as a drain on the resources of the company. The user of the technology is, therefore, interested in applying the most economical flue gas treatment system available.

Because process economics are paramount, it is worthwhile to look at the effect of each element on the total cost of a flue gas treatment system. There are major differences in capital equipment costs, operating costs, reagent costs, system reliability, waste disposal or regeneration requirements, and specific restrictions placed on the operation and design of the boiler for each flue gas treatment system. Similarly, each boiler installation has specific requirements for pollutant control that must be met by prospective flue gas treatment systems. Ultimately, the total cost of the system depends on the various advantages and disadvantages inherent in the chosen design, the impact of which can be found through further investigation of each factor affecting system cost.

1. Capital Equipment Costs: The initial investment made by a utility to control pollutant emissions is in the equipment comprising the flue gas treatment system. The amount of the investment in this equipment purchase is directly related to the size and complexity of the equipment itself. The vessels required in this application must be large because of the volume of flue gas that must be treated. Some equipment, such as spray dryers or absorbers, can be 20 to 50 feet in diameter, and spray towers can be over 100 feet in height. Considerable preparation must go into sizing these vessels properly in order to maximize gas-sorbent contact time and minimize scaling and other operational problems. Much of this equipment, especially in wet systems, must be constructed of costly corrosion-resistant materials. Elaborate valving systems must be set up to control flows to the system.

With the high cost of capital equipment in flue gas treatment systems, it is important to keep the amount of equipment to a minimum while maintaining the reliability of the system. Systems of high complexity, which are normally the case for regenerable systems, have more capital items and a high initial cost. In addition, the utility practice of financing capital charges over long periods of time (on the order of 30 years) increases the effect of these capital charges on the annual revenue requirement of the installation. Current discussions of legislation requiring the reduction of pollutant emissions from existing coal-fired electric power generating facilities require the consideration of additional factors in determining the most acceptable flue gas treatment system for a specific installation. Because of the shorter remaining life of these facilities (typically 15 years or less), capital investments must be recovered over shorter periods of time. This causes systems with a low capital cost to be preferred over higher capital cost systems even when operating costs are higher. In situations where existing facilities must be modified, the cost to replace existing equipment may be prohibitive. For example, the application of a spray drying or dry injection system to an existing facility should not overload existing dust control equipment nor should it require the replacement of an existing electrostatic precipitator with a baghouse.

2. Operating Costs: Once the flue gas treatment facility is in place, the company must incur the costs of operating it. Major contributors to the cost of operation are sorbent replacement or regeneration costs and waste disposal costs. In many systems the largest portion of the operating cost is the energy requirement of the system. For utility boilers, energy consumption by the flue gas treatment system is a drain on net boiler output, while for industrial boilers, this energy consumption cuts directly into profits because it requires additional purchase of electric power. The energy required in flue gas treatment systems is used to power motors and fans, and includes heat losses from the system. Most noteworthy of energy requirements in flue gas treatment systems are the fans required to overcome the pressure drop created by the system, and the energy required in some wet systems to reheat the flue gas for proper plume buoyancy. The energy consumed to overcome even a small increase in pressure drop is significant because of the large volumes of flue gas that must be treated. The typical energy required for a wet scrubber system amounts to three to five percent of the gross energy output from a boiler (6).

Other operating costs include the cost of maintaining the system, which depends on the system complexity and reliability. In applications to existing facilities, such as boiler limestone injection processes or dry injection processes, the boiler or certain boiler elements may require additional maintenance owing to their use in circumstances outside their original design. Water replacement requirements, which are large in some instances, add other costs to flue gas treatment systems. Many regenerable systems consume steam for regeneration. Water quality requirements for many systems prohibit the use of recycled water.

3. Sorbent Costs: These costs are actually part of capital or operating costs but because of their impact are worthy of discussion on their own. The actual cost of a sorbent for a flue

gas treatment system lies mainly in replacement costs. Sorbent replacement costs are affected by many factors, primary of which is the effectiveness or activity of the sorbent. While either lime or limestone may function as the sorbent in many flue gas treatment systems, the added shipping and replacement costs incurred by the relatively inactive limestone often somewhat compensate for the higher price of lime. In addition, some systems using relatively inactive sorbents such as limestone may incur additional costs due to additives required to enhance removal efficiencies. Sorbent replacement costs can often be reduced by sorbent recycle with or without separation of the unreacted sorbent from spent sorbent.

In some cases, however, sorbent costs are aggravated by other problems. While nahcolite (a mineral form of sodium bicarbonate) is effective for the removal of sulfur dioxide when injected directly into the duct, the mineral is only beginning to be mined commercially, which increases the costs associated with the supply of this mineral.

Many systems were designed primarily to remove only sulfur from the flue gas stream. In these cases, a second removal step must be incorporated in the facility if the removal of nitrogen oxides is required. This additional removal step can vary from burner modification to the application of selective catalytic reduction depending on the removal efficiencies that must be achieved. Other systems, such as those employing catalysts or supported metal oxide sorbents, are ideally designed for no sorbent or catalyst replacement. However, because of deactivation or sorbent attrition, some degree of sorbent replacement is required. In these systems, the initial sorbent or catalyst charge is basically a capital cost, and sorbent replacement costs are determined by the chemical or physical integrity of the catalyst or sorbent support.

4. <u>System Reliability</u>: The effect of system reliability on flue gas treatment system cost is greater than the cost of normal maintenance and can involve factors difficult to quantify. While the reliability of a system is directly related to its complexity, it can also involve specific operational problems inherent in each flue gas treatment system. Examples of these operational problems include the following: nozzle plugging, plenum erosion, and fly-ash buildup in spray-drying systems; slagging and fouling of boiler surfaces encountered in boiler sorbent injection; increased dust loading on particulate control systems for all dry flue gas treatment systems; corrosion and scaling in wet scrubbers using lime and limestone; and ammonium bisulfate formation in systems using ammonia.

5. <u>Waste Disposal and Sorbent Regeneration Requirements</u>: As discussed previously, flue gas treatment systems can be classified as either throwaway systems or regenerable systems depending on whether the spent sorbent must be disposed of or can be converted to fresh sorbent yielding a concentrated sulfur-containing stream. Most flue gas treatment systems operate as throwaway systems primarily because of the ease of operation and the lower cost of these systems. Credits from the sale of the by-products of regeneration (usually elemental sulfur or sulfuric acid) do not normally offset the capital and operating expenses associated with a regenerative system. Furthermore, owing to the size of flue gas treatment

systems, the amount of a chemical produced by a regenerative system could depress the price of the chemical and adversely effect the economics of the system.   For example, a single 500-MW(e) plant using one of several ammonia-based processes for the removal of sulfur dioxide would produce enough ammonium sulfate (a fertilizer) to supply 6 percent of the 1978 market (1).

A regenerable system brings added complexity to the flue gas treatment system, increasing capital and operating costs and concerns over system reliability.   Also, the increased space typically required for regenerable systems reduces their applicability for installation at existing facilities.

Throwaway systems are themselves not without problems. For many utility boilers, it is difficult to find enough land for proper disposal of the waste material produced.   For example, disposal of sludge from the 30-year operation of a scrubber system using lime or limestone on a 500-MW(e) boiler burning a medium-sulfur coal would require 200 acres for waste disposal ponds and dikes (1).   If this land is not available adjacent to the boiler site, there are additional transportation costs associated with disposal.   Indeed, some utilities must use regenerable systems because space is unavailable to handle the waste produced by throw-away processes.   In addition, special disposal techniques may be required for some sorbents.   All systems generating a sodium-containing waste material must include additional dikes and impermeable liners in the design of waste disposal facilities owing to the high solubility of the waste material.

Waste materials such as calcium sulfite are difficult to dewater and cannot support a load.   It is often desirable to stabilize such wastes before disposal.   Methods for the stabilization of these materials, such as oxidation of calcium sulfite to gypsum, have been developed.   In certain countries (such as W. Germany and Japan), waste materials like gypsum can be sold; however, this is not generally true in the United States.

All of the disadvantages of throwaway flue gas treatment systems can be lessened considerably by minimizing the amount of waste material produced.   This can be accomplished by the choice of an effective sorbent material and the use of sorbent recycle to increase utilization.   In turn, sorbent recycle can be optimized by the use of a separation process to remove the spent sorbent from unreacted sorbent.   As water usually contributes significantly to the mass of the waste produced, the dewatering characteristics of the waste material are important.   Efficient dewatering will not only minimize water losses but also reduce the disposal space required.

6.   <u>Restrictions Placed on the Boiler and Its Operation</u>: Many of the flue gas treatment system elements already discussed place restrictions on the boiler and its operation.   Some examples of flue gas treatment system requirements that could restrict boiler operations would be the necessity for flue gas reheat, the ability of the flue gas treatment system to follow boiler load, the increased dust loading of dry systems, and the increased size and complexity of the system.   In addition, many systems require a specific flue gas temperature for proper operation.   This temperature requirement determines the location where the flue gas is subjected to treatment, thus affecting the design of downstream

system components and the boiler. The effectiveness of flue gas treatment may place additional restrictions on the boiler and its operation, especially systems that cannot achieve 90 percent removal of sulfur dioxide. These boilers may be forced to burn low-sulfur coal to meet emissions standards. Moreover, ineffective or unreliable treatment systems may force the curtailment of electricity production because of an inability to meet emissions standards.

Sometimes the opposite is also the case, that is, the boiler itself restricts the type of flue gas treatment system that can be installed. Most electric power generating facilities have coal specifications required by the boiler design and the manufacturer's warranty. These sulfur and ash specifications are designed to optimize boiler performance and avoid fatigue of boiler materials. Boiler design and coal specifications can limit the type of system that can be applied. The construction date of a boiler determines the level of pollutant control required, and it also goes far toward determining the type of flue gas treatment system that can achieve this level of emissions control.

Research Strategy

It would be difficult to define the ideal flue gas treatment system that would perform optimally for all boilers under all circumstances. However, given a boiler and its specific criteria, an optimal flue gas treatment system would possess as many of the positive aspects of the elements described above as possible. Research funding applied in this area to obtain this optimal system would be best spent by improving flue gas treatment system performance for as many boiler-site combinations as possible. Toward this end, processes that are most broadly applicable to problems currently associated with emissions control in coal-fired electric power generating facilities become important candidates for future research.

In the development of new flue gas treatment processes or the improvement of existing processes, some general concepts may be applied. One important general area for research would include efforts to decrease sorbent costs. As discussed previously, sorbent costs are a significant portion of system operating costs. Research in this area should be directed toward increasing sorbent reactivity by the determination of optimal reaction conditions and toward improved sorbent preparation and handling. Sorbent effectiveness could be enhanced by the discovery and testing of sorbent additives that increase reactivity and utilization. The efficient use of less expensive sorbents (such as limestone or coal fly ash), perhaps together with additives, should be investigated and encouraged. Sorbent costs can also be cut by reducing sorbent losses. Research to reduce sorbent losses should be directed toward effecting the efficient separation of fresh and spent sorbent, investigating the effects of sorbent recycle, and reducing catalyst attrition or poisoning. An added advantage to reducing sorbent costs and increasing sorbent reactivity would be the greater applicability of these systems to electric power generating facilities using high-sulfur coal.

A related area of research would include efforts to reduce the water requirements of flue gas treatment systems. This would be especially important to the wet throwaway systems most commonly used today. Research to improve the dewatering properties of scrubber sludge could be combined with the development of techniques to separate spent and unused sorbent, thus reducing both water and sorbent consumption while also reducing the volume and mass of solid waste to be handled. The use of waste or recycled water in flue gas treatment systems would also reduce water needs. Improved sludge stabilization methods that also remove water could also lower costs associated with both waste disposal and water consumption.

Another general goal for research in this field would be the reduction of system complexity and the integration of environmental controls within the power generating plant. Even in relatively simple systems, additional reduction in system complexity would cut maintenance costs and increase system reliability. Research in this area could reduce capital costs for new boiler applications and permit cost-effective installation of emissions controls on existing facilities. Investigations of system optimization could minimize the number and size of the vessels required. The development of better gas-sorbent contacting methods could reduce the pressure drop and the size of the vessels associated with the treatment system and in turn reduce fan size and energy requirements. Studies to combine the removal of all pollutants of interest (sulfur dioxide, nitrogen oxides, and particulates) in one process should be pursued; while adding to the complexity necessary to remove an individual pollutant, an integrated process would in the final analysis reduce the total number of subsystems required to effect total pollutant control.

Dust control research could also reduce flue gas treatment system cost. Enhanced capabilities of electrostatic precipitators (ESP's) and baghouses would directly impact the reliability and increase the applicability of many flue gas treatment systems. Those systems requiring a clean (particulate-free) flue gas would be favorably impacted by research to develop efficient, effective, high-temperature dust control systems. The reliability of dry systems would be improved by research aimed at increasing the load on dust control systems while maintaining high efficiency. Particulate removal devices perform a dual function in dry flue gas treatment systems; they not only remove the spent sorbent material from the flue gas but also provide additional residence time for reaction. The energy requirements of all systems would be reduced through research to lower the power consumption of electrostatic precipitators and the pressure drop across baghouse systems while retaining their respective efficiencies.

Other research areas that could improve the effectiveness and economics of flue gas treatment are (1) the development of better instrumentation for system control and (2) the evaluation of superior corrosion-resistant materials. System optimization cannot occur without a good means of system control. Many existing flue gas treatment systems are particularly sensitive to instrument feedback and response. The ability to control closely the operation of these systems could enhance their effectiveness and reliability. The presence of water in flue gas treatment systems

creates a potential for corrosion. Corrosion in these systems is enhanced by the use of alkali sorbent materials. The development and use of corrosion-resistant materials and liners would improve system reliability and reduce maintenance costs.

The operability and reliability of processes using ammonia must also be studied. With the potential for increased ammonia use in these systems (in the selective catalytic reduction of nitrogen oxides and as an absorbent), research documenting ammonia emissions and the effects of ammonia on process equipment should be conducted. Furthermore, additional investigations should be performed to determine whether ammonium salts are formed and to document their effects on both the environment and the flue gas treatment system.

The acceptance of new technology requires that confidence in system reliability must be built through the intense large-scale testing of promising flue gas treatment systems. Such large-scale testing must be undertaken by both the public and private sectors at both utility and industrial boiler sites. The results of these tests must then be disseminated rapidly by all available means to utility companies, boiler manufacturers, and flue gas treatment process vendors. Responsibility for this research should be shared by all concerned.

The bench-scale experimentation and pilot-scale testing required to develop new flue gas treatment technology entail large expenditures. The funding sources available to meet this need are the state and federal governments, the combined utility industry through the Electric Power Research Institute (EPRI), and the major boiler and flue gas treatment system manufacturers. Each must play a productive role in the conduct of this research.

Summary

As society has become increasingly aware of the problems of air pollution, more stringent emissions controls have been required. The costs of controlling air pollutants are increasing with the degree of control required. New processes must be developed, or existing processes improved, to meet the challenge of stringent emissions controls efficiently and economically. The path toward commercialization of flue gas treatment processes can be long and costly. Eventual acceptance of a novel flue gas treatment system is based on the total cost of the system. Contributing to this total system cost are capital equipment costs, operating costs, sorbent costs, system reliability, and waste disposal or regeneration requirements. The effect that the flue gas system has on the boiler and its operation also contributes to the cost of the overall facility. While it would be ideal to reduce all costs associated with every boiler application, the most realistic and productive use of research funds would be to concentrate on investigations with the largest potential impact on the greatest number of coal-fired electric power generating facilities. The government, the utility industry, the boiler manufacturers, and the flue gas treatment equipment vendors can all play important roles, both individually and cooperatively, in the development of effective flue gas treatment processes.

Literature Cited

1. Behrens, G.P., G.D. Jones, N.P. Meserole, W.S. Seames, and
    J.C. Dickerman, "The Evaluation and Status of Flue Gas
    Desulfurization Systems," Electric Power Research Institute
    Report No. CS-3322, January, 1984.

2. Satriana, M., ed., "New Developments in Flue Gas Desulfuriza-
    tion Technology," Noyes Data Corporation, Park Ridge, N.J.,
    1981.

3. McIlvaine Scrubber Manual Volume 4, Flue Gas Scrubbing, The
    McIlvaine Company, Northbrook, Ill., October, 1978.

4. Catalano, L., "Industrial NSPS Likely to Force Scrubbing for
    SO_2 Reduction," Power, June, 1985, pp. 7-9.

5. Bromberg, J.P., Clean Air Act Handbook, "How to Comply with
    the Clean Air Act," Government Institute, Inc., Rockville,
    Md., 1983.

6. Yeager, K.E., "FGD Systems: History, Cost, and Retrofit,"
    Pollution Engineering, June, 1984, pp. 24-28.

Technical Analyses of a Wet Process for Flue Gas Simultaneous Desulfurization and Denitrification

S. G. Chang

Lawrence Berkeley Laboratory, University of California, Berkeley, CA 94720

The technical and economic aspects of wet flue gas
simultaneous desulfurization and denitrification
systems are presented so that their practicality for
utilization by utility industry can be assessed. The
emphasis is on the kinetics of the systems based on
the employment of ferrous chelates to promote the sol-
ubility of NO and the reactivity of NO with SO_2 in
scrubbing liquors. Analytical techniques are devel-
oped for characterizing reaction intermediates and
products. Alternative approaches and novel ideas that
could develop into a more efficient and cost-effective
scrubber system employing metal chelate additives are
discussed.

While the development of flue gas clean-up processes has been pro-
gressing for many years, a satisfactory process is not yet available.
Lime/limestone wet flue gas desulfurization (FGD) scrubber is the
most widely used process in the utility industry at present, owing to
the fact that it is the most technically developed and generally the
most economically attractive. In spite of this, it is expensive and
accounts for about 25-35% of the capital and operating costs of a
power plant. Techniques for the post combustion control of nitrogen
oxides emissions have not been developed as extensively as those for
control of sulfur dioxide emissions. Several approaches have been
proposed. Among these, ammonia-based selective catalytic reduction
(SCR) has received the most attention. But, SCR may not be suitable
for U.S. coal-fired power plants because of reliability concerns and
other unresolved technical issues (1). These include uncertain cat-
alyst life, water disposal requirements, and the effects of ammonia
by-products on plant components downstream from the reactor. The
sensitivity of SCR processes to the cost of NH_3 is also the subject
of some concern.
      The development of a process that is simple and can allow an ef-
ficient removal of both SO_2 and NO_x simultaneously in one system
could provide economical advantage. In the 1970's, the Japanese pursued

this approach and developed several wet flue gas simultaneous desulfurization and denitrification processes (2) which can be classified into two types.

The first type of process involves the injection of gaseous oxidant, such as ozone or chlorine dioxide, into the flue gas to selectively oxidize insoluble NO to the more soluble NO_2. Nitrite and nitrate ions are produced in the aqueous phase after NO_2 and/or N_2O_3 are absorbed into scrubbing liquors; and sulfite/bisulfite ions are formed when SO_2 dissolves in the solutions. Interaction between nitrite and bisulfite ions can take place (Figure 1) (3-7) to produce hydroxylamine disulfonate (HADS), hydroxylamine monosulfonate (HAMS), amine trisulfonate (ATS), amine disulfonate (ADS), sulfamate (SA), and hydroxylamine (HA). These nitrogen-sulfur compounds can be removed from the scrubbing liquors as potassium salt precipitates (2-8). The percentage of the absorbed NO_x converted to nitrate ion ranges from 10 to 50%. The two most common wastewater treatment methods for the soluble nitrate ion are evaporation and biological denitrification. Sulfate and sulfite ions can precipitate as calcium salts by reaction with lime/limestone. Processes of this type (2), such as Chiyoda, Ishikawajima-Harima Industries, Mitsubishi, Moretana Calcium, and Moretana Sodium, are in most cases simple modifications of commercially available FGD technology.

The second type of process is based on the addition of ferrous chelates to scrubbing liquors to enhance the absorption of NO by forming ferrous nitrosyl chelates in aqueous solutions (9-11). Ferrous nitrosyl chelate can then react with dissolved SO_2 to produce (12) N_2, N_2O, dithionate, sulfate and various nitrogen-sulfur compounds as mentioned previously, while some ferrous chelates are oxidized by reaction intermediates and residual oxygen in flue gas to ferric chelates, which are inactive. Therefore, this type of process requires regeneration of scrubbing liquors by removing dithionate, sulfate, and nitrogen-sulfur compounds from the solutions and reducing ferric chelates back to ferrous chelates. Processes such as Asahi, Chisso, Kureha, and Mitsui belong to this category (2).

Processes of both types were demonstrated to be highly efficient in SO_2 and NO_x removal (more than 95% for SO_2 and 85% for NO_x). However, these wet processes have not reached the commercial stage yet because they are uncompetitive economically, according to cost evaluation (13). These cost evaluations, however, were made based on design and knowledge available in the 1970's. Critiques (13) indicated that these wet processes were in their early stages of development, and with their maturation they could become competitive in cost. The major cost of the first type of process is associated with the requirement of costly gas phase oxidants. Significant amounts of corrosion-resistant material are required for this type of process, regardless of which oxidant is utilized. The development of cost-effective methods for the oxidation of less soluble NO to more soluble NO_2 is essential for the future of this type of process. An extensive review article on the kinetics and mechanisms of important reactions involved has been published by Chang et al. (3). The major cost of the second type of process is associated with the low solubility of NO, even in scrubbing liquor containing ferrous chelates, the oxidation of ferrous to ferric chelates by residual oxygen in flue gas, and the production of undesirable soluble products such

as dithionate ion and nitrogen-sulfur (N-S) compounds in the system.
The need to refurbish chelates for the loss in processing also con-
tributes to the costs.

A preliminary-level economic evaluation ($\underline{13}$) performed by EPRI
(Electric Power Research Institute) and TVA (Tennessee Valley Author-
ity) indicates that a combination of electrostatic precipitators (or
bag house), ammonia-based SCR system, and wet lime/limestone FGD
scrubber range between 20% to 185% cheaper than wet process for com-
plete control of particulates, NO_x and SO_2. The lower percentage is
for the second type and higher percentage for the first type of pro-
cess. Therefore, the second type of process appears to be more prom-
ising and will be the subject of further discussion in this paper.

Asahi process was chosen from among the second type processes
for the cost evaluation ($\underline{13}$). In the Asahi process, the flue gas
enters a packed-bed absorber where it flows countercurrent to a 6.3
pH sodium-salt scrubbing solution containing Fe^{2+} (EDTA). The liquid
effluent from the absorber is then pumped to a reducing tank where
Fe^{3+} (EDTA) is reduced by HSO_3^- to produce Fe^{2+} (EDTA) and dithionate
ion. Most of the scrubbing liquors leaving the reducing tank are re-
cycled to the absorber. Only about 10-20% of the liquor is pumped to
an evaporator system in the regeneration section. The concentrated
solution from the evaporators is then pumped to a cooling crystallizer
where hydrated sodium dithionate and sulfate crystals are produced
under vacuum. These crystals are separated from the mother liquor in
a screw decanter and sent to a dryer operating at 120-150 °C, in
which the hydrated crystals are converted to anhydrous sodium salts.
Most of the mother liquor from the decanter is recycled to the reduc-
ing tank and a smaller stream is passed through a N-S compounds treat-
ment section. The potassium salts of N-S compounds are separated in
a screw decanter and sent to a thermal cracker for the decomposition
at about 500 °C.

The high capital investment cost of the Asahi process is due to
the necessity for large absorbers, evaporators, crystallizers, dryers,
rotary kiln crackers and screw decanter separators. The major oper-
ating and maintenance costs are electricity, fuel oil, steam and
chemicals such as soda ash, EDTA and limestone. The requirement for
consumption of large amounts of utilities is associated with the oper-
ation principle and design of the Asahi process. According to the
economic evaluation, equipment required for NO_x and SO_2 absorption
(such as packed-bed absorbers) accounts for 20% of total direct cap-
ital investment; for treatment of dithionate ion (such as evaporator,
crystallizer, dryer, and cracker) it accounts for about 40%; and for
treatment of nitrogen-sulfur compounds (such as screw decanter and
cracker) it accounts for only 2%.

The development of more efficient ferrous chelates that can in-
crease the binding rate and equilibrium constant with NO, and also
the reaction rate of ferrous nitrosyl chelates with sulfite/bisulfite
ion, would allow the employment of smaller absorbers, reducing tanks,
and L/G (flow rate ratio of scrubbing liquors to flue gas) to achieve
the same scrubbing efficiencies. The determination of optimum scrub-
bing conditions and chemistry such that the formation of undesirable
products can be depressed or eliminated would allow the reduction of
cost in the area of scrubbing liquor regeneration. This paper ad-
dresses the kinetics and thermodynamics of important reactions in-

volved, the analytical techniques developed for the determination of
reaction intermediates and products, and the areas for further re-
search that could result in substantial improvement in efficiency and
cost-effectiveness of this type of process based on the addition of
metal chelate additives.

Kinetics and Thermodynamics

Reversible Reaction of NO with Ferrous Chelates. The binding of NO
to $Fe^{2+}(L)$ can be expressed by the following equation:

$$NO + Fe^{2+}(L) \rightleftharpoons Fe^{2+}(L)(NO) \tag{1}$$
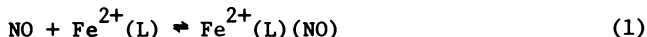
where L represents chelates. With the temperature-jump technique,
the formation and dissociation rate constants of several ferrous
nitrosyl chelates have been measured as shown in Table I. The tem-
perature-jump apparatus employed is similar to that described by
Czerlinski and Eigen (14).
     The result of $Fe^{2+}(H_2O)_5(NO)$ is in good agreement with that de-
termined by Kastin et al. (15) using the same experimental technique.
For both $Fe^{2+}(EDTA)(NO)$ and $Fe^{2+}(NTA)(NO)$, the relaxation times due
to the temperature jump were too fast to be measured. However, an
upper limit of 10 μs was established for the relaxation times for
both complexes. By use of this value with the equilibrium constants
determined for $Fe^{2+}(EDTA)(NO)$ (16) and $Fe^{2+}(NTA)(NO)$ (10), the lower
limits of formation rate constants were calculated to be 7 x 10^{7} and
6 x 10^{7} ℓ/mol-sec at 35 °C, which is in good agreement with that de-
termined by the temperature-jump technique. From the results listed
in Table I, we can conclude that the formation rate of $Fe^{2+}(EDTA)(NO)$
is at least 85 times faster than that of $Fe^{2+}(H_2O)_5(NO)$, whereas, the
dissociation rate of $Fe^{2+}(EDTA)(NO)$ is about 250 times slower than
that of $Fe^{2+}(H_2O)_5(NO)$ at 25 °C.

Reaction of NO with Sulfite and Bisulfite. We have recently studied
the reactions of $NO + SO_3^{2-}$ and $NO + HSO_3^-$ using rapid-mixing con-
tinuous-flow and stopped-flow techniques in conjunction with UV spec-
trophotometry for detection of the reaction's product, N-nitrosohy-
droxylamine-N-sulfonate (NHAS).
     In continuous-flow experiments, the UV spectrum was recorded
over a range of 200 to 400 nm, along with the pH of the reacting
solution. In stopped-flow experiments, the spectrometer was set at a
wavelength were NHAS absorbs. Wavelengths used for monitoring were
in the range of 257 to 295 nm, where no other species in the solution
were absorbed. A recording of the absorption was started and then
the flow was stopped abruptly. The record of the absorption vs. time
was used in rate constant determinations.
     A plot of the log of the rate constant vs. pH is shown in Figure
2 along with the log percent of sulfite and bisulfite vs. pH. From
the data we get the rate expression:

$$\frac{d[NHAS]}{dt} = k_a[NO][HSO_3^-] + k_a{}'[NO][SO_3^{2-}] \tag{a}$$

We obtain $k_a = 32 \pm 10$ M^{-1} sec^{-1} and $k_a{}' = 620 \pm 100$ M^{-1} sec^{-1} at

$$HNO_2 \xrightleftharpoons[]{HSO_3^-} HO_3SNO \xrightleftharpoons[]{HSO_3^-} (HO_3S)_2NOH \xrightleftharpoons[]{HSO_3^-} (HO_3S)_3N$$

Nitrous acid　　Nitrososulfonic　　Hydroxylamine　　Amine trisulfonic
　　　　　　　　　　acid　　　　　disulfonic acid　　　　　acid

$HNO_2 \downarrow$ 　$\downarrow H^+$ 　　　　$\downarrow H^+$ 　HSO_3^- 　$\downarrow H^+$

$NO + HSO_4^-$ 　HSO_4^- 　　　　HSO_4^- 　　　　HSO_4^-
　　　　　　　$+$ 　　　　　　$+$ 　　　　　　$+$
　　　　$H_2N_2O_2 \xleftarrow{HNO_2} (HO_3S)NHOH \xrightarrow{HSO_3^-} NH(HSO_3)_2$

　　　　Hyponitrous　　Hydroxylamine　　Amine
HNO_2 　　acid　　monosulfonic acid　disulfonic acid

$N_2 + HNO_3 + H_2O$ 　$\downarrow H^+$ 　HNO_2 　$\downarrow H^+$ 　HSO_3^- 　$\downarrow H^+$

　　　　　　N_2O 　　　　HSO_4^- 　　　　HSO_4^-
　　　　　　　　　　　　　$+$ 　　　　　　$+$
　　　　　　　$NH_2OH \xrightarrow{SO_2} (NH_2)(HSO_3)$
　　　　　　Hydroxylamine　　Sulfamic acid

　　　　　　　$\downarrow SO_2$ 　$H^+ \swarrow$ 　$\searrow HNO_2$

　　　　　$NH_4^+ + HSO_4^-$ 　$N_2 + HSO_4^-$

Figure 1. Summary of reactions that can take place as a result
of interactions between nitrite and bisulfite ions.

$$\frac{d(NHAS)}{dt} = k_a(NO)(HSO_3^-) + k_b(NO)(SO_3^=)$$

log k
(M^{-1} sec^{-1})

298 K

284 K

log percent of S^{IV} as $SO_3^=$

log percent of S^{IV} as HSO_3^-

pH
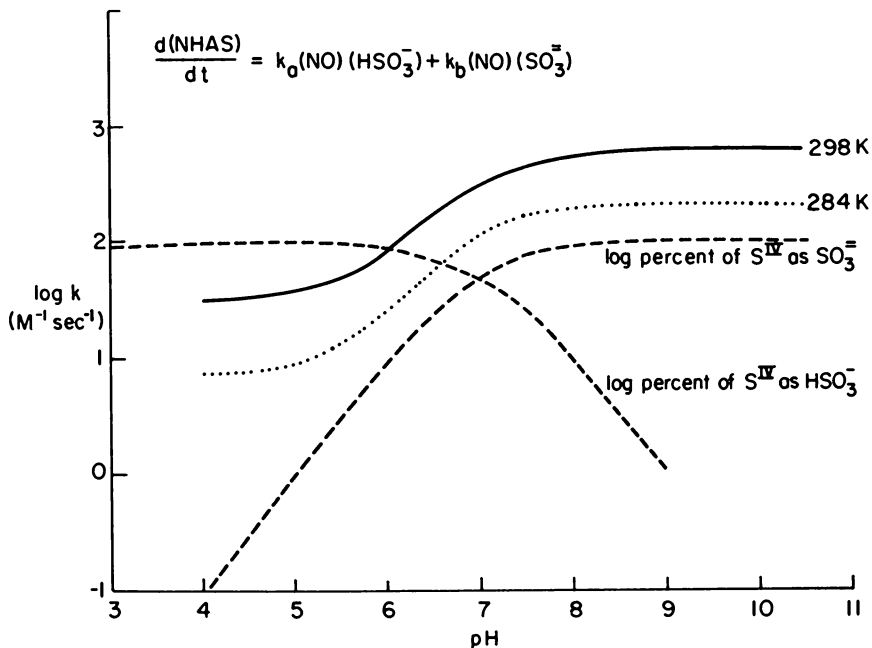
Figure 2. A plot of the log of the rate constant vs. pH for the
reaction between NO and $HSO_3^-/SO_3^=$.

Table I. Kinetic and Thermodynamic Data for
Reversible NO Coordination to Ferrous Chelates

Ferrous Chelates	k_1, mol/(L)	k_{-1}, s^{-1}	K.L/mol at 298 K	$\Delta H°$, kcal/mol	$\Delta S°$, eu
$Fe^{2+}(H_2O)_5(NO)$	$(7.1 \pm 1.0) \times 10^5$	$(1.5 \pm 0.6) \times 10^3$	$(4.7 \pm 2.0) \times 10^{2a}$		
$Fe^{2+}(acac)_2(NO)$	$(4.0 \pm 3.0) \times 10^2$	24 ± 2	17 ± 14		
$Fe^{2+}(oxal)(NO)$			$\sim 1.0 \times 10^5$		
$Fe^{2+}(cit)(NO)$			4.9×10^4	-8.6	-7.4
$Fe^{2+}(cit)(OH^-)(NO)$			2.1×10^5	-3.7	12.0
$Fe^{2+}(cit)(IDA)(NO)$			$\geqslant 3.3 \times 10^5$		
$Fe^{2+}(IDA)(NO)$			2.1×10^5	-9.1	-6.3
Chelex 100(Fe^{2+})(NO)			1.8×10^4	-7.3	-5.1
$Fe^{2+}(NTA)(NO)$	$\geqslant 7 \times 10^7$	$\geqslant 35$	2.14×10^6	-11.94	-11.0
$Fe^{2+}(EDTA)(NO)$	$\geqslant 6 \times 10^7$	$\geqslant 6$	1.15×10^7	-15.8	-20.7

where acac = acetylacetone, oxal = oxalate, cit = citrate, IDA = iminodiacetate,
NTA = nitrilotriacetate, EDTA = ethylenediaminetetraacetate, and Chelex 100 =
a crosslinked polystyrene divinylbenzene porous lattice with attached imino-
diacetate multidentate functional groups.

25°C. The curve for this rate expression is shown in Figure 2 also.
The rate constant for the reaction with sulfite ion is much larger
than that obtained by Nunes and Powell (18), who studied the reaction
using a stirred reactor by bubbling NO gas into a sulfite solution
and obtained an expression:

$$-\frac{d[NO]}{dt} = .132[NO] + .45[NO][SO_3^{2-}] \qquad (b)$$

in M sec^{-1} at 25 °C and pH 13 to 14. They attribute the first term
to the hydration of nitric oxide and the second term to the reaction
of dissolved nitric oxide with sulfite ion.

$$NO + xH_2O \qquad\qquad \rightarrow \quad NO(H_2O)_x \qquad\qquad (2)$$

$$NO(H_2O)_x + SO_3^{2-} \quad \rightarrow \quad {}^-ONSO_3^- \qquad\qquad (3)$$

$$NO + SO_3^{2-} \qquad\qquad \rightarrow \quad {}^-ONSO_3^- \qquad\qquad (4)$$
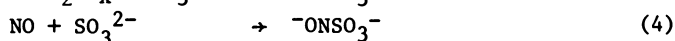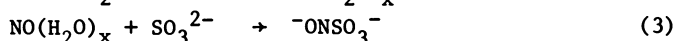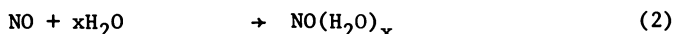
where NO and $NO(H_2O)_x$ represent dissolved and hydrated nitric oxide
respectively. The reaction of hydrated nitric oxide with sulfite ion
was assumed to be much faster than the reaction of dissolved nitric
oxide with sulfite ion. The $^-ONSO_3^-$ intermediate was believed to
react rapidly with a second molecule of nitric oxide to form NHAS.
They made no mention of whether the second nitric oxide needed to be
hydrated or not. Presumably, because of the rapidity by which the
intermediate reacts with nitric oxide, the nitric oxide could be
either in the dissolved or hydrated form. If this were not the case,
the rate expression would be more complex.

In our system, the hydrated form of nitric oxide is formed prior
to mixing, so the sulfite-independent term would not be observed, and
the rate constant we obtain is for the reaction of hydrated nitric
oxide with sulfite ion. The rate of the reaction of dissolved nitric
oxide with sulfite ion is sufficiently slow that it would not contrib-
ute significantly to the formation of NHAS in the time scales in which
we observed the reaction. In experiments where the original sulfite
ion concentration was in excess of that of nitric oxide, we observed
concentrations of NHAS equal to half the original nitric oxide concen-
tration shortly after mixing. This indicated that at least half of
the nitric oxide was in the hydrated form. Otherwise, the NHAS con-
centration would be lower because the dissolved nitric oxide could not
generate NHAS quickly. Other than measurements such as these, we have
no indication of what the equilibrium constant is for reaction (2).
In the analysis of experimental data and calculating rate constants,
it was necessary to correct the results for the hydrolysis of NHAS
whose kinetics follow.

Hydrolysis of N-nitrosohydroxylamine-N-sulfonate. NHAS hydrolyzes to
produce nitrous oxide and sulfate:

$$^-ON(NO)SO_3^- \quad \rightarrow \quad N_2O + SO_4^{2-} \qquad\qquad (5)$$
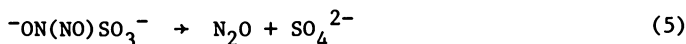
The rate of this hydrolysis was studied by Seel and Winkler (19)
at pH 6.8-7.6 and Ackermann (20) at pH 5.5-11, who found that hydrol-
ysis is catalyzed by acid as well as heavy metal ions. By adding EDTA

to the system it was possible to avoid the catalysis due to heavy metal ions. Seel and Winkler have obtained a hydrolysis rate equation:

$$- \frac{d[NHAS]}{dt} = k_5 [H^+][NHAS] \qquad (c)$$

with $k_5 = 1.1 \times 10^4$ M^{-1} sec^{-1}. The rate obtained by Ackermann and Powell without EDTA has a hydrogen ion dependence that is less than first order and can be expressed as:

$$\frac{d[NHAS]}{dt} = k_5' [H^+]^{0.86}[NHAS] \qquad (d)$$

where $k_5' = 1.6 \times 10^3$ sec^{-1}. The primary effect of trace heavy metal ions appears to be an increase of the decomposition rate at neutral and alkaline pH conditions.

Our kinetic results of the hydrolysis of NHAS between pH 4 and 5.8 were obtained from the analysis of rapid mixing stopped-flow experiments in the kinetic studies of NO reaction with HSO_3^-. Figure 3 shows the curve of absorption vs. time for a typical stopped-flow experiment at pH 4.6. The flow was stopped at 4 seconds on the scale shown in the figure. The absorbance initially rose due to the continued reaction of NO with HSO_3^- and SO_3^{2-}. As the reactants were depleted, the hydrolysis of NHAS caused the absorbance to decrease. The decaying absorbance curves obtained from these experiments were used to determine the hydrolysis rate constant for NHAS as a function of pH. Short intervals of the decay curve were used to calculate values of the rate constant. Intervals of the curve taken shortly after the flow was stopped yielded values which were low, due to the continuing formation of NHAS by NO + HSO_3^- and SO_3^-. At longer times, the values became consistent when the NHAS formation reaction no longer occurred at a significant rate. These values were averaged to obtain the hydrolysis rate constant. This is shown in Figure 4, along with results obtained at higher pH conditions by Ackermann (20) and Seel and Winkler (19).

Reaction of Ferrous Nitrosyl Chelates with SO_3^{2-}/HSO_3^-. The reaction is known to produce a large number of products (12), including N_2O, N_2, hydroxylamine disulfonates (HADS), SO_4^{2-}, $S_2O_6^{2-}$, and Fe^{3+}. Reports of the reaction have indicated that it is complicated. There are contradictions in the literature as to what the reaction products are, as well as the kinetic behavior.

Sada and co-workers (21) studied this reaction using a system where NO gas was continuously flowed into a Fe^{2+}(EDTA) + Na_2SO_3 solution. They conclude that the reaction proceeds by S(IV) reacting with NO coordinated to the ferrous complex to produce N_2O and Fe^{3+}. The basis for this conclusion is the appearance of higher concentration of N_2O in solutions of Na_2SO_3 and Fe^{2+}(EDTA) than in solutions of Na_2SO_3 alone when nitric oxide was bubbled through. They attribute NHAS to be the source of N_2O. No rate was given for the reactions of Fe^{2+}(EDTA)(NO) with either SO_3^{2-} or HSO_3^-.

In our study of the reaction degassed solutions of reagent grade sodium sulfite and/or sodium metabisulfite were added to the spectro-
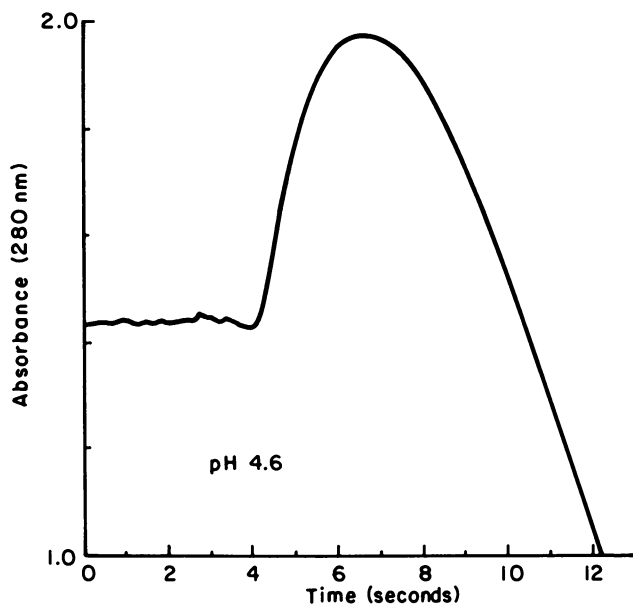
Figure 3. UV absorption at 280 nm vs. time for the reaction
between NO and HSO_3^-/SO_3^{2-} in a typical stopped-flow experiment at
pH 4.6.
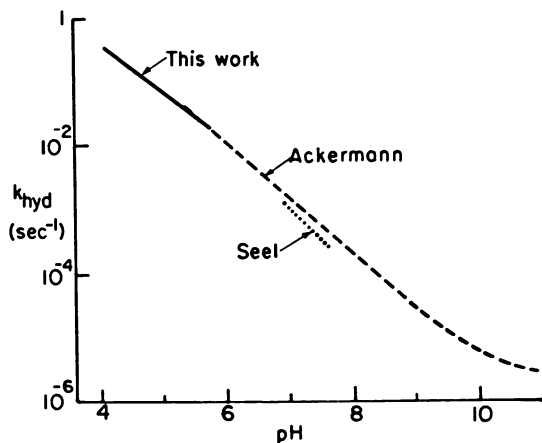
Figure 4. The pH dependence of the NHAS hydrolysis rate.

photometer cell and the cell was under vacuum. The solution contain-
ing the ferrous nitrosyl complex, which was prepared on a vacuum
line, was added and the solutions were mixed and placed in the spec-
trophotometer for monitoring.

The following reaction mechanism appears to be able to explain
the experimental data we obtained at high pH conditions where SO_3^{2-}
is the dominant species of S(IV) in solutions.

$$Fe^{2+}(L)(NO) \quad \underset{k_1}{\overset{k_{-1}}{\rightleftharpoons}} \quad Fe^{2+}(L) + NO \tag{1}$$

$$NO + xH_2O \quad = \quad NO(H_2O)_x \tag{2}$$

$$NO(H_2O)_x + SO_3^{2-} \quad \rightarrow \quad (ONSO_3)^{2-} \tag{3}$$

$$NO + SO_3^{2-} \quad \rightarrow \quad (ONSO_3)^{2-} \tag{4}$$

$$NO + (ONSO_3)^{2-} \quad \rightarrow \quad {}^-ON(NO)SO_3^- \tag{6}$$

$${}^-ON(NO)SO_3^- \quad \rightarrow \quad N_2O + SO_4^{2-} \tag{5}$$

$$2Fe^{2+} + (NO)_2SO_3^{2-} + H_2O \quad \rightarrow \quad 2Fe^{3+} + N_2O + SO_3^{2-} + 2OH^- \tag{7}$$
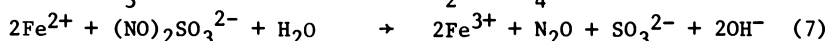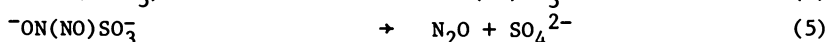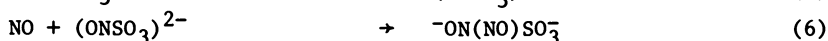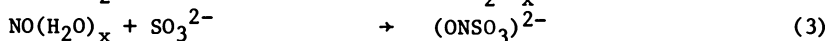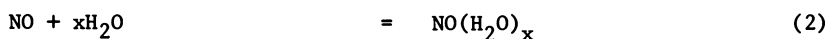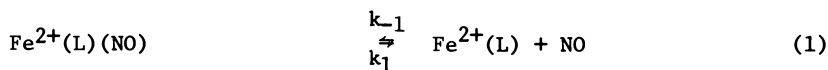
We did not include a direct reaction between $Fe^{2+}(L)(NO)$ and SO_3^{2-}
because it appears that the reactions listed account for disappear-
ance of $Fe^{2+}(L)(NO)$ when mixed with SO_3^{2-}.

While there is uncertainty in k_1 and k_{-1} for $Fe^{2+}(NTA)(NO)$ and
Fe(II)(EDTA)(NO), the rate constants for reaction (1), Littlejohn and
Chang (9), and Teramoto et al. (17) indicate that k_1 is on the order
of 10^7 M^{-1} sec^{-1}. The equilibrium constants $K_{eq} = k_1/k_{-1}$ are fairly
well established (10) as being about 10^6 M^{-1} at 25 °C, indicating
that k_{-1} is about 10 sec^{-1}. From this approximate value of k_{-1} and
the consumption rate equation for $NO + SO_3^{2-}$, we can calculate a
consumption rate for $Fe^{2+}(L)(NO)$. However, the calculated rate is
considerably faster than the observed rate. The calculated rate was
obtained assuming that the nitric oxide released by the ferrous chel-
ate reacts at the rate for hydrated nitric oxide.

A more likely assumption would be that the nitric oxide is not
hydrated until it is released by the ferrous chelate. Since the hy-
dration rate is so slow (18) (k ~0.14 at 25 °C), the rate of reaction
of $Fe^{2+}(L)(NO) + SO_3^{2-}$ no longer depends on k_{-1}, but on K_{eq} and the
hydration rate constant. Using this methodology, the calculated
rates agree well with the observed rates for both $Fe^{2+}(EDTA)(NO)$ and
$Fe^{2+}(NTA)(NO)$. For example, with initial concentrations of
$[Fe^{2+}(NTA)(NO)] = 1$ x 10^{-3} M and $[SO_3^{2-}] = 1$ x 10^{-2} M, the observed
rate is 1.3 x 10^{-6} M sec^{-1}. Using $K_{eq} = 2.0$ x 10^6 M^{-1}, the calcu-
lated rate is 1.4 x 10^{-6} M sec^{-1}. The calculated rate for
$Fe^{2+}(EDTA)(NO)$ is slightly larger, in agreement with what is ob-
served.

Measurements of the absorption of nitric oxide by $Fe^{2+}(EDTA)$
solutions done by Teramoto et al. (17) allowed them to estimate k_1 to
be on the order of 10^8 M^{-1} sec^{-1} for the EDTA complex. This indi-
cates that NO does not need to become hydrated to bind to the ferrous
chelate. This explains why Sada et al. (22) saw much more N_2O from
the $Fe^{2+}(EDTA) + SO_3^{2-}$ solutions than from solutions of SO_3^{2-} alone.
In the limited time available to extract NO from a gas bubble, the

solution with $Fe^{2+}(EDTA)$ could collect much more because of the relative rates of $Fe^{2+}(EDTA)$ + NO and SO_3^{2-} + NO (dissolved). This led to their erroneous conclusion that the sulfite ion reacted with coordinated nitric oxide.

At lower pH conditions, where HSO_3^- is the predominant S(IV) species, somewhat different chemistry occurs in the reaction between $Fe^{2+}(L)(NO)$ + S(IV). The rate is slower and this can be attributed to the slower rate of NO + HSO_3^- relative to NO + SO_3^{2-}. HADS and $S_2O_6^{2-}$ is produced by the reaction of Fe^{2+} with HSO_3^-. This does not occur at high pH conditions where HSO_3^- is not present.

The process by which HADS is produced appears to be somewhat more complicated. At present, the most plausible mechanism based on our experimental data obtained so far is:

$$Fe^{2+}(L)(NO) + HSO_3^- \;\; \rightleftharpoons \;\; Fe^{2+}(L)NOHSO_3^- \qquad (8)$$

$$2Fe^{2+}(L)NOHSO_3 \;\; \rightarrow \;\; 2Fe^{2+}(L) + HON(SO_3^-)_2 + HNO \qquad (9)$$

$$Fe^{2+}(L)NOHSO_3^- + Fe^{2+}(L)(NO) \;\; \rightarrow \;\; 2Fe^{2+}(L) + NOSO_3^- + HNO \qquad (10)$$

$$HSO_3^- + NOSO_3^- \;\; \rightarrow \;\; HON(SO_3^-)_2 \qquad (11)$$
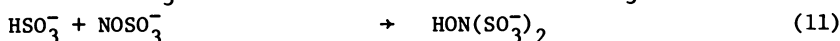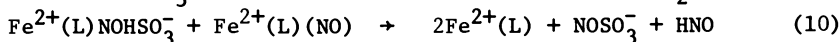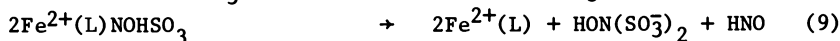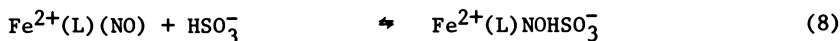
The last step of the process is the same as that proposed (3,4) for the preparation of HADS from bisulfite ion and nitrous acid. The nitrosyl ion, NO^-, could dimerize and decompose to N_2O. More work is required to clarify the HADS formation process.

Formation of Nitrogen-Sulfur Compounds. Once HADS is formed, it can further react to form other nitrogen-sulfur compounds (Figure 1). Chang et al. (3) have published an extensive review article on the kinetics and mechanisms of important reactions involved.

Oxidation of Ferrous Chelates to Ferric Chelates. Flue gas contains about 5% oxygen. When dissolved, oxygen can oxidize ferrous ions to ferric ions which are inactive for coordination with NO. The oxidation rate of ferrous ions is accelerated in the presence of chelating agents, e.g., EDTA and NTA. This acceleration may be ascribed to the stabilization of the oxidized form by the chelation.

Kurimura et al. (22) studied the oxidation of $Fe^{2+}(EDTA)$ and $Fe^{2+}(NTA)$ by dissolved oxygen in aqueous solutions and suggested that the oxidation proceeds by two parallel reaction paths, with both protonated and unprotonated chelates reacting. The reaction mechanisms suggested (22,23) are as follows:

$$Fe^{2+}(HL) + O_2 \;\; \xrightarrow{\;k_{22}\;} \;\; Fe^{3+}(L) + HO_2^- \qquad (12)$$

$$Fe^{2+}(L) + O_2 \;\; \xrightarrow{\;k_{23}\;} \;\; Fe^{3+}(L) + O_2^- \qquad (13)$$

$$O_2^- + H^+ \;\; \rightarrow \;\; HO_2 \qquad (14)$$

$$Fe(II) + HO_2 \;\; \rightarrow \;\; Fe(III) + HO_2^- \qquad (15)$$

$$HO_2^- + H^+ \;\; = \;\; H_2O_2 \qquad (16)$$

$$Fe(II) + H_2O_2 \quad\quad \rightarrow \quad Fe(III) + OH^- + OH \quad\quad (17)$$

$$Fe(II) + OH \quad\quad \rightarrow \quad Fe(III) + OH^- \quad\quad\quad\quad (18)$$
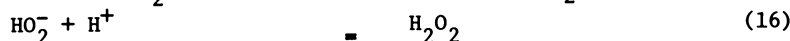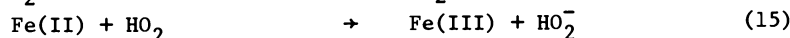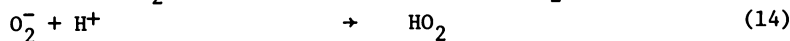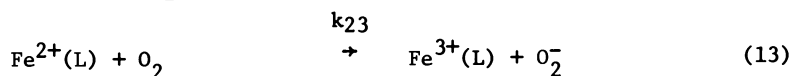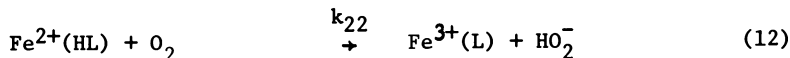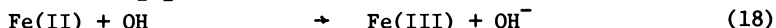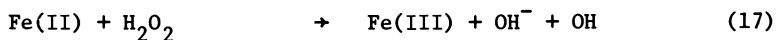
In these equations, Fe(II) and Fe(III) represent the ferrous and ferric ion species respectively. The rate equation for the oxidation is:

$$\frac{d[Fe^{3+}]}{dt} = 4k_{22}[Fe^{2+}(HL)][O_2] + 4k_{23}[Fe^{2+}(L)][O_2] \quad\quad (e)$$

For EDTA, $k_{22} = 6.8 \times 10^3$ and $k_{23} = 2.7 \times 10^2$ M^{-1} sec^{-1}, while for NTA, $k_{23} = 80$ M^{-1} sec^{-1} at 25 °C. As can be seen from these results, protonated chelates react more rapidly than the unprotonated ones.

In addition to oxidation by O_2, $Fe^{2+}(L)$ can be converted to $Fe^{3+}(L)$ in an aqueous system containing only $Fe^{2+}(L) + NO + SO_3^{2-}$. Preliminary experiments from our laboratory, performed by mixing $Fe^{2+}(NTA)$ or $Fe^{2+}(EDTA)$ with NHAS, have shown the formation of Fe^{3+} and the liberation of N_2O. The kinetic study of this reaction is in progress.

Reduction of Ferric Chelates by HSO_3^- and Formation of Dithionate.
$Fe^{3+}(EDTA)$ is reduced by HSO_3^-, producing dithionate and a small amount of SO_4^{2-} (24). The rate of reduction of $Fe^{3+}(EDTA)$ is first order in $[HSO_3^-]$ and $[Fe^{3+}(EDTA)]$, and inversely first order in $[Fe^{2+}(EDTA)]$.

$$-\frac{d[Fe^{3+}(EDTA)]}{dt} = k[Fe^{3+}(EDTA)][HSO_3^-]/[Fe^{2+}(EDTA)] \quad\quad (f)$$

The rate constant k is 8.8×10^{-6} sec^{-1} at 55 °C. The apparent activation energy is 21.3 kcal/mol. The following reaction mechanism was suggested:

$$Fe^{3+}(EDTA) + HSO_3^- \quad = \quad FeSO_3^+ + H^+ + EDTA \quad\quad (19)$$

$$FeSO_3^+ \quad\quad\quad = \quad Fe^{2+} + SO_3^- \quad\quad\quad\quad\quad (20)$$

$$Fe^{2+} + EDTA \quad\quad = \quad Fe^{2+}(EDTA) \quad\quad\quad\quad (21)$$

$$SO_3^- + H^+ \quad\quad\quad \rightarrow \quad HSO_3^- \quad\quad\quad\quad\quad\quad (22)$$

$$HSO_3 + HSO_3 \quad\quad \rightarrow \quad S_2O_6^{2-} + 2H^+ \quad\quad\quad (23)$$
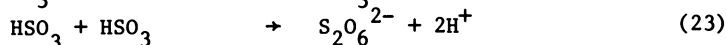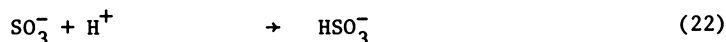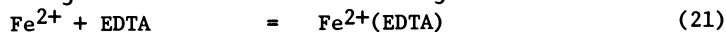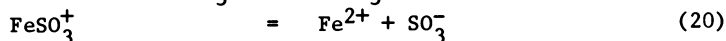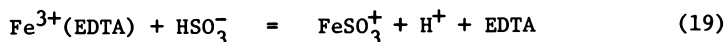
Analytical Techniques

One of the problems in studying the chemistry of wet processes for desulfurization and denitrification of flue gas in order to determine an optimum design and operating condition of scrubbers is the difficulty in quantitatively detecting all important species produced. Specifically, there was no methodology available for the convenient determination of the large number of N-S compounds that can be produced.

We have applied a laser Raman spectroscopic (25) and ion chromatographic (26) techniques to the determination of N-S compounds in reaction mixtures. Both techniques require only a small amount of

the sample and allow simple, rapid and simultaneous determination of these compounds. Table **II** shows Raman shifts and relative molar intensities of some species involved in flue gas scrubbers. The major limitation of Raman spectrometry is the lack of sensitivity. Samples with low concentrations (0.001-0.01 M) of the compounds of interest require very long data acquisition times. Using a Dionex 2010i ion chromatograph equipped with AG4 guard column, an AS4 anion separation column, and an anion fiber suppressor, we can make determinations of N-S compounds (Figure 5). For the determination of HAMS and sulfamate, a 1.5 mM bicarbonate eluent was used with a flow rate of 2.0 mL/min at a pressure of 700-800 psi. For the determination of HADS, ADS, and NHAS, the AG4 column alone was used as the separation column with 12 or 18 mM carbonate eluents. The flow rate was 1.5 mL/min at a pressure of 200-300 psi. Detection limits for the compounds, defined as the concentration that generated a peak with a height twice that of the background noise, are as follows: HAMS, 0.5×10^{-6} M; sulfamate, 0.6×10^{-6} M; ADS 1.4×10^{-6} M; HADS, 7.4×10^{-6} M; and NHAS, 0.5×10^{-6} M. As the retention time of a compound increases, the peak broadens and decreases in height. Thus it is advantageous to have as short a retention time as possible within the limitations of obtaining separation between the peaks of the chromatogram.

Future Research Areas

The improvement over the existing Japanese processes can be made by developing a more efficient ferrous chelate such that it can provide better absorption efficiency for NO, faster reaction rates between NO and SO_2, and better stability for the ferrous chelate toward oxidation, compared to Fe^{2+}(EDTA) or Fe^{2+}(NTA) employed in Japanese processes. The development of an efficient and cost-effective method for the reduction of ferric chelate to ferrous chelate without producing dithionate ions could make the process attractive. In addition to these areas, the study of several alternative approaches and novel ideas could develop into a much more efficient and cost-effective scrubber system employing metal chelate additives.

(1) Immobilization of the ferrous chelate onto a solid substrate (27). If an efficient immobilized ferrous-ion catalyst can be found, it could provide important improvements over the presently available Japanese processes. These improvements include simplification in processes design for species separation, reduction of water, energy, and catalyst consumption, and reduction of operating costs.

(2) Investigation of non-ferrous metal chelates that can efficiently absorb NO and provide stability toward oxidation. Many cobalt, copper, manganese, molybdenum, nickel, osmium, rhenium, rhodium, ruthenium and vanadium chelates have been demonstrated to be able to coordinate NO. Their application to flue gas scrubbing systems should be explored.

(3) Development of metal chelates suitable for employment in a spray drying system (28,29). Spray drying systems have been demonstrated to be more cost-effective than wet systems for control of SO_2 emissions from power plants.

Table II.   Raman Shifts and Relative Molar Intensities
of Some Species Involved in Flue Gas Scrubbers

Species	Raman shift (cm^{-1})	Relative molar intensity[a]
NO_2^-	818	0.053
	1240	~0.025
	1331	0.125
NO_3^-	1050	0.95
$N_2O_2^=$	692[b]	weak[b]
	1115[b]	weak[b]
	1383[b]	strong[b]
N_2O^-	1285	~0.18
$SO_3^=$	967	0.12
HSO_3^-	1023	0.10
$SO_4^=$	455	~0.07
	981	1.00
HSO_4^-	1055	~0.9
$S_2O_5^=$	1050	0.05
HADS	~700	~0.20
	1084	1.43
HAMS	~420	~0.13
	~760	~0.08
	1058	0.48
HA (pH $\leqslant$ 7)	1004	0.21
HA (pH $\geqslant$ 9)	918	0.09
ATS	1097	0.10
ADS	1084	0.056
SA (pH $\leqslant$ 1)	1063	c
SA (pH $\geqslant$ 3)	1049	0.41

[a] $SO_4^=$ 981 cm^{-1} line = 1.000

[b] Rauch, J. E.; Decius, J. C. Spectrochim. Acta 1966, 22, 1963.

[c] No value obtained.
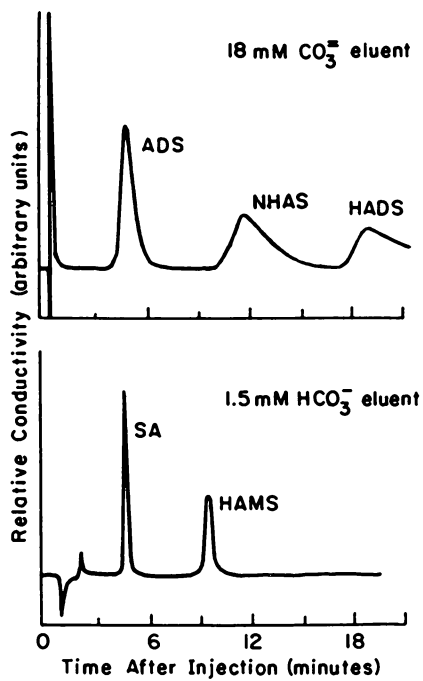
Figure 5.   Ion chromatogram of some nitrogen-sulfur compounds.

The addition of metal chelates to the alkali spray slurries for simultaneous control of SO_2 and NO_x could be very effective. The Fe^{2+}(EDTA) and Fe^{2+}(NTA) type metal chelates are not suitable for use in spray drying systems, however, because the metal chelates suitable for employment in spray drying systems must be able to absorb or react with NO irreversibly under the scrubbing conditions. As the droplet passes through the flue gas, it will heat up. This has the effect of reducing the liquid volume through evapora- tion and changing the kinetics due to the temperature dependence of the rate constants and equilibrium con- stants. The increase in temperature will also reduce the solubility of NO_x and SO_2. If the droplet loses all its water by evaporation, the NO attached to Fe^{2+}(EDTA) or Fe^{2+}(NTA) type ferrous chelates will dissociate and return to the gas phase. From the kin- etic information presented in this paper, one can cal- culate (30) that only a small fraction of absorbed NO will react with dissolved SO_2 during about 10 sec res- idence time of the droplet in spray drying chamber. A cost-effective method for the recovery of metal che- lates must be available for the process to be attrac- tive.

Acknowledgments

Literature Cited

1. Moore, T. EPRI Journal, November 1984, 26-33.
2. Faucett, H. L.; Maxwell, J. D.; Burnett, T. A. "Technical Assess- ment of NO_x Removal Processes for Utility Application"; EPRI-AF- 568, March 1978.
3. Chang, S. G.; Littlejohn, D.; Lin, N. H. ACS Symp. Ser. 1982, 188, No. 118, 127-152.
4. Oblath, S. G.; Markowitz, S. S.; Novakov, T.; Chang, S. G. J. Phys. Chem. 1981, 85, 1017.
5. Gomiscek, S.; Clem, R.; Novakov, T.; Chang, S. G. J. Phys. Chem. 1981, 85, 2567.
6. Oblath, S. B.; Markowitz, T.; Novakov, T.; Chang, S. G. J. Phys. Chem. 1982, 86, 4853.
7. Oblath, S. B.; Markowitz, S. S.; Novakov, T.; Chang, S. G. Inorg. Chem. 1983, 22, 579.
8. Martin, A. E., Ed.; "Emission Control Technology for Industrial Boilers"; Noyes Data Corp.: Park Ridge, NJ, 1981.
9. Littlejohn, D.; Chang, S. G. J. Phys. Chem. 1982, 86, 537.

10. Lin, N.; Littlejohn, D.; Chang, S. G. I & EC Proc. Design & Deveop. 1982, 1, 725.
11. Chang, S. G.,; Littlejohn, D.; Lynn, S. Environ. Sci. & Tech. 1983, 17, 649.
12. Littlejohn, D.; Chang, S. G. Lawrence Berkeley Laboratory report LBL-17962, submitted to Inorg. Chem., 1985.
13. Maxwell, J. D.; Tarkington, T. W.; Burnett, T. A. "Preliminary Economic Analysis of NO_x Flue Gas Treatment Processes Using TVA and EPRI Economic Premises" EPRI CS-2075, December 1981.
14. Czerlinski, G.; Eigen, M. Elektrochem. 1959, 63, 652.
15. Kustin, K.; Taub, I. A.; Weinstock, E. Inorg. Chem. 1966, 5, 1079.
16. Hishinuma, Y.; Kaji, R.; Akimoto, H.; Nakajima, F.; Mori, T.; Kamo, T.; Arikawa, Y.; Nozawa, S. Chem. Soc. Jap. Bull. 1979, 52, 2863.
17. Teramoto, M.; Hiramine, S.; Shimada, Y.; Sugimoto, Y.; Teranishi, H. J. Chem. Eng. of Japan 1978, 11, 450.
18. Nunes, T. L.; Powell, R. E. Inorg. Chem. 1970, 9, 1916.
19. Seel, F.; Winkler, R. Z. Naturforsch. 1963, 18a, 155.
20. Ackermann, M. N. "Alkaline Hydrolysis and Oxidation of Hydroxylamine-N-Sulfonate", Ph.D. Thesis, University of California, Berkeley, 1966.
21. Sada, E.; Kumazawa, H.; Takada, Y. IE & C Fundam. 1984, 23, 60.
22. Kurimura, Y.; Ochiai, R.; Matsuura, N. Chem. Soc. Jap. Bull. 1968, 41, 2234.
23. Kurimura, Y.; Kurizama, H. Chem. Soc. Jap. Bull. 1969, 42, 2238.
24. Sato, T.; Simizu, T.; Okabe, T. Nippon Kagakukaishi 1978, 361.
25. Littlejohn, D.; Chang, S. G. Environ. Sci. & Tech. 1984, 18, 305.
26. Littlejohn, D.; Chang, S. G. Anal. Chem. 1986, 58, 158.
27. Brodbeck, K.; Chang, S. G. "Study of Ferrous Ion on Chelex 100 for NO Absorption and Subsequent Reactivity with Oxygen", Lawrence Berkeley Laboratory report LBL-20132, 1985.
28. Chang, S. G.; Griffiths, E. "A Process for Combined Removal of SO_2 and NO_x from Flue Gas", LBL case no.: IB-612, U.S. patent pending.
29. Chang, S. G. "Spray Drying Process for Simultaneous Removal of SO_2, NO_x, and Particulates from Flue Gas", LBL case no.: IB-643, U.S. patent pending, 1986.
30. Chang, S. G.; Littlejohn, D. Lawrence Berkeley Laboratory report LBL-19398, 1985.

15

Effects of Magnesium and Chloride Ions on Limestone Dual Alkali System Performance

John C. S. Chang[1], Norman Kaplan[2], and Theodore G. Brna[2]

[1] Acurex Corporation, Research Triangle Park, NC 27709
[2] Industrial Environmental Research Laboratory, U.S. Environmental Protection Agency, Research Triangle Park, NC 27711

Pilot plant tests have been conducted to evaluate the effects of magnesium and chloride ions on system performance of limestone-regenerated dual alkali processes under closed-loop operating conditions. It was found that limestone reactivity and solids dewatering properties are very sensitive to magnesium ion concentrations. The total magnesium ion concentration should be maintained below 1000 ppm for satisfactory performance under normal operation. A model which assumes competitive surface adsorption of calcium and magnesium ions was used to interpret the data. Limestone reactivity decreased and solids dewatering properties worsened with the increase of chloride ion concentration. However, the effect of chloride ion accumulation was not significant until the concentration reached 80,000 ppm.

Sodium-based dual alkali (DA) flue gas desulfurization (FGD) processes have the features of clear solution scrubbing, high SO_2 removal efficiency, low liquid-to-gas (L/G) ratio, and high reliability[1]. Recent testing has demonstrated the feasibility of using limestone instead of lime for scrubbing liquor regeneration which makes DA processes more competitive with slurry scrubbing processes[2].

Since the limestone DA process uses concentrated sodium sulfite solution as the absorbent for SO_2 removal, closed water loops are desired to minimize the sodium makeup requirements. However, the closed-loop operation (i.e., the only water leaving the FGD system is through evaporation and filter cake moisture) also promotes the buildup of soluble salts in the recirculating scrubbing liquor. The primary sources of soluble salts include makeup water, reagents, and flue gas. Previous findings indicate that the accumulation of soluble salts, especially chloride ions, can have significant effects on system chemistry and scrubber performance of lime/limestone slurry FGD processes[3,4]. The most significant effects observed include decreases of equilibrium pH, SO_2 removal efficiency, and solids settling rate, and an increase in gypsum scaling potential.

In order to broaden the data base of the limestone DA process and to evaluate the impacts of closed-loop operation, a series of pilot plant tests was conducted under the sponsorship of U.S. Environmental Protection Agency's (EPA) Industrial Environmental Research Laboratory in Research Triangle Park, NC (IERL-RTP). The testing concentrated on evaluating the effects of magnesium and chloride ions since appreciable accumulations of soluble salts containing these two species are expected in a limestone DA system under closed-loop operating conditions.

The current trend in power plant design is to use plant waste water (e.g., cooling tower blowdown) for FGD system makeup. Magnesium and chloride are the primary ingredients of soluble salts which enter the FGD system with plant waste water. Additional chloride ions may enter the scrubbing liquor through the absorption of HCl produced during the coal combustion process. In addition to makeup water, limestone is also an important source of magnesium ions. If closed-loop operation is used, the dissolved salts from either of the above sources can be concentrated to levels which are considerably higher than those presently observed in most systems. This paper summarizes selected results from the pilot plant study of the limestone DA process with total magnesium ion concentration up to 2000 ppm and chloride ion concentration to 150,000 ppm.

Test Facilities

The IERL-RTP pilot facilities include a three-stage tray tower with 7.5 m^3/min (approximately 0.1 MW) flue gas capacity (Figure 1). The flue gas is drawn from a gas-fired boiler (no flyash is present). Pure SO_2 is injected to achieve the desired concentration in the flue gas. Regeneration of spent scrubbing liquor is performed in the four-tank-in-series reactor train with a total residence time of 80 minutes. Limestone is fed to the first reactor as 45% slurry. The feed rate is manually set as required for either pH or reactant stoichiometry control. Soda ash is added to the fourth reactor as sodium makeup. Reactor effluent slurry flows by gravity to the thickener centerwell. Clarified liquor overflows from the thickener to the forward feed hold tank from which it is pumped to the tray tower. A horizontal belt filter is used for further dewatering of the thickener underflow solids.

Ultraviolet spectrophotometry (DuPont 400 SO_2 analyzer) was used to monitor the gas phase SO_2 concentrations and SO_2 removal efficiencies. The pH of scrubbing liquor in each reactor was measured hourly during pilot testing. Solid dewatering properties were characterized by hold tank slurry settling rate and filter cake insoluble solids concentration. Detailed descriptions of the test facilities and analytical procedures were reported earlier[5].

Effects of Magnesium Ions

For the study of magnesium ion (Mg^{2+}) effects on the system performance of the limestone DA process, Epsom salt ($MgSO_4 \cdot 5H_2O$) was added to adjust the Mg^{2+} concentration in the scrubbing liquor. The base case system performance was established without the addition of epsom salt; the steady-state concentration of Mg^{2+} was 355 ppm. In subsequent tests, all operating conditions -- except for Mg^{2+}
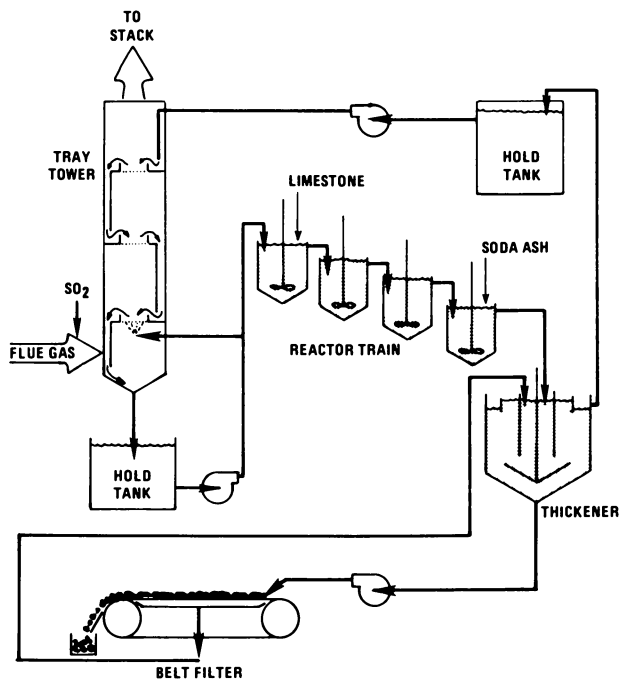
Figure 1.   Flow diagram of IERL-RTP dual alkali pilot plant.

concentration -- were maintained constant; the concentration of Mg^{2+} was gradually increased by Epsom salt addition to the first reactor. The maximum total Mg^{2+} concentration reached during this test series was 2000 ppm. The principal results of these tests are listed in Table I. Summaries of liquor and solid analyses are listed in Tables II and III, respectively.

Effects of 1000 ppm Mg^{2+}

A comparison of results obtained from run MG-1 with those from MG-2 indicated that the most significant change observed with the increase of total Mg^{2+} concentration up to 1000 ppm is the deterioration of solids dewatering properties as reflected by the decrease of insoluble solids in the filter cake. The base case (run MG-1) filter cake contained 52% solids; however, only 45% solids was obtained in the filter cake generated at 1000 ppm total Mg^{2+} concentration.

No magnesium sulfate was added to the system for run MG-3. The objective of this run was to evaluate the system performance with decreasing Mg^{2+} concentration. The mass balance indicated that the total Mg^{2+} concentration should drift down to below 500 ppm. During the run, the total Mg^{2+} concentration decreased from 1000 ppm to about 625 ppm toward its end. A leak was discovered at the scrubber bleed/quench recirculation pump inlet which introduced air into the process stream and therefore caused high oxidation. The high oxidation, as confirmed by solids analysis results in Table 3, was reflected by increases of the sulfate-to-sulfite ratio to above 2.5. After the air leak problem was corrected, the sulfate-to-sulfite ratio decreased, but the test average was 2.4.

Very stable operation was maintained for run MG-4 without magnesium sulfate addition with the total Mg^{2+} concentration stabilizing at about 356 ppm. The sulfate-to-sulfite ratio decreased to 2.0, the filter cake insoluble solids reached 53%, and the slurry settling rate was 2.2 cm/min. The results confirmed the base case solids quality and scrubber performance obtained from run MG-1.

Effects of 2000 ppm Mg^{2+}

Epsom salt was then added to the first reactor to raise the Mg^{2+} concentration for run MG-5. No significant changes of system performance were observed except the deterioration of filter cake quality when the total Mg^{2+} concentration reached 1000 ppm. The filter cake insoluble solids dropped from 53% to 47% at 1000 ppm total Mg^{2+} concentration and confirmed the results observed during runs MG-1 and MG-2. However, a further increase of the Mg^{2+} concentration caused significant changes in system performance. When the total Mg^{2+} concentration exceeded 1500 ppm, pH decreases were observed throughout the system. The SO_2 removal efficiency also decreased. Filter cake quality deteriorated further to below 40% insoluble solids. The solids settling rate also began to drop. At 2000 ppm total Mg^{2+} concentration, a system upset with non-settling solids occurred. The solids settling rate dropped to below 0.1 cm/min, while only 28% insoluble solids were obtained from the filter cake. The pH of the regenerated liquor was 6.2 (base case pH was 6.6) and SO_2 removal efficiency was 85% (base case removal efficiency was 92.7%). The solids content of slurries in the

Table I. Magnesium-Ion-Effect Test Conditions

Run No.	MG-1	MG-2	MG-3	MG-4	MG-5
Mg^{2+} concentration, ppm	355	1060	625	356	2000
Tower pressure drop, in. H_2O	8.1	8.4	7.9	7.8	8.2
Liquor forward feed, gpm	1.4	1.4	1.4	1.4	1.4
Scrubber feed pH	6.6	6.6	6.6	6.6	6.2
Scrubber effluent pH	6.2	6.2	6.2	6.2	5.6
Inlet SO_2 concentration, ppm	3010	2990	2990	3050	3020
SO_2 feed rate, lb/hr	6.7	6.7	6.6	6.7	6.6
SO_2 absorption, wt. %	92.7	91.8	91.0	92	85
SO_2 make-per-pass, mmol/l	139	137	132	138	125
Limestone slurry feed rate, lb/hr	23	23	22	22	22
Limestone slurry solids, wt. %	45	45	45	45	45
Flue gas O_2, vol. %	6.4	7.0	6.1	6.9	7.2
Thickener solids, wt. %	19	18	16	20.1	7.8
Filter cake solids, wt. % (insoluble)	52	45	48	53	28
Filter wash rate (nominal), gph	3	3	3	3	3
Na concentration, g/l	57	55.6	57.4	54.0	49.7
TOS, gmol/l	0.72	0.67	0.70	0.74	0.67
Ca concentration, ppm	88	52	74	62	58
Total alkalinity, gmol/l ⎫ (V-113)	0.42	0.41	0.38	0.42	0.28
Na in filter cake, mg/g(a) ⎭	15.5	18.6	16.9	12.6	(d)
Run time, hours	81	78	85	92	67
Limestone stoichiometry(b)	1.07	1.08	1.06	1.03	1.13
Settling rate (reactor), cm/min	2.0	1.9	2.2	2.2	<0.1
Settling test % solids	2.1	2.1	2.6	2.1	4.7
Active Na, gmol/l(c)	1.14	1.08	1.08	1.16	0.95
SO_4/sulfite	2.05	2.15	2.4	2.0	3.2

(a)Washed in the belt filter
(b)Mass balance
(c)Active Na = TOS + Total Alkalinity, gmol/l
(d)Data not available

Table II. Summary of Thickener Liquor Analysis
from Magnesium-Ion-Effect Tests

Run No.	MG-1	MG-2	MG-3	MG-4	MG-5
Component, g/l					
Ca	0.088	0.052	0.074	0.062	0.058
Mg	0.355	1.06	0.625	0.356	2.02
Na	57.0	55.6	57.4	54.0	49.7
TOS as SO_3	57.6	53.6	55.6	59.3	53.6
SO_4	82.6	84.5	86.4	80.6	86.4
CO_3	2.73	2.54	2.35	2.1	2.03
Cl	0.165	0.174	0.192	0.182	0.175
pH	6.7	6.7	6.6	6.7	6.2

Table III. Summary of Filter Cake Analysis
from Magnesium-Ion-Effect Tests

Run No.	MG-1	MG-2	MG-3	MG-4	MG-5
Component, mg/g					
Total S as SO_3	529	522	525	509	511
TOS as SO_2	379	378	363	382	376
Carbonate as CO_2	42	47	43	42	56
Ca	294	297	298	296	298
Mg	2.6	3.4	2.8	2.5	3.6
Na	5.7	5.8	5.8	4.4	5.3
Oxidation, %	10.4	9.5	13.6	6.2	8.0
L/S Utilization, %[a]	89.9	87.8	88.1	86.0	85.7

[a]SO_3/Ca

reactors reached 4.7% (base case solids content was 2.1%) due to the solids carryover in the thickener overflow.

Results of Chemical Analysis

Several sets of samples were taken from each reactor and hold tank for liquid and solids analyses to characterize the system chemistry at various Mg^{2+} concentrations. Results of the chemical analyses are shown in Figures 2 to 8. Figure 2 shows the profile of total Mg^{2+} concentration across the pilot plant system. A slight drop of Mg^{2+} concentration was observed from the scrubber bleed hold tank (V-102) to the first reactor (V-105), especially for the high Mg^{2+} concentration runs. The concentration drop was not very significant since the changes were within $\pm 5\%$ (the range of experimental error). However, a magnesium loss across the reactors is implied. Magnesium lost in this manner is probably coprecipitated with calcium sulfite/sulfate.

The pH profile is shown in Figure 3. A significant drop in the system pH was obtained when the total Mg^{2+} concentration was increased from 1060 to 2000 ppm. The scrubber bleed hold tank pH decreased from 6.3 to 5.6 and the forward feed hold tank pH also decreased from 6.7 to 6.2. However, the increase of pH across the reactors was observed even at 2000 ppm total Mg^{2+} concentration, indicating that the limestone dissolution was not completely stopped by increasing the Mg^{2+} concentration.

The total oxidizable sulfur (TOS) and sulfate ion concentrations are shown in Figures 4 and 5, respectively. Similar concentration levels and concentration trends were observed for both species at the three Mg^{2+} concentrations tested. Figures 4 and 5 confirm that the concentrations of important species, such as TOS and sulfate ion, were not altered by increasing the Mg^{2+} concentration by Epsom salt addition.

Figure 6 shows the total alkalinity concentrations across the system. Since the TOS concentrations were maintained at about the same levels for all runs (Figure 4), the decrease of total alkalinity when total Mg^{2+} concentration was increased from 1060 to 2000 ppm reflects the pH drop caused by the increase of magnesium ion concentrations.

The calcium ion (Ca^{2+}) and total carbonate concentrations are shown in Figures 7 and 8, respectively. The concentration levels and the trends of Ca^{2+} and total carbonate profiles obtained at the three Mg^{2+} concentrations are very similar.

Solids Analysis

The product solids obtained at various magnesium ion concentrations were examined under a scanning electron microscope (SEM) to observe the detailed morphology of the individual solid particles. As can be seen in the SEM photomicrographs reproduced in Figures 9 through 11, the product solids were physically different. Figure 9 shows the solids taken at the base case conditions where the particles gave a 50 to 55% solids filter cake with agglomerates of well-defined platelets. The thickness of each platelet can be seen clearly in Figure 9b which was taken at a magnification of 5000x.

Photomicrographs of solids produced at the 1000 ppm total Mg^{2+} concentration are shown in Figure 10. Compared with the base case
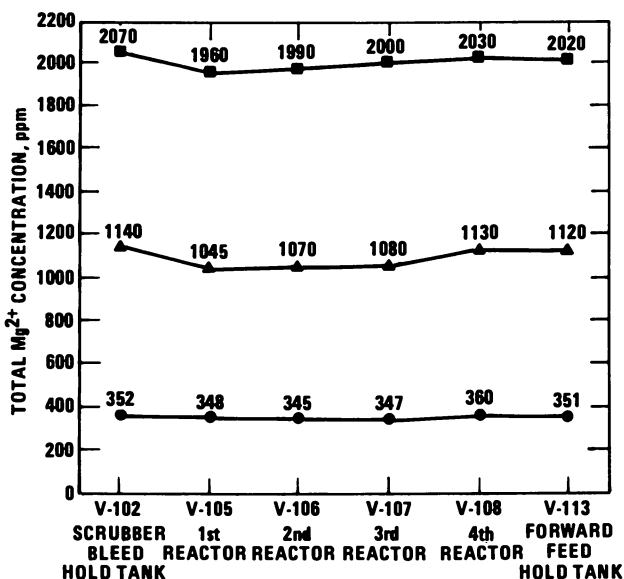
Figure 2. Distribution of magnesium ion concentration in limestone DA pilot plant.
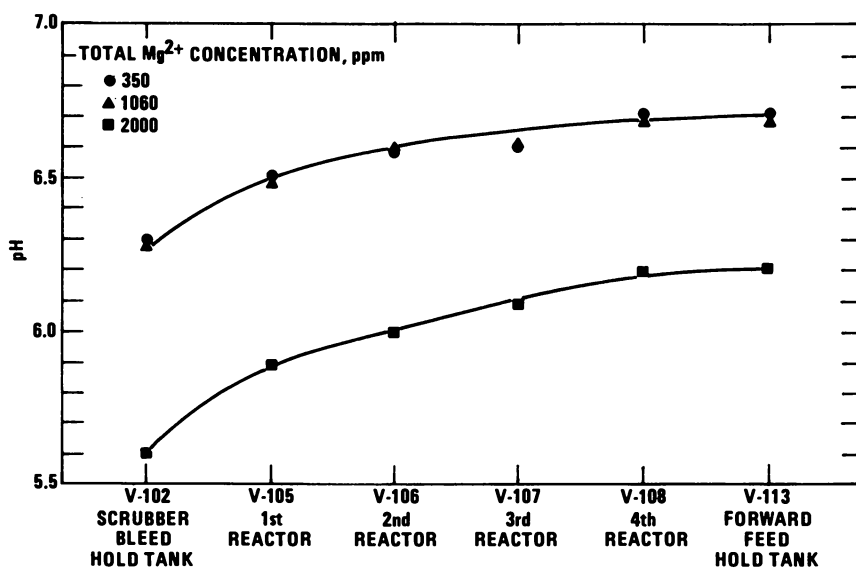
Figure 3. Profiles of pH values in limestone DA pilot plant.
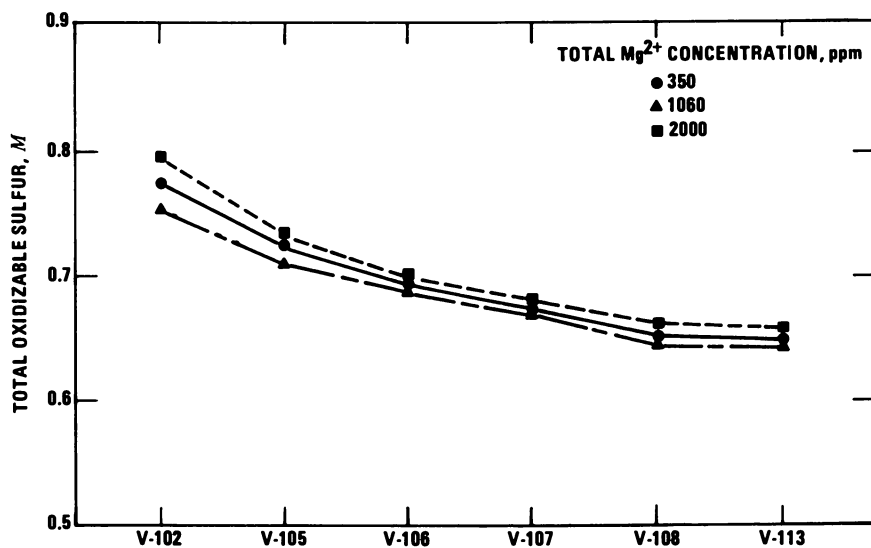
Figure 4. Total oxidizable sulfur concentrations in limestone DA pilot plant.
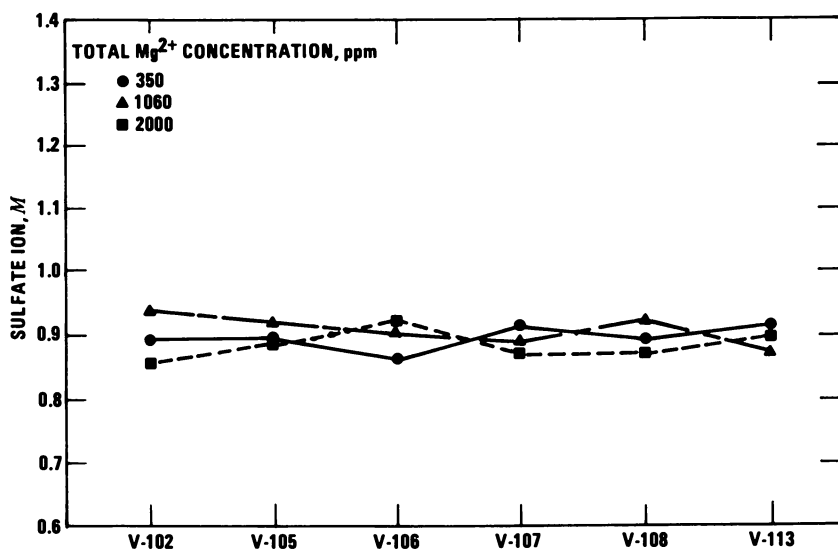
Figure 5. Distribution of sulfate ion concentration in limestone DA pilot plant.
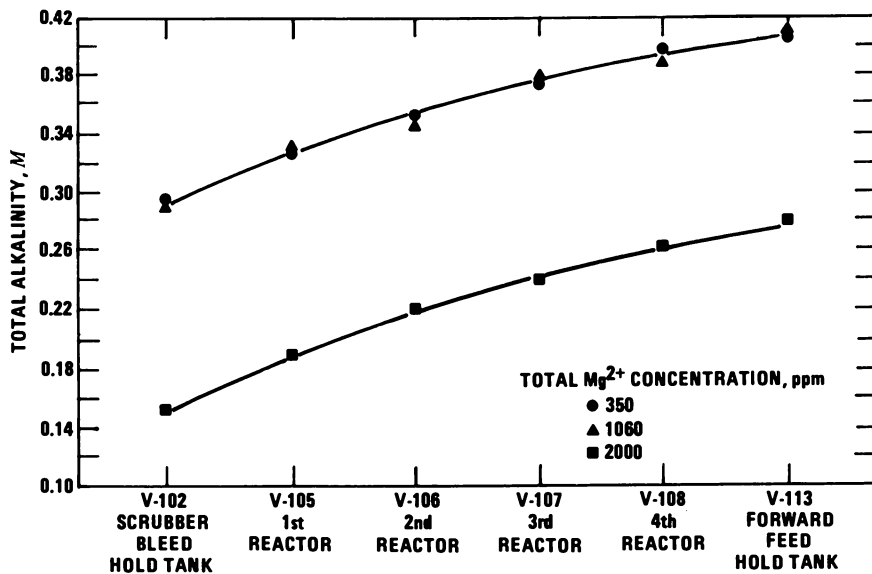
Figure 6. Total alkalinity concentrations in limestone DA pilot plant.
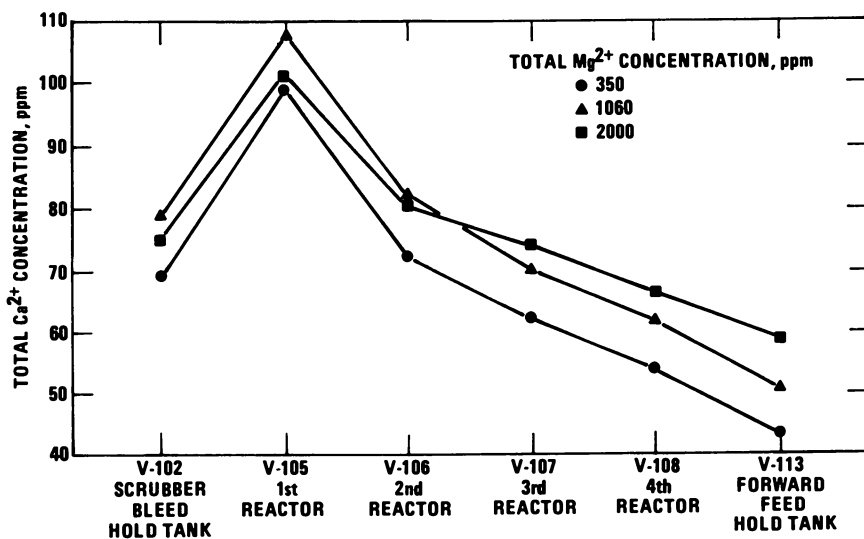
Figure 7. Distribution of total calcium ion concentration in limestone DA pilot plant.
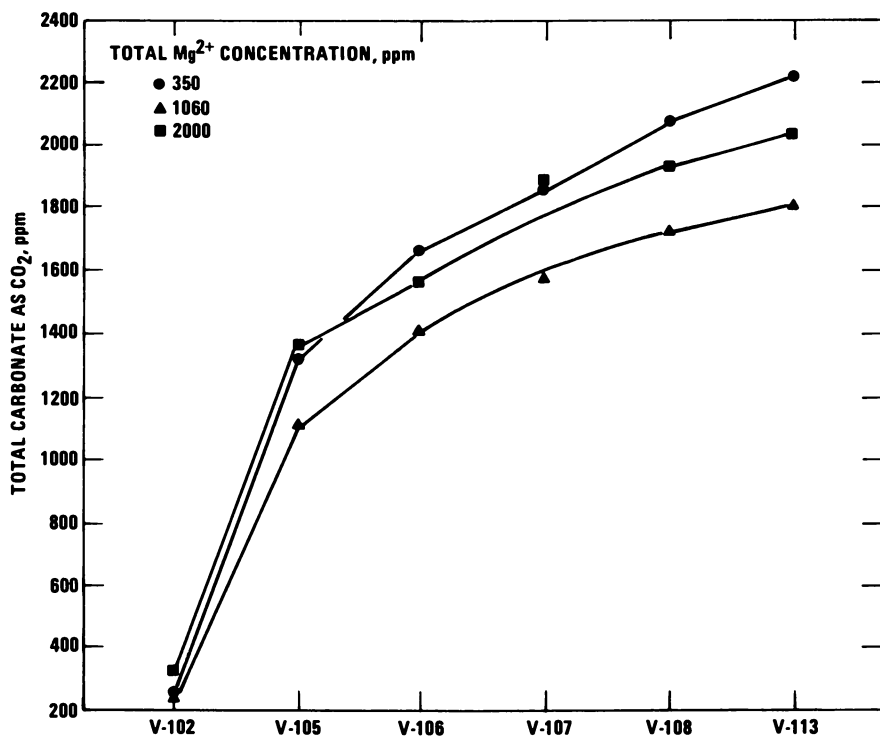
Figure 8. Distribution of carbonate ion concentration in limestone DA pilot plant.
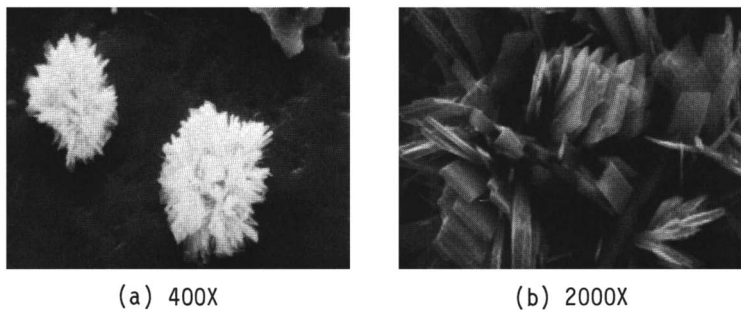
(a) 400X

(b) 2000X

Figure 9. Scanning electron micrograph of base case solid products.
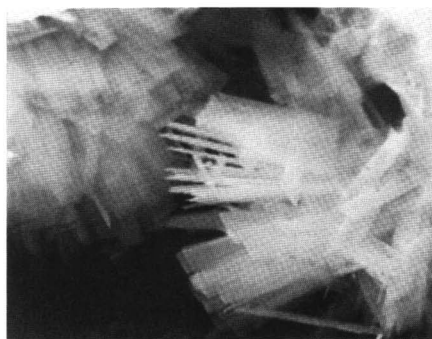
(a) 400X   (b) 2000X

Figure 10.   Scanning electron micrograph of solid products at 1000 ppm Mg^{2+} concentration.
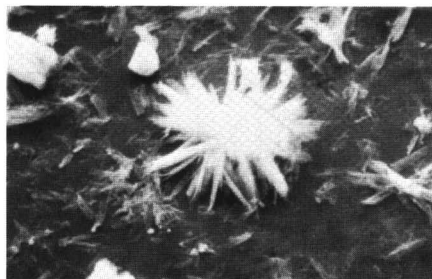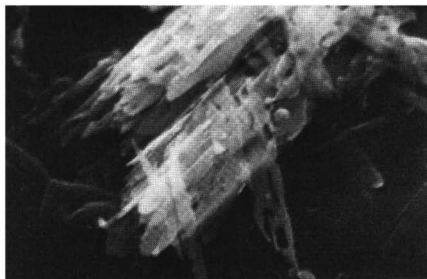
(a) 400X   (b) 2000X

Figure 11.   Scanning electron micrograph of solid products at 2000 ppm Mg^{2+} concentration.

solids (Figure 9), the solid particles in Figure 10 were composed of thinner, smaller platelets. This was reflected in poorer filter cake qualities (45 to 50% insoluble solids).

Photomicrographs of solids produced at 2000 ppm total Mg^{2+} concentration are shown in Figure 11 which indicates that the solid particles are composed of ill-defined, needle-like platelets. Furthermore, Figure 11b reveals serious crystal defects. The poor crystal properties were evidenced by an extremely low settling rate (less than 0.1 cm/min) and very few filter cake insoluble solids (less than 30%).

In summary, two significant effects of Mg^{2+} concentration on DA system performance were observed. First, the pilot plant data indicated that the solid product dewatering properties are very sensitive to Mg^{2+} concentration. Photomicrographs show that the deterioration of solids dewatering properties is caused by crystal morphology changes comprising crystal size decreases and crystal defects. Second, the limestone dissolution rate decreased as reflected by the system pH drop. This effect is not very significant until the total Mg^{2+} concentration reaches about 1000 ppm.

Surface Adsorption Model

The effect of Mg^{2+} on the dissolution rate of $CaCO_3$ has been investigated by laboratory experiments with a pH-stat[6]. Results indicated that the presence of Mg^{2+} in the solution reduces the $CaCO_3$ dissolution rate. To interpret the data, it was assumed that Mg^{2+} can be adsorbed on the surface of $CaCO_3$ particles to form a surface Ca-Mg-carbonate. The adsorption reduces the dissolution rate since the surface is partially blinded by adsorbed Mg^{2+}. It was also assumed that the reduction of the dissolution rate is proportional to the fraction of the surface (θ) occupied by the adsorbed Mg^{2+}, which can be expressed by the Langmuir adsorption isotherm:

$$\theta = ac/(1 + bc) \tag{1}$$

where a and b are constants and c is the concentration of adsorbed species.

The dissolution rate (R) can be determined from:

$$R = kA (1 - r^{1/2})^n \tag{2}$$

where k is the apparent rate constant, A is the active surface area, r is the degree of $CaCO_3$ saturation, and n is a constant. In the presence of Mg^{2+}, the active surface area A is related to θ by:

$$A = A_0(1 - \theta) \tag{3}$$

where A_0 is the total surface area. The inhibition effect of Mg^{2+} on $CaCO_3$ dissolution rate can be described by the following correlation derived from Equations (1), (2), and (3):

$$(1 - R/R_0) = 1.38 \times 10^5 \, [Mg^{2+}]/(1 + 1.68 \times 10^5 \, [Mg^{2+}]) \tag{4}$$

where R_0 is the dissolution rate in the absence of Mg^{2+} and $[Mg^{2+}]$ is the concentration of total magnesium in moles per cubic centimeter.

In wet FGD processes, either DA or limestone slurry, the combined effects of calcium and magnesium actually determine the limestone dissolution rate. Sjoberg's results[6] indicated that Ca^{2+} can inhibit the $CaCO_3$ dissolution rate much more effectively than Mg^{2+} by the same surface adsorption phenomenon. The combined effects of Ca^{2+} and Mg^{2+} can be described as competitive adsorption, and the limestone surface will act as an ion-exchanger. The fraction of surface occupied by adsorbed Ca^{2+} and Mg^{2+} can be expressed as:

$$\theta = \theta_{Ca} + \theta_{Mg} \qquad (5)$$
$$= \sum_{i=1}^{n} a_i c_i / (1 + \sum_{i=1}^{n} b_i c_i)$$

where a_i and b_i are constants and c_i is the concentration of the adsorbed species i. The reduction of dissolution rate is proportional to θ, or:

$$(1 - R/R_0) \alpha \theta \qquad (6)$$

In the ideal case, a_i and b_i are constants independent of c_i. Therefore,

$$\frac{\theta_{Mg}}{\theta_{Ca}} = K' \frac{[Mg^{2+}]}{[Ca^{2+}]} \qquad (7)$$

where K' is a constant with a value of 0.033 as obtained by Sjoberg[6].

Equation (7) indicates that the relative effectiveness of Mg^{2+} and Ca^{2+} in inhibiting the limestone dissolution rate depends on the ratio of Mg^{2+} concentration to Ca^{2+} concentration. On the other hand, the sensitivity of limestone dissolution rate to the Mg^{2+} concentration is determined by the Ca^{2+} concentration. As indicated by Equation (7), when the minimum ratio (θ_{Mg}/θ_{Ca}) of 0.5 is required for Mg^{2+} to effectively inhibit the limestone dissolution rate, dual alkali processes need only 908 ppm Mg^{2+} since the normal Ca^{2+} concentration in the first reactor is about 100 ppm. Furthermore, if competitive adsorption of Mg^{2+} and Ca^{2+} also occurred on the $CaSO_3$ surface, the adsorbed Mg^{2+} can act as an impurity which causes crystal defects and inhibits crystal growth. As a result, the properties of the solid product deteriorate with the increase of Mg^{2+} concentration as reflected by the decrease of slurry settling rate and filter cake insoluble solids obtained from pilot plant testing.

Effects of Chloride Ions

Chloride ions (Cl^-) accumulating in the scrubbing liquor will be balanced by cations such as sodium (Na^+) and Mg^{2+}. Since previous data indicated that high Mg^{2+} concentrations are not desirable, it is expected that Na^+ will be the cation associated with the Cl^- in limestone DA scrubbing solutions.

The pilot evaluation test was started on the base case (no chloride addition) conditions with 183 ppm Cl^- concentration. Industrial grade sodium chloride was then added to the third reactor to raise the Cl^- concentration to 20,000, 50,000, and 80,000 ppm,

respectively. The principal results of these tests are listed in Table IV. Summaries of liquor and solids analyses are listed in Tables V and VI. The most significant change observed with the increase of Cl^- concentration was the decrease of system pH. While all the other variables (limestone feed rate, SO_2 feed rate, active sodium concentration, sulfate-to-sulfite ratio, etc.) were maintained at approximately constant levels, the pH of regenerated liquor decreased from 6.6 to 6.5, 6.3, and 6.2 as the Cl^- concentration increased from the base case to 20,000, 50,000, and 80,000 ppm, respectively. Correspondingly, the SO_2 removal efficiency also dropped slightly from 93 to 92, 91, and 90%, respectively. In order to maintain constant total alkalinity concentrations, the soda ash makeup rate was increased by more than 50%. No significant changes in solids quality were observed with the increase of Cl^- concentration when the Cl^- concentration was below 80,000 ppm. The filter cake insoluble solids content fluctuated between 50 and 55% and the sulfate-to-sulfite ratio dropped slightly from 1.9 to 1.8. Filter cake analyses indicated that the overall oxidation decreased from 6.9% to 4.0% as the Cl^- concentration increased from the base case level to 80,000 ppm.

Chloride ion concentrations of 100,000 ppm and 150,000 ppm were also tested. Corresponding to these Cl^- concentrations, the Na^+ concentrations reached 116,900 ppm and 140,500 ppm, respectively. As observed in previous runs, the system pH dropped with the increase of Cl^- concentration. The base case (no chloride addition) regenerated liquor pH was 6.6. At 100,000 ppm Cl^- concentration, the regenerated liquor pH fell to 6.1. The regenerated liquor pH further decreased to 5.9 when the Cl^- concentration was increased to 150,000 ppm.

The most significant operating problem encountered during runs with 100,000 and 150,000 ppm Cl^- was scaling in the absorber. The quench nozzle scaled and plugged, and a very high pressure drop (over 10 in. H_2O) across the absorber was obtained. Layers of hard scale composed of $CaSO_3/SO_4$ were found on the absorber walls. A large quantity of water soluble sodium scale was deposited beneath the middle and the bottom trays. Neither scale contained significant amounts of chloride.

In addition to scaling, system performance also deteriorated. Only 86% SO_2 removal efficiency was obtained at 150,000 ppm chloride, significantly lower than the 93% at base case conditions. Filter cake insoluble solids also decreased to 39% compared with 53% for the base case. Decreases of TOS and total alkalinity concentrations were observed and reflected the increased liquor loss and sodium consumption.

Summary

In summary, the pilot plant data indicate that:
o The solid product dewatering properties are very sensitive to Mg^{2+} concentration. Significant drops (5% or more) of filter cake insoluble solids concentrations were obtained with the increase of total Mg^{2+} concentration from 500 ppm to 1000 ppm. Solids quality deteriorated rapidly after the total magnesium ion concentration exceeded 1000 ppm. At a total Mg^{2+} concentration of 2000 ppm, a system upset with non-settling solids occurred. The solids settling rate

Table IV. Chloride-Ion-Effect Test Conditions

Run No.	CL-1	CL-2	CL-3	CL-4	CL-5	CL-6
Cl^- concentration, ppm	Base Case	20000	50000	80000	100000	150000
Tower pressure drop, in. H_2O	8.0	8.1	8.1	8.2	8.9	10.2
Liquor forward feed, gpm	1.4	1.4	-(d)	1.4	1.4	1.4
Scrubber feed pH	6.6	6.5	6.3	6.2	6.1	5.9
Scrubber effluent pH	6.2	6.1	5.9	5.8	5.7	5.5
Inlet SO_2 concentration, ppm	3040	3010	3060	3010	3030	3010
SO_2 feed rate, lb/hr	6.6	6.7	6.7	6.6	6.6	6.7
SO_2 absorption, %	93	92	91	90	89	86
SO_2 make-per-pass, mmol/l	137.1	137.7	-	122.7	131	129
Limestone slurry feed rate, lb/hr	22	22	22	22	22	22
Limestone slurry solids, wt. %	45	45	45	45	45	45
Flue gas O_2, vol. %	5.6	5.1	5.3	4.7	5.2	5.1
Thickener solids, wt. %	22.8	19.8	23.4	22.1	18.1	20.2
Filter cake solids, wt. % (insoluble)	53	52	51	52	48	39
Filter wash rate (nominal), gph	3	3	3	3	3	3
Na concentration, g/l	47.8	59.6	78.8	96.9	116.9	140.5
TOS, gmol/l	0.70	0.65	0.66	0.64	0.61	0.47
Ca concentration, ppm	61	57	58	49	51	36
Total alkalinity, gmol/l } (V-113)	0.44	0.41	0.40	0.39	0.34	0.29
Na in filter cake, mg/g(a) }	8.2	9.4	13.3	14.6	17.7	24.5
Run time, hours	85	62	68	58	84	72
Limestone stoichiometry(b)	1.03	1.03	1.04	1.07	1.08	1.10
Settling rate (reactor), cm/min	2.3	2.1	1.8	1.9	1.8	1.7
Settling test % solids	2.0	1.9	2.7	1.8	2.1	2.4
Active Na, gmol/l(c)	1.14	1.06	1.06	1.03	0.95	0.76
SO_4/Sulfite	1.9	1.9	1.8	1.8	1.84	1.72

a Washed in the belt filter
b Mass balance
c Active Na = TOS + Total Alkalinity, gmol/l
d Flowmeter not operational

Table V. Summary of Thickener Liquor Analysis from
Chloride-Ion-Effect Tests

Run No.	CL-1	CL-2	CL-3	CL-4	CL-5	CL-6
Component, g/l						
Ca	0.061	0.057	0.058 ·	0.049	0.051	0.036
Mg	0.344	0.298	0.333	0.247	0.176	0.072
Na	47.8	59.6	78.8	96.9	116.9	140.5
TOS as SO_3	56.0	52.0	52.8	51.2	48.6	37.6
SO_4	80.3	76.2	69.1	67.3	60.2	48.0
CO_3	2.68	2.25	2.12	1.95	1.25	0.96
Cl	0.183	20.1	50.3	80.2	100.0	150.0
pH	6.6	6.5	6.3	6.2	6.1	5.9

Table VI. Summary of Filter Cake Analysis from
Chloride-Ion-Effect Tests

Run No.	CL-1	CL-2	CL-3	CL-4	CL-5	CL-6
Component, mg/g						
Total S as SO_3	513	498	503	505	501	491
TOS as SO_2	382	372	381	388	383	372
Carbonate as CO_2	40	42	43	46	56	61
Ca	295	286	292	298	308	307
Mg	2.4	2.3	2.4	3.2	3.0	2.6
Na	5.9	(b)	6.2	5.8	6.5	5.9
Oxidation, %	6.9	6.6	5.3	4.0	4.4	5.3
L/S Utilization, %[a]	86.9	87.1	86.1	84.7	81.3	80.0

(a) SO_3/Ca
(b) data not available

dropped below 0.1 cm/min, and only 28% insoluble solids were obtained from the filter cake. Scanning electron micrographs showed that the deterioration of solids dewatering properties was caused by crystal morphology changes reflecting crystal size decreases and crystal defects.

o   The limestone dissolution rate decreased as shown by decreasing system pH with increasing Mg^{2+} concentration. This effect is relatively small until the total magnesium ion concentrations reach about 1000 ppm.

o   The effect of Mg^{2+} concentration on limestone dissolution rate can be explained by a surface adsorption model. The adsorption of Mg^{2+} reduces the limestone dissolution rate because the surface is partially blinded by the adsorbed magnesium ions. The competitive adsorption of calcium and magnesium ions was described by a mathematical model based on the Langmuir adsorption isotherm. The model was used to explain the sensitivity of limestone dissolution rate to magnesium ion concentration under limestone DA operating conditions.

o   When the chloride ion concentration is below 80,000 ppm, the most significant change observed with the increase of Cl^- concentration was the decrease of system pH. Correspondingly, slight drops of SO_2 removal efficiency were also obtained.

o   When the chloride ion concentration is above 100,000 ppm, system performance deteriorated with the increase of chloride ion concentration. In addition to the decreasing scrubbing solution pH and SO_2 removal efficiency, the filter cake insoluble solids also decreased and resulted in increased liquor losses and sodium consumptions.

Converting Units of Measure

Environmental Protection Agency policy is to express all measurements in SI units. When implementing this practice will result in undue costs or lack of clarity, conversion factors are provided for the non-SI units. This report uses British Engineering units of measure for some cases. For conversion to the SI system, use the following conversions:

To Convert From	To	Multiply By
gal/mcf	$1/m^3$	0.134
gpm	l/min	3.79
in	cm	2.54
in. H_2O	Pa	1.87
lb	g	454

Literature Cited

1. Kaplan, N., "Summary of Utility Dual Alkali Systems," In: Proceedings: Symposium on Flue Gas Desulfurization, Las Vegas, Nevada, March 1979, Volume II, EPA-600/7-79-167b (NTIS PB80-133176), July 1979.
2. Chang, J. C. S. and N. Kaplan, "Pilot Evaluation of Limestone Regenerated Dual Alkali Process," In: Proceedings: Eighth Symposium on Flue Gas Desulfurization, New Orleans, LA, November 1983, Volume 1, EPA-600/9-84-017a (NTIS PB84-223031), July 1984.
3. Chang, J. C. S., "Pilot Plant Tests of Chloride Ion Effects on Wet FGD System Performance," EPA-600/7-84-039 (NTIS PB84-167584), March 1984.
4. Laslo, D., J. C. S. Chang, and J. D. Mobley, "Pilot Plant Tests on the Effects of Dissolved Salts on Lime/Limestone FGD Chemistry," In: Proceedings: Eighth Symposium on Flue Gas Desulfurization, New Orleans, LA, November 1983, Volume 1, EPA-600/9-84-017a (NTIS PB84-223031), July 1984.
5. Chang, J. C. S., J. H. Dempsey, and N. Kaplan, "Pilot Testing of Limestone Regeneration in Dual Alkali Processes," In: Proceedings: Symposium on Flue Gas Desulfurization," Hollywood, FL, May 1982, Volume 1, EPA-600/9-83-020a (NTIS PB84-110576), October 1983.
6. Sjoberg, E. L., "Kinetics and Mechanism of Calcite Dissolution in Aqueous Solutions at Low Temperatures," Stockholm Contributions in Geology, 32(1), 1981.

Application of the Sodium Dual Alkali Scrubbing Process to High Chloride Gas Streams

William H. Mink[1]

Battelle Memorial Institute, Columbus Laboratories, Columbus, OH 43201

Pilot plant experiments on the sodium dual alkali process were conducted to determine the steady-state concentration of the major ions in the scrubbing solution and to determine the scrubbing efficiency of the solution for SO_2 and HCl when scrubbing a gas containing an HCl/SO_2 mixture. The results of the experiments suggest that the steady-state chloride concentrations in the scrubbing solution can be permitted to reach as high as about 9 percent before salt deposits cause plugging problems. Under these conditions, the filter cake will contain 35-40 percent moisture. The scrubbing efficiencies observed in the pilot plant experiments exceeded 99 percent for both SO_2 and HCl using an alkali-to-acid stoichiometric ratio of about 1.9.

The methods used for disposing of military chemical agents, such as VX, GB, and H (mustard), have been changed from land and sea burial to chemical neutralization and incineration due to environmental constraints and legislative restrictions.

As an approach to munitions disposal, the Army has developed a Chemical Agent Munitions Disposal System (CAMDS) facility at the Tooele Army Depot, Tooele, Utah. This is a prototype for other lethal chemical demilitarization plants expected to be built in the future.

The CAMDS facility was especially designed for the safe handling, disassembly, destruction, and decontamination of chemical agents VX, GB, and H, and munitions containing these chemical agents. These disposal operations must include adequate emission control technology. The emissions of concern include not only the agents themselves, but also certain species produced in the disposal process, such as sulfur oxides (SO_2 and SO_3), phosphorus oxides (e.g., P_2O_5), hydrogen chloride (HCl), and particulate matter.

[1]Current address: Panatec, Inc., Consulting Engineers, 3871 Rushmore Dr., Columbus, OH 43220

Although the present method of gas treatment is believed
to have excellent reliability, it is costly to operate because
of its raw material requirements and its material handling pro-
cedures. A particularly expensive step in the overall gas treat-
ment procedure is the required evaporative drying of salts which
result from the use of the CAMDS single alkali scrubbing system.
Alternatives to the evaporative drying of the salts have been
investigated in order to reduce the energy consumption of the
facility.

After demilitarization of a munition at the CAMDS facility,
the metal parts are conveyed into the metal parts furnace (MPF),
a roller hearth furnace, where residual agent on metal parts is
thermally destroyed. Bulk mustard is also destroyed in the MPF.
Exhaust from this furnace is treated in an extensive control system
comprising (a) an oxidizing section for thermally decomposing
any residual agents at 1600 F, (b) a quench venturi, and (c) a
packed column where the exhaust gases are contacted with NaOH
or Na_2CO_3 solution. Exhaust from the packed tower exits through
a stack to the atmosphere.

To avoid buildup of phosphates, sulfates, and chlorides
in the scrubber solution, a portion of the scrubber stream is
removed from the system and evaporated to dryness. The resultant
dry salts are then placed in drums for storage. The evaporation
step requires large amounts of energy. The use of dual alkali
scrubbing technology could avoid the need to evaporate large amounts
of water to produce a solid waste.

In the sodium-based dual alkali process, the acid gases
are absorbed by a solution of sodium salts at a pH range of 5-
8. The solution is regenerated outside the scrubber with lime
or limestone to produce a solid waste containing calcium sulfate
and calcium sulfite. Some sodium salts are lost with the waste
and must be made up by the addition of NaOH or Na_2CO_3. The prin-
cipal chemical reactions are as follows:

$$\text{Scrubber:}\quad 2NaOH + SO_2 \longrightarrow Na_2SO_3 + H_2O \qquad\qquad 1)$$
$$Na_2SO_3 + 1/2\ O_2 \longrightarrow Na_2SO_4 \qquad\qquad 2)$$
$$\text{Regenerator:}\quad Ca(OH)_2 + Na_2SO_3 \longrightarrow CaSO_3 + 2NaOH \qquad 3)$$
$$Ca(OH)_2 + Na_2SO_4 \longrightarrow CaSO_4 + 2NaOH. \qquad 4)$$
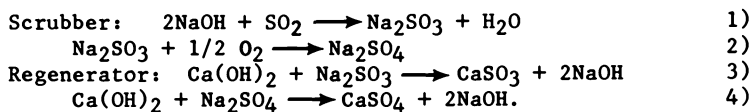
One consideration in specifying a dual alkali system for
the MPF is the relatively high concentration of HCl in the flue
gas during mustard operations. The NaCl resulting from the reac-
tion of NaOH and HCl cannot be regenerated with $Ca(OH)_2$ and must
be purged from the system. In order to avoid a liquid purge stream
which would have to be dried, the process in Figure 1 was designed
to remove the NaCl with the liquid in the filter cake.

Dual alkali systems have been extensively applied to scrub-
bing SO_2 from boiler flue gas. In most of these applications,
the objective in using a dual alkali system as compared to a
single alkali system, is to minimize the use of the more expensive
sodium as compared to the calcium in lime. However, the most
cost-effective operation for the system on the MPF is one that
will eliminate the expensive drying process. The design shown
in Figure 1 may actually require considerably more alkali than
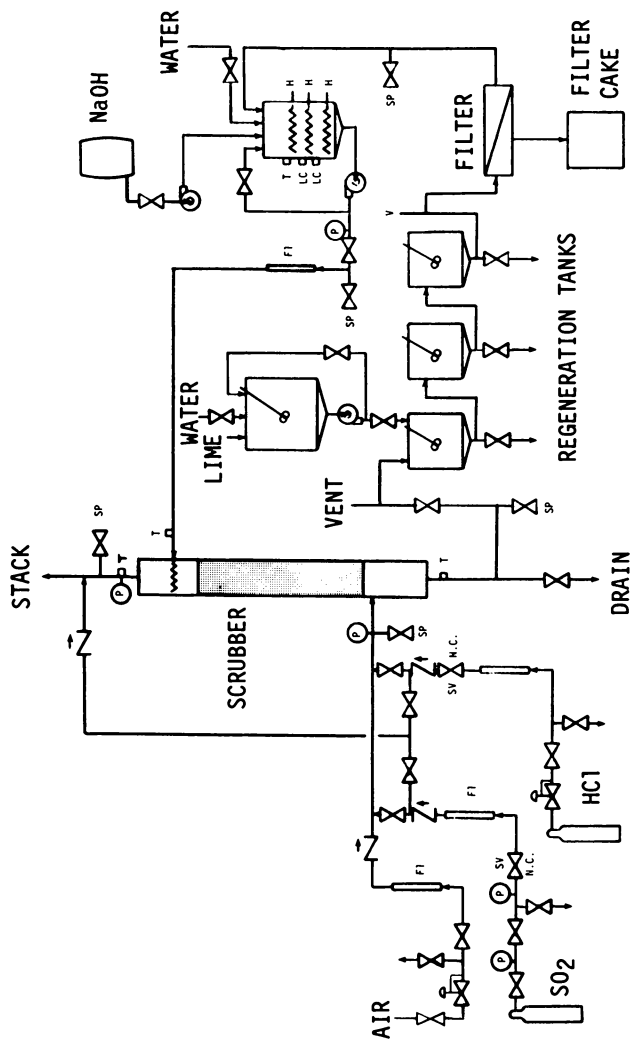
Figure 1. Pilot Plant Process Flow Diagram

the minimum required in order to increase the solids content in
the waste filter cake and thereby allow the NaCl to be purged
with the liquid attached to the filter cake. In order to minimize
this quantity of liquid, the chloride content is allowed to build
up to very high levels.

The principal advantage of a dual alkali process applied
to the MPF is the substitution of a relatively inexpensive filter-
ing step for the expensive drying step in the single alkali system.

Application of the sodium-based dual alkali process to
high chloride gas streams is of interest not only to the Army
but also to other operators of combustion systems using conven-
tional fuels such as coal where toxic chloride-containing wastes
are co-fired for destruction purposes.

Results and Discussion

After assembling the sodium dual alkali pilot plant shown in Figure
1, it was operated at several different conditions to explore
the scrubbing efficiency, the effect of chloride buildup in the
scrubbing liquor, and to obtain a material balance. Tables IA
and IB summarize the data obtained in the 13 runs made in the
pilot plant.

Scrubbing Efficiency. The effect of the stoichiometric ratio
of total alkali fed to the scrubber [Ca(OH)$_2$ plus NaOH] to total
acid gas (SO$_2$ plus HCl) is shown in Figure 2. The theoretical
limit for reaction of the alkali with the acid gases is indicated
in the figure. (Actually, some removal of HCl can be expected
with no alkali present.) Sulfur dioxide removal efficiencies
were found to exceed 99 percent when alkali/acid stoichiometric
ratios were greater than about 1.9. HCl removal efficiencies
generally exceed SO$_2$ removal efficiencies at any given alkali/
acid stoichiometric ratio.

Effect of Chloride Buildup

Removal Efficiency. The outlet stream from the regeneration tanks
was filtered to remove the solids. A typical filtrate composition
at the higher chloride concentration range is presented in Table
II. The filtrate was recycled to the system, mixed with additional
sodium hydroxide, and pumped back into the column as scrubbing
liquor. Chloride built up as the scrubbing reaction occurred.

Figure 3 shows percent SO$_2$ remaining in the scrubbed gas
as a function of alkali/acid gas stoichiometric ratio at steady-
state. The numbers beside each point are chloride concentration
in the scrubber liquor. From an examination of this figure, it
does not appear that chloride concentration has any significant
effect on SO$_2$ removal in the range studied.

Solids Precipitation. Although chloride concentration in the
scrubber liquor has little effect on removal efficiency, it has
a significant effect on the operation of the column. Chloride
concentrations greater than about 6.6 percent (see Table III),
lead to some deposit of salts in the scrubber column. Neverthe-
less, it appears that if chloride level is maintained below about
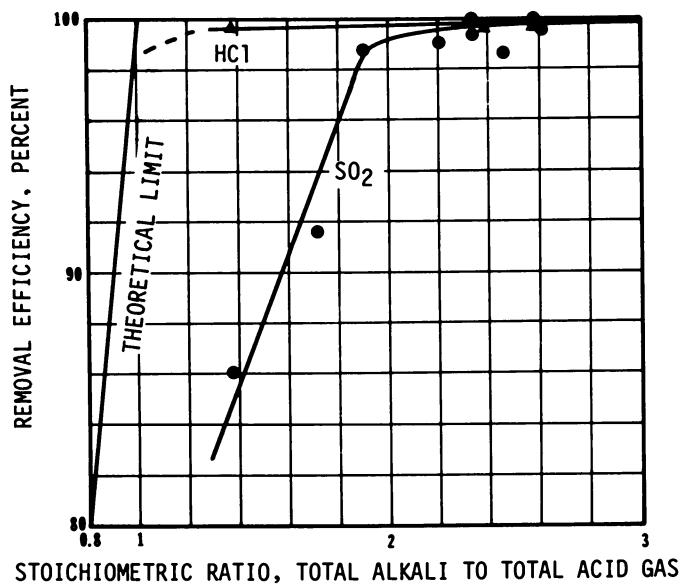
Figure 2. SO_2 and HCl Removal Efficiency

Table IA. Run Conditions

Run No.	Liquor Recirculation Rate GPM	Gas Rate CFM	Column Temperature		Column pH		Ca(OH)$_2$ Feed #/Hr	NaOH Feed #/Hr	Purpose of Run
			Inlet	Outlet	Inlet	Outlet			
1	1.0	31.4	158 F	108 F	10.4	--	5.46	*	a
2	1.7	31.0	158	108	9.5	--	10.98	*	a
3	1.4	30.6	160	99	12.0	10.4	6.18	3.9	a
4	0.9	30.6	160	96	10.9	5.2	9.44	4.2	a
5	1.3	30.6	158	106	10.9	2.3	6.18	0.0	b
6	0.9	31.1	163	94	11.0	1.3	6.18	4.25	c
7	1.2	31.1	162	95	10.4	1.2	7.72	3.65	c
8	0.9	31.1	159	95	12.0	4.2	9.44	4.65	c
9	0.6	31.1	161	96	12.1	4.1	10.98	4.75	c
10	0.4	31.1	159	96	12.1	1.9	9.44	4.65	d
11	1.1	32.4	161	--	12.1	0.2	9.44	11.5	e
12	0.6	32.4	163	--	12.2	0.6	9.44	11.5	e
13	0.7	32.4	160	--	12.1	3.5	9.44	5.4	e c

a To build concentration of liquor. b Build concentration and removal efficiency data.
c Obtain removal efficiency data. d Material Balance Run – removal efficiency data.
e Determine effect of high concentration of salts in liquor.

Table IB. Run Gas Concentrations and Results

Run No.	SO$_2$ Concentration PPM		HCl Concentration PPM		Stoichiometric Ratio total alkali/total acid gas	Removal Efficiency, %	
	In	Out	In	Out		SO$_2$	HCl
1	5,290	--	25,700	--	--	--	--
2	4,450	--	15,600	--	--	--	--
3	4,500	50	15,800	--	2.20	98.89	--
4	4,500	68	15,800	--	2.46	98.49	--
5	4,500	632	15,800	24	1.38	85.96	99.85
6	8,290	700	15,600	--	1.72	91.56	--
7	8,290	95	5,600	--	1.89	98.95	--
8	8,290	60	15,600	--	2.34	99.28	--
9	8,290	4	15,600	26	2.61	99.95	99.12
10	8,290	10	15,600	138	2.34	99.88	99.83
11	8,290	--	54,300	--	1.03	--	--
12	8,290	--	54,300	--	1.03	--	--
13	12,560	34	37,800	--	2.61	99.73	--

Table II.   Filtrate Composition
(Run 11)

Species	PPM
Ca^{++}	1,490
Na^+	41,200
Cl^-	83,200
$SO_3^=$	100
$SO_4^=$	1,300

8.5 to 9 percent, column operation would not be impaired. Figure
4 shows chloride concentration of the last nine runs together
with an indication of the degree of column plugging.
     Precipitation occurs when solubility limits of the compo-
nents in solution are exceeded. This is the case when chloride
concentration in the scrubbing liquor reaches values above 6.6
percent. These salts redissolve in the liquor, indicating that
they are most likely sodium salts.
     Chloride is removed with the moisture in the cake, thus
maintaining a steady-state concentration. Essentially no chloride
is removed as a solid as shown in a typical dry cake analysis
(Table IV).

Table IV.   Typical Dry Cake Solids Compositions
(Run 11)

A.   Analysis

Species	PPM
Ca^{++}	338,000
Na^+	32,100
Cl^-	512
$SO_3^=$	336,000
$SO_4^=$	390,000

B.   Postulated Dry Cake Composition

Species	%
NaCl	1.6
Na_2SO_4	7.9
Na_2SO_3	14.8
$Ca(OH)_2$	20.9
Unaccounted for	12.5
	100.0
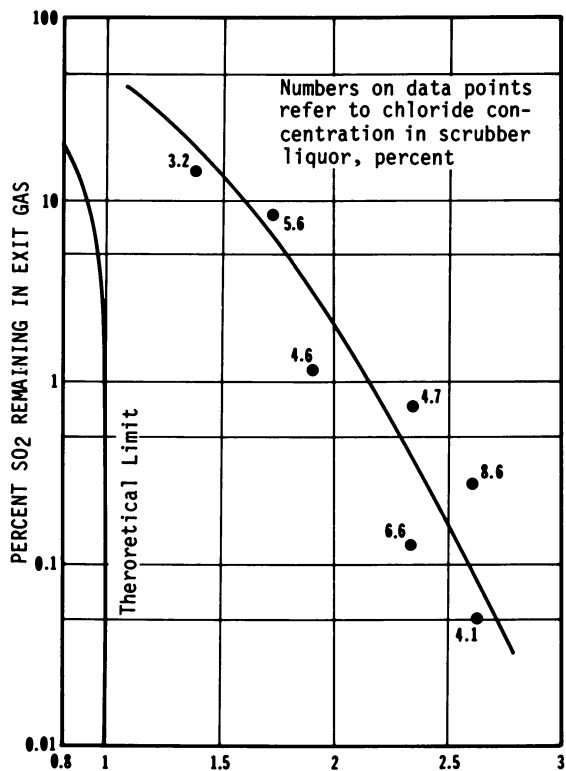
Figure 3. SO$_2$ Removal
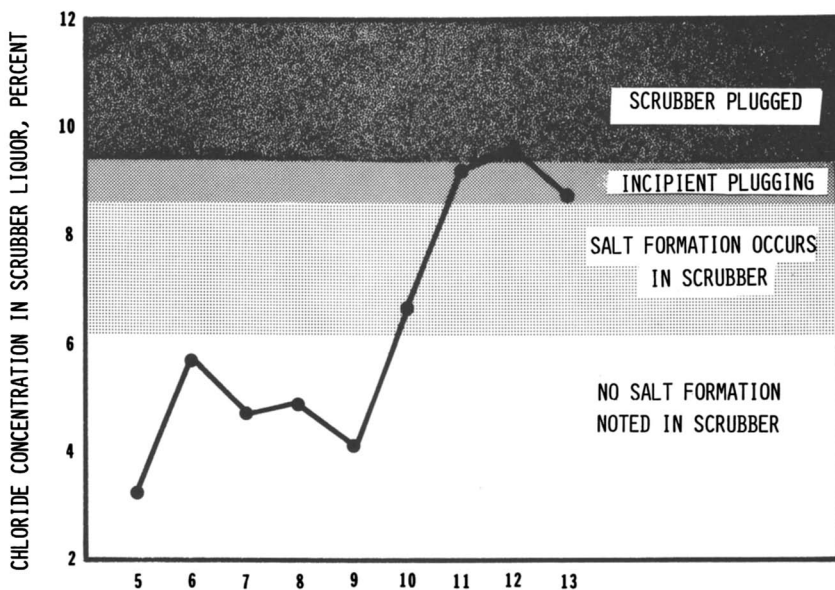
Figure 4. Effect of Chloride Concentration on Scrubber Operation

Table III. Chloride Concentration of Scrubber Liquor in Various Runs

Run No.	Cake Moisture, percent	Average Chloride Concentration in Scrubber Liquor, percent	Scrubber Liquor pH		Comments
			Scrubber Feed	Scrubber Discharge	
5	50.7	3.2	10.5	2.0	a
6	55.7	5.6	11.0	1.4	a
7	47.9	4.6	10.4	1.2	a
8	50.9	4.7	12.0	4.2	a
9	48.3	4.1	12.1	1.6	a
10	43.0	6.6	12.1	2.0	b
11	35.3	9.2	12.2	0.2	c
12	--	9.5	12.2	0.4	d
13	--	8.6	12.2	1.3	e

[a]No salt formation noted in scrubber. [b]Some salt formation noted. [c]Intermittent plugging in column.
[d]Scrubber full of salts. [e]Salt formation reduction noted.

        The other type of salt precipitating in the column is cal-
cium based. Elimination or reduction of calcium ions in the liquor
is critical if the temperature in the system drops. A larger
amount of precipitate was observed in the pilot plant when over-
night temperature dropped to about 60°F. Most of these salts
returned to solution after the system was reheated to operating
temperatures. This relationship between the temperature and precip-
itation must be taken into consideration in the design and operation
of a full-scale plant. As indicated by the analysis shown in
Table V, these salts are believed to be primarily calcium sulfite
and sulfate.
        Operation of a dual alkali plant would be significantly
impaired if precipitation is allowed in the system. For example,
as observed during pilot plant operation, precipitation present
at the nozzle and in the column sometimes limited the amount of
liquor input to the column.

Table V. Scrubber Deposit

Analysis

Species	Percent
Ca^{++}	24.3
Na^{+}	3.17
Cl^{-}	0.52
$SO_3^{=}$	23.4
$SO_4^{=}$	16.1
Total S	21.1

        Tower and packing designs also affect the accumulation
of insoluble matter in the column. A spray tower design would
considerably reduce the plugging potential, but at the expense
of scrubbing efficiency. The packing size, shape, and height
are also critical to the plugging problem. Large size, open shape,
and low packing height would all minimize plugging. However,
the large size has a reduced surface area per unit volume which
may cause a reduction in scrubbing efficiency. The low packing
height would also reduce the scrubbing efficiency. During the
pilot plant operation, no attempt was made to optimize the packing
material.
        The subject of scrubber plugging has been the subject of
intense study by investigators of conventional limestone and dual
alkali scrubbing systems.

Material Balance. In Pilot Plant Run No. 10, during two hours
of steady-state operation, all the materials in and out of the
system were accounted for in order to calculate a material balance.
The balance is shown in Table VI. Note that most of the values
closed to within 10 percent with the exception of calcium. The
discrepancy in calcium may have resulted from accumulation in
the scrubber column or other parts of the system and losses in
the filter washwater.

Table VI. Material Balance (lb/hr)
(Run 10)

	S	Cl	Ca	Na
IN				
Gas	1.32	2.68	0	0
Alkali	0	0	5.10	2.67
TOTAL	1.32	2.68	5.10	2.67
OUT				
Gas	0	0.02	0	0
Cake Solids	0.96	0	2.67	1.38
Cake Liquor	0.04	2.92	0.01	1.37
Wash Solids	0.39	0	1.08	0.05
TOTAL	1.39	2.94	3.76	2.80
OVER (UNDER) lb/hr	0.07	0.26	(1.34)	0.13
OVER (UNDER) percent of material in	5.3	9.7	(26.3)	4.9

Solids Removal. Some problems were found during the pilot plant
operation which were directly related to the filtration step. The
first problem was the filter cloth size. The initial filter cloth
installed plugged with the solids causing equipment malfunction.
This problem was overcome by using a coarser weave filter cloth.
     A second problem encountered with the filtration step was
the additional water introduced in the system most likely as a
result of the continuous washing of the filter cloth. This prob-
lem would probably be minimized with larger-scale equipment.
     An alternative to the horizontal belt filter for solids
separation is the use of a centrifuge or centrifugal filter.
A continuous decanter centrifuge may be acceptable for the opera-
tion. The separation of solids is controlled by the centrifugal
force, the bowel radius, and the effective length. The specifi-
cation depends on the desired product: maximum clarification,
classification, or solids dryness.
     The degree of dryness in this system is determined by the
amount of water necessary in the cake to carry out sufficient
chloride for an 8.5 to 9 percent chloride concentration in the
filtrate. A centrifugal filter was used in the pilot plant to
remove excess liquor from the cake collected in the material balance
run (Run 10) prior to analysis and disposal. The filter operated
well, reducing the wet cake to about 30 percent moisture.

pH Control and Monitoring. The pH of the scrubbing solution was
monitored during the pilot plant operation. An unsuccessful attempt
was made to control pH by use of pH controllers. The pH varied
greatly with small additions of NaOH until it reached a value
of about 12. At this level, the system appeared to be buffered.

Higher pH levels were not reached during operation. Because of
the difficulty in controlling the pH, the effect of pH on scrub-
bing was not determined and the method of NaOH addition changed
to pump feeding at a selected rate.

Continuous monitoring of the pH in the regeneration tank
was also accompanied with difficulties. Apparently, the higher
concentration of solids and extremely high pH values in localized
areas (from the lime feed) adversely affected the electrodes and
the meter. However, spot monitoring was accomplished with a por-
table unit.

The scrubber discharge pH (see Table III) varied from less
than 1 to over 4. This wide range probably resulted from the
absence of a strong buffering effect at the column discharge. The
discharge pH does not appear to correlate with either column plugging
or removal efficiency.

Corrosion. Soon after the pilot plant operation was started,
the column solution turned purple, dark green, and black. The
colors were a result of the corrosion occurring in the gas feed
lines. It was originally believed that the dry acid gases could
be retained in the stainless steel lines at least during the course
of the study. However, moisture from the compressed air, uniting
with the acid gases, caused corrosion at the point where the gases
and air mixed. To alleviate this problem, the junction of the
gas line and the air line was moved to just ahead of the column
inlet. This is an indication of the need for corrosion-resistant
pipes in a larger plant.

The column should also be made of corrosion-resistant material
to avoid corrosion problems. The pH in the tower is expected
to change from very basic at the top (pH 12) to acidic (down to
about pH 1) before the liquor reaches the bottom of the scrubber.

Conclusions

Laboratory and pilot plant studies on the sodium dual alkali scrub-
bing process indicate that it is a feasible method of scrubbing
the products of combustion of mustard agent. High removal effic-
iencies (over 99 percent) of both HCl and SO_2 may be obtained
at stoichiometric ratios of alkali-to-acid gas of about 1.9 or
higher. Removal efficiencies appear not to be affected by chlor-
ide in the scrubber liquor with loadings as high as 8.5 percent
chloride. Plugging of the scrubber occurs at chloride loadings
of over about 9 percent chloride; however, the solids redissolve
as the chloride content falls. Cake moisture content at this
chloride level was about 35 percent.

Acknowledgments

17

Effect of Deliquescent Salt Additives on the Reaction of SO$_2$ with Ca(OH)$_2$

Rosa N. Ruiz-Alsop and Gary T. Rochelle

Department of Chemical Engineering, The University of Texas at Austin, Austin, TX 78712

The effect of relative humidity, temperature, amount
of lime and SO$_2$ concentration on the reaction of SO$_2$
with Ca(OH)$_2$ solids dispersed in a sand reactor was
studied. Of these variables, relative humidity showed
the greatest impact on Ca(OH)$_2$ reactivity. Small
amounts of deliquescent salts (1 to 10 mole%) were
added to the Ca(OH)$_2$ by a slurrying and drying process,
and their effect on the reaction rate was investi-
gated. The reaction rate was studied at relative
humidities of 10% to 74%, with other conditions
similar to those encountered in bag filters during
flue gas desulfurization by spray drying. The
reaction solids were characterized by scanning
electron microscopy, powder x-ray diffraction,
coulter counter size distribution, BET (N$_2$) sur-
face area, energy dispersive x-ray spectrometry,
and differential scanning calorimetry. Most of
the deliquescent salts tested increased the
reactivity of the Ca(OH)$_2$ towards SO$_2$. The most
effective additives were: LiCl, KCl, NaCl, NaBr
and NaNO$_3$.

Spray drying has become increasingly important in recent years as an
alternative to wet scrubbing for sulfur dioxide control. In the
spray dryer the sulfur-containing flue gas is contacted with a fine
mist of an aqueous solution or a slurry of an alkali (typically
Ca(OH)$_2$ or soda ash). The sulfur dioxide is then absorbed in the
water droplets and neutralized by the alkali. Simultaneously, the
thermal energy of the gas evaporates the water in the droplets to
produce a dry powdered product. After leaving the spray dryer the
dry products, including the fly ash, are removed with collection
equipment such as fabric filters or electrostatic precipitators.
Fabric filters are the preferred collection equipment as addi-
tional sulfur dioxide removal takes place in the baghouse (1,2).
Typically, under conditions such that 80% of total inlet SO$_2$ is
removed, 60 to 70% of the removal takes place in the spray dryer
with 10 to 20% additional removal taking place in the bag filters

(3-6). Parametric studies in spray dryer pilot plants have demon-
strated that the main variable affecting SO_2 removal in the bag
filters, besides the stoichiometric ratio of $Ca(OH)_2$ to SO_2, is the
approach to the adiabatic saturation temperature of the flue gases
(3, 5-9). The approach to the adiabatic saturation temperature in
turn is correlated with the moisture content of the solids. Addi-
tives that will modify the moisture content of the $Ca(OH)_2$ solids
in equilibrium with a gas phase of a given relative humidity would
then be expected to change the reactivity of the $Ca(OH)_2$ towards
SO_2.

A few additives have been tested in spray drying systems.
Calcium chloride has proven effective in increasing the reactivity
of limestone and $Ca(OH)_2$ towards SO_2 (10, 11). Adipic acid was
also tested (12) with mixed results. Sodium sulfite, sodium hydro-
xide, Fe++ compounds, Ethylene-diamine-tetra-acetic-acetic acid
and disodium salt (EDTA) have been used as additives during simul-
taneous SO_2 and NO_x removal (Niro Process) (13). The emphasis in
the Niro process was to improve the removal of NO_x.

The present work was undertaken to investigate, in a systematic
manner, the kind of additives that could be used to improve $Ca(OH)_2$
reactivity towards SO_2. A small fixed bed reactor was used to simu-
late the conditions encountered in the bag filters during spray
drying flue gas desulfurization. Three different kind of additives
were tried: buffer acids, organic deliquescents and inorganic
deliquescents. The inorganic salts were selected according to their
deliquescent properties, or the lowering of the vapor pressure of
water over their saturated solutions. Of these three types of addi-
tives the deliquescent salts were the only substances that increased
the $Ca(OH)_2$ reactivity.

Experimental Apparatus

The general design of the experimental apparatus is given in Figure
1. A simulated flue gas was synthesized by combining nitrogen and
sulfur dioxide from gas cylinders. The gas flow rates were measured
using rotameters. Water was added by means of a syringe pump and
evaporated at 120°C before mixing with the gas stream. The glass
reactor (4 cm diameter, 12 cm height) was packed with a mixture of
silica sand and powdered reagent $Ca(OH)_2$ in a weight ratio of 40:1.
The addition of sand is necessary to avoid channeling caused by
$Ca(OH)_2$ agglomeration (10). The 100 mesh silica sand was obtained
from Martin Marietta Aggregates. The reactor was immersed in a
water bath that maintained the system temperature within 0.1°C.
Tubing upstream from the reactor was heated to prevent the conden-
sation of moisture on the walls. Before going to analysis the gas
was cooled and the water then condensed out by cooling water and an
ice bath. The gas was analyzed for SO_2 using a pulsed fluorescent
SO_2 analyzer (Thermoelectron Corporation model 40) and the concen-
tration continuously recorded. The reactor was equipped with a
bypass, to allow the bed to be preconditioned and to allow the gas
flow to be stabilized at the desired SO_2 concentration before begin-
ning the experimental run. Before each experimental run the bed
was humidified by flushing with pure nitrogen at a relative humidity
of about 98% for 10 minutes then later with pure nitrogen at the
relative humidity at which the experiment was to be performed for 8
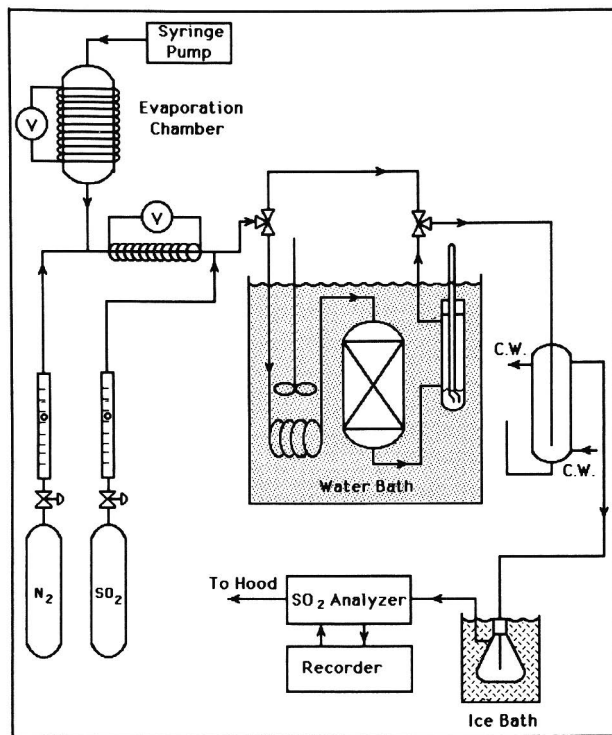
Figure 1. Experimental Apparatus

minutes. This was done to simulate better the moisture conditions
encountered in the bag filters because the solids leaving the spray
dryer were originally slurry droplets.

Preparation of the Samples with Additives

An aqueous solution containing the desired additive was prepared.
Five ml of this solution were then added to 1 g of $Ca(OH)_2$ and
slurried. The sample was placed in a oven to dry at 75°C for about
14 hours then later sieved to separate the individual $Ca(OH)_2$ parti-
cles prior to mixing with the silica sand and being placed in the
reactor.

Analysis

The fraction of $Ca(OH)_2$ reacted at any given time can be calculated
by integrating the SO_2 versus time curve obtained by the recorder on
the SO_2 analyzer and doing a mass balance in the reactor. As a
backup, the reacted solids are analyzed for sulfite and hydroxide
using acid/base and iodine titrations.

Characterization of the Reactant

The experimental work was done using reagant grade $Ca(OH)_2$ as a
reactant. Two batches of $Ca(OH)_2$ that will be identified as lime O
and lime A were used. These two batches of $Ca(OH)_2$ differ slightly
in particle size and BET surface area as shown in Table I. The use
of these two different batches of $Ca(OH)_2$ was not by choice, but
rather forced by the depletion of the first batch of $Ca(OH)_2$ (type O).
The particle size distribution of the $Ca(OH)_2$ was determined by means
of a Coulter Counter model T_{AII} using as electrolyte a solution of 4
wt% $CaCl_2$, saturated with $Ca(OH)_2$. The surface area was determined
using Brunauer, Emmett, and Teller (BET) nitrogen absorption iso-
therms. The BET surface area of a sample of 1 g of $Ca(OH)_2$ A, after
slurrying with 5 ml of distilled water and drying at 75°C is also
showed in Table I. The slurrying and drying process caused a slight
decrease in the surface area of $Ca(OH)_2$.

Figures 2 and 3 show Scanning Electron Micrographs of the two
types of $Ca(OH)_2$ used as the reactant. From these pictures it can be
seen that the $Ca(OH)_2$ particles are in the micrometer size range, are
highly nonspherical, and have considerable surface roughness.

The samples of $Ca(OH)_2$ with additives that were prepared in the
way discussed above were characterized using x-ray powder diffraction,
scanning electron microscopy (SEM), energy dispersive spectroscopy
(EDS), and BET surface area. According to x-ray diffraction analysis,
most of the additives precipitate as a separate phase after slurrying
with the $Ca(OH)_2$ then drying. The exception is $CaCl_2$, where a
$Ca(OH)_2 \cdot CaCL_2 \cdot H_2O$ phase is formed. This finding agrees with the
result reported in the literature for the equilibrium of the $Ca(OH)_2 \cdot$
$CaCl \cdot H_2O$ system (14). In the case of $Ca(NO_3)_2$, the formation of the
solid phase $Ca_2N_2O_7 \cdot 2H_2O$ has been reported (14). This could not be
confirmed using x-ray analysis as the diffraction pattern of the
$Ca_2N_2O_7 \cdot 2H_2O$ was not available. X-ray diffraction and scanning
differential calorimetry showed the reaction product to be
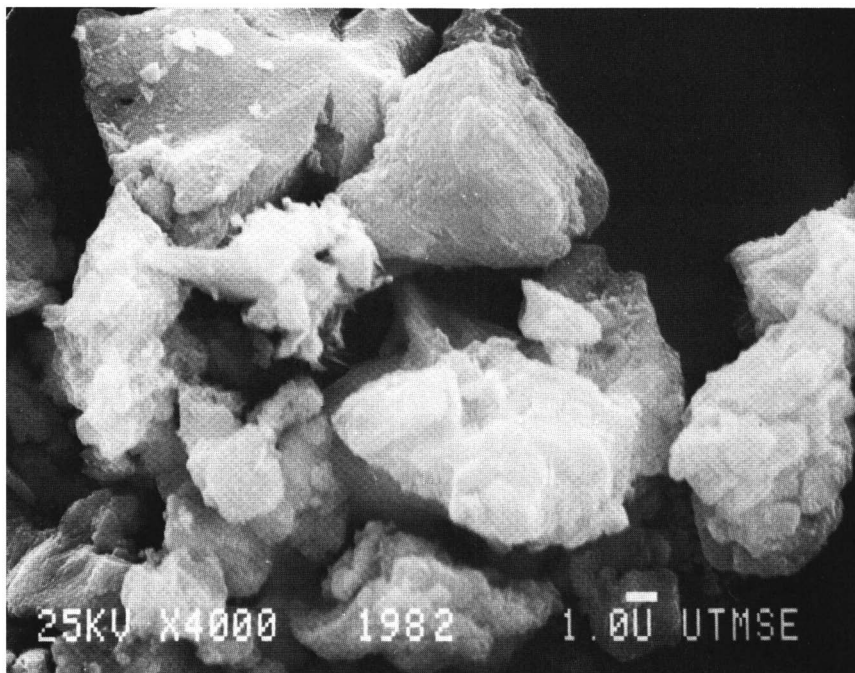
Figure 2. SEM picture, lime O, 4000 Magnification
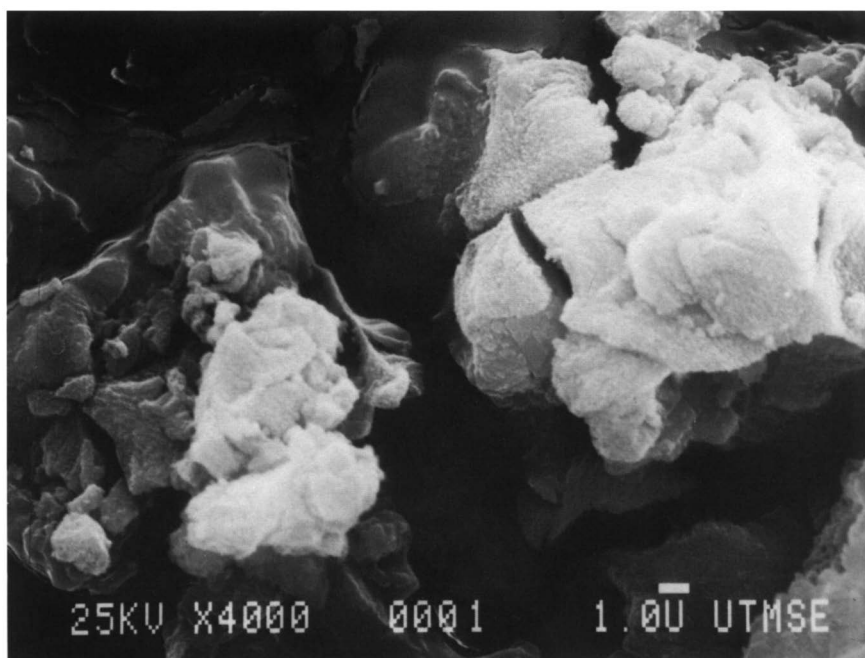
Figure 3. SEM picture, lime A, 4000 Magnification

$CaSO_3 \cdot \frac{1}{2}H_2O$. No gypsum or any other sulfate phase was detected either by x-ray diffraction or scanning differential calorimetry, suggesting that any sulfate produced in the reactor will be present in solid solution with the $CaSO_3 \cdot \frac{1}{2}H_2O$.

EDS was used to analyze individual particles and it was found that the additives precipitate together with the $Ca(OH)_2$ and are, more or less, uniformly distributed through the $Ca(OH)_2$ particles. SEM micrographs of the particles of $Ca(OH)_2$ with additives showed no significant difference in size or shape from the pure $Ca(OH)_2$ particles. The BET surface areas of the $Ca(OH)_2$ with different salt additives were also measured. The surface areas ranged from 7.0 to $9.6 m^2/g$ depending on the additive used. No correlation was found between $Ca(OH)_2$ reactivity and surface area.

Effect of Process Variables

Experiments were performed to determine the effect of relative humidity, temperature, inlet SO_2 concentration, and amount of $Ca(OH)_2$, on the reactivity of pure $Ca(OH)_2$ towards SO_2.

Relative humidity has the greatest impact on $Ca(OH)_2$ reactivity. Figure 4 shows $Ca(OH)_2$ conversion as a function of time at 19, 50 and 70% relative humidity. All three experiments were run at 2000 ppm inlet SO_2 and 66°C using 4 g of lime O. The discontinuous line in the figure corresponds to the $Ca(OH)_2$ that would be converted if all the SO_2 were being removed. For all relative humidities, 100% of the SO_2 is removed during the first one or two minutes of reaction, then the reaction rate decreases quickly at low relative humidities but slower at high relative humidities. The same kind of behavior was observed with the other batch of lime A which differs slightly in particle size and BET surface area.

Reactor temperature has a very moderate effect on $Ca(OH)_2$ reactivity, as illustrated by Figure 5 that shows the effect on $Ca(OH)_2$ conversion versus time when the temperature is increased from 30.4°C to 64.4°C while keeping all other variables constant.

The effect of the inlet SO_2 concentration on the reaction rate was found to depend on the relative humidity. At 70% relative humidity the $Ca(OH)_2$ conversion was practically independent of the inlet SO_2 concentration as illustrated in Figure 6. At lower relative

Table I: Particle Size and BET Surface Area of Reactant

Reactant	Coulter Counter Median Particle Size (μm)	BET Surface Area (m^2/g)
lime O	7.4	8.2
lime A	5.6	9.4
lime A (slurried)	–	8.8

humidity the reaction rate is not affected by the SO_2 concentration if the SO_2 concentration is high. However, at lower levels of SO_2
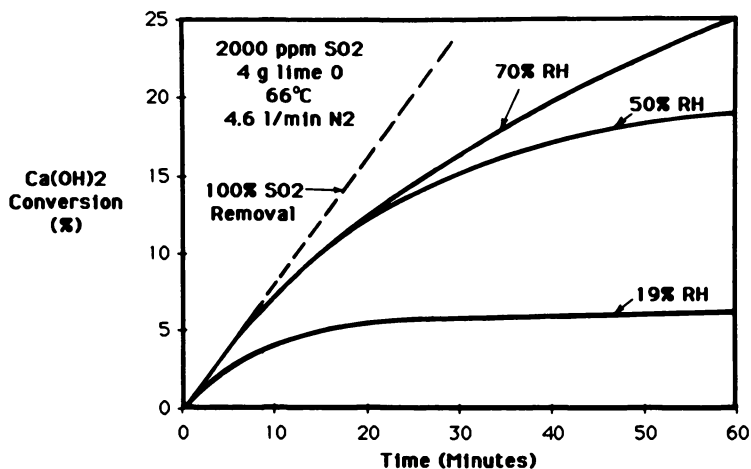
Figure 4.   Lime O, Effect of Relative Humidity
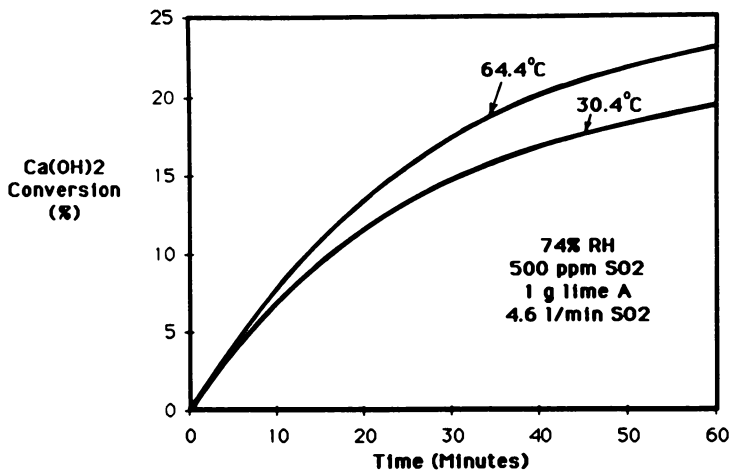
Figure 5.   Effect of Reactor Temperature, Lime A

the reaction rate is affected by the SO_2 concentration as illustrated by Figure 7 which shows the $Ca(OH)_2$ conversion at 50% relative humidity. The fact that at low relative humidities and low SO_2 levels the SO_2 concentration affects the reaction rate could be explained by assuming that the reaction has zero order kinetics in SO_2, but at low relative humidity and/or low SO_2 concentration, mass transfer through the product layer becomes the controlling step instead of chemical reaction.

     The effect on the average $Ca(OH)_2$ conversion of changing the amount of $Ca(OH)_2$ in the reactor is illustrated by Figure 8 which shows the $Ca(OH)_2$ conversion when the amount of $Ca(OH)_2$ in the reactor was reduced from 4 to 1 g, keeping the SO_2 concentration at 1000 ppm and the relative humidity at 50%. From Figure 8 it can be seen that the amount of $Ca(OH)_2$ present in the reactor makes a difference during the first minutes of reaction, but the effect is less marked at later times. These results are consistent with the effect of SO_2 concentration discussed above. When more $Ca(OH)_2$ is present in the reactor, more SO_2 is removed at the entrance of the reactor, so the $Ca(OH)_2$ present farther down in the reactor "sees" a lower concentration of SO_2, and the reaction rate is slower. At later times when the SO_2 removal is lower the amount of $Ca(OH)_2$ present will not be as important.

Effect of Organic Acids and Organic Deliquescents

Two organic acids were selected as test additives for $Ca(OH)_2$, adipic acid because of its extensive use in wet scrubbing, and glycolic acid, because of its deliquescent properties. Both of these acids proved to be detrimental to the reaction of SO_2 with $Ca(OH)_2$, as can be seen from Table II. At 74% relative humidity the average $Ca(OH)_2$ conversion in the reactor decreased from 22 to 11% when 5 wt% of glycolic acid was added to the $Ca(OH)_2$, and from 22 to 20% when 1 wt% adipic acid was used as additive.

Table II: Effect of Organic Acids and Organic Deliquescents on $Ca(OH)_2$ Reactivity

500 ppm SO_2, 1.0 g lime A, 74% RH, 64.4°C, 4.6 1/min N_2

Additive	Average $Ca(OH)_2$ conversion after 1 hour (%)
None	22.4
ORGANIC ACIDS	
5 wt% Glycolic Acid	11.3
1 wt% Adipic Acid	20.3
ORGANIC DELIQUESCENTS	
5 wt% Monoethanolamine	19.6
5 wt% Ethylene Glycol	20.3
5 wt% TEG	20.5
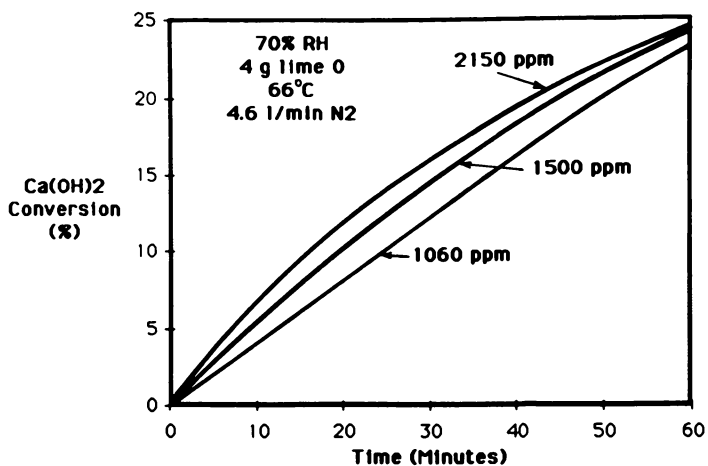
Figure 6.   Effect of SO_2 Concentration, High Relative Humidity
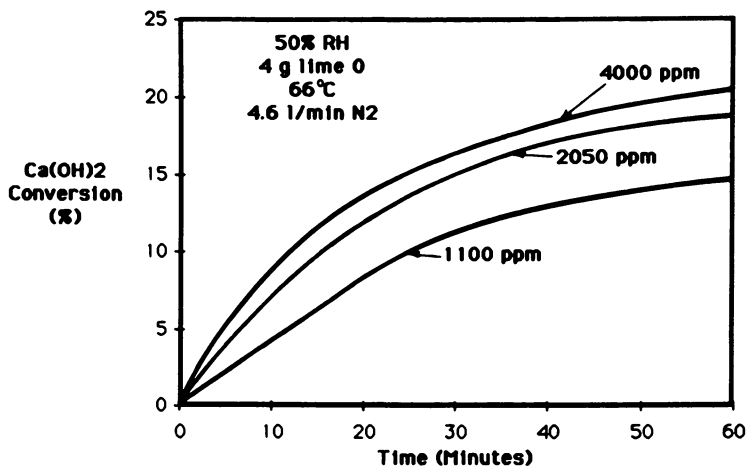
Figure 7.   Effect of SO_2 Concentration, Low Relative Humidity

The organic deliquescents tried were ethylene glycol (EG), tri-ethylene glycol (TEG), and mono-ethanolamine (MEA). The experimental runs made adding 5 wt% of EG, TEG, or MEA are presented in Table III. At 75% relative humidity, all three additives slightly decreased the $Ca(OH)_2$ converted after 1 hour of reaction, when compared with the conversion of pure $Ca(OH)_2$ at the same experimental conditions.

Effect of Deliquescent Salts Additives

Table III shows the experimental results of $Ca(OH)_2$ with deliquescent salts as additives, at 74 and 54% relative humidity. From the results presented in this table we can see that the beneficial effect of salts depends on the type of salt and the relative humidity. At high relative humidity (74%) all the deliquescent salts tried were successful in increasing the reactivity of the $Ca(OH)_2$ towards SO_2. At lower relative humidity (54%) some of the salts do not per-form as well, and some, such as $Ca(NO_3)_2$, do not have any beneficial effect at all.

Also presented in Table III is the water activity over saturated solutions of the salts at 25 and 100°C and 1 atm. The water activity is approximately equal to the relative humidity of the gaseous phase that would be in equilibrium with a saturated solution of the salt at that temperature and pressure. If one of these deliquescent salts is contacted with a gaseous phase of relative humidity greater than the water activity, the salt will capture water from the gas phase and become a solution. This tendency to capture water has been extensive-ly documented in the literature by studies of the growth of salt containing aerosols as a function of the atmospheric relative humi-dity (15-20). From the data presented in Table III it is clear that based in deliquescence alone most of the salts tested, specifically $NaNO_3$ and all the chlorides with exception of LiCl, should not have any beneficial effect at 54% relative humidity. Nevertheless, these salts are among the ones that behave the best at that low relative humidity. A possible explanation for these findings would be an hysteresis phenomenon, and this will be discussed later in the paper.

Influence of Salt Concentration. A series of experiments were per-formed to determine the influence of the salt concentration on the SO_2 reaction rate. The salts used were NaCl and $NaNO_3$ in concentra-tions ranging from 1 to 15 mole%. The experiments were carried out at a relative humidity of 54%, and a reactor temperature of 66°C. As can be seen from Figure 9, the conversion increases with increasing concentration of additive until about 10 mole%. After this the curve levels off. The optimum concentration of additive is then about 10 mole% for 1:1 electrolytes like NaCl and $NaNO_3$.

Effect of Prehumidification at 98% Relative Humidity. As was men-tioned in the Experimental Apparatus Section, before each experi-mental run the fixed bed was prehumidified by flushing with pure nitrogen at a relative humidity of about 98% for 10 minutes before flushing with nitrogen at the relative humidity at which the experi-ment was to be performed.

This prehumidification step could be the reason why some of the salts are still effective at a relative humidity lower than the one
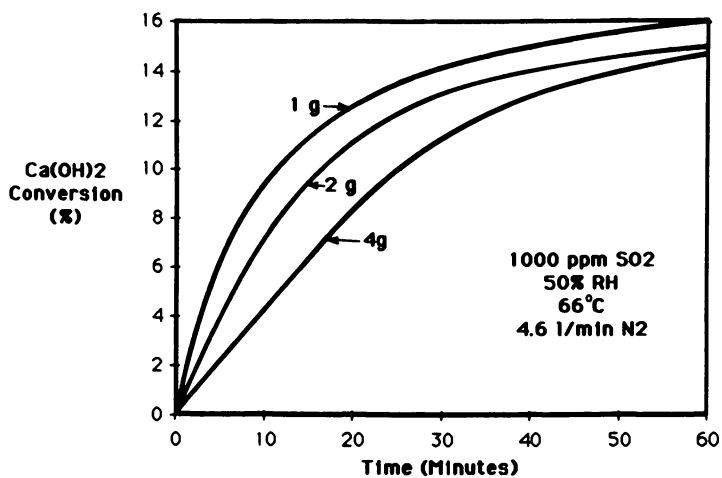
Figure 8.   Effect of Ca(OH)$_2$ loading, 1000 ppm SO$_2$
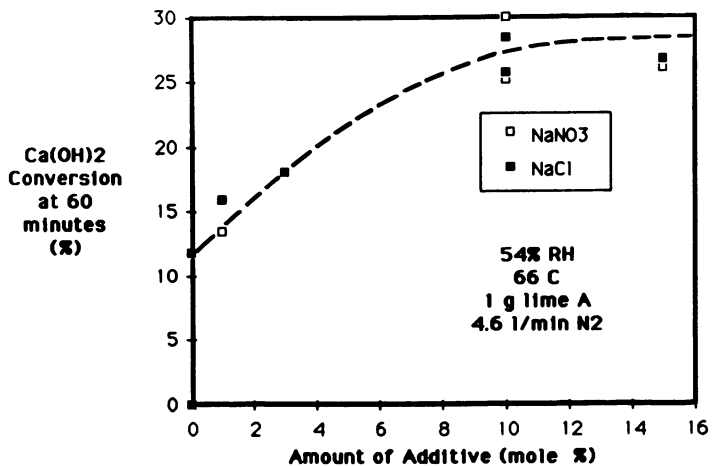
Figure 9.   Effect of Amount of Additive on Ca(OH)$_2$ Reactivity

Table III: Effect of Deliquescent Salts in $Ca(OH)_2$ Reactivity
and Deliquescent Properties of the Salts

500 ppm SO_2, 1.0 g $Ca(OH)_2$ A, 4.6 l/min (0°C, 1 atm) N_2

Additive (Mole%)	$Ca(OH)_2$ Conversion at 60 Minutes (%)		Water Activity Over Saturated Solutions	
	74% RH 64.4°C	54% RH 66°C	at 25°C	at 100°C
None	22.4	11.8	-	-
5% Na_2SO_4	28.3	-	-	.902 (1)
5% Na_2SO_3	29.8	16.1	-	-
5% $CaCL_2$(**)	34.6	16.4	.850 (1)	.686(*,1)
10% NaCL	38.5	27.0	.753 (3)	.735
5% $Ca(NO_3)_2$(**)	39.4	12.3	-	.553 (1)
5% $Co(NO_3)_2$	-	13.2	-	-
10% $NaNO_2$	40.0	-	-	.496 (2)
10% $NaNO_3$	41.5	27.2	.738 (3)	.549 (1)
5% $BaCl_2$	-	19.4	.902 (3)	.71 (2)
5% $Na_2S_2O_3$	-	21.6	-	.52 (2)
10% KCl	-	37.3	.842 (3)	.745 (1)
10% NaBr	-	42.0	.577 (3)	.502 (1)
10% LiCl	-	43.0	.112 (3)	.085 (1)
100% SO_2 Removal	48.2	48.2	-	-

(*)   data at 75°C
(**) Solids phases were $CaCL_2 \cdot Ca(OH)_2 \cdot H_2O$ and $Ca_2N_2O_7 \cdot 2H_2O$,
      respectively.
(1)   Source (15)
(2)   Extrapolated from (15)
(3)   Source (16)

predicted from equilibrium considerations. Due to hysteresis it is possible that when the relative humidity was lowered to the experimental conditions after the prehumidification, some excess water remains in the solids. Strong hysteresis effects have been reported in NaCl aerosols (21).

To check if hysteresis was responsible for the beneficial effect of some salts at low relative humidities, experimental runs were made omitting this step. Table IV shows the results obtained at 54 and 17.4% relative humidity with and without prehumidification of the bed at 98% relative humidity. The additives used were NaCl, NaNO3, and KCl. At 54% relative humidity even when some decrease of the Ca(OH)2 conversion was found without the prehumidification, the results are still far superior to the pure Ca(OH)2 case. Hysteresis then, can not explain all the beneficial effect observed at 54% relative humidity. At 17.4% relative humidity all the beneficial effect in the case of the NaCl appears to be due to the prehumidification of the bed, i.e., due to a hysteresis phenomenon.

Effect of Nitrogen Purity

When experiments using NaCl as an additive were performed it was found that the Ca(OH)2 conversion given by chemical analysis of the reacted solids was consistently lower than the Ca(OH)2 conversion calculated by integration of the SO2 versus time curve. This difference could be explained by the partial oxidation of the sulfite produced in the reaction by the oxygen present as an impurity in the nitrogen. To test this possibility some experiments were run using oxygen free nitrogen (purity of 99.998%) instead of the nitrogen previously used that has a purity of 99.5%.

Table IV: Effect of Prehumidification of the bed at 98% RH
on Ca(OH)2 Reactivity

500 ppm SO2, 1.0 g Ca(OH)2 A, 4.6 1/min (0°C, 1 atm) N2

Average Ca(OH)2 Conversion after 1 hr (%)

Additive (Mole%)	54% RH 66°C Prehumidified		17.4% RH 95°C Prehumidified	
	Yes	No	Yes	No
None	11.2	–	4.0	–
10% NaCl	27.0	23.2	9.7	4.0
10% NaNO3	27.2	23.7	11.9	–
10% KCl	37.3	19.3	3.4	–

Table V shows the comparison of two experiments run at the same experimental conditions but using the two different types of nitrogen. A much better agreement was found between the Ca(OH)2 conversion obtained by chemical analysis and the one obtained by integrating the SO2 curve when oxygen free nitrogen was used. The Ca(OH)2 conversion estimated by integration of the SO2 curve was the same in both experiments indicating that the rate of SO2 removal is not affected by the nitrogen purity even when some oxidation of the

Table V: Effect of Nitrogen Purity on Lime Reactivity

500 ppm SO_2, 54% Relative Humidity, 1.0g lime A, 4.6 1/min N_2

| | $Ca(OH)_2$ Conversion after 1 hour (%) | |
Type of Nitrogen	By Integrating SO_2 Curves	By Chemical Analysis
Common (99.5% purity)	27.0	19.7
O_2 Free (99.998% purity)	27.0	25.1

sulfite appears to be taking place when the less pure nitrogen was used.

Discussion

As shown in the results section, the relative humidity of the gaseous phase is the most important variable in the reaction of SO_2 with dry $Ca(OH)_2$ solids. These results are in agreement with results reported in the literature for SO_2 removal in the bag filters of spray dryer pilot and commercial plants (3, 5-9). In the spray dryer plants, the moisture content of the gases is normally indicated as approach to the adiabatic saturation temperature (difference between the tempera-ture of the gas and the adiabatic saturation temperature) rather than relative humidity.

The other variables tested, i.e. temperature, amount of $Ca(OH)_2$ and SO_2 concentration have a lower impact on the reaction rate. The different effect of SO_2 concentration at low and high relative humi-dity can be explained by assuming that the reaction has zero order kinetics in SO_2 and that at low relative humidity the reaction rate is mass transfer controlled while at high relative humidities the reaction is controlled by reaction kinetics.

Most of the deliquescent salts tried were effective in increasing $Ca(OH)_2$ reactivity towards SO_2. The extent of the beneficial effect being a function of the type of salt, the salt concentration, and the relative humidity. Some salts are effective at a lower relative humidity than would be predicted from their deliquescent properties. Hysteresis due to the prehumification of the bed appears to be partially responsible for this behavior. In other words some water remained absorbed in the solids after the relative humidity was reduced because of surface tension effects and formation of over-saturated solutions. From the results presented in Table IV, it can be concluded that even when the hysteresis effects can explain the improvement in reactivity at a very low relative humidity (17.4%) it can not explain all the improvement observed at 54% relative humidity. An alternate explanation proposed is that the chlorides and $NaNO_3$ modify the properties of the product $CaSO_3 \cdot 1/2H_2O$ layer that is formed as the reaction takes place thereby facilitating the access of the SO_2 to the unreacted $Ca(OH)_2$ which remains in the interior of the particle. NaCl and $CaCl_2$ have been reported to enhance the sulfur dioxide reactivity of limestones in fluidized bed combustion by affecting the pore structure of the lime during calcination which then increases the extent of sulfation of the limestone (23).

For an additive to be effective it is necessary that the hydroxide of the cation be very soluble, otherwise the cation will precipitate as the hydroxide and the anion as the Ca salt. For example, $Co(NO_3)_2$ is very deliquescent but $Co(OH)_2$ is insoluble so Co precipitates as $Co(OH)_2$ and adding cobalt nitrate becomes equivalent to adding calcium nitrate, which is not a very effective additive.

Literature Cited

1. Kelly, M.E.; Dickerman, J.C., Proc. Symp. on FGD, 1981, p. 761.
2. Kelly, M.E.; Kilgroe, J.D.; Brna, T.G., Proc. Symp. on FGD, 1983, p. 550.
3. Stevens, N.J., Proc. Symp. on FGD, 1981, p. 777.
4. Parsons, E.L.; Hemenway, L.L.F.; Krag, O.T.; Brna, T.G.; Ostop, R.L. Proc. Symp. on FGD, 1981, p. 801.
5. Bresowar, G.E.; Borsare, D.C.; Walki, K.W. "Dry Scrubber Design and Application. The C-E Approach", presented at Joint Power Generation Conference, 1981.
6. Robards, R.F.; Aldred, R.W.; Burnett, T.A.; Humphries, L.R.; Widico, M.J. Proc. The EPA/EPRI 9th Symp. on FGD, 1985.
7. Stevens, N.J.; Manavizadeh, G.B.; Taylor, G.W.; Widico, M.J. Proc. 3rd Symp. on Transfer and Utilization of Particulate Control Tech., 1982
8. Samuel, E.A.; Lugar, T.W.; Lapp, D.E.; Fortune, O.F.; Brna, T.G.; Ostop, R.L. Proc. Symp. on FGD, 1983, p. 574.
9. Blythe, G.M.; Rhudy, R.G. Proc. 8th Symp. on FGD, 1984, p. 708-734.
10. Karlsson, H.T.; Klingspor, J.; Linne, M.; Bjerle, I., APCA J., 1983, 33, 23.
11. Rhudy, R.G.; Blythe, G.M. Proc. 9th EPA/EPRI Symp. on FGD, 1985.
12. Parson, E.L.; Boscak, V.; Brna, T.G.; Ostop, R.L. "SO_2 Removal by Dry Injection and Spray Absorption Techniques", presented at the U.S. 3rd Symp. on the Transfer and Utilization of Particulate Control Tech., 1981.
13. Felsvang, K.; Morsing, P.; Veltman, P. Proc. 8th Symp. on FGD, 1984, p. 650-667.
14. Seidell, A.; Linke, W.F. "Solubilities of Inorganic and Metal Organic Compounds", Van Nostrand Co., Inc. Washington, D.C., 1958, Vol. 1.
15. National Research Council, International Critical Tables, McGraw-Hill, New York, Vol. 3, 1930.
16. Stokes, R.H.; Robinson, R.A., Ind. Eng. Chem., 1949, 41, 2013.
17. Winkler, P. J. Aerosol Sci., 1973, 4, 373-387.
18. Ferron, G.A. J. Aerosol Sci., 1977, 8, 251-267.
19. Tang, I.N. J. Aerosol Sci., 1976, 7, 361-371.
20. Tang, I.N.; Munkelwitz, H.R.; Davis, J.G. J. Aerosol Sci., 1977, 8, 149-159.
21. Tang, I.N.; Munkelwitz, H.R. J. Aerosol Sci., 1977, 8, 321-330.
22. Tang, I.N.; Munkelwitz, H.R.: Davis, J.G. J. Aerosol Sci., 1978, 9, 505-511.
23. Chopra, O.K.; Smith. G.W.; Lenc, J.F.; Shearer, K.M.; Myles, K.M.; Johnson, I. Proc. 6th Int'l Conf. Fluidized Bed Combustion, 1980.

Activity Coefficients Predicted by the Local Composition Model for Aqueous Solutions Used in Flue Gas Desulfurization

Charles E. Taylor and Gary T. Rochelle

Department of Chemical Engineering, The University of Texas at Austin, Austin, TX 78712

The goal of this research was to improve activity coeffi-
cient prediction, and hence, equilibrium calculations in
flue gas desulfurization (FGD) processes of both low and
high ionic strength. A data base and methods were devel-
oped to use the local composition model by Chen et al.
(MIT/Aspen Technology). The model was used to predict
solubilities in various multicomponent systems for gypsum,
magnesium sulfite, calcium sulfite, calcium carbonate,
and magnesium carbonate; SO_2 vapor pressure over sulfite/
bisulfite solutions; and, CO_2 vapor pressure over car-
bonate/bicarbonate solutions.

The major objective of this work is to extend the predictability of
solution equilibria models for flue gas desulfurization (FGD)
processes by employing an activity coefficient technique which is
accurate over a wide concentration range. Current FGD equilibrium
models use the Davies technique for activity coefficient prediction.
The Davies technique is useful only up to ionic strengths of 1 molal,
thus limiting the application of FGD equilibrium models to low ionic
strength. In this work a data base and methods have been developed
to use the local composition model (LCM) ($\underline{1},\underline{2},$) for the prediction
of activity coefficients in aqueous FGD solutions. The LCM was used
to predict the solubilities in various multicomponent systems for
gypsum, calcium sulfite, magnesium sulfite, calcium carbonate, and
magnesium carbonate, SO_2 vapor pressure over sulfite/bisulfite
solutions; and, CO_2 vapor pressure over carbonate/bicarbonate solu-
tions.

    Equilibrium calculations are useful in the design or operation
of a flue gas desulfurization (FGD) facility and provide the neces-
sary foundation for complex process simulation (e.g., absorber
modeling) ($\underline{3}$). Since SO_2 absorption into FGD slurries is a mass
transfer process which is primarily limited by liquid phase resis-
tance for most commercial applications, the solution composition, in
terms of alkaline species, is very critical to the performance of the
system. Accurate prediction of solution composition via equilibrium
models is essential to establishing driving forces for mass transfer,
and ultimately in predicting system performance.

By using the fundamental principles of conservation of mass and charge, and chemical equilibrium expressions, the concentration of individual species in solution (sometimes called the "species distribution") can be calculated. The available equilibrium models for lime or limestone based FGD are the Bechtel-modified Radian equilibrium program (BMREP) (4) and the species distribution model (SDM) (5). The SDM is the most current equilibrium model and has been improved considerably over earlier models to make it more general in nature. Some simple uses of equilibrium models include predicting the saturation or solubility of gypsum to indicate scaling potential, predicting SO_2 vapor pressure to trouble-shoot problems with SO_2 removal, and predicting dissolved alkalinity or capacity of a solution. However, the BMREP and SDM have limitations which restrict their use to low ionic strength processes.

The practical limit for using the BMREP, SDM, or any equilibrium model for electrolyte solutions normally stems from the lack of correlations for electrolyte thermodynamics (e.g., activity coefficient techniques). Although lime or limestone processes inherently operate with low ionic strength because the dissolved solids are of low solubility, there are a growing number of systems operating at higher ionic strength. Ionic strength of FGD systems is highly dependent on the type of process and certain parameters such as chloride content of coal, amount of free water purged from the process, and the addition of soluble additives to the scrubbing liquid.

The BMREP and SDM currently use the Davies technique for activity coefficient prediction. The Davies technique is a combination of the extended Debye-Huckel equation (6) and the Davies equation (7). The Davies technique (and hence both equilibrium models) is accurate up to ionic strengths of 0.2 molal and may be used for practical calculations up to ionic strengths of 1 molal (8). Ion-pair equilibria are incorporated for species that associate (e.g., 1-2 and 2-2 electrolytes). The activity coefficients (γ_i) are calculated as a simple function of ionic strength (I) and are represented as:

$$\log \gamma_i = A z_i^2 \left[\frac{-I^{1/2}}{1 + B a_i I^{1/2}} + b_i I \right] \qquad (1)$$

where A and B are constants at a given temperature. Depending on the input values of a_i and b_i, Equation 1 can represent either the extended Debye-Huckel or Davies equations, or an extension of the two.

Both the BMREP and SDM approximate activity coefficients of uncharged species (e.g., ion-pairs, molecular species) by the following expression:

$$\log \gamma_i = U_i I \qquad (2)$$

where U_i is an empirical constant.

To improve the BMREP and SDM in equilibrium calculations requires an activity coefficient technique which is accurate over a wide concentration range. Rosenblatt (9,10) identified the inherent

limitations of the BMREP and SDM and investigated the use of the modified Pitzer equation as an activity coefficient technique for FGD solutions. The modified Pitzer equation (11-13) was noted as the most elaborate and successful activity coefficient technique in use (14). Rosenblatt concluded that Pitzer's equations offered a promising approach for thermodynamic modeling of FGD chemistry. Currently, Radian is incorporating the Bromley method (15) as a new activity coefficient technique in the SDM (16). Recently, Chen and co-workers (1, 2, 17-19) developed the local composition model (LCM) for activity coefficient prediction.

The LCM is a semi-theoretical model with a minimum number of adjustable parameters and is based on the Non-Random Two Liquid (NRTL) model for nonelectrolytes (20). The LCM does not have the inherent drawbacks of virial-expansion type equations as the modified Pitzer, and it proved to be more accurate than the Bromley method. Some advantages of the LCM are that the binary parameters are well defined, have weak temperature dependence, and can be regressed from various thermodynamic data sources. Additionally, the LCM does not require ion-pair equilibria to correct for activity coefficient prediction at higher ionic strengths. Thus, the LCM avoids defining, and ultimately solving, ion-pair activity coefficients and equilibrium expressions necessary in the Davies technique. Overall, the LCM appears to be the most suitable activity coefficient technique for aqueous solutions used in FGD; hence, a data base and methods to use the LCM were developed.

The Local Composition Model

The local composition model (LCM) is an excess Gibbs energy model for electrolyte systems from which activity coefficients can be derived. Chen and co-workers (17-19) presented the original LCM activity coefficient equations for binary and multicomponent systems. The LCM equations were subsequently modified (1, 2) and used in the ASPEN process simulator (Aspen Technology Inc.) as a means of handling chemical processes with electrolytes. The LCM activity coefficient equations are explicit functions, and require computational methods. Due to length and complexity, only the salient features of the LCM equations will be reviewed in this paper. The "Aspen Plus Electrolyte Manual" (1) and Taylor (21) present the final form of the LCM binary and multicomponent equations used in this work.

The approach taken by Chen and his co-workers in developing the LCM was to account for the excess Gibbs energy of electrolyte systems as the sum of long-range (ion-ion) interactions and short-range (ion-ion, ion-molecule, and molecule-molecule) interactions. The extended Debye-Huckel equation proposed by Pitzer (22) was used to account for the long-range interactions, and the local composition concept was used to account for the short-range interactions of all kinds. The excess Gibbs energy expression is therefore the sum of the unsymmetric local composition expression. The equation has the general form:

$$\frac{g^{ex^*}}{RT} = \frac{g^{ex^*,pdh}}{RT} + \frac{g^{ex^*,lc}}{RT}$$

Similarly, the activity coefficient equations (which can be derived from the excess Gibbs energy expression) have the general form:

$$\ln\gamma_i^* = \ln\gamma_i^{pdh*} = \ln\gamma_i^{lc*} \tag{4}$$

The long-range Pitzer-Debye-Huckel equation calculates activity coefficients as a function of ion strength, and no adjustable parameters are necessary. The short-range local composition equation calculates activity coefficients by accounting for all short-range interactions and requires a minimum of adjustable parameters. For binary systems, two adjustable binary parameters are necessary: salt-molecule and molecule-salt. For multicomponent systems three types of adjustable parameters are necessary: salt-molecule, molecule-salt, and salt-salt. Therefore, the regressed parameters of the LCM data base are specifically for the short-range contribution to the activity coefficient equation.

The approach to using the LCM for FGD applications involves some assumptions and simplifications. Since the concentrations of all molecular species in solution are negligible with respect to water, only salt-water and water-salt binary parameters are necessary. All salt-molecule and molecule-salt binary parameters for molecular species other than water are set equal to salt-water and water-salt binary parameters. All molecule-molecule interactions are assumed equivalent to water-water interactions and are set equal to zero. Additionally, all salt-salt parameters are set to zero. Lastly, the temperature dependence of all binary parameters is neglected.

Results and Discussions

The results of applying the LCM to typical FGD solutions are summarized in Tables I and Table II. Table I presents the final regressed LCM binary parameters for typical FGD solutions. The implied formation reactions, and temperature dependent parameters for the equilibrium constants are shown in Table II.

Regression of the necessary LCM binary parameters required various thermodynamic data. The Power method (23), an unconstrained nonlinear code, was used to minimize a nonlinear function f(x) = f($x, \ldots, x_n$) of n variables. The function f(x) normally represented the standard deviation of the thermodynamic property (e.g., activity coefficients, osmotic coefficients, solubility products, or vapor pressure) being regressed using the LCM for activity coefficient prediction. The n variables represent the final regressed binary parameters. Default values were used for binary parameters representing interactions of species present in low concentration, or when no thermodynamic data were available. Default values were determined by averaging binary prarmeters regressed by Chen and co-workers (18) for each type of electrolyte (elg., 1-1, 1-2, 2-1, and 2-2). This approach should yield a minimum error, since the binary parameters were well defined for each type of electrolyte.

The LCM has proven to be useful in predicting data of molal ionic activity coefficients and vapor pressure depression of various single electrolyte, single solvent systems. The standard deviation of the natural logarithm of the mean activity coefficient was 0.01 for uni-univalent aqueous single electrolytes (17). Similar results

Table I. LCM Data Base: Final Regressed Binary Parameters.
(A-Activity coefficient data, D-default parameters,
O-osmotic coefficient data, V-vapor pressure data)

Cation	Anion	$\tau_{ca,m}$	$\tau_{m,ca}$	Data Type	Ref.
H+	SO3-2	-4.667	8.452	D	19
H+	SO4-2	-4.667	8.452	D	19
H+	HSO3-	-4.279	8.489	D	19
H+	CL-	-5.212	10.090	A	24
H+	HCO3-	-4.279	8.489	D	19
H+	CO3-2	-4.667	8.452	D	19
H+	OH-	-4.279	8.489	D	19
H+	HSO4-	-5.448	11.045	V	36
H+	AD-2	-4.667	8.452	D	19
H+	HAD-	-4.279	8.489	D	19
H+	S2O3-2	-4.667	8.452	D	19
H+	S3O6-2	-4.667	8.452	D	19
CA+2	SO3-2	-6.861	11.398	D	19
CA+2	SO4-2	-3.795	7.343	S	25
CA+2	HSO3-	-5.685	11.748	V	31
CA+2	CL-	-4.125	8.319	S	27
CA+2	HCO3-	-6.958	9.467	V	34
CA+2	CO3-2	-6.861	11.398	D	19
CA+2	OH-	-5.799	10.441	D	19
CA+2	HSO4-	-5.799	10.441	D	19
CA+2	AD-2	-6.861	11.398	D	19
CA+2	HAD-	-5.799	10.441	D	19
CA+2	S2O3-2	-4.795	9.542	V	37
CA+2	S3O6-2	-6.861	11.398	D	19
MG+2	SO3-2	-3.857	7.814	S	29
MG+2	SO4-2	-4.205	8.492	S	26
MG+2	HSO3-	-4.137	8.292	V	32
MG+2	CL-	-5.400	11.217	V	37
MG+2	HCO3-	-5.437	10.691	V	38
MG+2	CO3-2	-6.861	11.398	D	19
MG+2	OH-	-5.799	10.441	D	19
MG+2	HSO4-	-5.174	10.044	V	37
MG+2	AD-2	-6.861	11.398	D	19
MG+2	HAD-	-5.799	10.441	D	19
MG+2	S2O3-2	-6.861	11.398	D	19
MG+2	S3O6-2	-6.861	11.398	D	19
NA+	SO3-2	-2.745	5.703	V	30
NA+	SO4-2	-3.830	7.824	A,O,V	36,37,24
NA+	HSO3-	-2.735	7.779	V	30
NA+	CL-	-4.125	6.988	S	28
NA+	HCO3-	-7.196	13.109	V	33
NA+	CO3-2	-4.041	8.077	V	37
NA+	OH-	-4.816	9.644	A,O,V	36,37,24
NA+	HSO4-	-3.987	7.622	V	36,37
NA+	AD-2	-4.667	8.452	D	19
NA+	HAD-	-3.108	5.631	A,O	24
NA+	S2O3-2	-4.218	8.643	A,O,V	36,37,24
NA+	S3O6-2	-4.144	8.214	V	37

Table II. LCM Data Base: Implied Formation Reactions and Temperature
Dependent Parameters for Equilibrium Constants. Equation form:

$$-\log K = A/T + B \log T + CT + D$$

Equilibrium Constant	Implied Formation Reaction	Temperature Dependent Parameters			
		A	B	C	D
Ksp1	CaSO4*2H2O = Ca+2 + SO4-2 + 2H2O	4096.0521	31.3476	0.0	-86.9037
Ksp2	CaSO3*½H2O = Ca+2 + SO3-2 + ½H2O	-4636.4154	-31.8594	0.0	100.2073
Ksp3	MgSO3*6H2O = Mg+2 + SO3-2 + 6H2O	8121.4199	54.1774	0.0	-157.5713
Ksp4	MgSO3*3H2O = Mg+2 + SO3-2 + 3H2O	-3181.3288	-16.6579	0.0	55.3001
Ksp5	CaCO3 (calcite) = Ca+2 + CO3-2	13797.9724	108.4748	0.0	-306.2902
Ksp6	MgCO3*3H2O = Mg+2 + CO3-2 + 3H2O	-21134.1076	-143.5699	0.0	431.1240
K1	SO3-2 + SO2(aq) + H2O = 2HSO3-	2280.8662	19.6510	0.0	-60.6891
K2	SO2(aq) + H2O = H+ + HSO3-	276.8176	0.0000	0.006572	0.8521
K3	HSO3- = H+ + SO3-2	-2004.0486	-19.6510	0.006572	61.5412
HSO2	SO2(aq) = SO2(gas)	2422.8421	8.7615	0.0	-29.7136
K4	CO3-2 + CO2(aq) + H2O = 2HCO3-	-147.4864	1.2997	0.0	-6.6947
K5	CO2(aq) + H2O = H+ + HCO3-	5251.5323	36.7816	0.0	-102.2685
K6	HCO3- = H+ + CO3-2	5399.0187	35.4819	0.0	-95.5739
HCO2	CO2(aq) = CO2(gas)	2948.4426	11.4519	0.004540	-41.0371

were found for uni-bivalent and bi-bivalent electrolyte activity
coefficient prediction. Figure 1 compares the LCM with the Davies
technique for a sodium sulfate-water system (24). The LCM is accu-
rate over the entire concentration range of 0-4 molal. Two curves
are shown for the Davies technique. The upper curve assumes the
salt to be totally dissociated, and activity coefficients are calcu-
lated directly from Equation 1. The lower curve assumes the ion-
pair $NaSO_4^-$ is present, and activity coefficients are calculated from
the SDM, which incorporates the additional ion-pair equilibrium.
Figure 1 demonstrates the necessity of ion-pair equilibria to insure
an accurate activity coefficient prediction in the low concentration
range (0-0.2 molal) for salts that associate.

The LCM also predicted activity coefficients of bi-univalent
electrolytes (e.g., $MgCl_2$ and $CaCl_2$), which exhibit the experimental-
ly observed reversal of slope and dramatic increase in the activity
coefficient at higher ionic strengths. For bi-univalent electrolytes
regressing binary parameters over a 0-6 molal range causes some
inaccuracy in the low concentration region. However, regressing
the LCM binary parameters over a smaller concentration range (0-
2.5 molal) improves the LCM accuracy.

The solubility of gypsum in various salt solutions, ranging in
ionic strength from 0-6 molal, was predicted accurately by the LCM.
Figure 2 compares the LCM and SDM in predicting gypsum solubility
with the addition of sodium sulfate at 25, 50, and 75°C (25). A
relative saturation of unity would indicate accurate prediction of
the experimental data, since the solutions are known to be saturated
with gypsum. The LCM predicted the solubility of gypsum in sodium
sulfate solutions within 10 percent error in relative saturation at
50 and 70°C, and within 20-30 percent error in relative saturation
at 25°C. In magnesium sulfate solutions at 25°C (26), the LCM pre-
dicts gypsum relative saturation from 0-6 molal within 30 percent
error. The solubility of gypsum in calcium chloride (27) and sodium
chloride at 25°C (28) was predicted within 10 percent error in rela-
tive saturation from 0-6 molal. In general, the Davies technique,
and hence the SDM, gives accurate prediction of gypsum relative
saturation only in the low concentration range (0-1 molal). Increas-
ing the ionic strength causes the SDM to yield high relative satura-
tion (as seen in Figure 2).

The solubility of magnesium sulfite hexahydrate in water with
the addition of magnesium sulfate was accurately predicted by the
LCM for 0-6 molal (29). The relative saturation of the magnesium
sulfite hexhydrate was predicted within 10 percent error at 40 and
50°C, and within 20 percent error at 60°C.

The LCM accurately predicted the vapor pressure of SO_2 and CO_2
over sulfite/bisulfite and carbonate/bicarbonate solutions, respec-
tively, for salts of sodium, calcium, and magnesium. Figure 3 plots
the LCM predictions of SO_2 vapor pressure as a function of the total
SO_2 to sodium ratio for a sodium sulfite/bisulfite system at 50°C
(30). The LCM was accurate within 20 percent error in SO_2 vapor pres-
sure for the 50°C data, as well as data at 35, 70, and 90°C. The
solid line shows the general trend of the LCM predictions. Figure 4
plots the apparent equilibrium constant as a function of ionic
strength for a calcium sulfite/bisulfite system at 25, 50, and 60°C
(31). The LCM predicts the SO_2 vapor pressure within 6 percent error
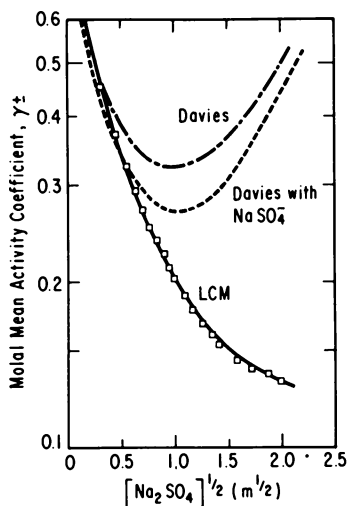
Figure 1 (left). Comparison of SDM Davies Technique and LCM in Predicting Molal Mean Activity Coefficient (1-2 electrolyte) at 25°C. Data from Robinson and Stokes (24).
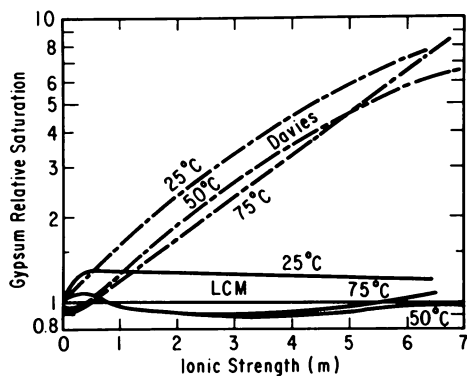
Figure 2 (right). Comparison of SDM Davies Technique and LCM in Predicting Gypsum Relative Saturation with the Addition of Sodium Sulfate. Data from Hill and Wills (25).
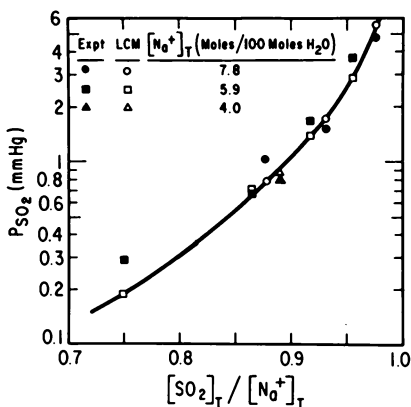
Figure 3 (left). LCM Prediction of SO_2 Vapor Pressure Over Sodium Sulfite/Bisulfite Solutions at 50°C. Data from Johnstone, et al. (30).
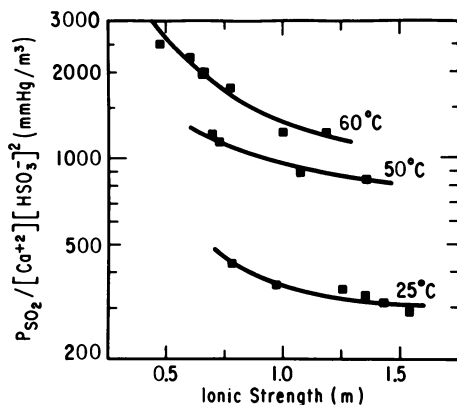
Figure 4 (right). LCM Prediction of Apparent Equilibrium Constant in Calcium Sulfite/Bisulfite Solutions. Data from Kuzminykh and Babushkina (31).

for this system at all temperatures. Similar results were obtained for a system of magnesium sulfite/bisulfite with the addition of magnesium sulfate at 48.3 and 70.6°C ($\underline{32}$). The SO_2 vapor pressure was predicted with 17 percent error for this system. Data for CO_2 vapor pressure analogous to the SO_2 systems discussed are available to a lesser extent. CO_2 vapor pressure over sodium carbonate/bicarbonate solutions ($\underline{33}$) from 35 - 65°C at constant ionic strength (1 molal) were predicted within 10 percent error. CO_2 vapor pressure over calcium ($\underline{34}$) and magnesium ($\underline{35}$) carbonate/bicarbonate solutions varying in temperature from 25 - 70°C, and at low ionic strength (<1.5 molal), were predicted within 5 percent error.

Overall, it is important to note that the data base presented in Tables I and II represent regressed LCM parameters from the best of available thermodynamic data analogous to FGD chemistry. The assumptions used in developing the data base were introduced to simplify the treatment of data correlation. Increased accuracy in activity coefficient prediction would be expected if LCM parameters such as salt-molecule (e.g., salt-Co_2, salt-SO_2) and salt-salt were regressed, or the temperature dependence of LCM parameters was introduced. Additionally, including ion-pairing and the necessary equilibria during LCM parameter regression may result in increased accuracy, especially for systems of high concentration.

Conclusions and Significance

Accurate prediction of activity coefficients over a 0-6 molal ionic strength range will allow for improvement of available FGD equilibrium models. This will provide accurate equilibrium calculations for low ionic strength lime/limestone processes and higher ionic strength processes such as dual alkali or regenerative sodium scrubbing. Additionally, improved accuracy will be available for more complex FGD simulations which use equilibrium models as a means of establishing the inlet scrubber solution composition and to calculate driving forces for rate processes.

A data base of necessary binary parameters and equilibrium constants for activity coefficient prediction by the LCM is presented. The LCM has proven to be accurate from 0-6 molal ionic strength for typical FGD aqueous solutions. In general, the LCM is slightly less accurate than the Davies technique for 0-1 molal ionic strength. The advantages of the LCM over the current Davies technique are clearly seen when predicting over the entire concentration range.

NOTATION

A	Debye-Huckel constant for osmotic coefficient
B	Temperature dependent parameter
I	Ionic Strength
R	Gas constant
T	Temperature (°K)
Z	Absolute value of ionic charge

a   Mean distance of closest approach

b   Empirical constant (normally 0.3)

g^{ex} Molar excess Gibbs free energy

m   Molality

Greek Letters

γ Activity coefficient

τ LCM binary interaction parameter

Subscripts

ca   Salt "ca" of cation c and anion a

m   Molecular species

Superscripts

*   Unsymmetric convention

lc   Short-range local composition contribution

pdh   Long-range Pitzer-Debye-Huckel contribution

Literature Cited

1. Aspen Technology Inc., "Aspen Plus Electrolytes Manual", 1984.
2. Chen, C-C, et al., "A Local Composition Model for the Excess
    Gibbs Energy of Multicomponent Aqueous Systems", AIChE Annual
    Meeting, San Francisco, 1984.
3. Chan, P.K. and G.T. Rochelle, "Modeling of SO_2 Removal by
    Limestone Slurry Scrubbing: Effects of Chlorides", EPA/EPRI
    Symposium on Flue Gas Desulfurization, New Orleans, 1983.
4. Epstein, H., U.S. EPA, Environmental Protection Technology
    Series, EPA-650/2-75/047, PB-244901, 1975.
5. Faist, M.B., et al., Radian Corporation, DOE Contract No.
    DE-AC21-80mc14549, 1981.
6. Harned, H.S. and B.B. Owens; "The Physical Chemistry of Electro-
    lyte Solutions", 3rd ed., Reinhold Publishing Corp., 1958.
7. Davies, C.W.; "Ion Association", Butterworths, Washington, D.C.,
    1962.
8. Lowell, P.S., et al., Radian Corporation, Final Report for
    Contract PHS CPA-22-69-138 to National Air Pollution Administra-
    tion (HEW), PB 193-029, 1970.
9. Rosenblatt, G.M., AIChE J. 1981, 27, 619.
10. Rosenblatt, G.M., ACS Symp. Ser. 1980, 188, 57.
11. Pitzer, K.S., J. Phys. Chem. 1973, 77, 268.
12. Pitzer, K.S.; G. Mayorga, J. Phy. Chem. 1973, 77, 2300.
13. Pitzer, K.S.; J.J. Kim, J. Am. Chem. Soc. 1974, 96, 5701
14. Maurer, G., Fluid Phase Equilibria 1983, 13, 269.
15. Bromley, L.A., AIChE J. 1973, 19, 313.

16. Radian Corporation, Communication with M.B. Faist, 1984.
17. Chen, C-C. Sc.D. Thesis, Dept. of Chem. Eng., Mass. Inst. of Tech., 1980.
18. Chen, C-C. et al., AIChE J. 1979, 25, 820.
19. Chen, C-C. et al., AIChE J. 1982, 28, 588.
20. Renon, H.; J.M. Prausnitz, AIChE J. 1968, 14, 135.
21. Taylor, C.E. M.S. Thesis, Dept. of Chem. Eng., Univ. of Texas at Austin, Texas, 1984.
22. Pitzer, K.S., ACS Symp. Ser. 1980, 133, 451.
23. Himmelblau, D.M.; "Applied Nonlinear Programming"; McGraw-Hill, New York, 1972.
24. Robinson, R.A.; R.H. Stokes; "Electrolyte Solutions", 2nd ed., Butterworths, 1959.
25. Hill, A.E.; J.H. Wills; J. Amer. Chem. Soc. 1902, 24, 674.
26. Cameron, F.K.; J.M. Bell, J. Phys. Chem. 1906, 10, 210.
27. Cameron, F.K.; A. Seidell; J. Phys. Chem. 1901, 5, 643.
28. Marshall, W.L.; R. Slusher; J. Phys. Chem. 1966, 70, 12.
29. Pinaev, V.A.; J. Appl. Chem. USSR 1964, 37, 1953.
30. Johnstone, H.F. et al.; Ind. Eng. Chem. 1938, 30, 101.
31. Kuzminykh, I.N.: M.D. Babushkina; J. Appl. Chem. USSR 1956, 29, 1601.
32. Kuzminykh, I.N.; M.D. Babushkina; J. Appl. Chem. USSR 1957, 30, 495.
33. Mai, K.L.; A.L. Babb; Ind. Eng. Chem. 1955, 47, 1749.
34. Miller, J.P.; Am. J. Sci. 1952, 250, 161.
35. Kline, W.D.; J. Am. Chem. Soc. 1929, 51, 2093.
36. CRC, "Handbook of Chemistry and Physics"; 59th ed., The Chemical Rubber Co., Cleveland, OH, 1978-79.
37. ICT, "International Critical Tables of Numerical Data, Physics, Chemistry and Technology"; Vols. I-VII, McGraw-Hill Book Co., Inc., New York and London, 1933.
38. Haehnel, O.; J. Prakt. Chem. [2] 1924, 107, 165.

19

Acoustic Agglomeration of Power Plant Fly Ash for Environmental and Hot Gas Cleanup

Gerhard Reethof

Noise Control Laboratory, The Pennsylvania State University, University Park, PA 16802

The paper shows that the imposition of a high
intensity acoustic field (140-160 db) at the proper
frequency (typically 1000-4000 Hz) on an aerosol
containing micrometer and smaller size particles
(fly ash in this case) with an exposure time of 2 to
4 seconds results in significant coagulation of
these particles into much larger particles which can
then be removed efficiently by conventional particle
removal devices. Recent advances in agglomeration
theory are described. The resulting computer based
simulation of the agglomeration processes is shown
to agree quite well with experimental results
achieved by the author. Two acoustics agglomeration
facilities are described; one for fly ash
agglomeration at up to 700°F and atmospheric
pressure; the other at up to 1600°F and 10
atmospheres to test at pressurized, fluidized bed
conditions.

Introduction and Statement of Problem. Current techniques to
remove particulates in coal fired power plant flues are based on
electrostatic precipitators, bag houses, cyclones and wet
scrubbers. Typical collection efficiencies of such devices and
the far less efficient cyclones are shown in Figure 1 (1). Of
interest is the fact that below 1 micrometer the efficiencies drop
off rather precipitously. Work presented by Davies (2), Figure 2,
has shown that the human lower pulmonary system is unfortunately
most efficient in absorbing and retaining particles in the 1
micrometer range. These particles are the primary cause of such
respiratory ailments as bronchitis, emphysema and lung cancer.
    Observations indicate that currently, approximately 50% of
the particles suspended in an urban atmosphere are smaller than 1
μm (3). This fact appears to be in part the result of the low
efficiency of particle collection devices for the removal of these
small particles. Therefore, legislation has been under
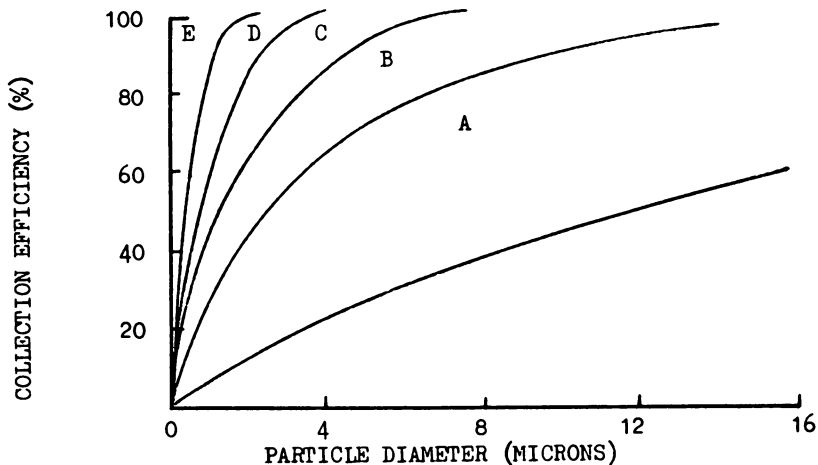
Figure 1. Typical Collection Efficiency Curves for Various Types of Collectors: A - high Throughput Cyclone; B - High Efficiency Cyclone; C - Dry Electrostatic Precipitator; D - Spray Tower; E - Venturi Scrubber
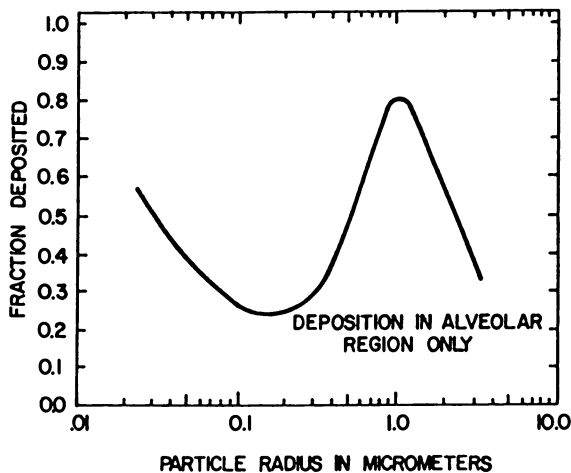
Figure 2. Deposition efficiency of particles in the human respiratory tract.

consideration at the Federal level which will include recognition of particle size rather than just mass removal which is the sole criterion in current Federal legislation. California and Maryland have already legislation in effect which, as a result of a "no visible emission" statement, provides some control of submicron particulates.

The agglomeration or growth of the submicrometer and low micrometer sized particles into 5 to 20 micrometer sized agglomerates using high intensity acoustic fields for subsequent efficient removal by conventional particle removal devices, such as those mentioned earlier, is one of the most attractive alternatives and the subject of this paper. Acoustic agglomerators would, therefore, be aerosol conditioning devices in clean-up trains consisting, for example, of a first stage of cyclones to remove the largest particles followed by an acoustic agglomeration device with the resulting enlarged particles being removed by any one of the conventional cleaning devices.

Accelerated agglomeration of particles in sound fields is not a new idea. Notable among the early studies is the work of Smoluchowski (4), in Germany in 1915; Andrade (5); Brandt, Freund and Hiedeman in Germany (6,7) in 1936; St. Clair (8) in the United States between 1938 and 1950; Stokes (9) in the United States in 1950. Of much interest is the work of Neumann, et al. (10-15), at Ultrasonic Corporation in Cambridge, Massachusetts during the early 1950s, who developed commercially available acoustic coagulators for such diverse applications as cement plants, open hearth gas dust removal, calcinated soda removal, molybdenum disulfate, ammonium chloride, carbon black and other dust as well as liquid aerosol agglomeration. Very thorough and often quoted work was done by Mednikov and others (16), and other in Russia in the 1960's. More recent work by Volk (17,18) in the United States at Penn State University has shown significant agglomeration of carbon black, white lead, kaolin clay and fly ash dusts at rather modest acoustic levels, between 100 and 120 dB with frequencies in the 1000 to 6000 Hz range, representative dust loadings between 0.5 to 2 g/m^3, and exposure times varying from 10 to 40 seconds. Scott (19), in Canada performed very interesting and important studies on the effect of nonlinear acoustic effects on agglomeration. Shaw (20-22), and his associates at the State University of New York at Buffalo have performed research of both a theoretical and experimental nature on acoustic agglomeration with special emphasis on the phenomena of acoustically induced turbulence at very high levels of acoustic intensities and also the effects of acoustically induced shock waves (22). Research at Penn State over the last two years under the author's direction has not been able to identify such high acoustically generated turbulence levels under similar conditions (23). On the other hand, very effective agglomeration of submicrometer sized particles of fly ash at flue temperatures was obtained by us with similar acoustic levels of 155-165 dB but at frequencies in the 2500 Hz range and exposure times of about 4 seconds (24).

Recent very successful demonstrations of the high efficiencies that can be achieved with combined cycle gas turbine-steam turbine power plants using pressurized, fluidized

bed coal combustion heat sources have shown that gas turbine life
is severely limited because even the most efficient available hot
clean-up devices cannot remove the small erosive particles from
the 6 to 10 atmosphere, 1600°F gas streams. Acoustic
agglomeration in conjunction with high efficiency cyclone trains
appears to be the only viable means of making this promising new
power plant concept feasible.   We must also mention the
acoustic agglomeration experiments conducted by the Braxton
Corporation (25) in 1974 which did not give good results. In
fact, essentially no agglomeration was experienced in this rather
large scale facility. These tests which were supported by EPA,
were performed at a frequency of 366 Hz and intensities of 165 dB.
Redispersed cupola dust of about 4 micrometer mean size and fly
ash of about 6 micrometer mean size were used as dusts. The
results of our research (26) and Dr. Shaw's work (20-22) clearly
show that for the type and size of dust used, frequencies on the
order of 2500 Hz and 3000 Hz provide optimum agglomeration. It
is, therefore, not surprising that very poor results were obtained
by the Braxton experiments.

From these introductory remarks it is apparent that much work
has been done on both the theoretical and the practical aspects of
acoustic agglomeration. The research results to date at Penn
State University show conclusively that acoustic agglomeration of
fly ash can be accomplished yet further research is required on
several important acoustic and coagulation phenomena before large
scale demonstration of the technical and economic viability of the
process can be accomplished. The work reported has been supported
by the Pittsburgh and Morgantown Energy Technology centers of the
U.S. Department of Energy.

The Fundamentals of Acoustic Agglomeration of Small Particulates.
Let us consider a polydisperse aerosol consisting of submicrometer
and micron sized particles. The mean separation distance between
particles would typically be about 100 micrometers. Brownian
movement of the particles is caused by the collision of the
thermally agitated air molecules with the particles. Also any
convection currents or turbulence in the carrier gas will of
course cause the particles to be partially entrained and moved in
the air. If we next impose an acoustic field of acoustic pressure
p, the acoustic velocity u will be given by

$$u = \frac{p}{\rho_0 c} \qquad \qquad 1)$$

where ρ_0 is the air density and c is the speed of sound in the air.
For a typical acoustic sound pressure level of 160 dB the acoustic
velocity will be about 5 m/sec (for 150 dB the acoustic velocity
will drop to 0.5 m/sec, one tenth this value). For a typical
acoustic frequency of 2000 Hz, a fully entrained particle might
flit back and forth 2000 times a second over a distance of about
600 µm.

We shall next develop a simple relationship for the
entrainment of a small particle of diameter d_p in an acoustic
field. The entrainment factor η is defined as the ratio of

particle velocity amplitude U_p to gas velocity amplitude U_g.
Since the Reynolds number of the flow is less than about 10 we can
apply Stokes' Law to obtain an expression for the viscous drag
flow on the particle

$$F_d = 3\pi\mu \ d_p \ (u_g - u_p) \qquad\qquad 2)$$

where μ is the gas dynamic viscosity, u_g and u_p are the time
varying gas and particle velocities respectively. Applying
Newton's second law to a particle of density ρ_p we obtain

$$\left(\frac{\rho_p \pi d_p^3}{6}\right) \ \frac{du_p}{dt} = 3\pi\mu dp \ (u_g - u_p) \qquad\qquad 3)$$

which is put into the form of 4) where the relaxation time τ is
given by 5)

$$\tau \ \frac{du_p}{dt} + u_p = u_g \qquad\qquad 4)$$

$$\tau = \frac{\rho_p \ d_p^2}{18\mu} \qquad\qquad 5)$$

since the gas velocity in a sound field of frequency ω is given by
6)

$$u_g = U_g \ \sin\omega t \qquad\qquad 6)$$

and entrainment factor was defined earlier and given by 7)

$$\eta_p = \frac{U_p}{U_g} \qquad\qquad 7)$$

Thus for $\eta_p = 1$ full entrainment occurs and $\eta_p = 0$ is no entrainment
occurs, meaning the solution of 4) in the form of 8)

$$u_p = \eta_p \ U_g \ \sin \ (\omega t - \phi) \qquad\qquad 8)$$

which means that the steady state solution of 4) is given by 9)

$$\eta_p = \frac{U_g \ \sin \ (\omega t - \phi)}{\sqrt{1 + \omega^2 \tau^2}} \qquad\qquad 9)$$

and the entrainment factor becomes

$$\eta_p = \frac{1}{\sqrt{1 + \dfrac{\rho_p d_p^2 \pi f \ 2}{9\mu}}} = \frac{1}{\sqrt{1 + \omega^2 \tau^2}}$$

where frequency $f = 2\pi\omega$.
    For a particle density of 2300 kg/m^3 corresponding to fly ash
dust and frequencies of 500, 1000 2000, 5000, 10,000 Hz, the
entrainment factor η_p is plotted for various particle diameters in
Figure 3. For each of the frequencies there is a cut particle

size (the size for which n_p = 0.5) below which particles are
almost fully entrained. For example, for the 2000 Hz case the cut
particle size is about 4.5 micrometers. The large particles
compared to the cut size are essentially still, the small
particles are moving through large displacements colliding with
the large particles, adhering to these particles because of the
large Van der Waal forces. In a slowly convecting field we can,
therefore, think of the large particles as cleaning out the small
particles thereby generating empty spaces. One of the long
standing unanswered questions in this field has been how the
refill of these swept out volumes occurs. Every investigator in
this country and abroad has assumed either explicitly or tacitly
that the swept out volume would be refilled in just one cycle
without giving a justification. Penn State's most recent
agglomeration analytical model also is based on this premise and,
as will be shown later, gives good agreement between our
measurements and prediction.

We recently completed an analytical investigation of the flow
field near slowly drifting spheres at Reynolds numbers from 0-10
(24). The interaction of flow fields between two moving spherical
particles of unequal size required the solution of the uncoupled
Navier Stokes Equations and applying experimentally obtained
expressions for the drag coefficient as a function of Reynolds
number. Typical results are shown in Figure 4 for a 10 micrometer
and a 1 micrometer particle exposed to an acoustic field of 150 dB
at 2500 Hz for several acoustic cycles. The 10 micrometer
particle remains essentially stationary and is shown at the origin
of the plot. The trajectory of the central position of 9
different (one at the time) particles entering from the right side
are shown with each little circle depicting the particle after
each acoustic cycle. The larger the spacing between little
circles along a trajectory the larger the velocity. The important
conclusion to be drawn is that the flow field around the large
particle causes the small particles which are vertically higher
than 10 micrometers to assume a significant orthogonal velocity to
the acoustic velocity thereby being able to refill the swept-clear
volumes. Actually the particles sweep through about 250
micrometers during each cycle as shown in Figure 5. Our
calculations show that this phenomenon explains about 85% of the
refill, the rest resulting from gravitational and turbulent
diffusion processes.

In a separate investigation on the fragility of agglomerates,
we have determined that the agglomerates up to modest sizes are
sufficiently robust to withstand the rigors of the flow through
cyclones and electrostatic precipitators (27). The research is
based on experimental results with inertial separation devices
(impactors) and comparing the experienced shear stresses in
impactors as determined from theory, with the shear stresses
experienced in cyclones.

A further experimental investigation at Penn State has
established that acoustically generated turbulence at these high
acoustic intensities is not the dominant mechanism of
agglomeration and that the acoustic velocities as explained
earlier are the primary kinetic sources (23).
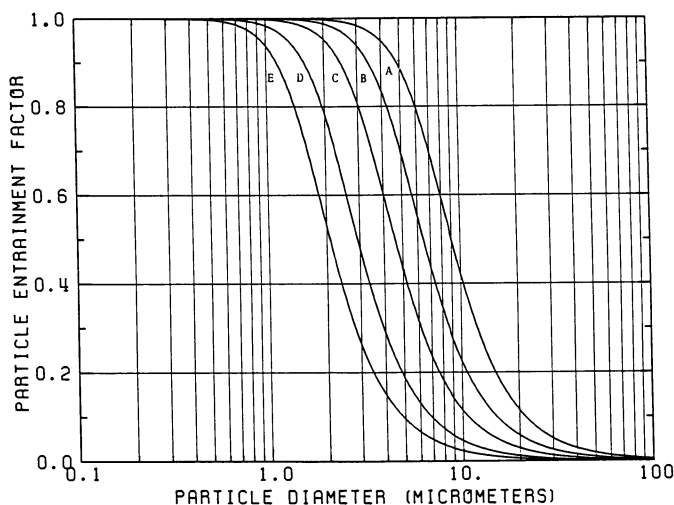
Figure 3.   Particle entrainment facotr.   Sound frequencies are:
(A) 500 Hz, (B) 1000 Hz, (C) 2000 Hz, (D) 5000 Hz and (E) 10000
Hz.
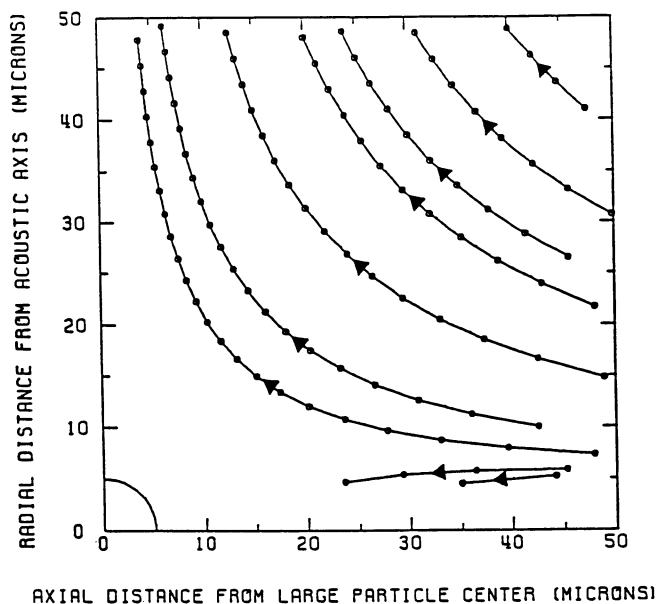
Figure 4.   Hydrodynamic interaction of particles shown for several
cycles.   Same conditions as in Figure 18.   The various lines show
trajectories of 1 micrometer particle for its different starting
locations and the small circles on the lines show the mean
positions of the 1 micrometer particle for successive acoustic
cycles.

We have recently developed a computer code for the simulation of the agglomeration processes using these just mentioned advances in our knowledge (28). The principal mechanism is the orthokinetic process including also Brownian movement and hydrodynamic particle-particle interaction. The code is in effect a simulation of the agglomeration process. The initially log normally distributed particle size distribution is divided into a number (75) of particle size ranges. As particles within ranges and particles from one range collide with particles from another range, the code moves the agglomerated particles into the range containing particles of the particular agglomerate size. The code assumes that all collisions result in agglomerations and that no break-up of agglomerates occur. Furthermore, the results of several other earlier investigations performed by us are included in the model. For example the results of our fragility study (27) permit us to exclude fractional agglomerate break-ups; the result that acoustically generated turbulence is not a significant contributor to agglomeration permits us to consider only acoustic velocity caused aerodynamic flow field; our recent results with the study of the fluid mechanics of the flow near spheres at low Reynold's numbers permit us to assume that refill of swept out volumes occurs within just a very few oscillatory periods (24). A typical result is given in Figure 6 comparing experimental results from impactor measurements with our prediction. The agreement is indeed most encouraging. What is also evident from this one example is that indeed we do obtain very significant agglomeration; in fact the particles smaller than 6 micrometers are essentially eliminated. We must point out, however, that the agreement between our idealized model and experiment is not as good for higher acoustic intensities and longer time exposures. We are continuing our research toward improving the model.

Description of the 700°F Acoustic Agglomerator. We have developed and used several acoustic agglomerators over the past 11 years that we have been working in this field. We are describing here the currently operating atmospheric pressure agglomerator which permits temperatures up to 700°F, sound pressure levels from 130-165 dB, sound frequencies from 1000-4000 Hz, dust loadings from 2 g/m^3 to 30 g/m^3, flow rates from 0.4 to 4 ft/sec in the 8 foot long agglomeration section. Noise exposure times therefore range from 2 seconds to 20 seconds.

The agglomerator is shown in the partial sectional view in Figure 7 and the system is shown in Figure 8. Starting from the left we have the 600 acoustic watt siren designed and built at Penn State. Compressed air is provided by a Roots-type blower. Pressure to the siren is controlled by means of a bypass valve. We note that the siren is acoustically coupled to the 8-inch internal diameter agglomerator chamber by an exponential type acoustic coupler. The 9.25 inch long tubular section has 16 - 0.5 inch diameter exhaust holes for the siren air. The acoustically transparent barrier prevents the cold siren air from flowing into the heater section. The sheet of felted, woven and sintered stainless steel has a low flow resistance rayls giving an acoustic transmission loss of only 4 dB. By automatically controlling the pressure drop across the barrier to about 1 inch of water, we are
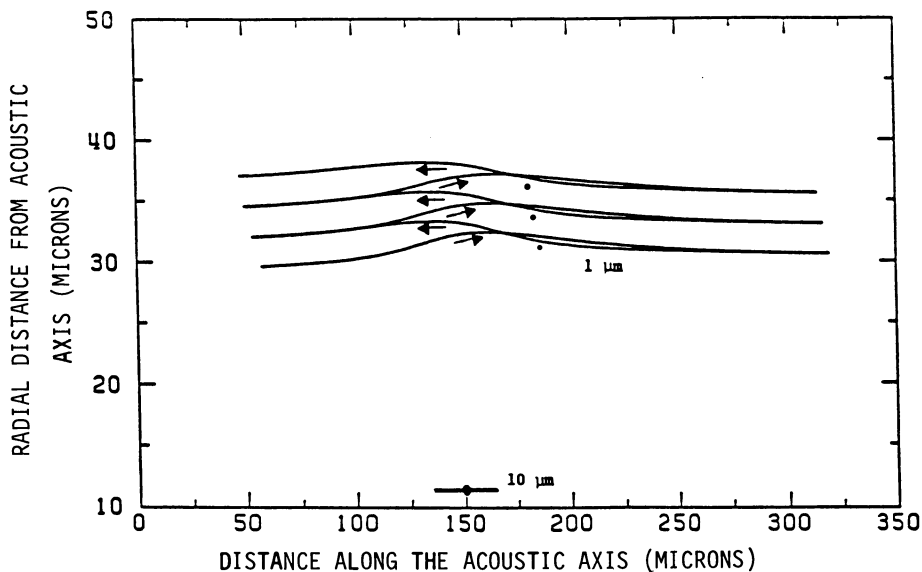
Figure 5.   Hydrodynamic interaction of particles for 3 acoustic
cycles.   Acoustc waves of 2500 Hz frequency and 150 dB sound
pressure level, particles of 1 and 10 micrometer diameter.   The
circles show mean positions during the acoustic cycles.
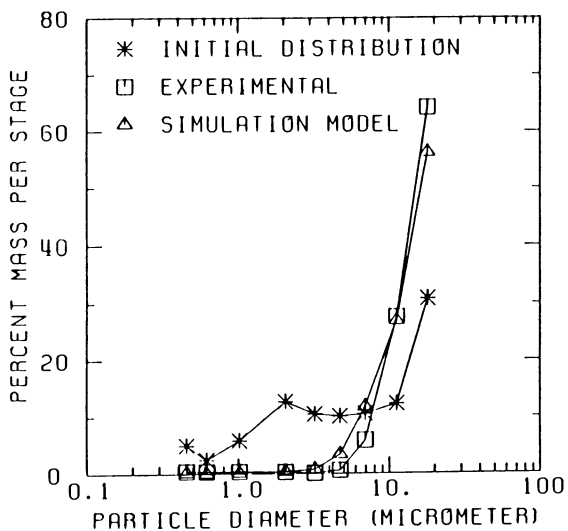
Figure 6.   Comparison at 149 dB sound pressure level and 2 second
exposure.   Mass loading 33.4 g/m^3 and frequency 2490 Hz.
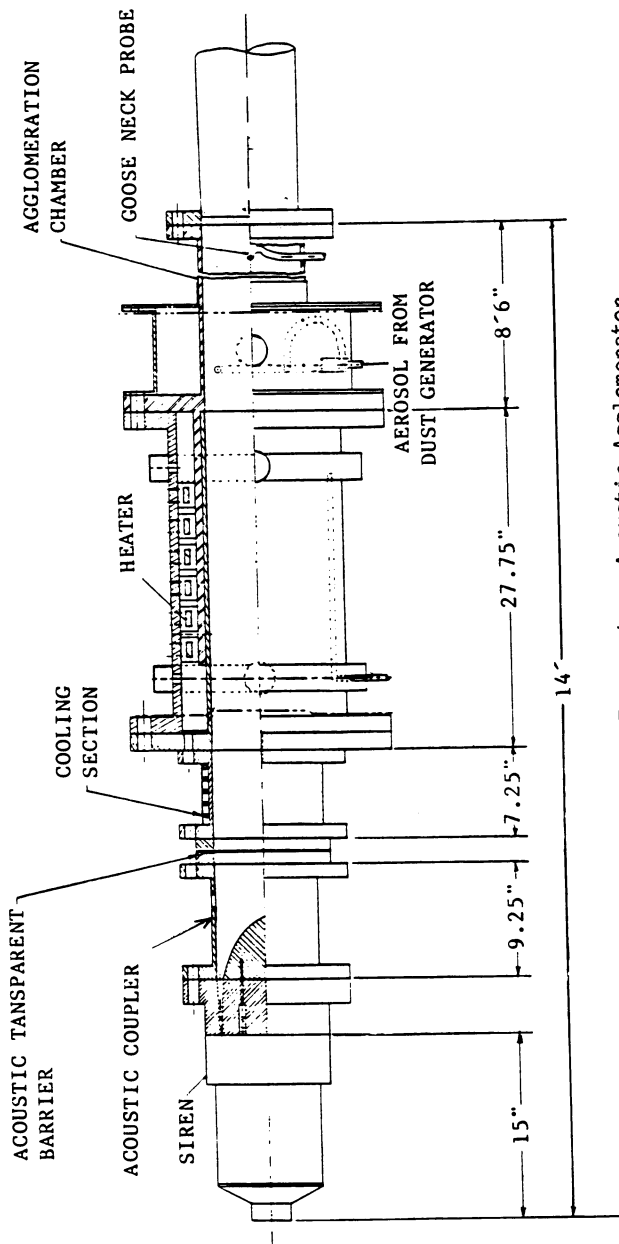
Figure 7.   Moderate Temperature Acoustic Agglomerator.
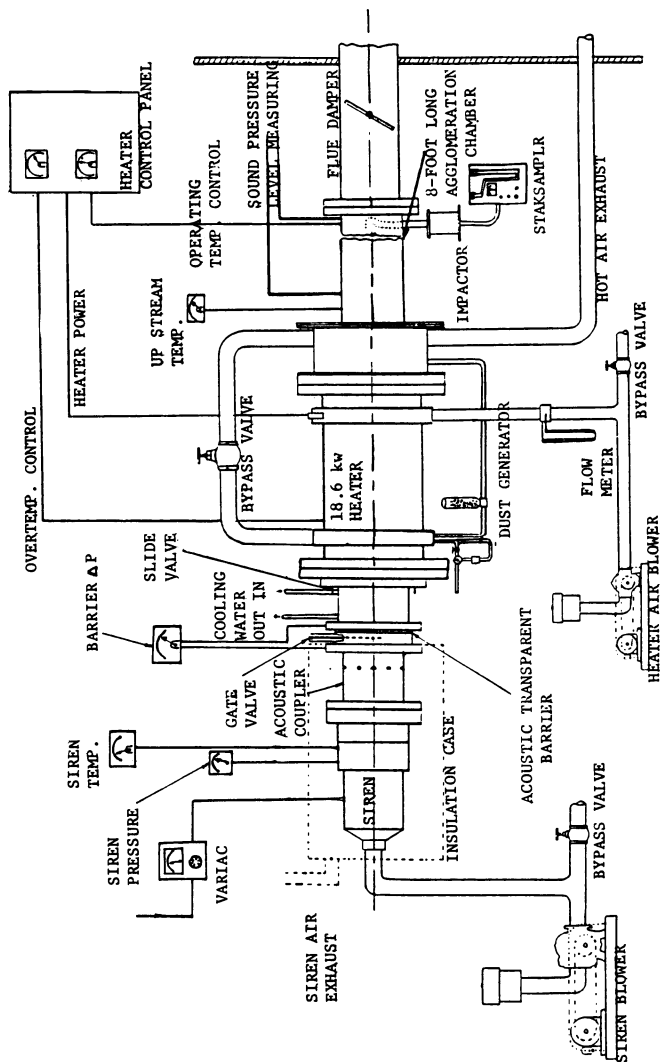
Figure 8.   Final Setup of Moderate Temperature Acoustic Agglomeration Facility.

able to minimize cold siren air flow into the agglomeration
chamber. Control is obtained by an automatically controlled
damper valve in the final exhaust section of the system. We sense
the pressure drop by means of a Valedyne differential pressure
sensor which in turn, through appropriate electronics, controls
the stepping motor activated damper valve. A sluice type gate
valve is installed as noted to prevent hot air backflow during the
many hours of heater-only time to reach the desired system
temperature.

       The 7.25 inch long jacketed, water cooled section prevents
heat conduction to the siren system thus protecting the wooden
horn and siren from over-temperature. The heater section consists
of a 14 inch schedule 40 pipe with 150 lb. flanges welded to each
end. Six Chromolox Model KSEF-Koilfin electric heating elements
generate 18.6 KW of heating power which is transferred to the
airflow by convection. The system can be cycled at 3 Hz holding
the temperature within just a few degrees. Air velocity over the
heaters is 10 ft/sec. to maintain proper heating element
temperatures. The system schematic diagram (Figure 8) shows the
Roots-type blower with bypass flow control and orifice meter flow
sensor providing the heating air to the system. Only about 10% to
20% of the heated air actually enters the agglomerator through
24-1/8 inch diameter angled holes. An adjustable sleeve valve
controls the exposure of these holes. The excess hot air is then
passed through the bypass control valve into the aerosol
distribution section to heat the aerosol to the gas temperature.
Finally the hot air is exhausted to the out-of-doors. The aerosol
concentrate distribution system is attached to the heater flange
as shown in Figure 7. Four equal length copper tubes from the
aerosol manifold are connected to the four 90° spaced holes on the
8-inch diameter tube.

       The aerosol generator is a simple plated standard aspirator
of the type used in laboratories to obtain a vacuum source from a
water supply. It is modified by removing the original vacuum
line attachment and is connected to a cylindrical glass tube as
the reservoir for the dust. A pulse of air traveling through the
aspirator creates a short time duration low pressure which causes
a controlled amount of dust from the reservoir to be sucked down
the pipe line and into the agglomeration chamber. The pulsed air
is produced by passing the compressed air through a solenoid valve.
The time that the air is permitted to flow through the aspirator
(pulse time) and the pulse frequency are controlled by a
Pulse/Lapse Timer connected to the solenoid valve.

       Agglomeration takes place in the 8-foot long, 8-inch schedule
40 pipe. A 1/2-inch gooseneck sampling probe is located in the
end of the section. Isokinetic samples were drawn by the RAC
Staksampler into an Anderson Mark III particle-sizing stack
impactor which is designed for use up to 1500°F. The impactor
consists of a series of plates with a number of holes arranged as
shown in Figure 9. The holes are displaced on successive plates
so that a gas stream, after going through the holes in a plate,
impacts a surface and must make a sharp turn to enter the holes in
the next plate. The impactor operates on the theory that at each
stage smaller particles flow with the air stream during the sharp
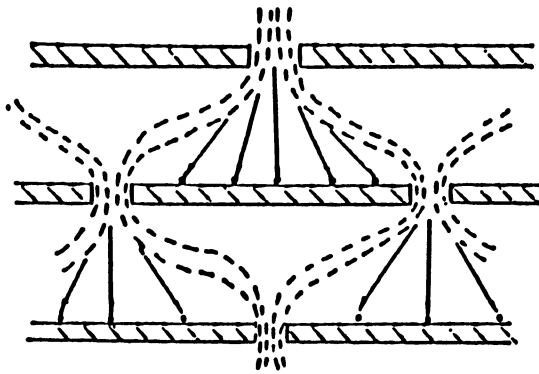
Figure 9.   Schematic of Impactor Stage

turn; larger particles, due to their greater inertia, will go straight and deposit on to the plate. As shown in Figure 9 each plate has holes smaller than those in the previous plate and, therefore, the velocity increases at each stage, depositing particles of given size ranges at each level. A final filter collects any particles which remain after the last plate. A glass fiber substrate with properly located cutouts is placed on each stage as the collection medium. Each substrate is weighed before and after exposure to determine the mass of particles of each size collected; and it is dehydrated before weighing to eliminate the factor of the weight of moisture. The range of particle diameters that will collect on a plate at each stage is determined by the aerosol flow rate through the impactor.

The impactors are preheated in a small furnace to the temperature of the aerosol being tested. The piping from the upstream heater flange to the end of the 8 foot agglomeration tube is covered completely with 2 inch thick thermal insulation (calcium silicate or Epytherm) and aluminum sheeting to reduce heat loss, increase acoustic transmission loss and reduce temperature gradients in the test section. The acoustic pressure sensors are attached to small water jacketed coolers which are screwed into the hot agglomeration chamber pipe wall to provide protection from the high temperatures.

Because of the importance of the sound source in terms of its overall efficiency, reliability and cost, we shall describe the siren design in somewhat greater detail. Before deciding on the siren as a very promising sound source, we investigated several other potential high acoustic sound pressure sources. Hartmann Whistles (generators) provide efficiencies of about 5%. Air powered, electrically driven oscillating sleeve valve type drivers are on the market with acoustic outputs in the 2 to 40 KW range. Their efficiencies are in the 8% to 10% range. These latter sound sources can provide the broad band sound required in the acoustic fatigue test installations for which they were designed. Generally, they are not designed for long life applications. These sources work at considerably lower frequencies than needed for acoustic agglomeration. Another well-known high power source is the St. Clair generator which is basically a resonant cylinder vibrating in an axial mode. Kilowatt range powers in the 1 to 15 KHz range have been produced with overall efficiencies in the vicinity of 6%. Sirens have been shown to be the only sound source which promises to provide the high overall efficiencies of from 50 to 60% required for economically viable acoustic agglomerators in power plant applications. Also, properly designed sirens offer the promise of the required long life, high reliability, low operating costs and relatively low initial cost compared to other systems.

Almost all commerical sirens are used for fire and air raid warning systems. They have frequencies in the 250-500 Hz range and produce acoustic power in the 100-1000 watt range and are not very efficient sound producers. We have, therefore, developed the technology to design high efficiency reliable sirens. A typical example of a 600 acoustic watt siren is shown in Figure 10. The

SHIMSTOCK

EXIT PORT

ROTOR

STATOR SECTION

PART G

FLOW GUIDE

PART F

FIELD WINDINGS
PART A

CAST INNER FRAME
PART C

MOTOR ARMATURE
PART B

PART D

PART E
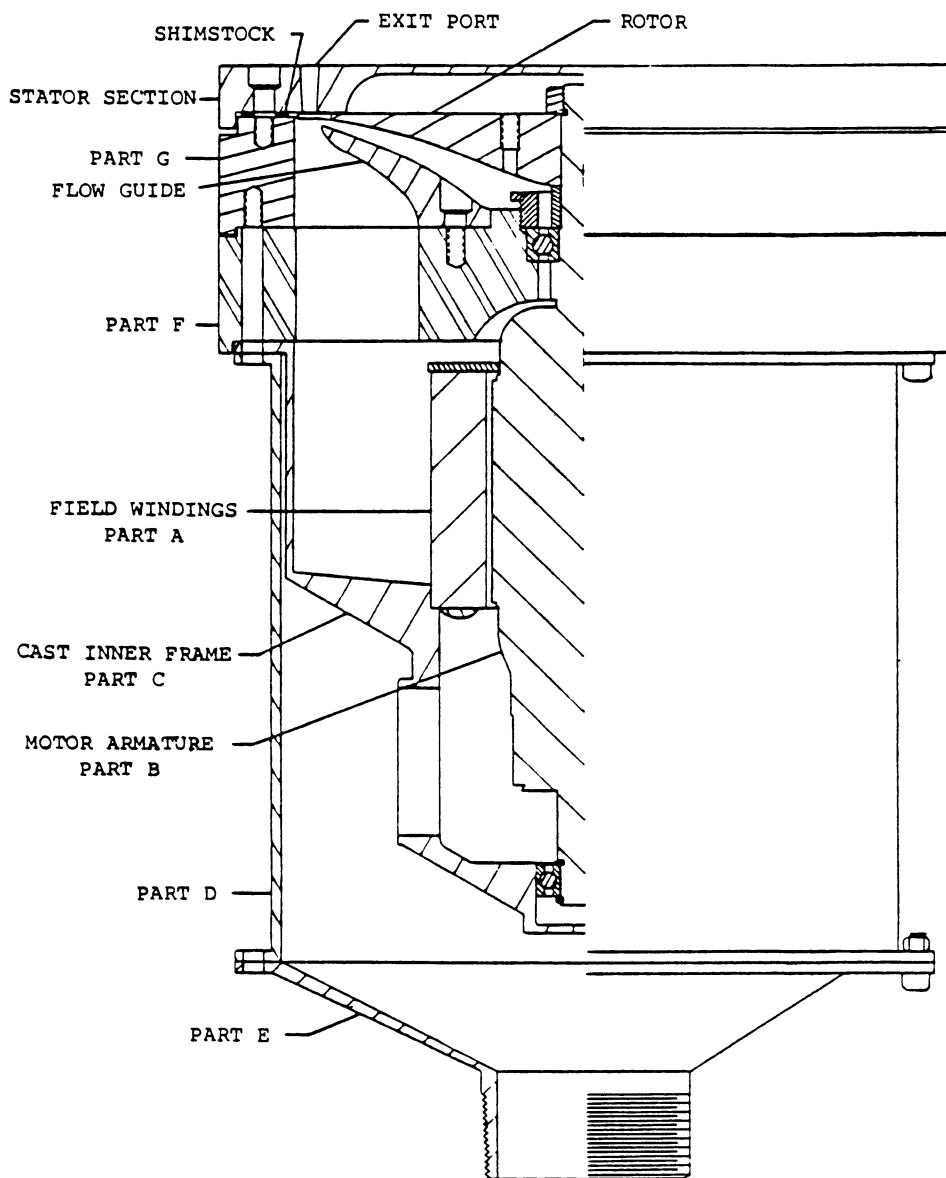
Figure 10. Full View of Siren

frequency range is from 1000-5000 Hz. Our work is built on a foundation of research at Penn State in the 1950s (29) and earlier work in the U.S.A. (30), some recent excellent work in Poland (31-33), and in Japan (34). The siren used in this research develops about 600 acoustic watts in the desired frequency range giving us sound pressure levels in the 8 inch duct up to 165 dB. Almost all the energy is contained in the fundamental frequency.

Recent Experimental Results. The agglomerator has performed reliably and the results were quite repeatable. We have used a processed fly ash dust consisting primarily of silica, alumina and iron oxide particles. A typical set of results is shown in Figure 11 for a dust loading of about 2 g/m^3 and an exposure time of 10 seconds. The results show that the maximum agglomeration for this density of dust and this particular size distribution does occur near the predicted value of 2500 Hz with clearly less agglomeration at 1290 Hz. Earlier experiments with heavier white lead dust followed prediction and gave an optimum frequency of about 1500 Hz.

Conclusions. Our theoretical and experimental work has shown conclusively that acoustic agglomeration does result in shifting the particle size distribution from submicrometer sizes into the 10 micrometers and above size range. In order to achieve the desired 150 to 160 dB, specific acoustic powers of from 0.1 to 1 watt/cm^2 are required for plane wave propagation and less than that for standing wave chambers.

We have reached an understanding of the fundamental processes and an ability to model the process permitting us to perform approximate trade-off studies for various clean-up train strategies involving various types of clean-up devices at different locations in the system. For example, a hot gas clean-up system consisting of a pressurized, fluidized bed coal burner producing 10 atmospheres, 1650°F gas with a loading of 10,000 ppm by weight with a particular size distribution followed by a Stairmand cyclone, an acoustic agglomerator which is followed by a high efficiency Van Tongeren cyclone. To meet the required 25 ppmw dust loading requirement, we predict exposure times of 9 seconds at 155 dB, 5 seconds at 160 dB and 3 seconds at 165 dB. Since long exposure times mean large agglomeration chambers and high acoustic intensities require more power from the power plant, cost trade-off optimization studies can be performed. As a general statement, we can say that the power required to operate the acoustic agglomeration system is about 0.02 to 0.5% of the power plant output. For a 250 megawatt power plant we would need anywhere from 50 KW to 1250 KW for the acoustic agglomeration system. At 50% overall efficiency the acoustic power would range from 25 to 625 kW. These are very large acoustic powers when compared to the acoustic power output of a 4 engine commercial jet aircraft of about 36 kW on take-off.

We are continuing our research with U.S. Department of Energy support to further improve our understanding of several important aspects of acoustic agglomeration such as acoustic energy absorption by hot gases and large particle concentrations,

Dp vs % MASS

+ No Sound, 10 Sec. Residence Time
× 2500 Hz, 161 Db, 10 Sec. Residence Time
□ 1290 Hz, 166 Db, 10 Sec. Residence Time
○ 3050 Hz, 158 Db, 10 Sec. Residence Time

MIDPOINT AERODYNAMIC DIAMETER (Micrometers)

% MASS
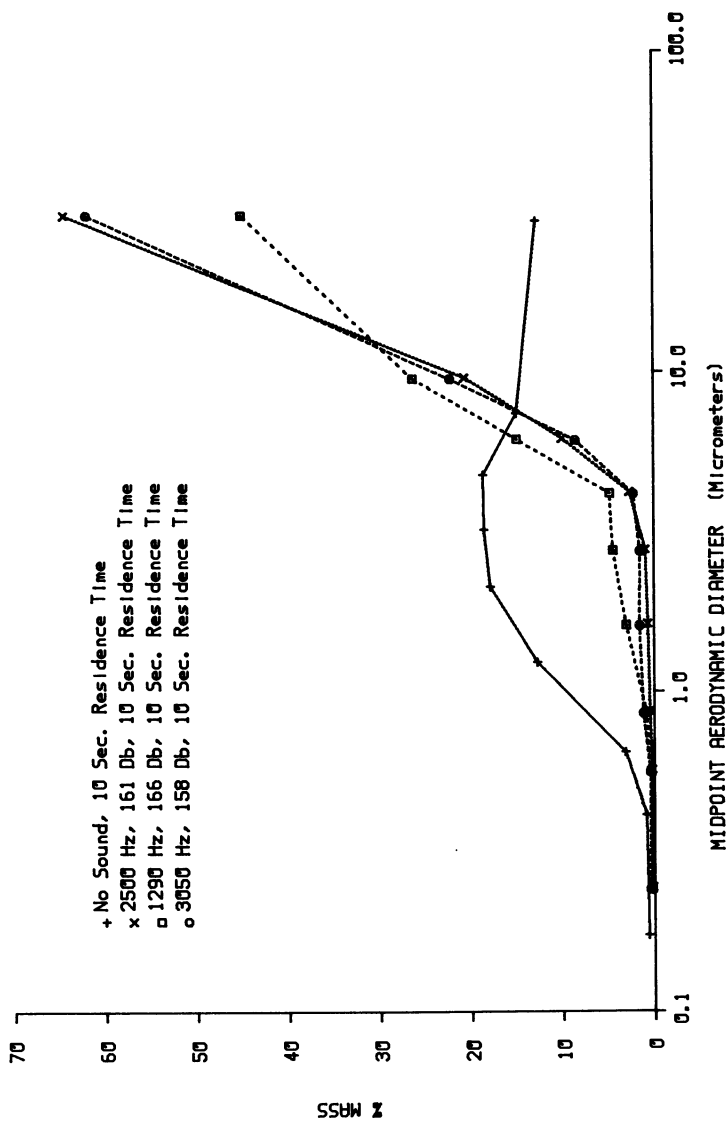
Figure 11. Acoustic Agglomeration Results for Fly Ash Aerosol

nonlinear acoustic phenomena, output and efficiency, the effect of acoustic agglomeration chamber geometry on the acoustic field. We are also involved in several other applications of acoustic agglomeration for dust control.

Literature Cited

1. Wark, K. and Warner, C., Air Pollution: Its Origin and Control, Harper and Row, New York, 1976, pp. 229.
2. Davies, R.N., "Dust is Dangerous", Faker & Faker Limited, London, 1953.
3. National Air Pollution Control Administration, "Air Quality Criteria for Particulate Matter", AP-69, 1969.
4. Smoluchowski, M.V., "Versuch Einer Mathematischen Theorie der Koagulationskinetik Kolloider Losungen", Z. Physik Chem., Vol. 195, 129-168, (1918).
5. Andrade, E.N. dac, "The Coagulation of Smoke by Supersonic Vibrations", Pro. Royal Society, Vol. 134, 1111-1115, (1936).
6. Brandt, O., Freund, H. and Heidemann, E., "Schwebstoffe im Schallfeld", Z. Phys., Vol. 104, No. (7-8), 511-533, (1937).
7. Brandt, O., Freund, H. and Hiedemann, E., "Zur Theorie der akustischen Koagulation", Kolloid Z, Vol. 77, No. 1, 103-115, (1936).
8. St. Clair, H.W., "Agglomeration of Smoke, Fog or Dust Particles by Sonic Waves", Industrial Engineering Chem., 2434-2438, (1949).
9. Stokes, C.A., "Sonic Agglomeration of Carbon Black Aerosols", Chemical Engineering Process, Vol. 46, No. 8, 423-432, (1950).
10. Neumann, E.P., Soderberg, C.R. and Fowle, A.R., "Design Application, Performance and Limitations of Sonic Type Flocculators and Collectors", International Committee on Air Pollution, Washington, D.C., Air Pollution Proc. - U.S. Technical Conference, 388-393, (1950).
11. Newmann, E.P. and Norton, R.L., "Application of Sonic Energy to Commercial Aerosol Collection Problems", Chem. Eng. Progr. Symp. Sec. 1, Vol. 47, No. 1, 4-10, (1951).
12. Danser, H.W., "Eliminate Stack Dusts and Mists", Chemical Engineering, 158-160, (1950).
13. Danser, H.W. and Newmann, E.P., "Industrial Sonic Agglomeration and Collection Systems", Industrial Engineering Chem., Vol. 41, No. 11, 2439-2442, (1949).
14. Soderberg, C,R., Jr., "Industrial Application of Sonic Energy", Iron Steel Engr., Vol. 29, No. 2, 87-94, (1952).
15. Neumann, E.P. and Norton, J.L., "Application of Sonic Energy to Commercial Aerosol Collection Problems", Chemical Engineering Symposium Series No. 1, Vol. 47, 4-10 (1951).
16. Mednikov, E.P., "Acoustic Coagulation and Precipitation of Aerosols", Translated from Russian, Consultants Bureau, (1965).
17. Volk, Jr., M and Moroz, W.J., "Aerosol Coagulation in an Acoustic Field", CAES Technical Report Number 354-74, The Pennsylvania State University, University Park, Pennsylvania, 80 pages, (1974).

18. Volk, Jr., M. and R. Hogg, "Sonic Agglomeration of Aerosol Particles", CAES Report 465-77, The Pennsylvania State University, March 1977.
19. Davidson, G.A. and Scott, D.S., "Finite-Amplitude Acoustics of Aerosols", J Acoustic Soc. AM. 53 (6), pp. 1717-1729, (1973).
20. Shaw, D.T., "Recent Developments in Aerosol Science", Wiley Inter-Science, pp. 279-319, (1978).
21. Shaw D. T., and Tu, K.W., "Acoustic Particle Agglomeration Due to Hydrodynamic Interaction Between Monodisperse Aerosols", SUNY at Buffalo, NY (1979).
22. Lee, P.S., Cheng, M.T. and Shaw, D.T., "The Acoustic and Hydrodynamic Turbulence-Turbulence Interaction and Its Influence on Acoustic Particle Agglomeration", Report DOE/MC/11842-T9, 1982.
23. Tiwary, R., and Reethof, G., "Acoustically Generated Turbulence and Its Effect on Acoustic Agglomeration", J. Acous. Soc. of Am., Vol. 76, pp. 841-849, (1984).
24. Reethof, G., "Acoustic Agglomeration of Power Plant Fly Ash", Final Report to Pittsburgh Energy Technology Center, U.S. Department of Energy, Contract #DE-AC22-83 PC 602070, December 1985.
25. Braxton Corporation, "Sonic Agglomeration", Report to Environmental Protection Agency, Report No. PB234146, 1974.
26. Tiwary, R., "Acoustic Agglomeration of Micron and Submicron Particles", Ph.D. Thesis, The Pennsylvania State University, May 1985.
27. George, W. and Reethof, G., "On the Fragility of Acoustically Agglomerated Submicron Fly Ash Particles", accepted for publication in the ASME Journal for Vibration, Acoustics, Stress and Reliability in Design, May 1985.
28. Tiwary, R. and Reethof, G., "Hydrodynamic Interaction Fill-Up of Acoustic Agglomeration Volume", accepted for publication in the J. of Sound and Vibration, May 1986.
29. Allen, C.H., and Rudnick, I., "A Powerful High Frequency Siren", The J. Acoust. Soc. Am., Vol, 19, No.5, pp, 857-865, 1947.
30. Jones, R.C., "A Fifty Horsepower Siren", J. Acoust. Soc. Am., Vol., 18, No. 2, pp. 371-387.
31. Puch A., and Wyrzykowski, R., "The Effect of the Shape of the Holes of the Rotor and Stator on the Acoustic Parameters of a Dynamic Generator", Proceedings of the 24th Open Seminar on Acoustics, Wladyslawowo, 1977.
32. Puch, A., "The Effect of the Shape of the Holes of the Rotor and Stator on the Acoustic Parameters of a Dynamic Axial Generator", Archives of Acoustics, Vol. 5, No. 4, pp. 369-380, 1980.
33. Wyrzykowski, R., Puch, A., Trzesniowski, J., Zamorski, R., "High-Duty Acoustical Siren", Contributed papers, V.2, IX International Congress on Acoustics, Madrid, 1977.
34. Oyama, Y., Okada, M., Sawahata, Y., and Inoue, I., "Design Note on Siren-Type Sound Generator", Journal of the Scientific Research Institute, Vol, 50, No. 1419, pp. 37-42, 1956.

20

Fossil Fuel Combustion and Forest Ecosystem Health

William H. Smith

School of Forestry and Environmental Studies, Yale University, New Haven, CT 06511

Historically, the combustion of fossil
fuels has directly or indirectly been the
source of air contaminants at three levels:
local, regional, and global. Pollutants of
importance at the local level have included
sulfur dioxide and trace metals. Local forest
damage is confined to a zone of a few km
immediately surrounding a facility and for a
distance of several to tens of km downwind.
Regional air pollutants may be deposited over
expansive forest areas because they are
transported tens or hundreds of km from point
of release due to small size or synthesis in
the atmosphere from precursors introduced into
the troposphere. Regional air pollutants of
potential influence for forests include:
oxidants, trace metals, and acid deposition.
Global pollutants influence the entire
atmosphere of the earth, e.g. halocarbons and
carbon dioxide. The latter is important
because of the potential it has to influence
global climate. Risks associated with
regional and global air pollution and forest
health are high. The evidence available to
describe the total boundaries of the problem
for all pollutants is incomplete.

A challenge of developed nations throughout the temperate zone is air
quality policies that protect natural resources as well as human
health. Throughout Europe and North America, the decade of the
eighties will be recorded as a period of profound decisions regarding
atmospheric contamination and natural resource quality. The central
issues for those interested in forest health are as follows. Is air
pollution influencing the growth of forests or individual species,
changing the species composition of forest communities or destroying
certain tree species, associated plants or animals over significant
forest areas? In an effort to answer this question, I shall discuss

the spatial scales of air pollution stress and what we know about
the response of trees to pollutants at these scales.

Local, regional and global-scale air pollutants

Local

During the first two thirds of the twentieth century, research and
regulatory efforts were focused on local air pollutants and acute
vegetative effects. Pollutants of primary concern were sulfur
dioxide, particulate and gaseous fluoride compounds and numerous
heavy metals such as lead, copper, and zinc. Occasional interest was
expressed in other inorganic gases including ammonia, hydrogen
sulfide and chloride, and chlorine. The sources of these pollutants
were and are typically discrete and stationary facilities for:
energy production, for example, fossil-fuel electric generating
plants, gas purification plants; metal related industries, for
example, copper, nickel, lead, zinc or iron smelters, aluminum
production plants; and diverse other industries, for example, cement
plants, chemical and fertilizer plants and pulp mills.
    It is appropriate for us to consider the above pollutants local-
scale because forest areas directly affected by these facilities are
typically confined to a zone of a few km immediately surrounding the
plant and for a distance of several to tens of km downwind. The
dimensions of the surrounding and downwind zones of influence are
variable and primarily controlled by source strength of the effluent,
local meteorology, regional topography and susceptibility of
vegetation. In any case, the forest influence is confined to a
region generally less than a thousand hectares.

Regional

During the past three decades we have become increasingly aware of
regional-scale air pollutants. The regional designation is applied
because these contaminants may affect forests tens, hundreds, or even
thousands of kilometers from their site of origin. The regional air
pollutants of greatest documented or potential influence for forests
include: oxidants, most importantly ozone; trace metals, most
importantly heavy metals (e.g., cadmium, iron, copper, lead,
manganese, chromium, mercury, molybdenum, nickel, thallium, vanadium,
and zinc); and acid deposition, most importantly the wet and dry
deposition of sulfuric and nitric acids. Ozone and sulfuric and
nitric acids are termed secondary air pollutants because they are
synthesized in the atmosphere rather than released directly into the
atmosphere. The precursor chemicals, released directly into the
atmosphere and causing secondary pollutant formation, include
hydrocarbons and nitrogen oxides in the case of ozone, and sulfur
dioxide and nitrogen oxides in the case of sulfuric and nitric acid.
The combustion of the fossil fuels (coal, oil, and gas)
hydrocarbons and sulfur dioxide. The heat of combustion causes
nitrogen and oxygen to react and form nitrogen oxides. Many
activities generate small particles (approximately 0.1 - 5 μm
diameter). Those activities associated with combustion (particularly

coal burning) can preferentially contaminate these small particles
with trace metals. Because the formation of secondary air pollutants
may occur over tens or hundreds of km from the site of precursor
release, and because small particles may remain airborne for days or
weeks, these pollutants may be transported 100 to more than 1000 km
from their origin. Eventual wet and dry deposition of the pollutants
onto lakes, fields, or forests may occur over large rather than small
areas.

The U.S. Environmental Protection Agency and the U.S. Department
of Agriculture's Forest Service established a network of air
monitoring stations to measure ozone concentrations in remote areas
of National Forests. Analysis of selected high ozone events during
1979 suggested that long-range transport of air masses contaminated
by urban centers contributed to peak concentrations at remote sites
(1). In a study of rural ozone episodes in the Upper Midwest by
Pratt et al. (2) presented evidence that ozone and precursors were
transported 275 km from Minneapolis-St. Paul. Studies of trace metal
concentrations in the atmosphere in remote northern and southern
hemispheric sites revealed that the natural sources include the
oceans and the weathering of the earth's crust, while the major
anthropogenic source is particulate air pollution (3). Murozumi et
al. (4) showed that long range transport of lead particles from
automobiles significantly polluted polar glaciers. We estimated the
annual lead deposition on a remote northern hardwood forest in New
Hampshire to be 266 g per hectare. This caused lead contamination of
the forest floor 5-10 times greater than the estimated pre-industrial
concentration (5).

Evidence is available from satellites, surface deposition of
aerosol sulfate and reduced visibility (6, 7, 8) for long-range
transport of acidifying pollutants from numerous sources. During
the winter, approximately 20 percent of the emissions from tall power
plant stacks in northeastern United States may remain elevated and
relatively coherent for more than a day and over 500 km (9).

The long distance transport of regional pollutants means they
may have interstate, international and even intercontinental
significance. It means further that the forests subject to their
deposition exceed tens of thousands of km^2.

Global

In the past 25 years, we have become concerned with a third scale of
air pollution--global. Global pollutants affect the entire
atmosphere of the earth. Two global air pollutants of special note
include carbon dioxide and halocarbons.

Careful monitoring of carbon dioxide during the past two decades
in Hawaii, Alaska, New York, Sweden, Austria and the South Pole has
firmly established that carbon dioxide is steadily increasing in the
global atmosphere. This increase is due to anthropogenic activities
including fossil fuel combustion. It may also be caused by altered
land use management, such as, forest destruction in the tropics.
The atmospheric carbon dioxide concentration has been estimated to
have been approximately 290 ppm ($5.2x10^4$ µg m^{-3}) in the middle of the
nineteenth century. Today, the carbon dioxide concentration

approximates 340 ppm (6.1×10^5 μg m^{-3}) and is increasing about one
ppm (1.8×10^3 μg m^{-3}) per year. In 1977-78 it increased 1.5 ppm (2.7×10^3 μg m^{-3}). In the year 2020, if the increasing rate continues,
the carbon dioxide amount in the global atmosphere may be nearly two
times the present value (10).

Naturally occurring stratospheric ozone is important because it
screens the earth from biologically damaging ultraviolet radiation --
light with wavelengths between 290 and 320 nanometers -- released by
the sun. Halocarbons released by humans can deplete the natural
ozone layer surrounding the earth. In summary, halocarbon molecules,
especially chlorofluoromethanes, released by various human
activities, are transported through the troposphere. They pass
through the tropopause and lower stratosphere and are decomposed in
the mid- to upper-atmosphere. Free chlorine, resulting from
decomposition, causes a rapid, catalytic destruction of ozone. In
1979, the National Academy of Sciences estimated that release of
halocarbons to the atmosphere, at rates inferred for 1977, would
eventually deplete stratospheric ozone 5 to 28 percent, most probably
17 percent (11). In 1982, the National Academy revised its previous
estimate and suggested a depletion from 5 to 9 percent (12).

Effect of local-scale, regional-scale and global-scale air pollution on forest ecosystems

Local

High deposition of local air pollutants has caused documented forest
destruction. High sulfur dioxide or fluoride doses severely injure
or kill forest trees. The ecosystems, of which the trees are a part,
are simplified, lose nutrients, sustain soil erosion, have
microclimates and hydrologic patterns altered, and ultimately they are
destroyed or converted to more resistant seral stages. Miller and
McBride (13) reviewed the forests destroyed by local air pollution.
Early in this century, it was clearly documented in numerous
locations throughout North America that sulfur dioxide and trace
metal pollution destroyed forests surrounding metal smelting
facilities. Smelting centered in Ducktown, Tennessee, devastated the
southern hardwood forest over 27 km^2 (10.5 mi^2) surrounding the
plant, converted an additional 68 km^2 (1 ,000A) to grassland and
created a 120 km^2 (30,000A) transition zone with altered species
composition. Smelters in the Sudbury, Ontario, Canada, area have
caused simplification of the surrounding mixed boreal forest and have
caused eastern white pine mortality in a 1865 km^2 (720 mi^2) zone to
the northeast.

Aluminum reduction plants have also caused local forest
destruction. In Montana, fluoride pollution killed or severely
injured ponderosa pine and lodgepole pine on 8 km^2 (2000A)
surrounding a plant. In Washington, ponderosa pine mortality and
morbidity resulted over a 130 km^2 (50 mi^2) area in the vicinity of an
aluminum plant.

Local pollution has caused extensive forest destruction in
Austria, Germany, Hungary, Norway, Poland and Sweden. Industrial
operations along the northern border of Czechoslovakia have caused
extensive forest destruction.

Regional

Deposition of regional pollutants subjects forests to different
perturbations than local- pollutants because the doses are less.
Rather than severe tree morbidity or mortality with dramatic
symptoms, regional pollutants subtly change tree metabolism and
ecosystem processes. Smith (14) provided a comprehensive review of
subtle air pollution forest stress.

        Regional air contaminants may influence reproductive processes,
nutrient uptake or retention, metabolic rates (especially
photosynthesis), and insect pest and pathogen interactions of
individual trees. At the ecosystem level, regional air pollutants
may influence nutrient cycling, population dynamics of arthropod or
microbial species, succession, species composition, and biomass
production. In the instance of high-dose local-scale pollution, the
symptoms are typically acute, dramatic and obvious (severe disease,
mortality, forest simplification). In the case of lower-dose
regional-scale pollution, the symptoms are typically not visible (at
least initially), undramatic and not easily measured. The
integration of regional pollutant stresses is slower growth, altered
competitive abilities and changed susceptibility to pests. Ecosystem
symptoms may include altered rates of succession, changed species
composition and biomass production. Symptom development is, of
course, much slower at the regional scale. Evidence of the relative
importance of regional pollutants is variable, caused in part by the
length of time that has been devoted to the study of individual
pollutants and in part by the subtleness and complexity of the
pollutant interactions. The toxicity of trace metals has been
studied for approximately 60 years, of ozone approximately 25 years
and of acid deposition approximately 10 years.
        Table 1 suggests the relative strength of evidence for forest
responses to regional pollutants. A review of the column totals
suggests we know most about the regional effects of oxidants, less
about regional effects of trace metals and least about regional
effects of acid deposition. A review of the row totals suggests tree
and ecosystem processes especially vulnerable to air pollution
stress. The processes with a total of five or more include; litter
decomposition, seedling survival, photosynthesis, foliar necrosis,
tree growth, microbial pathogen activity, and ecosystem succession
plus species composition. These are the tree and ecosystem processes
at particular risk from regional air pollution. Fig. 1 provides an
overview of regional air pollution influence on forest trees and
ecosystems.

Global

Increasing carbon dioxide concentration and decreasing stratospheric
ozone concentration of the atmosphere may alter global radiation
fluxes. Presumably a primary result of more carbon dioxide in the
air will be warming. While incoming solar radiation is not absorbed

by carbon dioxide, portions of infrared radiation from earth to space
are. Over time, the earth would become warmer. While the forces
controlling global temperature are varied and complex, the increase
of 0.5°C since the mid-1800s is generally agreed to be at least
partially caused by increased carbon dioxide. By 2000 it may
increase an additional 0.5°C. Numerous models advanced to estimate
the average global warming per doubling of carbon dioxide project 0.7
to 9.6°C. Natural impacts on climate, such as solar variability,
remain important and of unclear relationship to anthropogenic causes.
A mean global average surface warming, however, of 3 ± 1.5°C appears
reasonable (15, 16).

The consequences of a warmer global climate, with even a very
modest temperature increase, on the development of forest ecosystems,
could be profound. Warming, with increased carbon dioxide in the
atmosphere, might enhance forest growth. Manabe and Stouffer (17)
have estimated that a doubling of atmospheric carbon dioxide would
cause a 3°C warming at the U.S.-Canadian border, while Kellogg (18)
has suggested that a rise of 1°C in mean summer temperature extends
the growing season by approximately 10 days. Other changes
associated with global warming, however, may restrict forest growth.
Physiological processes of plants, especially photosynthesis,
transpiration, respiration and reproduction are sensitive to
temperature. With warming, respiration and decompositon may increase
faster than photosynthesis. Transpiration and evaporation increases
may enhance stress on drier sites. Reproduction may be altered by
changes in dynamics of pollinating insects, changes in flower, fruit
or seed set, or changes in seedling production and survival. The
geographic or host ranges of exotic microbial pathogens or insect
pests may expand. Previously innocuous endemic microbes or insects
may be elevated to important pest status following climatic warming.
Precipitation changes are associated with global warming, and certain
areas will receive more and others less. Those areas receiving less
precipitation will also experience increased evaporation and
transpiration. Waggoner (19) has estimated that the projected change
in weather by the year 2000, caused by increased atmospheric carbon
dioxide, will cause moderate decreases of 2-12 percent in yield of
wheat, corn and soybeans in the American grain belt due to increased
dryness. While agriculturists may be able to adopt new crop
varieties to a drier climate, forests cannot be similarly
manipulated. Increased drought stress over widespread forest areas
would be expected to initiate new rounds of progressive tree
deterioration termed dieback/decline disease. Drought is the most
common and important initiator of general forest tree decline.
Forest stresses caused by other air pollutants and other agents must
be evaluated against this background of forest change caused by
climatic warming.

A serious consequence of anthropogenic release of halocarbons to
the atmosphere is the depletion of naturally occurring stratospheric
ozone. Some reduction in halocarbon release has been achieved in the
United States and a few other countries. Immediate termination of
all release worldwide, however, would still leave the world with
important stratospheric ozone reductions during the next decade.
Reduced upper-air ozone would increase ultraviolet radiation reaching

Table 1. Relative strength of evidence (quantity/quality)* available to support forest ecosystem interaction with regional[+] air pollutants.

ecosystem process/component perturbation	air contaminants			
	oxidants	trace metals	acid deposition	TOTAL
I. nutrient cycling				
1. increase nutrient availability				
a. increase input (fertilization)	0	1	2	3
b. increase soil weathering	0	0	1	1
2. decrease nutrient availability				
a. reduce litter decomposition	0	4	1	5
b. increase soil acidification	0	0	2	2
c. increase soil (cation) leaching	0	0	2	2
d. decrease microbial symbioses	0	3	1	4
II. primary producers (trees)				
1. reproductive physiology				
a. reduce flowering	1	1	0	2
b. reduce pollen production/metabolism	2	1	1	4
c. reduce cone/seed set	2	0	0	2
d. reduce seedling survival	3	3	1	7
2. foliar physiology				
a. reduce photosynthesis	4	1	0	5
b. increase (cation) leaching	0	0	2	2
c. increase necrosis	4	2	0	6
3. root physiology				
a. decrease water/nutrient uptake	0	1	1	2
b. increase necrosis	0	1	2	3
4. reduce tree growth	4	1	1	6

III. consumers				
1. arthropod pest activity				
a. increase	4	0	0	4
b. decrease	0	0	0	0
2. microbial pathogen activity				
a. increase	6	1	1	4
b. decrease	3	0	2	1
3. other pest activity (viruses, bacteria, nematodes, mistletoes, weeds)				
a. increase	0	0	0	0
b. decrease	0	0	0	0
4. wildlife (bird/mammal) activity				
a. reduce food	2	0	0	2
b. reduce habitat	2	0	0	2
c. increase morbidity/mortality	2	0	2	0
IV. ecosystem succession/species composition (cause alteration)	5	0	1	4
V. ecosystem productivity (increase/decrease biomass accumulation)	4	0	0	4
TOTAL		18	25	41

*evidence scale

0 - extremely limited evidence or hypotheses only
1 - slight evidence
2 - more evidence
3 - greater evidence
4 - considerable evidence including field evidence

+exclusive of local air pollution effects within several km of point sources
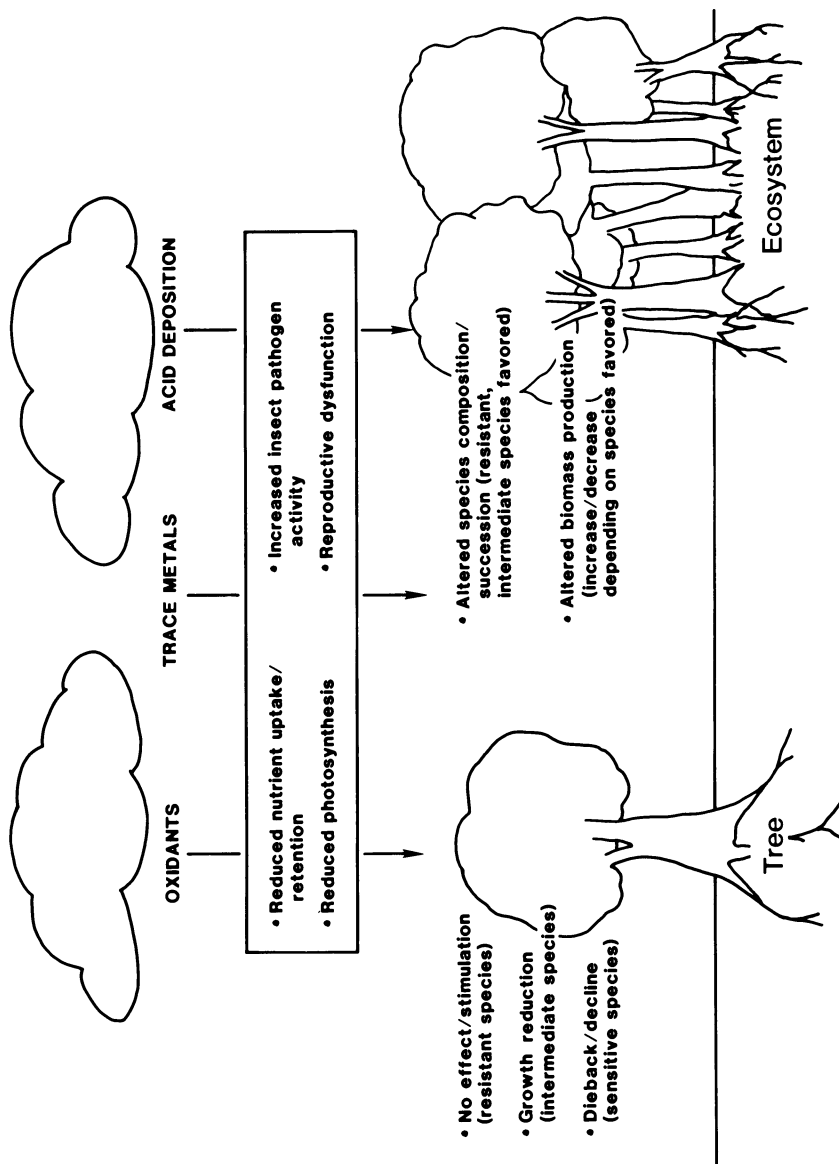
Fig. 1. Forest tree and ecosystem response to regional-scale air pollution stress.

the surface of the earth. Current understanding does not allow an
inventory of the impacts of increased ultraviolet radiation on
forests. Studies of more than 100 agricultural species showed that
increased ultraviolet exposure reduces plant dry weight and changes
the proportion of root, shoot and leaf tissue. Studies of more than
60 aquatic organisms showed that many were quite
sensitive to current levels of ultraviolet radiation at the water
surface (20). Chlorofluorocarbons can also contribute to global
warming in a manner similar to carbon dioxide.

Regional air pollutants are the most important concern

The effects of local air contaminants on forests have stabilized in
the vicinity of existing point-sources of air pollutants. In
numerous cases improvements have been achieved. In the case of
sulfur dioxide, increasing stack heights and use of scrubbers have
reduced ground level concentrations of sulfur dioxide. New
industries and electrical plants in the U.S. can employ the best
available air quality technology.

On the global-scale, the destruction of ozone by halocarbons was
addressed in the U.S. by banning chlorofluorocarbons in aerosol
products. The release of carbon dioxide to the atmosphere from
fossil fuel combustion will continue well into or through the
twenty-first century. Energy requirements of nations of the
temperate zone will require combustion of gas, oil and coal and the
atmospheric burden of carbon dioxide will continue to increase with
uncertain consequences.

Regional-scale air pollutants, on the other hand, exhibit both
increasing trends and known and probable effects on forest ecosystems
over large portions of the temperate region. The comprehensive study
of oxidant pollution in portions of the San Bernardino National
Forest, California, demonstrated regional scale air pollution effects
on forest growth and succession (21). Additional evidence of reduced
forest growth imposed by oxidant pollution in the west, mid-west and
east has been provided (22). For various forest ecosytems we are at,
or near, the threshold of trace metal impact on nutrient cycling
processes. Lead will continue to accumulate in forest floors as long
as it is released into the atmosphere (3). Although adverse effects
on forest ecosystems from acid deposition have not been conclusively
proven by existing evidence, we cannot conclude that adverse effects
are not occurring. Presently, tree mortality and tree morbidity and
growth rate reductions in European and North American regions do
occur where regional air pollution, including acid deposition, is
generally high. Temporal and spatial correlations between wet acidic
deposition and forest tree growth rates has been provided. Numerous
hypotheses for adverse forest effects from acid deposition, worthy of
testing, have been proposed (23, 24). Under natural conditions,
forest ecosystems are exposed to multiple air pollutants
simultaneously or sequentially and interactive and accumulative
influences are important. It is inappropriate to consider the
effects of any regional pollutant on forests in isolation. The
growth reductions and decline symptoms of the forests of the Federal
Republic of Germany are dramatic and should warn all nations that the

resiliency of forest ecosystems has limitations. Until the cause of
this decline is more clearly understood, prudent natural resource
science should not reject nor indict any single stress.

Conclusion

A sensitive and convenient forest parameter must be found to monitor
the extent and intensity of stress on expansive forest systems.
Waring (25, 26, 27) suggested that monitoring canopy leaf area and its
duration of display is a very appropriate general index of forest
ecosystem stress. Canopy quantity and quality is an indicator of
productivity. Inventory techniques from the air (multispectral
scanning, microwave transmission, radar, laser) and the ground
(correlations with stem diameter, sapwood cross-sectional area) for
canopy leaf area are available. At a given site, detection of an
increase in leaf area would suggest an improving environment, a
decrease in leaf area would infer the system is under stress. Baes
and McLaughlin (28) have proposed that trace metal analyses of tree
rings can provide information on temporal changes in air pollutant
deposition and tree health.
      Implementation of wide-area forest monitoring of any nature
involves two challenges. First, detection of stress does not suggest
cause. We are keenly aware that tree and forest health are
controlled by many factors in addition to air quality---age,
competition, environment (moisture, temperature, nutrition), insect
and pathogen activity. We desperately need procedures to partition
the relative importance of influencing variables for a given site.
Fortunately we are making research progress toward this resolution
(27, 29, 30). The second challenge is to convince foresters that the
time and cost of systematic forest health monitoring is justified. I
feel it is not only justified, but essential for intelligent
decisions regarding regulation of regional air pollutants.
      Air pollution has been killing trees locally for centuries. We
have been keenly aware of this in the United States for over 100
years. We now realize that in addition to mortality, regional air
pollutants may be capable of causing alterations in species
composition and growth-rate reductions in certain forest ecosystems
over large areas and across national boundaries.
      Forests are variable in species, topography, elevation, soils and
management. Air pollution deposition and influences are also
variable and poorly documented in the field. Monitoring of species
dynamics and productivity, necessary to detect effects of regional
air pollutants, or any other environmental stress, are presently
rarely available. Dendrochronological or other tree-ring analytical
techniques are subject to enormous difficulty when they attempt to
partition the relative importance of forces that may influence tree
growth. Growth is regulated by precipitation, temperature, length of
growing season, frost, drought, by developmental processes such as
succession and competition, and to stochastic events such as insect
outbreaks, disease epidemics, fire, windstorms and anthropogenic
activities such as thinning, fertilization, harvesting and, finally,
air quality.

For a long time, dieback and decline of specific forest species, somewhere in the temperate zone, has been common. Age, climate, or biotic stress factors have frequently been judged to be the principal causes for declines. Again, however, it is difficult to assign responsibility for specific cause and effect. Trees are large and long-lived and their health integrates all the stresses to which they are exposed over time.

The risks associated with regional and global air pollution stress and forest ecosystem health are high. The evidence available to describe the total boundaries of the problem for all pollutants is incomplete. There is enormous uncertainty about specific effects on forests of regional and global air pollutants. We do know, however, that coal combustion will provide more than 50 percent of America's electricity by 1990. We further know that without management or control, coal combustion is a source of numerous regional and global pollutants identified as important, or potentially important, to the health of forest ecosystems. Natural ecosystem health, along with human health, must be recognized in assessments, economic and otherwise, of pollution abatement strategies.

Literature Cited

1. Evans, G.; Finkelstein, P.; Martin, B.; Possiel, N.; Graves, M. Science 1983, 33, 291-6.
2. Pratt, G.C.; Hendrickson, R.C.; Chevone, B.I.; Christopherson, D.A.; O'Brien, M.V.; Krupa, S.V. Atmos. Environ. 1983, 17, 2013-23.
3. "Air Quality Criteria for Lead," U.S. Environmental Protection Agency, 1983a, Vol. I, Publica. No. 600/8-83-028A, 169 pp.
4. Murozumi, M.; Chow, T.; Patterson, C. Geochim. Cosmochim. Acta 1969, 33, 1247-94.
5. Smith, W.H.; Siccama, T.G. Jour. Environ. Qual. 1981, 10, 323-33.
6. Chung, Y.S. Atmos. Environ. 1978, 12, 1471-80.
7. Tong, E.Y.; Hidy, G.M.; Lavery, T.F.; Berlandi, F. Proceedings, Third Symposium on Turbulence, Diffusion and Air Quality, 1976.
8. Wolff, G.T.; Kelly, N.A.; Furman, M.A. Science 1981, 211, 703-5.
9. "The Acidic Deposition Phenomenon and Its Effects," U.S. Environmental Protection Agency, 1983b, Vol. I, Atmos. Sci. Publica. No. 600/8083-016A, p. 3-92.
10. Holdgate, M.W.; Kassas, M.; White, G.F. Environ. Conserva. 1982, 9, 11-29.
11. "Stratospheric Ozone Depletion by Halocarbons," National Academy of Sciences, 1979, 249 pp.
12. "Stratospheric Ozone Depletion by Halocarbons," National Academy of Sciences, 1982c, 92 pp.
13. Miller, P.R.; McBride, J.R. Academic Press, 1975, pp. 195-235.
14. Smith, W.H. "Air Pollution and Forests"; Springer-Verlag, 1981, 379 pp.
15. "Solar Variability, Weather, and Climate (Studies in Geophysics)", National Academy of Sciences, 1982a, 120 pp.

16. "Carbon Dioxide and Climate: A Second Assessment", National
    Academy of Sciences, 1982b, 92 pp.
17. Manabe, S.; Stouffer, R.J. Jour. Geophys. Res. 1980, 85, 5529–
    54.
18. Kellogg, W.W. World Meteorol. Org., Technical Note No. 156, WHO-
    No. 486.
19. Waggoner, P.E. Amer. Scient. 1984, 72, 179–184.
20. Maugh, T.H. Science 1980, 207, 394–95.
21. Miller, P.R.; Taylor, O.C.; Wilhour, R.G. U.S. Environmental
    Protection Agency 1982, Publica. No. EPA-600/D-82-276, 10 pp.
22. "Air Quality Criteria for Ozone and Other Photochemical Oxidants"
    U.S. Environmental Protection Agency, 1984, (in press).
23. Linthurst, R.A., Ed. In Direct and Indirect Effects of Acidic
    Deposition on Vegetation 1984, Vol. 5, Acid Precipitation
    Series, J.I. Teasley, Ed., 117 pp.
24. "Acid Deposition and Forest Ecosystems," Society of American
    Foresters, 1984, 51 pp.
25. Waring, R.H.; Newman, K.; Bell, J. Forestry, 1981, 54, 129–137.
26. Waring, R.H. Proc. Workshop held in Uppsala, Sweden 1983, in
    press.
27. Waring, R.H. For. Ecol. Manage., 1985, (in press).
28. Baes, C.F.; McLaughlin, S.B.; Science 1984, 224, 494–497.
29. McLaughlin, S.B.; Blasing, T.J.; Mann, L.K.; Duvick, D.N. Jour.
    Air Pollu. Cont. Assoc., 1983, 33, 1042–49.
30. Fritts, H.C.; Stokes, M.A. Tree-Ring Bull. 1975, 35, 15–24.

Carbon Isotopes as Tracers of Biogenic and Fossil-Fuel-Derived Carbon Transport in the Atmosphere

Roger L. Tanner and Jeffrey S. Gaffney[1]

Environmental Chemistry Division, Department of Applied Science, Brookhaven National Laboratory, Upton, NY 11973

Carbon-14 content and $^{13}C/^{12}C$ isotopic ratios were measured in ambient atmospheric aerosol samples which had been speciated into organic and elemental carbon fractions after collection in winter and summer seasons near Oak Ridge, TN. Major fractions of contemporary carbon were found in summer and winter aerosols, based on radiocarbon measurements, with biogenic source contributions to organic carbon exceeding that for elemental carbon. $^{13}C/^{12}C$ ratios were consistent with a mixture of fossil fuel and C-3 terrestrial plants as the source of the aerosol carbon. Extension to measurements of carbon isotopes in collected gaseous samples to aid in biogenic source identification is discussed.

Carbonaceous aerosols in the atmosphere are complex in nature and are found in both coarse particles (> about 2.5 μm) and fine particles (< about 2.5 μm). Sources of carbon-containing particles are varied and include resuspended soil particles, pollen, plant waxes, etc. in the coarse fraction, and soot particles, sorbed organics including PAHs, and secondary aerosols resulting from

[1]Current address: Los Alamos National Laboratory, Group INC-7, MS-J514, Los Alamos, NM 87545

gas-to-particle conversion in the fine fraction. An important
need in contemporary studies of the carbon cycle in the atmosphere
is to develop and apply improved techniques for characterization
of organic and elemental fractions of fine and coarse-sized
carbonaceous aerosols. Especially critical is the need to assess
the relative contributions to carbonaceous aerosols from biogenic
and fossil fuel-derived sources of their gaseous and primary
particulate precursors.

Several previous reports (1-5) have demonstrated the useful-
ness of measurements of ^{14}C (radiocarbon) and ^{13}C (stable isotope)
carbon isotopes in obtaining new information on carbon source
terms. Radioactive carbon-14 measurements of atmospheric samples
are made using microscale gas proportional counting techniques
(6,7) or by direct atom counting in high energy accelerators, a
technique referred to as Tandem Van de Graaff mass spectrometry
(8). Both techniques rely on the two-source, isotope dilution
assumption (9): carbonaceous material in the atmosphere is
derived from biogenic sources in equilibrium with the $^{14}CO_2$ in the
atmosphere, or from fossil fuel sources whose geological age is
long compared to the half-life of ^{14}C (ca 5800 yr). The principal
causes of the method-limiting variations of ^{14}C in the biosphere
are: (a) solar modulation of cosmic rays; (b) radiocarbon produc-
tion associated principally with nuclear tests; and (c) dilution
of radiocarbon in the atmosphere by fossil-fuel-derived CO_2. The
value of ^{14}C measurements, however, is that they directly trace
biogenic emissions; furthermore, the $^{14}C/^{12}C$ ratio is resistant to
changes during transport.

The additional measurement of $^{13}C/^{12}C$ ratios in carbonaceous
aerosols by isotope ratio mass spectrometry provides information
concerning fractionation during chemical conversion of carbon-
containing atmospheric species. However, $^{13}C/^{12}C$ ratios,
expressed in terms of the del value, $\delta^{13}C$,

$$\delta^{13}C = \left[\frac{(^{13}C/^{12}C)\text{sample}}{(^{13}C/^{12}C)\text{PDB standard}} - 1 \right] \times 10^3$$

i.e., the relative $^{13}C/^{12}C$ value in parts per thousand, vs. that
of CO_2 derived from standard calcium carbonate (Peedee formation
belemnite), differ widely between plants of the two major photo-
synthetic pathways (10). Biomass burning of C-4 terrestrial
plants (Hatch-Slack photosynthetic pathway, as for example, sugar
cane and corn) will produce carbonaceous aerosols with $^{13}C/^{12}C$
ratios, $\delta^{13}C$, 10 to 18 parts per thousand more positive than
material derived from C-3 terrestrial plants (Calvin-Benson photo-
synthetic pathway, as for example, wheat, potatoes, and most woody
plants); that is, $\delta^{13}C$ = -12 ± 2 vs the PDB standard for C-4
plants compared to $\delta^{13}C$ = -26 ± 3 for C-3 plants. Thus, major
biogenic contributions from slash burning of C-4 plants can be
differentiated using the $^{13}C/^{12}C$ data, although C-3 plants cannot
be differentiated from coals and oils.

Previous studies using ^{14}C and $^{13}C/^{12}C$ measurements in con-
nection with other source apportionment techniques have demon-
strated their value in assessing the importance of various sources
(3). In winter studies in Portland, OR, at a site in which the
impact from wood-burning is large, the fraction of contemporary
carbon was near 100%; urban plume values of ^{14}C for Denver samples
were substantially lower (10-54% contemporary) (8). Previous
values reported for Long Island, NY, and Barrow, AK, sites were in
the range of 30% contemporary carbon (5), with $^{13}C/^{12}C$ ratios con-
sistent with a combination of fossil fuel and C-3 plant biogenic
sources ($\delta^{13}C \sim -26$).

In this work we report organic and elemental carbon data, ^{14}C
content and $^{13}C/^{12}C$ isotopic ratios for samples obtained in a
larger set of measurements in the POLTERCAIST (POLlutant-TERpene
CAnopy Interaction STudy) taken at the Walker Branch experimental
site, Oak Ridge National Laboratory, Oak Ridge, TN, during a
summer period (July, 1983) and a late winter period (March,
1984). As an extension of these studies in which major impact
from biogenic sources is confirmed, we discuss the potential use
of carbon isotopes to identify aerosols from sugar cane-derived
fuels and to identify gaseous products of atmospheric

photooxidation (i.e., aldehydes) derived from precursor biogenic
hydrocarbon emissions.

Experimental

Organic/elemental carbon speciation is performed on µg-sized
samples using a thermal evolution technique (11) in which carbon
is evolved in 2 discrete steps at 400°C in He and at 650°C in 10%
O_2/He, then measured as CO_2 by nondispersive infrared (NDIR) spec-
troscopy (Beckman Model 865). $^{13}C/^{12}C$ measurements are made by
isotopic ratio mass spectrometry (Nuclide Corp) also after conver-
sion to CO_2; ratios in samples of as little as 0.5 mg can be
determined to ± 0.1 parts per thousand.

Carbon-14 content is measured by specially designed gas pro-
portional counters (7). Aerosol samples are first converted to
CO_2 by combustion in a macroscale version of the thermal evolution
technique. A clam shell oven was used to heat the sample for
sequential evolution of organic and elemental carbon under equiva-
lent conditions. Due to the possibility of thermal gradients,
conditions in the macroscale apparatus were adjusted to produce
the same recoveries of total carbon (µg C per cm^2 of filter area)
as for the microscale apparatus. Carbon-14 data are reported as %
contemporary carbon based on the 1978 $^{14}CO_2$ content in the atmo-
sphere. Aldehyde data referred to in this paper were obtained by
impinger sampling in dinitrophenylhydrazine/acetonitrile solution
and analysis of the derivatives by HPLC with UV detection (12).
Olefin measurements were made by a specially designed ozone-
chemiluminescence apparatus (13); difficulties in calibration
accuracy and background drift with temperature limit its use to
inferences of relative reactive hydrocarbon levels.

Results and Discussion

Summaries of the aerosol carbon data obtained as part of the
POLTERCAIST I and II conducted at the National Oceanographic and
Atmospheric Administration (NOAA) Atmospheric Turbulence and
Diffusion Laboratory (ATDL) Walker Branch site near Oak Ridge, TN,
in cooperation with NOAA-ATDL and Oak Ridge National Laboratory
(ORNL) staff are reported in Tables I and II. Concentrations of

organic and especially elemental carbon reported in Table I were
quite high compared to previously reported data (5) from North-
eastern U.S. sites. Organic/total C (total = organic + elemental)
ratios as determined by the microscale method (11) were somewhat
lower than reported data (5). This indicates relatively more
local aerosol sources at Walker Branch, since emitted elemental
aerosol carbon is conservative but additional secondary organic
aerosol carbon can be formed after emission into the atmosphere.

Some significant differences in measured organic/total C
ratios by macro- and microscale techniques were observed, with the
macroscale apparatus yielding higher ratios. This suggests that
improvements should be made in the macroscale technique to simu-
late better the rapid, uniform heating of the microscale appara-
tus. However, differences were not large enough to affect the
conclusion that local sources, possibly due to incineration, make
substantial contributions to local aerosol carbon levels at this
site. No aerosol size distribution or TSP data are available for
this study. Based on reported aerosol carbon size distributions
(14, 15) in which most (60-90%) of the carbonaceous aerosol was in
the fine fraction (< 2.5 μm diameter), the data reported here are
somewhat higher but consistent with the summertime results in the
nearby Great Smoky Mountains (16) and in more remote areas (17) in
which fine aerosol carbon levels and their contribution to visi-
bility reduction were much smaller than those produced by aerosol
sulfate levels. Summertime levels of aerosol sulfate were compa-
rably high in both studies.

Table II presents the data for $^{13}C/^{12}C$ ratios and ^{14}C content
of aerosols collected at the ATDL/Oak Ridge site. The ^{14}C results
for two samples in which both organic and element ^{14}C carbon were
measured on the same sample are in agreement with predictions that
elemental carbon (soot) in atmospheric aerosols is due to primary
emissions from combustion of fossil fuels to a greater extent than
is organic carbon in aerosols, leading to lower ^{14}C content. The
organic carbon may come from a large range of biomass materials of
recent origin (leaf litter, carbon in resuspended soil, pollen,

Table I
POLTERCAIST I and II
Organic/Elemental Carbon
Oak Ridge, TN; July, 1983 and March, 1984

Sample	Sampling Time	Sample Wt., mg	Microanalysis Org C µg/m³	Elem C µg/m³	Org/Total	Macroanalysis Org/Total C
POLTERCAIST I						
1-Organic 1-Elemental	} 1937, 7/14/83 to 2005, 7/15 {	7.5 6.2	} 5.26	5.32	0.50	0.55
2-Elemental	2015, 7/15 0843, 7/18	10.2a	3.52	4.63	0.43	NA
4-Totalb	1105, 7/20 to ~1000, 7/21	7.1	3.59	4.25	0.46	0.75
5-Total	1008, 7/21 to 0852, 7/22	11.4	5.02	4.42	0.53	0.62
POLTERCAIST II						
1-Total	2050, 3/8/84 to 0939, 3/10	10.1	3.30	7.2	0.31	0.54
2-Organic	0940, 3/10 to 1356, 3/12	6.5	5.9	6.2	0.49	0.59
(3+4)-Organic (3+4)-Elemental	{ 1357, 3/12 to 0933, 3/16 {	14.1 7.4	8.3 6.8	4.7 5.4	0.64 0.56 }	0.66

a Weight of elemental fraction only, organic fraction lost.
b Total samples are weight-averaged for elemental and organic carbon content.

Table II
POLTERCAIST I and II
Organic/Elemental Carbon, 13C/12C and 14C Data
Oak Ridge, TN; July, 1983 and March, 1984

Sample	Sample Wt., mg	Microanalysis Org/Total[a]	Macroanalysis Org/Total[a]	13C/12C, δ	14C, % Contemporary[b]
POLTERCAIST I					
1-Organic	7.5 }	0.50	0.55 {	−25.5	74 ± 1.8
1-Elemental	6.2	0.43	NA	−24.9	47 ± 2.0
2-Elemental	10.2	0.46	0.75	−25.0	63 ± 1.9
4-Total[c]	7.1	0.53	0.62	−25.2	99 ± 2.6
5-Total	11.4			−25.4	78 ± 1.7
POLTERCAIST II					
1-Total	10.1	0.31	0.54	−24.3	48 ± 1.5
2-Organic	6.5	0.49	0.59	−24.7	75 ± 2.1
(3+4)-Organic	14.1	0.64[d] }	0.66 {	−25.2	76 ± 2.0
(3+4)-Elemental	7.4	0.56[e]		−24.6	53 ± 1.8

a Org/Total = organic carbon/(organic + elemental carbon).
b Corrected to 1978 standard (6).
c Total samples are weight-averaged for elemental and organic carbon contents.
d Sample 3.
e Sample 4.

etc.) as well as primary and secondary combustion aerosols. In contrast, all soot must come from combustion sources and, although wood combustion (home heating, incineration, brush fires) makes a major impact on aerosol elemental carbon in some locations, especially in winter (3), most elemental carbon is thought to be derived from fossil fuel burning. The presence of ~ 50% contemporary carbon in elemental samples even during the summer season strongly suggests that there are local soot sources from combustion of biogenic fuels other than wood at this site. $^{13}C/^{12}C$ ratios are fully consistent with contributions from both fossil fuel and C-3 plants to the observed carbonaceous aerosols. As expected, C-4 plants do not make a major contribution to the observed aerosols, and coal-derived fossil material is more likely than oil-derived material based on reported $^{13}C/^{12}C$ ratios (18).

In addition to aerosol measurements within and above the canopy during POLTERCAIST I and II studies, reactive trace gases (HNO_3, O_3, NO_x, olefins, reduced sulfur compounds and aldehydes) were also measured (19). In the summer of 1983, increased levels of olefins (~ 2-fold) sampled after a significant rainfall were accompanied by increases in formaldehyde (HCHO) levels but not in acetaldehyde (CH_3CHO) levels. Isoprene emissions from the deciduous forest canopy are deduced to be the cause of increased HCHO levels, indicating that biogenic contributions to gas phase organic oxidant precursors were substantial, but that they probably did not contribute directly to organic aerosol carbon levels. Much lower ratios of $HCHO/CH_3CHO$ were observed during winter, 1984, sampling when the deciduous canopy was dormant. Additional measurements are required in coniferous forest canopies in which emissions are different in nature (terpenes vs. isoprene) and emitted in a more continuous pattern (20).

To study the impact of biogenic sources of hydrocarbons on gas phase photochemistry in the atmosphere, new isotopic ratio-based techniques are required. For example, ultra-high volume collection of aldehydes with separation of formaldehyde and acetaldehyde (or their derivatives), and subsequent ^{13}C and ^{14}C

measurements would confirm the tentative conclusions made from the
POLTERCAIST data. Ultimately, isotopic measurements of such
species as organic oxidants (peroxyacyl nitrates, alkyl hydroper-
oxides and peracids) and weak organic oxidants should be made to
trace the relative contributions of biogenic and anthropogenic
sources to organic carbon cycling through the atmosphere.

Acknowledgments

Literature Cited

1. Currie, L.A.; Kunen, S.M.; Voorhees, K.J.; Murphy, R.B.;
    Koch, W.F. Proc. Conf. Carbonaceous Particles in the
    Atmosphere, 1978, p. 36-48.
2. Currie, L.A.; Noakes, J. and Breiter, D. In: "Radiocarbon
    Dating"; Berger, R.; Suess, H.E., Eds; Univ. California
    Press; Berkeley, CA, 1979, p. 58-175.
3. Cooper, J.A.; Currie, L.A.; Klouda, G.A. Environ. Sci.
    Technol. 1981, 15, 1045-1050.
4. Gaffney, J.S., 1982. "Organic air pollutants: setting
    priorities for long-term research needs," Report BNL 51605
    UC-11, Brookhaven National Laboratory, 1982.
5. Gaffney, J.S.; Tanner, R.L.; Phillips, M. The Science of
    the Total Environment 1984, 36, 53-60.
6. Currie, L.A.; Klouda, G.A.; Cooper, J.A. Radiocarbon 1980,
    22, 349-362.
7. Harbottle, G.; Sayre, F.V.; Stoenner, R.W. Science 1979,
    206, 683-685.
8. Muller, R.A. Science 1977, 196, 489-494.
9. Currie, L.A. Contemporary Particulate Carbon, In:
    "Particulate Carbon: Atmospheric Life Cycle," Wolfe, G.T.;
    Klimisch, R.L., Eds., Plenum Pub. Co.: New York, 1982.
10. Gaffney, J.S.; Irsa, A.P.; Friedman, L.; Slatkin, D.N.
    Biomed. Mass. Spectr. 1978, 5, 495-497.
11. Tanner, R.L.; Gaffney, J.S.; Phillips, M. Anal. Chem. 1982,
    54, 1627-1630.
12. Tanner, R.L.; Meng, Z. Environ. Sci. Technol. 1984, 18,
    723-726.

13. Kelly, T.J.; Allar, W.J.; Premuzic, E.; Tanner, R.; Gaffney, J. "Temperature dependence of ozone-hydrocarbon chemiluminescence. Possible hydrocarbon class monitor." Presented at the Symp. on Atmospheric Chemistry, 182nd ACS National Meeting, New York, NY, 1981.
14. Wolff, G.T. J. Air Pollut. Contr. Assoc. 1981, 31, pp. 935-938.
15. Van Vaeck, L.; Van Cauwenberghe, K. Atmos. Environ. 1978, 12, pp. 2229-2239.
16. Stevens, R.K.; Dzubay, T.G.; Shaw, R.W.; McClenny, W.A.; Lewis, C.W.; Wilson, W.E. Environ. Sci. Technol. 1980, 14, 1491-1498.
17. Shaw, R.W., Jr.; Crittenden, A.L.; Stevens, R.K.; Cronn, D.R.; Titov, V.S. Environ. Sci. Technol. 17, 389-395.
18. McMullen, C.C.; Thode, H.G. Isotope Abundance Measurements and Their Application to Chemistry, In: "Mass Spectrometry", McDowell, C.D., Ed., McGraw-Hill: New York, 1963.
19. Tanner, R.L.; Gaffney, J.S. Proc. 77th Annual Mtg., Air Pollution Control Assoc., 1984, Paper No. 84-162.
20. Yokouchi, Y.; Okaniwa, M.; Ambe, Y.; Fuwa, K. Atmos. Environ. 1983, 17, 743-750.

Oxygen Isotopic Study of the Oxidation of SO_2 by H_2O_2 in the Atmosphere

B. D. Holt and R. Kumar

Argonne National Laboratory, Argonne, IL 60439

Dependence of the $^{18}O/^{16}O$ ratio in sulfate on the $^{18}O/^{16}O$ ratio in the H_2O_2 by which the sulfate was formed in aqueous oxidation of SO_2 was determined. From this and a previously determined dependence of the oxygen isotope ratio in sulfate on that of the solvent water, a comprehensive relationship $\delta^{18}O_{SO_4^{2-}} = 0.57\ \delta^{18}O_{H_2O} + 0.43\ \delta^{18}O_{H_2O_2} + 8.4‰$, was derived. This relationship was used to assess the relative importance of the H_2O_2-oxidation mechanism of sulfate formation from SO_2 in the atmosphere by measurement of the isotope ratios in the sulfate, water, and H_2O_2 in some preliminary experiments with rainwater. A new method was developed for the conversion of H_2O_2 in dilute aqueous solutions (ppm range) to CO_2 for mass spectrometric analysis.

Present efforts to control acid rain focus on controlling emissions of sulfur oxides and nitrogen oxides from coal-burning plants. The sulfate acidity arises from the oxidation of the emitted sulfur dioxide to sulfuric acid in the atmosphere. The key reactants responsible for this oxidation are not well known, although a large number of possible catalysts and oxidants exist in the atmosphere, including carbon, transition metal ions, hydroxyl and organic free radicals, hydrogen peroxide and ozone. Of these, the last two are the only ones believed to be present in sufficient quantity to produce the observed amounts of SO_4^{2-} in wet deposition. It has been postulated that the atmospheric oxidation of SO_2 is limited by the availability of one or both of these oxidants, rather than by the availability of SO_2 itself. This is the so-called phenomenon of non-linearity between the concentration (and, by implication, the emission) of SO_2 in the atmosphere and the conversion of this SO_2 to H_2SO_4. The potential importance of H_2O_2 lies in the view that aqueous-phase oxidation of SO_2 to H_2SO_4 probably accounts for a major fraction of the observed SO_4^{2-} in the acid precipitation occurring in the northeastern United States. If such is indeed the case, it is important to determine if H_2O_2 has a pivotal role in acid formation and deposition from the atmosphere.

Considerable interest has been shown in the possibility of using oxygen isotopy to elucidate the role of H_2O_2 in the oxidation of SO_2 to sulfates in the atmosphere ([1]). Oxygen isotopic studies are useful in distinguishing between

the different oxidation mechanisms effective in the atmosphere. Laboratory simulation of several different atmospheric reaction sequences has shown that the oxygen isotope ratio in the product SO_4^{2-} is uniquely related to the reaction pathway followed in its formation ([2]). It may, therefore, be possible to determine if the atmospheric hydrogen peroxide is responsible for significant oxidation of SO_2 to sulfate, and if it is this oxidant that limits the aqueous-phase formation of sulfuric acid. The results of these studies could have significant implications for energy technology, particularly if they indicate that, because of the non-linearity in SO_2 conversion discussed above, it may be more important to reduce the ambient concentrations of H_2O_2 than of SO_2.

In the 1981 JASON committee report to the U. S. Department of Energy ([1]), some recommendations for further research were based, at least in part, on our earlier work on SO_2 oxidation by H_2O_2 ([3]). According to our results, the $\delta^{18}O$ [deviation in parts per thousand (‰) of the $^{18}O/^{16}O$ ratio of the sample from that of the standard reference material, Standard Mean Ocean Water (SMOW)] of sulfates produced by H_2O_2 oxidation were significantly lower than the $\delta^{18}O$ of sulfates found in rainwater. However, the $\delta^{18}O$ of the reagent-grade H_2O_2 used in those experiments was not known. The results suggested the need for isotopic analysis of H_2O_2 in dilute solutions, and for a methodology whereby the $\delta^{18}O$ values of H_2O_2, H_2O, and SO_4^{2-} in rainwater could be compared in order to assess the importance of H_2O_2 in the formation of sulfate-constituted acid rain.

Experimental

The plan of this investigation was to develop a method for the determination of the $\delta^{18}O$ of H_2O_2 in dilute aqueous solutions (simulating rainwater); to prepare solutions of H_2O_2 of various ^{18}O enrichments; to use the freshly prepared solutions of H_2O_2 to oxidize SO_2 to SO_4^{2-} for evaluation of the relationship between $\delta^{18}O_{SO_4^{2-}}$ and $\delta^{18}O_{H_2O_2}$; and to apply this relationship to the measured $\delta^{18}O_{H_2O_2}$, $\delta^{18}O_{SO_4^{2-}}$, and $\delta^{18}O_{H_2O}$ in precipitation water, for assessment of the importance of H_2O_2 in the atmospheric transformation of SO_2 to sulfate.

Development of Analytical Method.   Since no suitable analytical method was available for the quantitative extraction of the oxygen in H_2O_2 (in water, ppb range) for isotopic analysis, a 4-step method was developed ([4]). It consisted of the removal of dissolved O_2 from 20-liter samples of water by a combination of evacuation, ultrasonic agitation, and sparging with helium; oxidation of the dissolved H_2O_2 to O_2 with $KMnO_4$; removal of the newly formed O_2 from the water in a carrier-gas stream; and conversion of the O_2 to CO_2 by reaction with platinum-catalyzed carbon at 600°C. The CO_2 was then mass spectrometrically analyzed for its $\delta^{18}O$ (identical to that of the oxygen in the original H_2O_2).

To confirm the absence of appreciable isotopic interference by oxygen exchange between the H_2O and either the H_2O_2 or the O_2, before, during, or after the oxidation reactions, the reaction was carried out in the presence of three different water supplies of various $\delta^{18}O$. The results in Figure 1 show that the $\delta^{18}O$ of the CO_2 product was unaffected by the $\delta^{18}O$ of the water solvent.

Synthesis of ^{18}O-enriched H_2O_2.   Hydrogen peroxides of various $\delta^{18}O$ were not commercially available. A suitable method of synthesis ($\underline{5}$) was successfully applied to the laboratory preparations of four stock solutions of H_2O_2 of different $\delta^{18}O$. By this method, H_2O_2 is formed by exposure of different supplies of water vapor (each differing in $\delta^{18}O$) to a high-voltage ($\sim$1.4 kV) discharge in $\sim$100 cm of 10-mm o.d. glass tubing between two water-cooled aluminum electrodes. Some of the HO radicals formed by the dissociative reaction

$$2H_2O \rightleftarrows 2HO + 2H \qquad (1)$$

are condensed in a liquid-nitrogen cold trap where they combine to form H_2O_2, leaving the H radicals to combine in formation of H_2 and be pumped away through the vacuum line.

Other techniques which we experimentally found to give inadequate yields of H_2O_2 were conduction of an electric arc across a stream of aerosolized water droplets ($\underline{6}$), excitation of water vapor by a radio-frequency silent discharge in a glass chamber (7.5 cm dia $\times$ 20 cm long) in a commercially available plasma cleaner unit, and excitation by a glow-discharge unit (4.8 cm dia $\times$ 70 cm long) that had uncooled aluminum disk electrodes ($\underline{7}$).

Oxidation of SO_2 to SO_4^{2-} by H_2O_2.   Using the four stock solutions of hydrogen peroxide, each of different $\delta^{18}O$, sulfate solutions of correspondingly different $\delta^{18}O$ were prepared by oxidation of SO_2 in water ($\delta^{18}O$, constant at $-7.9‰$). In Figure 2 the $\delta^{18}O$ of each resulting sulfate is plotted versus the $\delta^{18}O$ of the H_2O_2 and the equation of the best-fit regression curve is

$$\delta^{18}O_{SO_4^{2-}} = 0.43\, \delta^{18}O_{H_2O_2} + 3.5‰ \qquad (2)$$

The regression curve of the previously determined ($\underline{3}$) relationship between $\delta^{18}O_{SO_4^{2-}}$ and $\delta^{18}O_{H_2O}$ in aqueous-phase oxidation of SO_2 by H_2O_2 was

$$\delta^{18}O_{SO_4^{2-}} = 0.57\, \delta^{18}O_{H_2O} - 2.4‰ \qquad (3)$$

Assuming that all significant effects of the $\delta^{18}O$ of the SO_2 on the $\delta^{18}O$ of the SO_4^{2-} are lost by rapid isotopic exchange between the SO_2 and the large excess of water, prior to appreciable oxidation ($\underline{3}$), $\delta^{18}O_{H_2O}$ and $\delta^{18}O_{H_2O_2}$ remain as the only two complementary variables in the equation for $\delta^{18}O_{SO_4^{2-}}$.

Therefore, the comprehensive regression curve for $\delta^{18}O_{SO_4^{2-}}$ is

$$\delta^{18}O_{SO_4^{2-}} = 0.57\, \delta^{18}O_{H_2O} + 0.43\, \delta^{18}O_{H_2O_2} + C \qquad (4)$$

$$= \sim\frac{3}{5}\, \delta^{18}O_{H_2O} + \sim\frac{2}{5}\, \delta^{18}O_{H_2O_2} + C. \qquad (5)$$

The constant, C, was evaluated at 8.4‰ from the data given in Figure 2 by substituting the corresponding measured values for $\delta^{18}O_{SO_4^{2-}}$ and $\delta^{18}O_{H_2O_2}$,
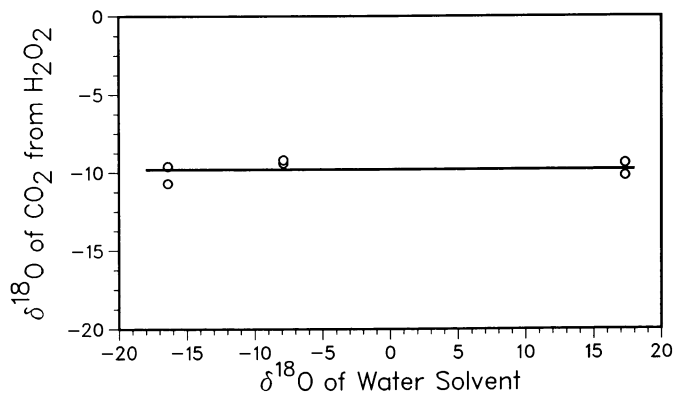
Figure 1.   Isotopic influence of water solvent on CO_2 of H_2O_2 origin.
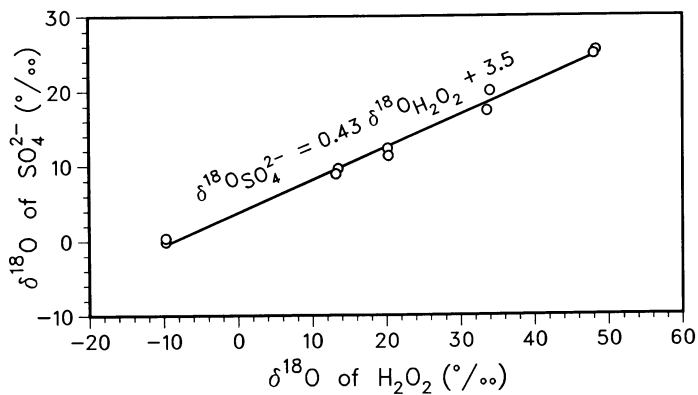
Figure 2.   Isotopic influence of the H_2O_2 oxidant on the SO_4^{2-} product.

and $-7.9\%_0$ for $\delta^{18}O_{H_2O}$.

The comprehensive equation then becomes

$$\delta^{18}O_{SO_4^{2-}} = 0.57\ \delta^{18}O_{H_2O} + 0.43\ \delta^{18}O_{H_2O_2} + 8.4\%_0 \qquad (6)$$

and can now be used to calculate $\delta^{18}O_{SO_4^{2-}}$ from $\delta^{18}O_{H_2O_2}$ and $\delta^{18}O_{H_2O}$ of rainwater for comparison with corresponding measured values of $\delta^{18}O_{SO_4^{2-}}$. This comparison may prove to be uniquely useful in the assessment of the importance of H_2O_2 in the oxidation of SO_2 to SO_4^{2-} in the atmosphere.

The slope of 0.43 (approximately 2/5) in Equation 2 of the regression curve through the data of Figure 2 confirms the evidence of the intermediate species, $H_2O_2 \cdot SO_3^{2-}$, which was previously proposed (3). Apparently, the $\delta^{18}O$ of the sulfate product is 2/5-controlled by the two oxygens in the H_2O_2 of the adduct, and 3/5-controlled by the HSO_3^-, which, in turn, is isotopically controlled by rapid oxygen exchange with the large excess of water with which it is associated.

Results and Discussion

Isotopic and H_2O_2-concentration analyses were completed on rainwater samples collected from seven precipitation events at Argonne, IL, during the period of September 1984 through April 1985. These results, presented in Table 1 and in Figure 3 are to be supplemented by additional results from precipitation samples collected in the remaining four or five months of the current program. The conclusions based on these limited data are therefore subject to change.

The $\delta^{18}O$ of H_2O_2 could not be determined on the snow sample of January 18 because the amount of H_2O_2 in the 20-liter sample did not exceed

Table 1. Isotopic results and H_2O_2 concentrations for precipitation samples, September 1984 through April 1985.

1	2	3	4	5	6	7	8
					$\delta^{18}O_{SO_4^{2-}}$		
	H_2O_2 Concen.	$\delta^{18}O_{H_2O_2}$	$\delta^{18}O_{H_2O}$	Calculated by H_2O_2 oxidation	by air oxidation	measured	% Oxidation by H_2O_2
Sample	(ppb)	(‰)	(‰)			(‰)	($\frac{7-6}{5-6} \times 100$)
R- 9/25/84	63	32	−4.1	19.9	6.7	16.2	72
R-10/18/84	35	33	−3.3	20.7	7.4	17.6	77
R-11/27/84	10	22	$\begin{cases} -2.3 \\ -3.6 \end{cases}$	16.3	7.6	11.1	40
S- 1/18/85	0	−	−12.2	−	0.2	7.8	−
S- 2/ 5/85	4	(41)	$\begin{cases} -13.1 \\ -13.5 \end{cases}$	(18.4)	−0.6	6.1	(35)
R-3/27−28/85	13	42	−4.9	23.7	6.1	17.0	62
R-4/23−24/85	1	(67)	$\begin{cases} -4.7 \\ -4.8 \end{cases}$	(34.5)	6.2	16.3	−
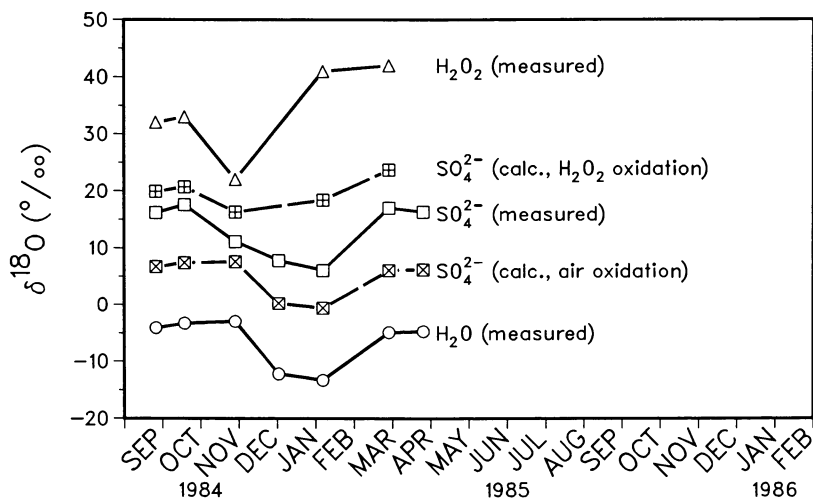
Figure 3.   Isotopic results for H_2O_2, SO_4^{2-}, and H_2O in rainwater.

the blank (6.5 μmole) of the analytical procedure in use at that time. Similarly, the $\delta^{18}O_{H_2O_2}$ of the sample of April 23–24 was uncertain because of the very low concentration. These very-low-to-zero concentrations of H_2O_2 during the colder months precluded the determination of whether there was a winter seasonal minimum in the $\delta^{18}O$ of H_2O_2, corresponding to those of H_2O and SO_4^{2-}, observed in these and in previously reported experiments (8).

Three sets of data for the $\delta^{18}O$ of SO_4^{2-} are given in Table 1 and plotted in Figure 3. One is measured; another is calculated by Equation 6 for the aqueous H_2O_2 oxidation of SO_2; and another is calculated by the previously developed relationship (3), $\delta^{18}O_{SO_4^{2-}} = 0.8\ \delta^{18}O_{H_2O} + 10$, for the aqueous air oxidation of SO_2. The curve for the measured data in Figure 3 is bracketed by these two curves of calculated data.

This comparison of measured *vs* calculated data suggests that by ignoring the possible presence of primary sulfates [the concentration of which may not be insignificant at the Argonne sampling site (2)], the sulfate in precipitation water is formed from SO_2 in the atmosphere, partly by aqueous-phase H_2O_2 oxidation and partly by aqueous-phase air oxidation. The relative deviations of the measured values from the two calculated values represent the relative amounts of each in the mixture.

Acknowledgments

Literature Cited

(1) Chamberlain, J. C., Foley, H., Hammer, D., MacDonald, G., Rothaus, O., and Ruderman, M., Technical Report JSR-81-25, prepared for the Office of Energy Research, U. S. Department of Energy (1981).

(2) Holt, B. D., Kumar, R., and Cunningham, P. T., *Science*, **217**, 51 (1981).

(3) Holt, B. D., Kumar, R., and Cunningham, P. T., *Atmos. Environ*, **15**, 557 (1981).

(4) Holt, B. D., to be published elsewhere.

(5) Vol'now, I. I., Tsentsiper, A. B., Chamova, V. N., Latysheva, E. I., and Kuznetsova, Z. I., *Russian J. Phys. Chem.* **38**, 645–648 (1964).

(6) Kok, G. L., "The Production of Hydrogen Peroxide by Lightning," presented at the 1982 American Geophysical Union Meeting, San Francisco.

(7) Jarnagin, R. C. and Wang, J. H., *J. Amer. Chem. Soc.* **80**, 786–787 (1958).

(8) Holt, B. D., Cunningham, P. T., and Kumar, R., *Environ. Sci. Tech.* **15**, 804 (1981).

23

Chemical Kinetics of Intermediates in the Autoxidation of SO$_2$

Robert E. Huie

National Bureau of Standards, Gaithersburg, MD 20899

The autoxidation of SO$_2$ solutions is known to involve free radicals. Recent work on the reaction of free radicals with sulfite and bisulfite and on the reaction of the sulfite and peroxysulfite radicals is beginning to allow this complex system to be understood better. This is particularly true of the effect of added chemicals on SO$_2$ autoxidation and chemical transformations induced by this system.

The autoxidation of aqueous solutions of sulfur dioxide (sulfite, bisulfite) is a classic problem in chemistry. Basic features of this reaction have been known since early in this century, when it was established that the reaction is trace metal ion catalyzed ([1]) and most likely involves free radicals ([2]). Certain chemical effects associated with sulfite autoxidation were noted also. Before the turn of the century, it was noted that sulfite would induce the oxidation of transition metal ions ([3]) and it was reported later that the oxidation of organic compounds was brought about during sulfite autoxidation ([4]). Conversly, organic compounds were also shown to serve as inhibitors of sulfite autoxidation ([5]).

Over the past century there have been a great many studies on sulfite autoxidation ([6]), including studies on the rate of the reaction in the presence of catalysts and inhibitors, measurements of the amounts of sulfate and dithionate found under various conditions, the determination of the products arising from the addition of organic (including biochemical) compounds, and studies on the effects of mixed catalysts. Yet, a quantitative understanding of the reaction has been elusive ([7],[8]). This is due largely to a lack of quantitative data on the elementary steps in the overall reaction, including data on the rates of the free radical reactions likely to be important. From the point of view of fossil fuel use and its effects on the environment, a knowledge of this chemistry is important for two reasons. First, wet scrubbers are still the most important means of removing SO$_2$ from flue gas; for the most efficient operation, the oxidation of SO$_2$ in the scrubber solution

needs to be controlled. Second, intermediates formed during the autoxidation of SO_2 may play a role in the environmental and health effects associated with SO_2 emission.

Recently, we have carried out studies on the free radical chemistry of sulfite. These studies have included kinetic measurements on the reactions of organic and inorganic free radicals with sulfite and bisulfite, and on the reactions of the sulfite derived radicals SO_3^- and SO_5^- with organic and inorganic substrates. In this paper, I will review some of our results and results from other laboratories on the radical chemistry of sulfite and discuss these results in relation to the problem of SO_2 autoxidation.

Rate constants for the radical reactions were carried out using pulse radiolysis. Briefly, a N_2O saturated solution is pulse irradiated, with high energy electrons, producing OH radicals.

$$H_2O \rightsquigarrow OH, H, e^-_{aq}$$

$$e^-_{aq} + N_2O + H_2O \rightarrow N_2 + OH + OH^-$$
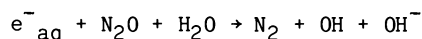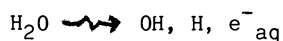
(The small amount of H atoms produced usually does not interfere.) The OH reacts with sulfite or bisulfite to produce the SO_3^- radical

$$OH + HSO_3^- \rightarrow H_2O + SO_3^-$$

$$OH + SO_3^{2-} \rightarrow OH^- + SO_3^-$$
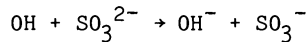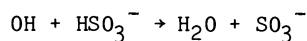
or with some other organic or inorganic substrate to produce another desired radical

$$OH + S \rightarrow OH^- + S^+$$
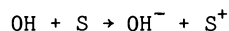
The optical absorption of SO_3^- exhibits λ_{max} = 225 nm with ε_{max} = 1000$M^{-1}cm^{-1}$ (9). This absorption is not convenient for most reactions of SO_3^- since the uv absorption of most other substrates or of their radicals mask this relatively weak absorption. Therefore, the optical absorption of the other radical product (or reactant) was monitored. For example, in the reaction of SO_3^- with ascorbate, the ascorbate radical absorption at 360 nm was monitored; the reaction of the radical I_2^- with HSO_3^-/SO_3^{2-} was monitored at 380 nm, the absorption maximum for I_2^-.

Oxidation of sulfite and bisulfite by free radicals

We have found that sulfite and bisulfite undergo one-electron oxidation by many free radicals to produce SO_3^-. Rate constants determined for selected radicals are given in Table 1. Measurement of the rate constant over a wide range of pH has, in some cases, allowed the separate determination of rate constants for the oxidation of sulfite and bisulfite. The very strong oxidant OH reacts very rapidly and oxidizes bisulfite faster than sulfite, possibly due to a contribution from hydrogen atom abstraction. For radicals which are relatively weaker oxidants, the reaction with sulfite is the faster. For example, with Br_2^- the ratio of rate constants for sulfite to bisulfite is about 4; for the even weaker

Table I .   Rate Constants for Reactions of Sulfite with Radicals

Reaction	pH	$k(M^{-1}s^{-1})$	reference
$OH + HSO_3^-$	~	9.5×10^9	10
$OH + SO_3^{2-}$	~	5.5×10^9	10
$SO_4^- + HSO_3^-$	~	$\geq 1 \times 10^9$	9
$Br_2^- + HSO_3^-$	4.2	6.9×10^7	12
$Br_2^- + SO_3^{2-}$	10	2.6×10^8	12
$I_2^- + HSO_3^-$	3	1.1×10^6	12
$I_2^- + HSO_3^-/SO_3^{2-}$	6.7	1×10^7	12
$I_2^- + SO_3^{2-}$	11	1.9×10^8	12
$NH_2 + SO_3^{2-}$	11	NR	12
$C_6H_5O + SO_3^2$	11	1×10^7	12
$C_6H_5NH_2^+ + HSO_3^-$	2.5	4.8×10^6	12
$C_6H_5NH_2^+ + SO_3^{2-}$	*	4×10^9	12
$C_6H_5NH + SO_3^{2-}$	13	$<3 \times 10^4$	12
$C_6H_5N(CH_3)_2^+ + HSO_3^-$	3.6	$<8 \times 10^5$	12
$C_6H_5N(CH_3)_2^+ + SO_3^{2-}$	10.9	9.9×10^8	12
$(chlorpromazine)^{\cdot +} + HSO_3^-$	3.6	$\sim 5 \times 10^5$	13
$(cystine)^{\cdot} + HSO_3^-, SO_3^{2-}$	7.4	5.4×10^7	14

NR No reaction detected ($k < 10^5 M^{-1}s^{-1}$). The redox potentials for NH_2
   and SO_3^- radicals appear to be very similar, judging from rate
   constants for their reactions with several reactants.

* Calculated from the pH dependence of the rate constant.

oxidant I_2^- the ratio is about 200. For the dimethylaniline radical
cation, the reaction with sulfite is very fast ($k \sim 10^9 M^{-1}s^{-1}$) while
the reaction with bisulfite is too slow to measure with the
technique employed ($k < 8 \times 10^5 M^{-1}s^{-1}$). This higher reactivity of
SO_3^{2-} toward one-electron oxidents compared to HSO_3^- results from its
lower reduction potential (see below).
     These observations on both the relative and absolute rates of
 reaction of radicals with sulfite and bisulfite can be compared with
observations made on the reactions of transition metal ions with SO_2
solutions. Typically, a strong, positive pH dependence is observed
for these reactions. This usually is interpreted as suggesting that
sulfite, not bisulfite, is the important reactant. Since these
metal ions are often relatively weak oxidants ($E < 1V$), this
conclusion would appear to be justified. For metal ion complexes
which are stronger oxidants, however, this assumption may be

unwarranted. Indeed, the kinetics of the reaction of Mn(III) ($E°$ ~ 1.4V) in strong acid could be explained as mainly due to reaction with bisulfite (15).

Oxidation of Sulfite by NO_2

We have measured rate constants for reactions of ClO_2 and NO_2 with a number of organic and inorganic compounds (16). In all cases but one, the rate constant for the ClO_2 reaction was greater than for the NO_2 reaction. This one exception was for the reaction of NO_2 with SO_3^{2-}. The typically greater rate constant for ClO_2 reactions compared to NO_2 is due to the much larger electron self-exchange rate for ClO_2 (4.4×10^2 $M^{-1}s^{-1}$) than NO_2 (1 $M^{-1}s^{-1}$). The exception in the case of the reaction of NO_2 with SO_3^{2-} is because this reaction is not a simple electron-transfer but, rather, involves an oxygen atom transfer

$$NO_2 + SO_3^{2-} \rightarrow NO + SO_4^{2-}$$
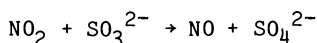
This result is important in modeling wet SO_x-NO_x flue-gas scrubbers. It shows that whereas NO_2 will oxygenate SO_3^{2-} rapidly, it will not initiate the free-radical autoxidation of sulfite (17). Further, since the slightly soluble gas NO is the product, this reaction could reduce the efficiency of NO_x removal (unless an NO scavenger is added).

Reactions of sulfite radicals

Rate constants for the reactions of SO_3^- with a wide variety of organic compounds are summarized in Table 2. The sulfite radical was found to oxidize ascorbate, trolox (a water soluble tocopherol derivative), methoxyphenol, hydroquinone and other phenolic compounds, sulfonated hydroquinones, phenylenediamines, and phenothiazines with rate constants ranging to $10^9 M^{-1}s^{-1}$.

Rate constants for one-electron redox reactions depend upon the relative reduction potentials of the reactants. We have been able to derive the one-electron reduction potential of SO_3^- by measuring the equilibrium constant for its reaction with chlorpromazine (ClP_Z)

$$SO_3^- + ClPz \rightleftharpoons SO_3^{2-} + ClPz^+$$
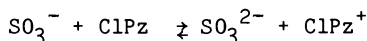
This led to a reduction potential of 0.84V v. NHE at pH 3.6 for the couple SO_3^-/HSO_3^-. The reduction potential of the SO_3^-/SO_3^{2-} couple in basic solution is calculated [using pKa ($HSO_3^- \rightleftharpoons H^+ + SO_3^{2-}$)=7.2] to be 0.63V. This change in potential helps explain why SO_3^{2-} is oxidized by the same oxidant more readily than HSO_3^-.

Using the reduction potential for SO_3^- we can calculate the one-electron reduction potential for SO_4^{2-}. In basic solution, this can be done by subtracting $E(SO_3^-)$=0.63V from twice the two-electron reduction potential for sulfite

$$SO_4^{2-} + H_2O + 2e^- \rightarrow SO_3^{2-} + 2OH^-, E = -0.92V$$

This leads to

$$SO_4^{2-} + H_2O + e^- \rightarrow SO_3^- + 2OH^-, E = -2.47V$$
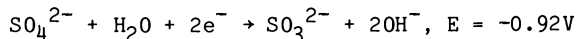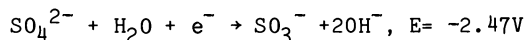
Table II.   Rate constants for Reactions of SO_3^- Radicals with
Various Reactants

Reactant	pH	$k(M^{-1}s^{-1})$	reference
ascorbic acid	<3	$<10^6$	18
ascorbate ion	5-10	9×10^6	18
ascorbate dianion	>12	3×10^8	18
trolox	9	$\sim 10^6$	18
phenol	11.1	6×10^5	13
p-methoxyphenol	9.2	4×10^7	13
p-methoxyphenol	12.4	1.2×10^8	13
hydroquinone	8.9	4.5×10^6	19
hydroquinone	10.5	5.4×10^7	19
hydroquinone	12.9	3.2×10^8	19
p-phenylenediamine	3.4	$<5 \times 10^5$	12
p-phenylenediamine	5.3	4.2×10^6	12
p-phenylenediamine	9.3	5.0×10^7	12
N,N,N',N'-tetramethyl-p-phenylenediamine	4.5	8.2×10^6	12
N,N,N',N'-tetramethyl-p-phenylenediamine	9.5	5.2×10^8	12
chlorpromazine	3.6	$\sim 5 \times 10^6$	13
O_2	6.8	1.5×10^9	13

Although this suggests that SO_3^- can act as a strong reductant,
this calculation possibly seriously overstates its actual reducing
power. This is because the initial product of the electron transfer
would be SO_3, not SO_4^{2-} which results from subsequent hydrolysis.
The enthalpy difference between $SO_3 \cdot_{aq}$ and SO_4^{2-} is not known, but
probably is greater than that between $SO_2 \cdot_{aq}$ and SO_3^{2-} (3.24V) (20).
If this is correct, the one electron potential for the SO_3/SO_3^-
couple would be greater than 0.77 V and SO_3^- would therefore be a
very poor reductant.

Possibly the most important reaction of the sulfite radical in
autoxidation systems is with molecular oxygen. The reaction has
been suggested to lead either to O_2^- or to the peroxy radical SO_5^-

$$SO_3^- + O_2 \rightarrow SO_3 + O_2^-$$

$$SO_3^- + O_2 \rightarrow SO_5^- \quad .$$
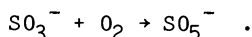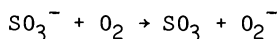
By determining the reactivity of the product radical with ascorbate
(18), we were able to demonstrate that the former reaction is very
unlikely and concluded that the product is the peroxy radical, SO_5^-.

Reactions of the Sulfate Radical

The SO_4^- radical could be produced as discussed below or by the
self-reaction of SO_5^-,

$$2SO_5^- \rightarrow 2SO_4^- + O_2$$

$$\rightarrow S_2O_8^{2-} + O_2$$
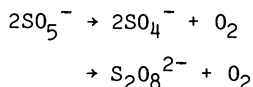
This is a very reactive radical which can abstract H atoms, add to double bonds, or oxidize by electron transfer quite rapidly. A few examples of rate constants for its reactions are given in Table 3; rate constants for over a hundred reactions of SO_4^- are given in a recent compilation (<u>21</u>)

Reactions of the peroxysulfate radical

In Table 3 are listed some rate constants for reactions of SO_5^-, along with some values for SO_3^- and SO_4^- for comparison. The results show that SO_5^- is a stronger oxidant than SO_3^- (but weaker than SO_4^-) and we have estimated its one-electron reduction potential to be about 1.1V at pH 7. Of particular interest is the ability of SO_5^- to oxidize certain substances (aniline and dimethylaniline, for example) which form radicals which are capable of oxidizing sulfite. This can lead to the enhancement of the autoxidation of sulfite through the chain

$$SO_5^- + X \rightarrow SO_5^{2-} + X^+$$

$$X^+ + SO_3^{2-} \rightarrow X + SO_3^- .$$

$$SO_3^- + O_2 \rightarrow SO_5^-$$
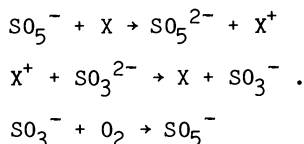
In sulfite autoxidation, an exceedingly important reaction is that of SO_5^- with SO_3^{2-}/HSO_3^-. We have been able to derive a rate constant of 3×10^6 $M^{-1}s^{-1}$ at pH 6.8 (<u>13</u>) for this reaction, but have not been able to establish its mechanism.
   Three paths are possible for this reaction

$$SO_5^- + SO_3^{2-} + H^+ \rightarrow HSO_5^- + SO_3^-$$

$$\rightarrow SO_4^- + SO_4^{2-} + H^+$$

$$\overset{H_2O}{\rightarrow} 2SO_4^{2-} + OH + 2H^+$$
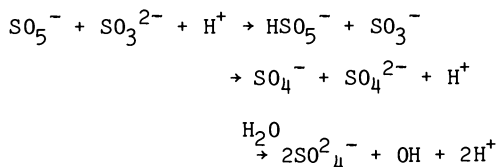
Since both OH and SO_4^- very rapidly oxidize SO_3^{2-} to SO_3^-, these paths are indistinguishable in our experiments, although the extensive rearrangement required makes the final path highly unlikely. The identity of the correct path is quite important since the production of HSO_5^- can lead to possible chain branching steps and the formation of SO_4^- has consequences for the effect of inhibitors on sulfite autoxidation.
   This product of the one-electron reduction of SO_5^- (HSO_5^-, peroxymonosulfate, Caro's acid), is a strong oxidant with a standard two-electron reduction potential of 1.82V (<u>22</u>). A product with the properties of peroxymonosulfate has been observed with a yield of up to 30% upon bubbling oxygen through a solution of sodium sulfite (<u>23</u>). This compound can undergo many possible subsequent reactions.

Table III. Comparison of Some Rate Constants for Reactions of SO_3^-, SO_5^-, and SO_4^- with Organic Compounds (in $M^{-1}s^{-1}$)

Reactant	SO_3^-	SO_5^-	SO_4^-
ascorbic	$<10^6$	2×10^{6a}	*
ascorbate	9×10^6	1.4×10^{8a}	*
trolox	$\sim10^6$	1.2×10^{7a}	*
aniline	(reverse)	3×10^{6b}	*
N,N-dimethylaniline	(reverse)	1×10^{7b}	*
tyrosine	$<10^6$		$\sim3\times10^{9c}$
tryptophan	8×10^4		$\sim2\times10^{9c}$
histidine	NR		$\sim2.5\times10^{9c}$
i-PrOH	$<10^3$		$\sim8\times10^{7c}$
ethanol		$<10^{3d}$	$\sim3\times10^{7c}$
fumarate	$<10^5$		$\sim2\times10^{7c}$
succinate	–	–	7.1×10^{6c}
allyl alcohol	NR		1.5×10^{9c}
glycine	$<10^3$		$\sim9\times10^{6c}$
HSO_3^-	–	3×10^{6e}	$\sim10^{9c}$

(a) Ref. 18
(b) Ref. 12
(c) Ref. 21
(d) Ref. 9
(e) Ref. 13

From the present point of view, the most important would be the
further production of free radicals, most likely upon reaction with
transition metal ions, for example

$$Fe^{2+} + HSO_5^- \rightarrow Fe^{3+} + OH + SO_4^{2-}$$

$$\rightarrow Fe^{3+} + OH^- + SO_4^-$$
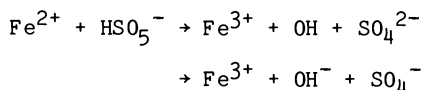
In a mechanism for the iron catalyzed autoxidation of sulfite, this
would be a chain branching step. We have some evidence that the
reaction of Fe^{2+} with HSO_5^-, in acid, does lead to free radicals,
but it is somewhat more complex than written above (24).

Conclusions

It has been apparent for some time that the inhibition of sulfite
autoxidation by organic compounds is due to their reactions with
free radical intermediates. Further, it seems likely that the
chemical effects associated with SO_2 autoxidation are due to these
radicals or, possibly, peroxymonosulfate. Now that the
reactivities of the likely free radical intermediates are known, the
mechanism of these effects can be begun to be understood. For many
organic compounds, like hydroquinone and other phenolic species,
reaction with SO_3^- and SO_5^- is possible. Indeed, they prove to be
the most efficient inhibitors of SO_2 autoxidation and the order of

their efficiency reflects their relative reactivity toward these radicals ($\underline{19}$). For other organic compounds like mannitol or fumarate, only reactions with SO_4^- or OH are likely. In some cases, inhibition by direct reaction with HSO_5^- might be possible.

The results we have obtained on the one-electron oxidation of sulfite and bisulfite by free radicals also are important in understanding possible chain-initiation and chain-carrying steps in SO_2 autoxidation. This is particularly true in systems which do not consist simply of SO_2 and a catalyst. For example, the production and subsequent reaction of halide free radicals could be important in any system containing halogen ions, and subsequent reactions of organic radicals with sulfite will be required to describe completely the effect of organic inhibitors.

Lee and Rochelle ($\underline{25}$) have investigated the effects of various additives on the degradation of carboxylic acids used as buffers in flue gas desulfurization systems, comparing the rates of decarboxylation to sulfite oxidation. It is apparent from Table 3 that, of the SO_x radicals, only SO_4^- is likely to react with aliphatic acids. Further, it has been shown that whereas SO_4^- efficiently decarboxylates these carboxylic acids, OH does not ($\underline{26}$). Therefore, it is apparent that SO_4^- is the active radical for this process. Upon addition of KBr or KI, SO_4^- is converted to the corresponding halide radical, Br_2^- or I_2^-, which will be relatively unreactive toward the carboxylic acids, but can still react with sulfite.

The formation of free radicals can be used as a means of promoting sulfite autoxidation. For example, NO_2 reacts with many compounds by one-electron oxidation ($\underline{16}$)

$$NO_2 + S \rightarrow NO_2^- + S^+$$
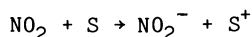
and the resulting free radical is capable of initiating SO_2 autoxidation

$$S^+ + SO_3^{2-} \rightarrow S + SO_3^- \ .$$
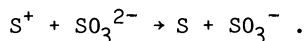
This could be important in some SO_x-NO_x scrubber systems ($\underline{27}$). Further, some organic free radicals are formed easily by reaction with molecular oxygen. Reaction of these radcials with sulfite also can be used to initiate SO_2 autoxidation ($\underline{12}$).

This rich chemistry associated with SO_2 autoxidation might also have consequences for the environmental effects of SO_2 emission. If, for example, SO_2 undergoes autoxidation on a wet leaf, the result might include not only acidification, but also the generation of highly reactive species, which should be considered when assessing the cause of such phenomena as forest dieback ($\underline{28}$).

Although the study of SO_2 autoxidation is over 100 years old, the direct study of the reactive intermediates is just beginning. In real-world systems, ranging from atmospheric droplets to flue-gas scrubbers, reactions take place over a wide range of pH, temperature, and ionic strength. Computer modeling incorporating the free radical chemistry of SO_2 autoxidation needs to be applied to these systems to identify gaps in our knowledge and determine which reactions deserve further study. These models should provide

a better understanding of all elements of the SO_2 problem, ranging from the behavior of flue-gas scrubbers to the effects of SO_2 in the environment.

Literature Cited

1. Titoff, A. Z. Phys. Chem. (Liepzig) 1903, 45, 641.
2. Mathews, J. H.; Weeks, M. E. J. Am. Chem. Soc. 1917, 39, 635.
3. For a discussion of some of this early work, see, Jorissen, W. P. "Induced Oxidation", Elsevier, Amsterdam, 1959.
4. Kharasch, M. S.; May, E. M.; Mayo, F. R., J. Org. Chem. 1938, 3, 175.
5. Bigelow, S. L., Z. Phys. Chem. 1898, 28, 493.
6. Westley, F., National Bureau of Standards Special Publication 630, 1982.
7. Huie, R. E.; Peterson, N. C. In "Trace Atmospheric Constituents", S. E. Schwartz, ed.; Wiley, New York, 1983; Chapter 2.
8. Hoffmann, M. R.; Boyce, S. D. In "Trace Atmospheric Constituents", S. E. Schwartz, ed.; Wiley, New York, 1983; Chapter 3.
9. Hayon, E.; Treinin, A.; Wilf, J. J. Am. Chem. Soc. 1972, 94, 47.
10. Adams, G. E.; Boag, J. W. Proc. Chem. Soc. 1964, 112.
11. Hasegawa, K; Neta, P. J. Phys. Chem. 1978, 82, 854.
12. Neta, P.; Huie, R. E. J. Phys. Chem. 1985, 89, 1783.
13. Huie, R. E.; Neta, P. J. Phys. Chem. 1984, 88, 5665.
14. Huie, R. E.; Neta, P. Unpublished result.
15. Siskos, P. A.; Peterson, N. C.; Huie, R. E. Inorg. Chem. 1984, 23, 1134.
16. Huie, R. E.; Neta, P. J. Phys. Chem. 1986, 90, 1193.
17. Ellison, T. K.; Eckert, C. A. J. Phys. Chem., 1984, 88, 2335.
18. Huie, R. E.; Neta, P. Chem. Biol. Interact., 1985, 53, 233.
19. Huie, R. E.; Neta, P. J. Phys. Chem., 1985, 89, 3918.
20. Wagman, D. D.; Evans, W. H.; Parker, V. B.; Halow, I.; Bailey, S. M.; Schumm, R. H. NBS Tech. Note 270-3, 1968.
21. Ross, A. B; Neta, P., NSRDS-NBS-65, 1979.
22. Steele, W. V., Appelman, E. H. J. Chem. Thermodynamics 1982, 14, 337.
23. Deuvyst, E. A.; Ettel, V. A.; Mosolu, M. A. CHEMTECH, 1979, 426.
24. Peterson, N. L; Ouellette, P. A; Huie, R. E. Unpublished work.
25. Lee, J. Y.; Rochelle, G. T. In "Environmental Concerns in Fossil Fuel Utilization," ACS Symposium Series, this volume.
26. Madhavan, V.; Levanon, H.; Neta, P., Rad. Res., 1978, 76, 15.
27. Chang, S. G.; Littlejohn, D. In "Environmental Concerns in Fossil Fuel Utilization", ACS Symposium, this volume.
28. Smith, W. H. In "Environmental Concerns in Fossil Fuel Utilization," ACS Symposium this volume.

Variability of Compositions of Particles Released by Coal-Fired Power Plants

Glen E. Gordon and Ann E. Sheffield

Department of Chemistry, The University of Maryland, College Park, MD 20742

Particulate emissions data for 21 studies of coal-fired power plants were compiled for use in receptor models. Enrichment factors were calculated (relative to Al) with respect to the earth's crust (EF_{crust}) and to the input coal (EF_{coal}). Enrichment factors for input coals relative to crustal material were also calculated. Enrichment factors for some elements that are most useful as tracers of coal emissions (e.g., As, Se) vary by more than ten-fold. The variability can be reduced by considering only the types of plants used in a given area, e.g., plants with electrostatic precipitators (ESPs) burning bituminous coal. For many elements (e.g., S, Se, As, V), EF_{crust} values are higher for plants with scrubbers than for plants with ESPs. For most lithophiles, EF_{crust} values are similar for the coarse (>2.5 μm) and fine (<2.5 μm) particle fractions. Many volatile elements (e.g., Cl, V, Ni, Cu, Zn, As, Br, Sb) are more enriched in the fine than in the coarse fractions. The few data available show similar trends for EF_{coal} values, which are comparable for plants burning eastern and western U.S. coal.

Accurate knowledge of compositions of particles released by pollution sources is required by receptor modelers, e.g., for Chemical Mass Balances (CMBs). To improve model calculations, we have developed a source-composition library of data from journals, reports, and unpublished work. The library makes the data readily available and also helps to identify what new data are most needed. The library includes data for 21 studies of coal-fired plants. These data were used to investigate effects of coal type, pollution control device, and particle size on plant emissions.

Table I summarizes the locations, capacities, and pollution-control devices of the coal-fired plants included in the library. In the library each data set includes a brief text giving details of the plant's characteristics, the sampling method and date, the analytical techniques used, and any other useful details.

Table I. Coal-Fired Power Plant Studies in
Source-Composition Library

Plant	Location	Poll. Control Device	Capacity (MW)	Study Type[a]
Allen (1)	Tennessee	ESP[b]	290X3	IS
Chalk Point (2)	Maryland	ESP	355X2	IS
ORV(A)[c] (3)	Ohio Valley	ESP	560	IS
ORV(B)[c] (3)	Ohio Valley	ESP	125	IS
ORV(C)[c] (3)	Ohio Valley	ESP	163	IS
ORV(D)[c] (3)	Ohio Valley	Scrubber	411	IS
ORV(E)[c] (3)	Ohio Valley	Scrubber	156	IS
Eddystone (4)	Pennsylvania	ESP	300	DSS
Dickerson (5)	Maryland	ESP	185X3	PL,IS
Mt. Tom (6)	Connecticut	ESP	155	IS
Beckjord (7)	Ohio	ESP	125	IS
Bridger (7)	Wyoming	ESP	475	IS
Johnston (7)	Wyoming	ESP	110	IS
Coles[c] (8)	Southwest	ESP	-	IS
Radian(1)[c] (9)	Wyoming coal	Scrubber	330	IS
Radian(2)[c] (9)	Wyoming coal	ESP	350	IS
Radian(3)[c] (9)	N. Dakota lignite	Cyclone	250	IS
Valmont (10)	Colorado	ESP Scrubber	180	IS
Wangen[c] (11)	New Mexico	ESP	800X2	PL
Davison[c] (12)	Indiana coal	Cyclone	-	IS

[a]IS = in-stack; DSS = dilution stack sampler; PL = plume study
[b]ESP = Electrostatic Precipitator
[c]Name of plant not identified in original reference, so we
have identified by investigator or general area.

Methods: Data Treatment

Some studies included data for different particle size fractions.
For these studies, we entered separately the compositions of "fine",
"coarse", and "total" particles. "Fine" particles are defined as
those of diam <2.5 μm, the cut-point of most dichotomous samplers.
"Coarse" particles are those with diameters between 2.5 μm and the
maximum collected (usually 15-20 μm). Many of the data were taken
with different size cuts, so it was necessary to group the data in
different ways and interpolate around the 2.5-μm region. "Total"
particles are either those collected without size segregation, or
else the sum of the collected size fractions weighted by the
relative mass loadings of each.
    Most recent data sets are accompanied by either estimates of
errors of the measurements or observed sample-to-sample fluctuations
which were entered into the library, as modern CMB programs (e.g.,
13) use uncertainties of the source compositions and in ambient
samples in weighted least-squares fitting procedures. Many older
data sets do not include estimates of analytical errors or fluctua-
tions of particle composition, so we attached estimates based on the

analytical methods used and other information given in the
original reports. We have tried to exclude fluctuations arising
from variations of mass loading of the stacks or errors in the
volume sampled. To avoid errors of an absolute nature in
comparing composition patterns from several coal-fired power
plants, we normalized concentrations of all elements to that of
Al. However, we retained available mass information by entering a
value for mass relative to Al.

We also calculated "enrichment factors" to simplify compari-
sons between different plants. About half of the particulate
matter in the atmosphere is suspended soil, so we have used
enrichment factors with respect to the earth's crust to help
identify potential coal tracer elements:

$$EF_{crust} = (X/Al)_{spl}/(X/Al)_{crust} \qquad (1)$$

where X and Al are the concentration of an element X and of Al in
a sample and in Wedepohl's crustal abundances (14), respectively.

As discussed below, some elements are highly enriched,
relative to the crust, on airborne particles from coal-fired
plants. In part, the compositions of the emitted particles are
determined by the compositions of the input coal and, in part, by
fractionation during the combustion process and subsequent passage
of stack gases and particles through pollution-control devices.
Some variability also arises from condensation of volatile species
as they leave the stack. Results of the very few studies
performed via dilution or plume sampling are not dramatically
different from those of in-stack measurements, suggesting that
this effect is not large; however, many more studies of particles
after release are needed to clarify this issue. In order to make a
crude separation of the two major effects, i.e., coal composition
and in-plant fractionation, we also calculate enrichment factors
of the coals themselves with respect to the crust, EF_{crust} (coal),
using Equation 1 with (X/Al) values for coal in the numerator, and
enrichment factors of the emitted particles with respect to the
input coal:

$$EF_{coal} = (X/Al)_{spl}/(X/Al)_{coal} \qquad (2)$$

where $(X/Al)_{coal}$ is the ratio of concentrations in the coal. For
a particular plant, the various enrichment factors for a given
element are related by:

$$EF_{crust} = EF_{crust}(coal) \cdot EF_{coal} \qquad (3)$$

Results

Before discussing the emitted particles, let us consider the
compositions of the coals themselves. Figures 1 and 2 show
enrichment factors for eastern and western coals relative to the
earth's crust, EF_{crust}(coal), respectively. Soluble elements such
as the alkali metals and Mn are depleted in coal, and apparently
are leached from it during its formation. Sodium, Ca, and Mn are
more depleted in eastern than in western coals, whereas K, Rb, and
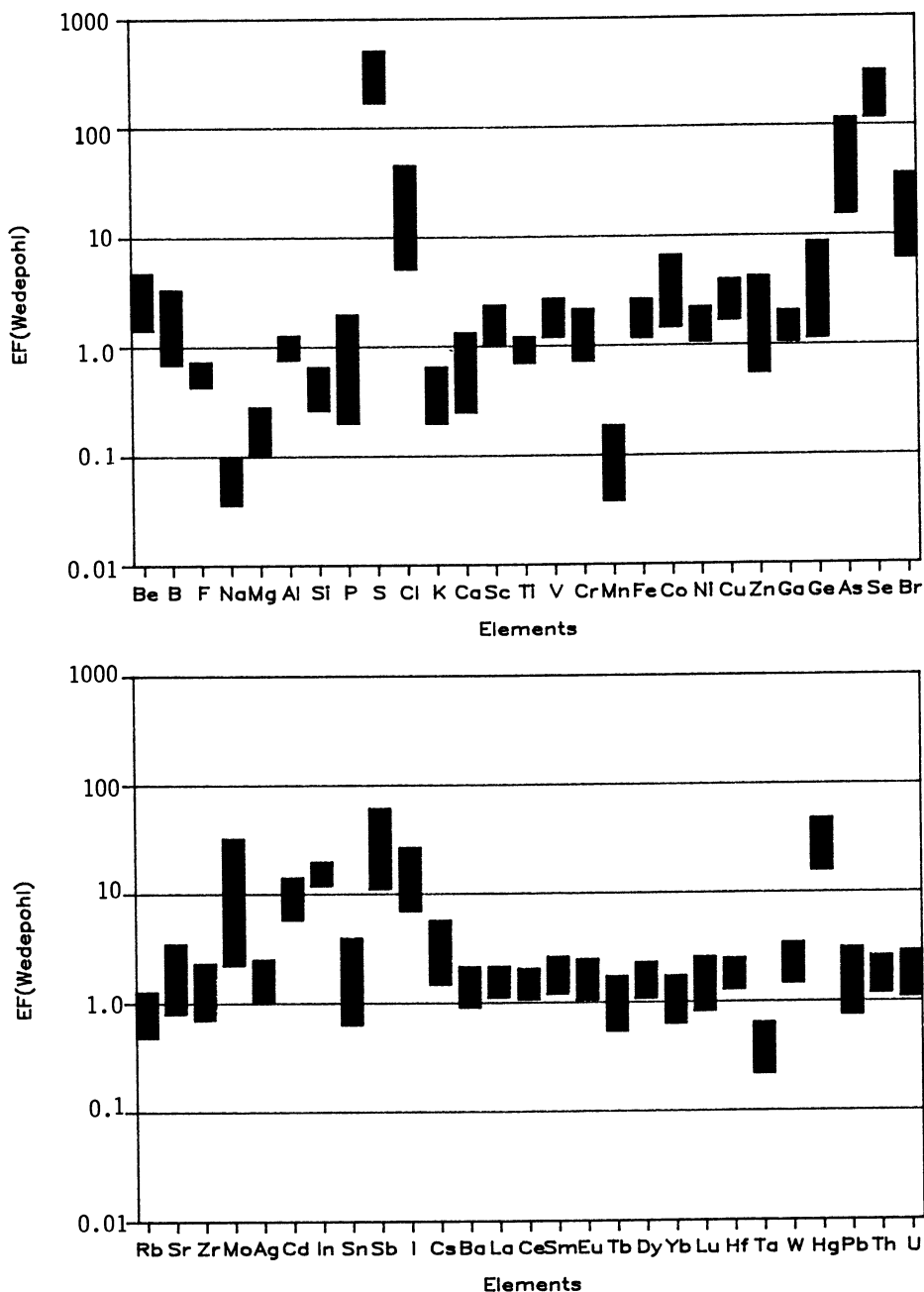
Figure 1.   Enrichment factors with respect to the earth's crust
(14) for coals from the eastern United States.   Based on coal com-
positions determined by the Illinois State Geological Survey (15).
Range shown for each element is from x_g/σ_g to $x_g \cdot \sigma_g$, where x_g and
σ_g are geometric means and standard deviations.
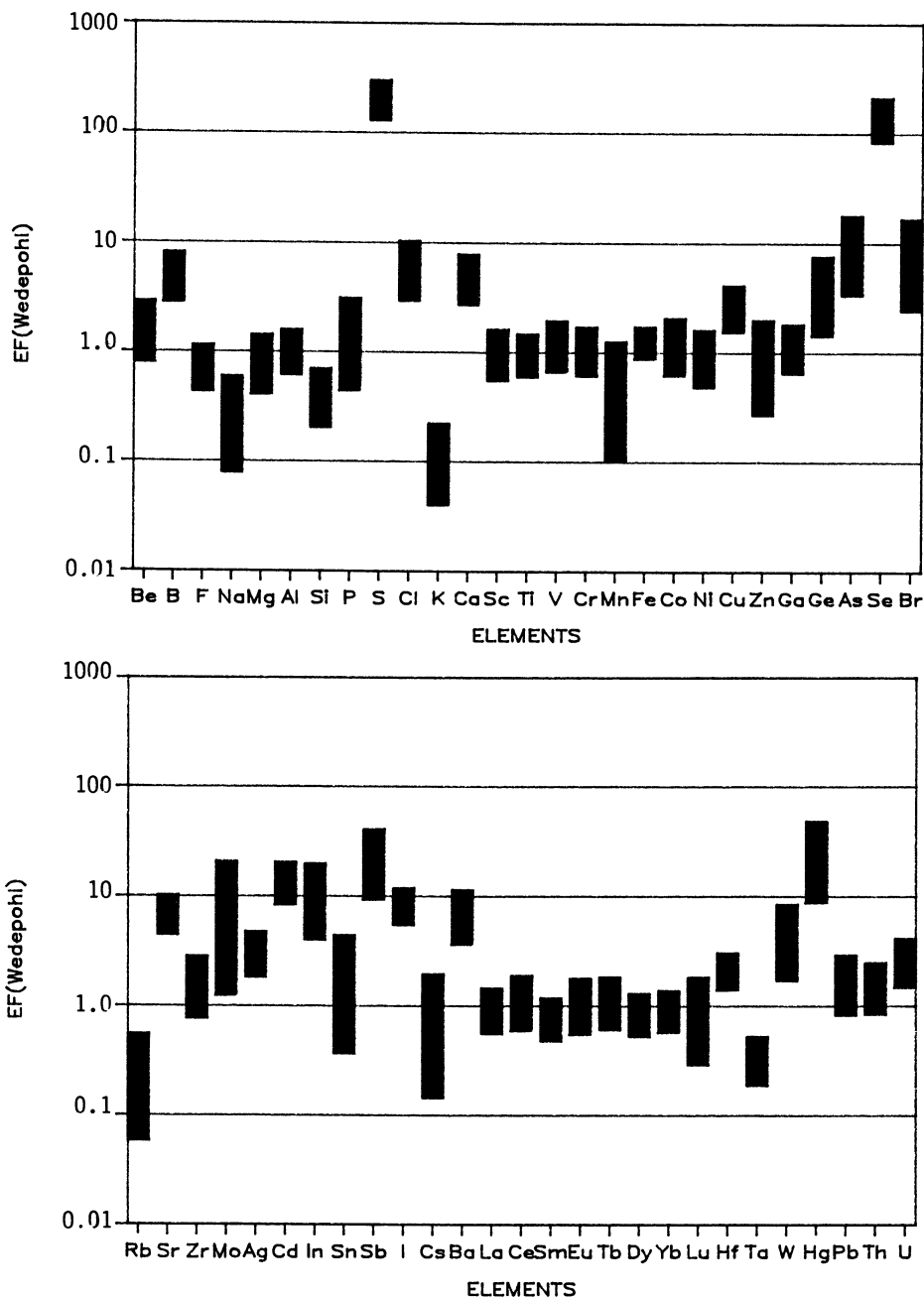
Figure 2. Enrichment factors with respect to the earth's crust (14) for coals from the western United States. Based on coal compositions determined by the Illinois State Geological Survey (15). Range shown for each element is from x_g/σ_g to $x_g \cdot \sigma_g$, where x_g and σ_g are geometric means and standard deviations.

Cs are more depleted in western coals. Silicon is also depleted in coal, probably because of the presence of clay minerals. Most lithophile elements (i.e., those normally associated with the earth's crust) have EF values near one, but it is interesting that the rare earth elements show slightly, but consistently higher enrichments in eastern coal. The apparent depletion of Ta is probably not real, but an artifact resulting from Wedepohl's use of too large a crustal abundance for it (14).

Most chalcophile elements (i.e, S and other elements with an affinity for S in nature such as Cu, As, Se, Cd, In, and W), boron, and the halogens are enriched in coal with respect to soil, and this accounts in part for their enrichment in emitted particles. Differences between eastern and western coals are apparent for many elements, especially the alkali and alkaline earth metals, As, and In. This accounts for some of the large plant-to-plant variability that we observe below.

Enrichment factors for stack emissions relative to the earth's crust are shown in Figure 3 for 56 elements. Averages are based on all available data from the 21 studies. An EF_{crust} of about 1 indicates that an element is at about the same relative concentration in coal-fired plant emissions as in soil. An EF_{crust} of less than 1 indicates that an element is depleted relative to soil, while a value greater than one indicates an enrichment of the element in coal-fired plant emissions. Elements such as Na, K, Si, Ca, Rb and Mn are depleted relative to the crust because of depletion in the input coals. Most lithophiles, e.g., Sc, Ti, Fe, and rare earths, have EFs of about 1.

Many chalcophile elements such as S, As, Se, Cu, Sb, Mo, Ni, Zn, Ag, Cd, In, W, and Pb are enriched with respect to crustal material, as are boron and the halogens F, Br, and I, in part because of enrichment in coals. Note that the errors for many of these elements are distressingly large. The important elements S, As, and Se have relative errors of over 100%. These large fluctuations are due in part to the inclusion in the averages of all plants regardless of coal type, pollution-control device or sampling method. The larger errors for Br, I and, especially, Hg are probably due to the high volatility of these elements. Their concentrations on particles depend on their particle/vapor-phase phase distributions and are therefore, highly sensitive to temperature and sampling conditions.

To remove the effect of coal type on emissions, EF_{crust} values are compared to EF_{coal} values for 22 elements in Table II. For lithophiles such as Sc, V, Cs, Fe and Hf, whose EF_{crust} values are near one, the EF_{coal} values are also near one, but generally have somewhat smaller fluctuations. Sodium and Mn, which are depleted with respect to soil, have EF_{coal} values of about 1, as is expected from the depletion of these elements in coal. Many enriched elements, such as S, Co, Zn, As, Se, Mo, Cd, Sb, I, W and Pb, are much less enriched with respect to coal than to soil because of the considerable enrichment of these elements in the coal itself relative to crustal material. However, most of these, especially S, As, Se, Mo and Cd, are still more enriched in plant emissions than in coal, so a knowledge of coal composition does not suffice to explain their behavior in stack emissions.

Table II. Enrichment Factors with Respect to the Earth's Crust
and to Input Coal for All Plants and for Eastern
Plants with ESPs. Geometric Ranges are given for
22 Selected Elements on Total Particles.

Element	All Plants				Eastern Plants with ESPs	
	EF_{crust}	n	EF_{coal}	n	EF_{crust}	n
Na	0.04-0.34	15	0.7-1.5	8	0.03-0.15	9
Si	0.36-0.52	8	-		0.32-0.49	4
S	7.4-6800	11	9.4-263	3	5.4-15	4
Sc	0.80-3.1	7	1.1-1.8	5	1.3-3.4	5
V	1.3-10	15	1.2-5.6	8	1.5-5.5	8
Cr	1.5-14	19	0.8-10	11	1.3-5.8	9
Mn	0.18-0.92	19	1.0-2.1	11	0.14-0.47	9
Fe	0.50-2.2	21	0.6-1.4	13	0.5-2.2	9
Co	1.9-4.7	14	0.8-3.6	11	2.6-4.6	6
Ni	1.3-10	16	0.8-10	9	1.6-3.8	7
Zn	2.7-26	20	2.3-11	12	2.0-25	8
As	20-390	18	0.5-19	8	65-270	8
Se	200-7000	18	3.3-15	9	350-1380	8
Br	3.9-175	6	0.2-2.8	2	1.8-92	3
Mo	17-350	9	2.7-36	6	25-43[a]	1
Cd	24-490	5	2.1-33	4	210-840[a]	1
Sb	34-140	12	2.7-7.4	8	52-250	4
I	27-1300	3	1.8-4.5	2	410-770	2
Hf	0.91-3.5	6	0.8-1.5	4	0.9-1.6	4
W	3.3-4.8	4	1.6-2.7	2	4.0-4.1	2
Pb	3.0-31	19	1.0-1.8	9	1.6-24	8
U	1.0-7.0	5	0.8-3.7	4	-	

[a]Only 1 value available - analytical range given.

Many elements with high EF_{coal} values are moderately volatile and, hence, expected to be enriched during combustion. According to the models of Natusch and coworkers (12,16) and Smith (17,18), volatile elements are vaporized during combustion and condense on particle surfaces. As fine particles have a larger surface area per unit mass than do coarser particles, and as pollution-control devices generally remove large particles more efficiently than smaller ones (19), there is a net enrichment of more volatile elements in the stack emissions.

A comparison of fine and coarse particle compositions supports this hypothesis. Figure 4 shows EF_{crust} values for fine and coarse particles from six eastern-coal-burning plants equipped with ESPs. (We wanted to emphasize size-fraction differences without the additional effects of coal type and pollution control device.) For
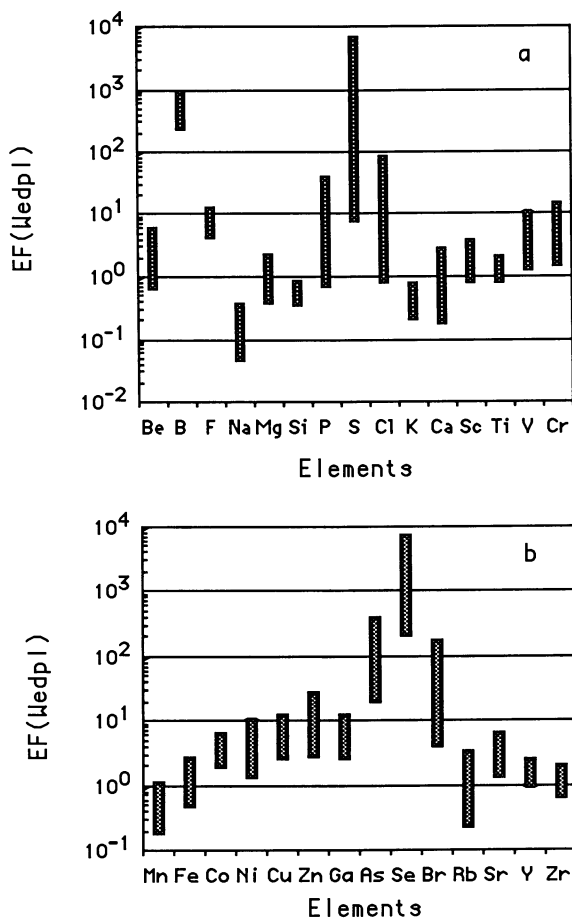
Figure 3. Enrichment factors with respect to the earth's crust (14) for total particles based on results from 21 studies. Range shown for each element is from x_g/σ_g to $x_g \cdot \sigma_g$, where x_g and σ_g are geometric means and standard deviations. (a) Be-Cr; (b) Mn-Zn.
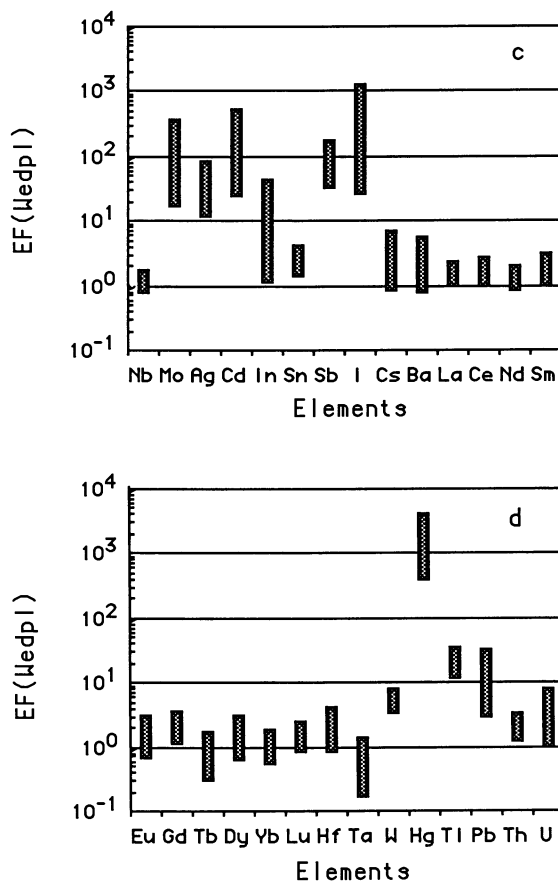
Figure 3. Continued. Enrichment factors with respect to the earth's crust (14) for total particles based on results from 21 studies. Range shown for each element is from x_g/σ_g to $x_g \cdot \sigma_g$, where x_g and σ_g are geometric means and standard deviations. (c) Nb-Sm; (d) Eu-U.
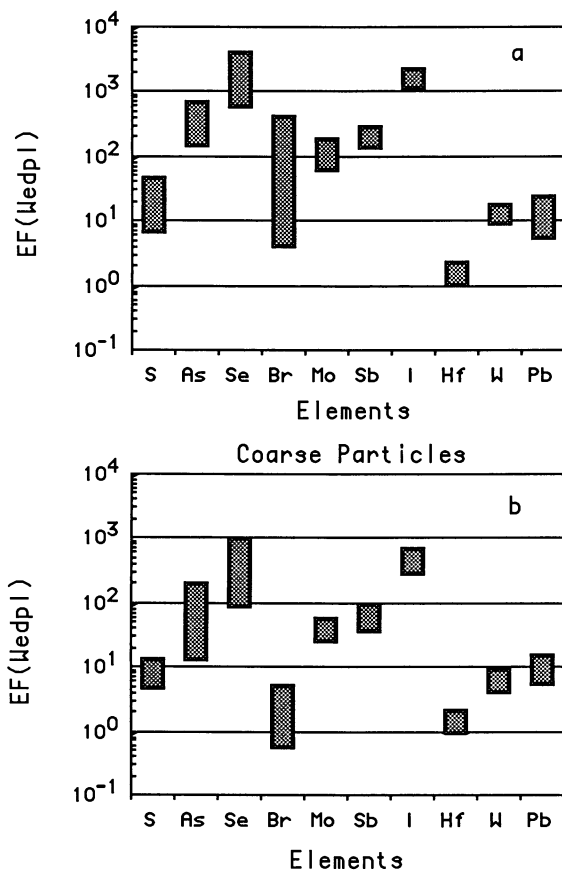
Figure 4. Enrichment factors for fine and coarse particles from eastern U.S. plants equipped with ESPs. Plants included are ORV(A), (B), and (C); Chalk Point; and Eddystone for coarse particles, and the same plants plus Dickerson for coarse particles. Note that the y-scale is logarithmic for the more enriched elements. Range shown for each element is from x_g/σ_g to $x_g \cdot \sigma_g$, where x_g and σ_g are geometric means and standard deviations.
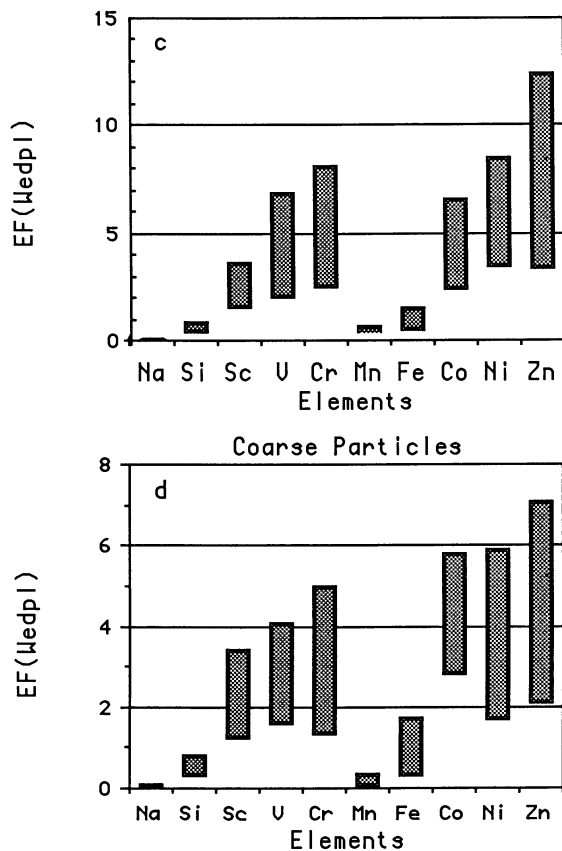
Figure 4. <u>Continued.</u> Enrichment factors for fine and coarse
particles from eastern U.S. plants equipped with ESPs.

depleted elements, e.g. Na and Mn, and for those, such as Si, Sc, V, Fe and Hf, with EFs near unity, little or no difference between the fine and coarse fractions is generally seen. Some slightly enriched elements (Cr, Co, Zn) also show little size fractionation, but most enriched elements are more highly enriched in the fine than in the coarse fraction, as expected. The difference is most pronounced for the most highly enriched elements: S, As, Se, Mo, Sb, I, and Pb. These are from 2 to 9 times more enriched in fine than in coarse particles. Use of fine-fraction samples in receptor modeling should, therefore, increase the resolving power of these elements as tracers. In particular, As, a good potential coal tracer, is 4 times more abundant in fine than in coarse particles for eastern plants with ESPs. Other potential tracers are Se and I, but both are volatile enough to have significant gas-phase concentrations (20,21).

We now further examine the effects of coal type and pollution control device on plant emissions. Table III gives individual values from each of 18 studies for the important elements S, As, and Se. As expected from the results in Table II, coal type has some effect on emissions of these elements, but the presence of a scrubber vs. an electrostatic precipitator (ESP) has a far greater influence. Except for the anomalous Radian(2) plant, and despite some overlap between the two groups, scrubber-equipped plants generally emit far more As, Se and, especially, S than do plants with ESPs. The total particulate mass emitted by plants with scrubbers (≈ 25 mg/m^3; sulfate ≈ 4 mg/m^3) is comparable to that emitted by plants with ESPs (≈ 47 mg/m^3; sulfate ≈ 0.5 mg/m^3), so scrubber-equipped plants release much more primary sulfate than do plants with ESPs. Scrubbers are designed to remove gas-phase SO$_2$. They accomplish this partly by converting SO$_2$ to sulfate droplets or particles, some of which escape from the plant.

If only plants using the same type of pollution-control device and burning the same type of coal are considered, fluctuations in the compositions of emitted particles are considerably reduced. The final column in Table II shows EF$_{crust}$ values for eastern plants with ESPs. For most elements, especially the highly enriched ones, the fluctuations are much smaller than for the 21-study group which lumps all plants together.

Conclusions

Using a source-composition library containing data from 21 studies of coal-fired power plants, we have investigated the effects of particle size, coal type, and pollution control device on the composition of particles emitted from coal-fired power plants.

Because of the nature of the enrichment process during combustion, potential tracer elements such as As, Se, and I are more enriched on fine than on coarse particles. Therefore, analyzing the fine particle fraction of source emissions and ambient aerosols increases the source-discriminating power of receptor models.

Both the type of coal burned and the emission control device used affect the composition of emitted particles. If plants appropriate to the area under study (e.g., plants burning eastern

Table III. Comparison of As, Se, and S Concentrations (Relative to Al = 1.0) among Individual Plants.

Plant	S	As($\times 10^3$)	Se($\times 10^3$)
Plants with ESPs:			
Eastern Coal			
Allen	NR[a]	5.8 ± 0.5	1.16 ± 0.08
Chalk Point	NR	10 ± 3	1.6 ± 0.4
ORV(A)	0.023 ± 0.006	2.1 ± 0.4	0.42 ± 0.08
ORV(B)	0.041 ± 0.026	2.3 ± 2.2	0.76 ± 0.90
ORV(C)	0.025 ± 0.010	1.1 ± 0.4	0.30 ± 0.12
Eddystone	0.068 ± 0.010	1.7 ± 0.5	0.40 ± 0.07
Dickerson	NR	3.4 ± 3.2	1.5 ± 0.6
Mt. Tom	NR	2.4 ± 1.3	1.6 ± 0.9
Western Coal			
Coles	0.025 ± 0.004	0.46 ± 0.06	0.55 ± 0.03
Radian (2)	76 ± 11	0.024 ± 0.003	4.0 ± 0.6
Valmont (ESP)	NR	1.6 ± 0.4	0.67 ± 0.24
Wangen	NR	0.36 ± 0.08	0.59 ± 0.57
Plants with Scrubbers:			
Eastern Coal			
ORV(D)	37 ± 14	18 ± 9	340 ± 170
ORV(E)	3.0 ± 2.3	5.8 ± 2.8	15 ± 19
Western Coal			
Radian (1)	72 ± 10	1.3 ± 0.2	1.0 ± 0.1
Valmont (scrubber)	NR	3.8 ± 0.9	6.0 ± 1.1
Plants with Cyclones:			
Eastern Coal			
Davison	0.91 ± 0.19	5.9 ± 1.7	0.14 ± 0.04
Western Coal			
Radian (3)	12 ± 2	1.6 ± 0.2	0.49 ± 0.07

[a]NR = not reported in reference.

U.S. coal and equipped with ESPs for the northeastern U.S.) are selected, the variability of the emitted particle composition is reduced substantially. As an example of component constructed using these principles and data in the library, we give in Table IV the fine-particle component for eastern U.S. plants with ESPs. Here we have used arithmetic means and standard deviations, as that is the form in which components are normally entered into CMB calculations (13). A better representation of the particles as received at ambient sampling sites could, in principle, be obtained

Table IV. Receptor-Modeling Component for Fine Particles
           from Eastern Plants with ESPs.

Element	n	Conc.[a]	Element	n	Conc.
Be[b]	1	$(1.7 \pm 0.3) \times 10^{-4}$	Zr	2	$(3.4 \pm 1.9) \times 10^{-3}$
Na	6	0.019 ± 0.003	Mo[b]	1	$(1.2 \pm 0.5) \times 10^{-3}$
Mg	4	$0.14 + 0.06$	In	2	$(5.0 \pm 0.2) \times 10^{-6}$
Si	4	1.68 ± 0.09	Sb	2	$(3.9 \pm 0.5) \times 10^{-4}$
P[b]	1	0.047 ± 0.007	I	2	$(7.6 \pm 0.3) \times 10^{-3}$
S	4	0.10 ± 0.11	Cs	2	$(7.5 \pm 1.5) \times 10^{-5}$
Cl	3	0.024 ± 0.030	Ba	3	0.018 ± 0.008
K	5	0.10 ± 0.010	La	3	$(7.2 \pm 1.1) \times 10^{-4}$
Ca	6	0.073 ± 0.020	Ce	3	$(1.3 \pm 0.4) \times 10^{-3}$
Sc	3	$(3.2 \pm 0.6) \times 10^{-4}$	Nd[b]	1	$(5.5 \pm 1.9) \times 10^{-4}$
Ti	6	0.066 ± 0.008	Sm	3	$(1.4 \pm 0.2) \times 10^{-4}$
V	6	$(4.1 \pm 1.5) \times 10^{-3}$	Eu	3	$(3.2 \pm 0.4) \times 10^{-5}$
Cr	6	$(3.6 \pm 1.6) \times 10^{-3}$	Tb[b]	1	$(2.5 \pm 0.4) \times 10^{-5}$
Mn	6	$(3.0 \pm 1.0) \times 10^{-3}$	Yb	3	$(5.7 \pm 1.5) \times 10^{-5}$
Fe	6	0.34 ± 0.16	Lu	2	$(1.1 \pm 0.5) \times 10^{-5}$
Co	3	$(5.0 \pm 1.4) \times 10^{-4}$	Hf	3	$(4.5 \pm 0.8) \times 10^{-5}$
Ni	5	$(2.4 \pm 0.5) \times 10^{-3}$	Ta	2	$(1.2 \pm 0.3) \times 10^{-5}$
Cu	5	$(2.5 \pm 0.07) \times 10^{-3}$	W	2	$(1.5 \pm 0.1) \times 10^{-4}$
Zn	6	$(4.7 \pm 2.6) \times 10^{-3}$	Pb	4	$(2.2 \pm 1.2) \times 10^{-3}$
Ga[b]	1	$(1.1 \pm 0.3) \times 10^{-3}$	Th	3	$(1.9 \pm 0.2) \times 10^{-4}$
As	6	$(7.6 \pm 6.5) \times 10^{-3}$	Mass	4	9.5 ± 2.1
Se	6	$(2.3 \pm 2.3) \times 10^{-3}$			
Br	3	0.007 ± 0.012			
Rb	2	$(1.2 \pm 0.1) \times 10^{-3}$			
Sr	3	$(7.4 \pm 2.0) \times 10^{-3}$			

[a] Concentrations relative to $Al = 1$; arithmetic means and standard deviations reported unless otherwise noted.
[b] Only 1 value reported. Value is reported as concentration with analytical error.

by confining the average to data obtained by dilution or plume
sampling; however, there are presently so few data of these types
available that the need for statistics was more important than the
insistence on studies of a particular type. This type of component,
constructed only from fine particle measurements, is ideal for CMBs
of particles transported over long distances, but would not be
appropriate for local studies in which particles are collected
without size segregation because of the size dependence of enrich-
ment.
        By analyzing and presenting data in fundamental terms involv-
ing the use of EF values, we have attempted to provide users of
the data with quantities of more universal value than raw stack
concentrations. In this regard, we should note that it would help
one separate the effects of of coal composition and in-plant
fractionation if more investigators would analyze samples of

input coal (and, possibly, ash fractions) when they analyze released particles.

If one is performing CMBs of an area in which particulate emissions from coal combustion are dominated by those from one to several plants, it is obviously desirable to use a coal component based on measurements of compositions of the particles released by those specific plants, preferably particles collected in their plumes. However, as those data are rarely available, we have placed data from as many multielement studies as possible in the library so the user can construct a component from results of the most appropriate studies that have been done.

In publishing these results from the library, we do not imply that adequate data are now available. The data are better than in a similar, earlier paper from this group (22), but still far from adequate. Many more studies are needed to determine the compositions of particles of various sizes released by plants of different types having differing types of coal and equipped with various types of pollution-control devices. A very large area of uncertainty is the question of what fractions of various elements remain in the gas phase after release into ambient air. The only obvious way in which to answer these questions is by analysis of particles and gases collected at various distances downwind in plumes. We cannot know if dilution samples adequately simulate effects in the plume until results from dilution sampling are compared directly with those of plume measurements. Also, very little data are available on the typical time variability of the compositions of particles from typical plants. Such data, on time scales ranging from hours to years, are needed. In lieu of such detailed results, we have assembled the best data presently available, limited though they are.

Literature Cited

1. Klein, D. H.; Andren, A. W.; Carter, J. A.; Emery, J. F.; Feldman, C., Fulkerson, W., Lyon, W. S., Ogle, J. C., Talmi, Y., Van Hook, R. I.; Bolton N. E. Environ. Sci. Technol. 1975, 9, 973-9.
2. Gladney, E. S.; Small, J. A.; Gordon, G. E; Zoller, W. H. Atmos. Environ. 1976, 10, 1071-77.
3. Baker, G.; Clarke, P.; Gerstle, R.; Mason, W.; Phillips, M., "Emission Characteristics of Major Fossil Fuel Power Plants in the Ohio River Valley," Knapp, K. T., Project Officer; EPA Contract No. 68-02-3271, U. S. Environmental Protection Agency, Research Triangle Park, NC, 1984.
4. Houck, J. E.; Pritchett, L. C.; Cooper, J. A.; Olmez, I.; Sheffield, A. E.; Gordon, G. E.; Dzubay, T. G.; Bennett, R. L. "Elemental Profiles of Selected Sources in Philadelphia for Receptor Modeling Applications", in preparation.
5. Small, J. A. Ph.D. Thesis, University of Maryland, College Park, 1976.
6. Kowalczyk, G. S., "Emission and Atmospheric Impact of Trace Elements from a Reconverted Coal-Fired Power Plant," Preprint for 77th Annual Meeting of the Air Pollution Control Association, San Francisco, CA, June 24-29, 1984.

7. Que Hee, S. S.; Finelli, V. N.; Fricke, F. L.; Wolmik, K. A.
    Int. J. Environ. Anal. Chem. 1982, 13, 1-18.
8. Coles, D. G.; Ragaini, R. C., Ondov, J. M.; Fisher, G. L.,
    Silberman, D.; Prentice, B. A. Environ. Sci. Technol. 1979, 13,
    455-9.
9. "Coal Fired Power Plant Trace Element Study," Vols. II-IV,
    prepared for U. S. Environmental Protection Agency by Radian
    Corp., Austin, TX, 1975.
10. Kaakinen, J. W.; Jorden, R. M.; Lawasani, M. H; West, R. E.;
    Environ. Sci. Technol. 1975, 9, 862-9.
11. Wangen, L. E. Environ. Sci. Technol. 1981, 15, 1080-88.
12. Davison, R. L.; Natusch, D. F. S.; Wallace, J. R.; Evans, C.
    A., Jr. Environ. Sci. Technol. 1974, 8, 1107-13.
13. Watson, J. G., Jr. Ph.D. Thesis, Oregon Graduate Center,
    Beaverton, 1979.
14. Wedepohl, K. H., In "Origin and Distribution of the Elements";
    Ahrens, L. H., Ed.; Pergamon Press: London, 1968; pp. 999-
    1016.
15. Gluskoter, J. J.; Ruch, R. R.; Miller, W. G.; Cahill, R. A.;
    Dreher, G. B.; Kuhn, J. R.; "Trace Elements in Coal:
    Occurrence and Distribution" Ill. Geological Survey Circular
    No. 499, 1977.
16. Natusch, D. F. S.; Wallace, J. R.; Evans, C. A. Science, 1974,
    183, 202-4.
17. Smith, R. D. Prog. Energ. Combust. Sci. 1980, 6, 53-119.
18. Smith, R. D.; Campbell, J. A.; Nielson, K. K. Atmos. Environ.
    1979, 13, 607-17.
19. "Controlling Airborne Particles," National Academy of
    Sciences, 1980.
20. Andren, A. W.; Klein, D. H.; Talmi, Y. Environ. Sci. Technol.
    1975, 9, 856-8.
21. Germani, M. S. Ph.D. Thesis, University of Maryland,
    College Park, 1980.
22. Gordon, G. E.; Zoller, W. H.; Kowalczyk, G. S.; Rheingrover,
    S. W., In Atmospheric Aerosol: Source/Air Quality Relation-
    ships, Macias, E. S.; Hopke, P. K., eds., ACS Symp. Ser. #167,
    1981, pp. 51-74.

Cascade Impactors in the Chemical and Physical Characterization of Coal-Combustion Aerosol Particles

John M. Ondov

Department of Chemistry, The University of Maryland, College Park, MD 20742

Aerosol particles from combustion of pulverized coal are
typically distributed bimodally with respect to size, and
contain particles ranging from about 0.01 μm to over 100 μm
in diameter. Development of control technology, emissions
testing, and prediction of health and environmental effects
often require characterization of the size distributions or
aerosol particulate mass or the various chemical components.
Cascade impaction provides a relatively simple and fundamen-
tal measurement of the mass-vs-size distribution and can
yield size-segregated material in quantities adequate for
determining the distributions of chemical, physical, or
biologically active constituents. This paper briefly
reviews impactor theory, considers the merits and short-
comings of four cascade impactors, and reviews the principal
problems involved in using cascade impactors to measure pro-
perties of coal combustion aerosols. These problems include
errors in measuring narrow distributions, effects of par-
ticle bounce and reentrainment, diffusive deposition of fine
particles, and deposition of condensible/adsorbable gases.
Ambiguities in data reduction are also discussed.

Cascade impactors have been used extensively to provide size-
segregated particulate samples for characterizing the distributions
of mass and chemical constituents in both ambient and source aero-
sols. In principle, conventional inertial impactors can provide
accurate data on particle distributions in the range of 0.2 to 50 μm
(1,2). The lower size limit has been reduced to 0.05 μm with low-
pressure impactors (3,4,5) and, more recently, to 0.026 μm with a
microorifice impactor (6,7,8). Large errors in estimates of the
distribution parameters can result, however, in cases where the size
distribution is narrow (such as that for aerosols modified by highly
efficient particulate-control devices), from the effects of particle
bounce and reentrainment, and from the deposition of particles and
gases from boundary streams onto impaction substrates. These
problems are especially important in sampling the bimodal aerosols
produced in the combusion of pulverized coal, which contain conden-
sible gases, enormous concentrations of submicrometer particles, and
predominantly dry, glassy aluminosilicate spheres that tend to stick
poorly to impaction substrates. Because of particle bounce, con-

tamination of submicrometer-particle fractions with larger particles is an especially important problem in sampling both source and ambient aerosols. These problems are reviewed below.

The Principle of Inertial Impaction

The underlying principle of inertial impaction is embodied in the concepts of relaxation time and stopping distance. When the velocity of a particle-containing gas is changed, for example, by accelerating the gas through a nozzle or by changing the direction of its flow, the suspended particle, with its greater inertia, lags behind the gas. The time required for equilibrium to become reestablished is known as the relaxation time, and the distance the particle travels while equilibrating is known as the stopping distance. In an impactor, placement of an obstruction (impaction plate) normal to the direction of flow forces the gas to change direction. A particle is deposited (i.e., collected) on the impaction plate if the size of the plate is large with respect to the stopping distance of the particle.

The stopping distance (S) of an aerosol particle is a function of the diameter (D_p), velocity (V_p), and density (ρ_p) of the particle, and the viscosity of the gas (μ), as shown in Equation 1 (9):

$$S = \frac{\rho_p V_p C D_p^2}{18\mu} \qquad (1)$$

where C is the Cunningham slip correction factor, which accounts for discontinuity in the transfer of momentum to the particle (as a result of collisions with gas molecules at the particle surface) that occurs for particles of size near that of the mean free path of the gas molecules (9).

Typical cascade impactors consist of a series of nozzle plates, each followed by an impaction plate; each set of nozzle plate plus impaction plate is termed a stage. The sizing characteristics of an inertial impactor stage are determined by the efficiency with which the stage collects particles of various sizes. Collection efficiency is a function of three dimensionless parameters: the inertial parameter (Stokes number, Stk), the ratio of the jet-to-plate spacing to the jet width, and the jet Reynolds number. The most important of these is the inertial parameter, which is defined by Equation 2) as the ratio of the stopping distance to some characteristic dimension of the impaction stage (10), typically the radius of the nozzle or jet (D_j).

$$\text{Stk} = \frac{\rho_p V_p C D_p^2/18\mu}{D_j/2} \qquad (2)$$

Particle collection efficiency is a monotonically increasing function of the inertial parameter and has been determined experimentally (1,11,12). Customarily, this function is represented by a single value, that is, the value of the Stokes number (Stk) that corresponds to a collection efficiency of 50%. Thus by rearranging Equation 2), the diameter of the particle collected with 50% efficiency (D_{50}) is

expressed in terms of the Stokes number for 50% collection (Stk$_{50}$) as follows:

$$D_{50} = \sqrt{Stk_{50}} \quad x \quad \sqrt{\frac{9\mu D_j}{\rho_p V_p C}} \tag{3}$$

Particles with large enough stopping distances will be deposited on the first impaction plate; those with somewhat smaller stopping distances will be carried to the next stage; and so on. By increasing the velocity of the aerosol in successive stages, the stopping distance of the particle is likewise increased, and progressively smaller particles are collected. The jet velocity can be increased either by reducing the number of size of the jets or by increasing the overall flow rate of the aerosol.

Data Reduction

In typical aerosols, particle size is distributed lognormally. The distribution parameters (median and the geometric standard deviation) may be estimated graphically from cumulative plots of mass vs particle size on log-probability paper, or mathematically, by fitting the data to a lognormal distribution function. By convention the mass median aerodynamic diameter of an aerosol is abbrivated as MMAD, where as the mass median aerodynamic diameter of a population of particles that is a subset of an aerosol is abbreviated mmad. The latter convention is used, for example, to indicate the median particle collected on a single impaction stage.
     Gravimetric or chemical analysis of the individual impaction plates is used to determine the aerosol mass or the amount of some chemical constituent associated with the range of particle sizes collected on the plate. The size distribution of the measured variable can then be deduced by plotting the data against the appropriate impactor stage parameter, usually the D$_{50}$ as determined by Equation 3). The D$_{50}$, however, is a measure of the diameter of a particle collected with 50% efficiency, and not the size of the particle collected on the impactor stage. The true distribution of particles actually collected on the stage is a function of the distribution of the aerosol sampled and the efficiency-vs-size curves for the individual stages; only by chance would the D$_{50}$ be equal to the mediam diameter of particles on the stage. The use of D$_{50}$s in determining actual distributions therefore contains an intrinsic error. If efficiency curves are available, this intrinsic error can be reduced by using data-inversion techniques (13,14). These techniques determine the distribution that, after multiplication by the appropriate sets of calibration curves, best reproduces the amounts of particulate mass collected on each impactor stage.
     In general, if the aerosol distribution is wide enough and the mass mediam diameter (MMD) is within the range of the device, D$_{50}$s can provide reasonably accurate estimates of the aerosol-distribution parameters. Efficiency curves for impactors are sigmoidal, however, and collection efficiency for particles of all sizes is non-zero. Thus, when the size distribution is narrow, as in aerosols modified by particulate-control devices, the amount of mass attributed to the larger particles may be incorrect. As a rule, the size of the

largest particle collected on the first stage of the impactor should be determined by microscopy or by inference from other measurements. Additional sizing errors, resulting from nonideal behavior, are discussed below.

Nonideal Behavior

The principal problems in determining size distribution parameters with cascade impactors are wall losses, inefficient collection due to particle bounce, deposition of gas-phase species on impaction substrates, and deposition of fine particles from boundary layers. As discussed above, an intrinsic error can result from using D_{50}s to infer size distributions from the impactor data. Depending on the sampling conditions and on the chemical and physical properties of the aerosol sampled, each of the other errors can also be significant, and generally must be considered in sampling coal combustion aerosols.

Wall losses. Ideally, all of the aerosol sampled in an impactor should be deposited on the collection plates or be captured by the after-filter. In practice, some of the particles collect on other interior surfaces and are typically excluded from the analysis. Wall losses result from diffusion of particles in turbulent eddies, from sedimentation of large particles (especially in large-particle stages with large internal volume and corresponding low gas velocities), from electrostatic effects, and from particle bounce. Wall losses appear to depend on size and hence on stage. Therefore, if they are significant, both the total mass concentration of the aerosol and its inferred size distribution will contain an error. Experience has shown that wall losses are greater for large, hard, dry particles, typically composed of aluminosilicate materials, than for small (submicrometer) carbonaceous or sulfate particles.

Particle bounce. When particles bounce off the collection surface, they may be carried to subsequent stages, where they may stick or again bounce off. The result is that subsequent stages collect more mass than is appropriate, and the inferred particle-size distribution is biased towards the smaller particles. Apparently, because of increasing velocity, particles that bounce off one stage continue to bounce off the subsequent stages and are finally collected on the afterfilter. As discussed below, such collection can severely limit the utility of afterfilter data. Typically, sticky substances are applied to impaction surfaces to reduce particle bounce. Compounds that can be "wicked" by the collected particles tend to be the most effective.
    The significance of these and other real-world difficulties are discussed below for sampling coal combustion aerosols.

Problems in Measuring Coal Combustion Aerosols

In an earlier study (15) we addressed some of the problems in obtaining accurate concentration-vs-particle-size distributions for elements in stack aerosols collected downstream of an electrostatic precipitator and a Venturi wet scrubber at a coal-fired power plant. The problems investigated were error associated with the use of the

D_{50}s, wall losses, and contamination of afterfilters by particle
bounce. In a later study, we observed the artifactual deposition of
gas-phase components during sampling (16). In both studies we used
the University of Washington Mark III and Mark V Source Test Cascade
Impactors (17). Our specific objectives were to verify the sizes of
particles collected on impaction stages and afterfilters and to esti-
mate impactor efficiency relative to collection on filters. The
ultimate goal was to determine elemental emission rates as a function
of particle size.

The Mark III and Mark V impactors used in these studies are,
respectively, 7- and 11-stage multicircular jet units with integral
backup filters. These were operated isokinetically, in-stack, with
Nuclepore polycarbonate impaction substrates coated with vacuum
grease. Elemental constituents of the particles collected were
determined by neutron activation analysis, and number-size distribu-
tions (for each stage) were determined by counting particles in
discrete size ranges after sonic dispersion in hexane. Particle
sizes were determined from scanning electron microscope (SEM) pho-
tographs or by use of a Quantimet image analyzer with an interface to
the SEM.

Impactor stage data. In Figure 1 are plotted both the cumulative
mass distributions of Al in fly-ash particles as determined from
stage D_{50}s and the distribution parameters for each stage as deter-
mined from SEM analyses. The SEM number-distribution (nmd) parame-
ters for each stage were transformed to the corresponding volume
parameters and adjusted for the measured particle density (2.44
g/cm^3) and slip correction factor to obtain estimates of the mass
mediam aerodynamic diameters (mmad) for the stage. Neither the nmds
nor the mmads determined from the microscopy analysis are directly
comparable to the D_{50} stage parameters. Values corresponding to the
D_{50}s can, however, be interpolated from the cumulative curves (Figure
1) and are listed in Table I. Comparison of these data shows that
use of the D_{50}s supplied with the impactor (these are calculated
values, and generally agree well with calibrations) results in
serious overestimation of the amount of mass associated with large
particles. As indicated in Figure 1, aerosol MMAD was overestimated
by a factor of two when the D_{50}s were used, and the estimated
geometric standard deviation was 40% too large. In this case, the
aerosol contained relatively few particles with diameters comparable
to the D_{50}s of the first impactor stages. The presence of particles
with diameters much smaller than the D_{50}s is attributed to their low,
but significant, collection efficiency.

Wall losses were estimated by comparing the mass concentrations
of various elemental constituents of aerosols collected with a series
of alternately collected filter and impactor samplers. For samples
collected downstream of an electrostatic precipitator (ESP), where
the aerosol MMAD was 11.5 µm, the average amount of mass collected in
the impactors was about 60% of that collected by the filters (Table
II). When fine (MMAD <2 µm), wet particles were collected downstream
of a Venturi wet scrubber, the impactor and filter data typically
agreed to within 20% which was well within the uncertainty of the
comparison. We concluded, therefore, that wall losses were lower for
small, wet particles than for larger, dry fly-ash particles.

Afterfilter data. As indicated in Table I, the minimum D_{50} in this study was about 0.5 μm, and particles smaller than this were collected on an afterfilter. Aerosols from combustion of pulverized coal typically are distributed bimodally, with a fine-particle mode at about 0.1 μm and a large-particle mode at supermicrometer sizes; the modal diameter of the latter depends strongly on the efficiency characteristics of the control device. The elemental concentrations in the fine-particle mode are of interest in health-impact and source-apportionment studies because of the typically high enrichment of the concentrations of many potentially toxic elements and useful tracer elements in particles in this size range. Large-particle contaimination of the afterfilter due to particle bounce can, however, limit the value of these data.

To investigate the importance of afterfilter contamination by particle bounce, particle-size distributions were determined by SEM techniques for afterfilters from three impactors (15). With a final-stage D_{50} of 0.5 μm, we would expect to see particles as large as about 0.94 μm on the afterfilters; however, the afterfilters actually contained particles as large as 4 μm. Cumulative mass distributions for the observed particles are plotted in Figure 2. Curves a and b represent data for samples collected downstream of an ESP. Impactor stages were coated with vacuum grease (curve a) or not coated (curve b). Curve c represents afterfilter data for a coated impactor run downstream of a Venturi wet scrubber. As indicated in Figure 2, large particles accounted for about 96% of the particulate mass on the afterfilter from the coated ESP impactor and 98% of that from the uncoated ESP impactor. A somewhat lower value (87%) for large-particle mass on the third afterfilter indicates that particle bounce and reeentrainment were only slightly reduced for the small (<2 μm), wet particles collected downstream of the Venturi scrubber.

The mmads for the distribution of particles on these after-filters, which ranged from about 1.4 to 3 μm, were far larger than the D_{50} for the final impactor stage and could not have been inferred without SEM measurement. Since neither the correct mass nor the correct particle size can be determined without SEM measurements, afterfilter data should usually be excluded from the analysis when SEM analyses are not made. However, there are some exceptions. For example, the concentrations of certain trace elements are typically much higher in submicrometer particles than in supermicrometer particles. In this study, the concentrations of Mo, Sb, As, and Se in the large particles were so low that a high degree of large-particle contaimination could be tolerated. As shown in Table III, we used the microscopy data and chemical analyses to estimate the true concentrations of elements in the fine-particle component of one of the afterfilters. Except for Mo, Sb, As, Se, and Ba, the elemental concentrations determined in particles on the afterfilter (which would normally be assigned a size less than the final-stage D_{50}) ranged from 40% to over 200% higher than our estimates of their bounce-off-corrected concentrations.

Diffusive deposition of gases. Although we have not formally investigated the deposition of condensible gases, the overall concentrations of Br and Se in impactor samples collected downstream of a hot-side ESP at a large western coal-fired power plant far exceeded their concentrations as determined by filter sampling (16). In addition, the concentrations of Br and Se were nearly uniform on all stages
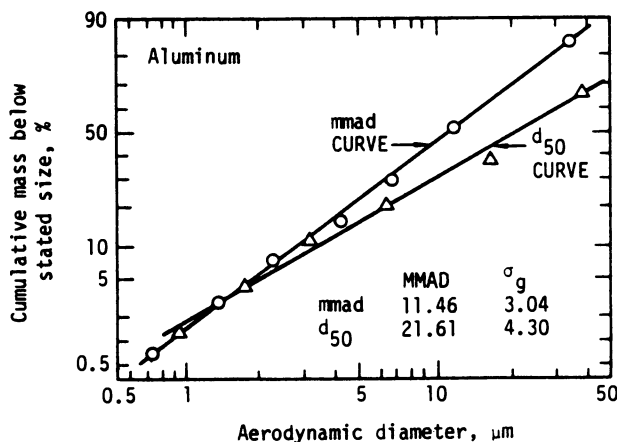
Figure 1. Cumulative mass distributions of the element Al plotted using impactor D_{50} values and mmads derived from scanning electron microscope analyses. The impactor was run down-stream from an electrostatic precipitator with uncoated impaction stages. Reproduced with permission from Ref. 15. Copyright 1978, Pergamon Press Ltd.
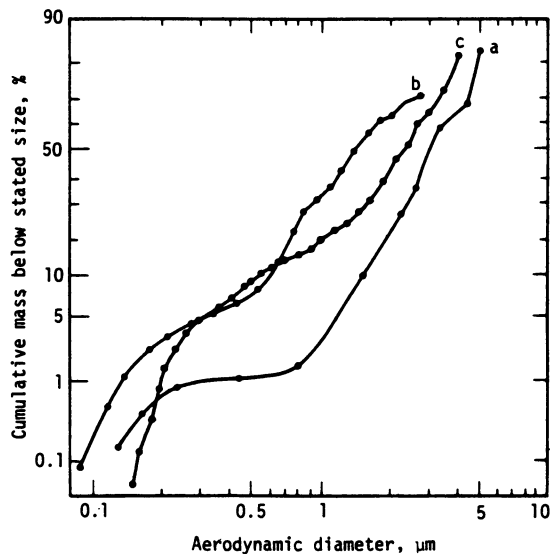
Figure 2. Curve a – cumulative mass distribution for coal combustion particles collected on an afterfilter of a coated impactor. Curve b – cumulative mass distribution for particles collected on an afterfilter of an uncoated impactor. Curve c – cumulative mass distribution for particles collected on an afterfilter at the outlet of a wet scrubber. Reproduced with permission from Ref. 15. Copyright 1978, Pergamon Press Ltd.

Table I.   Comparisons of D_{50} Values for a University of Washington
           Mark III In-Stack Impactor and Observed Particle Sizes in a
           Sample Collected Downstream from the Electrostatic Precipi-
           tator of a 750-MW Coal-Fired Electrical Power Unit (15).

Stage	mg AL	nmd[a]	σ_g	mmad	Interpolated[b] D_{50}	D_{50}
1	2.01	8.14	1.88	34.4	18.5	38.3
2	1.75	2.91	2.10	11.7	8.06	16.7
3	0.985	2.21	1.71	6.72	4.70	6.40
4	0.586	1.39	1.65	4.24	3.01	3.17
5	0.428	1.00	1.35	2.24	1.70	1.77
6	0.179	0.64	1.38	1.37	0.99	0.94
7	0.0837	0.34	1.35	0.73	d	0.50

[a]Number median diameters (nmd) determined from SEM observation.
[b]Diameter taken from mmad curve (Figure 1) corresponding to cumula-
 tive mass points of impactor D_{50} values.
[c]50% cutoff diameters taken from calibration curves provided with the
 impactor and adjusted to reflect a particle density of 2.44 $g \cdot cm^{-3}$.
[d]Value not determined.

Table II. Comparisons of Selected Elemental Concentrations in Samples
           Collected on Filters and on Impactors Located Downstream
           From the Electrostatic Precipitator of a 750-MW Coal-Fired
           Electrical Power Unit.

Al	230,000 ± 21,000	402,000 ± 46,000	0.57 ± 0.08
As	72.3 ± 4.9	118 ± 8	0.61 ± 0.06
Ba	3,640 ± 490	5,990 ± 420	0.62 ± 0.09
Br	10.2 ± 0.7	81 ± 34	0.13 ± 0.05
Ce	210 ∓ 29	381 ± 28	0.55 ± 0.09
Co	25.4 ∓ 3.9	43.1 ± 3.5	0.59 ± 0.10
Sb	12.4 ± 0.7	19.5 ± 1.2	0.63 ± 0.05
Sc	24.7 ± 2.7	45.9 ± 3.2	0.54 ± 0.07
Se	55 ± 18	44 ± 22	1.27 ± 0.75
Sr	738 ± 28	1,320 ± 20	0.56 ± 0.02
Ta	3.74 ± 0.14	7.73 ± 0.57	0.48 ± 0.04
Th	45.9 ± 5.7	86.5 ± 8.5	0.53 ± 0.08
Ti	10,500 ± 900	17,500 ± 2,300	0.60 ± 0.09
U	25.5 ± 2.4	42.0 ± 3.5	0.61 ± 0.08
V	268 ± 18	498 ± 28	0.54 ± 0.05

Average collection efficiency[a]   0.60 ± 0.05
($\pm\sigma$) (excluding Br and Se)

Range   0.47 - 0.71

[a]Includes additional data reported in reference 15.

of an impactor (16). Both of these elements tend to be distributed inversely with respect to particle size, and concentrations typically differ by a factor of 10 between particles of 0.1 μm and 1 μm diameter The surface area available for vapor adsorption is dominated by the substrates rather than by the particles collected on the substrates. Therefore we concluded that the flat concentration-vs-size distributions for Br and Se resulted from the adsorption of vapor-phase components of these elements. Artifacts from the deposition of gases can probably reduced if not eliminated by diluting the gas with clean cool air prior to impactor sampling, or by using a diffusion denuder (17) to remove the gas prior to impactor sampling.

Another phenomenon that we have observed in sampling coal-combustion aerosols is the collection of numerous fine particles on large-particle impaction stages. Figure 3 is an SEM photograph of the third stage of an impactor located downstream of an ESP at a large western coal-utility boiler. Although the D_{50} was 6 μm, hundreds of tenth-micrometer particles are visible. In treated off-gas streams from combustion of pulversized coal, concentrations of submicrometer particles are typically about $10^7/cm^3$, while supermicrometer particle concentrations are typically three or four orders of magnitude lower. We attribute the collection of these fine particles to diffusive deposition from flow streams passing near the collection surface. Since these fine particles typically contain much higher concentrations of many trace elements, their collection may significantly bias the reported size distributions of these elements towards large particles.

Submicrometer Aerosol Measurements

Impactors that size-segregate particles via a series of stages operating at successively higher nozzle velocities have been designed by numerous investigators (11,18,19,20). There is a practical upper limit to jet velocity (3,000-4,000 cm/s), above which small particles tend to rebound from the collection plate and no longer stick to it (3). The theory for particle capture at a surface suggests that the limiting capture velocity is a function of particle mass, the ratio of the incident and reflected particle velocities, and the particle surface adhesion energy (21). Limiting velocity is proportional to the square root of adhesion surface energy and thus also proportional to the square root of particle diameter. As limiting velocity is also inversely proportional to the square root of particle mass, the net effect for particles of uniform density is that the limiting velocity is inversely proportional to particle diameter. Thus larger velocities can be tolerated for smaller particles. Further, given conventional drilling techniques, it is difficult to make jets with diameters less than about 0.025 cm. As a result, the lower limit of sizing by these impactors is about 0.4 μm (3). Particles below this size are typically collected on a backup filter, but are not size-segregated. Fresh aerosols from high-temperature combustion sources typically contain accumulation modes with modal diameters of about 0.1 μm. Thus the distribution characteristics of these aerosols cannot be determined with conventional cascade impactors operated at near-atmospheric pressure.

From Equation 3), it is clear that the size of particles collected on an impaction stage can also be reduced by increasing the

Table III. Ratios of Observed Elemental Masses on a Typical After-
            Filter to Those Adjusted for Particle Bounce.

Element	Ratios
Mo, Sb, As, Ba	1.0±0.3; 1.18±0.08; 1.19±0.08; 1.3±0.1
Se, W, V, In	1.3±0.1; 1.4±0.2; 1.5±0.2; 1.9±0.3
Zn, Fe, U, Sr	2.1±1.1; 2.9±1.0; 2.5±1.2; 2.9±1.4
Mn	3.8±2.6
Ca, Ce, Co, Cr	
Hf, K, Lu, Sc	>1.0
Sm, Ta, Yb	
Ga, Ti, Eu, Al	>1.4, >1.7, >2.0, >2.1
Dy, Th, La, Na	>2.2, >2.6, >2.7, >3.3

Adapted from reference 15
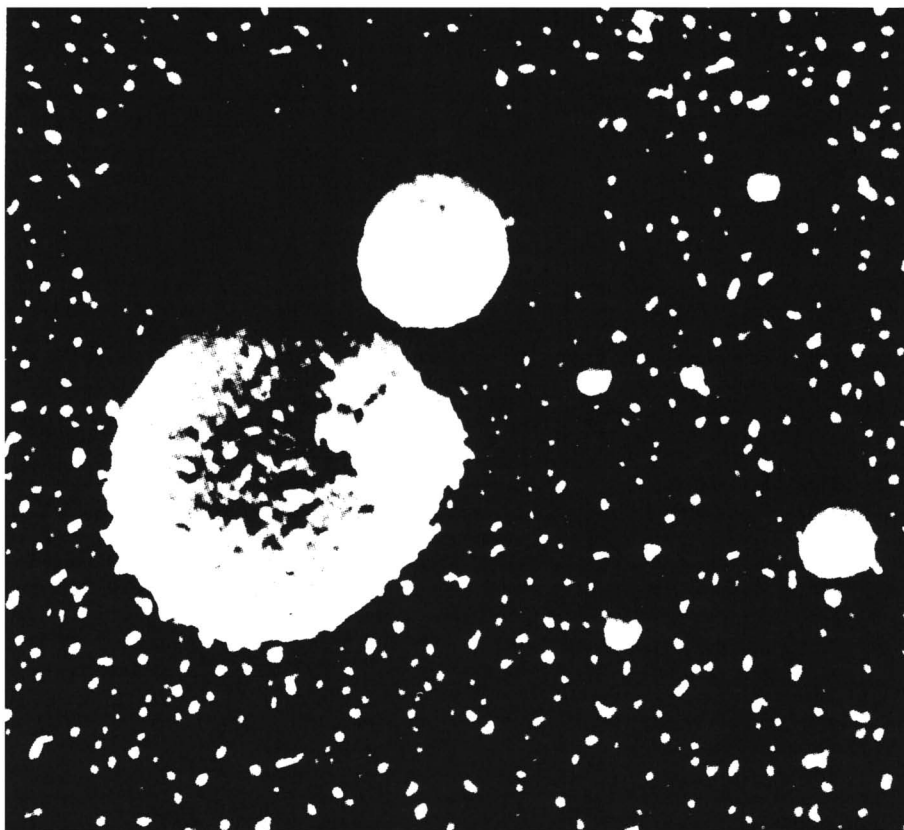
Figure 3. Particles collected on an impactor stage with a D_{50}
of 6.4 μm; scanning electron microscopy, 2,400X magnification.

value of the slip correction factor (C) or by reducing the diameter
of the jets. The value of C is increased by reducing the gas
pressure, and such an increase is the basis for low-pressure and high
pressure-drop impactors such as those designed by McFarland et al.
(3), Hering et al. (4), and Pilat et al. (5). Characteristics of the
final stage of each of these impactors are listed in Table IV. The
McFarland and Hering impactors use commercially available preimpac-
tors for supermicrometer sizing and have three and four additional
stages, respectively, for sizing submicrometer particles. The sub-
micrometer sizing stages operate at a final stage pressure of 24.3 mm
Hg (McFarland impactor) or 8 mm Hg (Hering impactor). The lower
limit diameter for both impactors is 0.05 μm. The McFarland impactor
samples at a rate of 28 ℓpm and, by using multiple jets (600 or
1,762), achieves jet velocities within the range required for accep-
table particle bounce. Unfortunately, however, the unit requires a
vaccum pump weighing between 400 and 500 lb to support the 28 ℓpm
sampling rate at the low final-stage pressure. Because of its large
size and power requirements, the unit has not been adopted for
routine field use and has never been fully evaluated.

   The Hering impactor is more portable and has been used to study
the distribution of submicrometer sulfate aerosols (22). In this
impactor a critical orifice separates the atmospheric and low-
pressure stages and determines the 1-ℓpm sampling rate. The low-
pressure stages each use a single jet, which even at the relatively
low sampling rate produces jet velocities ranging from 9,300 to
30,000 cm/s. These jet velocities are so high that particle bounce
is severe for the submicrometer particles (23). The single-jet
design is not conducive to analysis by x-ray fluoresence, and the low
flow-rate hampers the collection of sufficient material for analyses
of trace constituents in ambient air.

   In another study (24), we used a University of Washington Mark V
impactor to determine the distributions of trace elements in sub-
micrometer combustion aerosols from a 430-MW(e) coal-fired power
plant. The Mark V is similar in design to the Mark III, but it has
11 impactor stages and may be operated as a high pressure-drop impac-
tor. The orifice plates of the last four stages of the Mark V are
quite similar to those of the University of Washington Mark IV, which
was designed specifically for low-pressure operation. The unit can
provide up to six submicrometer particle-size fractions. The Mark V
was operated at flow rates of about 7 ℓpm at final-stage pressures no
lower than 345 mm Hg.

   Theoretical values of stage cutoff diameters can be calculated
for the impactor if the gas pressures can be accurately estimated or
measured. Pilat et al. (25) have extensively measured the pressures
on each stage of the Mark IV and have prepared theoretical curves
giving stage cutoff diameters as a function of gas temperature and
sampling rate for a specific final-stage pressure. Because of the
constraints of isokinetic sampling and the somewhat high pressure-
drop filter required for our chemical analyses, and possibly because
the amount of gas leakage around the jet stages in our study may have
differed from that in the study of Pilat et al. (25), we were unable
to obtain the final-stage pressures and sample flow rates called for
by the theoretical curves. Because the degree of leakage between
stages was unknown, and because the effects of particle bounce are
not accounted for by theory, we relied on SEM techniques to determine

the size distribution of particles collected on individual stages.
The mmds for individual stages that collected submicrometer particles
ranged from 0.77 to 0.11 μm. In this study we used Teflon-fiber
afterfilters to achieve the desired flow rate, but these could not be
analyzed by SEM. The size distributions observed for the last four
stages (Figure 4) were generally "well behaved" -- i.e., they fit
well the lognormal distribution function, and tended to be free of
the large particles that should have been collected on previous sta-
ges. We believe that the use of coated substrates and the numerous
impactor stages helped to minimize the effects of particle bounce.

        More recently, Kuhlmey, et al. (6) developed a uniform-deposit
micro-orifice impactor in which nozzles with diameters of 100 μm were
made in 50-μm-thick plates by a photochemical etching process. The
original impactor used 200 jets per stage and could collect 0.1 μm
particles at a flow rate of 10 ℓpm with an overall pressure drop of
only a few inches of Hg. Because of the large number of nozzles, the
relatively high flow rate is achieved at somewhat lower jet veloci-
ties than achieved in low pressure impactors. The nozzles were
placed in a spiral pattern and the collection plate was rotated to
achieve uniform deposition. The advantages of uniform deposition are
that particles do not pile up under the nozzles and alter the jet-to-
plate spacing, thus changing the cutoff diameter; and that x-ray
fluorescence can be used for analysis. A later, horizontally-
configured five-stage design with up to 2,000 jets per stage per-
mitted sampling at 30 ℓpm with a mimimum cutoff size of 0.06 μm.
Marple (8) has recently built two vertically configured microorifice
impactors having a final cutoff size of 0.026 μm (see Table V).
These vertically configured units use four-stage conventional
atmospheric-pressure preimpactors to remove supermicrometer par-
ticles, and they also operate at 30 ℓpm. All of these microorifice
impactors can be used with standard low-volume rotary carbon-vane
vacuum pumps.

        We have used both the horizontally and vertically configured
impactors to sample coal-combustion aerosols in elevated plumes and
in plumes at ground level near Deep Creek Lake in western Maryland.
Few problems were encountered in this study however, particle bounce
could not be evaluated for ambient samples because the individual
submicrometer particles could not be discerned. Marple and Rubow (8)
have performed extensive calibrations with monodisperse aerosols;
these show that impaction plates covered with aluminium foil have
slightly larger D_{50}s than plates covered with Teflon-fiber filters.

        Particle bounce problems in the microorifice impactor have not
been adequately evaluated with real-world aerosols. As jet veloci-
ties in the later few stages are greater than the 3000 to 4000 cm/sec
design criteria quoted by McFarland, et al. (3), particle bounce
problems may be expected for stages E, F, G. Note that even at lower
jet velocities, some amount of particle bounce is anticipated, and in
general, it is extremely difficult to obtain submicrometer particle
fractions completely free of larger particles. Particle bounce can
lead to very large errors in the total aerosol mass and the con-
centration of matrix-type elements (e.g., Al, Si, rare earths, etc.)
which are typically associated with supermicrometer particles. This
phenomenon is frequently overlooked by researchers investigating sub-
micrometer mass and composition. Consequently, much of the existing
information derived from impactors on elemental composition of fine

Table IV.   Characteristics of Three Reduced Pressure Impactors

Impactor	Jet Diameter cm	No. of Jets	Jet Velocity cm/sec	D$_{50}$ μm	Final Stage Pressure Torr	Flow Rate lpm
McFarland, et al.	0.0208	1762	4158	0.05	2.43	28
Hering, et al.	0.140	1	30,000	0.05	8	1.0
Pilat, et al.	0.0198	60	13,900	20.1	345	7

Table V.   The New Micro-Orifice Impactor Permits Submicrometer Sizing At High Flow Rates, Low Pressure Drops, and Lower Jet Velocities.

		Total Flow Rate 30 lpm			
Stage	Jet Width, cm	No. Jets	Jet Velocity cm/sec	D$_{50}$ μm	ΔP inches mercury
C	0.0123	2000	2,180	1.6	1.0
D	0.0100	2000	3,330	0.55	1.3
E	0.00694	2000	7,200	0.20	2.4
F	0.00551	2000	12,700	0.092	7
G	0.00371	2000	23,100	0.024	14

Adapted from Marple and Rubow (8).
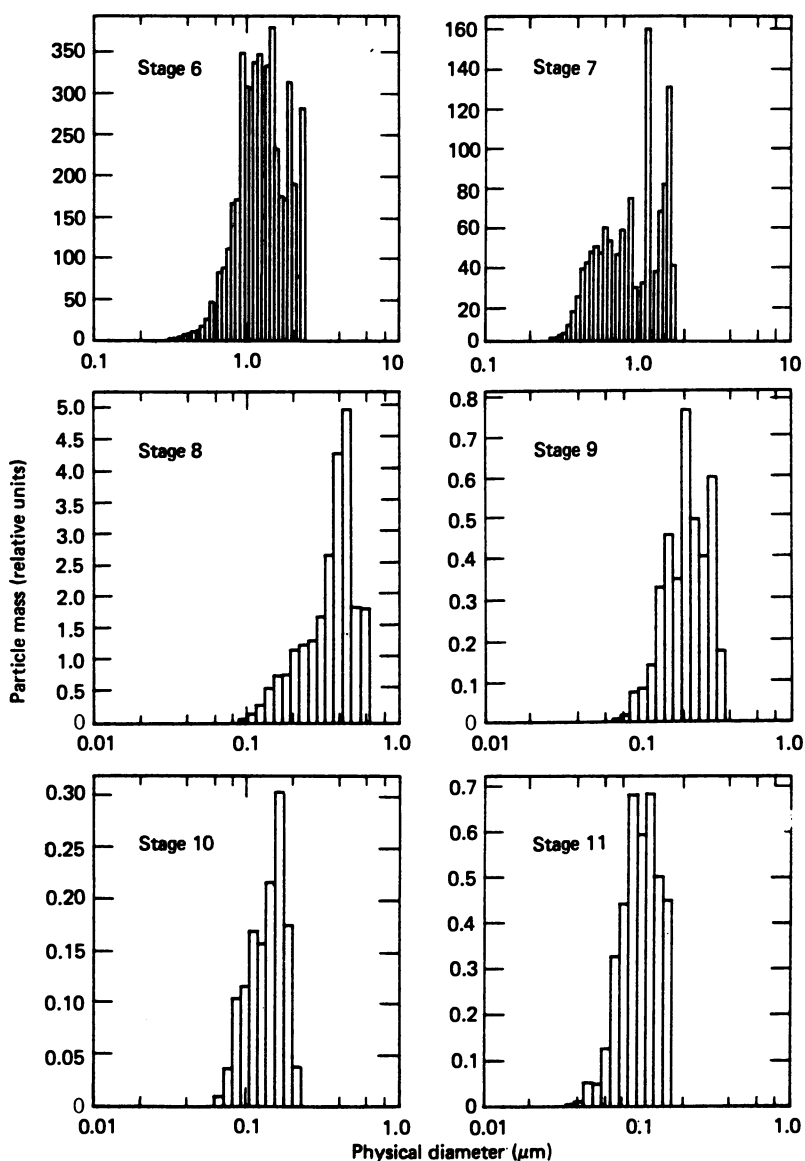
Figure 4. Distribution of particles on stages of a high pressure-drop impactor with submicrometer cutoff diameters.

particles should be viewed with skepticism unless the impact of particle bounce has been rigorously investigated. In general, submicrometer particle sizing and particle bounce off should be checked by microscopy techniques. Fine particle distribution parameters should also be obtained by auxiliary methods, for example, electric mobility analysis.

Literature Cited

1. Ranz, W.E., and Wong, J.B., Indust. Eng. Chem. 44, 1371-1381 (1952).
2. Mercer, T.T., Amer. Industr. Hyg. Assoc. J. 26, 236-241 (1965).
3. McFarland, A.R., Nye, H.S., Erikson, C.H., Development of a Low Pressure Impactor. U.S. Environmental Protection Agency, Report No. EPA-650/2-74-014 (1973).
4. Hering, S.V., Flagan, R.C., Friedlander, S.K., Environ. Sci. Technol. 12, 667-673 (1978).
5. Pilat, M.J., Powell, E.B., Carr, R.C., Proc. 70th Annual Meeting, Air Pollut. Control Assoc. 4, 35.2 (1977).
6. Kuhlmey, G.A., Liu, B.Y.H., Marple, V.A., Amer. Indust. Hyg. Assoc. J. 42, 790-795 (1981).
7. Marple, V.A., Liu, B.Y.H., Kuhlmey, G.A., J. Aerosol Sci. 12, 333-337 (1981).
8. Marple, V.A., Rubow, K.L., Development of a Microorifice Uniform Deposit Cascade Impactor. University of Minnesota, Particle Technology Laboratory Publ. No. 532 (1984).
9. Fuchs, N.A., The Mechanics of Aerosols. MacMillan Co., New York, (1964). p. 71.
10. Hidy, G.M., Brock, J.R., The Dynamics of Aerocolloidal Systems. Pergamon Press, Oxford (1970). Vol. 1, p. 72.
11. May, K.J., J. Sci. Instrument. 22, 187-195 (1945).
12. McFarland, A.R., Zeller, H.W., Study of a Large Volume Impactor for High Altitude Aerosol Collection. Report of the Division of Technical Information Extension of the U.S. Atomic Energy Commission, TID-18624 (1963).
13. Cooper, D.W., Spielman, L.A., Atmos. Environ. 10, 723-729 (1976).
14. Dzubay, T.G., Hasan, H., Size Distributions of Species in Fine Particles in Denver Using a Micro-Orifice Impactor. In preparation.
15. Ondov, J.M., Ragaini, R.C., Biermann, A.H., Atmos. Environ. 12, 1175-1185 (1978).
16. Ondov, J.M., Biermann, A.H., Ralston, H.R., Composition and Distribution Characteristics of Aerosols Emitted from a Coal-Utility Boiler Equipped with a Hot-Side Electrostatic Precipitator. Presented at the Annual ACS Meeting, Miami Beach, FL, September 10-15 (1979).
17. Allegrini, I., DeSantis, F., DiPalo, V., Liberti, A., J. Aerosol. Sci 15, 465-471 (1984).
18. Pilat, M.J., Ensor, D.S., Bosch, J.C., Atmos. Environ. 4, 671-679 (1970).
19. Andersen, A.A., Amer. Indust. Hyg. Assoc. J. 27, 160-165 (1966).
20. Marple, V.A., Amer. Ind. Hyg. Conf. Abs. N.P. p. 24 (1977).
21. Dahneke, B., J. Colloid Inter. Sci. 45, 584-590 (1973).
22. Hering, S.V., Friedlander, S.K., Atmos. Environ. 16, 2647-2656 (1982).
23. Hering, S.V., Personal communication (1981).

24. Ondov, J.M., Biermann, A.H., Heft, R.E., Koszykowski, R.F.,
    Elemental Composition of Atmospheric Fine Particles Emitted from
    Coal Burned in a Modern Electric Power Plant Equipped with a
    Flue-Gas Desulfurization System. American Chemical Society
    Symposium Series no. 167, 173-186 (1981).
25. Pilat, M.J., University of Washington, Personal communication
    (1979).

RECEIVED May 29, 1986

Chemical Reactivity of Polycyclic Aromatic Compounds Adsorbed on Coal Stack Ash

Arlene A. Garrison, Robert A. Yokley, Robert J. Engelbach, E. L. Wehry, and Gleb Mamantov

Department of Chemistry, The University of Tennessee, Knoxville, TN 37996

The photochemical reactivity of anthracene, phenanthrene, pyrene, benzo[a]pyrene, and benz[a]anthracene is examined. Each aromatic hydrocarbon was adsorbed onto the surface of each of a variety of coal stack ashes. The reactivity of each hydrocarbon was also studied on a variety of model adsorbents. All hydrocarbons are observed to be less photoreactive on coal ash surfaces than when adsorbed on alumina, silica, or glass surfaces. Different coal ashes stabilize poly- cyclic aromatic hydrocarbons to phototransformation with differing efficiencies. The role of the chemical composition of coal ashes (especially carbon and iron content) and physical properties of the ashes (especially color) is discussed.

The chemical reactivity of particle-associated polycyclic aromatic hydrocarbons (PAHs) under real or simulated atmospheric conditions is receiving greatly increased attention (1-4). The residence times of particle-adsorbed PAHs in the atmosphere obviously depend upon the susceptibility of the compounds to chemical transformation. We describe herein an investigation of the photochemical reactivity of five PAHs (anthracene, phenanthrene, pyrene, benzo[a]pyrene, and benz[a]anthracene) adsorbed on various coal ashes of widely diverse origin and composition. Each PAH was deposited on each coal ash from the vapor phase to attempt to simulate the adsorption of combustion-produced PAHs onto atmospheric particles (5).
     It is now clear that the photochemical behavior of PAHs adsorb- ed on coal ash tends to be significantly different from that of pure PAHs, PAHs in liquid solution, or PAHs adsorbed on "model" surfaces such as alumina and silica (6-10). The manner in which coal ash surfaces affect the behavior of adsorbed PAHs undoubtedly represents a complex combination of chemical and physical phenomena. The study of these phenomena is complicated by the complex (and heterogeneous) nature of coal ash.

Experimental Section

Aromatic Hydrocarbons. Anthracene (henceforth abbreviated "A"), phenanthrene (Ph), pyrene (Py), benzo[a]pyrene (BaP), and benz[a]-anthracene (BaA) were obtained from commercial sources and, when required, were purified by vacuum sublimation.

Adsorbents. Six coal ashes, from combustion of Eastern Appalachian (EA), East Tennessee (ET), Illinois (IL), and Western Kentucky (WK) bituminous coals; New Mexico (NM) subbituminous coal; and Texas (TX) lignite were acquired from the Oak Ridge National Laboratory. Each ash was obtained from a power plant stack emission control device. Sampling and chemical characterization of these ashes is described elsewhere (11). A seventh ash was an analytical standard, of unknown origin, obtained from Alpha Resources (AR), Stevensville, Mich. An eighth ash, Kaneb (KA), was a high-carbon ash obtained from the stacks of a power plant experiencing operating difficulties at the time of sampling. Elemental analyses of the ashes are listed in Table I.

Table I. Bulk Elemental Compositions of Coal Stack Ashes[a,b] (11)

Element	KA	EA	NM	ET	TX	WK	IL	AR
Silicon	na	23.4	28.1	30.0	25.7	23.4	22.7	29.0
Aluminum	na	13.6	13.1	15.5	7.5	10.1	9.1	11.4
Calcium	na	1.0	4.2	0.2	14.5	1.3	2.4	2.9
Magnesium	na	0.8	0.7	1.8	1.9	0.4	0.6	0.8
Sodium	na	0.3	1.4	0.2	0.4	0.2	1.7	0.8
Potassium	na	2.4	0.6	2.0	0.5	2.2	1.6	0.9
Carbon	2.8	1.8	1.0	0.5	0.5	0.3	0.3	0.3
Iron	na	10.9	2.5	1.7	3.4	16.9	16.5	4.0

a: All data as weight percentage of the indicated element.
b: Data not available indicated by "na".

Other adsorbents included alumina (neutral, Brockmann activity I); silica gel; controlled-pore glass (100 Å pore diameter, Pierce Chemical Co., Rockford, Ill.); and flaked graphite (Southwestern Graphite Co., Burnet, Tex.). Each adsorbent was sieved to pass a 45-μm screen prior to use. All adsorbents were stored in the dark, and degassed at elevated temperatures by passing high-purity nitrogen over them in an expanded bed (12) immediately before use. Porosities and specific surface areas were measured by BET nitrogen adsorption. Diffuse reflectance spectra were measured with a Varian Cary 14L spectrophotometer.

Adsorption and Illumination Procedures. PAHs were deposited onto the adsorbents from the vapor phase using a diffusion cell-expanded adsorbent bed apparatus described elsewhere (12).
Two photochemical illumination cells were used. The first was a rotatable quartz tube (7). The second was a fluidized-bed photo-reactor similar to that described previously by Daisey et al. (13).

When intercomparisons between results obtained by these two illumination systems were made, no significant differences were noted. Therefore, the rotary photoreactor (7) was used in the large majority of these studies.

The illumination source was a xenon illuminator (Cermax, ILC Technology, Sunnyvale, Cal.) operated at 180-320 W and situated 34-38 cm from the photolysis cell. The spectrum of the output of this lamp closely simulated the solar spectrum over the 300-700 nm wavelength region. To avoid thermal decomposition of samples undergoing illumination, the near-infrared component of the lamp output was attenuated by inserting a 20-cm water filter between the lamp and a sample. A portion of each sample of adsorbed PAH was stored in the dark, as a control, to ensure that no detectable non-photochemical decomposition of the PAH occurred during the duration of illumination.

Analytical Methods. Once a sample was illuminated, it was subjected to 24-hr micro-Soxhlet extraction in the dark with methanol or toluene. Both the illuminated and control samples were treated identically in all cases. All samples were subdivided into four portions after illumination but before extraction, and extractions were performed on each of these subdivided samples. The recovery of unreacted PAH for each sample (illuminated and control) could therefore be expressed as a 95% confidence interval for quadruplicate extractions. Decisions as to whether a particular PAH exhibited significant phototransformation on a particular adsorbent were based on whether the extraction recoveries for the illuminated and control samples (as 95% confidence intervals) were detectably different.

Results and Discussion

To simplify the presentation of the results, we use the following categories to classify the photoreactivity of adsorbed PAHs:

(a) ++: High photochemical reactivity (greater than 50% photodecomposition of adsorbed PAH upon 24-hr illumination);

(b) +: Moderate photochemical reactivity (10-50% photodecomposition of adsorbed PAH caused by 24-hr illumination); and

(c) 0: Little or no photochemical reactivity (less than 10% loss of adsorbed PAH caused by 24-hr illumination).

Based on these reactivity categories, the results are summarized in Table II (top of next page).

Several major generalizations emerge from an examination of these results. First, each PAH exhibits greater photochemical reactivity when adsorbed on silica gel, alumina, or controlled-pore glass than when adsorbed on any of the eight coal ashes examined in this study. This observation reinforces previous observations that, compared with substrates such as alumina or silica, coal ash surfaces stabilize adsorbed PAHs with respect to photochemical transformation (6-10). It is therefore evident that the residence times of PAHs in the atmosphere adsorbed on coal fly ash particles are likely to be significantly greater than heretofore presumed. Whether similar conditions pertain for other important classes of atmospheric particulate substrate has not yet been investigated.

Table II. Photochemical Reactivity of Adsorbed PAHs[a]

PAH	KA	EA	NM	ET	TX	WK	IL	AR	Silica	Alumina	Glass	Carbon
A	0	0	+	+	++	+	0	+	++	++	++	0
Ph	0	0	0	0	+	0	0	+	++	++	++	0
Py	0	0	0	0	+	0	0	++	++	++	++	0
BaP	0	0	0	0	++	0	0	+	++	++	++	0
BaA	0	0	na	+	++	+	na	+	++	++	++	0

a: Results not available for entries denoted "na".

There are two ashes (KA and EA) on which none of the five PAHs
exhibits detectable photoreactivity, and a third ash (IL) on which
none of the PAHs examined thus far (excluding BaA) exhibits detect-
able photodecomposition. At the other extreme, all five PAHs undergo
appreciable phototransformation when adsorbed on two ashes (TX and
AR). In fact, for each, greater photochemical reactivity is observed
on the Texas lignite ash than on any other ash (though less reactiv-
ity is observed on the TX ash than on alumina, silica, or glass
adsorbents).

It is obviously worthwhile to inquire into the characteristics
of the various ashes that may be responsible for these pronounced
differences in photoreactivities of adsorbed PAHs. We note first
from Table I that both KA and EA ashes are very high in carbon
content. We note further in Table II that none of the PAHs exhibits
measurable phototransformation when adsorbed on pure carbon (flaked
graphite). In contrast, those ashes on which all five PAHs are
photoreactive (TX and AR) are relatively low in carbon. It is
especially important to note in this context the observations of
Griest and Tomkins (14,15), who, in studies with radiolabeled PAHs
adsorbed from liquid solution onto various coal ashes and ash sub-
fractions, observed that the carbonaceous particles exhibited much
greater sorptivity for PAHs than did the magnetic or nonmagnetic
mineral ash particles. There appear to be specific chemical inter-
actions between carbonaceous particulate surfaces and adsorbed PAHs,
the nature of which is not yet fully understood. Whether such
chemical interactions are related to the apparent ability of carbon
(or high-carbon coal ash) surfaces to stabilize PAHs to photodegra-
dation is not yet clear, but is a matter of obvious importance re-
quiring additional study.

It is clear from Tables I and II that differences between photo-
reactivities of PAHs on different coal ash substrates cannot be re-
lated solely to differences in the carbon content of the ashes.
The NM ash, on which phenanthrene, pyrene, and BaP are unreactive,
is relatively high in carbon, but the ET, WK, and IL ashes are 0.5%
or less in C. However, both IL and WK are relatively high in iron
(>15%). Thus, of the ashes on which most PAHs are unreactive (KA,
EA, NM, ET, WK, and IL), all but ET are relatively high either in
carbon (>1%) or iron (>10%), or both. Whether this pattern of
results is chemically significant or merely adventitious cannot be
stated definitely at this time. In contrast, those ashes on which
all PAHs exhibit photoreactivity (TX and AR) are low both in carbon
and iron. ET is the only ash which deviates from this general trend.

It is conceivable that the relationship of carbon and iron content of coal ashes with their ability to suppress PAH phototransformation may be due in part to the fact that the ashes high in carbon and/or iron are relatively dark in color, whereas the TX and AR ashes (upon which all PAHs undergo photodecomposition) are much lighter in color. If the adsorbent is highly colored and relatively porous, it is possible for an adsorbate (PAH) molecule to become sequestered in the pore structure and be "shielded" from the incident light by the absorbing substrate. Such "inner-filter" effects are well known in photochemistry (16), and they have previously been presumed to play a role in the photochemistry of PAHs adsorbed on particulate solids (1).

We have used two techniques in an attempt to compare the "color" of the various adsorbents. First, they have been compared with Munsell soil color charts (17). Second, their diffuse reflectance spectra have been measured (vs. white filter paper as reference). These results are summarized in Tables III and IV, respectively.

Table III. Munsell Color Designations of Adsorbents

Adsorbent	Munsell Designation	Color Description
Silica gel	N 9/0	White
Alumina	N 9/0	White
Controlled-pore glass	N 9/0	White
ET ash	5Y 8/1	White
TX ash	5Y 7/2	Light gray
AR ash	5Y 6/2	Light olive gray
EA ash	5Y 5/1	Gray
NM ash	5Y 5/1	Gray
KA ash	5Y 3/1	Very dark gray
IL ash	10YR 3/2	Very dark grayish brown
WK ash	2.5Y 3/2	Very dark grayish brown
Graphite	N 3/0	Very dark gray

Table IV. Optical Absorbances of Substrates at Selected Wavelengths by Diffuse Reflectance[a]

Adsorbent	360	350	340	330	320	310	300	290	280	270	260 nm
Silica	0.2	0.0	−0.1	−0.1	−0.1	−0.1	−0.1	0.0	0.1	0.2	0.4
Alumina	−0.2	−0.2	−0.2	−0.2	−0.1	−0.1	−0.1	0.0	0.0	0.0	0.1
Glass	0.0	0.0	−0.1	−0.1	−0.1	−0.1	−0.1	−0.1	−0.1	−0.1	−0.1
ET ash	0.4	0.4	0.5	0.6	0.7	0.8	0.8	0.9	1.0	1.1	1.2
TX ash	0.6	0.6	0.6	0.7	0.7	0.8	0.9	0.9	0.9	1.0	1.0
AR ash	0.7	0.8	0.8	0.9	1.0	1.0	1.1	1.1	1.2	1.2	1.3
EA ash	0.8	0.9	1.0	1.0	1.1	1.1	1.2	1.2	1.3	1.3	1.4
NM ash	0.7	0.7	0.8	0.8	0.9	0.9	1.0	1.0	1.1	1.1	1.2
KA ash	1.1	1.1	1.1	1.1	1.1	1.1	1.2	1.2	1.2	1.3	1.3
IL ash	1.2	1.2	1.2	1.2	1.3	1.3	1.3	1.3	1.3	1.3	1.4
WK ash	1.2	1.2	1.2	1.3	1.3	1.3	1.3	1.3	1.3	1.4	1.4
Graphite	0.8	0.8	0.8	1.0	1.7	1.7	1.7	1.7	1.7	1.6	1.7

a: Absorbances vs. white filter paper reference. All wavelengths in nanometers.

(In Table IV, a negative absorbance means that the adsorbent in question was less strongly absorbing than the white filter paper reference).

Comparison of Tables III and IV shows a general correlation between adsorbent color (as defined by the Munsell indices) and optical absorbance. Note that the "darkest" adsorbents (graphite; WK, IL, KA, NM, EA) ashes are those on which PAH photoreactivity tends to be low, while the "lighest" adsorbents (silica, alumina, glass, TX and AR ashes) are those on which adsorbed PAHs are most photosensitive. Again, the ET ash is an exception (being a light-colored ash but one on which adsorbed PAHs are not especially susceptible to phototransformation).

BET surface-area and porosity measurements (using nitrogen) indicate that all adsorbents studied possessed pore structure in the 100-1000 Å size range. In order for the "inner-filter" effect to influence the susceptibility to photolysis of an adsorbed organic compound, the adsorbent must be porous as well as colored. Assuming an average molecular area for benzo[a]pyrene of 108.0 Å^2 (18), it appears safe to conclude that BaP, and all smaller PAHs, could be incorporated within the pore structures of all coal ashes examined in this study. These results, in combination with the color assignments and reflectance spectra of the ashes, do not "prove" unambiguously the importance of "inner-filter" effects. However, it seems highly unlikely that the relationships between coal ash color and the photoreactivity of adsorbed PAH can be totally accidental.

In addition to carbon and iron content and color, there are undoubtedly other properties of coal ashes, as yet not identified, that influence the photochemical reactivity of adsorbed PAHs (and other adsorbed organic compounds). The extent to which the behavior described in this paper arise from physical parameters (e.g., color) as opposed to chemical phenomena (e.g., strong binding of adsorbed PAHs to carbonaceous particles or domains) is thus far unclear, and conceivably will never be elucidated fully. The failure of the ET ash to conform to any of the correlations estab-lished for the other seven ashes is itself indicative of the fact that the influence of coal ash on the degradation of adsorbed environmentally-important organic compounds represents a complex combination of parameters and influences. On the basis of these results and those reported previously by us (6,7) and other investigators (8-10), there can now be little doubt that stabiliza-tion by coal ash surfaces of PAHs to photochemical oxidation is a general phenomenon, which should have significant influence on the residence times of particle-adsorbed PAHs in the atmosphere.

We note in conclusion that different PAHs exhibit differing levels of photoreactivity when adsorbed on coal ash, with the reactivity order in this case being anthracene, BaA > phenanthrene, pyrene, BaP. To the extent that this question has been addressed in other studies of PAH photolysis on coal ash substrates, our results are consistent with those previously reported (7-10).

Literature Cited

1. Nielsen, T.; Ramdahl, T.; Bjørseth, A. Environ. Health Perspect. 1983, 47, 103-114.
2. Pitts, J. N., Jr. Environ. Health Perspect. 1983, 47, 115-140.
3. Van Cauwenberghe, K.; Van Vaeck, L. Mutat. Res. 1983, 116, 1-20.
4. Nikolaou, K.; Masclet, P.; Mouvier, G. Sci. Total Environ. 1984, 32, 103-132.
5. Natusch, D. F. S.; Tomkins, B. A. In "Polynuclear Aromatic Hydrocarbons"; Jones, P. W.; Freudenthal, R. I., Eds.; Raven Press: New York, 1978; p. 145.
6. Korfmacher, W. A.; Natusch, D. F. S.; Taylor, D. R.; Mamantov, G.; Wehry, E. L. Science 1979, 205, 582-4.
7. Korfmacher, W. A.; Wehry, E. L.; Mamantov, G.; Natusch, D. F. S. Environ. Sci. Technol. 1980, 14, 1094-1099.
8. Dlugi, R.; Güsten, H. Atmos. Environ. 1983, 17, 1765-1771.
9. Güsten, H.; Bozicevic, Z.; Klasinc, L. Staub-Reinhalt. Luft 1984, 44, 448-451.
10. Behymer, T. D.; Hites, R. A., Indiana University, Bloomington, Ind., personal communication, November 1984.
11. Lauf, R. J., ORNL Report TM-7663, Oak Ridge National Laboratory, Oak Ridge, Tenn., 1981.
12. Miguel, A. H.; Korfmacher, W. A.; Wehry, E. L.; Mamantov, G.; Natusch, D. F. S. Environ. Sci. Technol. 1979, 13, 1229-1232.
13. Daisey, J. M.; Lewandowski, C. G.; Zorz, M. Environ. Sci. Technol. 1982, 16, 857-861.
14. Griest, W. H.; Tomkins, B. A. Sci. Total Environ. 1984, 36, 209-214.
15. Griest, W. H.; Tomkins, B. A. Environ. Sci. Technol., in press.
16. Wehry, E. L. In "Analytical Photochemistry and Photochemical Analysis"; Fitzgerald, J. M., Ed.; Marcel Dekker: New York, 1971; p. 173.
17. Munsell Soil Color Charts; Kollmorgen Corp.: Baltimore, 1975.
18. Schure, M. R. Ph.D. Dissertation, Colorado State University, Fort Collins, Col., 1981.

Sorbent and Leachate Characteristics of Fly Ash

John W. Liskowitz[1], Richard B. Trattner[1], James M. Grow[1], Mung S. Sheih[1], James A. King[2], John Kohut[3], and Melvin Zwillenberg[3]

[1]Industry/University Cooperative Center for Research in Hazardous and Toxic Substances, New Jersey Institute of Technology, Newark, NJ 07102
[2]Lincoln University, Lincoln, PA 19352
[3]Public Service Electric & Gas, Newark, NJ 07101

Coals from ten different mines were burned under monitored conditions in three different types of coal fired utility boilers in order to determine the influence of coal composition and boiler combustion conditions on the leaching and sorbent characteristics of the fly ash produced. The leaching and removal exhibited by the fly ashes with regard to pH, Cd, Sn, Ni, Pb, Mo, Cu, Fe, Cr, Zn, Mn, As and organics were examined.

Results indicate that the leachable elements are contained to some extent within a water soluble component in low and high fusion fly ashes. The leachable amounts of each element are in general related to the bulk composition of the elements in the coal from which the fly ash is produced and the size of the fly ash particles. Boiler temperatures also influence the leachable amounts of elements in low fusion fly ashes.

Aqueous washing of the fly ash provides a sorbent with the capacity to remove the elements in amounts in excess of that originally leached. The sorbent characteristic of fly ash is favored by combustion temperatures that lead to the fusion of the fly ash during its formation and the time it remains in the fused state. No correlation could be established between the sorbent characteristic of the fly ashes and their bulk major , minor, trace elemental compositions and the particle size of the fly ash particles. Only the carbon content of the fly ash could be related to its organic removal properties.

Increased reliance on coal combustion can give rise to significant fly ash storage or disposal problems. Most fly ash is presently used as a low cost material for construction purposes and also as cover material for landfills. Other, more economically advantegeous, uses for this inexpensive material would be desirable. One such use for fly ash could be to treat ash pond effluent for reuse by power plants as cooling tower makeup water. Another application could be as

sorbents for the treatment of the heavy metals, toxic anions and
organic substances commonly found in leachates emanating from land-
fills. Over the past several years, our laboratory has developed,
under EPA Grant R803-717 a method utilizing fly ash alone or in
combination with other inexpensive sorbents for the removal of heavy
metals, toxic anions and organics from industrial sludge leachates
and industrial waste stream effluents. During the course of these
investigations, two types of fly ash were repeatedly collected at
different times from the same electrostatic precipitator at a coal
burning boiler of a large east coast electric utility. These fly
ashes exhibited different leaching and sorbent characteristics.
Although both fly ashes initially leached both cations and anions,
the leaching eventually ceased and removal of these species
occurred. For example, one fly ash whose effluent was initially
acidic leached copper (0.69 micrograms/gram of fly ash) and zinc
(0.32 micrograms/gram of fly ash) when this material was placed in
a lysimeter and eluted with industrial sludge leachate. After a
period of time the leaching ceased and both copper and zinc in the
treated effluent were reduced from about 2.5 mg/L and 0.4 mg/L,
respectively, to 0.01 mg/L (1). Since each fly ash type exhibited
different sorbent characteristics, a mixture of both types was found
to be more effective in the treatment of industrial sludge leachates.
Up to this point, the availability of the different types of fly ash
from the power plant could not be predicted. One simply had to
collect what was available and determine its characteristics by
testing. This lack of an adequate supply of fly ashes with the
desired sorbent characteristics inhibited the further development
of this low cost technology for the treatment of industrial waste
effluent and leachate from industrial landfills. Therefore, this
investigation was carried out to correlate the sorbent and leaching
characteristics of fly ash produced with the composition of the coal
and the combustion conditions that existed during the production of
these fly ashes.

Experimental Boiler Types

Three different types of coal fired boilers were utilized in this
study. One type (A) was a dry bottom boiler with direct fired
burners located on opposite walls. The second type (B), wet bottom
boilers #11 and #12, was operated in parallel with the same coal
stream split to feed both boilers simultaneously. The third boiler
types (C & D) were dry bottom, tangentially fired boilers.

Samples and Their Analysis

Six high-fusion coals and five low-fusion coals were burned in the
three different boiler types under closely monitored conditions.
Well defined combustion conditions were followed to insure uniformity
in the evaluation of the test coals (2). Table I gives a listing of
these eleven coals by mine name and location.

Table I.   Coals burned under test conditions

Mine	Location
High Fusion Coal	
Militant	Pennsylvania
Deep Hollow	West Virginia
Upshur	West Virginia
Badger	West Virginia
Mine Mouth C	Pennsylvania
Mine Mouth D	Pennsylvania
Low Fusion Coal	
Wellmore Cactus	Virginia
Wellmore Ackiss	Virginia
Ellsworth	Pennsylvania
Nora	Pennsylvania
Blend	Not Known

During the combustion of each coal, samples were collected at the entrance to each pulverizer just prior to being burned. The collection of fly ash was timed to correspond to the coal being burned. Different size distributions of the fly ash were obtained by the collection of samples from both the front and back row of electrostatic precipitators. The coals and their ashes were analyzed for percent C, S, SiO_2, Al_2O_3, CaO, K_2O, Na_2O, and MgO, and ppm of Ti, Cd, Cu, Cr, Pb, Zn, Sn, Ni, and Mn, ash content and ash fusion temperatures according to ASTM procedures.

All boiler temperatures were measured just prior to and after the collection of the coal samples and their respective fly ashes, since it was physically impractical to collect the samples and measure the temperatures at the same times. In all cases, the temperatures remained essentially constant. An optical pyrometer was used to measure flame temperatures, and water-cooled jacketed thermocouples were used to monitor the boiler temperatures. The wall effects on the temperature measurements were minimized by insertion of the thermocouple into the boiler until temperatures remained constant with distance upon further insertion of the thermocouple into the boiler.

Surface Analysis

The surface composition of the fly ash samples was obtained using a Varian I.E.F. spectrometer operating at around 1×10^{-6} torr. The powder samples were mounted on the probe using two sided tape. The relative compositions were calculated using Weingle's photoelectric cross sections as a measure of relative intensities (3).

Lysimeter Studies

Lysimeters were used to evaluate the leaching and removal of Cd, Sn, Ni, Pb, Mo, Cu, Cr, Zn, Mn, Fe, As, and COD using 500 grams of fly ash under continuous flow conditions.

Laboratory lysimeters were constructed of plexiglass tubing (6.2 cm i.d.; 0.6 cm wall thickness; 90 cm length), supported in a vertical position. A 164 micron pore size corundum disc (6.10 cm diameter; 0.6 cm thickness) was placed in each column directly over the drain hole in order to support the fly ash sorbent and to prevent clogging of the outlet.

The leaching characteristics of the fly ashes generated under the various combustion conditions were evaluated as to the extent that each fly ash leaches Cd, Sn, Ni, Pb, Mo, Cu, Cr, Sn, Mn, and Fe. Deionized water was added to the lysimeters containing 500 grams of the fly ash and specific volumes of effluent leachates were collected and analyzed for the above elements until 4 liters had passed through each ash sample. It was observed that 500 grams of fly ash generally ceased to leach after passage of 4 liters of water through the column.

The packed columns were then slowly wetted with ash pond effluent to allow total saturation and to force all the air trapped in the voids out of the column packing. The column was then filled with ash pond effluent to the level of an overflowing drain, in order to permit a constant head condition. The ash pond effluent was fed to the top of the column through a valved manifold which distributed the effluent to all lysimeters, simultaneously, from a central reservoir. The central reservoir, a 100 liter polyethylene carboy, delivered the ash pond effluent to the manifold system by means of a gravity siphon feed arrangement. Any overflow from the constant head drains was collected and pumped back to the central reservoir. All tubing in the system was made of Tygon (3/8" i.d.). Tygon was used because analysis of ash pond effluent samples passed through this tubing revealed no leachable constituents. A constant hydraulic head was maintained in the lysimeters at all times and the volumes of effluent passing through the columns were continuously monitored. Samples of treated ash pond effluent were collected at intervals and analyzed to determine the concentration of all measurable constituents remaining in the effluent after a known volume had passed through the column. This was continued until breakthrough had occurred for all measurable contaminants or excessively low permeabilities were encountered. Breakthrough is defined as that condition when the concentrations of the species of concern in the lysimeter effluent sample approached or exceeded that in the pond effluent samples.

Results and Discussions

The temperature profiles monitored in the coal fired boilers during the collection of the coal and fly ash samples are listed in Table II for different power outputs. The limited temperature results obtained for the Militant and Deep Hollow fly ashes was the result of our thermocouple probes being unavailable for these test burns.

The three different type of boilers used in this study were found to exhibit different temperature profiles. The flame and boiler temperatures monitored in Boiler A, when measured, were observed to be well below the initial deformation temperature of the ash (see Table II). On the other hand, the flame temperatures encountered in the B and D boilers were above the initial deformation point of the ash, and in some cases above the temperature at which the ash becomes fluid. In addition, the temperatures monitored in

Table II: Relations of Boiler Conditions to Leachate pH

| Ash | Source | Power | Flame | Boiler Temp °F | | Ash Fusion °F | | | pH |
				Above Basket	Arch	Init. Def	Soft	Fluid	range
Boiler A: Militant	Front	Full				2555	2700+	2700+	3.5-6.6
Militant	Back	Full							3.8-6.8
Militant	Front	Full							4.2-6.7
Militant	Back	Full							3.6-6.9
Militant	Front	Int.							3.8-7.2
Militant	Back	Int.							3.8-5.9
Militant	Front	Min.							3.7-6.9
Militant	Back	Min.							3.7-7.3
Deep Hollow	Front	Full				2605	2700	2700+	3.7-5.1
Deep Hollow	Back	Full							3.8-5.5
Deep Hollow	Front	Int.		1550					4.0-6.1
Deep Hollow	Back	Int.							3.6-4.7
Deep Hollow	Front	Min.		1450					3.8-5.6
Deep Hollow	Back	Min.							6.3-7.0
Upshur	Back	Full	2470	1590	1565	2700+	2700+	2700+	2.7-4.5
Badger	Front	Full	2550	1750	1440	2700+	2700+	2700+	2.8-5.5
Back	Full	Full							3.6-4.6
Boiler B: Blend	No. 11	Full	3100	1815	2250	2143	2325	2665	7.7-9.1
	No. 12	Full	3100	1737	1835	2188	2325	2353	7.3-7.5
Wellmore	No. 11	Full	3150	1620	2080	2120	2285	2570	8.3-9.3
Cactus (1)	No. 12	Full	3150	1530	1480	2135	2310	2555	6.9-7.9
Nora	No. 11	Full	3100	1850	2175	2130	2230	2330	9.4-9.8
	No. 12	Full	3250	1700	1700	2145	2265	2480	4.1-6.4
Wellmore	No. 11	Full	3050	1900	2180	2135	2330	2625	7.3-8.6
Ackiss	No. 12	Full	2950	1725	1500	2110	2265	2440	5.1-6.8
Wellmore	No. 11	Min.	2870	1590	1780	2190	2400	2695	7.2-9.1
Ackiss	No. 12	Min.	2950	1620	1500	2155	2215	2510	5.6-5.8
Wellmore	No. 11	Full	3125	1400	1680	2150	2235	2445	9.8-11.5
Cactus (2)	No. 12	Full	2970	1400	1320	2155	2275	2470	8.2-9.0
Ellsworth	No. 11	Full	3100	1815	2240	2183	2520	2700+	10.5-12.3
	No. 12	Full	3100	1740	1820	2125	2503	2700+	8.5-9.4
Boiler C: Mine mouth		Full	2650	2600					6.6-8.1
Boiler D: Mine mouth		Full		2700	2700				7.1-10.0

the arch of boiler #11 was significantly higher than that measured
at the arch in boiler #12 even though they were burning the same
coal. Also, the C and D boiler temperatures above the flame basket
were observed to be greater than the softening temperatures of the
ash.
     The results of monitoring the temperature profiles and ash
fusion temperatures of the ash resulting from the test coals burned
in the different boilers indicated that the effect of boiler
temperature and ash fusion characteristics of the coal on the leach-
ing and sorbent characteristics should be examined. This could be
carried out through a comparison of the leaching and sorbent
characteristics of the fly ash produced in the #11 boiler with that
produced in #12 boiler and the fly ash produced in the A boiler with
that produced in the C and D Boilers, respectively.

Leaching

Factors Influencing Leachate pH

The pH for the fly ash leachates indicate that the ashes produced
basic and acidic leachates. The pH's of low fusion fly ash produced
in the wet bottom B boilers in general range from a minimum of about
4.1 up to a maximum of about 12.3 (see Table II). High boiler
temperatures accompanied by fusion of the ash appears to favor the
formation of fly ash that generates an alkaline leachate. In all
cases, the fly ashes generated in boiler #11 are significantly more
alkaline than those produced in #12 even though there is no signifi-
cant difference in the major and minor element contents of these
ashes (see Table III).

Table III.   Representative amounts of major and minor constituents
             (in %)

Ash	Source	CaO	K_2O	Na_2O	MgO	SiO_2	Al_2O_3	Fe_2O_3	S
Wellmore									
Cactus (1)	No.11	2.84	3.59	1.02	1.40	49.6	25.8	13.8	0.28
	No.12	3.36	3.39	0.94	1.50	48.1	26.1	14.6	0.63
Badger	Front ppt.	2.04	1.94	0.44	0.63	38.3	32.9	11.8	0.25
	Back ppt.	2.14	2.08	0.44	0.80	46.2	33.6	12.1	
Mine Mouth									
	Boiler C:	1.65	3.18	0.58	0.93	52.7	26.4	11.5	0.27
Mine Mouth									
	Boiler D:	2.18	2.76	0.58	0.81	46.4	29.7	18.3	0.20

     The boiler temperatures in the #11 boiler were observed to be
400-600 degrees higher than those measured in #12 boiler. The
difference in temperature was especially pronounced in the arch reg-
ion of the boilers. These temperatures indicate that the fly ash
in the #11 boiler was exposed to higher temperatures for longer
period of time in the fusion state than the fly ash in #12 boiler.
A comparison of flame temperatures encountered in both the #11 and
#12 boilers and the ash fluid temperatures exhibited by the fly ashes
indicates that the flame temperatures are some 500°F higher than that
required to melt the ash.

Similar events also seem to have occurred with the boiler C and
D fly ashes. Both fly ashes also generate alkaline leachates (see
Table II). A comparison of the boiler temperatures that produced
the boiler C and boiler D fly ashes and their ash fusion temperatures
suggest that the boiler temperatures were high enough to cause fusion
of their respective fly ashes within the boilers. Temperatures of
2600 and 2700°F were measured above the flame basket in the boiler C
and boiler D, respectively. This is some 200° above the softening
temperatures of the fly ashes. Apparently, the high temperatures
encountered by the fly ash in the B boilers, boiler C and boiler D,
have resulted in fusion reactions that have led to alkaline products
that can be dissolved upon contact with water to form alkaline
leachates.

It can be seen from Table II that the fly ashes produced in the
A boiler essentially form acidic leachates even though the major
element composition of these fly ashes were comparable to the amounts
found in the boiler C and boiler D fly ashes (see Table III). The
Militant, Deep Hollow, Upshur and Badger fly ashes produced in this
boiler encountered flame and boiler temperatures that are below even
the initial deformation temperatures of the fly ash. Hence, the
fusion reactions probably did not occur that might have led to
formation of products that generate an alkaline leachate.

Factors Influencing Leachate Composition

The different amounts of leaching exhibited by the fly ashes suggest
that the leachable elements are contained within a water soluble
component which is eventually removed when the fly ash is brought in
contact with sufficient quantities of water. In most cases, the
leachable elements in 500 grams of fly ash ceased to appear after
4 liters of water was passed through the fly ash samples.

The differences in leaching of Cd, Sn, Mo, Pb, Cu, Cr, Zn, and
Mn from the fly ashes, with the exception of Ni and Fe, were found
to be dependent upon the differences in the amounts of these elements
present in the fly ash. Also, the differences in boiler temperatures
encountered by the fly ashes during combustion were observed to
influence the leaching of the above elements.

A correlation between the differences in the amount of Ni and Fe
present in a majority of these ashes and their leachability was not
observed. This lack of correlation suggests that these elements are
in a matrix that is not readily solubilized by the water used to
generate the leachate. Hansen and Fisher (4) have shown the iron to
be primarily in the insoluble silicate matrix and nickel appears to
be associated with an acid insoluble phase. However, for all of the
other elements, the differences in amounts leached from the fly ashes
were correlated with the bulk differences found in the fly ashes.

The difference in the amounts of Cd, Sn, Mo, Pb, Cu, Zn, and Mn,
measured in the high fusion ashes can be related to their concentra-
tions in the coal and the size of the fly ash particles. The smaller
fly ash particles in general contained greater amounts of a given
element than the larger particles.

In comparison, the differences in the amount of specific ele-
ments found in the low fusion fly ashes were not only observed to be
related to the concentration of that element in the coal and its

particle size, but also boiler temperatures. The smaller low fusion fly ash particles and/or lower boiler temperatures, when compared to the larger particles and/or higher boiler temperatures, contained the greater amounts of the majority of the above elements.

Boiler temperatures probably influence the leaching characteristics of the fly ashes by fixation of the leachable elements. The different leaching results obtained with the low fusion fly ashes produced from the same coal at the same time, but in two boilers operated in parallel at different temperatures, indicated that operation of the boilers at temperatures above the ash fusion temperatures, along with the ash produced in the hotter boiler remaining in the fused state for longer lengths of time may explain these differences. Apparently, the high temperatures along with the ash remaining in the fuse state for different lengths of time lead to some fixation of these elements into a non-soluble portion of the fly ash.

Factors Influencing Sorbent Properties of Fly Ash

Four separate ash pond samples were used to evaluate the effectiveness of the fly ash in treating fly ash pond effluent. Results of the analyses of these ash pond samples are presented in Table IV.

Table IV. Elemental Concentration of Actual Ash Pond Samples Used in Fly Ash Sorbent Characterization.

Element	Sample A mg/l.	Sample B mg/l.	Sample C mg/l.	Sample D mg/l.
Cadmium	N.D.*	N.D.*	0.02	0.02
Tin	0.90	2.07	1.01	
Molybdenum	3.0	2.70	0.41	
Nickel	0.26	0.11	0.09	
Lead	1.80	0.35	0.62	0.30
Copper	0.01	0.01	0.09	0.07
Chromium	0.48	0.18	0.09	
Zinc	0.16	0.06	1.48	0.56
Manganese	0.24	0.24	0.40	
Iron	0.22	0.05	0.10	
Arsenic	0.16	0.15	0.13	0.10
COD				12.8

* N.D. =below measurable limits

Sample D, which was primarily used to measure COD removal by the fly ashes, was collected from a different ash pond than those ash ponds which provided Sample A, Sample B and Sample C. The COD in the latter ash ponds could not be determined because of high chloride interferences resulting from salt water contamination of the ash pond effluent.

The results show that fly ash can be used for treatment of Cd, Sn, Mo, Ni, Pb, Cu, Zn, Mn, Fe, As and organics in these ash pond effluents. Removals of greater than 75 percent were achieved for all of the above elements with the exception of Mo where removals of only 43% were obtained. For example, Figure 1 shows that the concentration of lead in the treated ash pond sample remained below detectable

levels with no indication of breakthrough even after passing 36
liters of ash pond sample through the fly ash generated from the
Nora coals. These removals were achieved even though the concentra-
tion of lead in the ash pond sample was increased to 3.0 mg/1 (see
dotted line in Figure 1). The maximum allowable primary drinking
standard for lead is 0.05 mg/1. The exceptional removal of lead does
not appear to be due to precipitation since the concentration of
lead in the ash pond sample was kept below the maximum solubility of
the lead as measured as a function of pH (see Figure 2). Also, the
pH measured in the treated ash pond effluent ranged from an alkaline
value of 10 down to an acidic value of 6 during the removal of lead
from 36 liters of ash pond sample (see Figure 3).

     The general sorbent characteristics of the fly ashes are
favored by low ash fusion temperatures, combustion temperatures that
favor the fusion of the fly ash during formation and the time that
the fly ash remain in the fused state. No correlation could be
established between the sorbent characteristic of the fly ashes and
their bulk major, minor and trace elemental compositions nor with
their major and minor elemental compositions. Also, no correlation
could be established between the adsorbtion achieved with the fly
ashes and size of the fly ash particles. Only the carbon content of
the fly ash could be related to its organic removal properties.

     The amount of carbon remaining in the fly ashes which have
undergone fusion appears to be a factor in COD removal. The amount
of carbon remaining in the Mine Mouth D, Blend and Nora fly ashes on
a dry basis was 2.5%, 1.8% and 1.0%, respectively. The decreasing
amounts of carbon remaining in the fly ashes correlated with the
removal of COD achieved. The Mine Mouth D, Blend and Nora fly ashes
reduce the COD in ash pond Sample D from 12.8 mg/L down to 1.0 mg/L,
2.0 mg/L and 2.5 mg/L, respectively. These results are in agreement
with those reported by Johnson et al. (5) and Mancy et al. (6),
who showed that fly ashes with high organic content are better ad-
sorbers. Apparently, the high boiler temperatures encountered by
these fly ashes in the molten state may lead to activation of the
carbon present in the fly ash. Activated carbon is regularly used
for the removal of organics from waste streams.

     The sobent capacities of the fly ashes, identified in this
investigation to provide the best treatment, average over 80 μg/g
for the Cu and Zn, 66 μg/gm for Cd, 3.4 μg/gm for As and about 700
μg/gm for the organics. Experimental evidence suggests that the
sorbent capacity for As may be increased with further washing of the
fly ashes. These sorbent capacities were independent of pH in the
range from about 6 to 10. Also, the removals of Cd, Cu, Pb, and Zn
were independent of their inlet concentration in the ranges from
0.52 mg/1 to 2.0 mg/1, 0.52 mg/1 to 3.5 mg/1, 0.30 mg/1 to 3.0 mg/1
and 0.56 mg/1 to 4.0 mg/1, respectively.

     Greater than 75 percent removals of the Cd, Cu and Zn present in
the ash pond samples were achieved within 15 minutes of contact time
between the fly ash and the sample. In addition, the results indica-
te that removal of the above elements in ash pond samples can be
achieved with the fly ash that originally leached these elements.
The washed fly ashes were observed to have a significant excess of
sorptive capacity beyond that required to treat the element origin-
ally leached from the fly ash (see Table V).
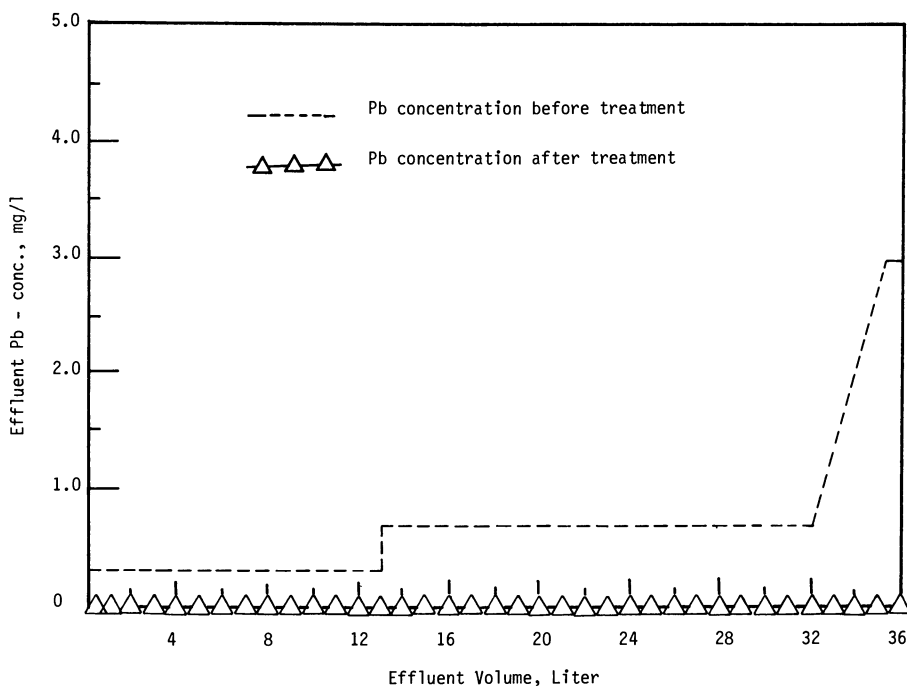
Figure 1. Concentration of Lead Remaining After Treatment with Nora Fly Ash, 500 grams.
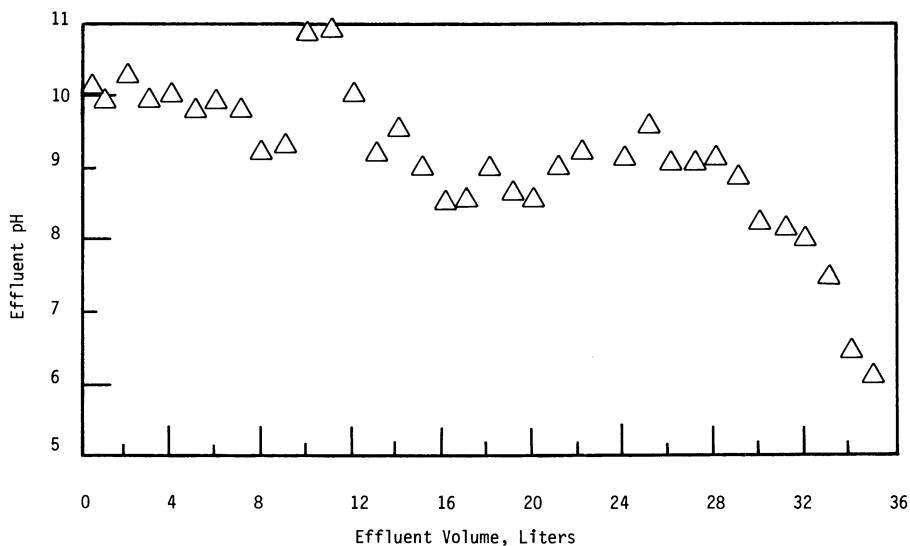
Figure 2. Influence of Treatment of Ash Pond Effluent with Nora Fly Ash on Resultant Treated Effluent pH.
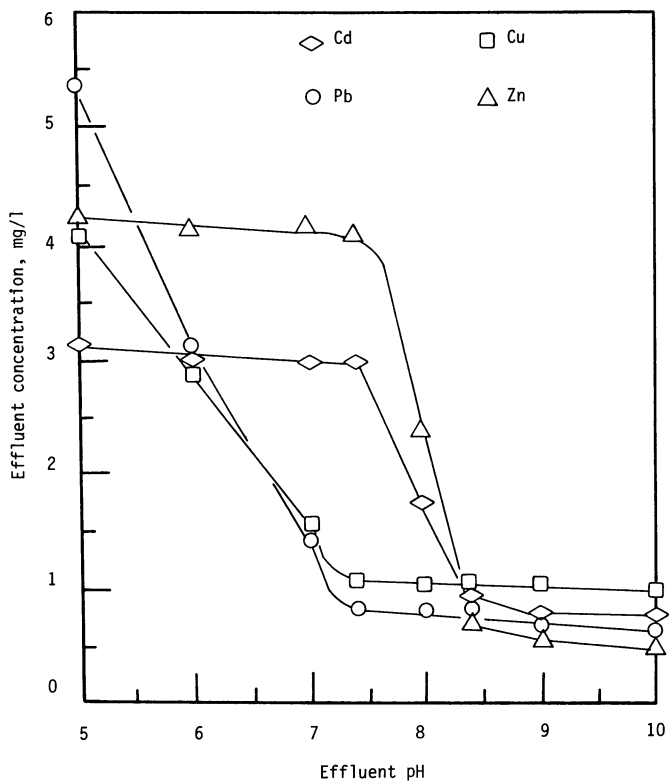
Figure 3. pH Effect on Cd, Cu, Pb and Zn Solubility in Ash Pond Sample D.

Table V.   Representative Element Leaching and Removals
             Exhibited by Selected Fly Ashes.

Fly Ash Samples	Leaching (ug/gm)		
	Cd	Cu	Zn
Militant	2	30	12
Blend	12	.04	.2
Nora	.2	.4	1
	Removals (ug/gm)		
Militant	41	34	51
Blend	66	83	86
Nora	56	70	60

Conclusion

The sorbent and leaching characteristics of fly ash can be related to
operating temperatures in the boiler and to coal ash compositions
that provide low ash fusion temperatures. Boiler temperatures that
favor the fusion of the ash and maintain the ash in the fused state
reduce the amount of trace elements leached from the fly ash and
improve the sorbent characteristics of the fly ash for removal of
these elements from ash pond effluents. In addition, the leachable
amounts of each of the elements analyzed in this study can be cor-
related with the fly ash particle area and with their bulk composi-
tions in the original coal. No correlation could be identified
between the sorbent characteristics of fly ashes and their particle
size and bulk, major, minor and trace elemental compositions, with
the exception of the carbon content. Only organic removals, as
measured by COD from ash pond effluent, could be correlated with the
carbon content of the fly ash particles.

Acknowledgments

Literature Cited

1. Chan, P., Dresnack, R, Liskowitz, J.W., Perna, A. and Trattner,
    R. "Sorbents for Fluoride Metal Finishing and Petroleum
    Sludge Leachate Contaminant Control", EPA 600/2-78-824.
    Match (1978)
2. "Sorbate Characteristics of Fly Ash", Volume II, Final Report,
    U.S. D.O.E. Grant DE-FG22-80PC30231, August, 1983, page 212.
3. Swingle, R.S. and Riggs W.M. "ESCA" Critical Reviews in
    Analytical Chemistry 5. 267 (1975)
4. Hansen, R.D., and Fisher, G.L. "Elemental Distribution in Coal
    Fly Ashes", Env. Sci. & Tech., 14, pp. 1111-1117, 1980.
5. Johnson, G.E., Kunka, L.M. and Field, J.H., "Use of Coal and
    Fly Ash as Absorbents for Removing Organic Contaminants from
    Secondary Municipal Effluents", I & EC, Process Design and
    Development 4, 323-327, 1965.
6. Mancy, K.H., Gates, W.E., Eye, J.D. and Deb, P.K., "The
    Adsorption Kinetics of ABC on Fly Ash", Purdue University Engineering
    Bulletin, Ext. Ser. 117, pt. 1, pp. 146-160, 1964.

28

Electron Microscopical and Chemical Characterization

Airborne Coal Fly Ash from a Remote Site
in the Northeastern United States

Liaquat Husain, James S. Webber, Vincent A. Dutkiewicz, Edmondo Canelli, and
Pravin P. Parekh

Wadsworth Center for Laboratories and Research, New York State Department of Health,
Albany, NY 12201

    Individual airborne microparticles collected before,
    during and after an episode of high sulfate concentra-
    tion at Whiteface Mountain, NY (26-30 July 1983) were
    characterized by scanning, transmission and high-voltage
    electron microscopy. Consistent with findings from an
    earlier episode, submicrometer spheres commonly identi-
    fied in coal fly ash were abundant during the high-
    sulfate period but were sparse before or after the epi-
    sode. Minerals identified in iron-rich spheres by
    electron diffraction were magnetite, maghemite, and
    hematite. Equally abundant at the same time were sili-
    con spheres which were probably glass because they
    yielded no diffraction patterns. Also common in high-
    sulfate samples were submicrometer spheres composed of
    varying proportions of iron, silicon, aluminum, potas-
    sium, calcium and titanium. Oil fly ash was not
    detected during the high-sulfate period. The chemical
    tracers Se and V revealed that oil-combustion aerosols
    had decreased while coal-combustion aerosols had
    increased during the high-sulfate period. Additional
    support for coal combustion as the source of the high-
    sulfate air mass at Whiteface Mountain and other NY
    sites was given by Mn/V ratios which were consistent
    with air from the coal-burning Midwest rather than the
    oil-burning East Coast. Prevailing meteorologic condi-
    tions also indicated air flow from the Midwest. Prelim-
    inary evaluation of a new chemical signature, V/Ni
    ratio, is also presented. Although observed ratios
    were also consistent with coal rather than oil combus-
    tion, additional evaluation of this tracer is needed.

Sections of eastern North America are being adversely affected by de-
position of acidic precipitation and aerosols, generally termed
''acid rain''. Most severely affected are ecosystems which overlie
the Canadian Shield, a silicate bedrock with low Mg and Ca

concentrations and hence low buffering capacity. Acid deposition here can quickly decrease pH in lakes, streams and soils. The Adirondack Mountains of New York are in such a position, with hundreds of lakes sustaining pH decreases that have severely depleted or eradicated fish populations (1). Coniferous forests may also be stressed as decreased soil pH alters metal ion balance (2). Human health may be affected directly by respirable sulfates and by the increased solubility of trace metals in acidified drinking water (3,4). An investigation of sediments in a remote Adirondack lake indicated that significant increases in sulfur deposition did not occur until about 1930 (5).

Approximately two thirds of airborne acids in the Northeast are sulfate with wet or dry deposition contributing equally to sulfates reaching the ground (6). Coal combustion in the industrial Midwest produces most of the SO_2 (sulfate precursor) emitted east of the Mississippi River. Indeed, eight coal-burning midwestern states (Illinois, Indiana, Kentucky, Michigan, Ohio, Pennsylvania, Tennessee, West Virginia) cumulatively produce 13,440 kilotons of SO_x annually versus only 1,481 kilotons from eight northeastern states (Connecticut, Massachusetts, Maine, New Hampshire, New Jersey, New York, Rhode Island, Vermont) (7). This, coupled with its location upwind of the acid-stressed Northeast, makes the Midwest the most likely source of sulfates reaching the Northeast. Indeed, studies that related daily aerosol sulfate concentrations ($[SO_4^{2-}]$) with backward air trajectories at Whiteface Mountain, NY, have invariably found that the highest $[SO_4^{2-}]$ were associated with air masses passing through the Midwest (8,9,10). A similar pattern has been observed in precipitation at Whiteface Mountain (11). While trajectory-based studies themselves do not unequivocally prove this assumption, more recent investigations have shown with increasing clarity that coal-burning in the industrial Midwest is indeed the major source of SO_4^{2-} aerosols reaching the acid-stressed Adirondack region. Husain et al. (12) used samples collected at 6-hour intervals from a network of sites to trace high-SO_4^{2-} air masses from the Midwest across New York State. These air masses retained Mn/V ratios characteristic of the Midwest ($\gg$ 1) even after traveling more than 500 km. Conversely, when trajectories passed through coastal regions, Mn/V ratios were distinctly lower ($<$ 0.5), consistent with that region's dependence on oil. Although the Mn/V ratio technique has some limitations (13), it can be a very useful indicator of air mass history, particularly at rural sites when used in conjunction with other tracers. Coal burning has been implicated by a high correlation of SO_4^{2-} and Se, a trace metal greatly enriched in coal-combustion emissions, in aerosols reaching Shenandoah Valley, VA, and New York State (14,15). This Se and SO_4^{2-} enrichment is caused by similarities in physical and chemical transformations. Sulfur is emitted primarily as gas, SO_2, and Se is emitted partially in the gaseous phase and also on the surfaces of the smallest particles which pass through precipitators and scrubbers. Recently, electron microscopy was used to identify coal fly ash in a high-SO_4^{2-} air mass at Whiteface Mountain during June, 1983 (16). Submicrometer magnetite and glass spheres were abundant when $[SO_4^{2-}]$ peaked but were absent 12 hours before and 12 hours after. Both the meteorology and the Mn/V ratios indicated a midwestern origin for this air mass. The combination of microparticle identification, meteorology and

chemical tracers has provided the clearest fingerprint to date of the
sources of SO_4^{2-} in northern New York.

   During the summer sampling campaign in 1983, a second high-SO_4^{2-}
episode was seen at Whiteface Mountain. Electron-microscopical (EM)
analysis of samples collected during this episode are presented and
discussed along with the measurement at Whiteface Mountain and other
NY sites of selected trace metals (V, Se, Mn, Ni) in relation to
source regions.

Experimental

During summer 1983 airborne particulate samples were collected with
high-volume samplers on Whatman 41 filters at the summit of Whiteface
Mountain (WFM), at Mayville (MAY) in the southwestern corner of New
York, at Alexandria Bay (AXB) on the northeastern shore of Lake
Ontario, and at West Haverstraw (WHV) in the lower Hudson River
Valley (Figure 1). While the first three sites are rural, West
Haverstraw is a suburban site located near the metropolitan New York
City area. This site was selected primarily to characterize East-
Coast aerosols because of its proximity to two oil-burning power
plants. Samples were collected for 6-hour intervals at Whiteface
Mountain and Mayville and for 12-hour intervals at West Haverstraw
and Alexandria Bay. These were analyzed for SO_4^{2-} by ion chromatog-
raphy and for Al, Mn, V, and Ni by atomic absorption spectrophoto-
metry as detailed elsewhere (12). Selenium concentrations were
measured by neutron activation analysis. Simultaneously with the
high-volume samples at Whiteface Mountain, microparticles were
collected on carbon-coated Nuclepore filters in an automatic dichoto-
mous sampler (16). These filters with collected particles were
transported in airtight containers to the lab where a thin carbon
film was vacuum evaporated over the collection surface to immobilize
the particles and to reduce excess charge produced by the electron
beam. In addition to the morphological, electron diffraction and
elemental EM analyses performed on the earlier samples (16), sections
of filter were shadowed with Au-Pd at an angle of ~30 degrees to
allow 3-dimensional interpretation of particle morphology by
transmission EM (17).

   During the period of interest (26-30 July 1983), air flow across
New York State was dominated by a slow-moving high-pressure system
from the Great Lakes. Although air trajectories were not available
at the time of writing, this pattern in the past has produced air
flow from the Midwest across the state and is generally associated
with high-SO_4^{2-} periods in upstate New York (18). This high pressure
system centered over southern Pennsylvania early on 27 July should
have produced air flow from the Midwest at Mayville while Alexandria
Bay and Whiteface Mountain should have been under the influence of
Canadian air. By the next day, the high had moved off the coast of
Virginia, where it remained stationary for two days (Figure 1) and
surface winds probably followed the pressure isobars. A cold front
with a large mass of leading showers was trailing the high. (The
leading edge of the showers can be seen in the upper left hand corner
of Figure 1.) During 28 July, precipitation began in the western
part of the state and by the next day was widespread throughout the
upstate area.
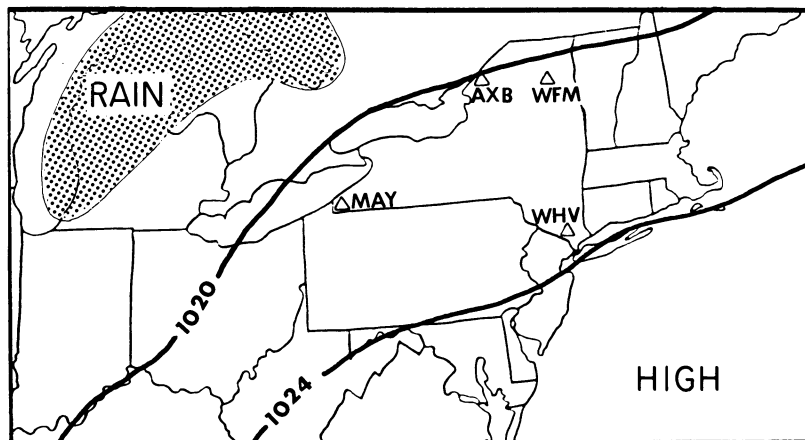
Figure 1. Simplified surface meteorologic conditions in the north-eastern United States at 0730 EST on 28 July 1983. Sampling sites are Mayville (MAY), Alexandria Bay (AXB), Whiteface Mountain (WFM) and West Haverstraw (WHV).

Results

Chemistry. On 27 July, [SO_4^{2-}] began to increase throughout the
state, first at Mayville and 12 hours later at Alexandria Bay and
Whiteface Mountain (Figure 2). This is consistent with the beginning
of midwestern air flow on the backside (western edge) of the high
pressure system. At Alexandria Bay and Whiteface Mountain, maximum
concentrations, 46 and 49 µg/m³ respectively, were observed late on
28 July but decreased dramatically on 29 July when precipitation was
widespread throughout the state. The onset of precipitation is also
indicated by the trace metal data. Aluminum concentrations at
Whiteface Mountain, for example, were ~340 ng/m³ during the peak
[SO_4^{2-}] period but decreased abruptly to 90 ng/m³ for the first sample
on 29 July. Such an abrupt decrease is consistent with the washout
of aerosols. At Mayville, [SO_4^{2-}] leveled off at ~25 µg/m³ for 30
hours beginning with the first sample on 28 July. However, the lead-
ing edge of showers shown in Figure 1, which began affecting the
western part of the state on the 28th, may have significantly lowered
the [SO_4^{2-}] at Mayville. The variations in trace metal concentrations
are consistent with this assumption. [SO_4^{2-}] at West Haverstraw also
peaked in the last sample on 28 July, but the concentration was much
lower, 15 µg/m³. Because this site was much closer to the center of
the high, it may very well have been influenced by air from a differ-
ent area than the upstate sites. This has been the case in episodes
previously studied (12).
        Trace element data can shed some light on the source of this SO_4^{2-}
episode; oil-combustion emissions are enriched in vanadium and coal-
combustion emissions, on the other hand, are enriched in selenium.
The variations of these elements can be related, at least qualita-
tively, to the presence of coal- and/or oil-combustion emissions.
        Since crustal contributions to vanadium can at times be a sig-
nificant proportion of the ambient concentrations, we have used the
vanadium enrichment factor (V_{ef}) rather than the vanadium concentra-
tion in Figure 2. (The enrichment factor is the ratio of an element
to aluminum in the sample relative to the ratio in the crust.) A
clear pattern of negative correlation between [SO_4^{2-}] and V_{ef} is seen
in Figure 2 for Whiteface Mountain and Mayville, indicating that oil
combustion was not the source of [SO_4^{2-}] increases. The pattern at
Alexandria Bay is less obvious, and may be due to a large, intermit-
tently operating oil-fired power plant located approximately 100 km
southwest of the site on the southeastern shore of Lake Ontario.
However, the fact that peak [SO_4^{2-}] at Whiteface Mountain and
Alexandria Bay on 28 July are essentially the same and that V_{ef} at
Whiteface Mountain indicates minimal influence from oil combustion
suggests that oil combustion did not significantly contribute to the
[SO_4^{2-}] at Alexandria Bay.
        Selenium concentrations were measured on 24-hour composite sam-
ples at Mayville and Whiteface Mountain. These results are compared
to 24-hour average [SO_4^{2-}] in Figure 3. At both sites [Se] and [SO_4^{2-}]
vary proportionately; [Se] increased markedly during the high [SO_4^{2-}]
period. This together with the negative correlation of V_{ef} and
[SO_4^{2-}] indicates that coal combustion was the dominant source of
[SO_4^{2-}] during this episode. Note that the Se scale at Whiteface
Mountain is half that at Mayville because the ratio of SO_4^{2-}/Se at
Whiteface Mountain (~ 8,000) is approximately twice that at Mayville
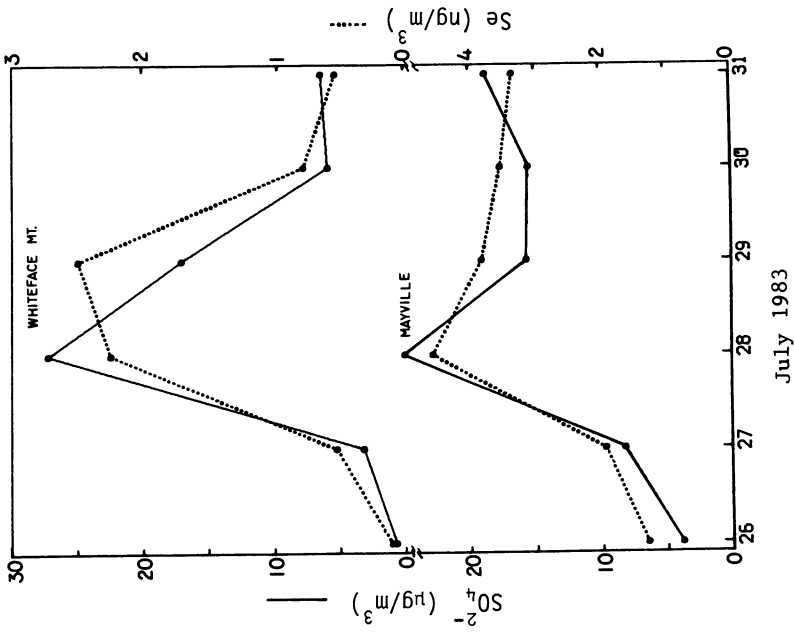
Figure 3. Mean daily sulfate and selenium concentrations at Mayville and Whiteface Mountain.
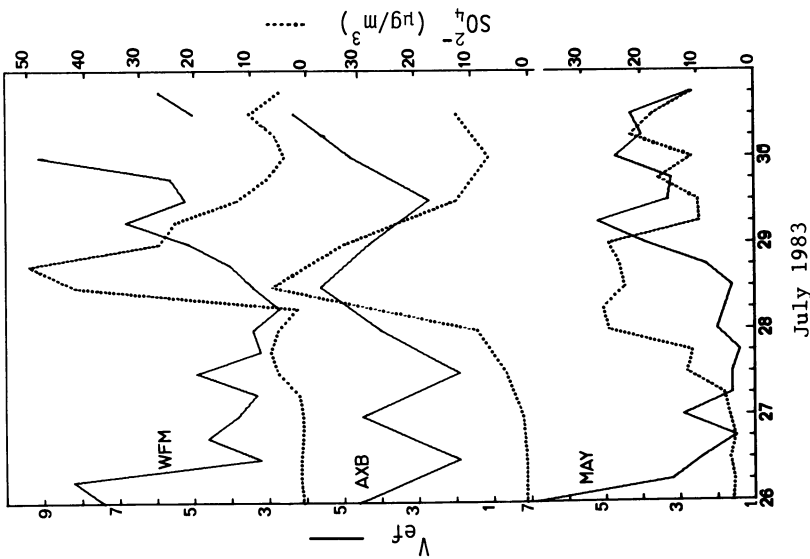
Figure 2. Sulfate concentrations and vanadium enrichment factors at three upstate New York sites in 1983.

($\sim$ 4,000). An increase in the proportion of $[SO_4^{2-}]$ to [Se] during transport across New York State has been generally observed during summer (15) and appears to be related to atmospheric conversion of SO_2 to SO_4^{2-}.

The ranges of Mn/V ratios (crustal corrected as described earlier (12)) are presented in Table 1. Throughout the episode, Mn/V ratios at the three upstate sites were consistently >2. While $[SO_4^{2-}]$ was >20 µg/m³ at Mayville, Mn/V ratios ranged from 3.3 to 21 and averaged 11. During 26 and 27 July Mn/V ratios were very high, often >20. V_{ef} from Figure 2 is very low, generally <2, indicating that the non-crustal component was very small. At these low levels, crustal correction of V can have large uncertainties and the magnitude of the Mn/V ratios are not significant. In spite of this, the data clearly indicate the lack of any significant contributions from oil combustion during this period. At Mayville on 29 July, however, the increase in V_{ef} coupled with a decrease in Mn/V ratios indicates a contribution from oil emissions at this time. At Whiteface Mountain during the peak $[SO_4^{2-}]$ period, Mn/V ratios averaged 6, which is within the range of values observed at Mayville although only about half the mean. Larger ratios at Mayville compared to Whiteface Mountain are, however, consistent with previous data (12,15). At both sites the Mn/V ratios were clearly within the range for midwestern air and much too high to suggest significant influence from oil-burning areas. However, on 29 July V_{ef} increased to between 5 and 7 and Mn/V ratios were much lower, at times <1, suggesting a contribution from oil emissions at this time. The fact that [Se] was still elevated indicates that a combination of coal and oil emissions were present during the latter stages of the SO_4^{2-} episode. We do not, however, feel that quantitative apportionment is appropriate at this time. The relationship between SO_4^{2-} and trace elements has not yet been sufficiently characterized, particularly in light of recently noted differences in the transport of SO_4^{2-} and trace elements during a detailed multi-site study (15). At Alexandria Bay, Mn/V ratios were only slightly >2, much lower than at Whiteface Mountain. While $[SO_4^{2-}]$ were comparable at the two sites, Vef at Alexandria Bay was much higher (Figure 2). Although the Mn/V ratios at Alexandria Bay were within the range of coal-burning regions, the fact that the ratios were much lower than at Whiteface Mountain suggests a larger influence from oil-combustion at Alexandria Bay. As discussed earlier the $[SO_4^{2-}]$ still seemed to be dominated by coal-combustion aerosols at Alexandria Bay.

While Mn/V ratios at West Haverstraw have been included for completeness, the site is situated within a few km of 2 oil-burning power plants and this precludes the usefulness of Mn/V ratios as tracers at West Haverstraw (13). In previous studies (12,16), Mn/V ratios at West Haverstraw were almost invariably <0.2 as a result of very high [V], which averaged $\sim$ 30 ng/m³. On 28 July the Mn/V ratio increased to 0.53 suggesting that a component from coal-combustion sources was also present at this site.

To reinforce the Mn/V ratio data we also considered V/Ni ratios in these samples. V/Ni ratios are different in coal and oil fly ash. [V] is markedly enriched in oil fly ash while [Ni] is enriched to a smaller extent (19). In contrast, [Ni] is increasingly enriched with decreasing particle size in coal fly ash whereas [V] is not (20,21). From 6 oil fly ash samples and 6 coal fly ash samples analyzed by

Table I. Airborne sulfate concentrations, Mn/V and V/Ni ratios at 4 New York sites during July 1983.

Date	Mayville			Whiteface Mountain			Alexandria Bay			West Haverstraw		
	SO_4^{2-}	Mn/V*	V/Ni	SO_4^{2-}	Mn/V*	V/Ni	SO_4^{2-}	Mn/V*	V/Ni	SO_4^{2-}	Mn/V*	V/Ni
26 July I	3.9	10.6	ND+	0.45	4.3	2.8	0.77	15	2.1	6.9	0.10	2.9
II	3.6	8.2	4.7	0.90	4.7	5.2	0.77	31	2.4	2.9	0.22	2.8
III	4.4	9.7	2.4	0.90	8.3	0.76						
IV	3.4	46	ND	0.45	0.67	2.3						
27 July I	4.5	58	ND	0.45	2.5	ND	1.4	2.6	3.1	3.3	0.46	3.1
II	5.4	40	1.5	1.1	4.7	0.22	4.4	9.5	1.6	NS#	NS	NS
III	12	21	1.9	4.9	2.0	1.1						
IV	11	62	1.5	6.2	5.5	0.81						
28 July I	26	9.9	1.4	4.9	5.5	1.0	9.5	2.8	2.3	12	0.53	1.6
II	27	22	0.72	14	9.2	1.3	46	2.1	1.9	15	0.47	1.7
III	23	12	1.0	41	7.6	1.0						
IV	24	7.9	2.1	49	5.7	1.7						
29 July I	26	3.3	0.97	26	2.6	1.3	33	2.1	2.1	6.7	0.44	1.7
II	9.9	1.9	ND	23	1.6	1.4	13	3.1	1.9	8.9	0.35	1.4
III	10	8.8	ND	12	0.28	2.1						
IV	17	7.9	1.5	6.7	0.78	0.26						
30 July I	11	4.1	ND	3.6	0.98	0.35	7.3	2.5	2.4	7.7	0.39	2.4
II	22	4.5	1.7	5.4	ND	ND	13	1.4	2.9	22	1.3	2.9
III	18	2.1	3.8	9.8	2.6	ND						
IV	11	4.8	ND	4.5	1.0	ND						

* Crustal corrections made according to reference (12).
+ ND, could not be determined accurately because of large crustal correction or low [Ni].
# NS, sample not collected.

Henry and Knapp (22), average V/Ni ratios are calculated to be 5.2 and 1.2 respectively. Analysis of the data of Davison et al. (21) reveals that V/Ni is very low (<0.5) in coal fly ash particles smaller than 2 μm. This is the particle size range expected to be transported long distances.

At West Haverstraw on 26-27 July, the V/Ni ratio averaged 3.0 (Table 1). This site is strongly influenced by oil emissions ([V] averaged 30 ng/m³) and the V/Ni ratio approached that measured in oil fly ash. On 28 July, however, when [SO_4^{2-}] increased to 10-15 μg/m³, V/Ni decreased to 1.6 but returned to near 3 on the 30th. The decreased V/Ni ratios are consistent with increased influence from coal-burning regions during the high-SO_4^{2-} period. At Whiteface Mountain, episodic ratios averaged 1.2 and nonepisodic ratios averaged 1.3, near that for coal, again indicating that oil-combustion aerosols were not dominant at these times. However, on 29 July when the Mn/V ratio was 0.28 the V/Ni ratio increased to 2.1, consistent with the earlier observation of increased contributions from oil combustion at this time. Trends in V/Ni ratios at Mayville and Alexandria Bay were similar to West Haverstraw with nonepisodic ratios averaging 2.1 and 2.4, respectively, and episodic ratios averaging 1.4 and 2.0. At none of the sites was the episodic V/Ni ratio large enough to be associated with purely oil-fired combustion products and, except at Whiteface Mountain where the ratio was already near that of coal, the V/Ni ratio decreased during the high-SO_4^{2-} episode, as expected for increased contributions from coal-burning areas. Consistent with Mn/V ratios, V/Ni ratios were higher at Alexandria Bay than at Whiteface Mountain during the episode, supporting the earlier conclusion that Alexandria Bay has an oil-derived aerosol component. While further study is needed, these data suggest that V/Ni ratios may provide another useful indicator of coal and oil combustion emissions.

Microparticles. More than 200 particles collected at Whiteface Mountain in the fine fraction (<2.5 μm) on 27 July I and IV, 28 July II, III and IV and 29 July I (where I=0000-0600 hours, II=0600-1200 hours, III=1200-1800 hours, IV=1800-2400 hours) were characterized by electron diffraction, energy-dispersive x-ray spectroscopy (EDXRS) and morphology with transmission and high-voltage EM.

The most abundant particles were S-rich particles, usually much smaller than 0.8 μm. These particles were electron translucent and occasionally the S x-ray peaks were accompanied by much smaller K, Ca or Fe x-ray peaks. Electron-difraction patterns disappeared too rapidly in the high-energy beams to be recorded on film. Interesting morphological features were highlighted by Au-Pd shadowing (Figure 4). Sulfur particles collected on 27 July IV ([SO_4^{2-}]=6μg/m³) and 29 July I ([SO_4^{2-}]=29 μg/m³) were dome shaped and generally larger than in other periods. Those collected in 28 July II and III samples ([SO_4^{2-}]=14 and 41 μg/m³, respectively) were not flattened, but rather had cluster morphologies similar to N in Figure 4b. Ferek et al. (17) revealed that aerosol (NH_4)$_2$$SO_4$ collected on SiO films with an impactor had dome-like morphologies. Particles were collected in the present study at a face velocity orders of magnitude lower than that encountered with an impactor. Hence, the S-rich clusters seen by us were probably (NH_4)$_2$$SO_4$ clusters which had retained their solid morphology rather than being flattened by high-velocity impaction.
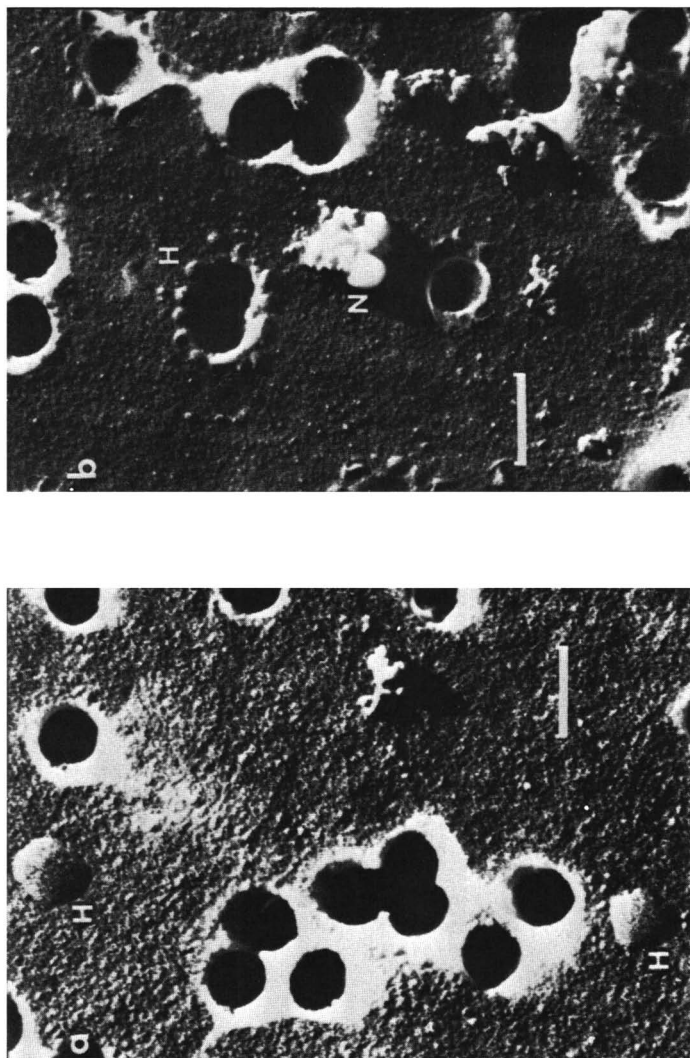
Figure 4. Transmission electron micrograph of sulfate particles collected on Nuclepore filters at Whiteface Mountain and shadowed with Au/Pd. Scale bars equal 0.5 μm. (a) 27 July IV 1983. H denotes caplike particles which are probably H_2SO_4. (b) 28 July IV 1983. N denotes cluster which is probably $(NH_4)_2SO_4$.

Ferek et al. also found that impacted H_2SO_4 on SiO films formed a
large central drop with multiple satellite droplets. This phenomenon
had been reported earlier by Frank and Lodge (23), who concluded that
this was caused by dehydration of the H_2SO_4 on the hydrophobic SiO
rather than by impaction forces. One reason that dome-like spheres
with satellites were not seen by us might be that the carbon film
used for collection was less hydrophobic than SiO and thus satellite
formation was not favored during desiccation. Furthermore, our
samples were given a second carbon coat soon after collection and
this probably slowed desiccation and prevented changes in morphology
during any subsequent desiccation/oxidation. Hence the dome-like
spheres were probably H_2SO_4. This hypothesis is reinforced by the
bubbling seen within these domes during electron-beam heating. This
bubbling was not evident in the clusters thought to be $(NH_4)_2SO_4$.
The S particles collected during the peak $[SO_4^{2-}]$ ranged from clusters
to domes, with small domes often concentrated around the 0.4 μm pores
(Figure 4b). This collection pattern is not unusual for smaller
particles which have insufficient inertia to be impacted uniformly on
the filter face but have too much inertia to pass over the lip of the
pore (24). These small domes are morphologically similar to the
H_2SO_4 and their contents did bubble in the electron beam. The
collection of the smaller H_2SO_4 near the pores during peak $[SO_4^{2-}]$ as
compared to the collection of the larger H_2SO_4 between the pores in
the earlier and later samples may indicate a less aged SO_4^{2-} component
in the aerosol during the peak period (25).

Spheres similar to those seen in the episode one month earlier
and identified as coal fly ash (16) were less numerous than the SO_4^{2-}
particles. The total number of spheres is larger than shown in
Figure 3 because spheres in clusters were often too small or too
agglomerated to allow individual enumeration. The abundance of these
spheres varied dramatically, ranging over more than two orders of
magnitude. Spheres were almost absent before the episode but were
abundant during the high-SO_4^{2-} period. A strictly quantitative
relationship between $[SO_4^{2-}]$ and fly-ash particles was not expected
because of opposing forces during transport: fly ash spheres could
only decrease during transport because of sedimentation whereas
$[SO_4^{2-}]$ could increase because of SO_2 oxidation.

All spheres and sphere clusters were <1 μm. This would suggest
a distant source in that larger spheres would have settled out during
extended transport. Their spherical morphology points to combustion
evolution, e.g., cooled silicate and metal droplets.

The abundance of spheres composed primarily of Fe (and called
ferrospheres after Lauf (26)) generally followed $[SO_4^{2-}]$ but peaked 12
hours earlier. Whereas magnetite (Fe_3O_4) was the most common ferro-
sphere mineral in the episode studied earlier, maghemite (γ-Fe_2O_3)
was the most abundant mineral in ferrospheres in this episode (Figure
5a,b). Magnetite (or Fe-rich spinels) and hematite (α-Fe_2O_3) were
also present. These minerals have been commonly reported in coal fly
ash studies (27,28,29). The x-ray spectra of these spheres occa-
sionally revealed traces of Mn, Zn, Si, K, Ca, Cr or Se. The first-
row transition metals are possibly isomorphic substitutions in the
spinel structure (29) whereas Se may be a surface-enriched volatile
as reported by others (21).

Spheres composed primarily of Si were as abundant as the
ferrospheres and their numbers correlated with $[SO_4^{2-}]$. In addition
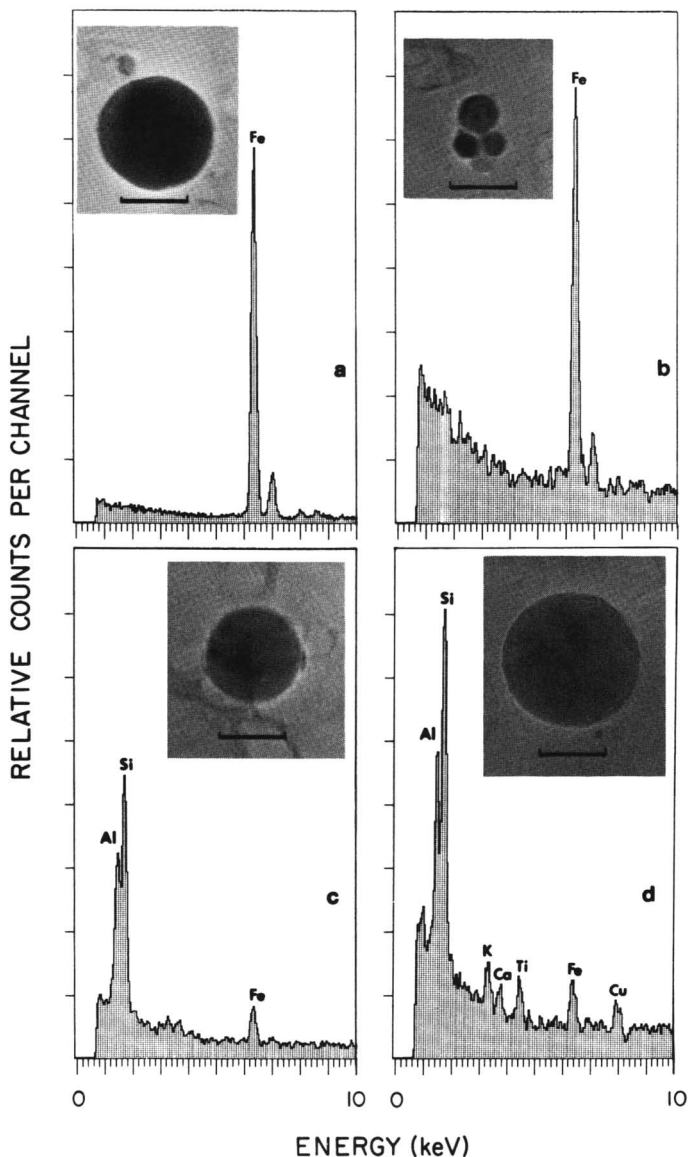
Figure 5.   High-voltage electron micrographs and x-ray spectra of microparticles collected at Whiteface Mountain in 1983.   Scale bars equal 0.5 μm.   (a) γ-Fe₂O₃ sphere collected 28 July II.   (b) γ-Fe₂O₃ sphere cluster collected 28 July IV. (c) Mullite sphere collected 28 July IV.   (d).   Mixed-element sphere collected 28 July III.

to the Si x-rays, these spheres often yielded smaller x ray peaks of
Fe, K, Ti, Al, Mn, Zn, Cd or Se. Like the Si spheres collected one
month earlier, these did not yield diffraction patterns, again making
them likely candidates for the glass spheres found in coal fly ash
(26,29).

Spheres which did not fit neatly into the Fe or Si group usually
were composed of a mixture of Al, Si, Fe and/or Ti. One sphere
(Figure 5c) was identified by its EDXRS and electron diffraction as
mullite $(3(Al_2O_3).2SiO_2)$, a high-temperature mineral found in coal
fly ash (26,27,28). Fe has been previously identified in mullite
coal fly ash (29). The mixed-element sphere in Figure 5d is the
largest sphere collected and identified at Whiteface Mountain.

There was no microparticle evidence of increased oil-combustion
emissions in the high-$[SO_4^{2-}]$ air mass. Oil fly ash is generally
platy or honeycombed carbon which is enriched in V and Ni (19,22,30).
Two particles yielded very small V x-ray peaks but these peaks were
not associated with a specific particle type or elemental
combination.

Common, though never abundant, were Si-rich fragments which were
identified from ED patterns as quartz, K feldspars and plagioclase
(Figure 6). These ranged in size from submicrometer to 3 μm.
Although more numerous during the high-$[SO_4^{2-}]$ period, abundance
varied only a little more than an order of magnitude. These were
probably local crustal fragments since the three identified mineral
groups are the most common minerals in the Adirondack region (31).

Pb-rich particles ranging from 0.1 to 1.0 μm were detected in
the episodic samples (Figure 7). These Pb x-ray peaks were always
associated with larger S peaks and $PbSO_4$ was the most commonly
identified mineral. The source of the particles is unceratin. Some
undoubtedly arose from automotive emissions even though Br x-ray
peaks were not seen. The more volatile Br may have been lost by
aging or by the heat of the electron beam. Whatever the source, the
association of SO_4^{2-} with Pb probably results in large part from
heterogeneous oxidation of SO_2 during atmospheric transport.
These particles were seen only when [Pb] exceeded 30 ng/m³ and the
concentration of Pb particles correlated closely with [Pb].

Conclusion

The variety of evidence outlined above demonstrated that SO_2
emissions from the industrial Midwest rather than emissions in the
Northeast were the major source of a high-SO_4^{2-} episode in the acid-
sensitive regions of New York State. The movement of a high-pressure
system during this episode was similar to previous meteorologic
conditions when trajectory analyses revealed flow of air masses from
the Midwest across the state. Vanadium enrichment factors revealed
decreased influence by oil combustion during peak $[SO_4^{2-}]$ at most
sites whereas selenium concentrations indicated that coal combustion
played an increased role. Mn/V ratios were distinctly midwestern
during this episode. V/Ni ratios reinforced the interpretation of
Mn/V ratios and hold promise as another regional signature. The
mineralogy, morphology and elemental composition of spheres collected
during the episode were typical of coal fly ash but not of oil fly
ash. The submicrometer size range of these spheres pointed to a
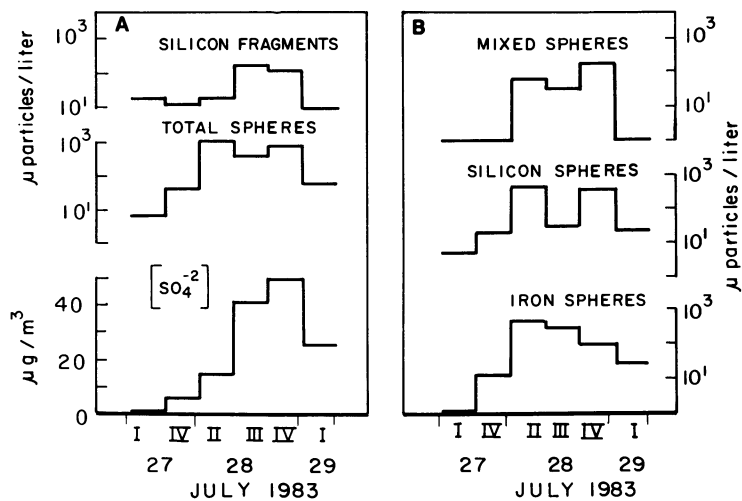
Figure 6. Sulfate and microparticle concentrations at Whiteface Mountain during selected periods from 27-29 July 1983.
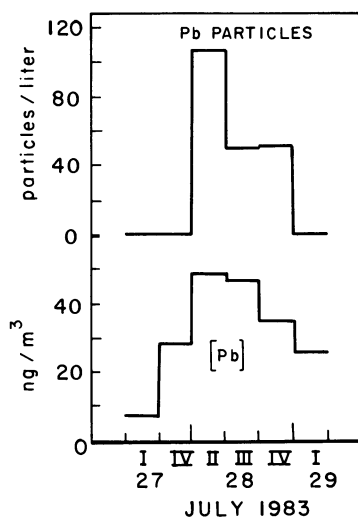
Figure 7. Lead concentrations at Whiteface Mountain during selected periods from 27-29 July 1983.

distant source. While this coal fly ash was virtually absent before
the episode, it became abundant when $[SO_4^{2-}]$ increased.

Acknowledgments

Literature Cited

1. Scofield, C.L. Ambio 1976, 10, 228.
2. Johnson, A.H., Siccama, T.G., Environ. Sci. Technol. 1983, 17,
   294A.
3. Alink, G.M. Mutation Res. 1983, 116, 21.
4. Mumford, J.L., Lewtas, J. J. Toxicol. Environ. Health, 1982, 10,
   565.
5. Holdren Jr., G.R., Brunelle, T.M., Matisoff, G., Wahlen, M.
   Nature, 1984, 311, 245.
6. Ragland, K.W., Wilkening, K.E. Relationship between Mesoscale
   Acid Precipitation and Meteorological Factors, Initial Draft of
   the Effects of Acid Precipitation and Ecological Systems,
   Michigan State University, East Lansing, MI, 1981.
7. Benkowitz, C.M. Atmos. Environ., 1982, 16, 1551.
8. Galvin, P.J., Samson, P.J., Coffey, P.E. Environ. Sci. Technol.
   1978, 12, 580.
9. Samson, P.J. Atmos. Environ. 1978, 12, 1889.
10. Parekh, P.P., Husain, L. Geophys. Res. Lett. 1982, 9, 79.
11. Wilson, J.W., Mohnen, V.A., Kadlacek, J.A., Atmos. Environ.
    1982, 16, 1667.
12. Husain, L., Webber, J.S., Canelli, E., Dutkiewicz, V.A.,
    Halstead, J.A. Atmos. Environ. 1984, 18, 1059.
13. Husain, L., Webber, J.S., Canelli, E. J. Air Poll. Control
    Assoc. 1983, 33, 1185.
14. Tuncel, S.G., Olmez, I., Parrington, J.R., Gordon, G.E., Stevens,
    R.K. Environ. Sci. Technol., 1985, 19, 529.
15. Husain, L., Dutkiewicz, V.A., Canelli, E., Parekh, P.P., Webber,
    J.S. Relationship between Aerosol Sulfate and Trace Elements
    during 500-km Transport, Middle Atlantic Regional Meeting, ACS,
    May 19, 1985.
16. Webber, J.S., Dutkiewicz, V.A., Husain, L. Atmos. Environ.
    1985, 19, 285.

17. Ferek, R.J., Lazrus, A.L., Winchester, J.W. Atmos. Environ. 1983, 17, 1545.
18. Dutkiewicz, V.A., Halstead, J.A., Parekh, P.P., Khan, A., Husain, L. Atmos. Environ. 1983, 17, 1475.
19. Cheng, R.J., Mohnen, V.A., Shen, T.T., Current, M., Hudson, J.B. J. Air Poll. Control Assoc. 1976, 26, 787.
20. Weissman, S.H., Carpenter, R.L., Newton, G.J. Environ. Sci. Technol 1983, 17, 65.
21. Davison, R.L., Natusch, D.F.S., Wallace, J.R., Evans, C.A. Jr. Environ. Sci. Technol. 1974, 8, 1107.
22. Henry, W.M., Knapp, K.T. Environ. Sci. Technol. 1980, 14, 450.
23. Frank, E.R., Lodge, J.P. Jr. J. Microscopie 1967, 6, 449.
24. Hinds, W.C., ''Aerosol Technology'', John Wiley and Sons, New York, NY, 1982.
25. Whitby, K.B. Atmos. Environ. 1978, 12, 135.
26. Lauf, R.J. Application of Materials Characterization Techniques to Coal and Coal Wastes, ORNL/TM-7663, Oak Ridge National Laboratory, TN, 1981.
27. Hansen, L.D., Silberman, C., Fisher, G.L. Environ. Sci. Technol. 1981, 5, 1057.
28. Cabaniss, G.E., Linton, R.W. Environ. Sci. Technol. 1984, 18, 271.
29. Hulett, L.D. Jr., Weinburger, A.J., Northcutt, K.J., Ferguson, M. Science 1980, 210, 1356.
30. McCrone, W.C., Delly, J.G. ''The Electron Microscopy Atlas'', In The Particle Atlas, Ed. Two, V. III, Ann Arbor Science, Ann Arbor, MI., 1973, 773-789.
31. Whitney, P., N.Y. State Geol. Survey, personal communication.

29

Modeling Future Emissions of Atmospheric Pollutants

Kristin Graves, Edward H. Pechan, and Donna L. Turner

E. H. Pechan & Associates, Inc., 5537 Hempstead Way, Springfield, VA 22151

This paper provides an overview of the techniques
used by policy analysts to estimate air pollution
emission from anthropogenic sources. The development
of an inventory of emissions from a large number of
emission sources by direct measurement would be
prohibitively expensive. Therefore, estimation
techniques are used which, although somewhat less
reliable at the specific unit or boiler level,
provide a reasonable assessment of emissions on
average. Although no physical measurement is used,
policy analysts are able to generate historic and
current estimates, and future forecasts, of air
pollutant emissions. This paper provides an overview
of the techniques used to provide such estimates and
forecasts.

Each year, millions of dollars are expended to fund research on the
causes and effects of environmental air pollution. While chemists
and biologists quantify and measure the physical relationships
between emission sources, emissions, and deposition, policy analysts
attempt to estimate historic, current, or future emissions and
deposition without making measurements at each emission source or
deposition site. The work of each group is quite dependent upon the
work of the other. For example, policy analysts use the results
obtained by chemists and biologists as an input to their
calculations. In turn, the estimates provided by the policy analysts
provide information to policy-makers regarding which pollutants are
likely to be the cause of current or future problems -- these problem
areas are those for which basic research, such as that conducted by
the biologists and chemists, will be funded.

The purpose of this paper is to provide chemists with an
overview of the techniques used by policy analysts to estimate future
air pollutant emissions. A comparison of modeling techniques for
future periods is also made with techniques for historical and
current periods. In addition, sample estimates of forecasted sulfur
dioxide (SO_2) emissions provide an illustration of the
uncertainty inherent in such estimates.

Environmental Estimation Methodology

General Methodology. The following is a schematic equation of the procedure used to estimate emissions:

$$EMIS = ACTLEV * EMISCOEFF * (1 - CONTEFF) \qquad (1)$$

where   EMIS = emission level of pollutant of interest, e.g., metric tons SO_2 per year

ACTLEV = level of activity relevant to estimated emission, e.g., coal use by utilities (for utility SO_2 emissions) or vehicle miles traveled (for transportation nitrogen oxides emissions)

EMISCOEFF = uncontrolled emissions per unit of activity level (e.g., tons of SO_2 emitted per ton of coal burned)

CONTEFF = proportion of uncontrolled emissions removed by emission control device

This general procedure is used to obtain emissions estimates for historic, current, and future years. The primary difference between emission estimates for historic, current, and future years is the use of historically available, currently reported, or future estimated values of the required input information.

The specific information used to provide estimates of activity levels varies with the emission source sector being examined. For utilities, fuel use is desired. For the industrial sector, information on fuel use alone is not adequate since many industrial process emissions do not result from fuel combustion. Usually, some approximation for product output, such as estimates of value added or earnings, is often used. For motor vehicle emissions, estimates of vehicle miles traveled is more useful than fuel use because most emissions are unrelated to vehicle efficiency, i.e., a small car emits about the same amount of pollution per mile as a larger car.

Emission coefficients are estimates of emissions per unit of activity level. These coefficients are generally estimated using actual measurements of emissions and information about activity levels from a subset of representative sources. The emission measurements used as an input to these coefficients are subject to considerable uncertainty, being based on measurements at ten sources or, at most, at a few hundred sources. Usually, no direct estimates of associated variability or uncertainty, are available. Depending upon the level of detail in the model being used to make the emission estimates, emission coefficients may be assumed constant over time or across regions, or new combustion and other technologies may be assumed to be available.

Multiplying activity levels by emission coefficients provides information on uncontrolled emissions over time. To obtain information on controlled emissions, the uncontrolled emissions total

can be multiplied by the quantity one minus the control efficiency.
Estimates of control efficiency can be obtained from the manufacturer
or from independent tests. As with emission coefficient estimates,
control efficiency information is generally somewhat crude with
little known about its variability over time or uncertainty.

Differences Between Estimates. The combination of these three
factors results in estimates of emissions that may be, as evidenced
here, somewhat crude. The general methodology described above may be
embellished or used at finer levels of detail to provide an
appropriate level of resolution in the generated emission estimates.
For example, EPA's National Emissions Data System (NEDS), a major
emission inventory covering point and area sources, uses such
calculations at the point or boiler level; other less-detailed data
files would use emissions calculated at a county or regional level
(1). It is important to stress, however, that the fate of
billions of dollars hinges on analyses such as these. Estimates of
emissions obtained similarly to those described here are used in the
analysis of proposed legislation and regulation. For example, under
House of Representatives bill number H.R. 3400 (also known as the
Sikorski-Waxman bill), the 50 highest emitting plants in 1980 were
targeted for scrubber installation; methods akin to those described
here, albeit in finer detail, would likely be used to identify those
plants. In fact, E.H. Pechan & Associates, Inc., identified the top
coal-fired utility SO_2 emitters for the U.S. Environmental
Protection Agency (EPA) in 1982 using a similar methodology
(2,3). For that study, information on the coal quantity and
quality (sulfur content) were available, as well as information on
existing control technologies.
     In general, the greatest resolution can be obtained in estimates
of current or recent historical (within the last 10 to 15 years)
emissions. This is because reliable data on fuel use (both quality
and quantity) and other activity levels are available, and good
estimates of emission coefficients and control efficiencies are
available. As one goes further back in time, the data needed for
detailed emission estimates are either not available or are less
reliable. Recently, SO_2 and nitrogen oxide emissions were
estimated for EPA for the period 1900 to 1980 at the state level by
fuel and source sector (4,5). It was particularly difficult to
obtain reliable estimates of pre-1940 fuel use and quality, control
efficiency, and emission coefficients. Obviously, the less data that
are available, the simpler the methodology that must be used. A
discussion of a data set required for detailed analysis of emissions
and deposition is beyond the scope of this paper, but is available
elsewhere (6).
     Obviously for future periods, no measured data are available and
all variables must be estimated. Some models, such as the Advanced
Utility Simulation Model (7) being developed for EPA, use complex
algorithms and modeling structures to internally simulate the
operations of a sector or sectors of the economy to obtain estimates
of activity levels, control efficiencies, and emission coefficients.
Other models, such as the Environmental Trends Analysis Model II
(8,9), originally developed for the U.S. Department of Energy,
use exogenous forecasts of activity levels and assumed values of
control efficiencies and emission coefficients. The uses for these

various types of forecasting models are discussed more fully in the
next section of this paper.

Emissions Forecasting

Introduction. Environmental projections are needed for three
primary reasons. The first reason is the long lag time between
beginning the process of setting of environmental standards and the
change in environmental conditions associated with the new standards.
The procedures needed to pass legislation or establish agency
standards take months or years to complete, and the lag time between
completion of those procedures and their implementation may be even
longer. During that entire period of time, it is important to be
able to predict the effects of the new standards so that it can be
determined whether or not additional controls may be necessary.
Furthermore, the longer the lag time, the greater the likelihood that
other relevant factors may also change, thereby having an impact on
the expected effect of the standards. For example, changing fuel
costs may encourage fuel switching, say from coal to oil, and thus
reduce the need for additional controls on coal-fired boilers.
        The second reason for environmental projections is the
significance of control costs. For example, proposed acid rain
legislation could cost utilities and their customers billions of
dollars. Before this money is spent, it is important to be able to
evaluate the effects that controls may have on emissions, on
employment, in different regions of the country, and the like. A
large share of SO_2 emissions are from older, dirtier, coal-fired
power plants. If these plants are retiring in a few years, it may
not make economic sense to spend millions or billions of dollars to
retrofit them with controls. On the other hand, if such plants will
be operating for many years to come, the benefits may be considered
worth the expense.
        The third reason for environmental projections is that they may
be able to identify emerging issues of importance. For example, the
increased use of scrubbers over time may result in a problem in the
disposal of scrubber sludge. As another example, the increasing
importance of certain high-tech industries over time may indicate
emerging hazardous waste disposal problems in certain regions of the
country.

Differences Between Models. As described above, there are several
reasons for making emission forecasts. A number of models exist that
have been developed to provide such forecasts. The differences
between the models cause one model to be more appropriate for certain
types of analyses than another model.
        In general, policy analysts use two structural types of models
to make forecasts of future activity levels: econometric and
engineering or process models. Econometric models use historic data
and relationships to estimate future trends in variables of interest.
Engineering or process models use the physical relationships of
production processes (i.e., the relationship between inputs to a
production process and its outputs) to predict levels of the
dependent variables. In general, the use of econometric modeling
techniques to forecast activity levels provides a better long-term
(beyond 20 years) trend because it relies on long-term, historical

trend analysis, and thus can capture the general upward or downward trends. For shorter-term forecasts, engineering or process models may provide a more accurate picture; in addition, use of engineering or process models facilitates the pin-pointing of the cause of a particular trend or change in a trend.

For some types of analyses, it may be important to examine individual utilities or even individual power plants. For other analyses, it may be sufficient to examine effects at the state level. Factors affecting the level of detail in a model include the data contained in the model and the types of calculations used. Generally, less-detailed models are appropriate for use in scoping analyses for time periods further into the future, say 50 years, to identify major trends that may be of future importance. The more detailed models can then be used to examine those identified trends in greater depth.

Associated with the level of detail in a model, the costs of development and use vary considerably among models. Some models, usually those attempting to provide extremely detailed results, may be developed over periods of ten years or more at a multi-million dollar cost. Other models, usually providing less detailed results, have been developed in a period of a few months at a cost of several thousand dollars. The cost of model use, in terms of computer time and expense, also varies considerably among models. Model runs may take a few hours in turn-around time and cost tens of dollars, or turn-around and analysis time may be several weeks and cost hundreds to thousands of dollars. As with development costs, the costs of model use generally vary with the level of detail. As with the level of detail, the less costly models are best used to identify major trends, which can (in terms of time and cost) then be examined in additional detail by the more expensive models.

In determining which model to use, the analyst needs to determine what outputs or results are needed to successfully accomplish the desired objectives of the study. Factors that should be considered include the level of regional detail, the forecast period, the pollutants to be considered, and the sectoral detail desired. Available funds and resources for running a model also need to be taken into account. For example, if a control strategy affecting all emission sectors is proposed, then a model examining only, say industrial emissions may not be sufficient. Interaction between emission source sectors and the capability of the models needs to be considered.

The treatment of uncertainty varies considerably from one model to another. Simpler models allow uncertainty in the input data to be treated through the use of alternative estimates of uncertain variables. For example, in the next section of this paper, uncertainty about the length of utility coal plant lifetimes is addressed by comparing results of two assumptions about the lifetime -- 60 years and 40 years. In that way, ranges of emission estimates are obtained that, it is hoped, provide reasonable upper and lower bounds on emissions. More sophisticated models allow users to specify percentage ranges of uncertainty for input data; the model then incorporates these uncertainty estimates into upper and lower bounds on estimated emissions. The Electric Power Research Institute has sponsored a number of such models (10).

Sample Emission Estimates

For illustrative purposes, results from the Environmental Trends
Analysis Model II (ETAM II) are presented here. ETAM II is an
engineering and process model that uses exogenous activity level
information (i.e., supplied from outside the model rather than
produced within it), to which production relationships are applied as
a means of generating estimates of pollutant emissions. ETAM II was
originally developed to provide environmental trend analyses in
support of DOE's 1983 National Energy Policy Plan (NEPP). ETAM II is
one example of a simple model, designed for use as an aid in
long-term emission trends analysis. In fact, it has been used for
policy and sensitivity analysis in support of such programs as the
Interagency Visibility Task Force and the Interagency Prevention of
Significant Deterioration Task Force.
    To provide an illustration of the type of ouputs provided by
these models, Figure 1 presents results based on the examination of
alternative coal plant lifetimes for facilities operated by the
electric utility industry. Figure 1 shows a comparison of assumed 40
and 60 year utility plant lifetimes on emissions to 2030. As can be
seen, these assumptions have no effect on emissions from non-utility
sectors, but have a tremendous effect on both the pattern and the
magnitude of total emissions.
    The significant impact of a plant lifetime assumption is due to
the stringent controls placed on new plants through new source
performance standard requirements; with earlier retirement of plants,
the newer and more stringently regulated plants come on-line much
sooner. For SO_2 emissions, the assumption regarding coal plant
lifetime affects the year in which industrial emissions become the
primary contributor to total emissions. Under the 40-year lifetime
assumption, utility SO_2 emissions fall below industrial emissions
by 2010. If a 60-year lifetime is assumed, this switch will not
occur until about 2030. As indicated earlier, the difference caused
by utility plant lifetime assumptions, identified here, could be
examined in greater detail by a more-detailed model.

Summary

Although measured levels of emissions are used as a basis for
calculating emissions in future years, such measurements are not used
as directly as one might think. Rather, combinations of estimated or
average emission factors, activity levels, and control efficiencies
are used to obtain estimates of emissions. The level of detail at
which these emission estimates are provided varies considerably. The
choice of a projection model for use in analysis is dependent upon
the desired detail in and the intended use for the results.

SO2 EMISSIONS (MILLION TONS PER YEAR)

LO = 40 YEARS; HI = 60 YEARS
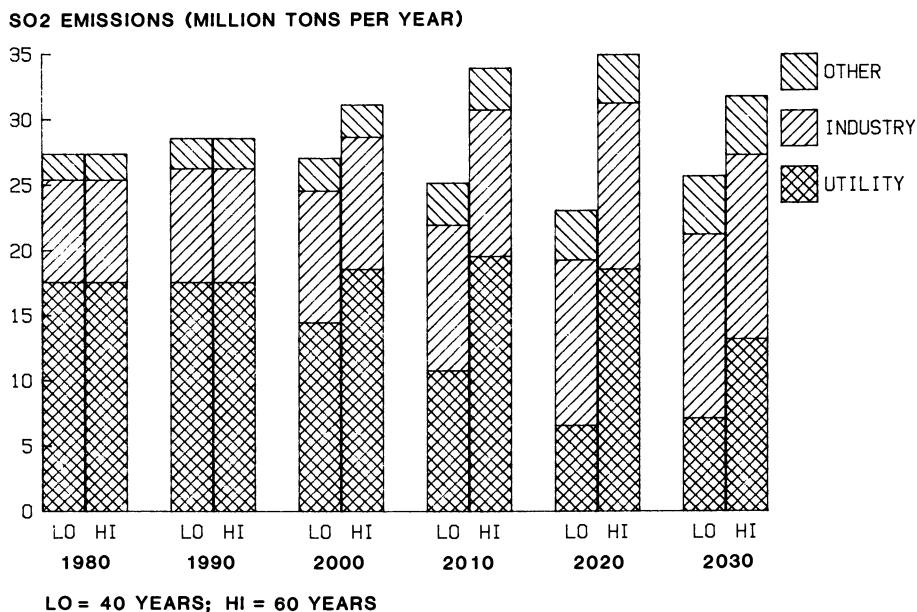
Figure 1. Emission forecasts under alternative utility coal plant lifetime assumptions.

Literature Cited

1. "National Air Pollutant Emission Estimates, 1940-1984." U.S. Environmental Protection Agency. EPA-450/4-85-014. January 1986.

2. E.H. Pechan & Associates, Inc. "Estimates of Sulfur Oxide Emissions from the Electric Utility Industry," Volume I - Summary and Analysis. Prepared for U.S. Environmental Protection Agency; EPA-600/7-82-061a. July 1982.

3. E.H. Pechan & Associates, Inc. "Estimates of Sulfur Oxide Emissions from the Electric Utility Industry," Volume II - Databook. Prepared for U.S. Environmental Protection Agency; EPA-600/7-82-061b. July 1982.

4. Gschwandtner, G.; Gschwandtner, K.; Eldridge, K.; Mann, C.; Mobley, D. "Historic Emissions of Sulfur and Nitrogen Oxides in the United States from 1900 to 1980." *Journal of the Air Pollution Control Association*. Vol. 36, No. 2. February 1986; p. 139-149.

5. "Historic Emissions of Sulfur and Nitrogen Oxides in the United States from 1900 to 1980," Volume I - Results. U.S. Environmental Protection Agency, Air and Energy Engineering Research Laboratory; EPA-600/7-85-009a. April 1985.

6. Saxena, P.; Seigneur, C.; Pollack, A.K. "A Critical Assessment of Existing Data Bases for Acid Deposition Modeling Studies," *Journal of the Air Pollution Control Association*. Vol. 36, No. 1. January 1986; p. 48-54.

7. "AUSM - Analytical Documentation," Volumes I, II, and III. Assembled by U.S. Environmental Protection Agency, Industrial and Environmental Research Laboratory, prepared by Universities Research Group on Energy. March 1983.

8. E.H. Pechan & Associates, Inc. "The Environmental Trends Analysis Model: Technical Documentation." March 1984.

9. E.H. Pechan & Associates, Inc. "The Environmental Trends Analysis Model: User Documentation." March 1984.

10. Electric Power Research Institute. "Air Quality Models Update: Decision Frameworks and Risk Assessment Models." Energy Analysis and Environment Division Technical Newsletter, Issue #1. February 10, 1984.

Author Index

Subject Index

370

Author Index

Subject Index

370

M

Magnesium
  effect on solids analysis, limestone
      DA desulfurization process, 182
  effects on performance of limestone
      DA process, 177–188
  limestone DA pilot plant,
      distribution of ion
      concentration, 183f
  surface adsorption on calcium
      carbonate, model, 188
Magnesium ion effect, test conditions,
    limestone DA process, 180t,191t
Magnesium sulfite hexahydrate, LCM
    prediction of solubility, FGD, 229
Metal parts furnace (MPF), munitions,
    chemical agent disposal, 196
Meteorology, chemical tracers,
    microparticle identification, SO_2
    sources, 345
Methanol, supercritical, organic
    sulfur removal, gas and liquid
    product analysis, 81
Microbial desulfurization
  coals, 86
  experiments in two-inch pipeline, 91
  literature review, organic
      sulfur, 87
  mechanism, 87
Microbubble flotation, advanced PCC
    processes, 16
Microparticles
  characterization, identification of
      source of sulfates in airborne
      particulates, 352–356
  meteorology, and chemical tracers,
      identification of SO_2
      sources, 345
Mineral matter
  effect of gravimelt process,
      coal, 46
  removal, caustics, 52
  sulfur, two-step process for
      extracting from coal, 39
Moisture, role in sulfur removal from
    coal, 60
Molal ionic activity coefficients, LCM
    prediction, FGD, 226

N

Nitrate ion, precipitation, 1980, 6f
Nitrite ion, bisulfite ion, summary of
    interactions between, 162f
Nitrogen
  content effect on combustion of coal
      liquid fuels, 124

Nitrogen--Continued
  purity effect on $Ca(OH)_2$
      reactivity, 220
Nitrogen oxides
  coal liquid fuels
    diesel combustion, 130
    effect of excess oxygen, 141f,143f
    emissions reduction, 137,138–144
  coal-fired power plants, federal
      emissions regulations, 149
  ferrous chelates
    kinetics and thermodynamics of
        reversible reaction, 162
    simultaneous desulfurization, 161
  formation in FBC, 102–104
  history, emission control, 2
  kinetics and thermodynamics of
      reactions with sulfite and
      bisulfite, , 162
  oxidation of sulfite, 287
  potential for emissions reduction in
      FBC, 101
  simultaneous desulfurization,
      analytical methods, 170
  sulfur dioxides, U.S. current and
      projected emissions, 3t
Nitrogen-sulfur compounds
  ion chromatogram, 173f
  kinetics and thermodynamics of
      formation, 169

O

Oil agglomeration, coal, trace element
    removal, PCC, 65
Oil fly ash, sulfates, airborne
    microparticles, 344
Oil-combustion emissions, trace
    element data, 348
Organic acids, effect on $Ca(OH)_2$
    reactivity, 215
Organic compounds present in
    effluents, coal combustion, 116t
Organic deliquescents
  effect on $Ca(OH)_2$ reactivity, 215
  effect on reactions of SO_2 with
      $Ca(OH)_2$, 209
Organic pollutants
  coal combustion, gas
      chromatograms, 118f
  extraction procedures, 113
  fly ash, sampling procedures, 112
  grate ash, sampling procedures, 112
  particulate effluents,
      discussion, 120
  partitioning procedures, 113
  release from coal combustion, 109
  stack ash, sampling procedures, 112

Production by Cara Aldridge Young
Indexing by Susan Robinson
Jacket design by Pamela Lewis

Elements typeset by Hot Type Ltd., Washington, DC
Printed and bound by Maple Press Co., York, PA